

Electrochemical C–H Activation by Ruthenium and Palladium Catalysis

Dissertation
for the award of the degree
“Doctor rerum naturalium”
of the Georg-August-Universität Göttingen



within the doctoral program of chemistry
of the Georg-August-Universität School of Science (GAUSS)

Submitted by
Xiaoyan Hou
From Shijiazhuang, China

Göttingen, 2024

Thesis Committee

Prof. Dr. Lutz Ackermann

Institute of Organic and Biomolecular Chemistry, Georg-August-Universität Göttingen

Prof. Dr. Konrad Koszinowski

Institute of Organic and Biomolecular Chemistry, Georg-August-Universität Göttingen

Prof. Dr. Dietmar Stalke

Institute of Inorganic Chemistry, Georg-August-Universität Göttingen

Members of Examination Board

Reviewer: Prof. Dr. Lutz Ackermann

Institute of Organic and Biomolecular Chemistry, Georg-August-Universität Göttingen

2nd Reviewer: Prof. Dr. Konrad Koszinowski

Institute of Organic and Biomolecular Chemistry, Georg-August-Universität Göttingen

Further members of the Examination Board

Prof. Dr. Dietmar Stalke

Institute of Inorganic Chemistry, Georg-August-Universität Göttingen

Prof. Dr. Jun.-Prof. Dr. Nadja A. Simeth

Institute of Organic and Biomolecular Chemistry, Georg-August-Universität Göttingen

Dr. Michael John

Institute of Organic and Biomolecular Chemistry, Georg-August-Universität Göttingen

Dr. Holm Frauendorf

Institute of Organic and Biomolecular Chemistry, Georg-August-Universität Göttingen

Date of the oral examination: 19.03.2024

List of Abbreviations

| | |
|-------------|---|
| A | Ampere |
| Ac | acetyl |
| Alk | alkyl |
| AMLA | ambiphilic metal-ligand activation |
| aq. | aqueous |
| Ar | aryl |
| atm | atmospheric pressure |
| BG | Bagging |
| BIES | base-assisted internal electrophilic substitution |
| Bn | benzyl |
| BQ | 1,4-benzoquinone |
| Boc | <i>tert</i> -butyloxycarbonyl |
| Bu | butyl |
| Bz | benzoyl |
| calc. | calculated |
| <i>cat.</i> | catalytic |
| CMD | concerted metalation deprotonation |
| conv. | conversion |
| Cp* | cyclopentadienyl |
| Cy | cyclohexyl |
| δ | chemical shift |
| d | doublet |
| DCE | 1,2-dichloroethane |
| DCM | dichloromethane |
| dd | doublet of doublet |
| DFT | density functional theory |
| DG | directing group |
| DME | dimethoxyethane |
| DMF | <i>N,N</i> -dimethylformamide |
| DMSO | dimethyl sulfoxide |
| DT | Decision Tree |
| dt | doublet of triplet |

List of Abbreviations

| | |
|------------------|--|
| EI | electron ionization |
| Equiv. | equivalent |
| ES | electrophilic substitution |
| ESI | electrospray ionization |
| ET | Extra-Trees |
| Et | ethyl |
| Fc | ferrocene |
| FG | functional group |
| g | gram |
| GB | Gradient Boosting |
| GC | gas chromatography |
| h | hour |
| Hal | halogen |
| Het | hetero atom |
| Hept | heptyl |
| Hex | hexyl |
| HPLC | high performance liquid chromatography |
| HR-MS | high resolution mass spectrometry |
| Hz | Hertz |
| <i>i</i> | <i>iso</i> |
| IR | infrared spectroscopy |
| IES | internal electrophilic substitution |
| <i>J</i> | coupling constant |
| KIE | kinetic isotope effect |
| KNR | k-Nearest Neighbors Regression |
| KRR | Kernel Ridge Regression |
| L | ligand |
| LSVR | Linear Support Vector Regression |
| <i>m</i> | <i>meta</i> |
| m | multiplet |
| M | molar |
| [M] ⁺ | molecular ion peak |
| Me | methyl |

List of Abbreviations

| | |
|------------|--|
| Mes | mesityl |
| mg | milligram |
| MHz | megahertz |
| min | minute |
| mL | milliliter |
| ML | Machine learning |
| mmol | millimol |
| M. p. | melting point |
| MS | mass spectrometry |
| <i>m/z</i> | mass-to-charge ratio |
| NCTS | <i>N</i> -cyano-4-methyl- <i>N</i> -phenyl benzenesulfonamide |
| NMTS | <i>N</i> -cyano- <i>N</i> -(4-methoxy)phenyl- <i>p</i> -toluenesulfonamide |
| NMP | <i>N</i> -methylpyrrolidinone |
| NMR | nuclear magnetic resonance |
| <i>o</i> | <i>ortho</i> |
| OA | oxidative addition |
| OPV | oil pump vacuum |
| <i>p</i> | <i>para</i> |
| Ph | phenyl |
| Piv | pivaloyl |
| ppm | parts per million |
| Pr | propyl |
| Py | pyridyl |
| Pym | pyrimidine |
| q | quartet |
| RF | Random Forest |
| RT | room temperature |
| s | singlet |
| sat. | saturated |
| SPS | solvent purification system |
| SVR | Support Vector Machine |
| <i>t</i> | <i>tert</i> |
| t | triplet |

List of Abbreviations

| | |
|------------|------------------------------|
| T | temperature |
| THF | tetrahydrofuran |
| TLC | thin layer chromatography |
| TM | transition metal |
| TMS | trimethylsilyl |
| Ts | <i>para</i> -toluenesulfonyl |
| TS | transition state |
| V | Volt |
| <i>wt%</i> | weight by volume |
| XGB | XGBoost |

Contents

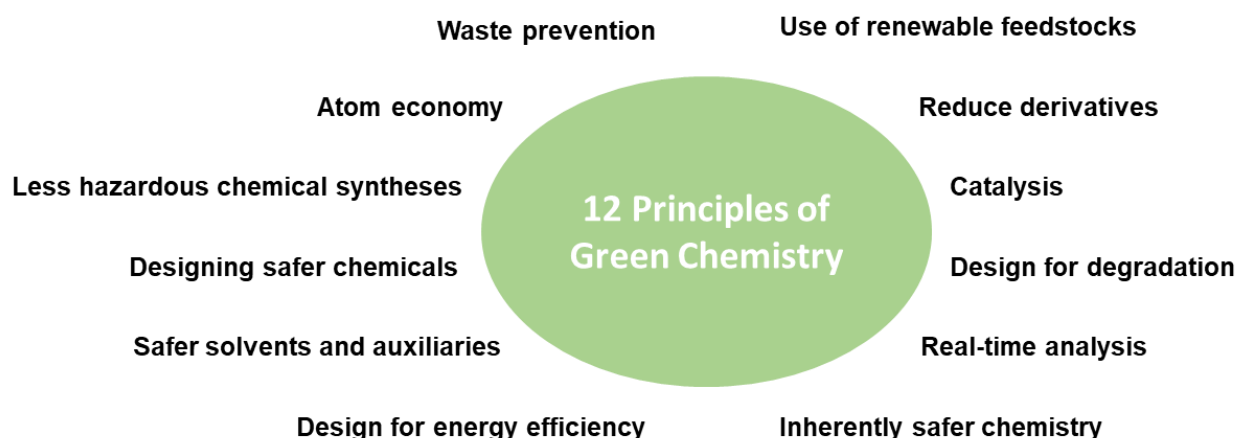
| | |
|--|----|
| 1 Introduction | 1 |
| 1.1 Metal-Catalyzed C–H Activation | 1 |
| 1.1.1 Metal-Catalyzed Cross-Coupling <i>versus</i> C–H Activation | 1 |
| 1.1.2 Mechanistic Manifolds | 2 |
| 1.1.3 Selectivity Control | 4 |
| 1.2 Ruthenium-Catalyzed C–H Activation | 6 |
| 1.2.1 Ruthenium-Catalyzed Alkyne Annulation Reactions | 8 |
| 1.2.2 Ruthenium-Catalyzed C–H Acyloxylation | 10 |
| 1.3 Palladium-Catalyzed Enantioselective C–H Activation | 13 |
| 1.3.1 Monoprotected Amino Acids as Chiral Ligands | 14 |
| 1.3.2 Chiral Transient Directing Group | 18 |
| 1.4 Transition Metal-Catalyzed Electrochemical C–H Activation | 21 |
| 1.4.1 Palladium Catalyzed Electrochemical C–H Activation | 21 |
| 1.4.2 Ruthenium Catalyzed Electrochemical C–H Activation | 25 |
| 1.5 Machine Learning in Synthetic Organic Chemistry | 28 |
| 1.5.1 General Introduction of ML | 28 |
| 1.5.2 ML for Reaction Prediction and Optimization | 29 |
| 2 Objective | 31 |
| 3 Results and Discussion | 34 |
| 3.1 Ruthenaelectro-Catalyzed Three-Component C–H Annulation | 34 |
| 3.1.1 Optimization and Substrate Scope of Annulation Reaction | 34 |
| 3.1.2 Mechanism Study | 36 |
| 3.1.3 Proposed Catalytic Cycle | 39 |
| 3.2 Ruthenaelectro-Catalyzed C–H Acyloxylation for Late-stage Tyrosine and Oligopeptide Diversification | 40 |
| 3.2.1 Optimization Study | 40 |
| 3.2.2 Scope and Removal of Pyridyl Group | 41 |
| 3.2.3 Mechanistic Study | 46 |
| 3.2.4 Proposed Catalytic Cycle | 50 |
| 3.3 Palladaelectro-Catalyzed C–H Olefination for N–C Axial Chirality <i>via</i> Chiral Transient Directing Group Strategy | 52 |
| 3.3.1 Optimization and Scope | 52 |
| 3.3.2 Cyclic Voltammetry Studies | 56 |

| | |
|--|-----|
| 3.3.3 Plausible Catalytic Cycle | 57 |
| 3.4 Palladaelectro-Catalyzed C–H Olefinations for Axially Chiral Anilides Mediated by the Mono- <i>N</i> -Protected Amino Acid | 59 |
| 3.4.1 Optimization Studies..... | 59 |
| 3.4.2 Substrate Scope and Limitations | 59 |
| 3.4.3 Proposed Catalytic Cycle | 62 |
| 3.5 Yield Optimization of Palladaelectro-Catalyzed C–H Annulation using Machine Learning..... | 64 |
| 3.5.1 Workflow Design for Reaction Optimization | 64 |
| 3.5.2 Results of ML-Guided Yield Optimization | 66 |
| 3.5.3 Scope of ML-Guided Palladaelectro-Catalyzed C–H Annulation..... | 69 |
| 3.6 Enantioselectivity Prediction for Palladaelectro-Catalyzed C–H Olefination using Machine Learning | 73 |
| 3.6.1 Workflow of ML Process..... | 73 |
| 3.6.2 Model Training Results..... | 74 |
| 4 Summary and Outlook | 80 |
| 5 Experimental Data | 85 |
| 5.1 General Remarks..... | 85 |
| 5.2 General Procedures..... | 89 |
| 5.3 Ruthenaelectro-Catalyzed Three-Component C–H Annulation | 94 |
| 5.3.1 Characterization Data..... | 94 |
| 5.3.2 Cyclic Voltammetry Studies..... | 98 |
| 5.4 Ruthenaelectro-Catalyzed C–H Acyloxylation for Late-stage Tyrosine and Oligopeptide Diversification | 100 |
| 5.4.1 Characterization Data..... | 100 |
| 5.4.2 Removal of Pyridyl Group..... | 126 |
| 5.4.3 Mechanistic Study | 127 |
| 5.5 Palladaelectro-Catalyzed C–H Olefination for N–C Axial Chirality <i>via</i> Chiral Transient Directing Group Strategy | 142 |
| 5.5.1 Characterization Data..... | 142 |
| 5.5.2 On/off Experiment..... | 144 |
| 5.5.3 Cyclic Voltammetry Study..... | 145 |
| 5.6 Palladaelectro-Catalyzed C–H Olefinations for Axially Chiral Anilides Mediated by the Mono- <i>N</i> -Protected Amino Acid | 148 |
| 5.6.1 Characterization Data..... | 148 |

| | |
|--|-----|
| 5.6.2 Cyclic Voltammetry Study..... | 164 |
| 5.7 Yield Optimization for Palladaelectro-Catalyzed C–H Annulation using Machine Learning..... | 166 |
| 5.7.1 Details of Dataset | 166 |
| 5.7.2 Details of Descriptors | 168 |
| 5.7.3 Results of Yield Optimization..... | 171 |
| 5.7.4 Characterization Data..... | 178 |
| 5.8 Enantioselectivity Prediction of Palladaelectro-Catalyzed C–H Olefination using Machine Learning | 208 |
| 5.8.1 Characterization Data..... | 208 |
| 6 References | 220 |
| 7 Acknowledgements | 228 |
| 8 NMR Spectra | 230 |

1 Introduction

Since the discovery of the urea synthesis reported by Wöhler in Germany in 1828,^[1] enormous progress in organic chemistry has been made during the last century, ranging from drug development to materials science.^[2] Nevertheless, there is a growing need for resource-, step- and atom- efficient synthetic methods.^[3] In 1998, Anastas and Warner put forward the “12 Principles of Green Chemistry”, providing a general guideline for designing sustainable organic synthetic processes (Scheme 1-1).^[4] In this regard, catalysis helps to operate the chemical reactions with catalytic amounts of catalysts instead of stoichiometric reagents, thus setting the stage for resource-economical chemistry. In addition, the direct activation of inert C–H bonds without pre-functionalization allows for step- and atom-efficient chemical processes.^[5] Furthermore, using electricity in place of toxic chemicals can enable more chemical transformations with reduced waste generation under mild exceedingly reaction conditions.^[6]



Scheme 1-1 12 Principles of green chemistry.

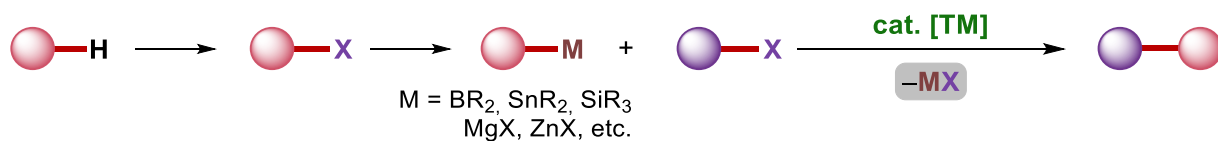
1.1 Metal-Catalyzed C–H Activation

1.1.1 Metal-Catalyzed Cross-Coupling *versus* C–H Activation

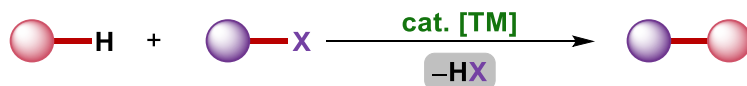
Transition metal-catalyzed cross-coupling reactions have been widely used in organic synthesis for the robust construction of C–C and C–heteroatom bonds (Scheme 1-2a).^[7] Evolving from homo-coupling reactions, as pioneered by Glaser^[8] and Ullman,^[9] a diverse array of transition metal-catalyzed cross-coupling reactions has been developed, including Mizoroki-Heck,^[10] Kumada-Corriu,^[11] Negishi,^[12] Stille,^[13] Hiyama,^[14] Suzuki-Miyaura,^[15] and Sonogashira-Hagihara^[16] reactions. The significant impact and practical applications of these discoveries in both academia and industry were recognized with awarding the 2010 Chemistry Nobel Prize to Heck, Negishi and Suzuki for their pioneering work on palladium-catalyzed cross-coupling reactions.^[17]

Despite the tremendous progress achieved through transition metal-catalyzed cross-couplings, several limitations, such as the requirement for pre-functionalized starting materials and the use of air- and moisture-sensitive organometallic coupling partners, can compromise their overall atom-economy and sustainability. Moreover, the generation of stoichiometric and potentially toxic by-products is undesirable and violates the principles of green chemistry. To address these limitations, C–H activation has emerged as an alternative in modern organic synthesis.^[18] It allows for the direct utilization of an otherwise inert C–H bond to form a new C–C or C–Het bond in the absence of any leaving groups (Scheme 1-2b).^[19] Additionally, oxidative twofold C–H activation enables the direct transformation of two inert C–H or C–H/Het–H bonds into C–C or C–Het bonds with molecular hydrogen as the sole by-product, thus being rendered as a promising atom- and step- economic approach (Scheme 1-2c).^[6a, 6d, 20]

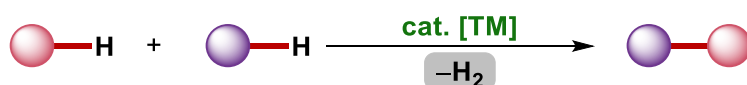
a) Traditional cross coupling



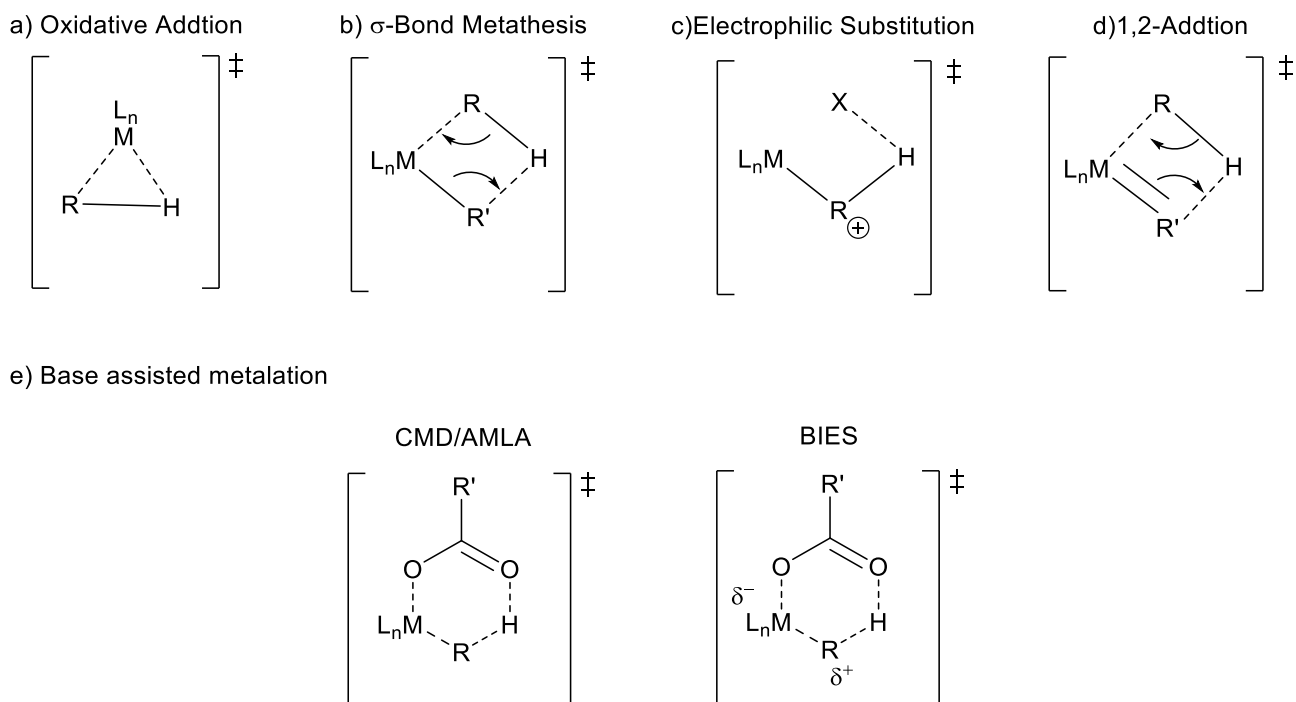
b) C-H activation



c) Oxidative C-H/C-H activation

**Scheme 1-2 Metal-catalyzed cross coupling versus C-H activation.****1.1.2 Mechanistic Manifolds**

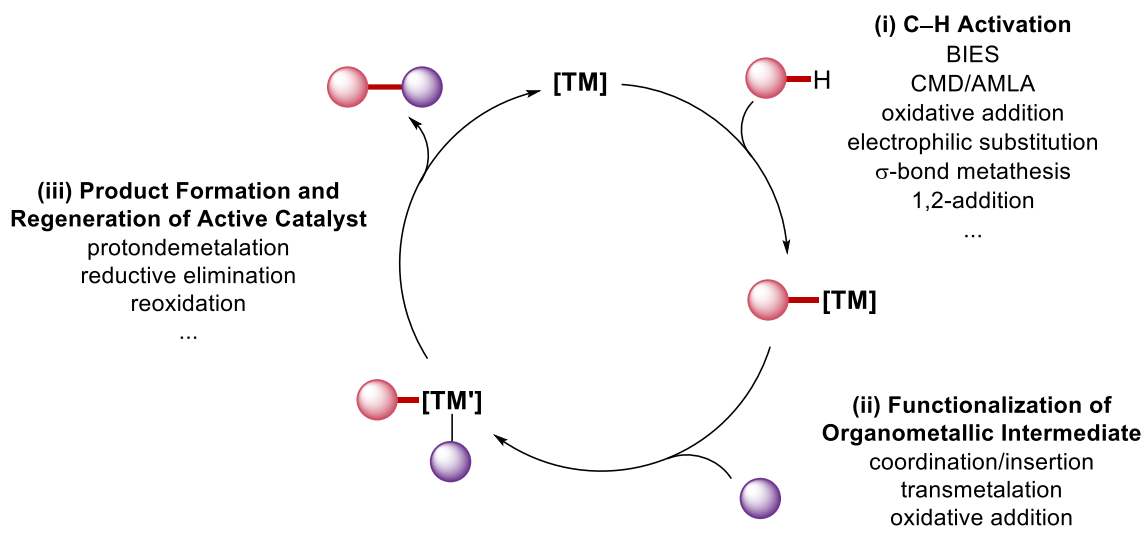
Despite significant advantages of transition metal-catalyzed C-H activation, the formation of a C-Metal bond from a C-H bond is far more difficult, since the C-H bond is generally stronger than the C-X bond.^[21] Thus, significant efforts have been directed towards understanding the mechanistic pathways involved in the C-H activation step. Aside from metalloradical or metal carbene/nitrene outer-sphere mechanisms, five different possible pathways are mainly proposed:^[22] a) oxidative addition; b) σ -bond metathesis; c) electrophilic substitution; d) 1,2-addition and e) base-assisted metalation (Scheme 1-3).



Scheme 1-3 C–H activation modes of action.

Among these pathways, the base-assisted metalation model has garnered significant research attention, and it was classified into 2 types (Scheme 1-3e). One is the CMD pathway proposed by Fagnou and Gorelsky, including the simultaneous coordination of a metal atom and deprotonation of a proton from a C–H bond.^[23] The similar pathway, known as AMLA, was introduced by Macgregor and Davies through computational studies.^[24] The BIES mechanism introduced by Ackermann involves electrophilic substitution-type C–H activation with the assistance of coordinated ligands, such as carboxylate.^[25] In contrast to the CMD/AMLA, the selectivity of BIES-type C–H activation is not controlled by kinetic C–H acidity.^[26] BIES-type reactions typically exhibit a preference for the more electron-rich substrates (Scheme 1-3e).

Based on these proposals, the general catalytic cycles for organometallic catalyzed C–H functionalization reactions can be envisioned (Scheme 1-4), although the specific details of the mechanisms may differ according to the specific reaction. The first step is the coordination of the substrate to the metal center, which is followed by a C–H activation to generate an organometallic intermediate. Then, this organometallic species undergoes functionalization and reductive elimination to afford the final product, and the catalyst is regenerated for subsequent cycles of substrate coordination, activation, and functionalization.

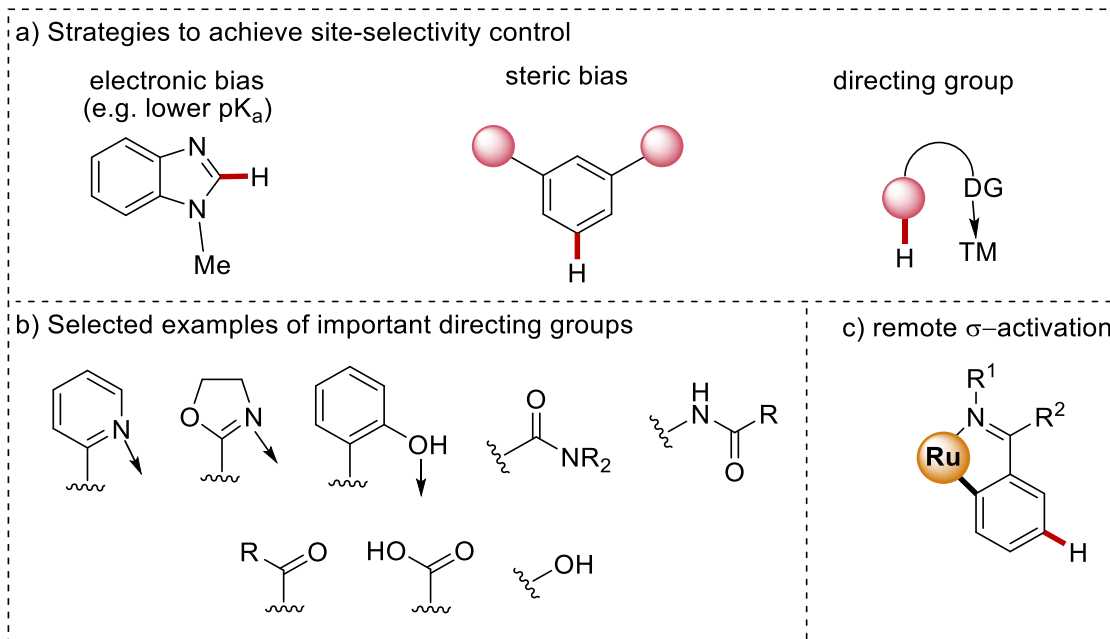


Scheme 1-4 General catalytic pathway for transition metal-catalyzed C–H activation reactions.

1.1.3 Selectivity Control

Controlling the position selectivity is the main challenge of C–H functionalization due to the difficulty in differentiating multiple C–H bonds in one molecule. In this respect, several strategies have been developed, such as (Scheme 1-5a): a) exploiting the inherent electronic bias of the substrate to activate more acidic positions, and b) using steric bias to activate the less hindered C–H bond. Unfortunately, these strategies are substrate-dependent and may not be generally applicable. To overcome this limitation, c) the introduction of directing groups (DGs) with Lewis basic functionalities has been shown with excellent regioselectivity. Thus, significant efforts have been devoted to develop different DGs (Scheme 1-5b).

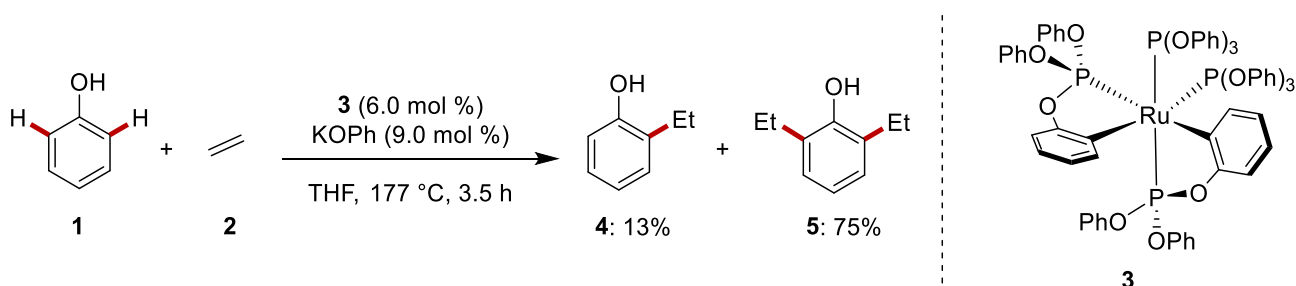
While there is an abundance of research on *ortho*-C–H transformations, investigations into C–H activations at the *meta/para* position have been more challenging. The most prominent strategies require either the use of mediators, for example norbornene in a Catellani-type manifold,^[27] or the installation of elaborate templates^[28] that direct the transition metal to the proximity of *meta* or even *para* C–H bond of the arene. A mechanistically different approach was unravelled by Ackermann in 2011 for *meta*-C–H functionalization,^[29] prompting the establishment of a robust platform for ruthenium-catalyzed *meta*-C–H functionalizations *via* unique σ - activation (Scheme 1-5c).



Scheme 1-5 Strategies for site-selectivity control.

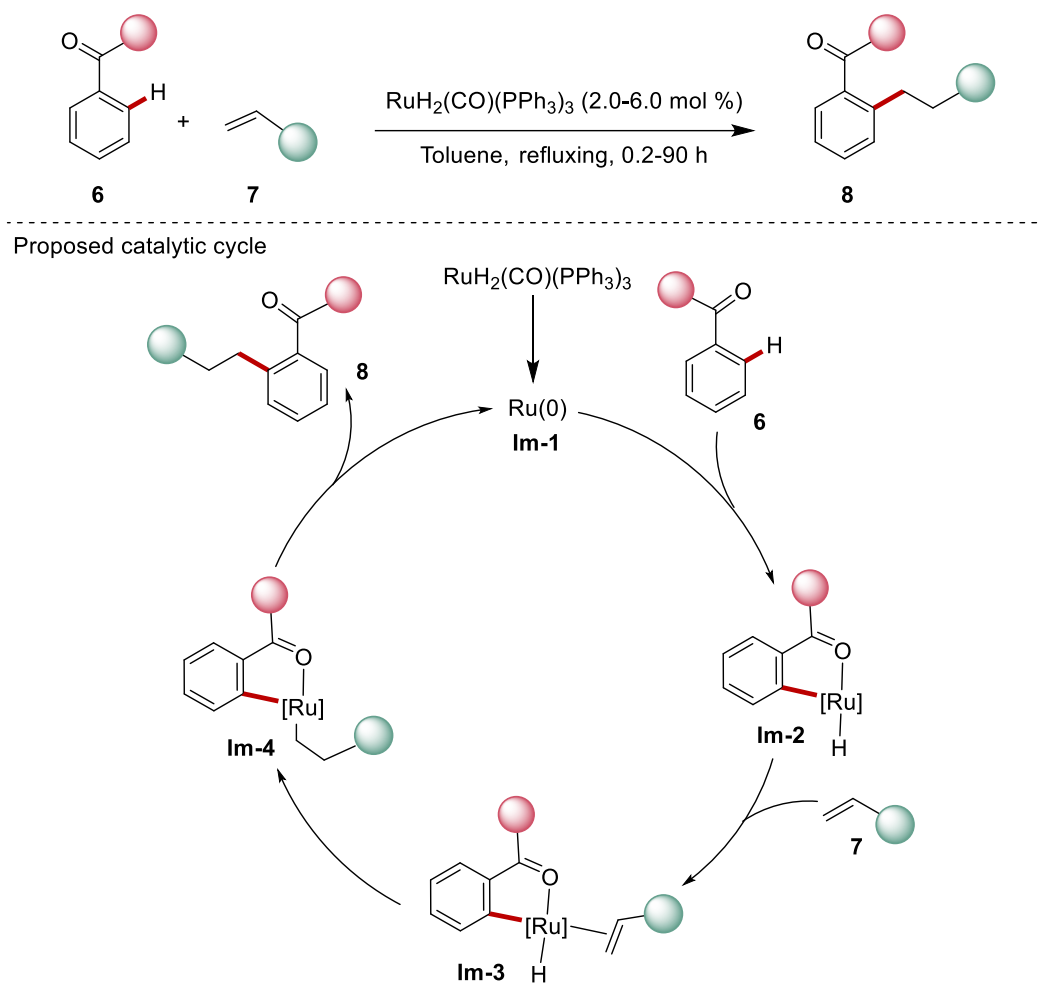
1.2 Ruthenium-Catalyzed C–H Activation

In recent decades, the use of ruthenium as catalyst has led to significant achievements in C–H functionalization.^[30] Inspired by earlier stoichiometric C–H activation with ruthenium complex by Chatt,^[31] Lewis and Smith^[32] reported the earliest instance of ruthenium-catalyzed C–H activation in 1986. An unprecedented transient directing group approach was employed in this study to achieve the ruthenium-catalyzed hydroarylation of ethylene gas **2** with phenol **1**, yielding a mixture of mono- and disubstituted products **4** and **5** (Scheme 1-6). The reaction was performed under a pressure of 6.6 bar and at a temperature of 177 °C.



Scheme 1-6 First ruthenium catalyzed C–H alkylation.

Almost a decade later, a seminal reaction was developed by Murai, Kakiuchi, and Chatani on ruthenium(0)-catalyzed alkylation of ketones **6** under elevated temperature (Scheme 1-7).^[33] The ruthenium precatalyst RuH₂(CO)(PPh₃)₃ underwent a transformation, yielding a ruthenium(0) compound **Im-1**. The new species **Im-1** facilitated C–H cleavage *via* oxidative addition, giving rise to a C–Ru–H species **Im-2**. It, then, underwent insertion with the olefin followed by reductive elimination, ultimately yielding the linear anti-Markovnikov addition products **8**. This methodology exhibited a broad scope, revealing for the first time the extensive versatility of ruthenium-catalyzed C–H activation.



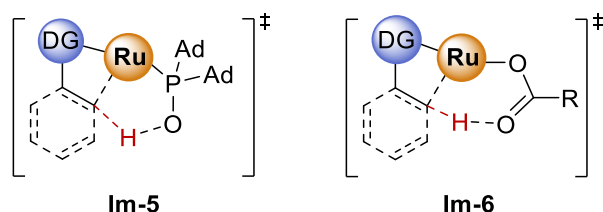
Scheme 1-7 Ruthenium-catalyzed C–H alkylation of ketones.

Building upon these studies, a wide range of ruthenium-catalyzed C–H activation reactions have been reported, encompassing diverse transformations such as arylations,^[34] alkylations,^[29, 35] aminations/amidations,^[36] oxygenations,^[37] and more. Significantly, the readily accessible $[\text{RuCl}_2(p\text{-cymene})]_2$ and its analogous complexes, which exhibit user-friendly characteristics, such as stability towards air and moisture, have emerged as highly robust and efficient catalyst, even when employed on a larger scale.

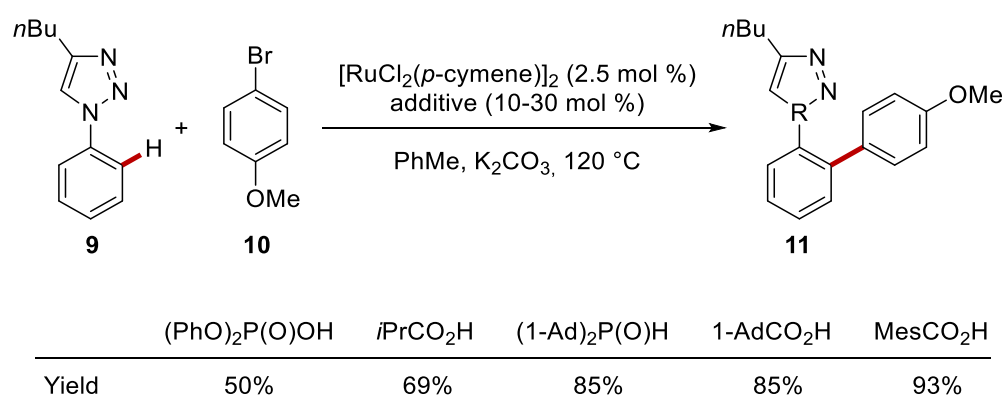
In 2005, Ackermann reported the first widely applicable method for directly arylating functionalized arenes with ruthenium(II) catalysts.^[38] This breakthrough was achieved by employing air-stable 1-adamantyl-substituted secondary phosphine oxide (SPO) $(1\text{-Ad})_2\text{P}(\text{O})\text{H}$, which exhibited superior efficiency in activating the ruthenium(II) catalyst, when compared to tertiary phosphine ligands. The SPO-based ruthenium(II) catalysis was operating *via* a proposed base-assisted metalation mechanism with a five-membered transition state **Im-5** (Scheme 1-8a). The proposed mechanism paved the way for the development of C–H activations facilitated by the carboxylate group, which share a similar

bifunctional nature. In a study conducted in 2008, Ackermann successfully demonstrated that this carboxylate group exhibited comparable or superior performance over the phosphine ligands in direct arylations of arenes **9**, involving the possible generation of a six-membered ruthenium-carboxylate species **Im-6** (Scheme 1-8b).^[39]

a) Postulated transition state



b) Acerkman, 2008



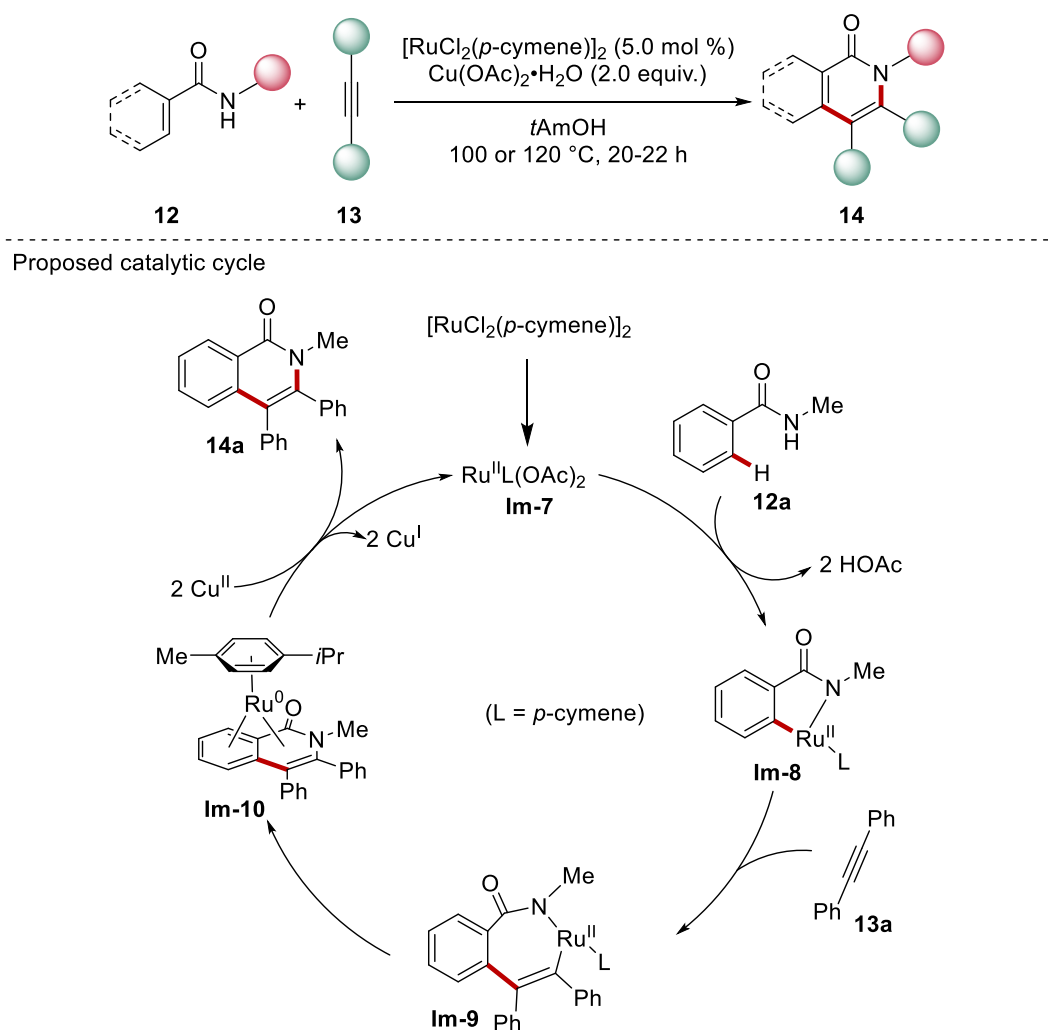
Scheme 1-8 Bifunctional ligand assistance for ruthenium-catalyzed C–H activation.

The introduction of carboxylic acid ligands has brought about a revolution in C–H bond functionalization by transition metals, particularly for ruthenium catalysis. This approach allows for mild reaction conditions and even permits the use of water as a reaction medium. Over the years, there has been significant progress in developing flexible and robust methods that utilize carboxylate-assisted *ortho*-ruthenation, enabling the functionalization of diverse types of molecules.^[40]

1.2.1 Ruthenium-Catalyzed Alkyne Annulation Reactions

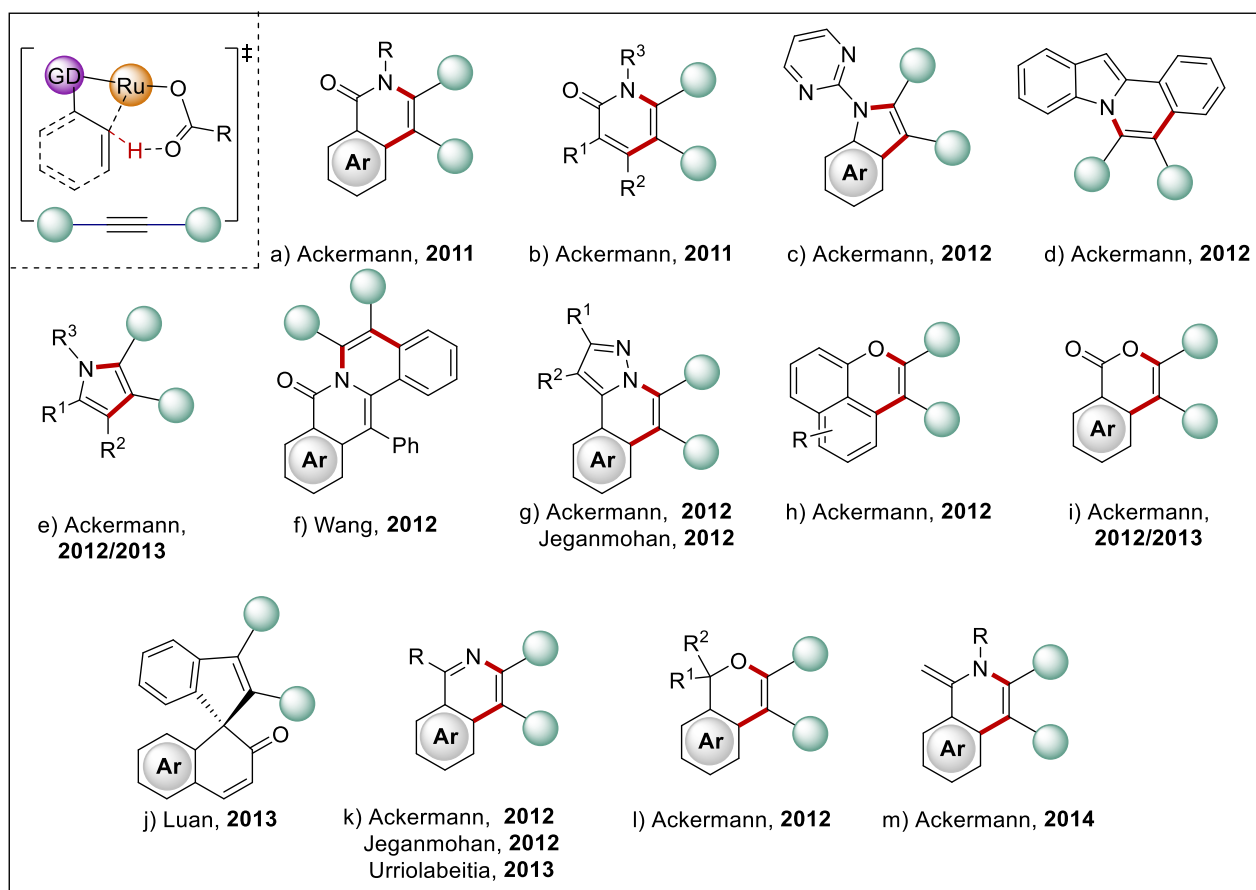
Annulations are convenient methods for synthesizing various heterocyclic compounds.^[41] Recently, an increasing number of reports focusing on annulation reactions catalyzed by various transition metal complexes has been published.^[42] Among them, rhodium has been demonstrated as an efficient catalyst for the catalytic C–H annulations due to its high reactivity and good functional group tolerance.^[43] However, the relatively high costs for rhodium has prompted researchers to actively explore more economical alternatives.

The Ackermann group was the first to employ the relatively economical ruthenium catalyst as a substitute for the costly rhodium catalyst for oxidative annulation processes. They employed a ruthenium(II) catalyst to realize the annulation of alkynes **13** by amides **12** via twofold C–H/N–H activation (Scheme 1-9).^[44] The catalytic cycle commenced with the C–H activation of substrate **12a**, forming the cyclic ruthenium complex **Im-8**. Then, this complex **Im-8** underwent alkyne insertion, followed by reductive elimination to afford the isoquinolone **14a**. The regeneration of the ruthenium catalyst is accomplished using a copper(II) salt as the sacrificed oxidant.



Scheme 1-9 Ruthenium(II)-catalyzed synthesis of isoquinolones and 2-pyridones.

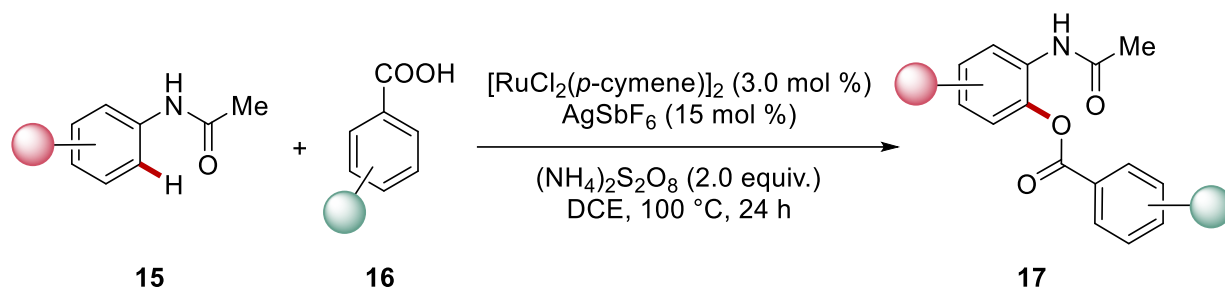
Moreover, ruthenium-catalyzed annulations with alkynes have been reported subsequently by several other groups, leading to the formation of pyrroles,^[45] indoles,^[46] isoquinolines,^[47] isocoumarins,^[48] and other heterocycles^[49] (Scheme 1-10).



Scheme 1-10 Overview of alkyne annulations by C–H/Het–H bond functionalization.

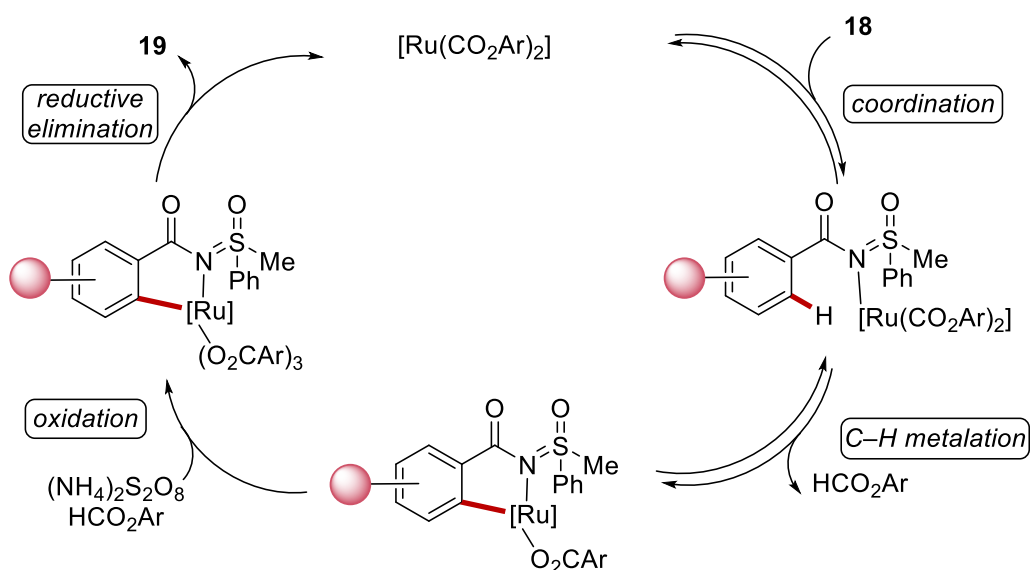
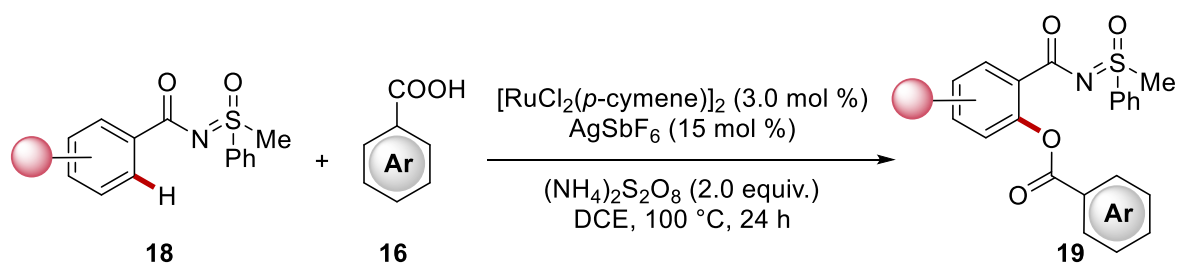
1.2.2 Ruthenium-Catalyzed C–H Acyloxylation

Compounds featuring C–acyloxy ester bonds, notably acetates, serve as ubiquitous scaffolds in diverse natural products, pharmaceuticals, biologically active compounds, agrochemicals, and marketed drugs.^[50] Thus, direct acyloxylation reactions are particularly attractive with palladium(II) complexes emerging as arguably the most versatile catalysts.^[51] However, rather inexpensive ruthenium complexes have been underappreciated for the acyloxylation reactions. In 2013, Padala and Jeganmohan reported for the first time the usefulness of ruthenium catalysts for the direct C–H acyloxylation of arene using carboxylic acids.^[52] Their catalytic system consisted of $[\text{RuCl}_2(p\text{-cymene})]_2/\text{AgSbF}_6/(\text{NH}_4)_2\text{S}_2\text{O}_8$ in DCE at 100 °C, leading to the formation of *ortho*-benzoxylated acetanilides **17** with moderate to good yields (Scheme 1-11). Following this, the same research team further extended this method to include *N*-alkyl benzamides as coupling partners.^[53]



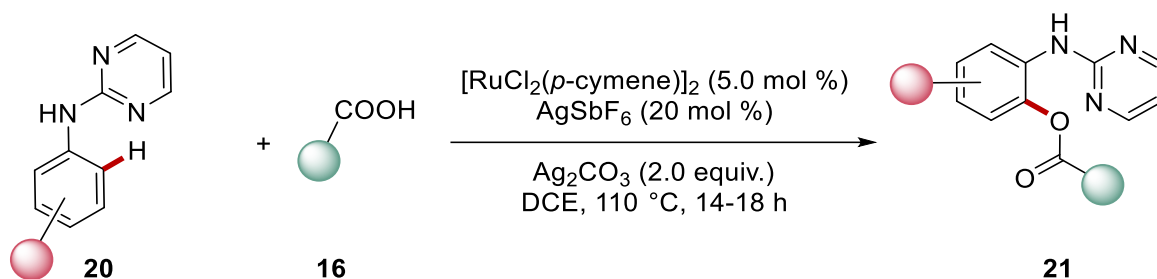
Scheme 1-11 Ruthenium-catalyzed synthesis of *ortho*-benzoxylated acetanilides.

The Ackermann group disclosed the ruthenium-catalyzed C–H benzoylation to sulfoximines.^[54] Through a series of control experiments, the authors proposed that the reaction followed a sequential process involving coordination, C–H metalation and oxidation-induced reductive elimination to give the products **19** (Scheme 1-12).

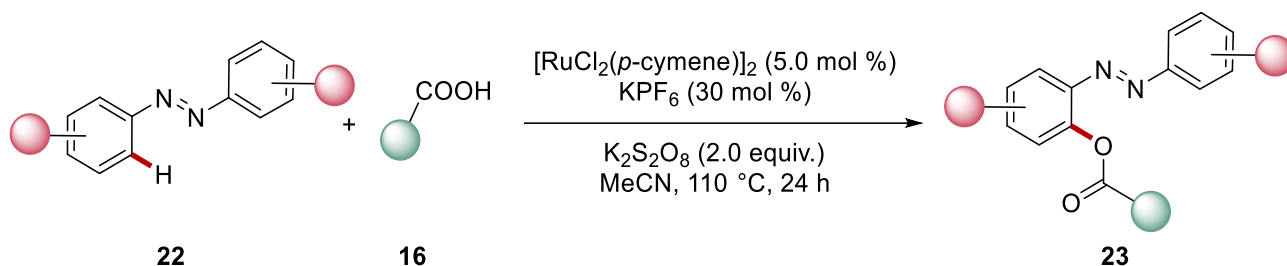


Scheme 1-12 Synthesis of *ortho*-benzoxylated sulfoximines.

Punniyamurthy group reported on ruthenium-catalyzed oxygenations of *N*-aryl-2-pyrimidines **20** using carboxylic acids **16** in the presence of AgSbF_6 as cocatalyst and Ag_2CO_3 as oxidant (Scheme 1-13).^[55] They found that the efficiency of the reaction was strongly influenced by the electronic nature of the substituents on the aromatic ring of **20**, where the electron-donating groups were favored.

**Scheme 1-13 Ru-catalyzed oxygenation of *ortho*-directed aromatic amines.**

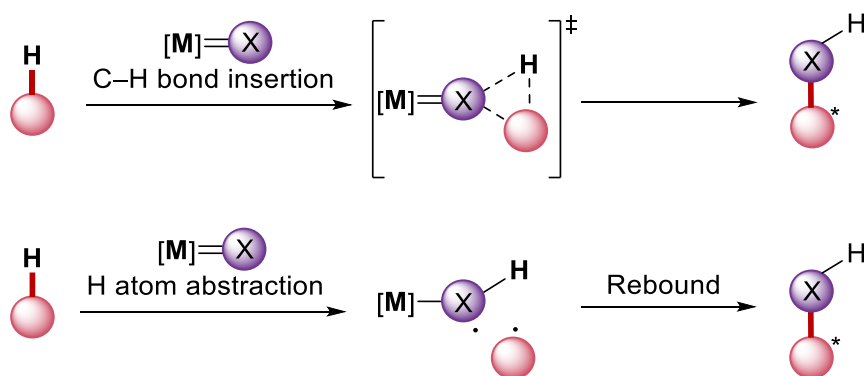
Recently, Kianmehr and Nasab utilized the standard $[\text{RuCl}_2(p\text{-cymene})]_2$ catalyst along with $\text{K}_2\text{S}_2\text{O}_8$ and KPF_6 for the regioselective *ortho*-acyloxylation of azoarenes **22**.^[56] The reaction was conducted in MeCN at 110 °C and resulted in the formation of *ortho*-acyloxyated azoarene derivatives **23** with moderate to high yields (Scheme 1-14). It is worth noting that other ruthenium catalysts, such as $\text{RuCl}_2(\text{PPh}_3)_2$ and $\text{RuCl}_3 \cdot \text{H}_2\text{O}$, were also capable of catalyzing this reaction, albeit with significantly lower efficiency.

**Scheme 1-14 *ortho*-Selective acyloxylation of azoarenes 22.**

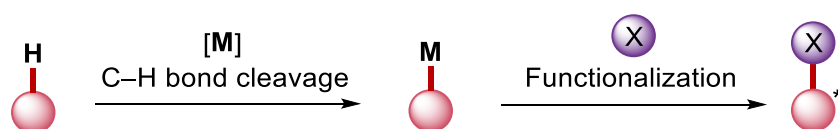
1.3 Palladium-Catalyzed Enantioselective C–H Activation

Asymmetric catalytic synthesis is among the most efficient methods for obtaining chiral molecules which are ubiquitous in biologically active molecules.^[57] Therefore, several strategies have been developed for the enantioselective C–H functionalizations, differing in operation mechanisms (Scheme 1-15).^[58] Processes that lack direct interaction between the C–H bond and the metal center are named outer-sphere or coordination mechanism, which is more prominent for metal-carbenoid and -nitrenoid insertion reactions,^[59] as well as radical transformations which proceed through hydrogen atom abstraction followed by radical rebound followed by radical relay^[61] mechanisms. In the inner-sphere approach, the C–H activation leads to an organometallic intermediate, which subsequently undergoes functionalization. So, our discussion is mainly focused on inner-sphere mechanisms.

a) Outer-sphere mechanism



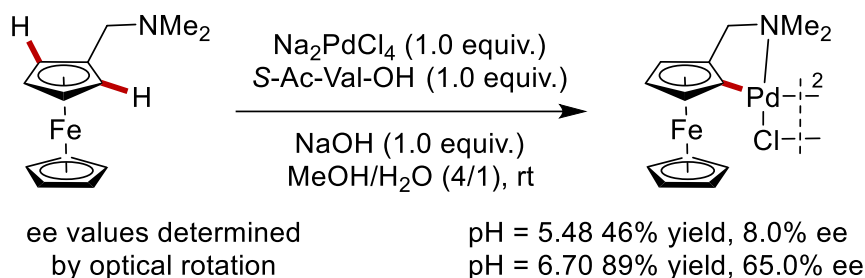
b) Inner-sphere mechanism



Scheme 1-15 Mechanistic classification for enantioselective C–H activations.

Since Sokolov's ground-breaking studies in 1977,^[62] which demonstrated the use of monoprotected chiral amino acids for achieving enantioselective stoichiometric C–H palladation (Scheme 1-16), palladium has emerged as the most widely employed transition metal for enantioselective organometallic C–H activations, enabling the synthesis of valuable organic molecules with precise stereo-control. The exceptional reactivity, remarkable versatility, and remarkable tolerance towards various functional groups make palladium indispensable in this field. Further experiments revealed the pivotal role of reaction pH (Scheme 1-16). Employing a 1:1 mixture of *S*-Ac-Val-OH and NaOH as the carboxylate source, lower pH (~5.5 before carboxylate addition) led to minimal

enantioselectivity (8.0% ee). However, at a higher pH (6.7), significantly improved yield (89%) and enantioselectivity (65.0% ee) were achieved.



Scheme 1-16 Diastereoselective cyclopalladation controlled by substrate chirality.

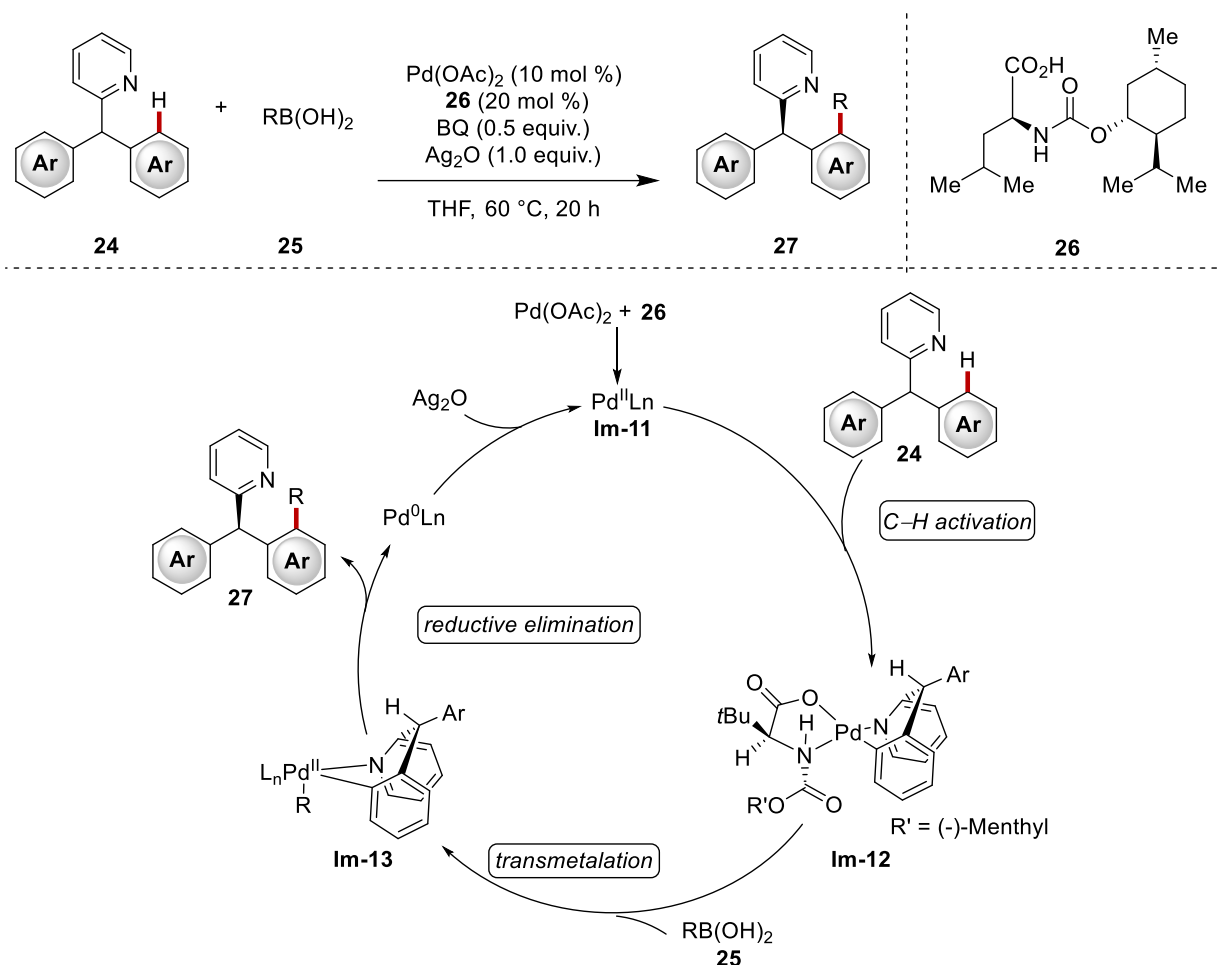
The effectiveness of palladium as a catalyst in enantioselective C–H functionalization is greatly enhanced by the discovery of innovative chiral ligands.^[63] By coordinating to palladium, ligands can modify the metal's reactivity and structure to reduce the activation energy of individual steps, improving site-selectivity and stereoselectivity of the palladium catalyst.^[64] Moreover, ligands contribute to higher solubility of palladium catalysts in organic solvents and enhance catalyst stability, ultimately increasing the concentration of active species in the reaction.^[65]

Chiral ligands can be either neutral, like chiral phosphoramidites,^[66] or anionic, such as chiral carboxylates^[65] and phosphates.^[67] Chiral anionic ligands can help maintain the electrophilicity of palladium(II) catalysts and serve as a base to facilitate enantioselective C–H cleavage.^[64] Recently a novel transient directing group strategy involving the *in-situ* generation and deconstruction of a chiral organocatalyst in a transient fashion has emerged as another efficient protocol to achieve enantioselective C–H functionalization, bypassing the extra steps in the classical installation and removal of directing groups.^[68]

1.3.1 Monoprotected Amino Acids as Chiral Ligands

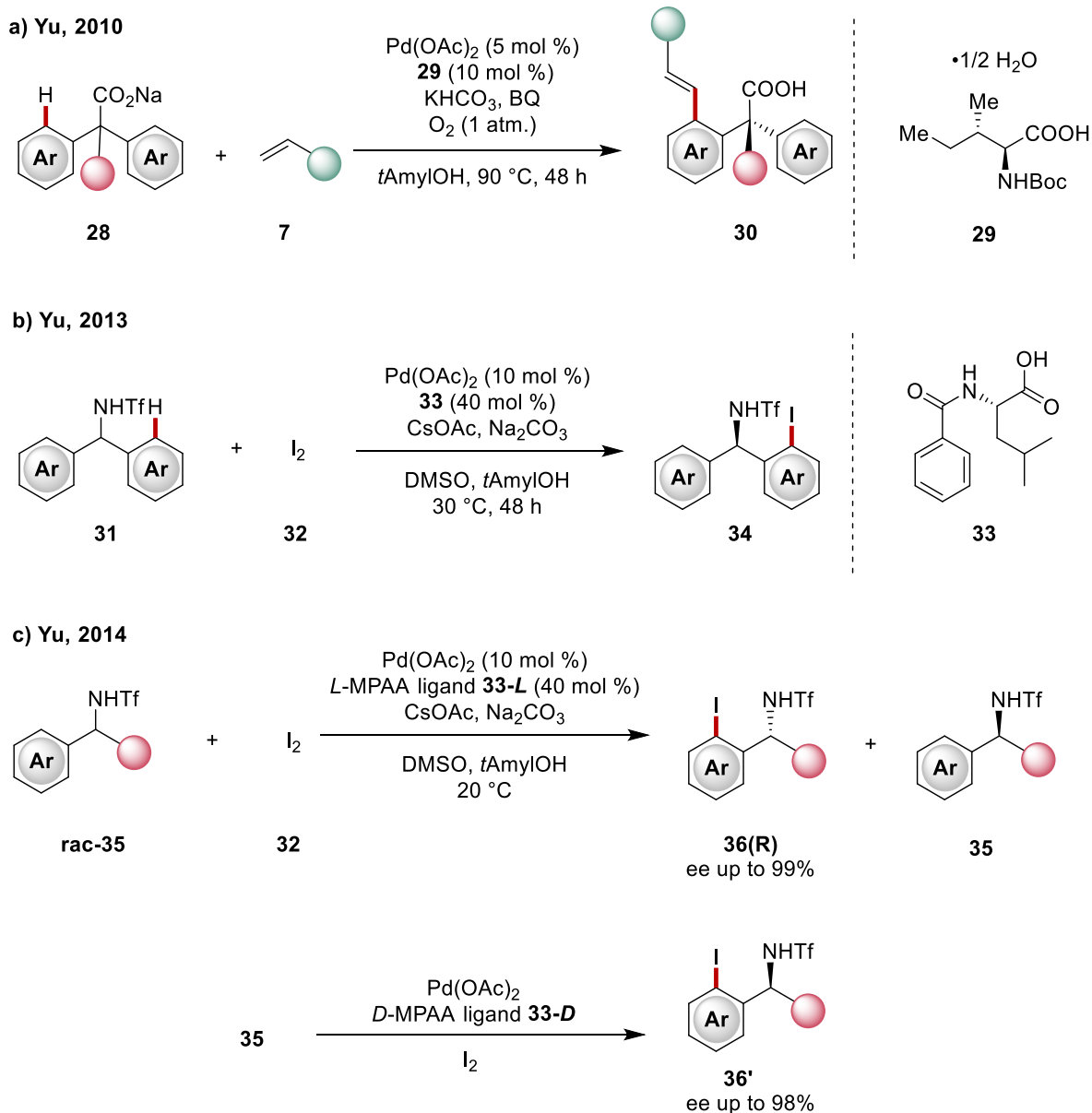
Inspired by the introduction of mono-protected amino acids (MPAA) as chiral ligands by Sokolov,^[62] Yu and co-workers reported the enantioselective C–H activation/cross-coupling enabled by the MPAA *via* a desymmetrization process in 2008.^[69] The bulky menthol-derived amino acid **26** in conjunction with Pd(OAc)₂ was employed to desymmetrize diaryl(2-pyridyl)methane derivatives **24** with alkyl boronic acids **25**, achieving products **27** with high enantioselectivity (Scheme 1-17). A potential catalytic cycle *via* palladium(II)/palladium(0) pathway was proposed, which commenced with the selective C–H activation of **24** using a Pd(II) catalyst in the presence of (–)-Men-Leu-OH **26**, giving rise to a cyclic Pd(II) intermediate **Im-12**. Subsequently, transmetalation occurred between **Im-12** and an alkyl boronic acid, leading to the formation of intermediate **Im-13**. Finally, reductive elimination

from **Im-13** released the desired chiral product **27** and a palladium(0) complex, which was reoxidized by Ag_2O to give the active catalyst **Im-11**.



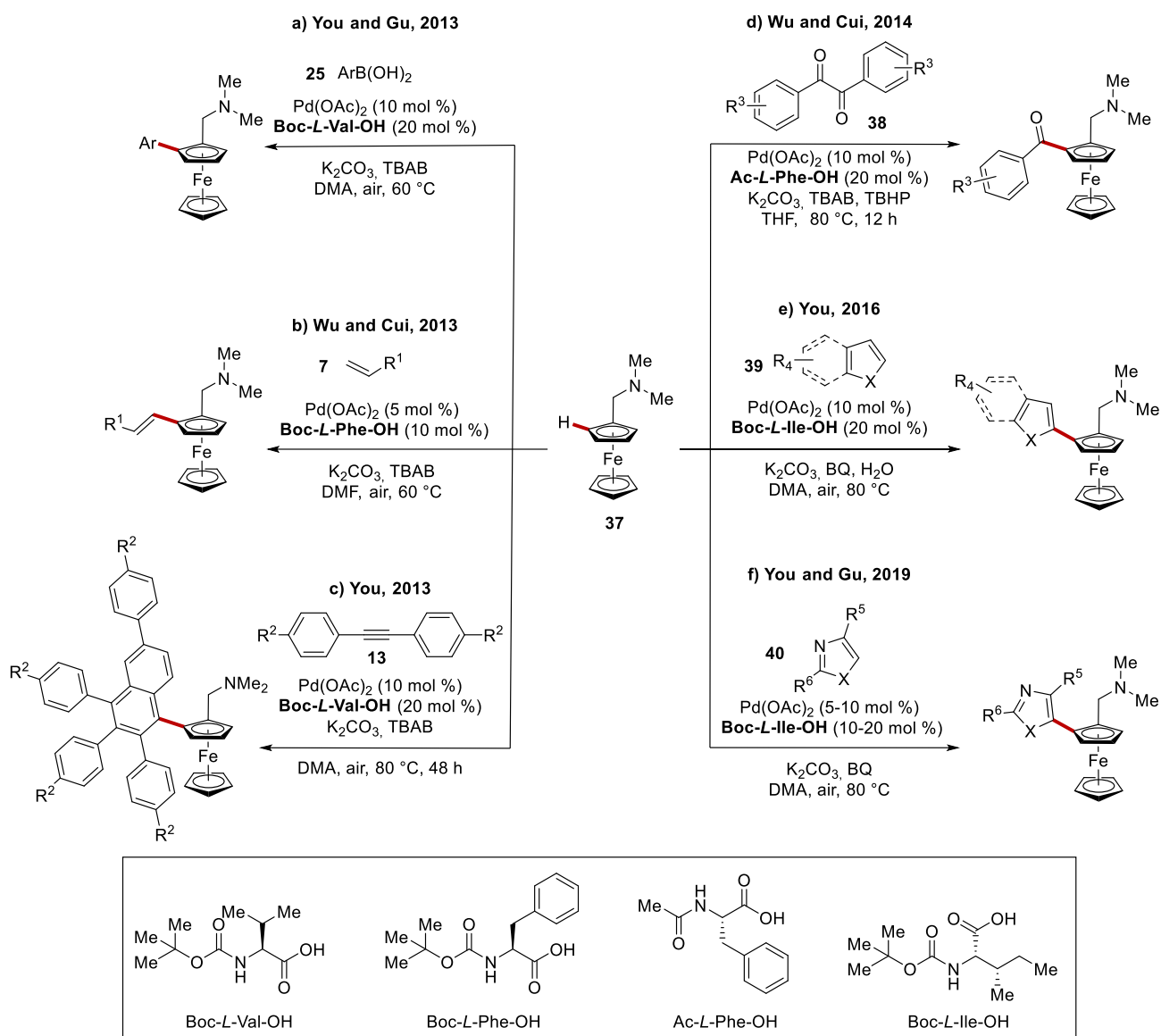
Scheme 1-17 Enantioselective $\text{C(sp}^2\text{)-H}$ activation enabled by MPAA ligand.

The same group also utilized MPAAAs to effectively obtain chiral acids^[70] and chiral amines^[71] *via* desymmetrization using α,α -diphenylacetates **28** and diarylmethylamines **31** as substrates, respectively (Scheme 1-18a and b). Soon after, they additionally accomplished the kinetic resolution of racemic amines **rac-35** by palladium catalysis in conjunction with MPAA **33-L** (Scheme 1-18c).^[72] In this case, when the remaining starting material **35** was recovered and subjected to the standard reaction conditions but with the MPAA ligand possessing the opposite configuration **33-D**, it gave rise to the iodinated benzylamines **36'** in high ees. This strategy was not restricted to the iodination, the same group also broadened the scope towards olefins^[73] and arylboronic acid pinacol esters^[74] as the coupling partners.



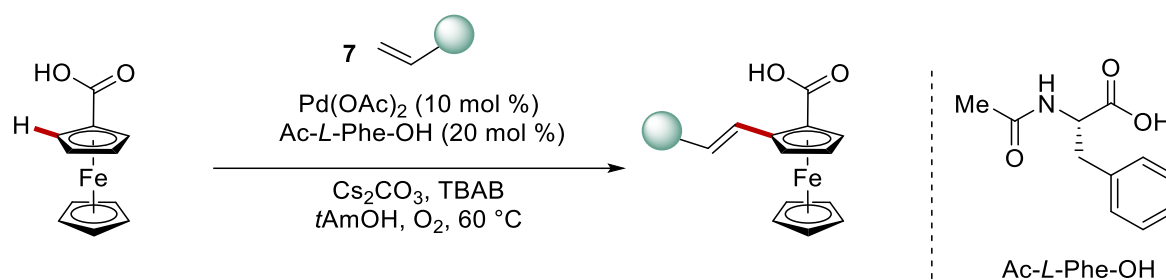
Scheme 1-18 Representative Pd/MPAA-catalyzed C–H functionalizations.

Taking inspiration from the pioneering studies conducted by Sokolov, Fujiwara, Moritani and Yu, You and co-workers successfully accomplished the enantioselective C–H arylation of dialkylaminomethylferrocene derivatives with arylboronic acids to access planer chirality in 2013 (Scheme 1-19a).^[75] Around the same time, the Wu and Cui groups independently reported an enantioselective oxidative *Heck* reaction employing a similar strategy (Scheme 1-19b).^[76] Subsequently, diverse coupling partners including diarylalkynes **13**,^[77] 1,2-diketones **38**,^[78] heteroarenes **39**,^[79] oxazoles and thiazoles **40**^[80] were employed to successfully achieve enantioselective transformations of dialkylaminomethylferrocenes **37** (Scheme 1-19c-f).



Scheme 1-19 Enantioselective palladium-catalyzed functionalization of ferrocenes 37.

In addition to the successful use of the dialkylaminomethyl group as a DG for the palladium(II)-catalyzed enantioselective C–H functionalizations of ferrocenes, other DGs have received relatively little attention. Recently, Wu, Cui, and their colleagues revealed that the carboxylic acid can act as a weakly coordinating DG in the Pd-catalyzed *ortho*-alkenylation reaction, leading to the formation of planar chiral 1,2-disubstituted ferrocenecarboxylic acid derivatives (Scheme 1-20).^[81]



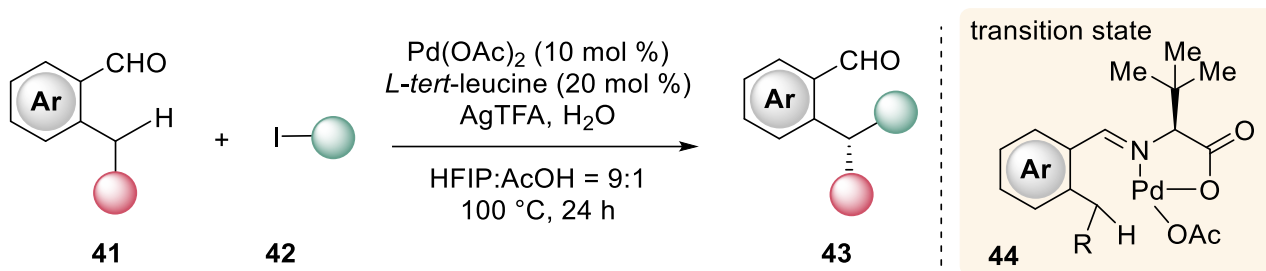
Scheme 1-20 Carboxylic acid-assisted C–H alkenylation.

The use of MPAAAs also allowed for the synthesis of axially chiral compounds by Pd(II)-catalyzed direct C–H iodination through kinetic resolution.^[82] Additionally, a similar strategy was applied to achieve atroposelective olefination of biaryls containing phosphorous based DGs.^[83] Recently, Shi utilized *L*-pyroglutamic acid as a chiral ligand for the synthesis of axially chiral styrenes^[84] and atroposelective anilides.^[85]

1.3.2 Chiral Transient Directing Group

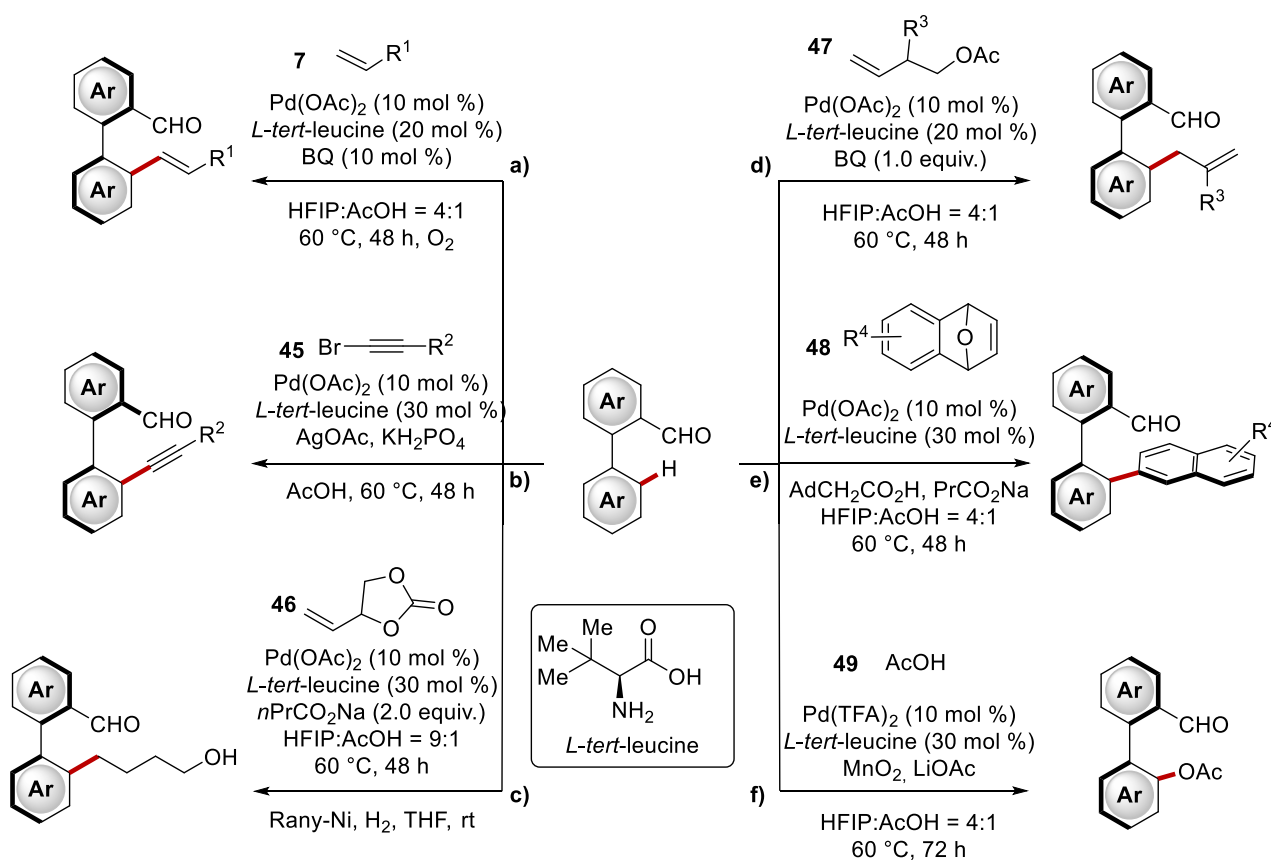
The strategy involving external chiral ligands for stereoselectivity control often requires the use of native DGs to facilitate binding to a metal center and guide the catalyst toward a specific C–H bond. However, the introduction and removal of these DGs can result in by-product waste, impacting the environmental sustainability. To tackle this issue, transient directing group (TDG) strategy has emerged as an effective tool, involving the generation of temporary and reversible DGs that enable directed C–H functionalization and subsequent cleavage of the TDG in one pot.^[68e, 86]

In 2016, chiral TDG enabled enantioselective C–H activation reaction was realized by Yu and co-workers (Scheme 1-21).^[87] *L-tert*-leucine played a crucial role as an efficient chiral organocatalyst in the reaction to facilitate the *in-situ* formation of a chiral imine intermediate with aldehydes **41**, which, then, acted as a bidentate directing group, coordinating with palladium(II) to form the intermediate **44**. This complex **44** underwent a stereo determining C–H activation followed by arylation, leading to the desired products **43** in high yields and excellent enantioselectivity. The same group then extended this approach towards fluorination with *N*-fluoro-2,4,6-trimethylpyridinium salts.^[88] Very recently, they developed a palladium(II)-catalyzed enantioselective C(sp³)–H arylation of aliphatic ketones assisted by *D*-valine as cTDG.^[89]



Scheme 1-21 Palladium(II)-catalyzed enantioselective benzylic C(sp³)-H arylation of aldehydes.

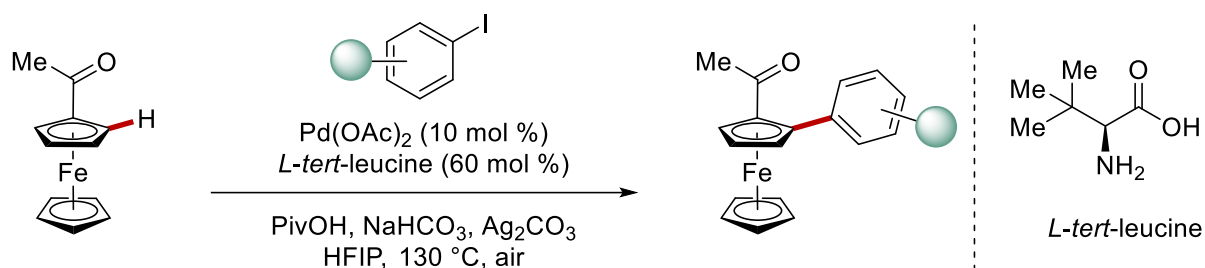
Motivated by the promising results of generating central chirality using cTDGs, Shi and his colleagues first developed an efficient route for the synthesis of axially chiral biaryls *via* olefination in the presence of commercially available *L-tert-leucine* as the chiral TDG and oxygen as the terminal oxidant in 2017 (Scheme 1-22a).^[90] Shortly afterwards, they successfully expanded this protocol to include other coupling partners such as protected alkynyl bromides **45**,^[91] 4-vinyl-1,1-dioxolan-2-one **46**,^[92] allyl acetate derivatives **47**,^[92] and 7-oxabenzonorbornadienes **48**^[93] (Scheme 1-22b-e). In 2022, Xie group introduced a palladium(II)-catalyzed atroposelective C-H acyloxylation strategy for the synthesis of biaryl aldehyde atropoisomers with the assistance of *L-tert-leucine* (Scheme 1-22f).^[94]



Scheme 1-22 Palladium-catalyzed atroposelective transformations of biaryls using cTDG strategy.

Alongside C–C bond as rotational axis, Shi^[95] and Xie^[96] groups also employed TDG strategy to synthesize N–C axially chiral scaffolds. More recently, Shi and coworkers reported the first Pd-catalyzed enantioselective C–H olefination to access axially chiral styrenes with cTDG.^[97]

In 2018, Xu, Jin and coworkers successfully employed the cTDG strategy to accomplish the planar chirality through the Pd catalyzed enantioselective C(sp²)–H arylation of ferrocenyl ketones,^[98] achieving good yields up to 75% and excellent ees ranging from 92% to 98% (Scheme 1-23).



Scheme 1-23 Enantioselective Pd-catalyzed C(sp²)-H arylation of ferrocenyl ketones.

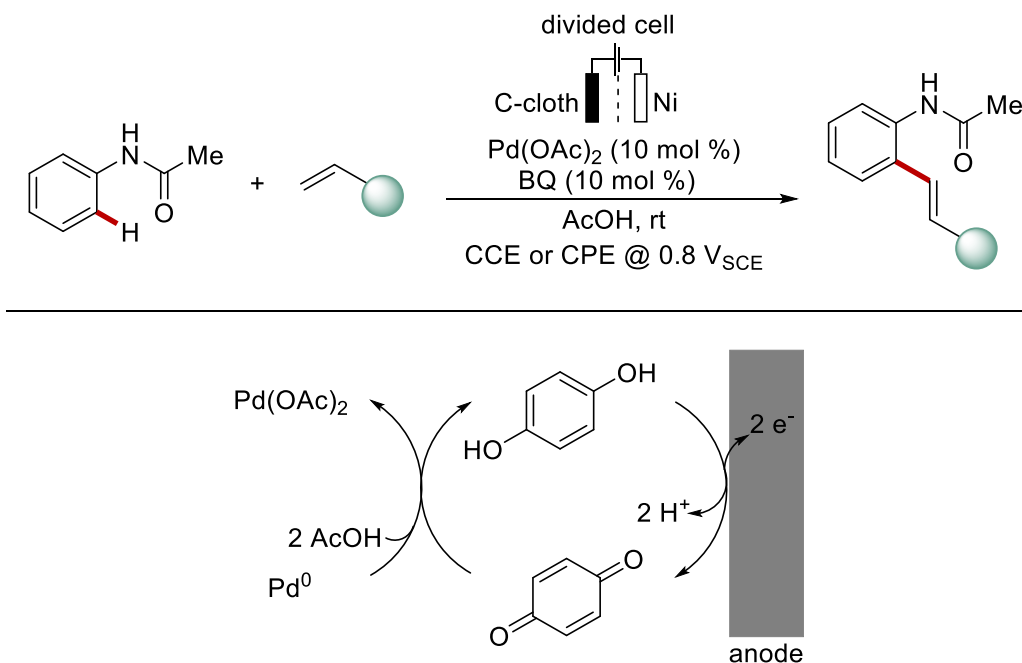
1.4 Transition Metal-Catalyzed Electrochemical C–H Activation

Transition metal-catalyzed C–H activation represents a sustainable approach for enabling direct functionalization reactions in molecules. While significant progress has been achieved, these reactions often rely on the use of stoichiometric chemical oxidants, resulting in the generation of unwanted metal waste and posing a challenge to the atom-efficient nature of the C–H activation strategy.^[6d] As a result, the merger of the C–H activation with electrocatalysis becomes increasingly desirable, as it provides an environmentally friendly approach to molecular synthesis.^[99] In metalla-electrocatalysis, electron transfers are predominantly utilized for catalyst regeneration or to facilitate oxidation state-dependent elementary steps in metalated intermediates.^[100] Unlike chemical oxidants with fixed oxidative ability, electricity allows for the adjustment of both potential and current, leading to improved selectivity in reactions and optimal resource utilization.^[101] This opens up new avenues for more sustainable and efficient processes in chemical synthesis.

The origin of electrocatalysis can be traced back to 1848, Kolbe from Göttingen performed the first electroorganic transformation^[102] based on the reports of Faraday on the laws of electrolysis and preliminary experiments.^[103] Building upon this pioneering work, electrocatalysis has made significant progress with the establishment of prominent reactions, such as the Shono oxidation,^[104] Simons fluorination^[105] or the Monsanto process.^[106]

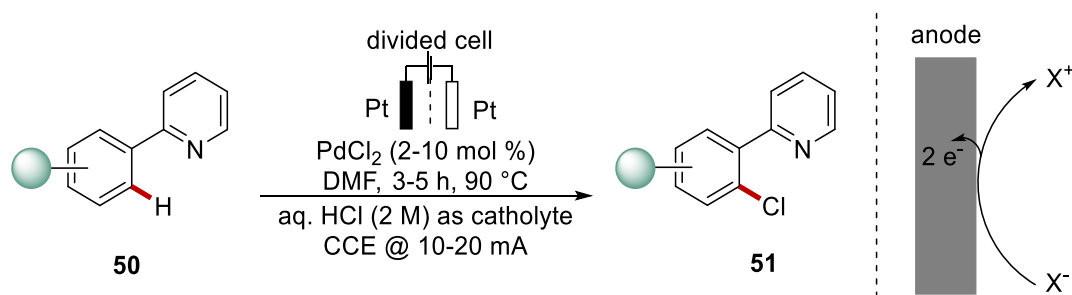
1.4.1 Palladium Catalyzed Electrochemical C–H Activation

In 2007, Amatore and Jutand reported on the first catalytic C–H activation using electricity in place of stoichiometric chemical oxidants, achieving the *Fujiwara-Moritani*-type reaction on benzamides (Scheme 1-24).^[107] The reaction required catalytic amounts of 1,4-benzoquinone (BQ) to mediate the reoxidation of palladium(0) to palladium(II).



Scheme 1-24 Electrochemical Pd-catalyzed alkenylation by Amatore and Jutand.

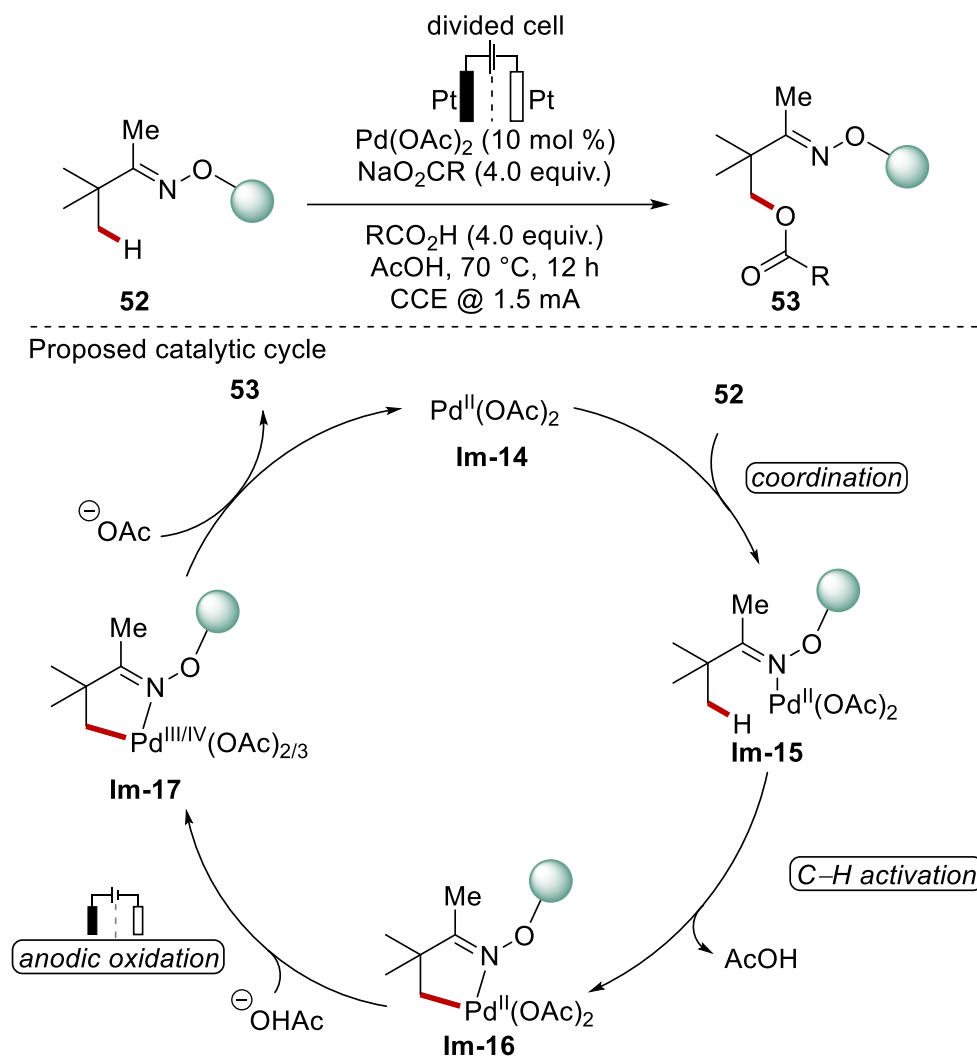
In 2009, Kakiuchi published a significant finding in which electrochemical palladium-catalyzed chlorination of phenylpyridines **50** was achieved (Scheme 1-25).^[108] Instead of relying on expensive halogenation reagents, electricity was employed to generate the halonium ion from mineral acids. The generated halonium cation subsequently reacted with the palladacycle, leading to the desired product **51**. Then, the same group extended this approach to iodinations using elemental iodine or potassium iodide as the iodine source.^[109] Additionally, Budnikova and Lei's groups developed protocols for pyridine-directed C(sp²)-H phosphonation^[110] and assembly of pyrido[1,2-a]benzimidazoles through intramolecular C(sp²)-H amination,^[111] respectively.



Scheme 1-25 Electrochemical palladium-catalyzed chlorination of phenylpyridines.

In 2017, a seminal report on an oxime-directed oxygenation for C(sp³)-H bonds through palladium catalysis was reported by Mei group (Scheme 1-26).^[112] The reaction employed the carboxylic acid coupling partner as the solvent and the corresponding sodium salt as a base. It proceeded through carboxylate-assisted C-H activation of the pre-coordinated

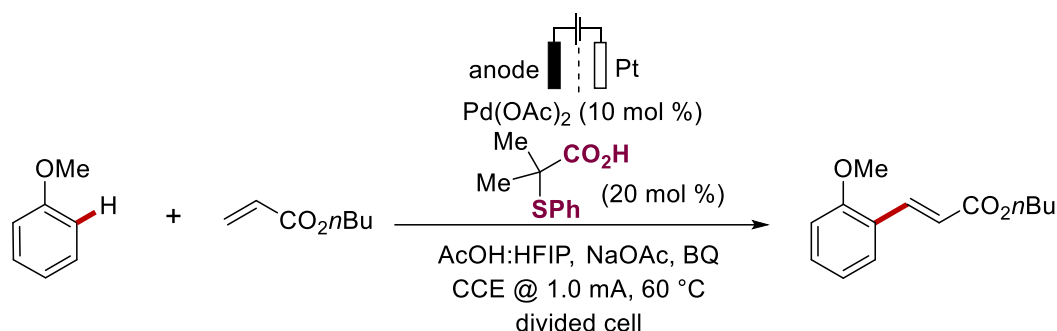
substrate **Im-15**, followed by anodic oxidation of intermediate **Im-16**. The generated high-valent palladium(III) or palladium(IV) species **Im-17** underwent reductive elimination to afford the desired product **53**. Thereafter, Mei also achieved C(sp²)-H acetoxylation of oximes,^[113] acylation with glyoxalic acids^[114] and alkylation with alkyl trifluoroborates^[115] through a similar mechanism.



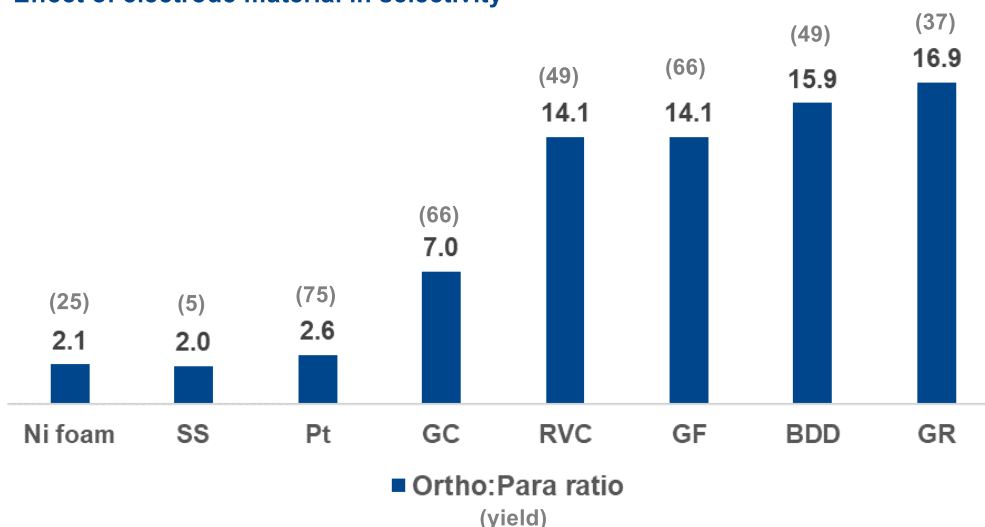
Scheme 1-26 Electrochemical palladium-catalyzed C(sp³)-H oxygenation and proposed catalytic cycle.

Very recently, the Ackermann group developed palladium-electrochemical catalyzed C-H olefinations of simple arenes devoid of directing groups (Scheme 1-27).^[116] The robust electrocatalysis proved amenable to a wide range of both electron-rich and electron-deficient arenes under exceedingly mild reaction conditions, avoiding chemical oxidants. Additionally, the outstanding position-selectivity in olefinations of the electron-rich substrates was achieved by the judicious choice of electrode materials. Furthermore, this strategy provided

a straightforward route for the late-stage functionalization of drug compounds and natural products.

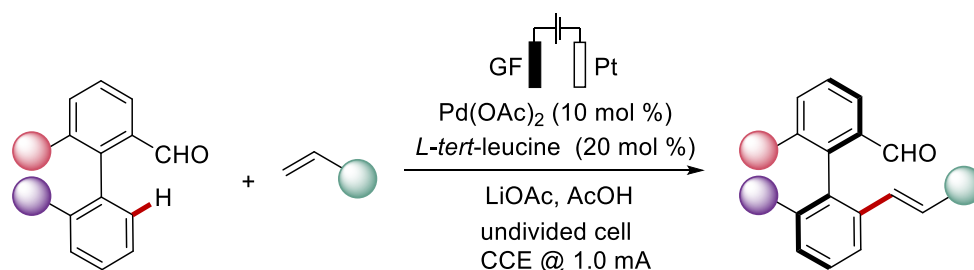


Effect of electrode material in selectivity



Scheme 1-27 Electrocatalyzed direct arene alkenylations without DGs.

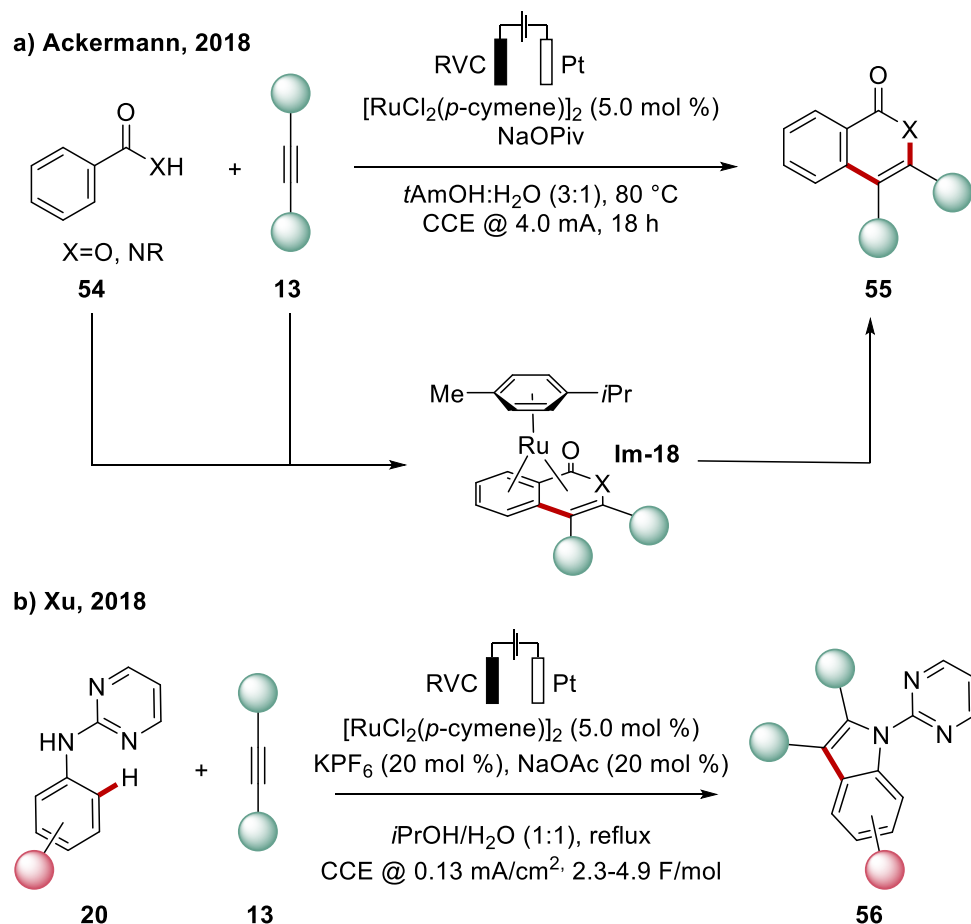
The Ackermann group also reported on the first enantioselective metalla-electrocatalyzed oxidative C–H activation, using palladium catalyst and a transient directing group manifold under mild reaction conditions for the synthesis of enantioenriched axially chiral biaryls and heterobiaryls (Scheme 1-28).^[117] Experimental and computational mechanistic studies on the pallada-electrocatalysis rationalized the key transition states. This strategy also set the stage for the efficient assembly of novel enantioenriched BINOLs, dicarboxylic acids and helicenes with good to excellent enantioselectivity.



Scheme 1-28 Enantioselective palladaelectro-catalyzed C–H activations by cTDG.

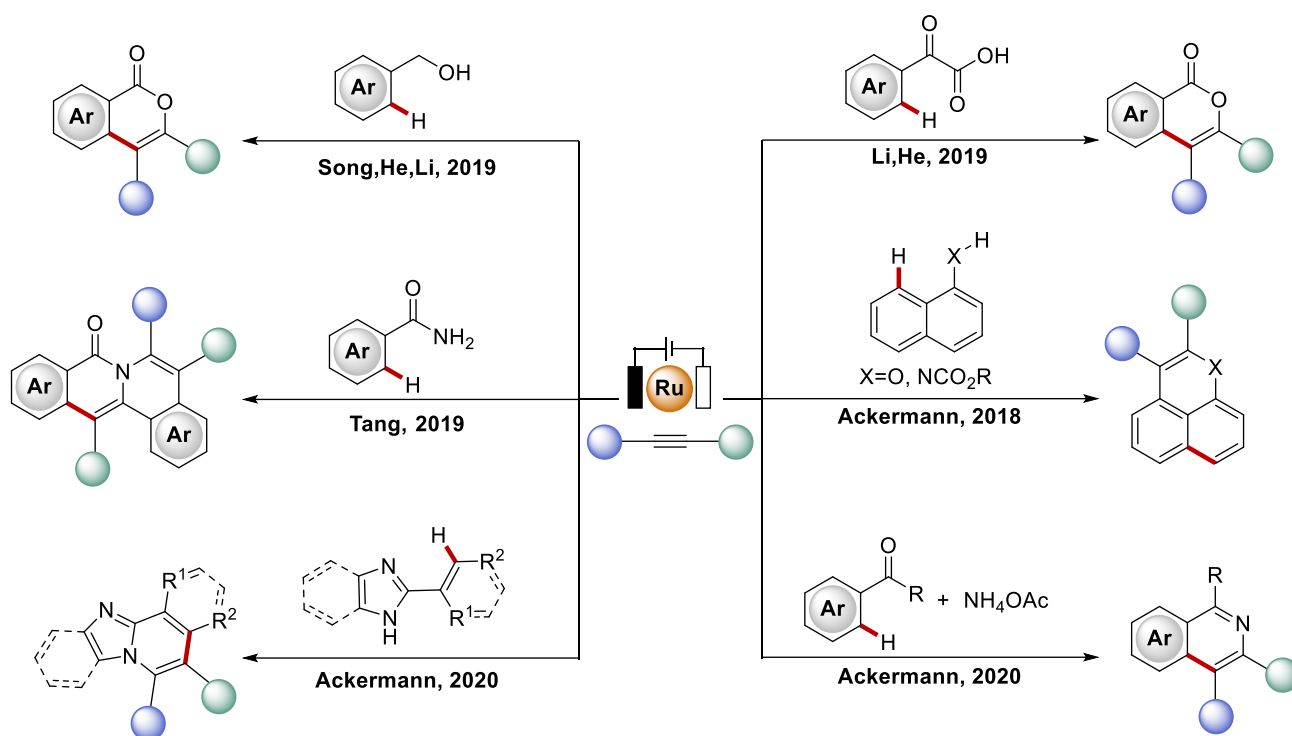
1.4.2 Ruthenium Catalyzed Electrochemical C–H Activation

In 2018, Ackermann and Xu independently demonstrated the potential of ruthenaelectrocatalysis with the alkyne annulation reactions, leading to the synthesis of **55** (Scheme 1-29a),^[118] as well as indole motifs **56** (Scheme 1-29b),^[119] respectively. In the study of Ackermann, C–H activation likely occurred through a BIES mechanism, as evidenced by the faster reaction rate with electron-rich benzoic acids **54**. The isolation of the key sandwich intermediate **Im-18** and experimental confirmation of oxidation-induced product decooordination supported their proposed mechanism. In Xu's research, electricity was utilized as a redox reagent to facilitate the ruthenium-catalyzed C–H/N–H activation for alkyne annulation, enabling the cost-effective synthesis of indole derivatives **56**. However, the reaction necessitated the use of the expensive KPF₆ salt.



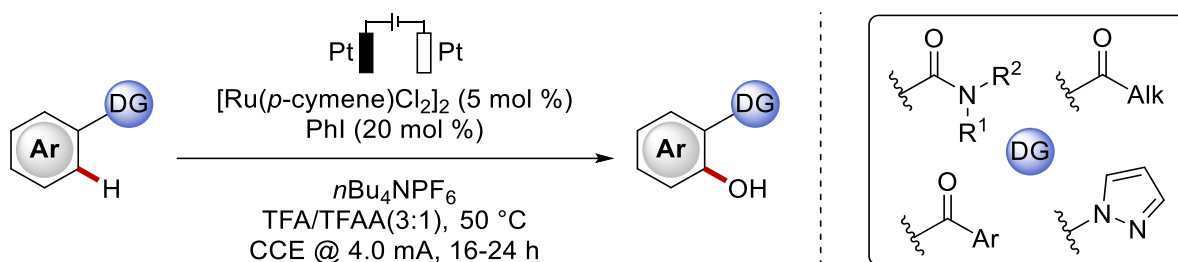
Scheme 1-29 First reports on ruthenaelectro-catalyzed C–H activation.

The robust ruthenium electrocatalysis was subsequently applied to several other substrates, for instance, benzylic alcohols,^[120] glyoxalic acids,^[121] *N*-unsubstituted benzamides,^[122] naphthylcarbamates,^[123] imidazoles^[124] and aryl ketones,^[125] to construct the isocoumarines or isoquinolones (Scheme 1-30).



Scheme 1-30 Ruthenaelectro-oxidative C–H/X–H annulation.

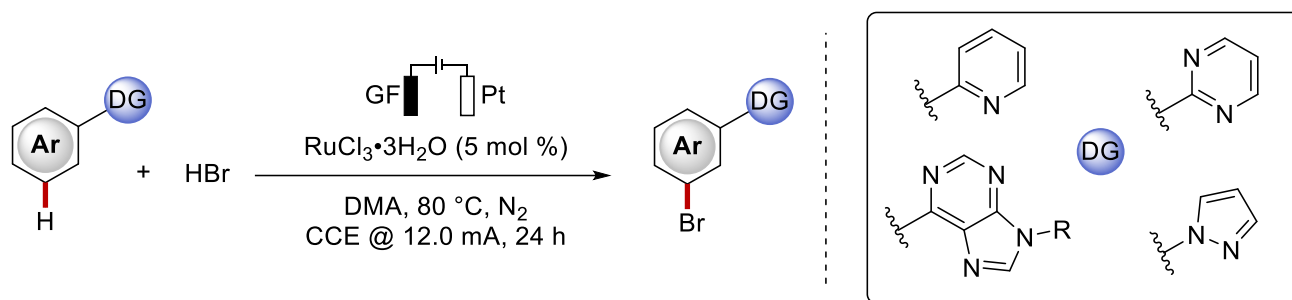
Ruthenaelectro-catalysis was also proved powerful in the formation of C–O bonds. In 2019, Ackermann group presented a strategy for the oxygenation of arenes with different directing groups (Scheme 1-31).^[37a] The versatile iodine(III)/ruthenium(II)-electrocatalyzed C–H oxygenation was achieved by merging the catalytic generation of hypervalent iodine(III) reagents using sustainable electricity as a cost-effective oxidant, with the molecular hydrogen as the sole by-product.



Scheme 1-31 Ruthenaelectro-catalyzed C–O bond formation.

In 2022, the Ackermann group achieved progress by successfully accomplishing the first *meta*-C–H functionalization (Scheme 1-32).^[126] They employed $\text{RuCl}_3 \cdot 3\text{H}_2\text{O}$ as the catalyst and aqueous HBr as a brominating agent to selectively brominate the starting materials without the need for additional ligands or electrolytes. The protocol exhibited *meta*-selectivity on the benzenoid position of pyrazolylarenes rather than the electron-rich pyrazole motif. Mechanistic studies suggested an initial ruthenacycle complex is formed through *ortho*-C–

H activation, followed by SET and LLHT process that leads to the liberation of the brominated product.



Scheme 1-32 Ruthenaelectro-catalyzed *meta*-C–H bromination.

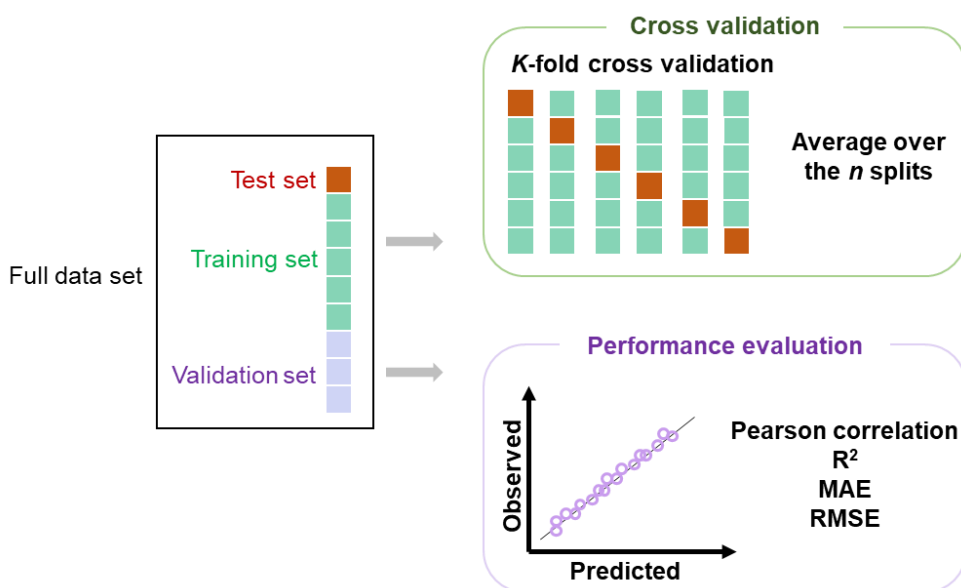
1.5 Machine Learning in Synthetic Organic Chemistry

1.5.1 General Introduction of ML

Machine learning (ML) is a subset of artificial intelligence (AI), which relies on statistical techniques and computational algorithms to analyze large datasets, enabling machines to identify patterns, make predictions, and enhance performance through experience. ML has permeated all aspects of contemporary life, ranging from everyday contexts like language translation and spam filtering to scientific and technological domains, such as medical diagnostics and materials design.

In the field of organic synthetic chemistry, ML algorithms can be separated into three main categories: reinforced, unsupervised, and supervised learning.^[127] In supervised learning, both the input (e.g., reaction) and output (e.g., yield, conversion, or ee) are provided, allowing algorithms to learn the correlation between them and make predictions on unseen data. This strategy was applied to the prediction of chemical reaction performance.^[128] Unsupervised learning focuses on analyzing input data without corresponding output, aiming to uncover underlying structures or patterns within the data. It has been employed in the generation of vector representations of molecular structures.^[129] Reinforcement learning, where models take certain actions and receive a reward at each step to maximize long-term benefits, has been utilized in the determination of catalytic reactions as well as in the optimization of molecular structures.^[130]

Supervised ML can be categorized into two primary branches: classification and regression algorithms. In classification, the given dataset is separated into classes by categorization. In contrast, regression algorithms are focused on quantitatively predicting the relationship between input features and a continuous target variable. In supervised ML algorithms, the full dataset is divided into three distinct subsets: the training set, the test set, and the validation set (Scheme 1-33). The training and test sets play a pivotal role in the creation of the predictive ML model. The validation set is utilized to evaluate the performance of the generated predictive model. When it comes to regression models, standard methods for assessing performance include the Pearson correlation coefficient, (R^2), the mean absolute error (MAE), and the root-mean-square error (RMSE). For classification models, the typical evaluation indexes include accuracy, precision, recall, and f1 score.

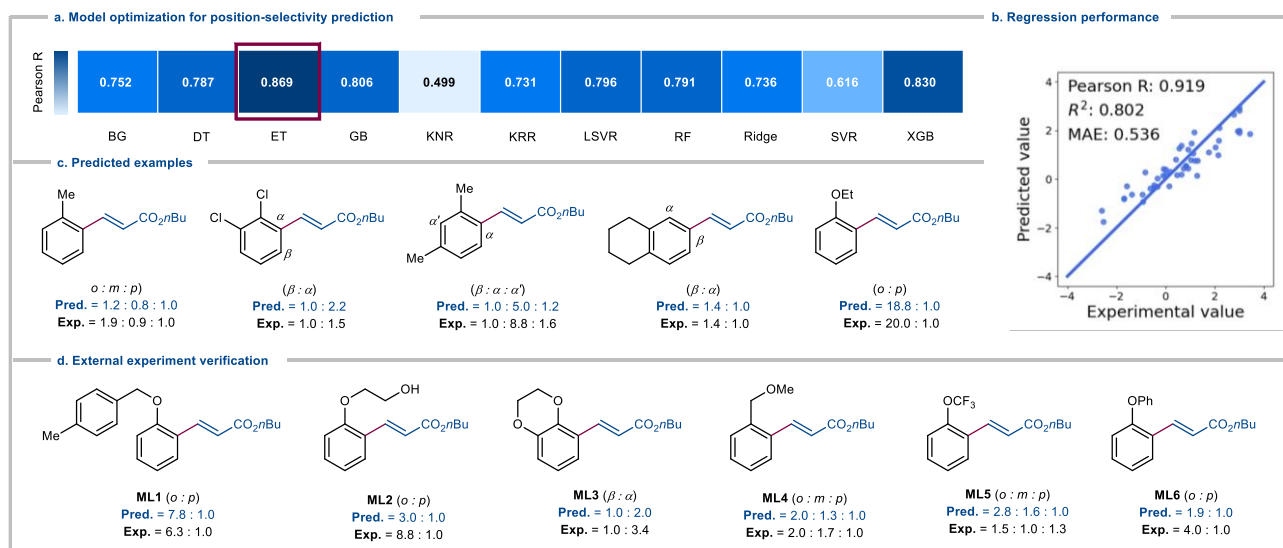


Scheme 1-33 Supervised ML model optimization and cross validation.

The model is validated based on the available data's quality through nested cross-validation, with one practical approach being K -fold cross-validation. In this approach, the full dataset excluding the validation set is divided into k subsets of equal dimensions. One subset is employed as the test set while the remaining $k - 1$ subsets are combined to form the training set. This process will iterate until each subset has served as the internal test set once.

1.5.2 ML for Reaction Prediction and Optimization

In 2023, Ackermann and Hong groups demonstrated the use of ML for the prediction of site-selectivity for palladaelectro-catalyzed C–H olefinations of simple arenes devoid of exogenous directing groups.^[116] The authors developed a statistical model by combining regioselectivity data from different aromatic compounds and encoded various molecular features using physical organic parameters. Additionally, they considered computed redox potentials due to the importance of the electro-oxidation. These descriptors, along with reaction temperature, formed a 28-dimensional code for each pair of competing regioisomeric sites. A series of ML algorithms was then tested and the Extra-Trees (ET) model was found to perform best (Pearson $R = 0.919$, mean absolute error = 0.536) (Scheme 1-34a and b). The model's effectiveness was validated with out-of-sample predictions for selected compounds, which matched experimental results well (Scheme 1-34c). Six new arenes were further experimentally tested to probe the predictions (Scheme 1-34d). This demonstrated the model's predictive potential in reducing experimental optimization efforts.

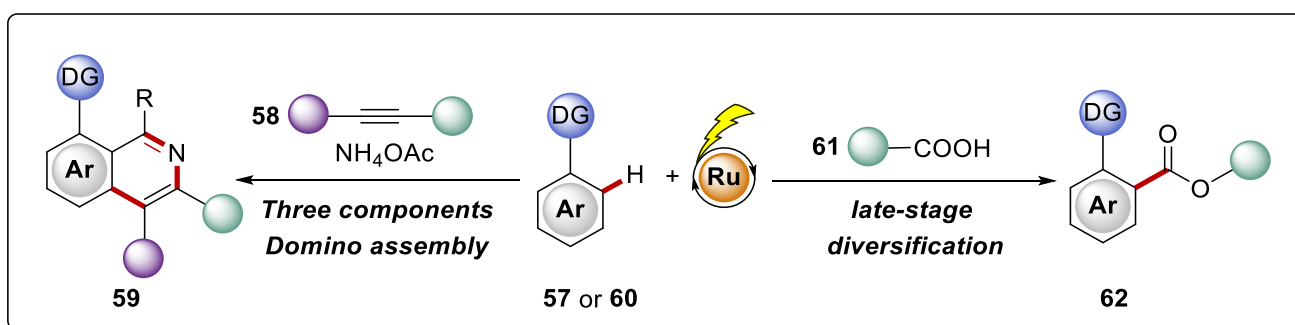


Scheme 1-34 Prediction of site-selectivity for palladaelectro-catalyzed C–H olefinations of simple undirected arenes using ML.

Cronin et al. employed One-Hot encoding to encode the reaction components of palladium-catalyzed *Suzuki-Miyaura* coupling reaction.^[131] By digitizing the synthetic space and employing ML regression of reaction yield, they were able to guide the iterative optimization of reaction conditions using a robotic platform. Recently, Doyle and colleagues highlighted the effectiveness of Bayesian optimization algorithms for reaction optimizations.^[132] They introduced a versatile Bayesian reaction optimization framework compatible with automated systems to optimize the palladium-catalyzed direct arylation reactions. The Bayesian reaction optimizer outperformed human decision-making in both consistency (variance between the results and initial available data) and efficiency (number of experiments). Zare and co-workers introduced a sophisticated deep reinforcement learning strategy to optimize chemical reactions.^[133] Their model demonstrated a significant advantage over conventional blackbox optimization algorithms, achieving a remarkable 71% reduction in the number of steps necessary for optimizing both simulation-based and real reactions.

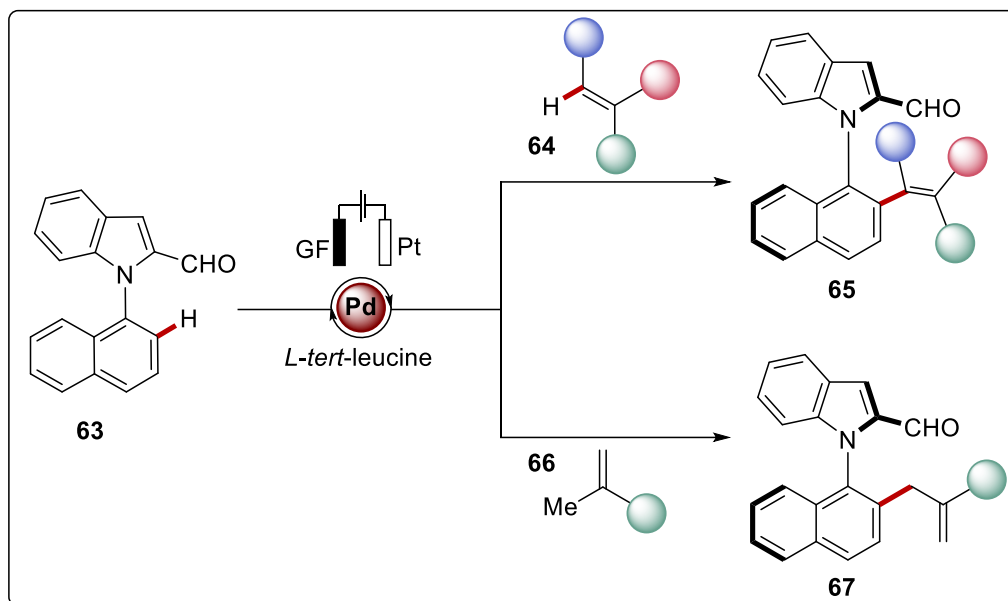
2 Objective

In recent years, the utilization of electrical energy as a redox reagent has gained recognition as a progressively feasible and environmentally conscious approach to facilitate chemical reactions.^[134] Significant development was gained by the merger of electrocatalysis with oxidative C–H activation, thus avoiding the use of often toxic metal oxidants. In this context, we became interested in exploiting the potential of ruthenium electrocatalysis for three-component C–H annulation of acetophenones. Moreover, the exploration of the electrochemical selective C–H acyloxylation of sensitive phenols would be highly desirable and of prime importance for *inter alia* late-stage diversification of tyrosine-derived peptides (Scheme 2-1).



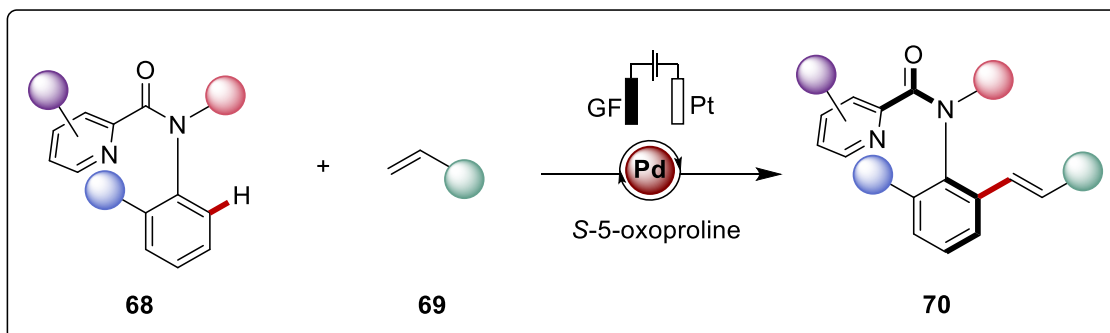
Scheme 2-1 Ruthenaelectro-catalyzed selective C–H activation with diverse chelating assistances.

Despite indisputable advances, full selectivity control in terms of enantioselective metallaelectro-catalyzed C–H activation is unfortunately elusive. In 2020, our group reported the first enantioselective pallada-electrocatalyzed C–H activation using a cTDG to access the C–C axially chiral compounds.^[117] Inspired by this study, we would like to extend this elegant cTDG strategy to the kinetic resolution of *N*-arylindoles, providing an alternative method for synthesis of the N–C axially chiral scaffold (Scheme 2-2).



Scheme 2-2 Enantioselective palladaelectro-catalyzed C–H olefinations and allylations for N–C axial chirality.

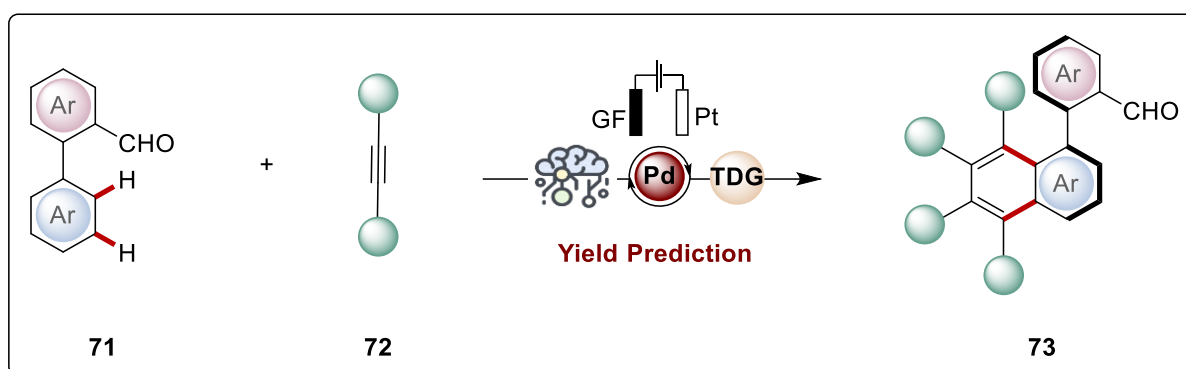
Compared with axially chiral biaryls, the enantioselective assembly of molecules featuring an acyclic anilide motif through C–H activation has gained less attraction, mainly due to the higher degree of rotational freedom than biaryls. In this context, we wished to explore atropoenantioselective pallada-electrocatalyzed C–H olefinations to access synthetically challenging axially chiral anilides with the assistance of an efficient chiral MPAA ligand (Scheme 2-3).



Scheme 2-3 Atropoenantioselective palladaelectro-catalyzed C–H olefinations using a MPAA chiral ligand.

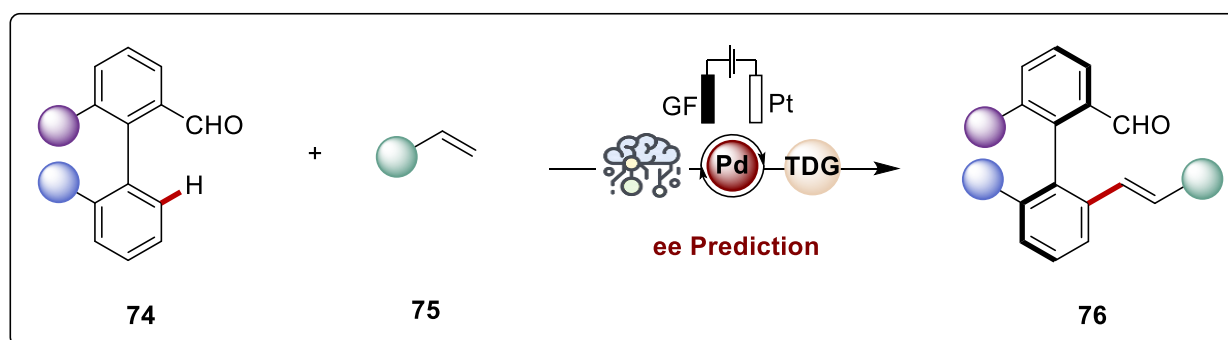
Due to the introduction of electricity, the dimensionality and complexity of electrochemical synthesis have significantly increased. More precisely, the parameter space is significantly increased by the addition of the electrochemical variables (e.g. electrochemical stability window of solvents and electrolytes, the redox potential of reactants, current/potential and electrodes). These parameters significantly impact the kinetics and thermodynamics of electron transfer,^[135] thus altering just one parameter,^[135] may result in remarkable and non-

intuitive effects on reaction productivity. In this context, ML showed tremendous potential in data-driven reaction optimization, which allows the investigation of the relationship between the various reaction parameters in a digitalized chemical space, thus avoiding the dependency on chemist's empirical knowledge and mechanistic studies in traditional screenings. Hence, we planned to establish a ML workflow to guide us in optimizing the palladaelectro-catalyzed annulation reaction (Scheme 2-4).



Scheme 2-4 ML guided yield optimization of the palladaelectro-catalyzed annulation reaction.

In addition to the yield optimization for metallaelectro-catalyzed C–H activation, we are also keen on harnessing ML for predicting the enantioselectivity, which is one of the main challenges in enantioselective catalysis due to the high-dimensional structure–enantioselectivity relationship. To address this challenge, we planned to design a ML-workflow combining the benefits of the mechanism-based and data-driven approaches to predict the enantioselectivity in the palladaelectro-catalyzed oxidative C–H activation reaction (Scheme 2-5).



Scheme 2-5 Enantioselectivity prediction of palladaelectro-catalyzed C–H activation using ML.

3 Results and Discussion

3.1 Ruthenaelectro-Catalyzed Three-Component C–H Annulation

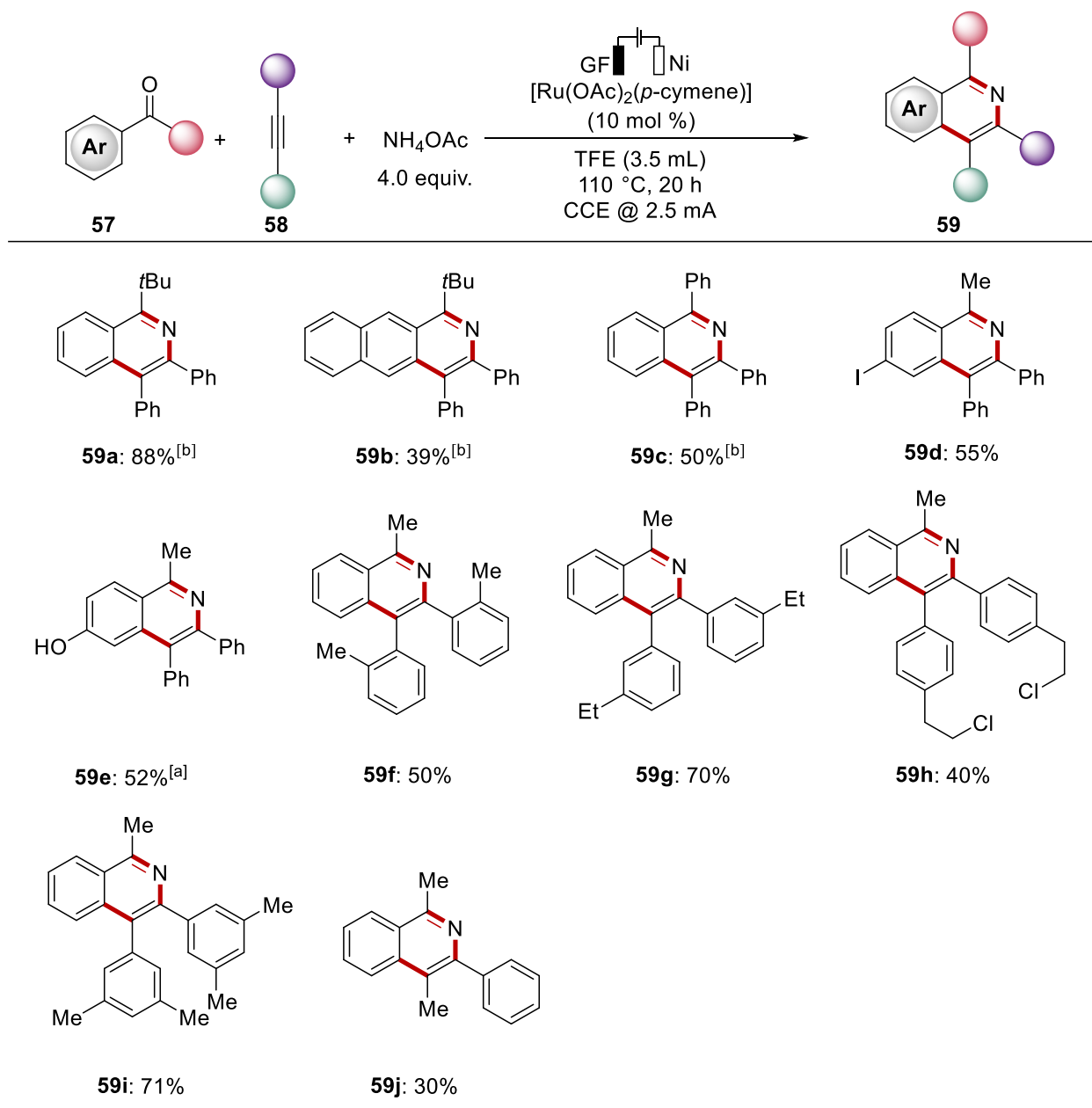
Nitrogen-containing heterocycles, which are commonly found in bioactive molecules, have been of particular interest to medicinal chemists and pharmaceutical industries.^[136] Among these heterocycles, isoquinolines exhibit diverse activities, including cardiovascular, *anti*-tumor, *anti*-inflammatory, and *anti*-malaria properties.^[137] One efficient strategy to construct isoquinolines is transition metal-catalyzed imino group-directed C–H activation followed by annulation of alkynes.^[30a, 138] However, this approach often requires the use of stoichiometric amounts of chemical oxidants, such as copper or silver salts. Additionally, the imines are basically not commercially available and need to be isolated prior to catalysis.^[139] Therefore, we intended to develop a ruthenaelectro-catalyzed oxidative C–H annulation reaction that overcomes these drawbacks, achieving a more sustainable and practical catalysis manifold.

3.1.1 Optimization and Substrate Scope of Annulation Reaction

The optimized reaction conditions were identified by Dr. Xuefeng Tan. The optimization process involved several key aspects, including the assessment of different ruthenium sources as catalysts and the evaluation of various solvents. Additionally, the impact of reaction temperature was investigated, and control experiments were conducted to optimize the loading of the coupling partner, applied current, and reaction time. As a result, using [Ru(OAc)₂(*p*-cymene)] (10 mol %), NH₄OAc (2.0 equiv.) in TFE at 110 °C for 20 h, under a constant current electrolysis of 2.5 mA on a 0.30 mmol substrate scale, gave the best yield. Graphite felt (GF) and nickel foam (Ni) were identified as the best choices for the anode and the cathode, respectively. The NH₄OAc served both as a NH source to generate the imine intermediate and as an electrolyte in this reaction.

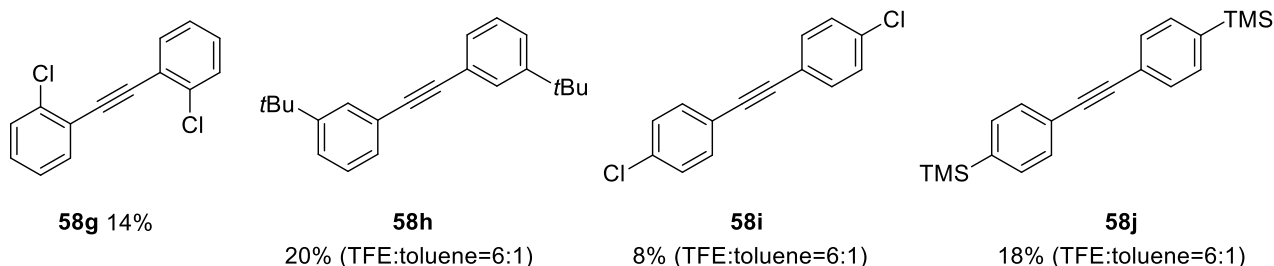
With the optimized reaction conditions in hand, we next examined the substrate scope of the ruthenaelectro-catalyzed three-component annulation with diverse ketones **57** and different alkynes **58** (Scheme 3-1). 2,2-Dimethyl-1-phenylpropan-1-one **57a** furnished the corresponding isoquinoline **59a** in 88% yield. The site-selectivity for *meta*-substituted ketone **57b** was governed by steric hindrance to afford the product **59b**. Benzophenone **57c** was also identified as a suitable substrate for this electrocatalysis. Iodide and acetoxy groups were well tolerated by the electrochemical conditions (**59d** and **59e**), highlighting a notable potential for further late-stage diversification. Next, electron-rich and electron-deficient alkynes **58** were carefully investigated, while electron-rich alkynes exhibited a slightly higher innate reactivity (**59f**, **59g** and **59i**). In addition to the symmetric aryl alkynes, asymmetric

alkyne featuring an alkyl group **58f** was also tested for our ruthenaelectro-catalyzed annulation reaction, albeit with a lower yield.



Scheme 3-1 Scope of the ruthenaelectro-catalyzed annulation. ^[a] Starting material is 4-acetoxyacetophenone. ^[b] by Dr. Xuefeng Tan.

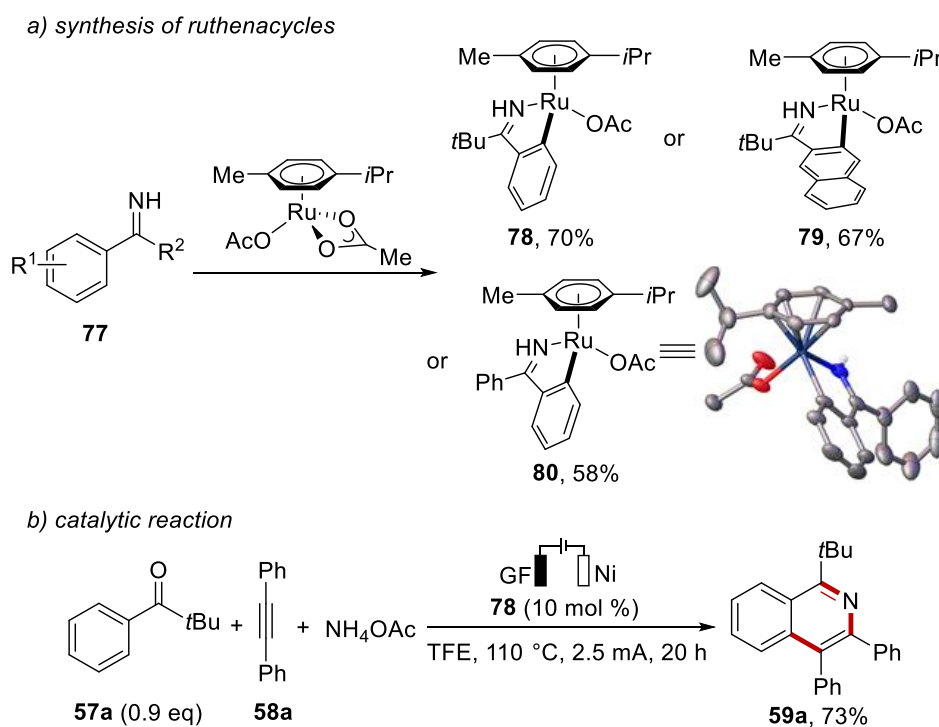
Under otherwise identical standard reaction conditions, diphenyl alkyne **58g** with Cl substituent in the *ortho* position proved to be challenging in the optimized condition probably due to the electronic effect. Other alkynes **58h-j** have poor solubility in the polar solvent TFE, so a solvent mixture consisting of TFE and toluene was employed but still gave a relatively poor reactivity in the transformation.



Scheme 3-2 Alkynes giving inefficient results.

3.1.2 Mechanism Study

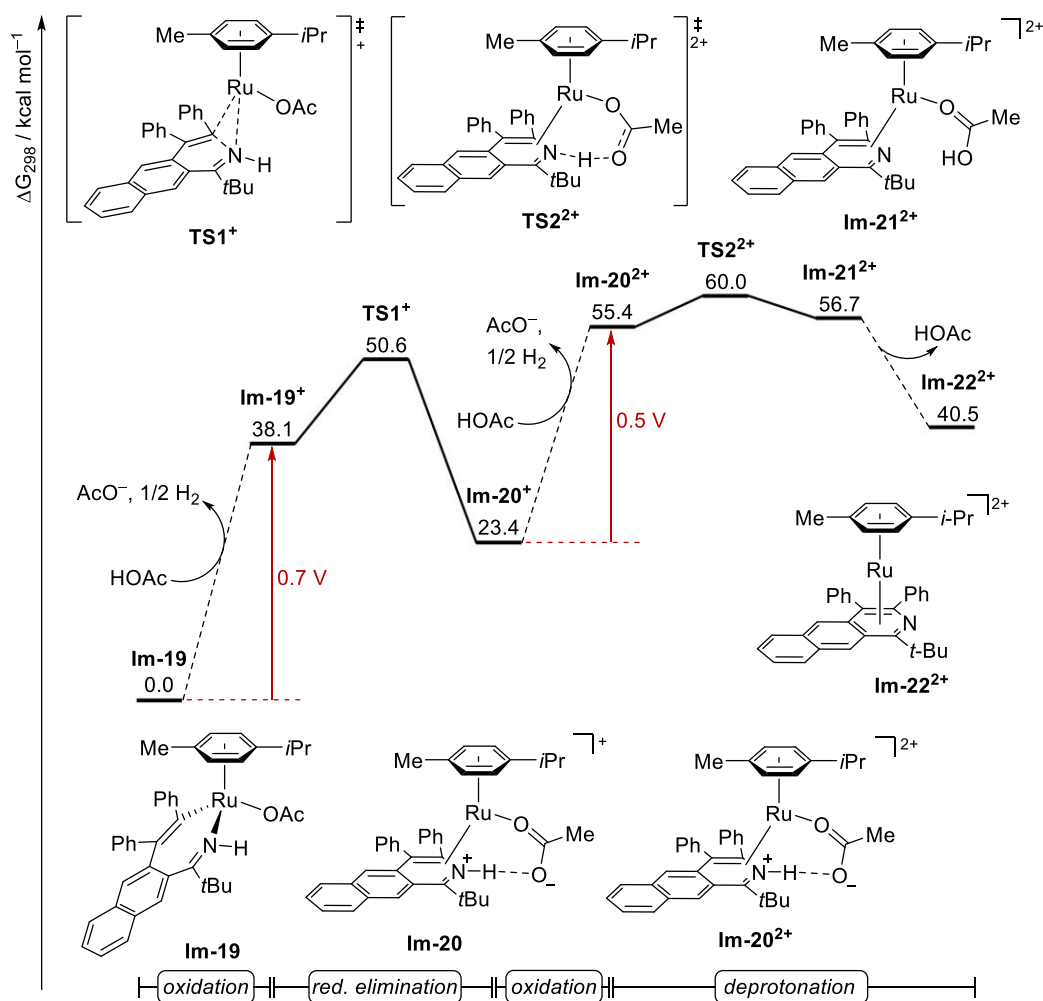
Various mechanistic studies were performed in order to elucidate the mode of action of the ruthenium catalysis. First, we attempted to identify possible intermediates in the reaction. Therefore, three ruthenacycle complexes **78**, **79**, and **80** were synthesized by Dr. Xuefeng Tan and complex **80** was unambiguously characterized by X-ray diffraction analysis (Scheme 3-3a). Notably, the metallacycle **78** was found to be competent under the catalytic reaction conditions (Scheme 3-3b).



Scheme 3-3 Study on ruthenacycle complexes (a) synthesis, (b) catalytic reaction.

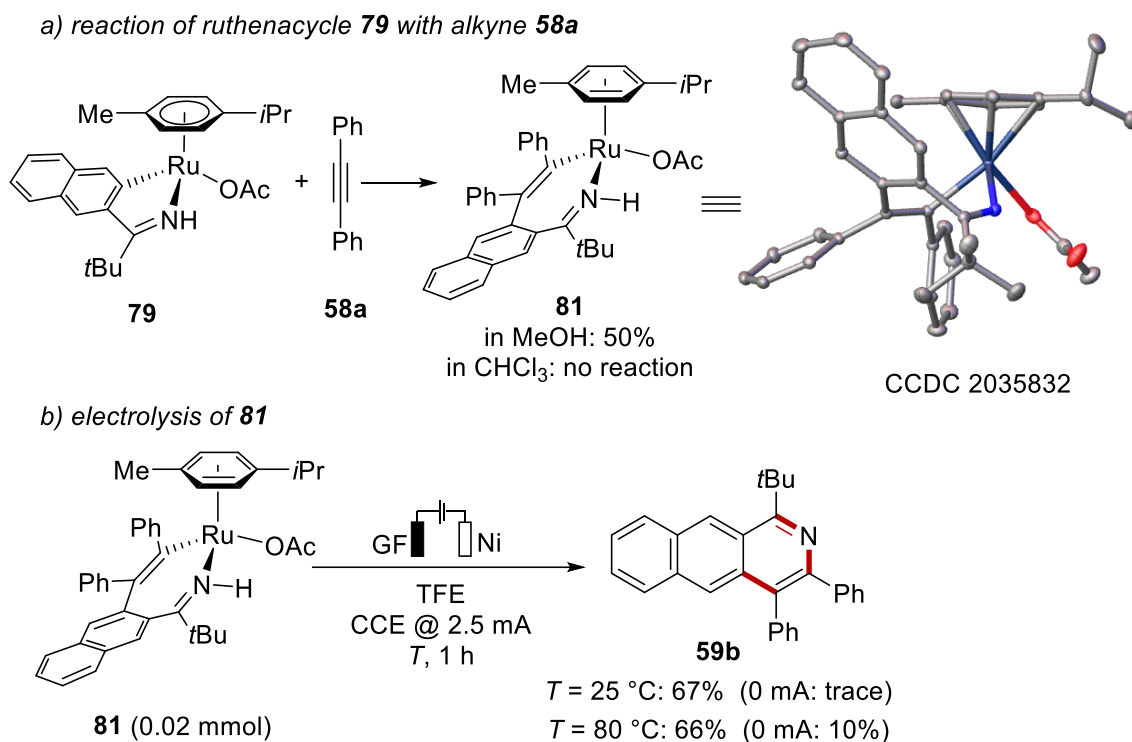
Next, Dr. Torben Rogge utilized density functional theory (DFT) studies to investigate the working mode of a catalyst at the ω B97X-V/def2-QZVP+SMD(TFE)//TPSS-D3(BJ)/def2-TZVP level of theory. The studies revealed a stepwise process: The initial one-electron oxidation of seven-membered ruthenacycle **Im-19** with an oxidation potential of 0.7 V *versus* $\text{Fc}^{+/0}$ takes place, leading to the formation of ruthenium(III) complex **Im-19⁺** (Scheme 3-4). Subsequently, reductive elimination occurs to generate **Im-20⁺**, which then undergoes a

second SET oxidation to a ruthenium(II) species with a calculated oxidation potential of 0.5 V. In the final step, facile deprotonation and decooordination of acetic acid takes place to deliver the 18-electron ruthenium sandwich-type complex **Im-22²⁺**.



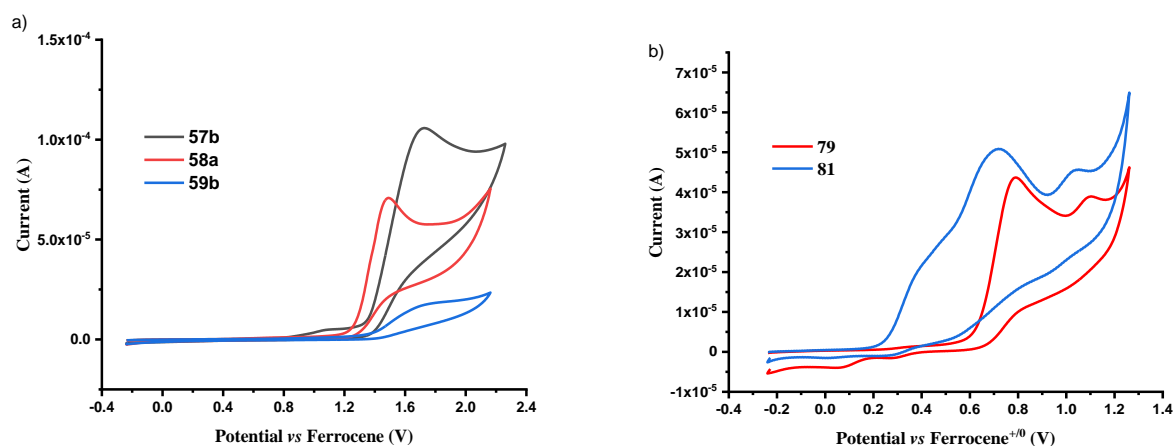
Scheme 3-4 Relative Gibbs free energy profile in kcal mol⁻¹ at the ω B97X-V/def2-QZVP+SMD(TFE)/TPSS-D3(BJ)/def2-TZVP level of theory. The given potential (red) corresponds to the half-wave potential versus $\text{Fc}^{+/0}$.

The insights gained from the DFT calculations were validated by the key intermediate **81** isolated from the reaction of ruthenacycle **79** and alkyne **58a** by Dr. Xuefeng Tan. The seven-membered ring compound **81** was characterized by X-ray diffraction analysis, providing unambiguous structural information (Scheme 3-5a). Regardless of the reaction temperature, the desired isoquinoline product **59b** could be obtained through direct electrolysis of intermediate **81** in TFE (Scheme 3-5b).



Scheme 3-5 Isolation of key intermediate ruthenacycle.

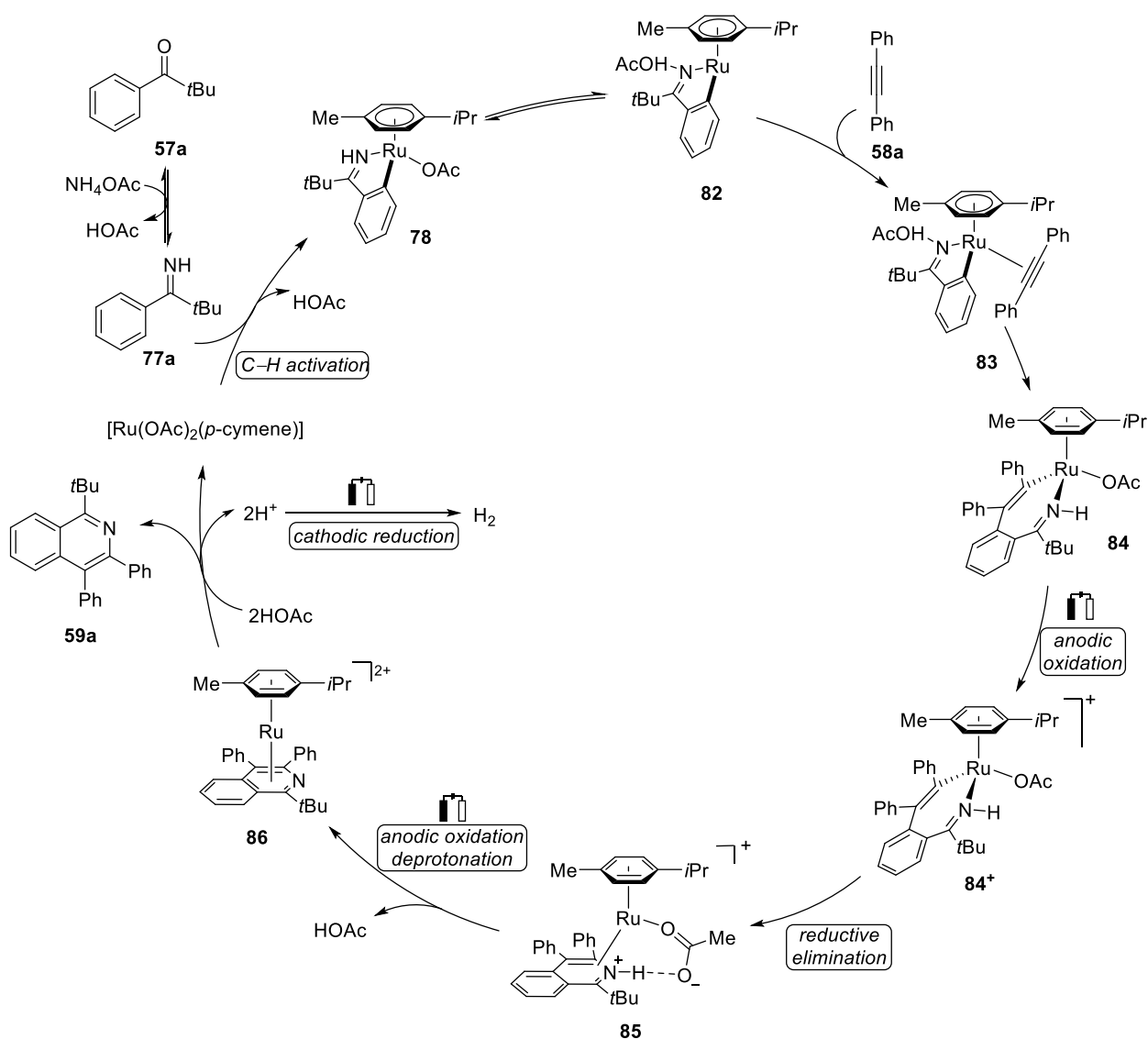
Furthermore, cyclic voltammetry experiments were performed to further investigate the electrochemical C–H activation mechanism. Substrates **57b** and **58a** as well as product **59b** all showed onset potentials higher than 1.2 V *versus* Fc⁺⁰ (Scheme 3-6a). In contrast, ruthenacycle **79** displayed two irreversible oxidation events with an onset potential of $E_{onset} = 0.60$ V *versus* Fc⁺⁰ (Scheme 3-6b). On the other hand, the seven-membered ruthenacycle **81** exhibited a significantly lower oxidation potential, with an onset potential of $E_{onset} = 0.20$ V *versus* Fc⁺⁰. This observation supports the hypothesis of oxidation-induced reductive elimination within a ruthenium(II/III) regime.



Scheme 3-6 Cyclic voltammogram in TFE under N₂.

3.1.3 Proposed Catalytic Cycle

Based on the detailed mechanistic studies, we proposed a catalytic cycle that begins with the *in-situ* generation of imine **77a**, followed by a rapid C–H activation, leading to the formation of ruthena(II)cycle **81** (Scheme 3-7). Subsequently, migratory insertion of **58a** takes place to form the intermediate **84**. Then, anodic oxidation-induced reductive elimination occurs through a ruthenium(II/III/I) manifold, giving rise to intermediate **85**. Further anodic oxidation and deprotonation of intermediate **85** generates a sandwich-type complex **86**, followed by ligand exchange to deliver the final product **59a** and regenerate the ruthenium(II) catalyst.



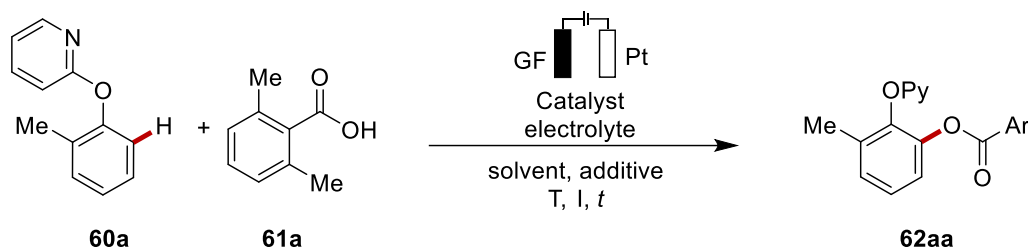
Scheme 3-7 Proposed catalytic cycle.

3.2 Ruthenaelectro-Catalyzed C–H Acyloxylation for Late-stage Tyrosine and Oligopeptide Diversification

Phenol derivatives, which are widely found in bioactive compounds related to crop protection,^[140] molecular syntheses,^[123, 141] and drug development,^[142] hold significant interest as target motifs. Thus, direct catalytic oxygenation to achieve phenol derivatives has captured numerous interest and significant developments have been achieved.^[143] In addition, the merger of C–H activation and electrooxidation was recently recognized as a particularly powerful strategy for molecular catalysis.^[6b, 144] However, the oxygenation of late-stage amino acid or peptide diversifications through electrocatalysis is still unprecedented. In this context, we were interested to achieve challenging electrochemical selective acyloxylation of sensitive phenols for late-stage tyrosine diversifications.

3.2.1 Optimization Study

The optimization study was commenced by probing various reaction conditions for the envisioned C–H acyloxylation with **60a** and **61a** in presence of a ruthenium catalyst and *n*Bu₄NBF₄ electrolyte (Table 3-1). A convenient undivided cell setup could be used, with a Pt cathode and a GF anode. Lower current with longer reaction time proved more efficient than higher current but shorter reaction time (entries 1 and 2). [Ru(OAc)₂(*p*-cymene)] was shown to be more reactive than [RuCl₂(*p*-cymene)]₂ (entry 3). Higher reaction temperatures improved the yield significantly (entries 4 and 5). EtOH and *t*AmOH/H₂O (3/1) failed to deliver the product, while DCE was demonstrated to be most efficient and gave the desired product in 87% yield (entries 6-8). The addition of PhI made no difference in the yield (entry 9). The electrolyte was found to be an important factor. *n*Bu₄NPF₆ provided a comparable yield of the desired product, while LiClO₄ and *n*Bu₄NOAc did not show any reactivity (entry 10-12). *p*-Cymene free ruthenium catalyst [Ru₂(OAc)₄Cl] offered almost the same reactivity compared with [Ru(OAc)₂(*p*-cymene)] (entry 14). Commercially available RuCl₃·3H₂O could also be employed efficiently for the electrocatalysis, affording the product in 66% yield (entry 15). However, other metal catalysts, like rhodium(III), iridium(III) and cobalt(III) complexes, did not provide any catalytic activity (entries 16-19). Control experiments were conducted to confirm the importance of the ruthenium catalyst and electricity in the reaction (entries 20 and 21).

Table 3-1 Optimization of the annulation reaction.

| Entry | Solvent | Catalyst | Electrolyte | Additive | I (mA) | T (°C) | t (h) | Yield (%) |
|-------|---|--|---|----------|--------|---------|-------|--------------------|
| 1 | TFE | [RuCl ₂ (<i>p</i> -cymene)] ₂ | <i>n</i> Bu ₄ NBF ₄ | - | 5.0 | 80 | 8 | 12 ^[b] |
| 2 | TFE | [RuCl ₂ (<i>p</i> -cymene)] ₂ | <i>n</i> Bu ₄ NBF ₄ | - | 3.0 | 80 | 15 | 28 ^[b] |
| 3 | TFE | [Ru(OAc) ₂ (<i>p</i> -cymene)] | <i>n</i> Bu ₄ NBF ₄ | - | 3.0 | 80 | 15 | 36 |
| 4 | TFE | [RuCl ₂ (<i>p</i> -cymene)] ₂ | <i>n</i> Bu ₄ NBF ₄ | - | 3.0 | 100 | 15 | 40 ^[b] |
| 5 | TFE | [Ru(OAc) ₂ (<i>p</i> -cymene)] | <i>n</i> Bu ₄ NBF ₄ | - | 3.0 | 100 | 15 | 65 |
| 6 | EtOH | [Ru(OAc) ₂ (<i>p</i> -cymene)] | <i>n</i> Bu ₄ NBF ₄ | - | 3.0 | 100 | 15 | - |
| 7 | <i>t</i> AmOH/H ₂ O (3/1) | [Ru(OAc) ₂ (<i>p</i> -cymene)] | <i>n</i> Bu ₄ NBF ₄ | - | 3.0 | 100 | 15 | - |
| 8 | DCE | [Ru(OAc) ₂ (<i>p</i> -cymene)] | <i>n</i> Bu ₄ NBF ₄ | - | 3.0 | 100 | 15 | 87 |
| 9 | DCE | [Ru(OAc) ₂ (<i>p</i> -cymene)] | <i>n</i> Bu ₄ NBF ₄ | PhI | 3.0 | 100 | 15 | 87 |
| 10 | DCE | [Ru(OAc) ₂ (<i>p</i> -cymene)] | <i>n</i> Bu ₄ NPF ₆ | - | 3.0 | 100 | 15 | 86 |
| 11 | DCE | [Ru(OAc) ₂ (<i>p</i> -cymene)] | LiClO ₄ | - | 3.0 | 100 | 15 | - |
| 12 | DCE | [Ru(OAc) ₂ (<i>p</i> -cymene)] | <i>n</i> Bu ₄ NOAc | - | 3.0 | 100 | 15 | - |
| 13 | DCE | [RuCl ₂ (<i>p</i> -cymene)] ₂ | <i>n</i> Bu ₄ NBF ₄ | - | 3.0 | 100 | 15 | 78 ^[b] |
| 14 | DCE | [Ru ₂ (OAc) ₄ Cl] | <i>n</i> Bu ₄ NBF ₄ | - | 3.0 | 100 | 15 | 86 ^[b] |
| 15 | DCE | RuCl ₃ ·3H ₂ O | <i>n</i> Bu ₄ NBF ₄ | - | 3.0 | 100 | 15 | 66 |
| 16 | DCE | RhCl ₃ ·3H ₂ O | <i>n</i> Bu ₄ NBF ₄ | - | 3.0 | 100 | 15 | - |
| 17 | DCE | [Cp [*] RhCl ₂] ₂ | <i>n</i> Bu ₄ NBF ₄ | - | 3.0 | 100 | 15 | 15% ^[b] |
| 18 | DCE | [Cp [*] IrCl ₂] ₂ | <i>n</i> Bu ₄ NBF ₄ | - | 3.0 | 100 | 15 | <5% ^[b] |
| 19 | DCE | [Cp [*] CoI ₂ (CO)] | <i>n</i> Bu ₄ NBF ₄ | - | 3.0 | 100 | 15 | - |
| 20 | DCE | - | <i>n</i> Bu ₄ NBF ₄ | - | 3.0 | 100 | 15 | - |
| 21 | DCE | [Ru(OAc) ₂ (<i>p</i> -cymene)] | <i>n</i> Bu ₄ NBF ₄ | - | 3.0 | 100 | 15 | - ^[c] |

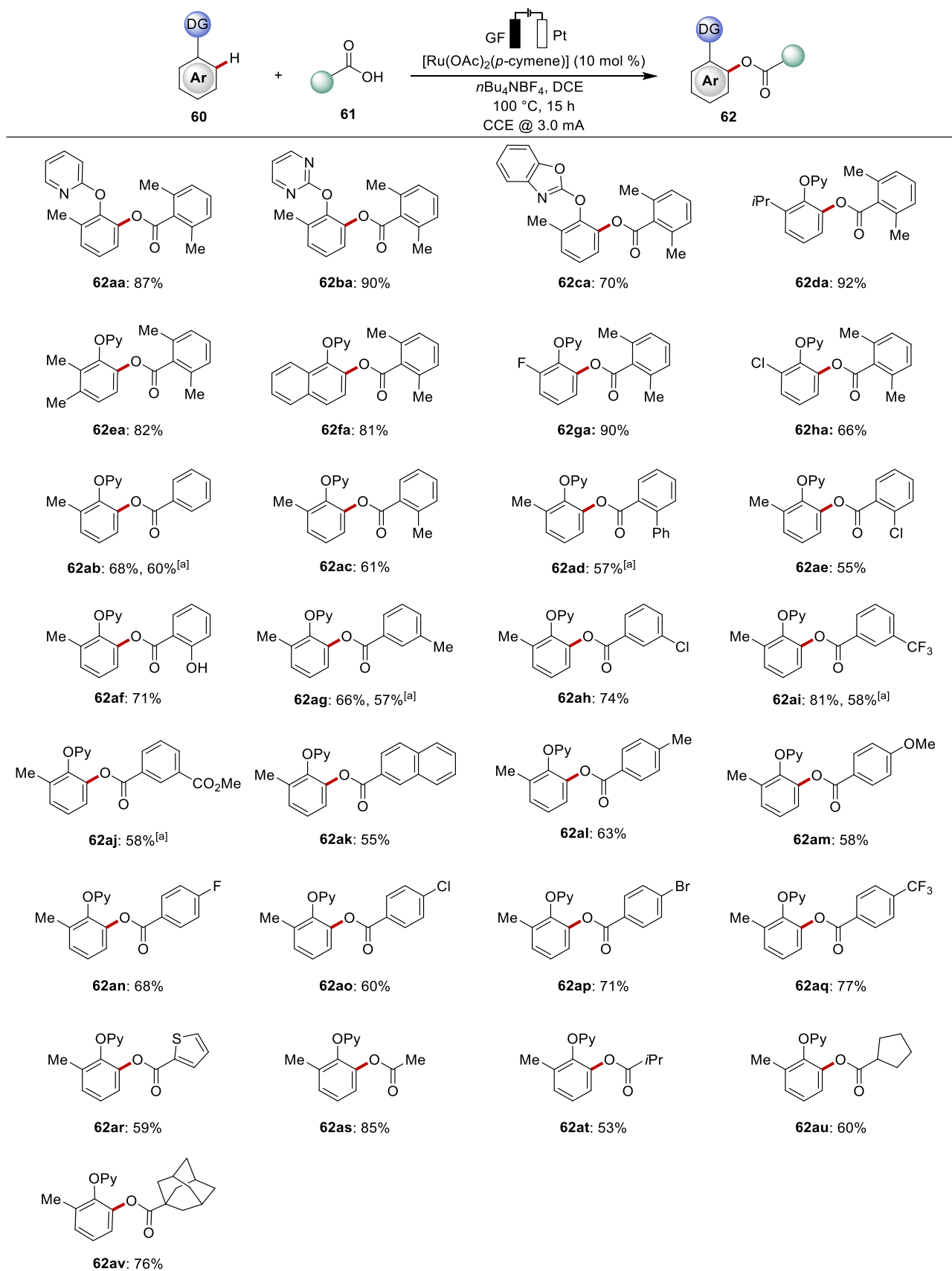
^[a] **60a** (0.25 mmol), **61a** (0.40 mmol), [Catalyst] (10 mol %), electrolyte (0.25 mmol), additive (10 mol %), solvent (4.0 mL), GF (10 x 15 x 6 mm³), Pt (10 x 15 x 0.25 mm³), air, reaction in a 25 mL Schlenk tube. ^[b] [Catalyst] (5 mol %). ^[c] no electricity. OPy = 2-pyridyloxy, TFE = 2,2,2-trifluoroethanol, DCE = 1,2-dichloroethane. Ar = 2,6-Me₂C₆H₃.

3.2.2 Scope and Removal of Pyridyl Group

With the optimized reaction conditions in hand, we proceeded to investigate alternative *N*-heterocycles as directing groups (Scheme 3-8). Both pyrimidine and benzo[*d*]oxazole demonstrated compatible reactivity for the oxygenation reaction (**62ba** and **62ca**). Then, the

substrate scope of the ruthenaelectro-catalyzed C–H acyloxylation was examined with a representative set of phenols **60**. Substrates with various substituents, such as isopropyl (**60d**), dimethyl (**60e**), naphthyl (**60f**), fluoro (**60g**), and chloro (**60h**), gave the corresponding products in good to excellent yields. Our attention was then shifted to explore viable carboxylic acids **61** for the ruthenaelectro-catalyzed acyloxylation (Scheme 3-8). Both electron-rich (**61c**, **61g**, **61k**, **61l** and **61m**) and electron-deficient (**61e**, **61h**, **61i**, **61k**, and **61n-61q**) benzoic acids delivered the products in good yields, with electron-deficient acids exhibiting slightly higher reactivity. Our electrocatalytic system also showed excellent tolerance towards delicate hydroxy group **61f**. Notably, a favorable reactivity was achieved upon employing the readily available catalyst $\text{RuCl}_3 \cdot 3\text{H}_2\text{O}$ in the ruthenium electro-catalyzed C–H acyloxylation (**62ab**, **62ad**, **62ag**, **62ai** and **62aj**). Furthermore, heteroaromatic thiophene acid **61r** was found to be a viable substrate. The efficacy of the ruthenaelectro-catalyzed oxygenation was further exemplified by the successful utilization of alkyl carboxylic acids, including acetic acid **61s**, isobutyric acid **61t**, cyclopentanoic acid **61u**, and 1-adamantanecarboxylic acid **61v**.

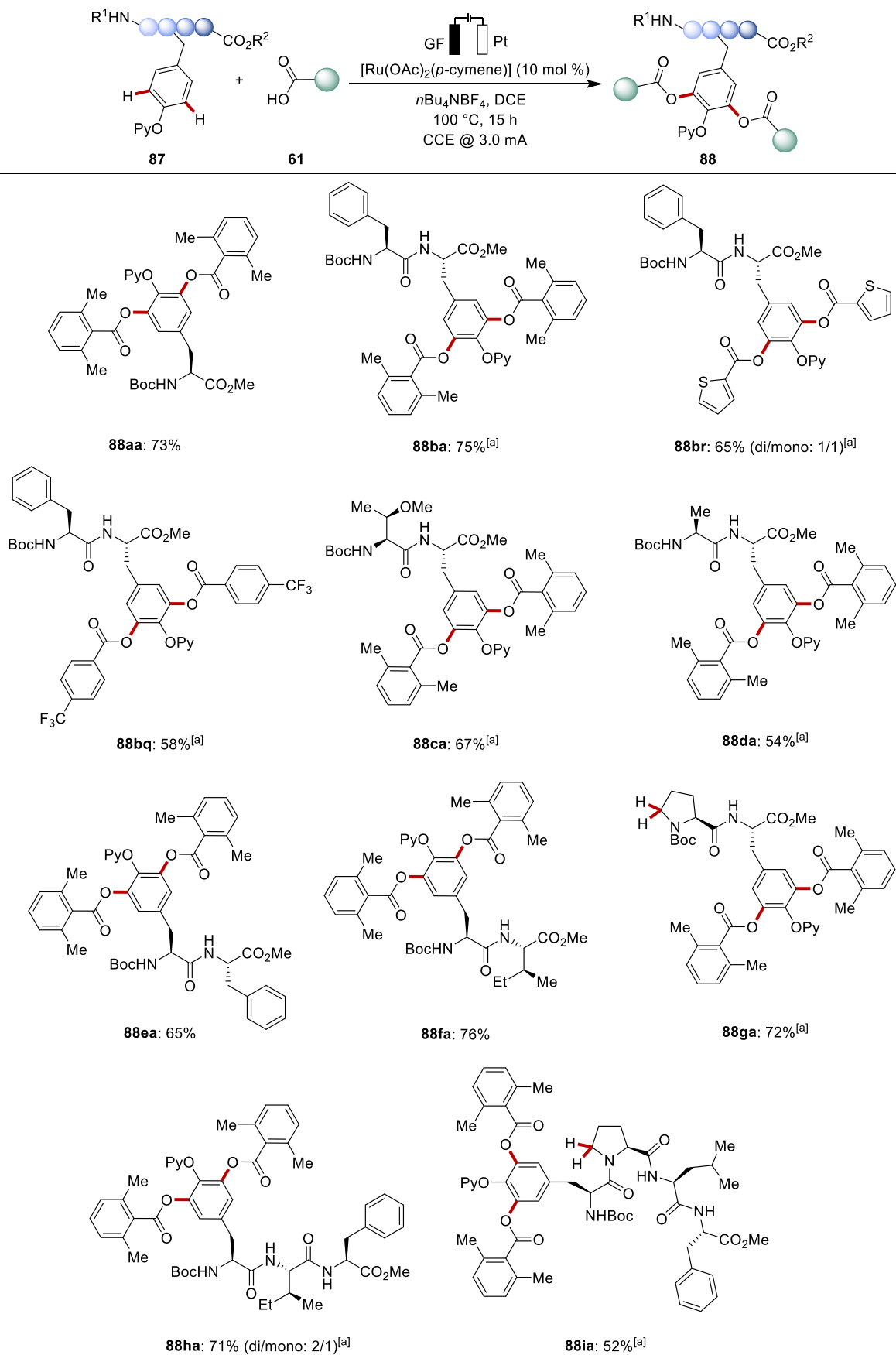
Results and Discussion



Scheme 3-8 Substrate scope of electro-C–H acyloxylation with phenols **60** and carboxylic acids **61**. ^[a] RuCl₃·3H₂O (10 mol %) as the catalyst.

The high efficiency and compatibility with diverse functional groups observed in our ruthena-electrocatalyzed acyloxylation of phenol derivatives motivated us to explore the late-stage functionalization of peptides containing tyrosine residues. When employing amino acid **87a**, we successfully obtained the desired acyloxylated tyrosine derivative **88aa** without racemization. Furthermore, various di-, tri-, and tetrapeptides **87b-87i** were effectively decorated with diverse (hetero)aromatic acids **61**, with no signs of any epimerization of the sensitive peptides. Notably, our mild electroxidative approach entirely circumvented Shono-type reactions, even in the presence of proline-containing di- and tetrapeptides **87g** and **87i**.

Results and Discussion



Scheme 3-9 Scope of viable peptides **87**. ^[a] Done by Dr. Nikolaos Kaplaneris.

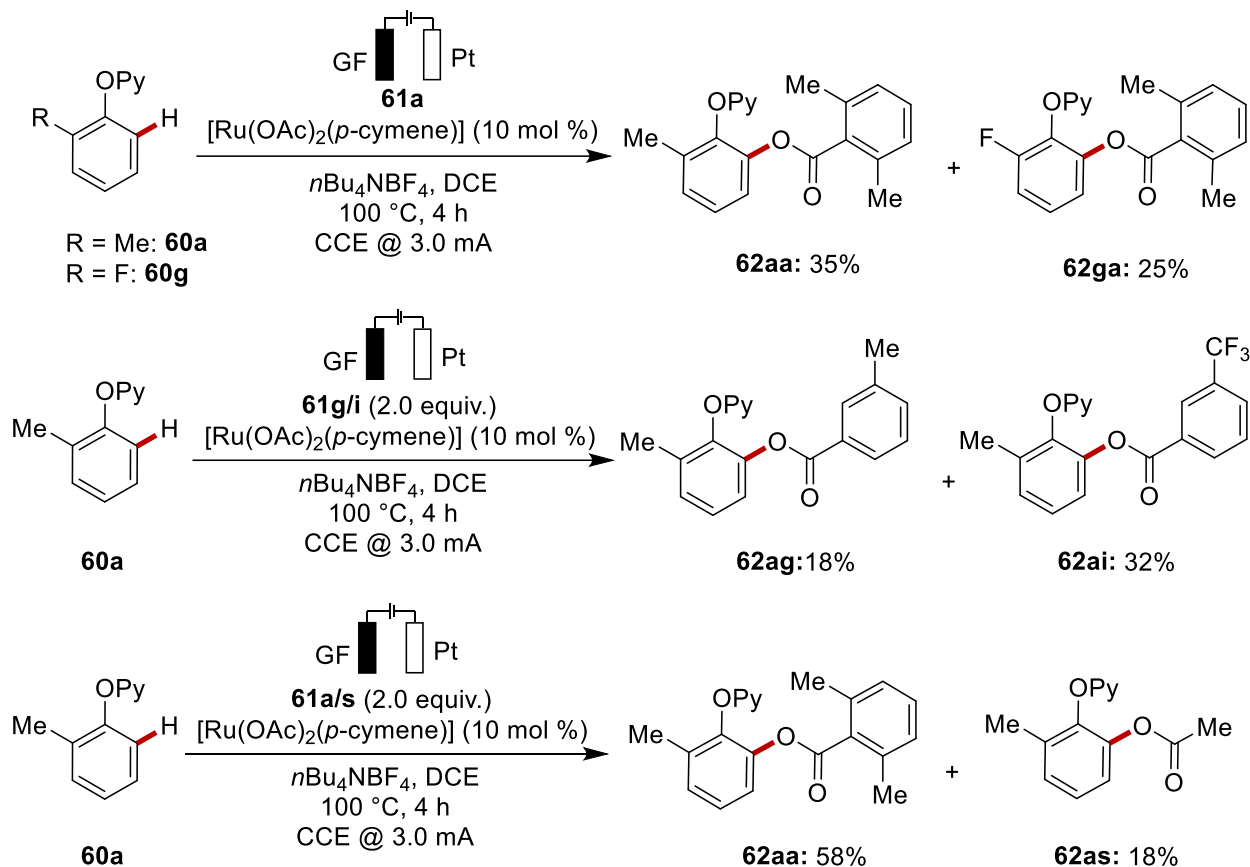
Moreover, we successfully achieved the complete removal of the pyridyl group through a selective methylation/hydrogenation protocol, resulting in the formation of *NH*-free tyrosine-containing acyloxylated amino acid **89** without racemization (Scheme 3-10).



Scheme 3-10 Removal of pyridyl group.

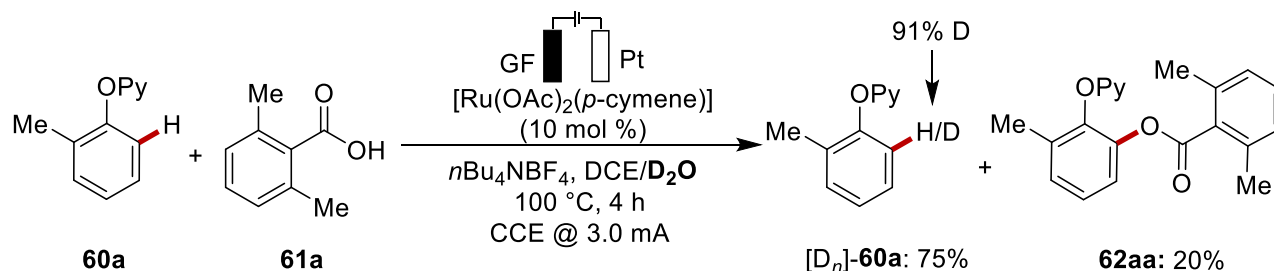
3.2.3 Mechanistic Study

Intrigued by the versatility of electrochemical C–H acyloxylation, we became motivated to investigate its mode of action. First, we conducted an intermolecular competition experiment involving phenols **60** with different electronic properties (Scheme 3-11). The electron-rich substrate **60a** exhibited higher reactivity compared to the electron-deficient substrate **60g**. This suggests that the reaction rate is primarily governed by nucleophilicity rather than the kinetic acidity of the C–H bond. These findings are inconsistent with a CMD mechanism. Instead, it is likely that a BIES mechanism is operative. Furthermore, competition experiments were designed to explore the relative reactivities of electronically differentiated carboxylic acids **61**. The electron-deficient aromatic carboxylic acids **61i** reacted at a faster rate than **61g**. Moreover, a competition experiment was performed between aryl carboxylic acid **61a** and alkyl carboxylic acid **61s**, which highlighted the enhanced reactivity of the aromatic derivatives over the alkyl counterparts.



Scheme 3-11 Competition experiments.

Furthermore, in the ruthenaelectrocatalysis with isotopically-labeled D_2O as cosolvent, a significant H/D-exchange was observed at the *ortho*-position, as evidenced by the re-isolation of the substrate $[\text{D}_n]\text{-60a}$, indicating a rapid C–H activation (Scheme 3-12).

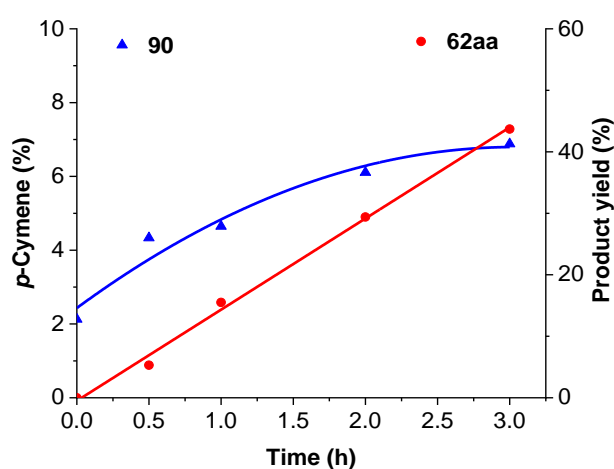
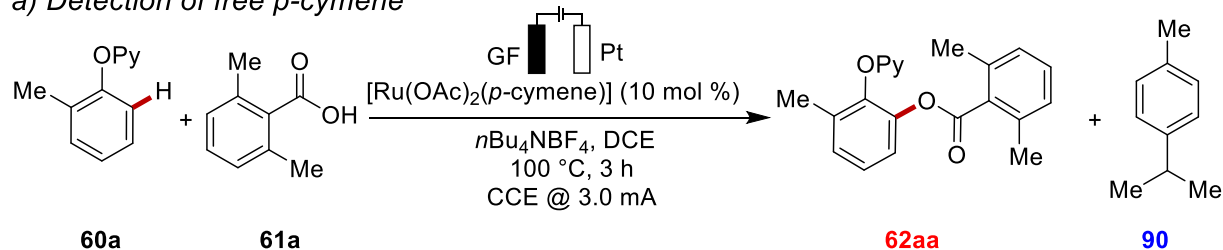


Scheme 3-12 H/D scrambling experiment.

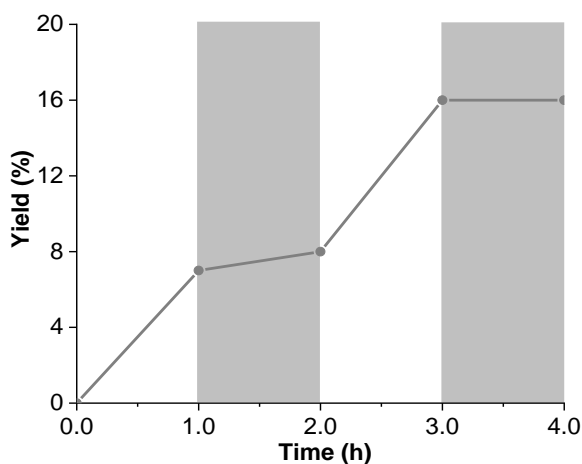
During the electrocatalysis process, a substantial release of free *p*-cymene **90** was observed from $[\text{Ru}(\text{OAc})_2(p\text{-cymene})]$ (Scheme 3-13a), implying the involvement of a *p*-cymene ligand-free complex in the catalytic reaction. This finding also aligns with our optimization process, where the ruthenium catalysts without *p*-cymene ligand exhibited high activity in this reaction. In addition, a linear relationship was observed between the time and product yield, indicating that the rate of the reaction did not depend on the catalyst or substrate concentration. The rate determining step should be the anodic oxidation step. This

hypothesis was further validated by the on/off electricity experiment (Scheme 3-13b). Notably, when the electric current was turned off, the formation of the acyloxylated product was effectively suppressed.

a) Detection of free *p*-cymene



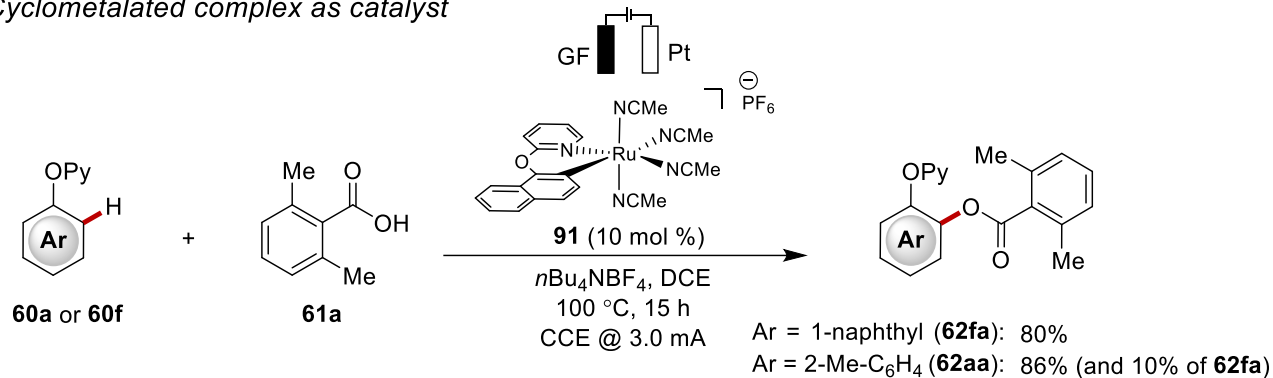
b) On/off electricity experiment



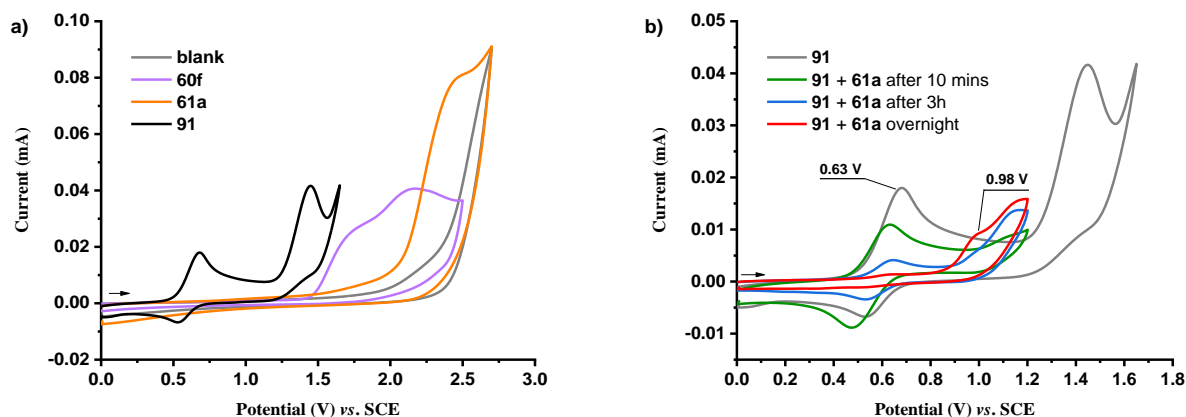
Scheme 3-13 (a) detection of free *p*-cymene, (b) On/off electricity experiment.

Next, a well-defined cationic cyclometalated ruthenium complex **91** was prepared. Remarkably, it exhibited high catalytic activity under otherwise identical reaction conditions (Scheme 3-14).

Cyclometalated complex as catalyst

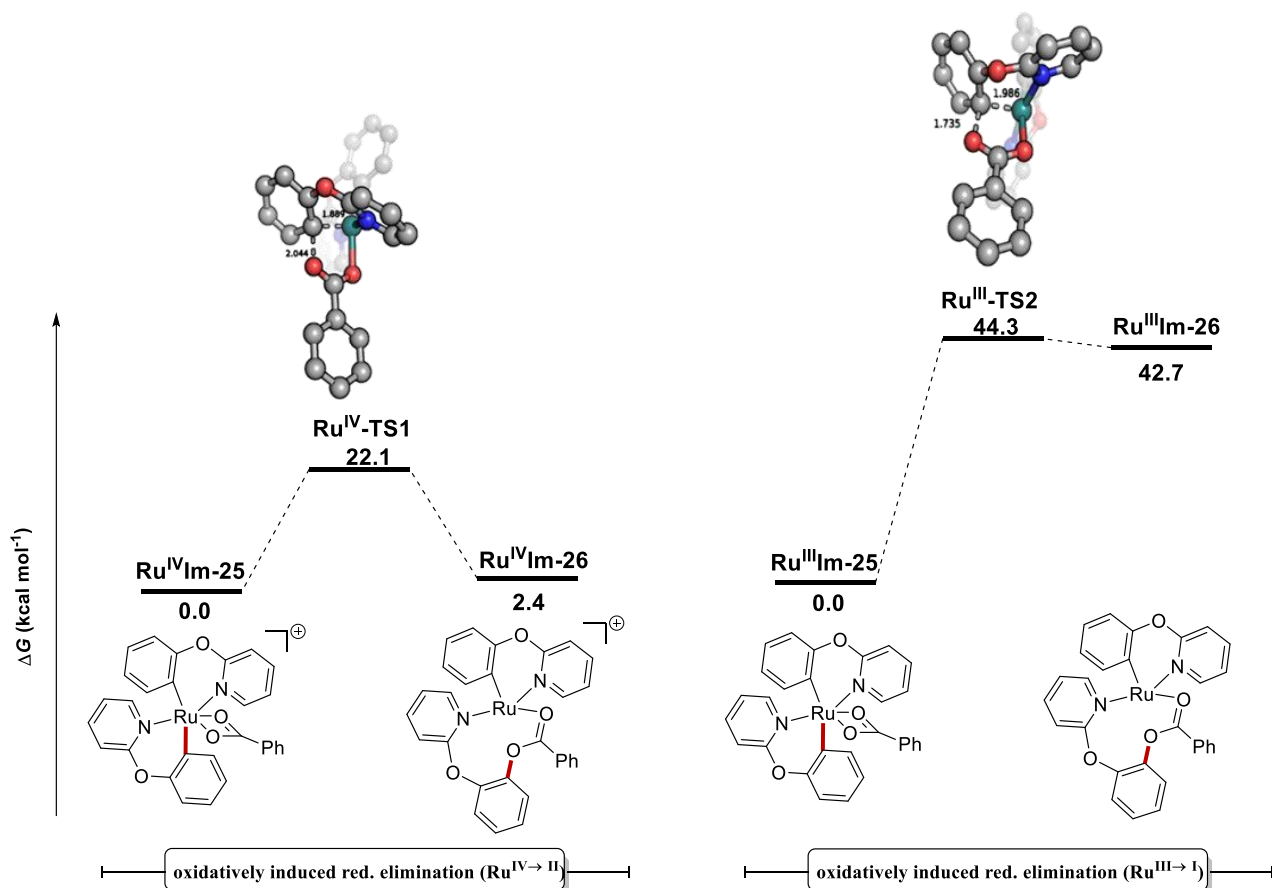
**Scheme 3-14 Cyclometalated complex as catalyst.**

We further investigated the redox properties of complex **91** by detailed cyclic voltammetry studies. As illustrated in Scheme 3-15a, complex **91** exhibited a reversible oxidation process to form ruthenium(III) at a potential of 0.63 V, which was significantly lower than the oxidative potentials observed for substrates **60f** or **61a**. Interestingly, the addition of carboxylic acid resulted in the gradual disappearance of the reversible peak at 0.63 V (Scheme 3-15b), and a new irreversible oxidation peak appeared at 0.98 V, which presumably resulted from the ligand exchange with the introduced acetic acid. Moreover, our analysis *via* high-resolution mass spectrometry of the solution after the CV experiment corroborated the replacement of acetonitrile by carboxylate ions to coordinate with the metal center (Scheme 5-10).

**Scheme 3-15 Cyclic voltammograms.**

In order to gain insights into the catalyst's mode of action, DFT calculations were conducted by MSc Binbin Yuan in the Ackermann group (Scheme 3-16). Three computational models were examined: (i) coordination of *p*-cymene and **60a** to the ruthenium center, (ii) coordination of two **60a**, with one serving solely as an *L*-type ligand, and (iii) C–H activation of both substrates, with only one involved in the reductive elimination process. The first two pathways were found to be energetically unfavorable due to high calculated barriers. These

findings align well with the experimental observations of free *p*-cymene being detected during the reaction. Additionally, the computational analysis indicated that the ruthenium(II/IV) manifold pathway was energetically preferred over the ruthenium(I/III) manifold pathway by 22.2 kcal mol⁻¹, suggesting a preferential oxidatively induced reductive elimination through bis-cyclometalated ruthenium(IV) species.

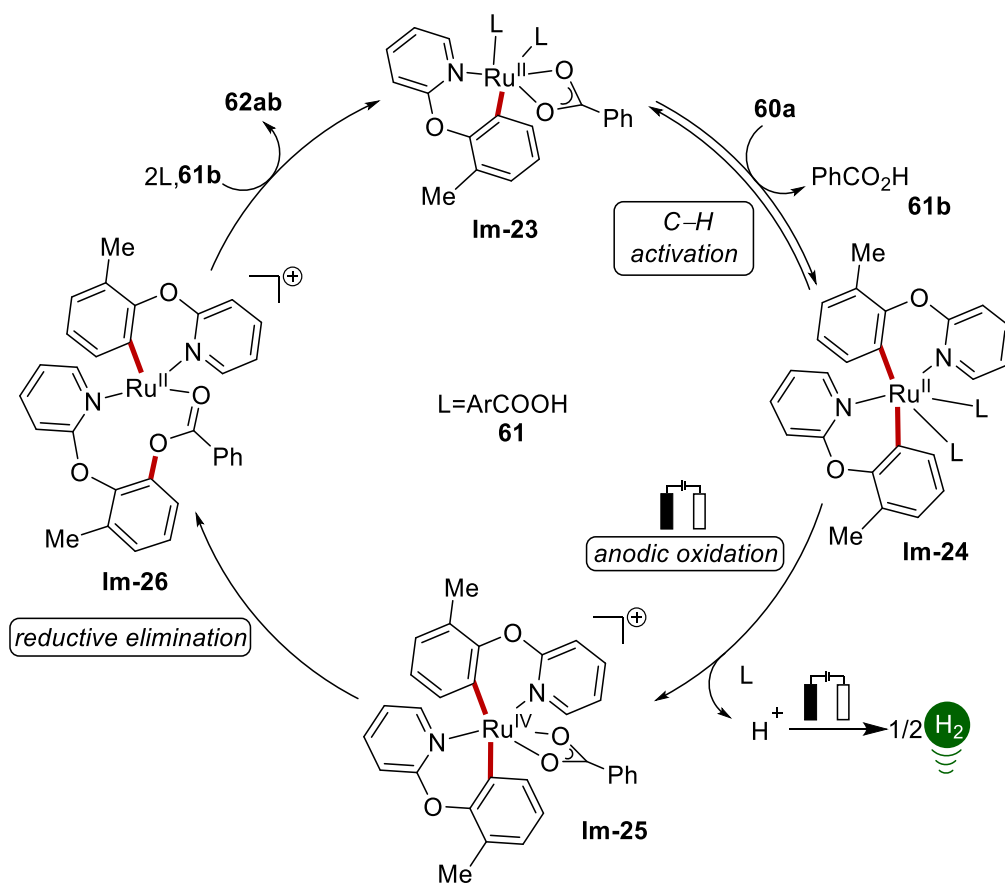


Scheme 3-16 Computed relative Gibbs free energy profile ($\Delta G_{373.15}$) in kcal mol⁻¹ for two distinct *p*-cymene free oxidatively induced reductive elimination pathways at the PW6B95-D4/def2-TZVP+SMD(DCE)//PBE0-D3BJ/def2-SVP level of theory. Nonparticipating hydrogen atoms were omitted for clarity.

3.2.4 Proposed Catalytic Cycle

Based on all the findings, the proposed catalytic cycle for the acyloxylation reaction begins with the BIES C–H metalation process and dissociation of *p*-cymene, resulting in the formation of a cyclometalated complex **Im-23** (Scheme 3-17). Next, another molecule of **60a** coordinates to the ruthenium complex **Im-23** and undergoes C–H activation, leading to the formation of a bis-cyclometalated complex **Im-24**. This complex **Im-24** then undergoes anodic oxidation, resulting in the generation of a ruthenium(IV) intermediate **Im-25**. Finally, reductive elimination and ligand exchange reactions take place, resulting in the formation of

the desired product **62ab**. Simultaneously, the ruthenacycle **Im-23** is regenerated, thus completing the catalytic cycle.



Scheme 3-17 Proposed catalytic cycle.

3.3 Palladaelectro-Catalyzed C–H Olefination for N–C Axial Chirality *via* Chiral Transient Directing Group Strategy

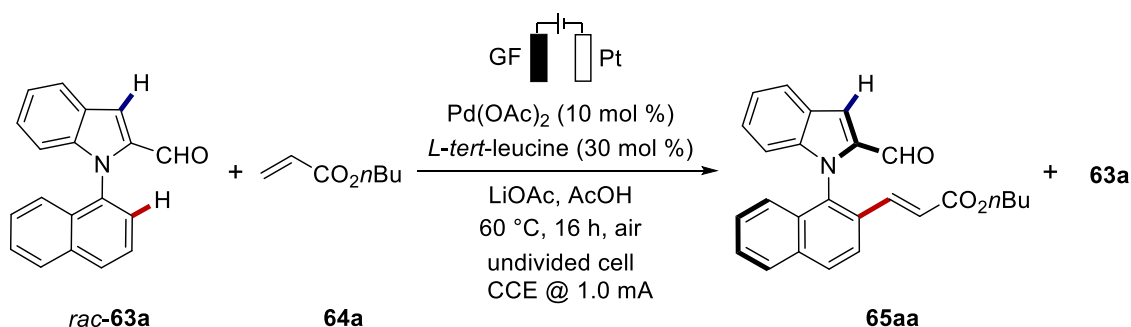
Axially chiral compounds have received considerable attention in recent years because they are found in natural products,^[145] drug discovery,^[146] or asymmetric catalysis.^[147] Particularly, chiral biaryls have been extensively investigated, resulting in significant developments.^[148] In this context, our group has recently merged enantioselective transition metal catalyzed C–H activation with electrocatalysis for the synthesis of C–C axially chiral binaphthyls.^[117] Despite notable progress in the assembly of chiral biaryls, the enantioselective synthesis of N–C axially chiral molecules continues to be undeveloped. As a consequence, recent attention has been shifted towards strategies for producing N–C axially chiral frameworks, with noteworthy contributions by Wencel-Delord and Colobert,^[149] Xie,^[96] as well as Shi,^[150] among others. However, the kinetic resolution^[151] of sterically hindered *N*-arylindoles has been constrained to the use of stoichiometric amounts of toxic and costly silver salts in expensive fluorinated solvents.^[96] Hence, we have currently developed a strategy for electrochemical kinetic resolution of *N*-arylindoles with the help of a transient chiral auxiliary.

3.3.1 Optimization and Scope

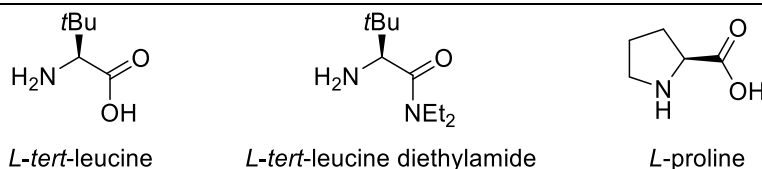
We initiated our studies with *L*-*tert*-leucine as a transient auxiliary for the envisioned atroposelective electrochemical kinetic resolution of racemic *N*-arylindoles **63** to synthesize N–C axially chiral motifs (Table 3-2). The optimal conditions were identified with Pd(OAc)₂ (10 mol %) as the precatalyst, *L*-*tert*-leucine (30 mol %), LiOAc (2 equiv.) as electrolyte, and *n*butyl acrylate **64a** (3 equiv.) in AcOH (4.5 mL) at 60 °C for 16 h. Under these conditions, racemic indole **63a** was kinetically resolved into the desired product **65aa** in 97% ee at a constant current of 1 mA, while the recovered starting material **63a** was obtained with 70% ee (entry 1). *L*-*tert*-leucine derived diethyl amide as the TDG provided a lower yield of 23%, albeit with an excellent selectivity factor (*S* = 264) (entry 2). In contrast, *L*-proline led to the C3-alkenylated product, highlighting the difficulties in addressing the inherent C3 reactivity of indole. (entry 3). No product was observed when TFE was used as the solvent (entry 4). Employing a solvent mixture of TFE and AcOH resulted in a lower yield and enantioselectivity (entry 5). When decreasing the amount of *L*-*tert*-leucine to 20 mol %, a diminished yield of 37% with unchanged enantio-induction was observed (entry 6). The importance of TDG is further proved by the formation of only C3-alkenylated product in the absence of TDG. (entry 7). Electricity demonstrated its significance in boosting the catalytic efficiency by an obvious decrease in yield without electricity (entry 8). Utilizing pure oxygen

as the oxidant also yielded comparable productivity in the reaction. (entry 9). Notably, the reaction proceeded efficiently under N₂ atmosphere, albeit with a reduced conversion (entry 10). Control experiment confirmed the necessity of the palladium catalyst for the atroposelective electrocatalysis of *N*-arylidole **63a** (entry 11), However, the addition of BQ as a redox mediator failed to improve the conversion (entry 12).

Table 3-2 Optimization of the N–C atroposelective C–H olefination^[a]

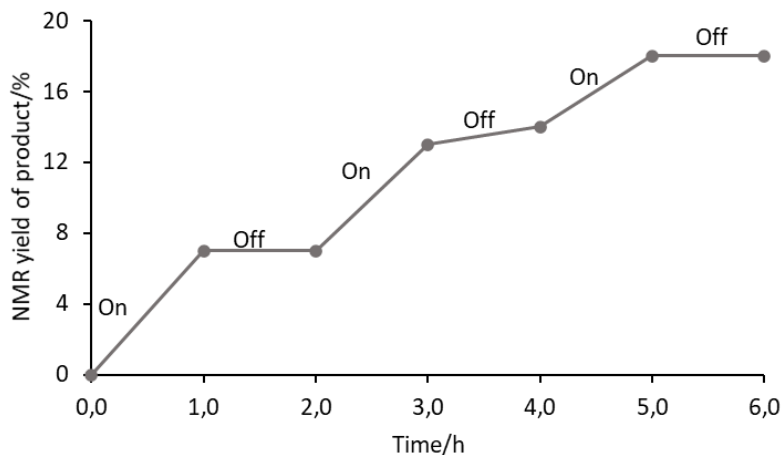


| Entry | Deviation from standard conditions | Conv. (%) ^[b] | ee (65aa) | S ^[c] |
|-------------------|--|--------------------------|--------------------|------------------|
| 1 ^[f] | none | 42 | 97 | 138 |
| 2 ^[f] | <i>L</i> -tert-leucine diethylamide as TDG | 23 | 99 | 264 |
| 3 ^[f] | <i>L</i> -proline as TDG | 30 ^[d] | --- | --- |
| 4 ^[f] | TFE as solvent, no LiOAc | --- | --- | --- |
| 5 ^[f] | TFE/AcOH as solvent, no LiOAc | 38 | 94 | 56 |
| 6 ^[f] | <i>L</i> -tert-leucine (20 mol %) | 37 | 97 | 118 |
| 7 ^[f] | No <i>L</i> -tert-leucine | 12 ^[d] | --- | --- |
| 8 ^[f] | No electricity | 29 | 97 | 97 |
| 9 | Under O ₂ , No electricity | 40 | 98 | 192 |
| 10 | Under N ₂ | 26 | 99 | 280 |
| 11 ^[f] | No palladium | --- | --- | --- |
| 12 | BQ | 36 ^[e] | 99 | 347 |



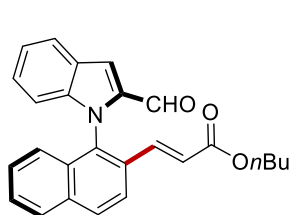
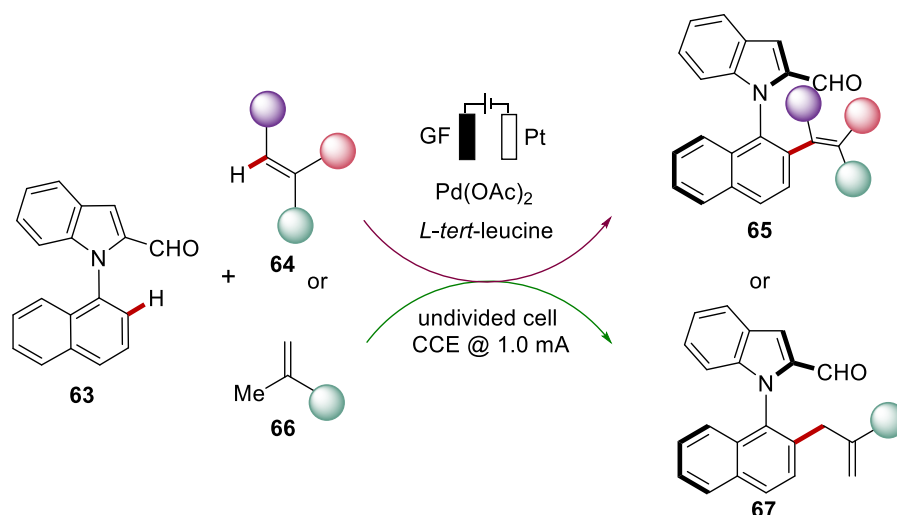
^[a] Reaction conditions: Undivided cell, *rac*-**63a** (0.20 mmol), **64a** (0.60 mmol), Pd(OAc)₂ (10 mol %), *L*-tert-leucine (30 mol %), LiOAc (2.0 equiv.), AcOH (4.5 mL), 60 °C, constant current at 1.0 mA, 16 h, graphite felt (GF) anode, Pt-plate cathode. ^[b] Calculated conversion, $C = ee_{1a}/(ee_{1a} + ee_{3a})$, $ee_{1a} = ee$ of **63a** and $ee_3 = ee$ of **65aa**. ^[c] $S = \ln[(1 - C)(1 - ee_{1a})]/\ln[(1 - C)(1 + ee_{1a})]$. ^[d] C3 alkenylated product was isolated. ^[e] BQ (10 mol %) as additive. ^[f] Done by Dr Uttam Dhawa or Dr Tomasz Wdowik.

Furthermore, an on/off experiment was conducted under N₂, which clearly demonstrated the essential role of electricity in enhancing the efficacy of the electrocatalytic C–H activation (Scheme 3-18).

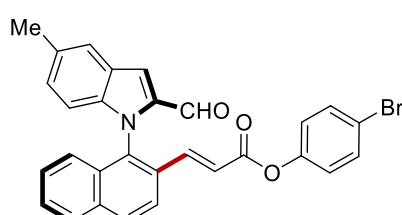


Scheme 3-18 On/off electricity experiment.

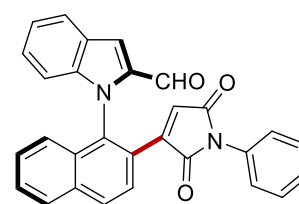
Based on the optimized reaction condition for the atroposelective palladaelectro-catalyzed N–C olefination in hand, we explored its versatility on a representative array of alkenes, as shown in Scheme 3-19. *n*Butyl acrylate **64a** was efficiently converted to the desired olefinated product **65aa** with 97% ee. Impressively, the bromophenyl-substituted acrylate **64b** with electron-rich 5-methyl substituted *N*-arylidole **63b** exhibited remarkable tolerance in the N–C atroposelective alkenylation to offer an outstanding *S*-factor of 158, suggesting its significant potential for subsequent late-stage modifications. Furthermore, we examined the versatility of the N–C atroposelective transformations with maleimides, which represent key structural motifs in several natural products and drug candidates.^[152] Phenyl-substituted maleimide **64c** delivered the desired product **65ac** in 30% yield and *S*-factor of 62. In addition, fluorinated alkenes, which have gained recent attention in pharmaceutical and agrochemical industries due to their improved lipophilicities,^[153] were also tolerated to this transformation. The presence of bromine in perfluoroalkylalkene **64d** did not affect the course of the electrocatalysis, leading to product **65ad** in 27% yield and 98% ee. Notably, unprecedented allylic selectivity was observed with 1,1-disubstituted alkenes.^[154] Thiophenyl methacrylate **66a** was identified as a suitable substrate for this electrocatalysis, delivering product **67aa** with complete allylic selectivity in 30% yield and 95% ee.



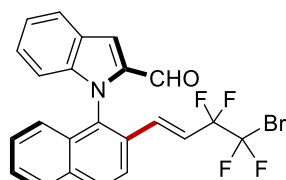
65aa^[a]: 40%, 97% ee
63a: 55%, 70% ee
 S = 138



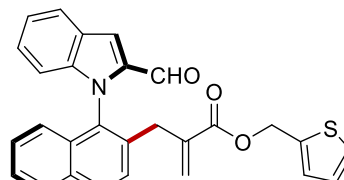
65bb^[a]: 30%, 98% ee
63b: 41%, 47% ee
 S = 158



65ac^[a]: 30%, 95% ee
63a: 59%, 47% ee
 S = 62



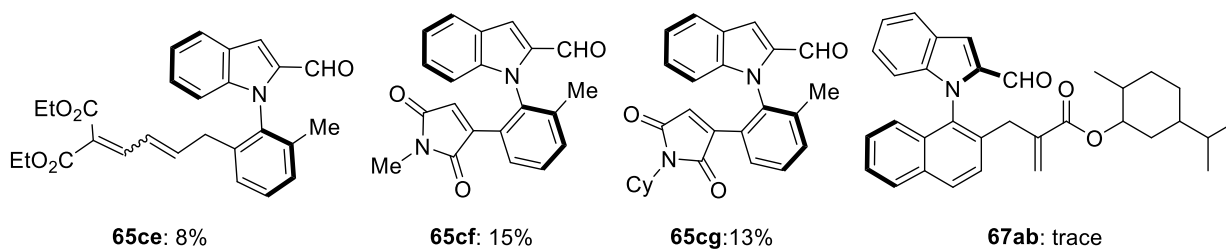
65ad^[a]: 27%, 98% ee
63a: 62%, 41% ee
 S = 148



67aa: 30%, 95% ee
63a: 41%, 54% ee
 S = 67

Scheme 3-19 Scope for the atroposelective palladaelectro-catalyzed C–H olefination. ^[a] done by Dr Uttam Dhawa and Dr Tomasz Wdowik.

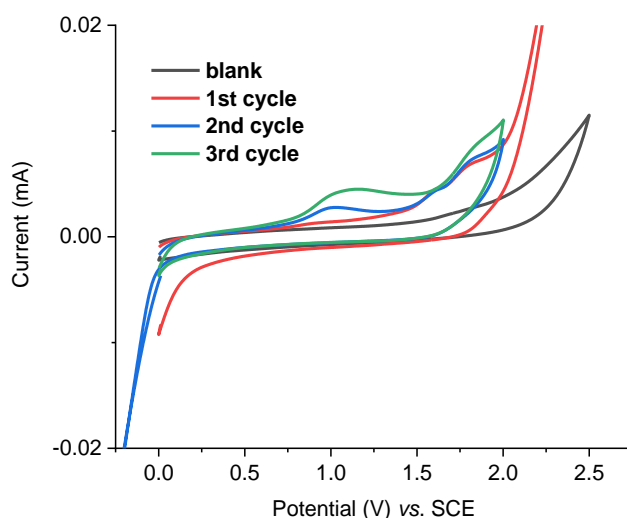
This asymmetric electrocatalysis way is not without limitations. Under otherwise identical standard reaction conditions, the application to 2-methyl substituted *N*-arylidoles **63c** or menthyl methacrylate **66b** proved to be challenging and yielded unsatisfactory results (Scheme 3-20).



Scheme 3-20 Examples with inefficient results.

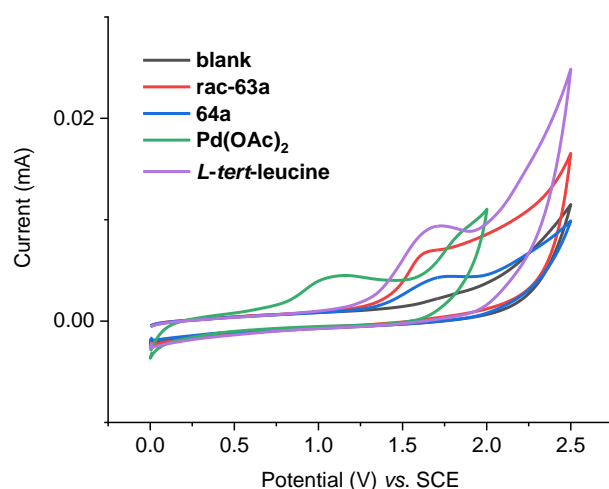
3.3.2 Cyclic Voltammetry Studies

In order to further understand the electrochemical C–H olefination process, we carried out CV studies (Scheme 3-21). Initially, we investigated the reactivity of Pd(OAc)₂ in the AcOH. In the first cycle's positive scan, we did not detect any oxidation peak; however, a reduction activity was observed within the voltage range of 0.4 V to 0 V. In the subsequent cycle, a small oxidation peak at around 1.1 V emerged. By expanding the negative scan range in the second cycle, a clear oxidation peak can be seen during the third positive scan. Thus, we hypothesized that it indicates the conversion of palladium(0) to palladium(II).



Scheme 3-21 Cyclic voltammogram of different scan cycles of Pd(OAc)₂ in AcOH with *n*Bu₄NPF₆ (0.1 M) at 100 mV/s.

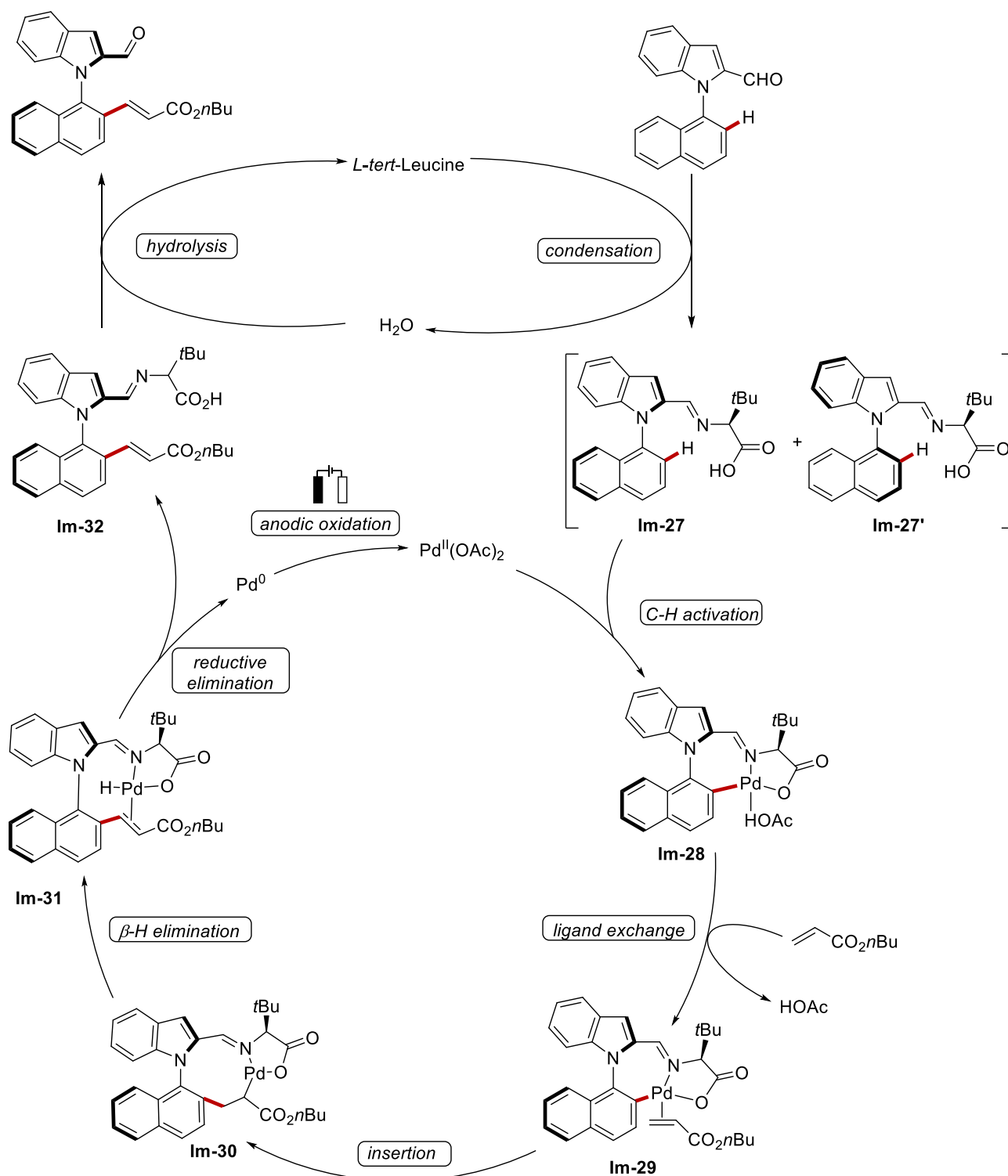
Next, we compared the oxidation curves of **63a**, **64a**, *L-tert*-leucine and the Pd(OAc)₂ (Scheme 3-22). Notably, the oxidation potential of palladium(0) to palladium(II) was significantly lower than that of the other reactants, indicating that the current applied in this transformation can readily regenerate the catalytically active species.



Scheme 3-22 Cyclic voltammogram of several reactants in AcOH with $n\text{Bu}_4\text{NPF}_6$ (0.1 M) at 100 mV/s.

3.3.3 Plausible Catalytic Cycle

Based on experimental and computational mechanistic studies, a plausible catalytic cycle is proposed (Scheme 3-23). The process initiates with the selective coordination of the *in-situ* generated imine **Im-27** with the catalyst, followed by C–H activation to deliver an axially stereo-enriched biaryl palladacycle intermediate **Im-28**. Thereafter, migratory insertion of the alkene occurs, which enables the formation of a nine-membered palladacycle **Im-30**. The final product is obtained through a sequence of steps involving β -hydride elimination and the dissociation of the TDG. To complete the cycle, the palladium(0) species undergoes anodic oxidation by electricity, and another condensed imine substrate coordinates to the catalyst, setting the stage for subsequent catalytic cycles to occur.



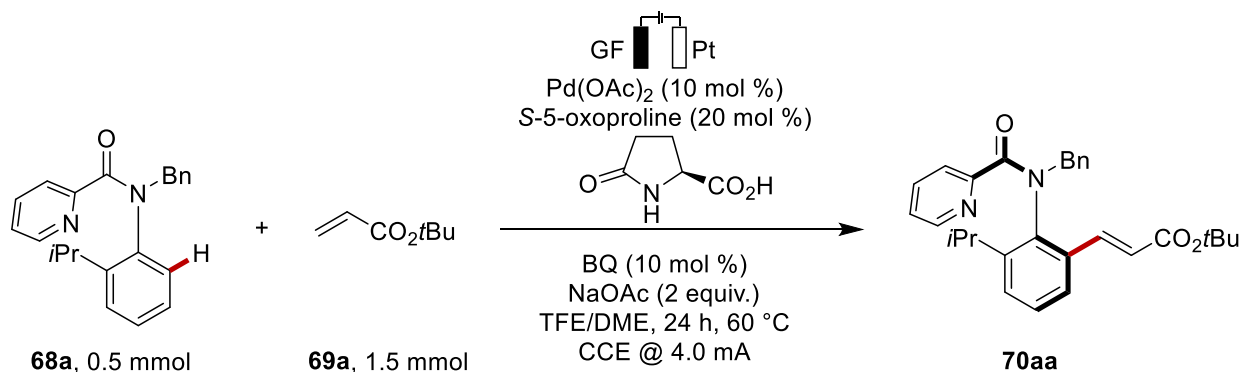
Scheme 3-23 Proposed catalytic cycle.

3.4 Palladaelectro-Catalyzed C–H Olefinations for Axially Chiral Anilides Mediated by the Mono-*N*-Protected Amino Acid

Compared to the heterobiaryls with N–C axial chirality, the enantioselective assembly of molecules bearing an acyclic chiral anilide motif is considerably more difficult as they have a higher degree of rotational freedom than biaryls. Pioneering work has been achieved by researchers, such as Curran and Taguchi, towards the efficient catalytic enantioselective synthesis of these compounds.^[155] Recently, significant contribution has been made in this area.^[85] We have now developed a DKR strategy for the synthesis of axially-chiral anilides through electrooxidative palladium(II)-catalyzed C–H activation with the help of mono-protected amino acid.

3.4.1 Optimization Studies

Initial optimized reaction conditions for the envisioned palladium-catalyzed electrochemical enantioselective C–H olefination are obtained by Dr. Johanna Frey, in that *N*-benzyl-*N*-(2-isopropylphenyl) picolinamide **68a** was reacted with *t*butyl acrylate **69a** in an undivided cell setup in the presence of 10 mol % of Pd(OAc)₂, 20 mol % of *S*-5-oxoproline, 10 mol % of BQ and 2 equiv. of NaOAc in 5.0 mL TFE:DME (1:1) solvent mixture at 60 °C with a combination of GF as anode and Pt as cathode. A constant current of 4.0 mA was applied to provide the desired olefinated product **70aa** with 90% yield, 98%ee (Scheme 3-24).

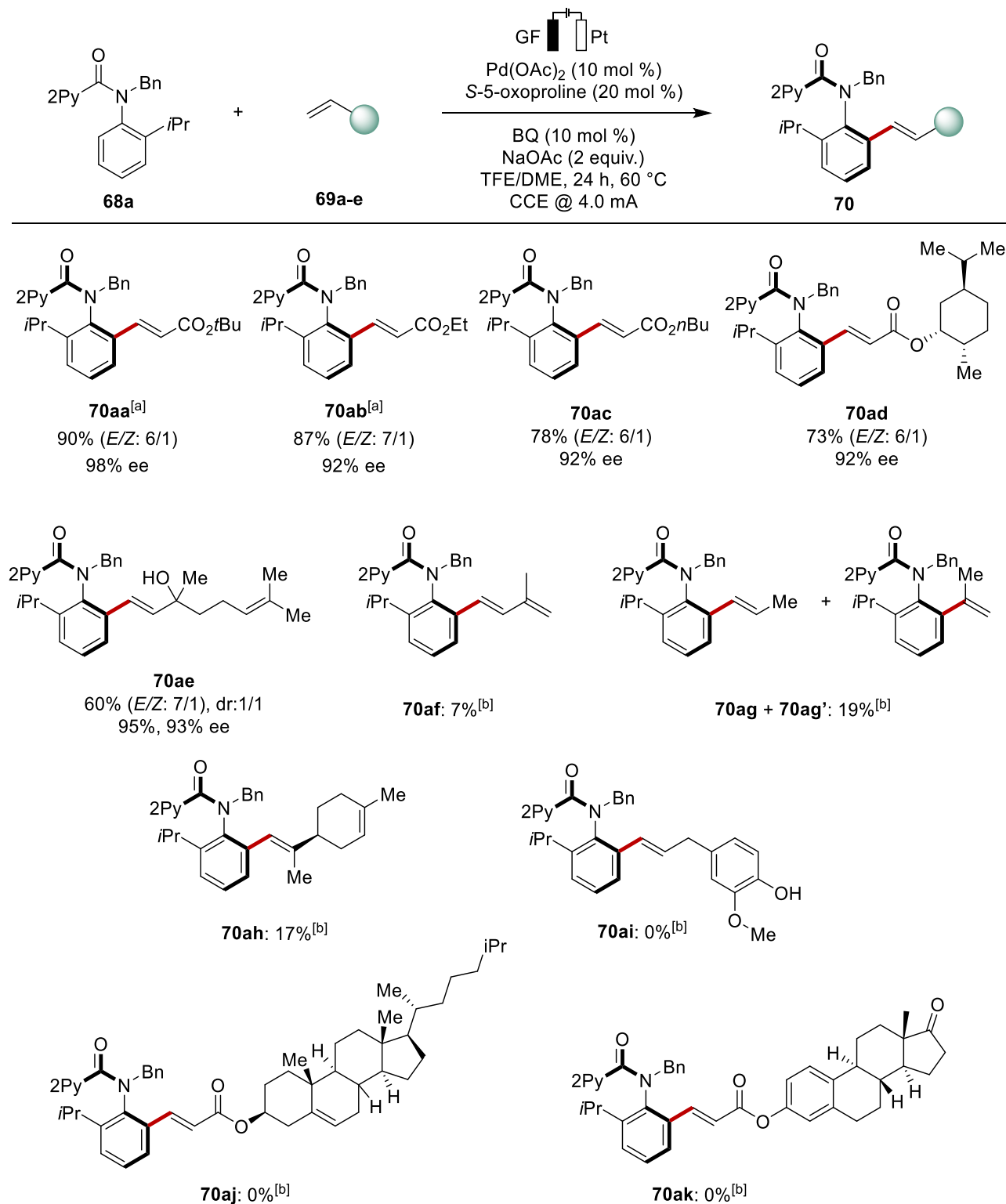


Scheme 3-24 Optimized condition of the atroposelective electrocatalyzed C–H olefination.

3.4.2 Substrate Scope and Limitations

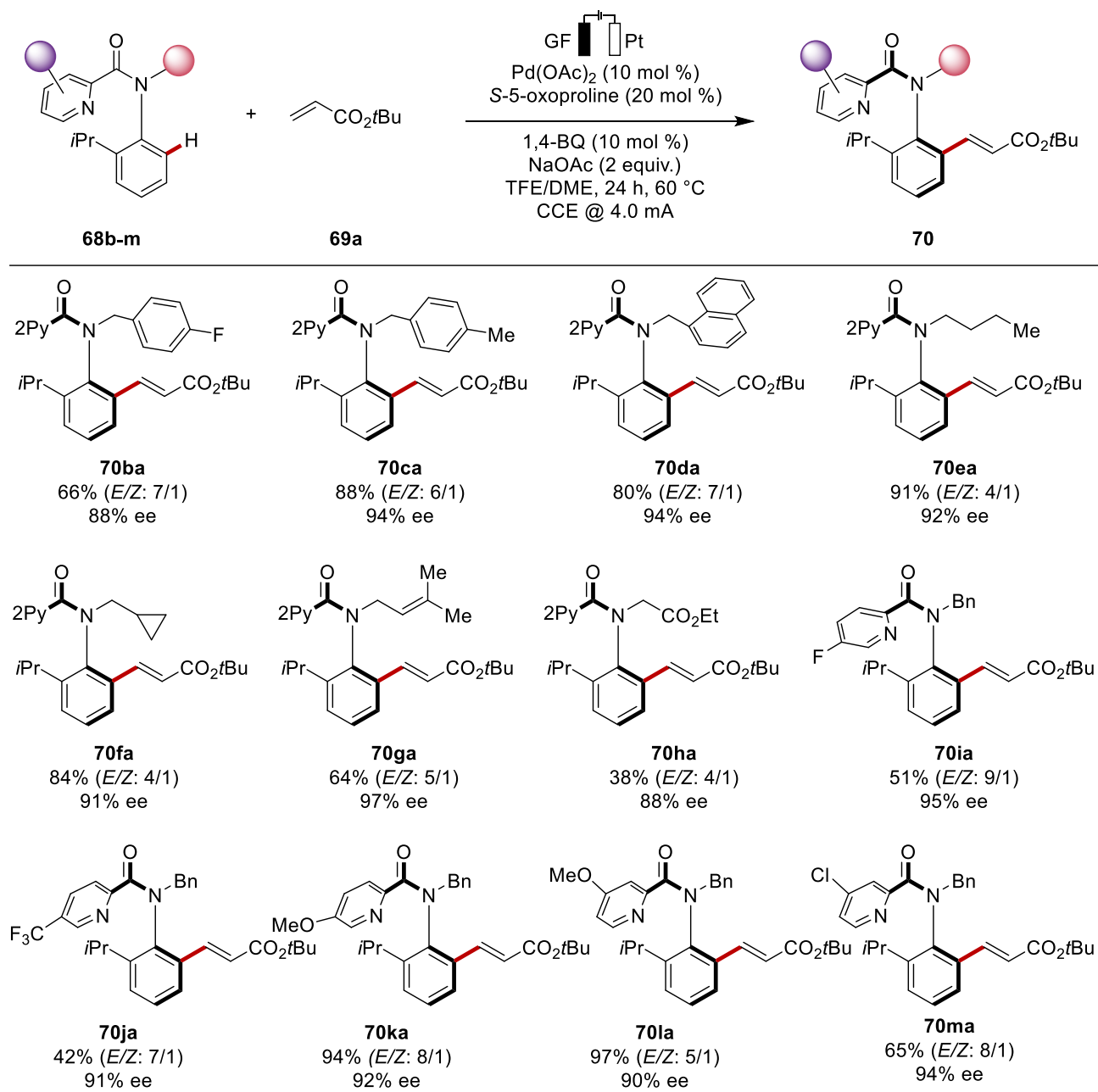
With the optimized reaction conditions in hand, we tested the versatility of the electrochemical palladium-catalyzed enantioselective C–H olefination with a wide variety of olefinic substrates **69** (Scheme 3-25). To our delight, acrylates **69a–69c** demonstrated their capability to produce desired products **70aa–70ac** with excellent yields and outstanding ees. Olefins obtained from natural sources, such as menthol **69d** and linalool **69e**, were also

found to be tolerated, giving 73% and 60% yield with 92% and 93% ee, respectively. However, this method was not without limitations, very simple alkenes **69f** and **69g** were ineffective, giving extremely low yields. Additionally, natural products derived olefins **69h-69k** led to either recovered starting materials or inseparable mixtures.



Scheme 3-25 Scope of the reaction regarding the olefin partner. ^[a] performed by Dr. Johanna Frey. ^[b] NMR yield.

Next, a broad range of substituted anilides **68b-h** was tested under our optimized electrochemical reaction condition to demonstrate the robustness of our electrocatalysis (Scheme 3-26). Various substituents on the anilide, including substituted benzyl **68b-68d**, alkyl **68e**, cyclopropylmethyl **68f**, isopentenyl **68g**, and acetate **68h** were well tolerated, giving the products with excellent enantiocontrol (**70ba-70ha**, 88% to 97% ee). Then we investigated the substituents on the pyridine ring. Electron-withdrawing groups, 5'-F **68i**, 5'-CF₃ **68j**, and 4'-Cl **68m**, as well as electron-donating groups, 5'-OMe **68k** and 4'-OMe **68l**, were compatible and gave the desired products in excellent enantioselectivities (90% to 95% ee). The substituents on the aryl ring were investigated by Dr. Johanna Frey in the Ackermann group. The *rac*-anilide with a naphthyl group gave the product in 65% yield and 88% ee, while a methyl group led to a slight decrease in the enantioselectivity.



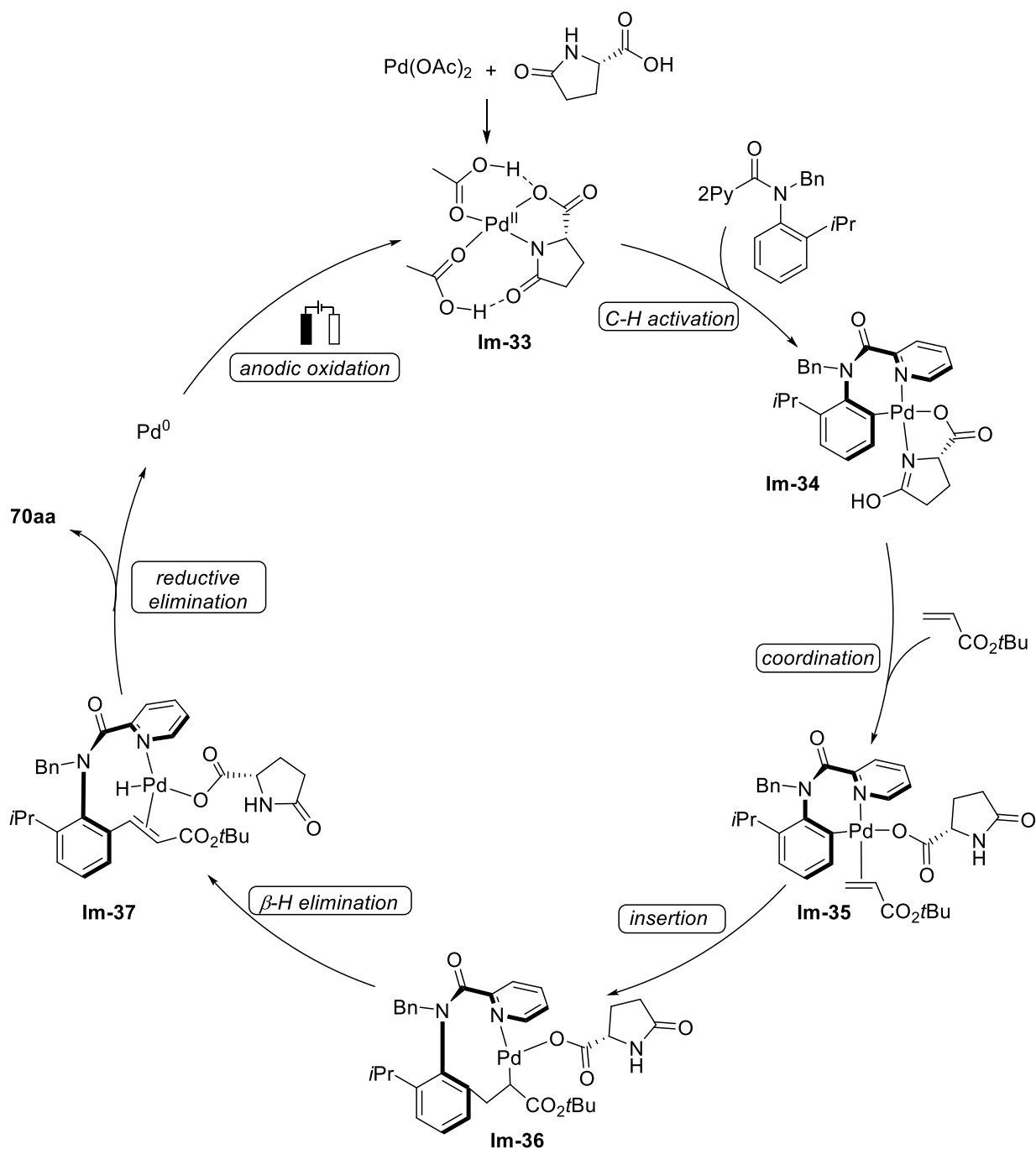
Scheme 3-26 Scope of the reaction regarding the anilide partner.

In order to significantly enhance the resource-economy of our strategy, Dr. Johanna Frey next performed the constant current electrolysis by renewable solar energy. Utilizing a commercially available photovoltaic cells as the power supply under natural sunlight, similar activity and enantioselectivity were achieved. Additionally, subsequent stirring of the electrocatalysis mixture under an atmosphere of hydrogen provided the alkylated products with high enantioselectivities.

3.4.3 Proposed Catalytic Cycle

On the basis of the mechanistic findings in experiments, a plausible catalytic cycle was proposed (Scheme 3-27), which commences by the coordination of palladium acetate

monomer complexes with *S*-5-oxoproline to form intermediate **Im-33**. Subsequent substrate coordination and C–H activation generate the arylpalladium species **Im-34**. The olefin coordination and subsequent insertion generate the intermediate **Im-36**, which then undergoes a β -hydride elimination and reductive elimination, leading to the palladium(0) and liberation of the product **70aa**. Palladium(0) is then anodically reoxidized, thereby regenerating the active catalyst **Im-33**.



Scheme 3-27 Proposed catalytic cycle.

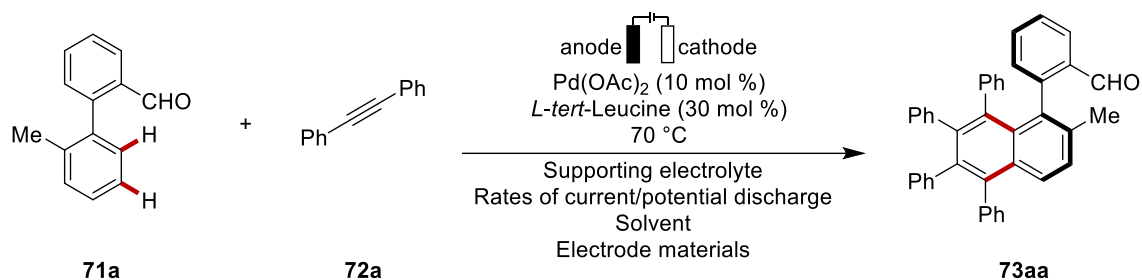
3.5 Yield Optimization of Palladaelectro-Catalyzed C–H Annulation using Machine Learning

Electrosynthesis has become an increasingly popular platform in modern organic chemistry, which has made a variety of new transformations possible by utilizing its distinctive features and reaction parameters like applied current/potential, electrodes, electrolyte system, and cell design. While these unique features give chemists new opportunities to control reactivity and selectivity, they also increase the dimensionalities of a reaction and complicate the interactions between variables, making the optimization more considerable challenging.

In recent years, the application of ML in molecular synthesis has brought new opportunities in high-dimensional synthetic space using data-driven approach.^[156] This strategy allows the investigation of the relationship between the various reaction parameters in a digitalized chemical space, thus avoiding the dependency on chemist's empirical knowledge and mechanistic studies in traditional screenings. However, the merger of ML and electrochemistry, two notable emerging frontiers, poses distinctive challenges due to the vast dimensions of the electrochemical space and the difficulty in determining the contribution of each dimension.^[157] This "curse of dimensionality" hampers the convergence of ideal prediction models, especially with the limited data in unsupervised optimization. To address this problem, we envisioned to develop a method that integrates data-driven yield optimization with classical orthogonal experimental design.

3.5.1 Workflow Design for Reaction Optimization

In our optimization study, we focused on enhancing the electrochemical reactivity of two model substrates, 2-(*ortho*-tolyl)benzaldehyde **1a** and diphenylacetylene **2a** (Scheme 3-28). We identified four crucial dimensions that greatly influence the reactivity and are closely related to electrochemical processes. These parameters include the electrode material (comprising 16 combinations of GF, Pt, Fe, and BDD as either the anode or cathode), the solvent (with 10 options such as acetic acid, TFE, and various 1:1 mixed solvents), the supporting electrolyte (consisting of 9 options including LiClO₄ and NaOPiv), and the electrochemical conditions (with 6 options involving different constant currents and constant voltages) (Scheme 3-25).

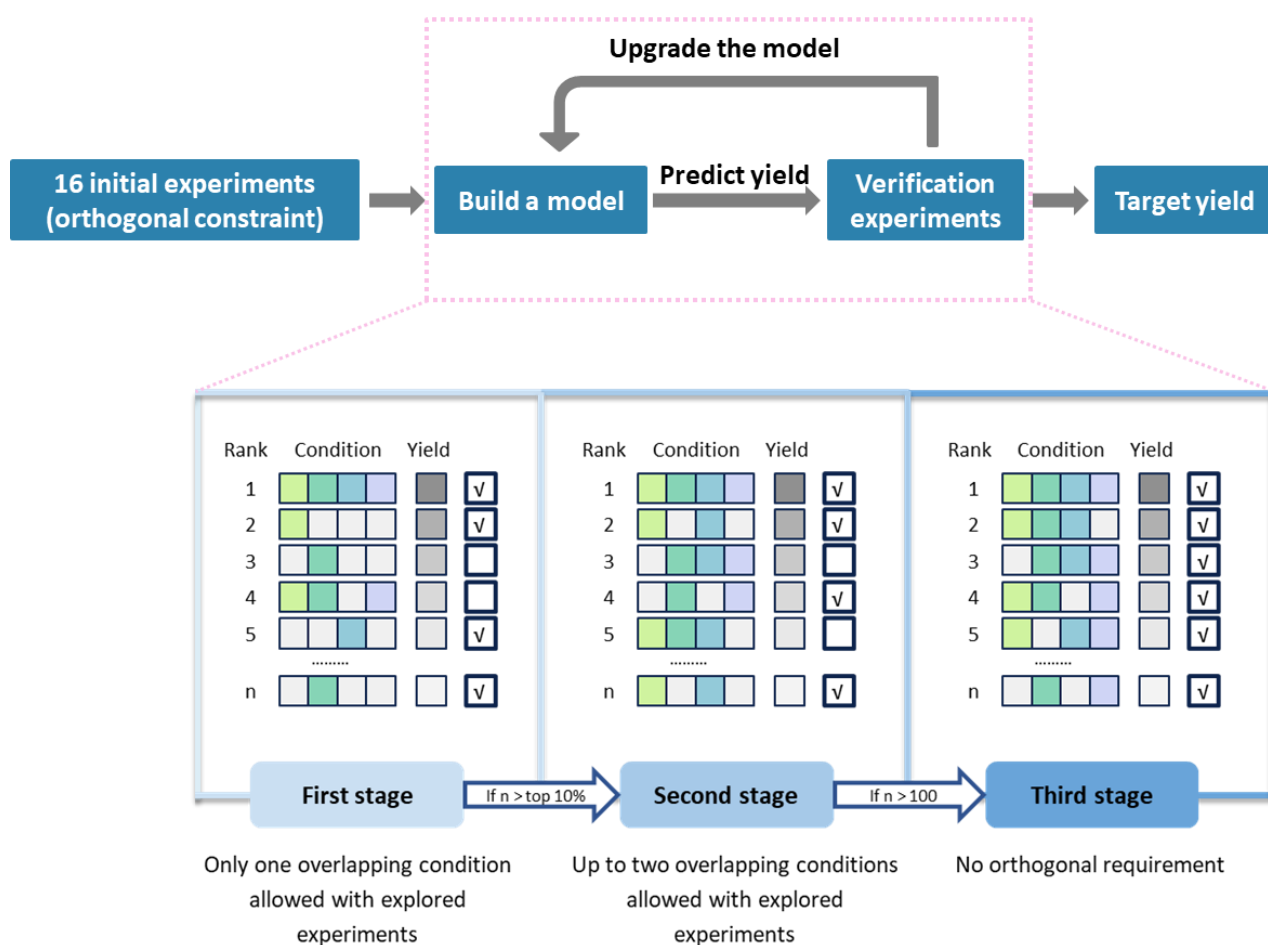


| Optimization space 16×10×9×6 = 8640 | | | | | |
|-------------------------------------|--------|--------------------------------|---|-----------|------------|
| Electrode materials: 16 | | | Solvents: 10 | | |
| Anode | | | Cathode | AcOH | AcOH: EtOH |
| BDD | | | BDD | TFE | AcOH: MeCN |
| GF | | | GF | EtOH | TFE: EtOH |
| Pt | | | Pt | MeCN | TFE: MeCN |
| Fe | | | Fe | AcOH: TFE | EtOH: MeCN |
| Supplied electricity: 6 | | | Supporting electrolytes: 9 | | |
| | I / mA | 0.3 | 0.6 | 0.9 | 1.2 |
| | U / V | 1.0 | 1.5 | | |
| | NaOAc | NaOPiv | NaO ₂ CAd | | |
| | KOAc | K ₃ PO ₄ | ⁿ Bu ₄ NPF ₆ | | |
| | LiOAc | LiClO ₄ | ⁿ Bu ₄ NOAc | | |

Scheme 3-28 Chemical space of the reaction.

The optimization workflow design (Scheme 3-29) in this study incorporates the use of orthogonal experimental design as a constraint requirement within the ML-based top-*K* sorting for yield prediction. By introducing the orthogonality constraint, we aim to enhance the diversity of experimental samplings. Initially, we conducted 16 experiments that covered different electrode material selections while evenly distributing the other dimensions. These 16 experiments strictly adhered to the orthogonality constraint, ensuring that only one dimension shared the same selection between any two experiments. Then Chen-Hang Chao and Shu-Wen Li constructed a ML model using the available experimental data to predict the reaction yield for the entire synthetic space in the optimization process. Based on the predicted yield and the orthogonality constraint, we selected four entries of conditions for experimental verification. The results obtained from these experiments were then fed back to update the ML model. This iterative process of validation and upgradation continued until optimal yield was achieved. We divided this part into three stages. In the first stage, we imposed the highest orthogonality constraint, mirroring the initial experimental samplings where only one dimension could be the same between any two tests. If no combination of conditions among the top 10% predicted selections satisfied the orthogonality constraint, we advanced to the next stage. The second stage followed the same optimization logic, but with

a relaxation of the orthogonality constraint. Here, two dimensions were allowed to be the same between any two experimental tests. This stage concluded when no combination of conditions among the top 100 predictions satisfied the orthogonality constraint. Finally, in the third stage, the orthogonality constraint was fully relaxed, allowing three dimensions to be the same. This stage represented a standard greedy optimization approach. We systematically evaluated a series of top- K reaction conditions based on the ML-predicted yield to identify the optimal reaction condition for the target palladaelectro-catalyzed annulation.

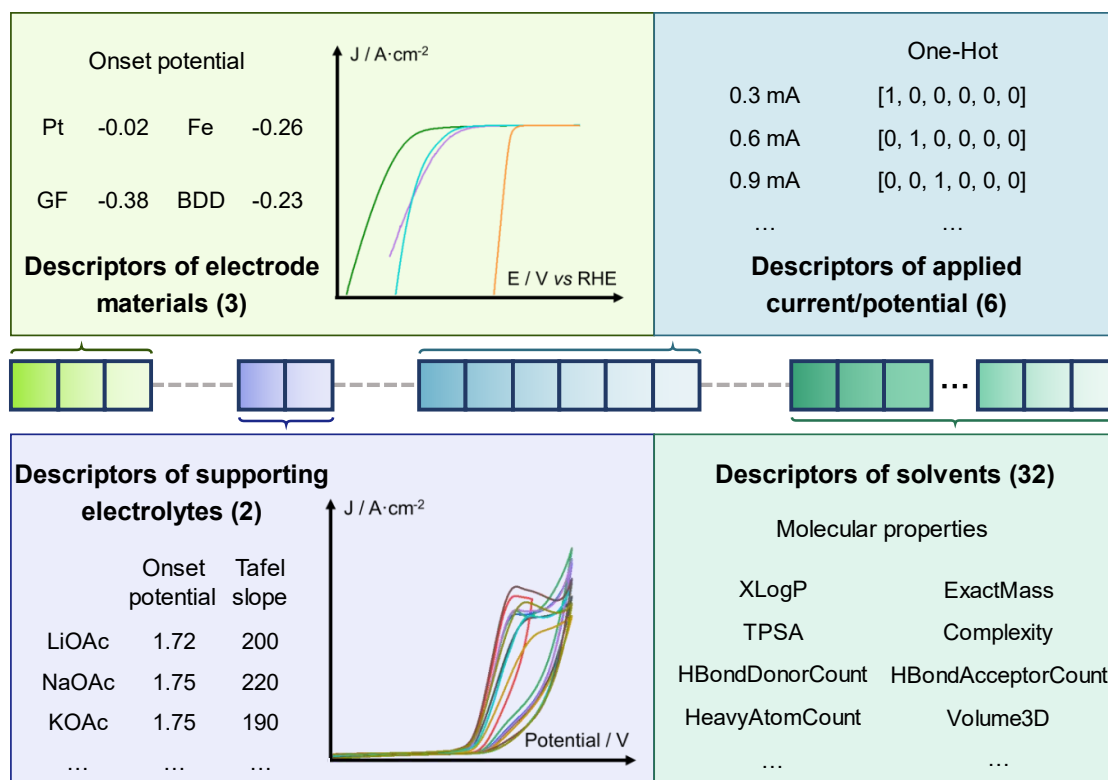


Scheme 3-29 Details of workflow.

3.5.2 Results of ML-Guided Yield Optimization

We employed a set of physical organic descriptors to represent the reaction system in our ML modelling (Scheme 3-30). To encode the electrode material, we utilized the onset potential of the hydrogen evolution reaction (HER). For the current and potential, we utilize One-Hot encoding to encode them, ensuring equal treatment. As for the solvent, we incorporated various physical organic parameters from the PubChem database, such as LogP, TPSA, and hydrogen bond donor, among others. Additionally, the onset potential and

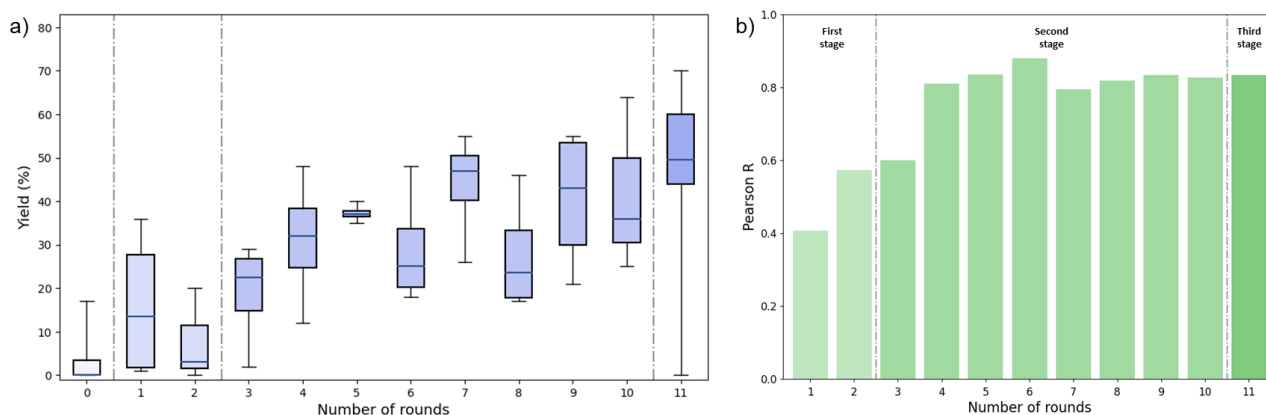
current-voltage profile at a scan rate of 5 mV/s from oxidation CV curves of **71a** were used as descriptors for the electrolyte. One-Hot encoding was used as the descriptor for six different discharge rates into the reaction. Collectively, these encodings constituted a 43-dimensional reaction vector, providing a digitized representation of the electroorganic reaction system. The following algorithms were examined for reaction prediction: Bagging (BG)^[158], Decision Tree (DT)^[159], Extra-Trees (ET)^[160], Gradient Boosting (GB)^[161], k-Nearest Neighbors Regression (KNR)^[162], Kernel Ridge Regression (KRR)^[163], Linear Support Vector Regression (LSVR)^[164], Random Forest (RF)^[165], Ridge^[166], Support Vector Machine (SVR)^[164], and XGBoost (XGB)^[167]. To mitigate the impact of ML modeling perturbations caused by data additions, we systematically re-evaluated algorithm performances using 10-fold cross-validation in each modeling round, ultimately recognizing the most accurate algorithm for predicting reactions. The model with the highest accuracy among the 11 models was selected to predict reaction yield and recommend the next-round reaction.



Scheme 3-30 Details of descriptors.

The results of ML modeling and experimental verifications in each round of optimization are shown in the Box Plot in Scheme 3-31a. Since Pearson's R is the typical statistical measure for evaluating the strength and direction of linear relationships between variables, it is used to assess the correlation between the predicted and actual outcomes throughout the

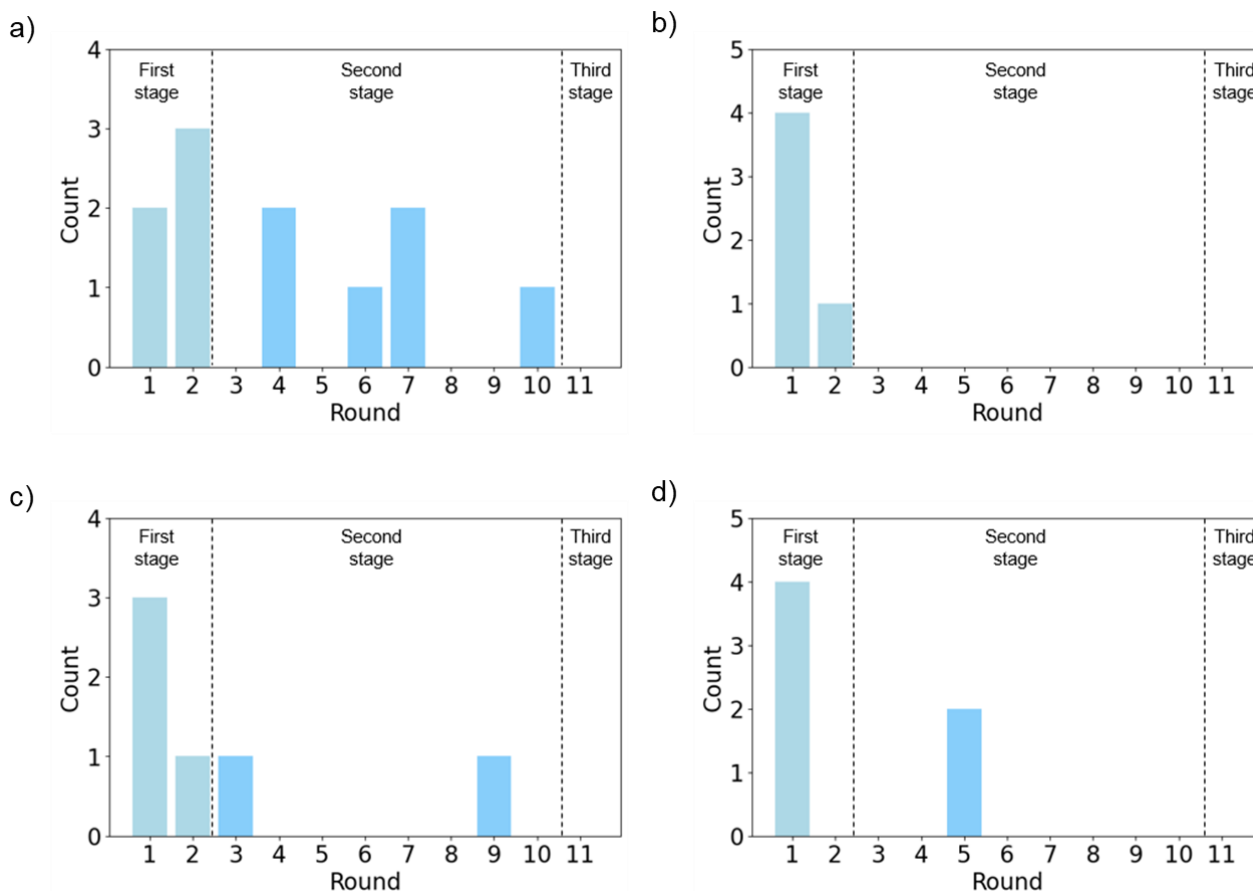
optimization process. By comparing each round of ML prediction results and the actual experimental yields, the prediction accuracy of ML models showed a steady improvement with each round of optimization feedback (Scheme 3-31b). The Pearson correlation coefficient increased from the initial 0.407 to around 0.8 and tended to converge in the end, indicating that the model had a relatively accurate and comprehensive understanding of the synthetic space with the iterative data collections. In addition, the yields of experimental verifications confirmed that the ML optimization provided the correct direction for searching the synthetic space. The maximum yield of each round increased from the initial 17% to 70%. This condition combination involves GF/Pt electrode material, AcOH/TFE mixed solvent, NaOPiv as supporting electrolyte, and 0.3 mA / 36 h. Since some starting materials were still observed to remain after the reaction, we increased the reaction time to 48 h while keeping all other parameters same, and eventually achieved an improved yield of 90%.



Scheme 3-31 a) Results of experimental verifications and ML predictions in each round. b) Pearson correlation coefficients between the ML predictions and the experimental yields in each round.

By analyzing the model sampling in each optimization round, we could also interpret the samplings of ML-guided optimization strategy (Scheme 3-32). Regarding the important anode/cathode selection, the model continued to explore options until the third stage. As for solvents, the model quickly identified AcOH: TFE (1:1) as the best solvent. Similarly, for electrolyte, the model continued exploring options until the third stage and discovered the selection of a new electrolyte in the 9th round. For currents and potentials, the model explored new options until the 5th round. It is important to note that in the final stage, instead of exploring new chemical possibilities, the model focused on finding better combinations within the explored conditions, highlighting the difference between ML-guided optimization and traditional empirical-based control variable methods. These results underscore the

effectiveness of our designed optimization approach and showcase the advantages of ML-guided navigation within the synthetic space.

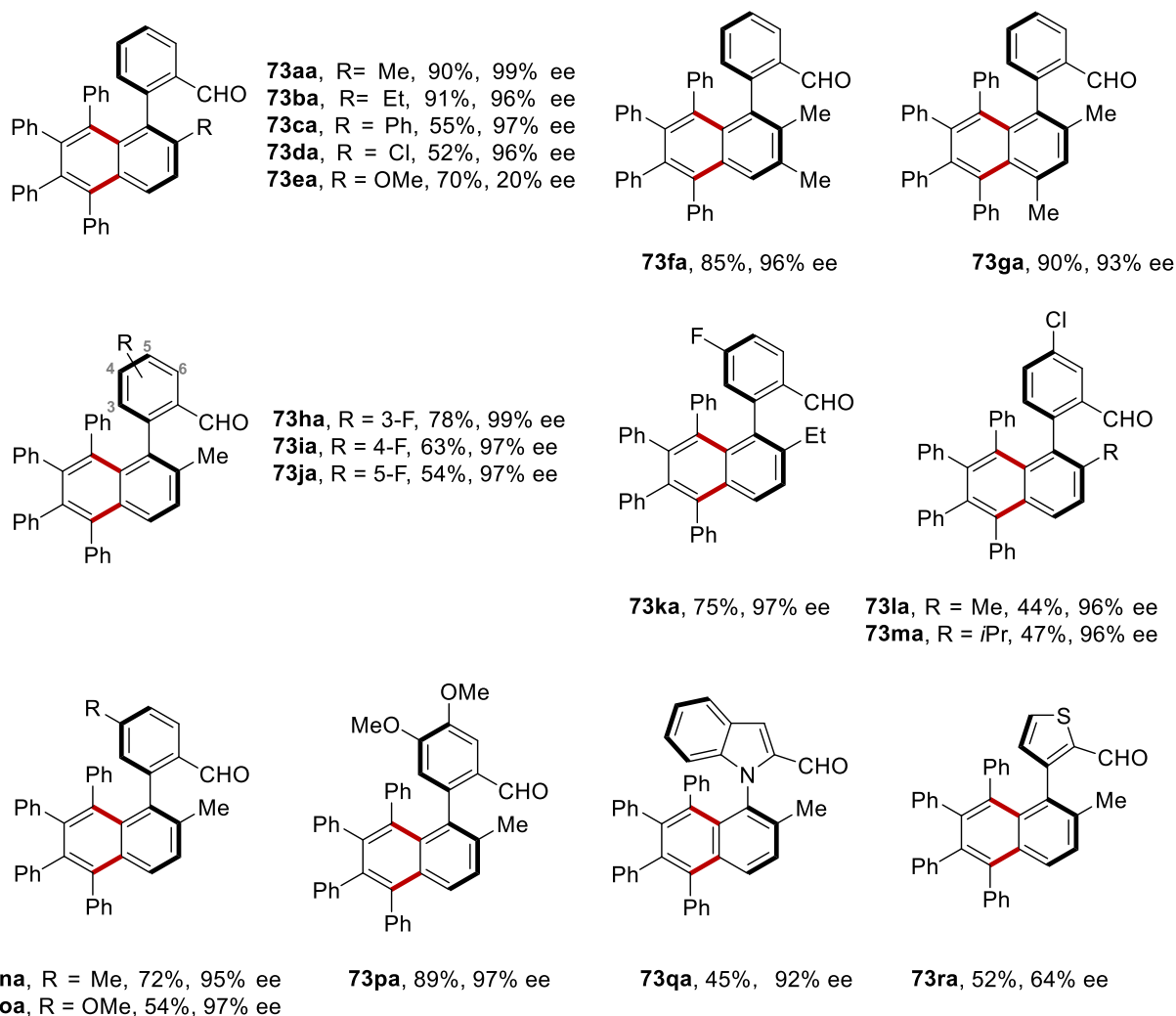
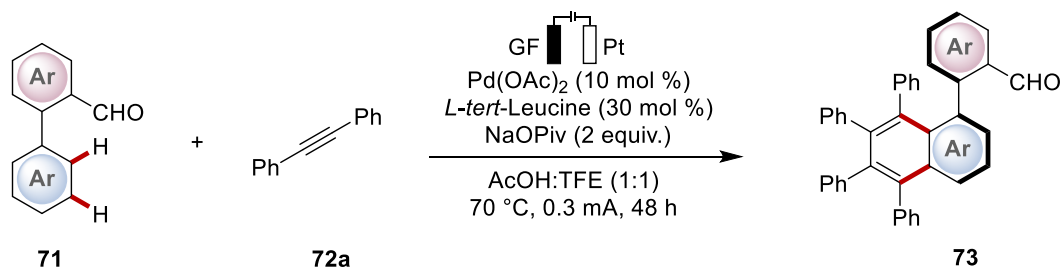


Scheme 3-32 The exploration process of reaction conditions in yield optimization. a) The counts of new electrodes explored in each round of exploration. b) The counts of new solvents explored in each round of exploration. c) The counts of new electrolytes explored in each round of exploration. d) The counts of new current and voltage selections explored in each round of exploration.

3.5.3 Scope of ML-Guided Palladaelectro-Catalyzed C–H Annulation

After successfully optimizing the electrocatalysis conditions guided by ML, our focus shifted towards exploring the versatility and robustness of the enantioselective palladaelectrocatalysis. A range of biaryls containing both electron-donating and electron-withdrawing groups was tested, yielding the desired axially chiral biaryls with outstanding enantioselectivities (Scheme 3-33). Biaryls bearing substituents at the 2'-position, such as methyl, ethyl, phenyl, and chloride, were compatible with the condition, furnishing the desired axially chiral biaryl aldehydes (**73aa-73da**) in good yields and excellent atroposelectivity. However, OMe group resulted in a significant decrease in the enantioselectivity (**73ea**). Additionally, multifunctionalized substrates were efficiently transferred into desired products (**73fa**, **73ga**) with up to 90% yield and 96% ee. The

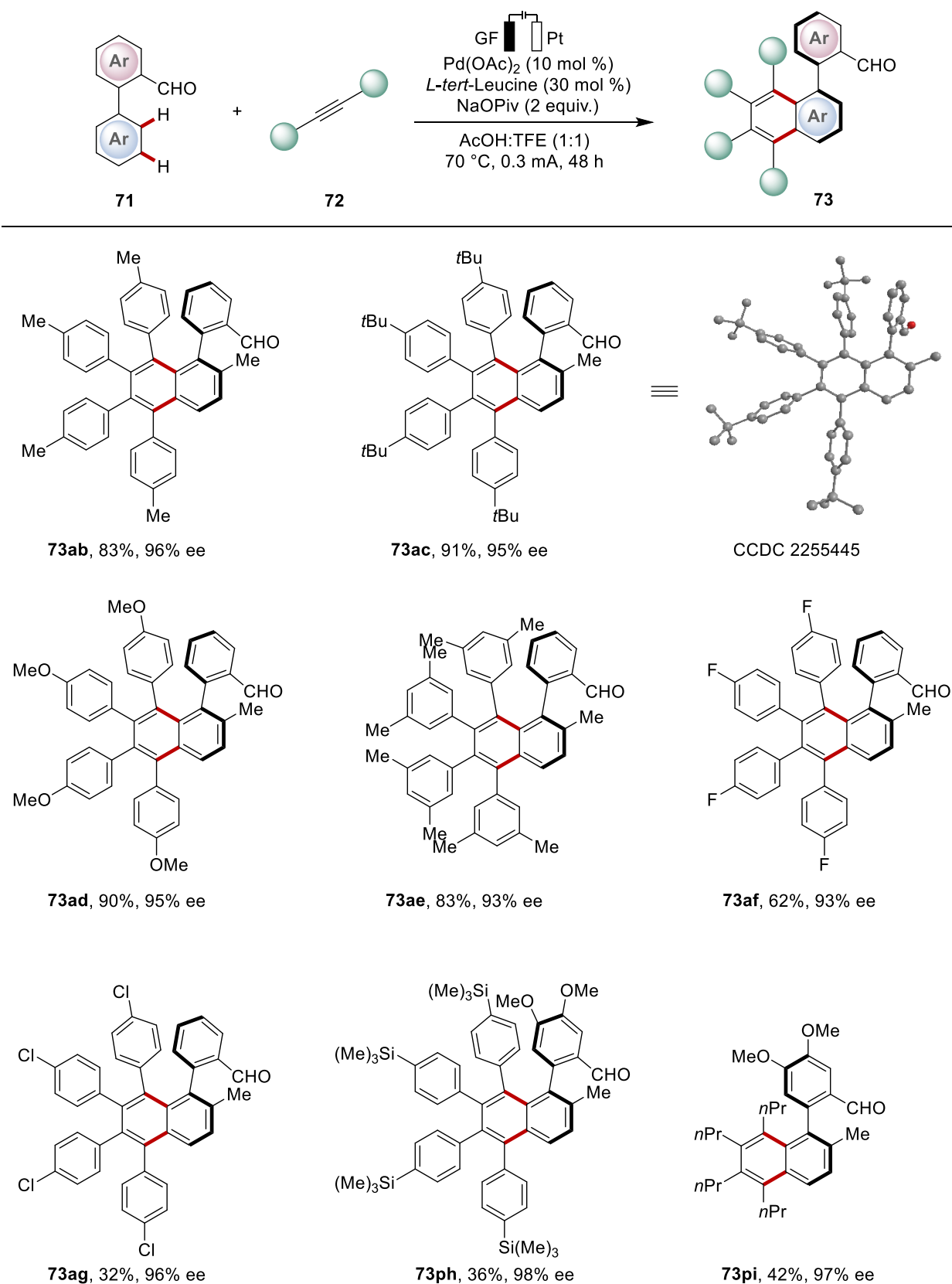
transformation also proceeded smoothly for the aldehydes with electron-deficient or electron-rich groups in aromatic ring, leading to the desired enantiomers (**73ha-73pa**) in moderate to excellent yields (44-90%) and excellent ee (95-99% ee). Encouragingly, *N*-arylindole-based aldehydes were well tolerated in the annulation, resulting in the corresponding product (**73qa**) with 92% ee. Furthermore, arylthiophene was successfully converted to desired product **73ra** under the optimized condition, albeit with reduced enantioselectivity due to decreased steric hindrance.



Scheme 3-33 Scope of biaryls. (**73ca**, **73da** and **73ea** were done by Dr. Johanna Frey).

Next, various alkynes **72** were investigated (Scheme 3-34). Substrates bearing electron-donating groups, such as alkyl and methoxy substituents, underwent the reaction with remarkable yields and excellent enantiomeric excess, affording products **73ab-73ae**. The crystal of product **73ac** was obtained and the configuration was unambiguously confirmed by X-ray crystallographic analysis. Alkynes with electron-deficient halogen groups **72f** and **72g** were also amenable to electrocatalysis, albeit with reduced yields. Notably, the trimethylsilyl group was well tolerated under the electrolysis conditions (**73ah**), providing a convenient handle for subsequent transformations, such as Hiyama cross-coupling. Encouragingly, alkyl alkyne 4-Octyne was also compatible and product **73ai** could be furnished in moderate yield and 97% ee.

Results and Discussion



Scheme 3-34 Scope of alkynes.

3.6 Enantioselectivity Prediction for Palladaelectro-Catalyzed C–H Olefination using Machine Learning

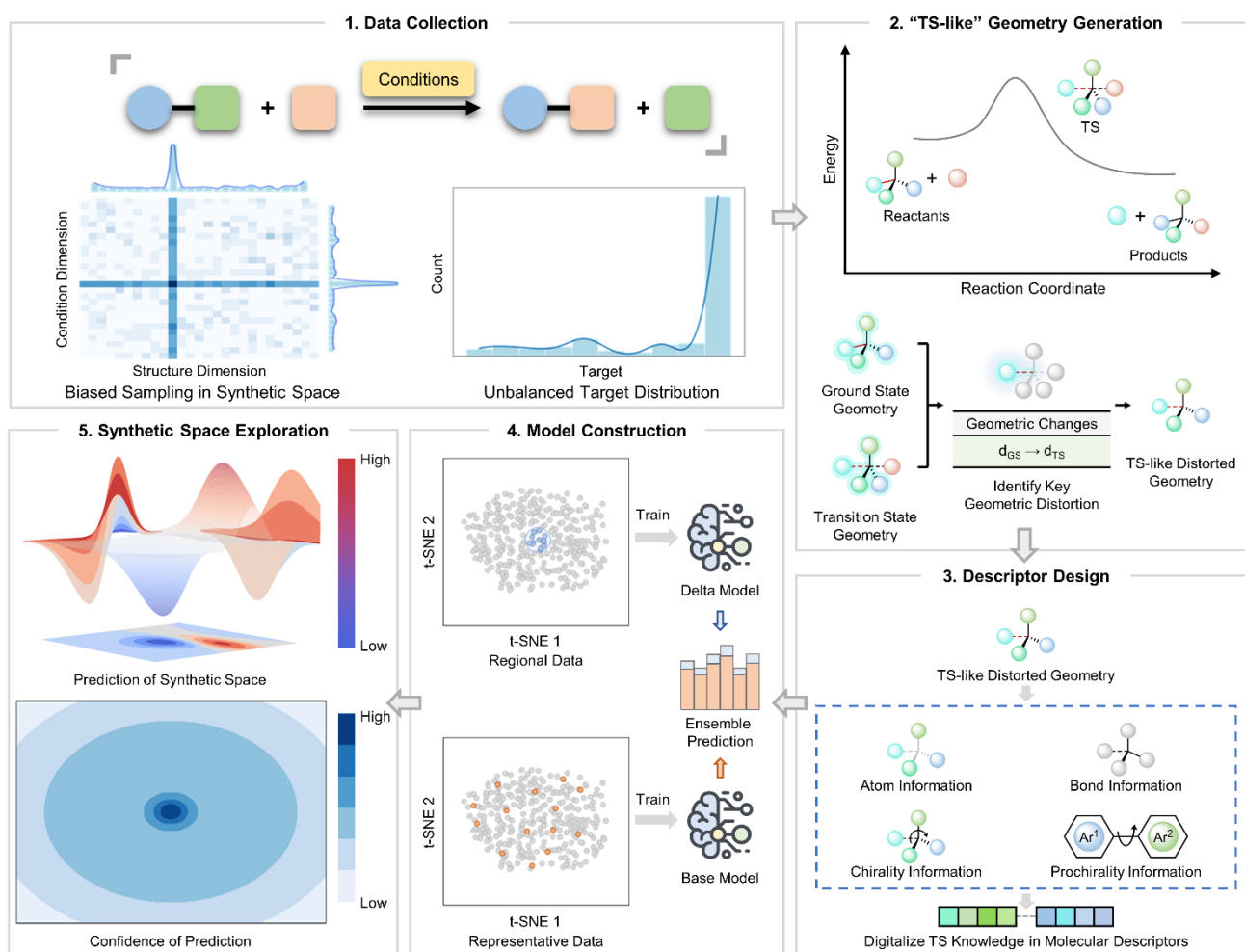
Enantioselective catalysis holds significant importance in molecular synthesis. The traditional mechanism-based approach^[168] for designing and refining enantioselective catalysis faces complexities arising from high-dimensional nature of the structure-enantioselectivity relationship. Even minor structural alterations in substrates can lead to non-intuitive effects on stereoselectivity outcomes,^[169] resulting in time-consuming screening efforts in current enantioselective catalysis research. To overcome these challenges, the data-driven approach was proposed, which involves digitalizing the catalytic system and training statistical models to predict chemical patterns.^[170] However, due to the lack of quantified and holistic understanding of the synthetic space, the predictive capability of data-driven models continues to be hindered.

In this context, a ML workflow will be developed to achieve a comprehensive prediction of the synthetic space, focusing on the palladium-catalyzed electrooxidative C–H bond activation. The goal is to accurately predict enantioselectivity by integrating the advantages of both mechanism-based and data-driven approaches through the incorporation of transition state knowledge into machine learning. Furthermore, the reliability of the model will be assessed for specific regions of interest within the synthetic space.

3.6.1 Workflow of ML Process

In order to achieve accurate prediction of the synthetic space, Li-Cheng Xu has developed a well-defined workflow that leverages the reported catalysis data and transition state knowledge (Scheme 3-35). The first step involves collecting the catalysis results in a structured manner. Due to the greedy nature of catalysis development, the collected data are typically unbalanced in the label space of synthetic performance. To address this, the next step is to generate “transition state (TS)-like” distorted geometries, which serve as the structural basis for vectorizing the transition state knowledge. In step three, a set of distinct molecular descriptors is generated using these “TS-like” geometries. To improve the predictive capability towards the target transformation, we have proposed a series of guidelines for implementing the transition state model in descriptor design. These designed descriptors also provide a digital representation of the synthetic space and the distribution of available samplings. Utilizing this information, in step four, ML models are trained to make enantioselectivity predictions and evaluate the reliability of the results. The base model aims to capture the general structure-performance relationship (SPR) by utilizing representative

data from the explored synthetic space. Furthermore, for specific regions within the synthetic space, a delta model is trained using neighboring data to learn the regional perturbations of the general SPR. By employing these ensemble predictions, one can explore the synthetic space with quantified synthetic performance and prediction reliability for any possible combinations. These five steps can be iteratively practiced as a feedback loop, allowing for further experimentation to achieve the desired accuracy and confidence.



Scheme 3-35 Workflow design for synthetic space prediction.

In order to incorporate transition state knowledge into the training process, Li-Cheng Xu next established “transition state-like” distorted geometries and digitalized them into a set of molecular descriptors, providing a vectorized representation of the target chemical process.

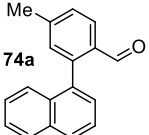
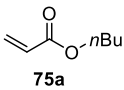
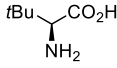
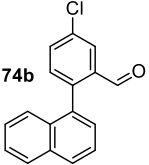
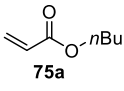
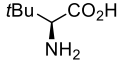
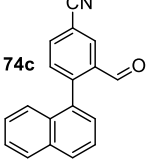
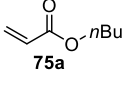
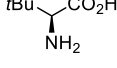
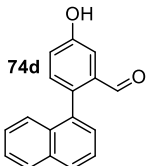
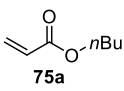
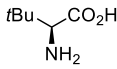
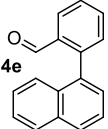
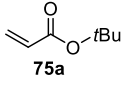
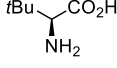
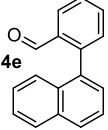
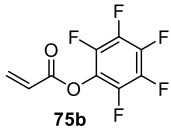
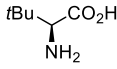
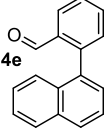
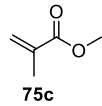
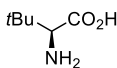
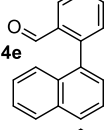
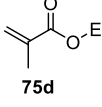
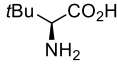
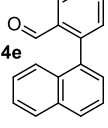
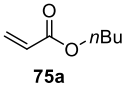
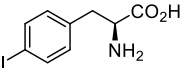
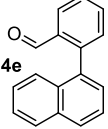
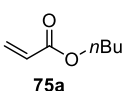
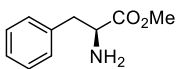
3.6.2 Model Training Results

3.6.2.1 External Test

To evaluate the model's predictive capability, we conducted an external test by synthesizing a series of new biaryl aldehydes, olefins, and TDGs (Table 3-3). By comparing the ML-

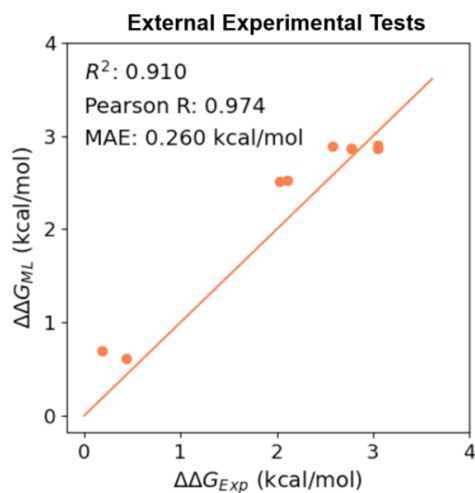
predicted and observed enantioselectivities, the model successfully captured the unexpected structural influence on synthetic performance.

Table 3-3 The detailed reaction information of the external experimental test set. (entries 1-4 and 9-10 were done by Dr. Johanna Frey and Dr. Uttam Dhawa)

| Entry | Biaryl | Olefin | TDG | Electrolyte | ee_{Exp} (%) | $\Delta\Delta G_{Exp}$ (kcal/mol) | ee_{ML} (%) | $\Delta\Delta G_{ML}$ (kcal/mol) |
|-------|---|---|---|-------------|----------------|-----------------------------------|---------------|----------------------------------|
| 1 |  |  |  | LiOAc | 97 | 2.77 | 97 | 2.86 |
| 2 |  |  |  | LiOAc | 97 | 2.77 | 97 | 2.86 |
| 3 |  |  |  | LiOAc | 98 | 3.04 | 97 | 2.86 |
| 4 |  |  |  | LiOAc | 98 | 3.04 | 97 | 2.86 |
| 5 |  |  |  | LiOAc | 96 | 2.58 | 97 | 2.90 |
| 6 |  |  |  | LiOAc | 98 | 3.04 | 98 | 2.90 |
| 7 |  |  |  | LiOAc | 92 | 2.11 | 96 | 2.53 |
| 8 |  |  |  | KOAc | 91 | 2.02 | 96 | 2.51 |
| 9 |  |  |  | LiOAc | 32 | 0.44 | 43 | 0.61 |
| 10 |  |  |  | LiOAc | 14 | 0.19 | 48 | 0.70 |

Solvent: AcOH, current: 1.0 mA, temperature: 60 °C

The knowledge-based model exhibited strong performance, demonstrating a convincing correlation (R^2 of 0.910, MAE of 0.260 kcal/mol, Scheme 3-36).



Scheme 3-36 External experimental tests.

3.6.2.2 Synthetic Space Prediction

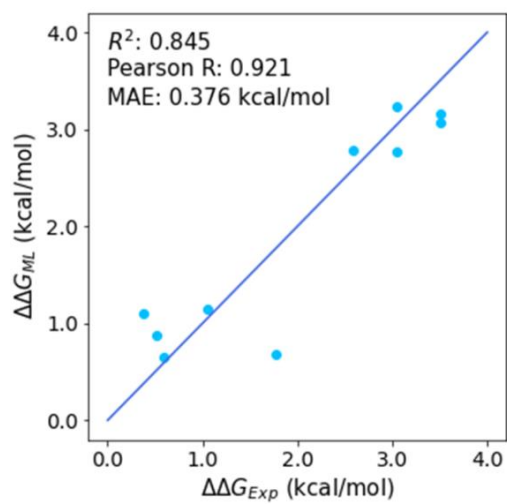
To assess the model's reliability and accuracy in predicting synthetic outcomes within the synthetic space, ten random cases were subsequently experimentally tested. These cases were specifically selected to cover a broad range of predicted ee values (Table 3-4).

Table 3-4 The detailed reaction information of the experimental validation of synthetic space.

| Entry | Biaryl | Olefin | TDG | Additive | ee_{Exp} (%) | $\Delta\Delta G_{Exp}$ (kcal/mol) | ee_{ML} (%) | $\Delta\Delta G_{ML}$ (kcal/mol) |
|-------|--------|--------|-----|---------------------------------|----------------|-----------------------------------|---------------|----------------------------------|
| 1 | | | | LiOAc | 96 | 2.58 | 97 | 2.79 |
| 2 | | | | quinone | 99 | 3.51 | 98 | 3.07 |
| 3 | | | | quinone | 99 | 3.51 | 98 | 3.16 |
| 4 | | | | quinone | 98 | 3.04 | 98 | 3.23 |
| 5 | | | | KH ₂ PO ₄ | 98 | 3.04 | 97 | 2.77 |
| 6 | | | | ---- | 28 | 0.38 | 68 | 1.09 |
| 7 | | | | sodium benzoate | 37 | 0.51 | 58 | 0.87 |
| 8 | | | | K ₂ CO ₃ | 66 | 1.05 | 70 | 1.15 |
| 9 | | | | ---- | 42 | 0.59 | 45 | 0.65 |
| 10 | | | | quinone | 87 | 1.77 | 47 | 0.68 |

Solvent: AcOH, current: 1.0 mA, temperature: 60 °C

These experimental results aligned well with the ML predictions (Scheme 3-37), indicating the model's reliability and accuracy in predicting synthetic outcomes. The model achieved a high R^2 value of 0.845 and a low MAE of 0.376 kcal/mol, demonstrating its capability to provide robust support for targeted exploration of candidate transformations within the synthetic space.

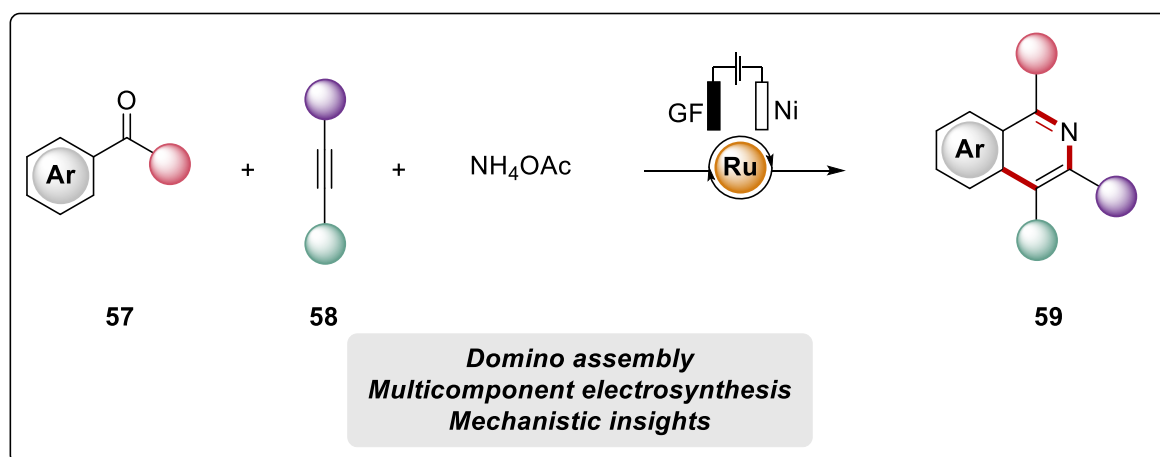


Scheme 3-37 Model performances in the synthetic space predictions.

4 Summary and Outlook

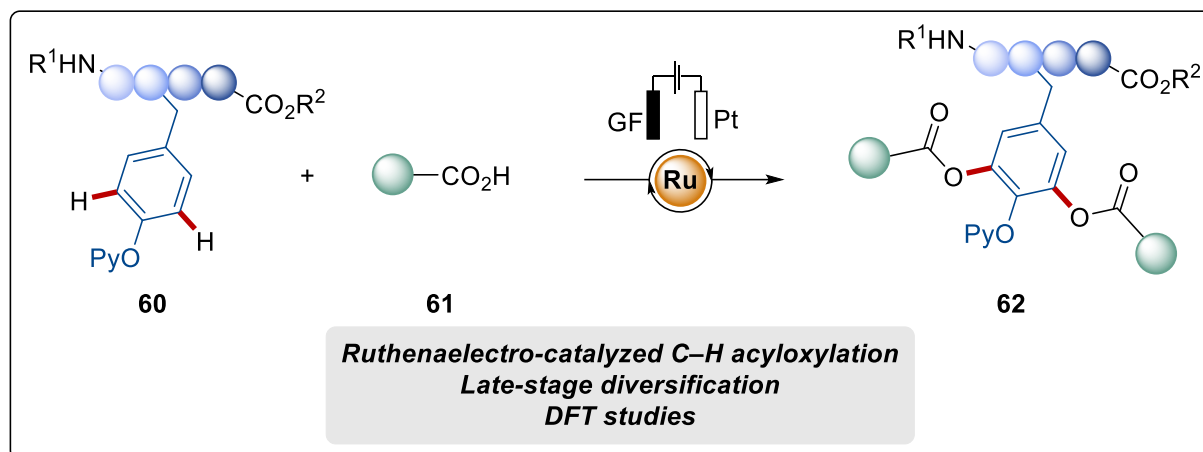
Transition metal-catalyzed C–H activation has emerged as a highly efficient tool for molecular synthesis. However, current methods for catalytic oxidative C–H activation often rely on super stoichiometric amount of toxic copper(II) and silver(I) salts as sacrificial oxidants. Recently, electrooxidation has been identified as an increasingly powerful strategy for TM catalyzed C–H activations. Despite of significant progress, there is strong demand on in-depth investigations of this field.

In the first project, the unprecedented ruthenium-catalyzed three-component electrochemical domino assembly of isoquinolines with electricity as the oxidant was achieved, generating H₂ as sole byproduct. (Scheme 4-1). The robustness of the electrocatalysis was reflected in sufficient substrate scope, efficient electrooxidation, and operator-friendly procedures. Well-defined ruthenacycles and a seven-membered ring intermediate were isolated and fully characterized by X-ray diffraction analysis, DFT calculations, and CV studies, providing strong support for a fast C–H activation and a ruthenium(II/III) manifold.



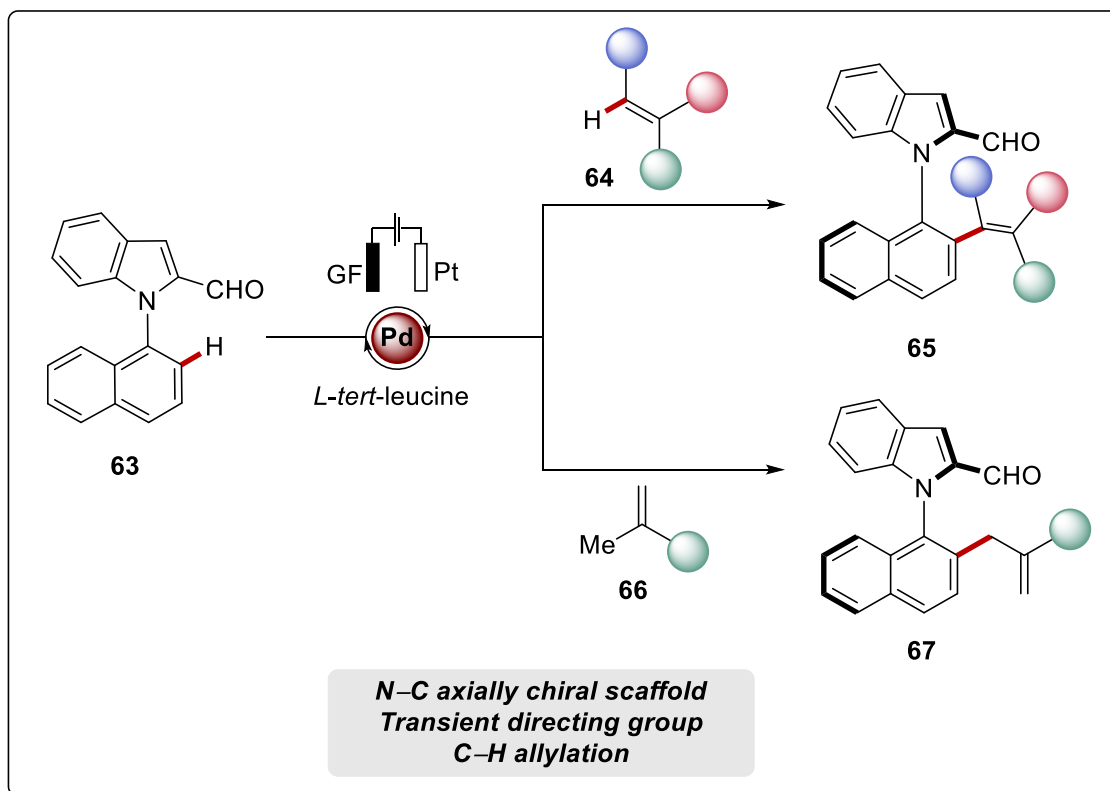
Scheme 4-1 Ruthenium-catalyzed electrochemical three-component synthesis of isoquinoline.

In the second project, the robust ruthenium catalysis was enabled for C–H acyloxylation of phenols with a broad substrate scope (Scheme 4-2). Experimental and computational studies unraveled a mechanism involving the formation of an arene-ligand-free bis-cyclometalated ruthenium complex followed by an oxidation-induced reductive elimination process through a ruthenium(II/IV/II) pathway. Importantly, this approach allowed for efficient late-stage diversification of tyrosine-derived peptides through electrocatalyzed bioorthogonal C–H acyloxylation.



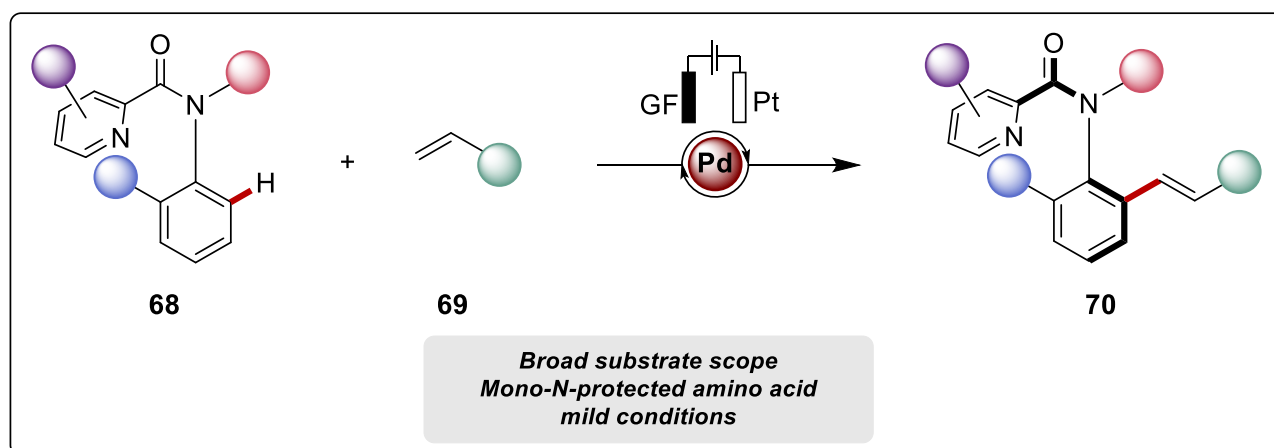
Scheme 4-2 Ruthenium-catalyzed electrochemical C–H acyloxylation for late-stage oligopeptide diversification.

The integration of electrosynthesis and transition metal catalysis offers immense potential in achieving a sustainable and green chemistry. Despite significant advances, studies in enantioselective metallaelectro-catalyzed C–H activation had been unknown. Thus, in the next project, we accomplished the first enantioselective palladaelectro-catalyzed C–H alkenylations and allylations utilizing an easily accessible amino acid as TDG, allowing the synthesis of highly enantiomerically-enriched N–C axially chiral biaryl scaffolds under exceptionally mild reaction conditions. A variety of alkenes was found to be compatible with this electrocatalysis, including nonactivated and perfluorinated alkenes. Remarkably, allylic selectivity was observed with 1,1-disubstituted alkenes in this transformation. Furthermore, computational studies provided valuable insights into a C–H activation through a seven-membered palladacycle (Scheme 4-3).



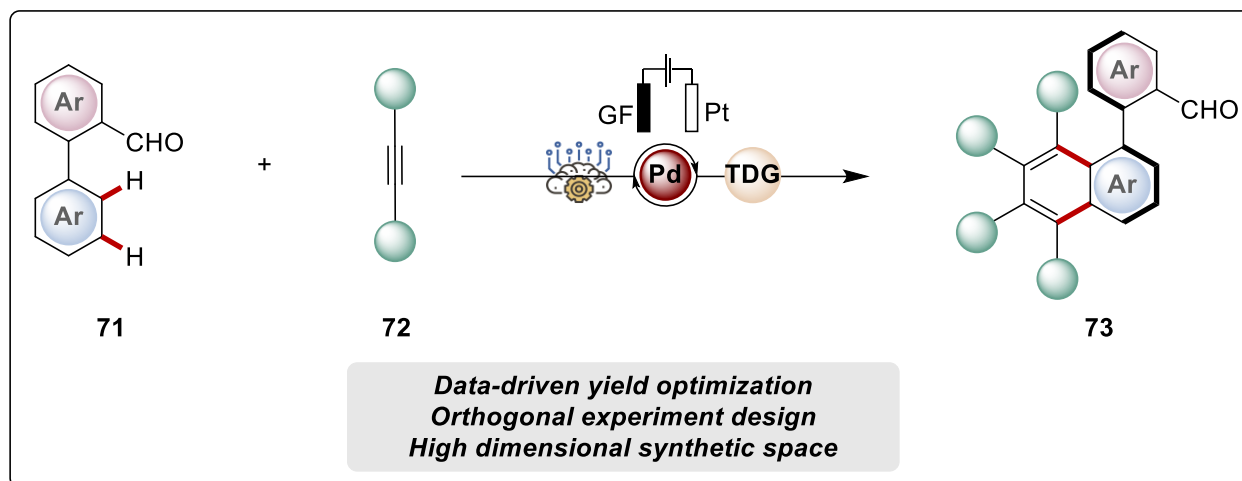
Scheme 4-3 Palladaelectro-catalyzed enantioselective C–H activation *via* cTDG strategy.

In addition, we achieved the enantioselective assembly of molecules bearing an acyclic anilide motif with challenging axial chirality *via* electrooxidative palladium(II)-catalyzed C–H olefination using a readily available mono-*N*-protected amino acid as a chiral ligand. With a quinone as catalytic redox-mediator in conjugation, we avoided the use of expensive and toxic silver salts, making the transformation more sustainable and environmentally-sound. The use of bifunctional sodium acetate as a base and a supporting electrolyte avoided electrochemical degradation of the catalyst. The robust electrochemical catalysis provided axially chiral anilides with high enantioselectivity under mild reaction conditions. Moreover, the feasibility of dual catalysis was showcased, allowing for the electrocatalytic C–H olefination, followed by subsequent hydrogenation. The enantioselective electrocatalysis could even be carried out with electricity generated by a commercial solar panel under natural sunlight (Scheme 4-4).



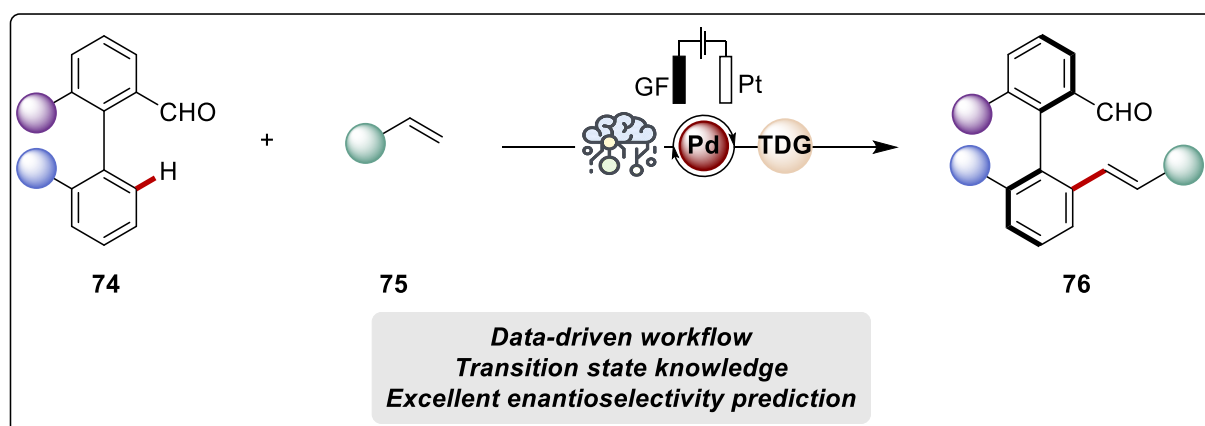
Scheme 4-4 Atropenantioselective palladaelectro-catalyzed anilide C–H olefinations mediated by the mono-*N*-protected amino acid.

Despite the advance in electrocatalysis, electrochemical reaction optimization remains a challenge, because of the vast dimensions of the electrochemical space and the difficulty in determining the contribution of each dimension. To address this, we developed an innovative workflow that combined machine learning and orthogonal experimental design to assist the optimization of electrocatalyzed C–H activation reactions. By integrating data-driven yield prediction modeling and setting a threshold for optimization progress, we achieved a balance between diverse sampling and target improvement in the high-dimensional synthetic space. This workflow successfully guided us to obtain the optimal reaction conditions for palladaelectro-catalyzed C–H annulation reaction among 8640 possibilities through only 74 experiments, facilitating the synthesis of atropoisomers with exceptional yields and enantioselectivities. This work shows the potential of synergizing organic electrochemistry and data-driven approach to tackle multi-dimensional chemical optimization problems (Scheme 4-5).



Scheme 4-5 ML-guided yield optimization for palladaelectro-catalyzed annulation reaction

Besides the yield optimization by ML, data-driven approach guided enantioselectivity prediction in enantioselective electrocatalysis is also of our interest due to the challenge in understanding the complex nature of the structure-enantioselectivity relationship. Thus, we designed a data-driven workflow implementing transition state knowledge in ML to achieve holistic enantioselectivity prediction of enantioselective palladaelectro-catalyzed C–H activation. The ML model are properly described and extrapolated by vectorizing of transition state knowledge, allowing the quantitative evaluation of 846,720 possibilities. This study highlighted the synergy between knowledge-based ML and interpretation-driven mechanistic study, offering a way to leverage existing screening data and transition state models for molecular synthesis.



Scheme 4-6 Enantioselectivity prediction of palladaelectro-catalyzed C–H activation using ML.

5 Experimental Data

5.1 General Remarks

All reactions involving air- and/or moisture-sensitive compounds were conducted under a dry nitrogen atmosphere using pre-dried glassware and standard Schlenk techniques. If not otherwise noted, yields refer to isolated compounds which were estimated to be >95% pure based on ¹H-NMR.

Vacuum

The following average pressure was measured on the used rotary vane pump RD4 from Vacuubrand®: 0.8×10^{-1} mbar (uncorrected value).

Melting points (M.p.)

Melting points were measured on a Stuart® Melting Point Apparatus SMP3 from Barloworld Scientific. All values are uncorrected.

Column Chromatography

Analytical thin layer chromatography (TLC) was performed on silica gel 60 F254 aluminium sheets from Merck. Plates were either visualized under irradiation at 254 nm or 365 nm or developed by treatment with a potassium permanganate solution followed by careful warming. Chromatographic purifications were accomplished by column chromatography on Merck Geduran® silica gel, grade 60 (40–63 μm, 70–230 mesh ASTM).

Gel Permeation Chromatography (GPC)

GPC purifications were performed on a JAI system (JAI-LC-9260 II NEXT) equipped with two sequential columns (JAIGEL-2HR, gradient rate: 5.000; JAIGEL-2.5HR, gradient rate: 20.000; internal diameter = 20 mm; length = 600 mm; Flush rate = 10.0 mL/min and chloroform (HPLC-quality with 0.6% ethanol as stabilizer) was used as the eluent.

Gas Chromatography

Monitoring of reaction process *via* gas chromatography or coupled gas chromatography-mass spectrometry was performed using a 7890 GC-system with/without mass detector 5975C (Triple-Axis-Detector) or a 7890B GC-system coupled with a 5977A mass detector, both from Agilent Technologies®.

Mass Spectrometry

Electron ionization (EI) and EI high resolution mass spectra (HR-MS) were measured on a time-of-flight mass spectrometer AccuTOF from JEOL. Electrospray ionization (ESI) mass spectra were recorded on an Io-Trap mass spectrometer LCQ from Finnigan, a quadrupole time-of-flight maXis from Bruker Daltonic or on a time-of-flight mass spectrometer microTOF from Bruker Daltonic. ESI-HR-MS spectra were recorded on a Bruker Apex IV or Bruker Daltonic 7T, Fourier transform ion cyclotron resonance (FTICR) mass spectrometer. The ratios of mass to charge (m/z) are indicated, intensities relative to the base peak ($I = 100$) are written in parentheses.

Infrared Spectroscopy

IR spectra were recorded using a Bruker® Alpha-P ATR spectrometer. Liquid samples were measured as film and solid samples neat. Spectra were recorded in the range from 4000 to 400 cm^{-1} . Analysis of the spectral data was carried out using Opus 6. Absorption is given in wave numbers (cm^{-1}).

Nuclear Magnetic Resonance Spectroscopy

Nuclear magnetic resonance (NMR) spectra were recorded on Avance III 300, Avance III HD 300, Avance Neo 400, Avance III 400, Avance III HD 400, Avance III HD 500 and Avance Neo 600 from Bruker®. Unless stated otherwise, all measurements were performed at 298 K. Chemical shifts are reported in δ -values in ppm relative to the residual proton peak or carbon peak of the deuterated solvent.

The coupling constants J are reported in hertz (Hz). Analysis of the recorded spectra was carried out using MestReNova 14.0 software.

Table 5-1 Chemical shifts of common deuterated solvents.

| Solvent | $^1\text{H-NMR}$ | $^{13}\text{C-NMR}$ |
|-----------------------|------------------|---------------------|
| CDCl_3 | 7.26 ppm | 77.16 ppm |
| DMSO- d_6 | 2.50 ppm | 39.52 ppm |
| Acetone- d_6 | 2.05 ppm | 206.7, 29.92 ppm |
| MeCN- d_3 | 1.94 ppm | 118.26, 1.32 ppm |

X-ray Crystallographic Analyses

X-ray diffraction experiments for all compounds were carried out by Dr. Christopher Golz at 100(2) K on a BRUKER *D8 Venture* four-circle-diffractometer from BRUKER AXS equipped

with a Photon II detector purchased from BRUKER AXS and using microfocus $1\mu\text{S}$ Cu/Mo radiation from INCOATEC with HELIOS mirror optics and single-hole collimator from BRUKER AXS.

Chiral HPLC

Chiral HPLC chromatograms were recorded on an Agilent 1290 Infinity using CHIRALPAK® IA-3, IB-3, IC-3, ID-3, IE-3 and IF-3 columns (3.0 μm particle size; \varnothing : 4.6 mm and 250 mm length) at ambient temperature.

Specific Rotations

Optical rotations were measured on an Anton Paar MCP 150 polarimeter using a 10 cm cell with a Na 589 nm filter. Concentrations are indicated in g/100 mL.

Solvents

Solvents used in reactions involving air- or moisture-sensitive compounds were dried and stored under an inert atmosphere of nitrogen or argon according to the following standard procedures.

Tetrahydrofuran is purified by solvent purification system (SPS-800) from M. Braun.

dimethoxyethane (DME) is dried and distilled over CaH_2 .

Acetic acid, trifluoroethanol, 1,2-Dichloroethane, ethanol, acetonitrile, and toluene are obtained from commercial sources, and were used without further purification.

Electrochemistry

Pt electrodes (10 mm \times 25 mm \times 0.125 mm, 99.9%; obtained from ChemPur® Karlsruhe, Germany) and GF electrodes (10 mm \times 10 mm \times 6 mm, SIGRACELL®GFA 6 EA, obtained from SGL Carbon, Wiesbaden, Germany), Nickel foam electrodes (20 mm \times 10 mm \times 1.4 mm, RCM-Ni5763; obtained from Recemat BV, Germany), Fe electrodes (10 mm \times 15 mm \times 0.50 mm, 99.9%; obtained from ChemPur® Karlsruhe, Germany) and BDD electrodes (20 mm \times 10 mm \times 3 mm, DIACHEM®, 15 μm boron-doped diamond layer on 3 mm silicon support/wafer, were purchased from CONDIAS GmbH, Itzhoer, Germany) were connected using stainless steel adapters. Electrolysis was conducted using an AXIOMET AX-3003P potentiostat in constant current mode, CV studies were performed using a Metrohm Autolab

PGSTAT204 workstation and Nova 2.0 software. Divided cells, separated by a P4 glass frit, were custom-made from the glass workshop of the Georg-August-Universität Göttingen. For the electrocatalysis powered by sunlight, the commercially available amorphous silicon photovoltaic cell TPS-103 from CONRAD ELECTRONIC (6 W, 17.5 V max. voltage, 428 mA max. current, 467 mm × 161 mm × 19 mm) was used. The output current was controlled with a customized and normalized constant current regulator and regularly double checked with an ammeter.

Reagents

Reagents obtained from commercial sources with a purity >95% were used without further purification unless stated otherwise.

The following compounds were synthesized according to previously reported procedures: Alkynes **58** and **72**,^[171] phenols **60**,^[172] phenol derived peptides **88**,^[173] *N*-arylindoles **63**,^[174] 4-bromophenyl acrylate,^[175] anilides **68**,^[85] biaryl aldehydes **71** and **74**,^[90, 176]

The following compounds were kindly synthesized and/or provided by the persons listed below:

Karsten Rauch: [RuCl₂(*p*-cymene)]₂, [Ru(OAc)₂*p*-cymene], [Cp*RhCl₂]₂, dry and/or degassed solvents.

Simon Homöller: **72d**, **72e**

Hendrik Simon: **72c**

Zhigao Shen: **72h**

5.2 General Procedures

General procedure A: Ruthenaelectro-Catalyzed Three-Component Annulation

The electrocatalysis was carried out in a 25 mL Schlenk tube with a GF anode (10 mm × 15 mm × 6.0 mm) and a nickel foam electrode (Ni, 20 mm × 10 mm × 1.4 mm). Diarylacetylene **58** (0.60 mmol), NH₄OAc (92.4 mg, 1.2 mmol) and [Ru(OAc)₂(*p*-cymene)] (10.6 mg, 0.03 mmol, 10 mol %) were added in the tube, which was then evacuated and purged with N₂ three times. Subsequently, ketone **57** (0.30 mmol) and TFE (3.5 mL) were successively added. An oil bulb was attached to the system by using a needle. The electrocatalysis was performed at 110 °C with a constant current of 2.5 mA maintained for 20 h. Then, the DC-power supply was stopped, and the reaction mixture was diluted with EtOAc (2.0 mL). The Ni cathode and the GF anode were washed with EtOAc. The solvents were combined with the reaction mixture, silica gel was added, and the solvents were removed *in vacuo*. Subsequent column chromatography on silica gel afforded the corresponding products.

General Procedure B: Ruthenaelectro-Catalyzed Three-Component Annulation

The electrocatalysis was carried out in a 25 mL Schlenk tube with a GF anode (10 mm × 15 mm × 6.0 mm) and a nickel foam electrode (20 mm × 10 mm × 1.4 mm). Diarylacetylene **58** (0.60 mmol), NH₄OAc (92.4 mg, 1.2 mmol) and [Ru(OAc)₂(*p*-cymene)] (10.6 mg, 0.03 mmol, 10 mol %) were added in the tube, which was then evacuated and purged with N₂ three times. Subsequently, ketone **57** (0.30 mmol) and TFE/Toluene (3.0/0.5 mL) were successively added. An oil bulb was attached to the system by using a needle. The electrocatalysis was performed at 110 °C with a constant current of 2.5 mA maintained for 20 h. Then, the DC-power supply was stopped, and the reaction mixture was diluted with EtOAc (2.0 mL). The Ni cathode and the GF anode were washed with EtOAc. The solvents were combined with the reaction mixture, silica gel was added, and the solvents were removed *in vacuo*. Subsequent column chromatography on silica gel afforded the corresponding products.

General Procedure C: Ruthenaelectro-Catalyzed C–H Acyloxylation of Phenols

The electrocatalysis was carried out in a 25 mL Schlenk tube with a GF anode (10 mm × 15 mm × 6.0 mm) and a Pt cathode (10 mm × 15 mm × 0.25 mm). Phenols **60** (0.25 mmol), acids **61** (0.40 mmol), [Ru(OAc)₂(*p*-cymene)] (8.8 mg, 10 mol %) and *n*Bu₄NBF₄ (82.3 mg, 0.25 mmol) were dissolved in DCE (4.0 mL). An oil bulb was attached to the system using a needle. The electrocatalysis was performed at 100 °C with a constant current of 3.0 mA maintained for 15 h. Then, the DC-power supply was stopped, and the reaction mixture was

diluted with EtOAc (2.0 mL). The Pt cathode and the GF anode were washed with EtOAc. The solvents were combined with the reaction mixture, silica gel was added, and the solvents were removed *in vacuo*. Subsequent column chromatography on silica gel afforded the corresponding products.

General Procedure D: Ruthenaelectro-Catalyzed C–H Acyloxylation of Phenols

The electrocatalysis was carried out in a 25 mL Schlenk tube with a GF anode (10 mm × 15 mm × 6.0 mm) and a Pt cathode (10 mm × 15 mm × 0.25 mm). Phenols **60** (0.25 mmol), acids **61** (0.40 mmol), RuCl₃·3H₂O (6.5 mg, 10 mol %) and *n*Bu₄NBF₄ (82.3 mg, 0.25 mmol) were dissolved in DCE (4.0 mL). An oil bulb was attached to the system using a needle. The electrocatalysis was performed at 100 °C with a constant current of 3.0 mA maintained for 15 h. Then, the DC-power supply was stopped, and the reaction mixture was diluted with EtOAc (2.0 mL). The Pt cathode and the GF anode were washed with EtOAc. The solvents were combined with the reaction mixture, silica gel was added, and the solvents were removed *in vacuo*. Subsequent column chromatography on silica gel afforded the corresponding products.

General Procedure E: Ruthenaelectro-Catalyzed C–H Acyloxylation of Peptides Derivatives

The electrocatalysis was carried out in a 25 mL Schlenk tube with a GF anode (10 mm × 15 mm × 6.0 mm) and a Pt cathode (10 mm × 15 mm × 0.25 mm). Peptides derivatives **87** (0.25 mmol), acids **61** (0.40 mmol), [Ru(OAc)₂(*p*-cymene)] (8.8 mg, 10 mol %) and *n*Bu₄NBF₄ (82.3 mg, 0.25 mmol) were dissolved in DCE (4.0 mL). An oil bulb was attached to the system using a needle. The electrocatalysis was performed at 100 °C with a constant current of 3.0 mA maintained for 15 h. Then, the DC-power supply was stopped, and the reaction mixture was diluted with EtOAc (2.0 mL). The Pt cathode and the GF anode were washed with EtOAc. The solvents were combined with the reaction mixture, silica gel was added, and the solvents were removed *in vacuo*. Subsequent column chromatography on silica gel afforded the corresponding products.

General Procedure F: Palladaelectro-Catalyzed C–H Activation for N–C Axial Chirality

The electrocatalysis was carried out in an undivided cell with a GF anode (10 mm × 15 mm × 6.0 mm) and a Pt cathode (10 mm × 15 mm × 0.25 mm). Hetero aryls aldehydes **63** (0.20 mmol, 1.0 equiv.), alkenes **64/66** (0.60 mmol, 3.0 equiv.), Pd(OAc)₂ (4.49 mg, 10 mol %), *L*-*tert*-leucine (7.9 mg, 30 mol %) and LiOAc (26.4 mg, 2.0 equiv.) were dissolved in AcOH (4.5 mL). The electrocatalysis was performed at 60 °C with a constant current of 1.0 mA maintained for 16 h. Then, the DC-power supply was stopped, and the reaction mixture was

diluted with EtOAc (2.0 mL). The Pt cathode and the GF anode were washed with EtOAc. The solvents were combined with the reaction mixture, silica gel was added, and the solvents were removed *in vacuo*. Subsequent column chromatography on silica gel afforded the corresponding product.

General Procedure G: The Synthesis of Racemic Arylindoles

The electrocatalysis was carried out in an undivided cell with a GF anode (10 mm × 15 mm × 6.0 mm) and a Pt cathode (10 mm × 15 mm × 0.25 mm). Hetero aryls aldehydes **63** (0.20 mmol, 1.0 equiv.), alkenes **64/66** (0.60 mmol, 3.0 equiv.), Pd(OAc)₂ (4.49 mg, 10 mol %), D/L-valine (7.0 mg, 30 mol %) and LiOAc (26.4 mg, 2.0 equiv.) were dissolved in AcOH (4.5 mL). The electrocatalysis was performed at 60 °C with a constant current of 1.0 mA maintained for 16 h. Then, the DC-power supply was stopped, and the reaction mixture was diluted with EtOAc (2.0 mL). The Pt cathode and the GF anode were washed with EtOAc. The solvents were combined with the reaction mixture, silica gel was added, and the solvents were removed *in vacuo*. Subsequent column chromatography on silica gel afforded the corresponding product.

General Procedure H: Palladaelectro-Catalyzed C–H Activation for Chiral Anilides

The electrocatalysis was carried out in an undivided cell with a GF anode (10 mm × 15 mm × 6.0 mm) and a Pt cathode (10 mm × 15 mm × 0.25 mm). anilide **68** (0.5 mmol, 1.0 equiv.), Pd(OAc)₂ (11.3 mg, 10 mol %), S-5-oxoproline (12.9 mg, 20 mol %), BQ (5.4 mg, 10 mol %) and NaOAc (82 mg, 1.0 mmol, 2.0 equiv.) and the olefin (1.5 mmol, 3.0 equiv.) were dissolved in 5 mL TFE/DME (1/1) solvent mixture. The electrocatalysis was performed at 60 °C with a constant current of 4.0 mA maintained for 24 h. The resulting mixture was filtered through a celite pad, eluted with EtOAc and concentrated *in vacuo*. The residue was purified by column chromatography to afford the title compound.

General procedure I: The Synthesis for Racemic Anilides Products

The electrocatalysis was carried out in an undivided cell with a GF anode (10 mm × 15 mm × 6.0 mm) and a Pt cathode (10 mm × 15 mm × 0.25 mm). anilide **68** (0.5 mmol, 1.0 equiv.), Pd(OAc)₂ (11.3 mg, 10 mol %), *rac*-S/R-5-oxoproline (12.9 mg, 20 mol %), BQ (5.4 mg, 10 mol %) and NaOAc (82 mg, 1.0 mmol, 2.0 equiv.) and the olefin (1.5 mmol, 3.0 equiv.) were dissolved in 5 mL TFE/DME (1/1) solvent mixture. The electrocatalysis was performed at 60 °C with a constant current of 4.0 mA maintained for 24 h. The resulting mixture was filtered through a celite pad, eluted with EtOAc and concentrated *in vacuo*. The residue was purified by column chromatography to afford the title compound.

General procedure J: 3.5 Yield Optimization of Palladaelectro-Catalyzed C–H Annulation by ML

Constant current reaction setup J_{CC} : The electrocatalysis was carried out in an undivided cell equipped with an anode and a cathode. Biaryl **71a** (0.20 mmol, 1.0 equiv.), alkyne **72a** (0.60 mmol, 3.0 equiv.), Pd(OAc)₂ (10 mol %), *L*-tert-leucine (30 mol %) and the electrolyte (2.0 equiv.) were placed in the undivided cell and dissolved in 4.0 mL of solvent. Electrocatalysis was performed at 70 °C with different constant current for different time (make the total discharge into the reaction is 10.8 mA·h = 38.8 C) with a stirring rate of 500 rpm. At ambient temperature, after removal of the solvent *in vacuo*, the crude mixture was diluted with EtOAc (20 mL) and washed with water (3 × 20 mL), then the organic layer was dried over Na₂SO₄. The yield was determined by ¹H-NMR spectroscopy with CH₂Br₂ (0.20 mmol) as internal standard.

Constant potential reaction setup J_{CP} : The electrocatalysis was carried out in an undivided cell, equipped with an anode, a cathode and a silver wire as the pseudo-reference electrode. Biaryl **71a** (0.20 mmol, 1.0 equiv.), alkyne **72a** (0.60 mmol, 3.0 equiv.), Pd(OAc)₂ (10 mol %), *L*-tert-leucine (30 mol %) and the electrolyte (2.0 equiv.) were placed in the undivided cell and dissolved in 4.0 mL of solvent. Electrocatalysis was performed at 70 °C with different constant potential for different time (make sure the total discharge into the reaction is 10.8 mA·h = 38.8 C) with a stirring rate of 500 rpm. At ambient temperature, after removal of the solvent *in vacuo*, the crude mixture was diluted with EtOAc (20 mL) and washed with water (3 × 20 mL), then the organic layer was dried over Na₂SO₄. The yield was determined by ¹H-NMR spectroscopy with CH₂Br₂ (0.20 mmol) as internal standard.

General Procedure K: Optimized Condition of Palladaelectro-Catalyzed C–H Annulation by ML

The electrocatalysis was carried out in an undivided cell, equipped with a GF anode (10 mm × 15 mm × 6 mm) and a Pt cathode (25 mm × 10 mm × 0.125 mm). Biaryls **71** (0.20 mmol, 1.0 equiv.), alkynes **72** (3.0 equiv.), Pd(OAc)₂ (10 mol %), *L*-tert-leucine (30 mol %) and NaOPiv (2.0 equiv.) were dissolved in 4.0 mL of AcOH:TFE (1:1) solvent mixture. The reaction was performed at 70 °C with a constant current 0.3 mA for 36 h with a stirring rate of 500 rpm. After completion of the reaction, the reaction mixture was diluted with EtOAc. After removal of the solvent *in vacuo*, the crude mixture was purified by column chromatography on silica gel to yield the products.

General Procedure L: Synthesis of Racemic Products for Yield Optimization

The electrocatalysis was carried out in an undivided cell, equipped with a GF anode (10 mm × 15 mm × 6 mm) and a Pt cathode (25 mm × 10 mm × 0.125 mm). Biaryls **71** (0.20 mmol, 1.0 equiv.), alkynes **72** (3.0 equiv.), Pd(OAc)₂ (10 mol %), D/L-valine (7.0 mg, 30 mol %) and NaOPiv (2.0 equiv.) were dissolved in 4.0 mL of AcOH:TFE (1:1) solvent mixture. The reaction was performed at 70 °C with a constant current 0.3 mA for 36 h with a stirring rate of 500 rpm. After completion of the reaction, the reaction mixture was diluted with EtOAc. After removal of the solvent *in vacuo*, the crude mixture was purified by column chromatography on silica gel to yield the products.

General procedure M: Enantioselectivity Prediction of Palladaelectro-Catalyzed C–H Activation using ML

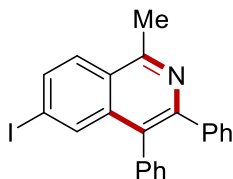
The electrocatalysis was carried out in an undivided cell, with a GF anode (10 mm × 15 mm × 6 mm) and a Pt cathode (10 mm × 15 mm × 0.25 mm). Biaryls **74** (0.20 mmol, 1.0 equiv.), acrylates **75** (0.60 mmol, 3 equiv.), Pd(OAc)₂ (4.49 mg, 10 mol %), transient directing group (20 mol %) and additive (2 equiv.) were placed in a 10 mL cell and dissolved in 4.5 mL of solvent. Electrocatalysis was performed at 60 °C with a constant current of 1.0 mA maintained for 20 h. At ambient temperature, the reaction mixture was diluted with EtOAc. The GF anode was washed with EtOAc. The solvents were removed *in vacuo*. The crude mixture was purified by column chromatography on silica gel to yield the expected product **76**.

General Procedure N: Synthesis of Racemic Products for Enantioselectivity Prediction

The electrocatalysis was carried out in an undivided cell, with a GF anode (10 mm × 15 mm × 6 mm) and a Pt cathode (10 mm × 15 mm × 0.25 mm). Biaryls **74** (0.20 mmol, 1.0 equiv.), acrylates **75** (0.60 mmol, 3 equiv.), Pd(OAc)₂ (4.49 mg, 10 mol %), D/L-valine (20 mol %) and additive (2 equiv.) were placed in a 10 mL cell and dissolved in 4.5 mL of solvent. Electrocatalysis was performed at 60 °C with a constant current of 1.0 mA maintained for 20 h. At ambient temperature, the reaction mixture was diluted with EtOAc. The GF anode was washed with EtOAc. The solvents were removed *in vacuo*. The crude mixture was purified by column chromatography on silica gel to yield the expected product **76**.

5.3 Ruthenaelectro-Catalyzed Three-Component C–H Annulation

5.3.1 Characterization Data



6-Iodo-1-methyl-3,4-diphenylisoquinoline 59d: The general procedure **A** was followed using 1-(4-iodophenyl)ethan-1-one **57d** (73.8 mg, 0.30 mmol) and 1,2-diphenylethyne **58a** (107 mg, 0.60 mmol). Purification by column chromatography on silica gel (*n*hexane/EtOAc: 30/1→10/1) yielded **59d** (70.2 mg, 55%) as a white solid.

M.p.: 180–182 °C.

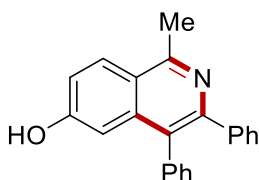
¹H-NMR (400 MHz, CDCl₃) δ = 8.02 (d, *J* = 1.6 Hz, 1H), 7.88 (d, *J* = 8.8 Hz, 1H), 7.83 (dd, *J* = 8.8, 1.7 Hz, 1H), 7.36 – 7.30 (m, 5H), 7.21 – 7.14 (m, 5H), 3.02 (s, 3H).

¹³C-NMR (101 MHz, CDCl₃) δ = 157.8 (C_q), 150.4 (C_q), 140.6 (C_q), 137.5 (C_q), 136.7 (C_q), 135.3 (CH), 135.0 (CH), 131.3 (CH), 130.1 (CH), 128.4 (CH), 127.9 (C_q), 127.6 (CH), 127.4 (CH), 127.1 (CH), 126.9 (CH), 124.8 (C_q), 97.6 (C_q), 22.6 (CH₃).

IR (ATR): 3057, 1683, 1589, 1561, 1386, 1326, 1028, 766, 698, 617 cm⁻¹.

MS (ESI) *m/z* (relative intensity): 422 (100) [M+H]⁺. **HR-MS** (ESI) *m/z* calc. for C₂₂H₁₇IN⁺ [M+H]⁺ 422.0400, found 422.0405.

The analytical data are in accordance with those reported in the literature.^[177]



1-methyl-3,4-diphenylisoquinolin-6-ol 59e: The general procedure **A** was followed using 4-acetoxyacetophenone **57e** (53.5 mg, 0.30 mmol) and 1,2-diphenylethyne **58a** (107 mg, 0.60 mmol). Purification by column chromatography on silica gel (*n*hexane/EtOAc: 3/1→1/1) yielded **59e** (48.5 mg, 52%) as yellow solid.

M.p.: 139–141 °C.

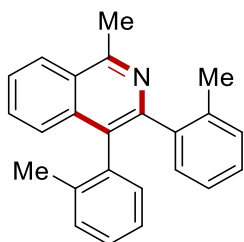
¹H-NMR (400 MHz, CDCl₃) δ = 10.23 (s, 1H), 8.14 (d, *J* = 9.0 Hz, 1H), 7.40 – 7.35 (m, 2H), 7.35 – 7.30 (m, 1H), 7.30 – 7.26 (m, 2H), 7.20 – 7.13 (m, 6H), 6.78 (d, *J* = 2.4 Hz, 1H), 2.88 (s, 3H).

¹³C-NMR (101 MHz, CDCl₃) δ = 158.9 (C_q), 156.5 (C_q), 148.7 (C_q), 141.1 (C_q), 137.8 (C_q), 137.7 (C_q), 131.0 (CH), 123.0 (CH), 128.3 (CH), 127.9 (CH), 127.4 (C_q), 127.2 (CH), 127.1 (CH), 126.7 (CH), 120.5 (C_q), 119.0 (CH), 106.9 (CH), 22.2 (CH₃).

IR (ATR): 3402, 1606, 1440, 1407, 1258, 1234, 1023, 996, 757, 611 cm⁻¹.

MS (ESI) m/z (relative intensity): 312 (100) [M+H]⁺. **HR-MS** (ESI) m/z calc. for C₂₂H₁₈NO⁺ [M+H]⁺ 312.1383, found 312.1387.

The analytical data are in accordance with those reported in the literature.^[178]



1-methyl-3,4-di-*o*-tolylisoquinoline 59f: The general procedure **A** was followed using acetophenone **57f** (36.0 mg, 0.30 mmol) and 1,2-di-*o*-tolylethyne **58b** (124 mg, 0.60 mmol). Purification by column chromatography on silica gel (*n*hexane/EtOAc: 30/1→5/1) yielded **59f** (48 mg, 50%) as a white solid.

M.p.: 153–155 °C.

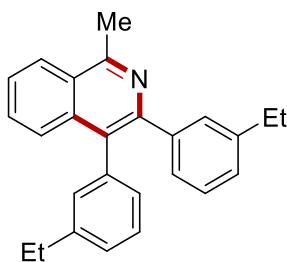
¹H-NMR (400 MHz, CDCl₃) δ = 8.25 – 8.18 (m, 1H), 7.63 – 7.53 (m, 2H), 7.40 – 7.35 (m, 1H), 7.20 – 7.11 (m, 3H), 7.11 – 1.00 (m, 3H), 7.00 – 6.88 (m, 2H), 3.06 (s, 3H), 2.23 (s, 3H), 1.97 (s, 3H).

¹³C-NMR (101 MHz, CDCl₃) δ = 157.1 (C_q), 150.5 (C_q), 140.2 (C_q), 136.9 (C_q), 136.5 (C_q), 136.2 (C_q), 135.8 (C_q), 131.0 (CH), 130.1 (CH), 129.9 (CH), 129.7 (CH), 129.5 (CH), 129.3 (C_q), 127.4 (CH), 127.3 (CH), 126.5 (CH), 126.1 (CH), 126.0 (C_q), 125.6 (CH), 125.3 (CH), 124.8 (CH), 22.5 (CH₃), 20.2 (CH₃), 20.1 (CH₃).

IR (ATR): 2921, 1735, 1549, 1501, 1387, 1336, 1043, 759, 728, 617 cm⁻¹.

MS (ESI) m/z (relative intensity): 324 (100) [M+H]⁺. **HR-MS** (ESI) m/z calc. for C₂₄H₂₂N⁺ [M+H]⁺ 324.1747, found 324.1753.

The analytical data are in accordance with those reported in the literature.^[179]



3,4-bis(3-ethylphenyl)-1-methylisoquinoline 59g: The general procedure **A** was followed using acetophenone **57f** (36.0 mg, 0.30 mmol) and 1,2-bis(3-ethylphenyl)ethyne **58c** (141 mg, 0.60 mmol) Purification by column chromatography on silica gel (*n*hexane/EtOAc: 50/1→10/1) yielded **59g** (74.0 mg, 70%) as a light yellow solid.

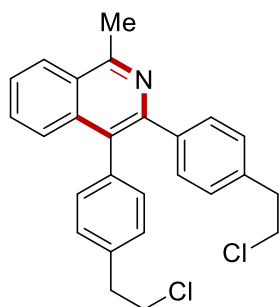
M.p.: 87–89 °C.

¹H-NMR (400 MHz, CDCl₃) δ = 8.22 – 8.15 (m, 1H), 7.77 – 7.69 (m, 1H), 7.62 – 7.51 (m, 2H), 7.30 – 7.22 (m, 2H), 7.17 – 7.10 (m, 3H), 7.09 – 7.02 (m, 2H), 6.99 (d, *J* = 7.6 Hz, 1H), 3.08 (s, 3H), 2.58 (q, *J* = 7.6 Hz, 2H), 2.48 (q, *J* = 7.6 Hz, 2H), 1.11 (t, *J* = 7.6 Hz, 3H), 1.04 (t, *J* = 7.6 Hz, 3H).

¹³C-NMR (101 MHz, CDCl₃) δ = 157.4 (C_q), 149.7 (C_q), 144.1 (C_q), 143.1 (C_q), 140.9 (C_q), 137.5 (C_q), 135.9 (C_q), 131.1 (CH), 129.9 (CH), 129.7 (CH), 129.3 (C_q), 128.6 (CH), 128.0 (CH), 127.5 (CH), 127.5 (CH), 126.5 (CH), 126.4 (CH), 126.3 (CH), 126.3 (CH), 126.1 (C_q), 125.4 (CH), 28.7 (CH₂), 28.7 (CH₂), 22.7 (CH₃), 15.7 (CH₃), 15.5 (CH₃).

IR (ATR): 3060, 2961, 1602, 1569, 1550, 1389, 1025, 799, 761, 618 cm⁻¹.

MS (ESI) *m/z* (relative intensity): 352 (100) [M+H]⁺. **HR-MS** (ESI) *m/z* calc. for C₂₆H₂₆N⁺ [M+H]⁺ 352.2060, found 352.2063.



3,4-bis(4-(2-chloroethyl)phenyl)-1-methylisoquinoline 59h: The general procedure **B** was followed using acetophenone **57f** (36.0 mg, 0.30 mmol) and 1,2-bis(4-(2-chloroethyl)phenyl)ethyne **58d** (106.9 mg, 0.6 mmol). Isolation by column chromatography (*n*hexane/EtOAc: 50/1→10/1) yielded **59h** (50.4 mg, 40%) as a white solid.

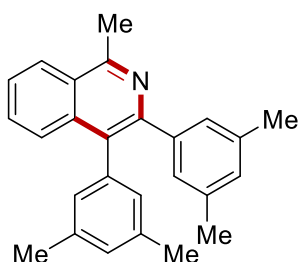
M.p.: 146 – 148 °C.

¹H-NMR (400 MHz, CDCl₃) δ 8.20 – 8.15 (m, 1H), 7.69 – 7.62 (m, 1H), 7.60 – 7.55 (m, 2H), 7.33 – 7.28 (m, 2H), 7.22 – 7.14 (m, 4H), 7.06 – 7.00 (m, 2H), 3.74 (t, *J* = 7.4 Hz, 2H), 3.62 (t, *J* = 7.6 Hz, 2H), 3.09 (t, *J* = 7.4 Hz, 2H), 3.05 (s, 3H), 2.98 (t, *J* = 7.6 Hz, 2H).

¹³C-NMR (101 MHz, CDCl₃) δ 157.8 (C_q), 149.1 (C_q), 139.66 (C_q), 137.04 (C_q), 136.73 (C_q), 136.16 (C_q), 136.02 (C_q), 131.60 (CH), 130.51 (CH), 129.99 (CH), 128.81 (C_q), 128.77 (CH), 128.16 (CH), 126.60 (CH), 126.21 (CH), 126.17 (C_q), 125.59 (CH), 45.00 (C_q), 44.90 (C_q), 39.04 (C_q), 38.94 (C_q), 22.79 (CH₃).

IR (ATR): 2955, 1761, 1568, 1513, 1391, 1332, 1182, 1022, 760, 612 cm^{-1} .

MS (ESI) m/z (relative intensity): 420 (100) $[\text{M}+\text{H}]^+$. **HR-MS** (ESI) m/z calc. for $\text{C}_{26}\text{H}_{24}\text{Cl}_2\text{N}^+$ $[\text{M}+\text{H}]^+$ 420.1280, found 420.1282.



3,4-bis(3,5-dimethylphenyl)-1-methylisoquinoline 59i: The general procedure **A** was followed using acetophenone **57a** (36.0 mg, 0.30 mmol) and 1,2-bis(3,5-dimethylphenyl)ethyne **58e** (141 mg, 0.60 mmol) Purification by column chromatography on silica gel (*n*hexane/EtOAc: 50/1→10/1) yielded **59i** (74.0 mg, 70%) as a light yellow solid.

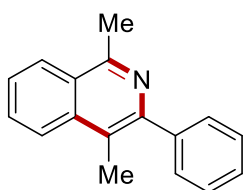
M.p.: 127–129 °C.

$^1\text{H-NMR}$ (400 MHz, CDCl_3) δ = 8.19 – 8.13 (m, 1H), 7.69 – 7.64 (m, 1H), 7.60 – 7.50 (m, 2H), 7.03 (s, 2H), 6.95 (s, 1H), 6.85 (s, 2H), 6.80 (s, 1H), 3.07 (s, 3H), 2.29 – 2.26 (m, 6H), 2.19 (d, J = 0.9 Hz, 6H).

$^{13}\text{C-NMR}$ (101 MHz, CDCl_3) δ = 157.1 (C_q), 149.4 (C_q), 140.7 (C_q), 137.4 (C_q), 137.3 (C_q), 136.5 (C_q), 136.2 (C_q), 129.6 (CH), 129.3 (C_q), 129.0 (CH), 128.4 (CH), 128.4 (CH), 128.0 (CH), 126.4 (CH), 126.2 (CH), 125.9 (C_q), 125.3 (CH), 22.7 (CH_3), 21.2 (CH_3), 21.2 (CH_3).

IR (ATR): 2947, 2912, 2022, 1597, 1554, 1391, 1027, 848, 756, 618 cm^{-1} .

MS (ESI) m/z (relative intensity): 352 (100) $[\text{M}+\text{H}]^+$. **HR-MS** (ESI) m/z calc. for $\text{C}_{26}\text{H}_{26}\text{N}^+$ $[\text{M}+\text{H}]^+$ 352.2060, found 352.2064.



1,4-dimethyl-3-phenylisoquinoline 59j: The general procedure **A** was followed using acetophenone **57f** (36.0 mg, 0.30 mmol) and prop-1-yn-1-ylbenzene **58f** (69.7 mg, 0.6 mmol). Isolation by column chromatography (*n*hexane/EtOAc: 30/1→5/1) yielded **59j** (20.9 mg, 82%) as a white solid.

M.p.: 101–103 °C.

$^1\text{H-NMR}$ (400 MHz, CDCl_3) δ 8.15 (dd, J = 8.3, 1.3, 1H), 8.04 (dd, J = 8.5, 1.2, 1H), 7.77 – 7.69 (m, 1H), 7.62 – 7.58 (m, 1H), 7.58 – 7.56 (m, 1H), 7.56 – 7.54 (m, 1H), 7.49 – 7.42 (m, 2H), 7.40 – 7.34 (m, 1H), 2.97 (s, 3H), 2.59 (s, 3H).

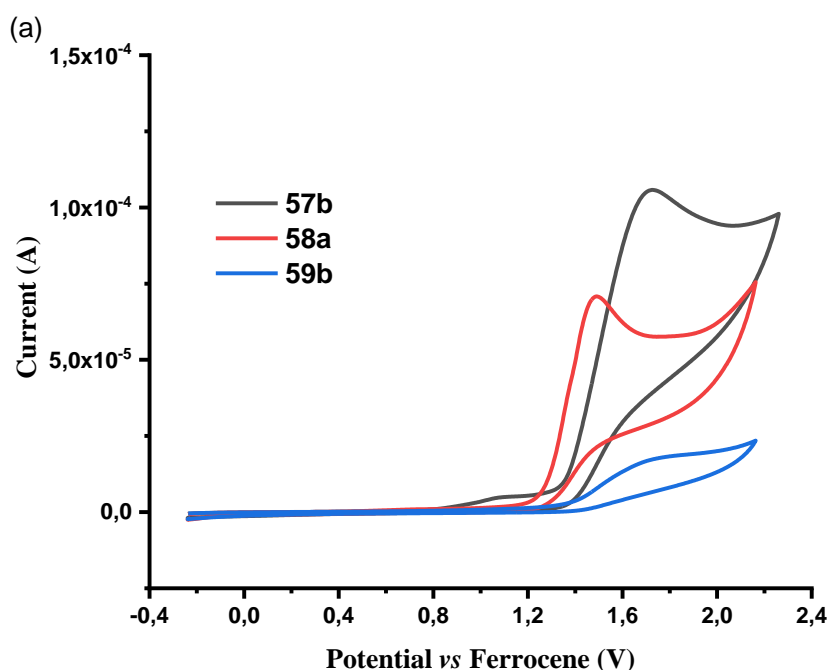
$^{13}\text{C-NMR}$ (101 MHz, CDCl_3) δ 155.85 (C_q), 150.64 (C_q), 141.59 (C_q), 136.23 (C_q), 129.84 (CH), 129.82 (CH), 128.07 (CH), 127.37 (CH), 126.21 (CH), 126.15 (C_q), 126.04 (CH), 124.11 (CH), 122.13 (C_q), 22.48 (CH_3), 15.40 (CH_3).

IR (ATR): 2948, 1610, 1560, 1437, 1387, 1336, 1019, 765, 699, 539 cm^{-1} .

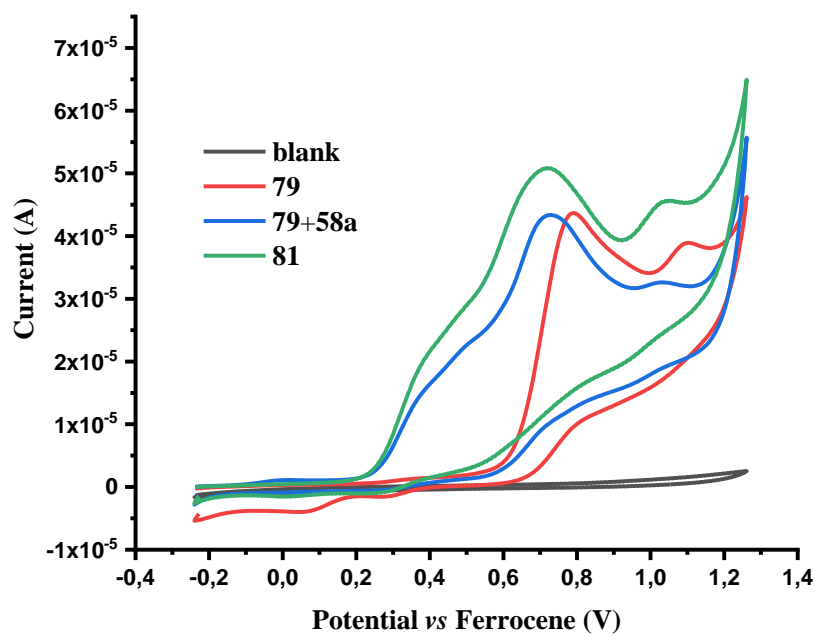
MS (ESI) m/z (relative intensity): 234 (100) $[\text{M}+\text{H}]^+$. **HR-MS** (ESI) m/z calc. for $\text{C}_{17}\text{H}_{16}\text{N}^+$ $[\text{M}+\text{H}]^+$ 234.1277, found 234.1277.

5.3.2 Cyclic Voltammetry Studies

The cyclic voltammetry measurements were carried out using a Metrohm Autolab PGSTAT204 workstation and following analysis was performed with the Nova 2.1 software. For all experiments a glassy-carbon (GC) electrode (3 mm-diameter, disc-electrode) was used as the working electrode, a Pt wire was used as the counter electrode and an Ag/Ag^+ electrode with ferrocene as an internal reference was employed. The measurements were done in 0.10 M of $n\text{Bu}_4\text{NBF}_4$ in 3.0 mL TFE and recorded at a scan rate of 100 mVs^{-1} . Substrate concentration is 5.0 mM if not indicated otherwise.



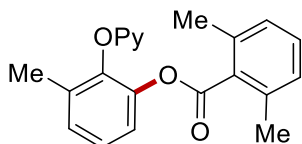
Scheme 5-1 Cyclic voltammograms for substrates and products. 57b (black), 58a (red), 59b (blue).



Scheme 5-2 Cyclic voltammograms for intermediates. blank (black), 79 (red), 79:58a = 1:1 mixture stirred for 0.5 h (blue), 81 (green).

5.4 Ruthenaelectro-Catalyzed C–H Acyloxylation for Late-stage Tyrosine and Oligopeptide Diversification

5.4.1 Characterization Data



3-methyl-2-(pyridin-2-yloxy)phenyl 2,6-dimethylbenzoate 62aa: The general procedure **C** was followed using **60a** (46.3 mg, 0.25 mmol) and **61a** (60.1 mg, 0.40 mmol). Isolation by column chromatography on silica gel (*n*hexane/EtOAc: 10:1→5:1) yielded **62aa** (72.5 mg, 87%) as a white solid.

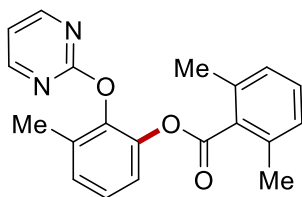
M. p. = 95–97 °C.

¹H-NMR (400 MHz, CDCl₃) δ = 8.13 (ddd, *J* = 5.0, 2.0, 0.8 Hz, 1H), 7.64 (ddd, *J* = 8.3, 7.2, 2.0 Hz, 1H), 7.28 – 7.16 (m, 4H), 7.04 – 6.98 (m, 2H), 6.95 – 6.89 (m, 2H), 2.34 (s, 6H), 2.18 (s, 3H).

¹³C-NMR (101 MHz, CDCl₃) δ = 167.9 (C_q), 162.8 (C_q), 147.8 (CH), 143.7 (C_q), 143.6 (C_q), 139.4 (CH), 135.5 (C_q), 133.7 (C_q), 132.9 (C_q), 129.7 (CH), 128.9 (CH), 127.7 (CH), 125.9 (CH), 121.1 (CH), 118.2 (CH), 110.2 (CH), 19.8 (CH₃), 16.7 (CH₃).

IR (ATR): 2966, 2924, 2868, 1742, 1595, 1426, 1231, 1055, 883, 774 cm⁻¹.

MS (ESI) *m/z* (relative intensity): 334 (90) [M+H]⁺, 356 (100) [M+Na]⁺. **HR-MS** (ESI) *m/z* calcd. for C₂₁H₂₀NO₃⁺ [M+H]⁺ 334.1438, found 334.1438.



3-methyl-2-(pyrimidin-2-yloxy)phenyl 2,6-dimethylbenzoate 62ba: The general procedure **C** was followed using **60b** (46.6 mg, 0.25 mmol) and **61a** (60.1 mg, 0.40 mmol). Isolation by column chromatography on silica gel (*n*hexane/EtOAc: 10:1→5:1) yielded **62ba** (75.1 mg, 90%) as a white solid.

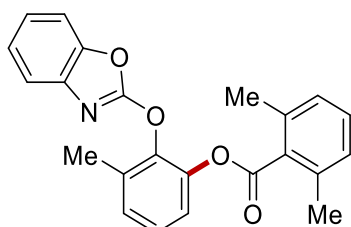
M. p. = 113–115 °C.

¹H-NMR (400 MHz, CDCl₃) δ = 8.49 (d, *J* = 4.8 Hz, 2H), 7.28 – 7.18 (m, 3H), 7.18 – 7.13 (m, 1H), 7.01 – 6.93 (m, 3H), 2.34 (s, 6H), 2.20 (s, 3H).

¹³C-NMR (101 MHz, CDCl₃) δ = 167.8 (C_q), 164.5 (C_q), 159.9 (CH), 143.2 (C_q), 143.1 (C_q), 135.6 (C_q), 133.3 (C_q), 132.8 (C_q), 129.8 (CH), 128.9 (CH), 127.7 (CH), 126.2 (CH), 121.2 (CH), 116.3 (CH), 19.9 (CH₃), 16.5 (CH₃).

IR (ATR): 1752, 1569, 1470, 1397, 1299, 1236, 1049, 900, 764 cm⁻¹.

MS (ESI) m/z (relative intensity): 357 (100) [M+Na]⁺. **HR-MS** (ESI) m/z calcd. for C₂₀H₁₈N₂O₃Na⁺ [M+Na]⁺ 357.1210, found 357.1209.



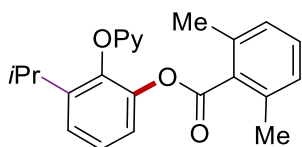
2-(benzo[d]oxazol-2-yloxy)-3-methylphenyl 2,6-dimethylbenzoate 62ca: The general procedure **C** was followed using **60c** (56.3 mg, 0.25 mmol) and **61a** (60.1 mg, 0.40 mmol). Isolation by column chromatography on silica gel (*n*hexane/EtOAc: 20:1→10:1) yielded **62ca** (65.0 mg, 70%) as a colorless oil.

¹H-NMR (400 MHz, CDCl₃) δ = 7.48 – 7.44 (m, 1H), 7.40 – 7.36 (m, 1H), 7.35 – 7.31 (m, 1H), 7.27 – 7.25 (m, 1H), 7.25 – 7.23 (m, 1H), 7.23 – 7.19 (m, 2H), 7.18 – 7.14 (m, 1H), 7.02 – 6.98 (m, 2H), 2.38 (s, 6H), 2.34 (s, 3H).

¹³C-NMR (101 MHz, CDCl₃) δ = 167.6 (C_q), 161.5 (C_q), 148.9 (C_q), 143.0 (C_q), 142.5 (C_q), 140.9 (C_q), 135.6 (C_q), 132.6 (C_q), 132.4 (C_q), 130.0 (CH), 129.3 (CH), 127.8 (CH), 127.5 (CH), 124.7 (CH), 123.5 (CH), 121.6 (CH), 119.0 (CH), 110.0 (CH), 19.8 (CH₃), 16.2 (CH₃).

IR (ATR): 2925, 1753, 1626, 1569, 1465, 1317, 1231, 1173, 1044, 749 cm⁻¹.

MS (ESI) m/z (relative intensity): 374 (10) [M+H]⁺, 396 (100) [M+Na]⁺. **HR-MS** (ESI) m/z calcd. for C₂₃H₂₀NO₄⁺ [M+H]⁺ 374.1387, found 374.1372.



3-isopropyl-2-(pyridin-2-yloxy)phenyl 2,6-dimethylbenzoate 62da: The general procedure **C** was followed using **60d** (53.3 mg, 0.25 mmol) and **61a** (60.1 mg, 0.40 mmol). Isolation by column chromatography on silica gel (*n*hexane/EtOAc: 10:1→5:1) yielded **62da** (83.1 mg, 92%) as a white solid.

M. p. = 122–124 °C.

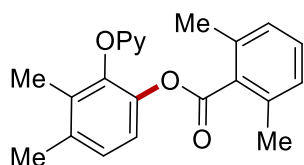
¹H-NMR (400 MHz, CDCl₃) δ = 8.12 (ddd, J = 5.0, 2.0, 0.8 Hz, 1H), 7.62 (ddd, J = 8.3, 7.2, 2.0 Hz, 1H), 7.36 – 7.31 (m, 2H), 7.23 (dd, J = 7.2, 2.5 Hz, 1H), 7.20 – 7.13 (m, 1H), 7.00

(d, $J = 7.6$, 2H), 6.94 – 6.88 (m, 2H), 3.10 (hept, $J = 6.9$ Hz, 1H), 2.30 (s, 6H), 1.19 (d, $J = 6.9$ Hz, 6H).

$^{13}\text{C-NMR}$ (101 MHz, CDCl_3) $\delta = 167.9$ (C_q), 163.4 (C_q), 147.8 (CH), 143.8 (C_q), 143.6 (C_q), 142.4 (C_q), 139.3 (CH), 135.5 (C_q), 132.9 (C_q), 129.7 (CH), 127.6 (CH), 126.2 (CH), 124.5 (CH), 120.8 (CH), 118.2 (CH), 110.1 (CH), 27.4 (CH), 23.2 (CH_3), 19.8 (CH_3).

IR (ATR): 2966, 2924, 1739, 1595, 1461, 1428, 1230, 1048, 884, 780 cm^{-1} .

MS (ESI) m/z (relative intensity): 362 (100) $[\text{M}+\text{H}]^+$, 384 (65) $[\text{M}+\text{Na}]^+$. **HR-MS** (ESI) m/z calcd. for $\text{C}_{23}\text{H}_{24}\text{NO}_3^+$ $[\text{M}+\text{H}]^+$ 362.1751, found 362.1753.



3,4-dimethyl-2-(pyridin-2-yloxy)phenyl 2,6-dimethylbenzoate 62ea: The general procedure **C** was followed using **60e** (50.0 mg, 0.25 mmol) and **61a** (60.1 mg, 0.40 mmol). Isolation by column chromatography on silica gel (*n*hexane/EtOAc: 10:1→5:1) yielded **62ea** (71.2 mg, 82%) as a white solid.

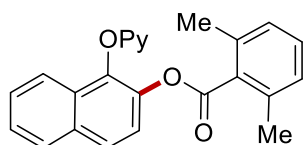
M. p. = 116–118 °C.

$^1\text{H-NMR}$ (400 MHz, CDCl_3) $\delta = 8.13$ (ddd, $J = 5.0, 2.0, 0.9$ Hz, 1H), 7.64 (ddd, $J = 8.3, 7.2, 2.0$ Hz, 1H), 7.20 – 7.15 (m, 2H), 7.12 (d, $J = 8.2$ Hz, 1H), 7.01 (d, $J = 7.6$ Hz, 2H), 6.93 – 6.90 (m, 2H), 2.36 – 2.33 (m, 9H), 2.09 (s, 3H).

$^{13}\text{C-NMR}$ (101 MHz, CDCl_3) $\delta = 168.1$ (C_q), 163.0 (C_q), 147.8 (CH), 143.3 (C_q), 141.5 (C_q), 139.3 (CH), 136.2 (C_q), 135.4 (C_q), 133.0 (C_q), 132.0 (C_q), 129.6 (CH), 127.6 (CH), 127.2 (CH), 120.1 (CH), 118.1 (CH), 110.2 (CH), 20.0 (CH_3), 19.7 (CH_3), 13.2 (CH_3).

IR (ATR): 2921, 1745, 1573, 1467, 1426, 1271, 1231, 1055, 838, 779 cm^{-1} .

MS (ESI) m/z (relative intensity): 348 (100) $[\text{M}+\text{H}]^+$, 370 (85) $[\text{M}+\text{Na}]^+$. **HR-MS** (ESI) m/z calcd. for $\text{C}_{22}\text{H}_{22}\text{NO}_3^+$ $[\text{M}+\text{H}]^+$ 348.1594, found 348.1597.



1-(pyridin-2-yloxy)naphthalen-2-yl 2,6-dimethylbenzoate 62fa: The general procedure **C** was followed using **60f** (55.3 mg, 0.25 mmol) and **61a** (60.1 mg, 0.40 mmol). Isolation by column chromatography on silica gel (*n*hexane/EtOAc: 10:1→5:1) yielded **62fa** (74.8 mg, 81%) as a white solid.

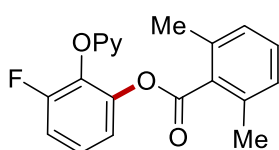
M. p. = 165–167 °C.

¹H-NMR (400 MHz, CDCl₃) δ = 8.10 (ddd, J = 5.0, 2.0, 0.8 Hz, 1H), 7.96 – 7.85 (m, 3H), 7.66 (ddd, J = 8.4, 7.2, 2.0 Hz, 1H), 7.55 – 7.44 (m, 3H), 7.22 (dd, J = 8.0, 7.3 Hz, 1H), 7.07 – 6.98 (m, 3H), 6.94 (ddd, J = 7.2, 5.0, 0.9 Hz, 1H), 2.40 (s, 6H).

¹³C-NMR (101 MHz, CDCl₃) δ = 168.0 (C_q), 163.6 (C_q), 147.9 (CH), 140.2 (C_q), 139.9 (C_q), 139.5 (CH), 135.5 (C_q), 133.0 (C_q), 132.7 (C_q), 129.8 (CH), 128.8 (C_q), 128.2 (CH), 127.7 (CH), 126.8 (CH), 126.5 (CH), 126.3 (CH), 122.3 (CH), 122.0 (CH), 118.5 (CH), 110.1 (CH), 19.8 (CH₃).

IR (ATR): 2923, 2853, 1753, 1589, 1464, 1426, 1374, 1240, 1050, 774 cm⁻¹.

MS (ESI) m/z (relative intensity): 370 (100) [M+H]⁺, 392 (50) [M+Na]⁺. **HR-MS** (ESI) m/z calcd. for C₂₄H₂₀NO₃⁺ [M+H]⁺ 370.1438, found 370.1437.



3-fluoro-2-(pyridin-2-yloxy)phenyl 2,6-dimethylbenzoate 62ga: The general procedure **C** was followed using **60g** (47.3 mg, 0.25 mmol) and **61a** (60.1 mg, 0.40 mmol). Isolation by column chromatography on silica gel (*n*hexane/EtOAc: 10:1→5:1) yielded **62ga** (75.9 mg, 90%) as a white solid.

M. p. = 113–115 °C.

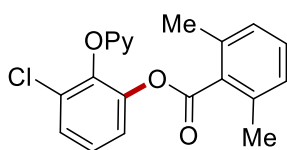
¹H-NMR (400 MHz, CDCl₃) δ = 8.13 (ddd, J = 4.9, 2.0, 0.8 Hz, 1H), 7.68 (ddd, J = 8.3, 7.2, 2.0 Hz, 1H), 7.33 – 7.25 (m, 1H), 7.25 – 7.14 (m, 3H), 7.07 – 6.96 (m, 4H), 2.39 (s, 6H).

¹³C-NMR (101 MHz, CDCl₃) δ = 167.4 (C_q), 162.1 (C_q), 156.2 (d, ¹ J_{C-F} = 250.6 Hz, C_q), 147.5 (CH), 144.7 (d, ³ J_{C-F} = 3.8 Hz, C_q), 139.5 (CH), 135.6 (C_q), 134.1 (d, ² J_{C-F} = 14.6 Hz, C_q), 132.4 (C_q), 130.0 (CH), 127.8 (CH), 125.6 (d, ³ J_{C-F} = 8.8 Hz, CH), 119.0 (d, ⁴ J_{C-F} = 2.8 Hz, CH), 119.0 (CH), 114.5 (d, ² J_{C-F} = 18.8 Hz, CH), 110.5 (CH), 19.9 (CH₃).

¹⁹F-NMR (376 MHz, CDCl₃) δ = -124.19.

IR (ATR): 2924, 1754, 1592, 1475, 1429, 1279, 1229, 1099, 1040, 772 cm⁻¹.

MS (ESI) m/z (relative intensity): 338 (100) [M+H]⁺, 360 (90) [M+Na]⁺. **HR-MS** (ESI) m/z calcd. for C₂₀H₁₇FNO₃⁺ [M+H]⁺ 338.1187, found 338.1189.



3-chloro-2-(pyridin-2-yloxy)phenyl 2,6-dimethylbenzoate 62ha: The general procedure **C** was followed using **60h** (51.3 mg, 0.25 mmol) and **61a** (60.1 mg, 0.40 mmol). Isolation by

column chromatography on silica gel (*n*hexane/EtOAc: 10:1→5:1) yielded **62ha** (58.4 mg, 66%) as a white solid.

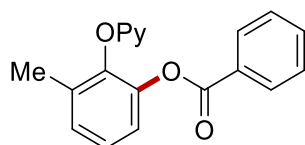
M. p. = 121–123 °C.

¹H-NMR (400 MHz, CDCl₃) δ = 8.11 (ddd, *J* = 5.0, 2.0, 0.8 Hz, 1H), 7.68 (ddd, *J* = 8.3, 7.2, 2.0 Hz, 1H), 7.43 (dd, *J* = 6.2, 3.4 Hz, 1H), 7.32 – 7.26 (m, 2H), 7.23 – 7.17 (m, 1H), 7.04 – 6.95 (m, 4H), 2.34 (s, 6H).

¹³C-NMR (101 MHz, CDCl₃) δ = 167.5 (C_q), 162.2 (C_q), 147.6 (CH), 145.0 (C_q), 142.4 (C_q), 139.6 (CH), 135.6 (C_q), 132.4 (C_q), 130.0 (CH), 129.7 (C_q), 128.1 (CH), 127.8 (CH), 126.2 (CH), 122.3 (CH), 118.8 (CH), 110.6 (CH), 19.8 (CH₃).

IR (ATR): 2923, 1749, 1575, 1464, 1427, 1228, 1172, 1043, 880, 771 cm⁻¹.

MS (ESI) *m/z* (relative intensity): 354 (100) [M+H]⁺, 376 (90) [M+Na]⁺. **HR-MS** (ESI) *m/z* calcd. for C₂₀H₁₇ClNO₃⁺ [M+H]⁺ 354.0891, found 354.0894.



3-methyl-2-(pyridin-2-yloxy)phenyl benzoate 62ab: The general procedure **C/D** was followed using **60a** (46.3 mg, 0.25 mmol) and **61b** (48.8 mg, 0.40 mmol). Isolation by column chromatography on silica gel (*n*hexane/EtOAc: 10:1→5:1) yielded **62ab** (51.9 mg, 68%, procedure **C**) (45.7 mg, 60%, procedure **D**) as a white solid.

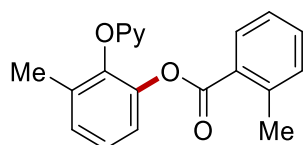
M. p. = 82–88 °C.

¹H-NMR (400 MHz, CDCl₃) δ = 8.12 (ddd, *J* = 5.0, 2.0, 0.8 Hz, 1H), 7.86 – 7.79 (m, 2H), 7.57 – 7.49 (m, 2H), 7.38 – 7.31 (m, 2H), 7.24 – 7.18 (m, 3H), 6.92 – 6.87 (m, 1H), 6.84 – 6.79 (m, 1H), 2.27 (s, 3H).

¹³C-NMR (101 MHz, CDCl₃) δ = 164.4 (C_q), 163.0 (C_q), 147.7 (CH), 143.7 (C_q), 143.4 (C_q), 139.3 (CH), 133.5 (CH), 133.2 (C_q), 130.1 (CH), 129.2 (C_q), 128.6 (CH), 128.4 (CH), 125.5 (CH), 121.2 (CH), 118.2 (CH), 110.4 (CH), 16.5 (CH₃).

IR (ATR): 3031, 2924, 1731, 1597, 1464, 1427, 1264, 1237, 1063, 774 cm⁻¹.

MS (ESI) *m/z* (relative intensity): 306 (100) [M+H]⁺, 328 (65) [M+Na]⁺. **HR-MS** (ESI) *m/z* calcd. for C₁₉H₁₆NO₃⁺ [M+H]⁺ 306.1125, found 306.1122.



3-methyl-2-(pyridin-2-yloxy)phenyl 2-methylbenzoate 62ac: The general procedure **C** was followed using **60a** (46.3 mg, 0.25 mmol) and **61c** (54.4 mg, 0.40 mmol). Isolation by column chromatography on silica gel (*n*hexane/EtOAc: 10:1→5:1) yielded **62ac** (48.7 mg, 61%) as a white solid.

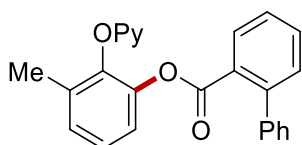
M. p. = 90–92 °C.

¹H-NMR (400 MHz, CDCl₃) δ = 8.13 (ddd, *J* = 5.0, 2.0, 0.8 Hz, 1H), 7.62 – 7.53 (m, 2H), 7.40 – 7.34 (m, 1H), 7.24 – 7.19 (m, 3H), 7.17 (dd, *J* = 6.9, 2.9 Hz, 1H), 7.12 – 7.06 (m, 1H), 6.91 (ddd, *J* = 7.2, 5.0, 1.0 Hz, 1H), 6.85 – 6.82 (m, 1H), 2.53 (s, 3H), 2.25 (s, 3H).

¹³C-NMR (101 MHz, CDCl₃) δ = 165.0 (C_q), 163.0 (C_q), 147.8 (CH), 143.8 (C_q), 143.5 (C_q), 141.4 (C_q), 139.4 (CH), 133.4 (C_q), 132.6 (CH), 131.8 (CH), 131.1 (CH), 128.6 (CH), 128.2 (C_q), 125.7 (CH), 125.6 (CH), 121.3 (CH), 118.3 (CH), 110.4 (CH), 21.8 (CH₃), 16.6 (CH₃).

IR (ATR): 3054, 2921, 1734, 1570, 1464, 1427, 1232, 1187, 1042, 775 cm⁻¹.

MS (ESI) *m/z* (relative intensity): 320 (100) [M+H]⁺, 342 (40) [M+Na]⁺. **HR-MS** (ESI) *m/z* calcd. for C₂₀H₁₈NO₃⁺ [M+H]⁺ 320.1281, found 320.1285.



3-methyl-2-(pyridin-2-yloxy)phenyl [1,1'-biphenyl]-2-carboxylate 62ad: The general procedure **D** was followed using **60a** (46.3 mg, 0.25 mmol) and **61d** (79.3 mg, 0.40 mmol). Isolation by column chromatography on silica gel (*n*hexane/EtOAc: 10:1→5:1) yielded **62ad** (53.4 mg, 56%) as a white solid.

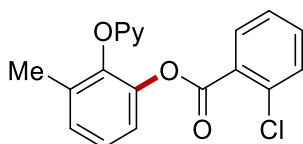
M. p. = 176–178 °C.

¹H-NMR (400 MHz, CDCl₃) δ = 8.14 (ddd, *J* = 5.0, 2.0, 0.8 Hz, 1H), 7.64 – 7.54 (m, 2H), 7.50 (ddd, *J* = 7.6, 7.6, 1.4 Hz, 1H), 7.39 – 7.27 (m, 7H), 7.15 – 7.08 (m, 2H), 6.94 (ddd, *J* = 7.2, 5.0, 0.9 Hz, 1H), 6.91 – 6.86 (m, 1H), 6.86 – 6.82 (m, 1H), 2.18 (s, 3H).

¹³C-NMR (101 MHz, CDCl₃) δ = 165.7 (C_q), 163.0 (C_q), 147.8 (CH), 143.6 (C_q), 143.4 (C_q), 143.4 (C_q), 141.0 (C_q), 139.4 (CH), 133.2 (C_q), 131.7 (CH), 131.0 (CH), 139.1 (CH), 129.6 (C_q), 128.7 (CH), 128.5 (CH), 128.1 (CH), 127.4 (CH), 127.1 (CH), 125.5 (CH), 120.8 (CH), 118.2 (CH), 110.2 (CH), 16.5 (CH₃).

IR (ATR): 3059, 2922, 1740, 1570, 1464, 1427, 1232, 1187, 1042, 752 cm⁻¹.

MS (ESI) *m/z* (relative intensity): 382 (100) [M+H]⁺, 404 (30) [M+Na]⁺. **HR-MS** (ESI) *m/z* calcd. for C₂₅H₂₀NO₃⁺ [M+H]⁺ 382.1438, found 382.1440.



3-methyl-2-(pyridin-2-yloxy)phenyl 2-chlorobenzoate 62ae: The general procedure **C** was followed using **60a** (46.3 mg, 0.25 mmol) and **61e** (62.4 mg, 0.40 mmol). Isolation by column chromatography on silica gel (*n*hexane/EtOAc: 10:1→5:1) yielded **62ae** (46.7 mg, 55%) as a white solid.

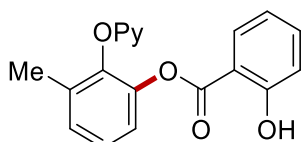
M. p. = 100–102 °C.

¹H-NMR (400 MHz, CDCl₃) δ = 8.12 (ddd, J = 5.0, 2.0, 0.8 Hz, 1H), 7.59 (ddd, J = 8.3, 7.2, 2.0 Hz, 1H), 7.55 – 7.50 (m, 1H), 7.44 – 7.34 (m, 2H), 7.24 – 7.20 (m, 3H), 7.17 (ddd, J = 7.8, 6.8, 1.7 Hz, 1H), 6.92 (ddd, J = 7.2, 5.0, 0.9 Hz, 1H), 6.89 – 6.86 (m, 1H), 2.24 (s, 3H).

¹³C-NMR (101 MHz, CDCl₃) δ = 163.0 (C_q), 162.9 (C_q), 147.8 (CH), 143.5 (C_q), 143.3 (C_q), 139.4 (CH), 134.6 (C_q), 133.4 (C_q), 133.1 (CH), 131.8 (CH), 131.3 (CH), 128.8 (CH), 128.8 (C_q), 126.5 (CH), 125.6 (CH), 121.1 (CH), 118.3 (CH), 110.3 (CH), 16.5 (CH₃).

IR (ATR): 2927, 2853, 1718, 1591, 1467, 1425, 1273, 1233, 1109, 774 cm⁻¹.

MS (ESI) m/z (relative intensity): 340 (100) [M+H]⁺, 362 (30) [M+Na]⁺. **HR-MS** (ESI) m/z calcd. for C₁₉H₁₅³⁵ClNO₃⁺ [M+H]⁺ 340.0735, found 340.0742.



3-methyl-2-(pyridin-2-yloxy)phenyl 2-hydroxybenzoate 62af: The general procedure **C** was followed using **60a** (46.3 mg, 0.25 mmol) and **61f** (55.2 mg, 0.40 mmol). Isolation by column chromatography on silica gel (*n*hexane/EtOAc: 10:1→5:1) yielded **62af** (57.0 mg, 71%) as a white solid.

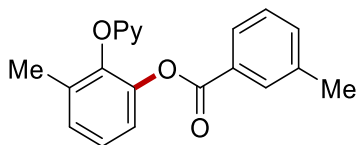
M. p. = 111–113 °C.

¹H-NMR (400 MHz, CDCl₃) δ = 10.37 (s, 1H), 8.11 (ddd, J = 5.0, 2.0, 0.8 Hz, 1H), 7.55 (ddd, J = 8.3, 7.2, 2.0 Hz, 1H), 7.49 – 7.40 (m, 2H), 7.26 – 7.16 (m, 3H), 6.96 (ddd, J = 8.4, 1.2, 0.5 Hz, 1H), 6.90 (ddd, J = 7.2, 5.0, 0.9 Hz, 1H), 6.86 – 6.82 (m, 1H), 6.73 (ddd, J = 8.0, 7.2, 1.1 Hz, 1H), 2.28 (s, 3H).

¹³C-NMR (101 MHz, CDCl₃) δ = 168.2 (C_q), 162.8 (C_q), 162.0 (C_q), 147.6 (CH), 143.6 (C_q), 142.6 (C_q), 139.5 (CH), 136.4 (CH), 133.5 (C_q), 130.2 (CH), 129.0 (CH), 125.5 (CH), 121.0 (CH), 119.3 (CH), 118.4 (CH), 117.6 (CH), 111.6 (C_q), 110.4 (CH), 16.5 (CH₃).

IR (ATR): 3271, 2920, 1686, 1573, 1461, 1425, 1230, 1154, 1064, 778 cm⁻¹.

MS (ESI) m/z (relative intensity): 322 (100) $[M+H]^+$, 344 (90) $[M+Na]^+$. **HR-MS** (ESI) m/z calcd. for $C_{19}H_{16}NO_4^+$ $[M+H]^+$ 322.1074, found 322.1074.



3-methyl-2-(pyridin-2-yloxy)phenyl 3-methylbenzoate 62ag: The general procedure **C/D** was followed using **60a** (46.3 mg, 0.25 mmol) and **61g** (54.4 mg, 0.40 mmol). Isolation by column chromatography on silica gel (*n*hexane/EtOAc: 10:1→5:1) yielded **62ag** (52.7 mg, 66%, procedure **C**) (45.6 mg, 57%, procedure **D**) as a white solid.

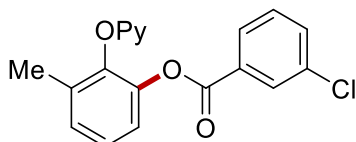
M. p. = 70–73 °C.

¹H-NMR (400 MHz, $CDCl_3$) δ = 8.14 (ddd, J = 5.0, 2.0, 0.8 Hz, 1H), 7.65 – 7.61 (m, 1H), 7.60 – 7.52 (m, 2H), 7.35 – 7.31 (m, 1H), 7.27 – 7.17 (m, 4H), 6.91 (ddd, J = 7.1, 5.0, 1.0 Hz, 1H), 6.84 – 6.81 (m, 1H), 2.31 (s, 3H), 2.27 (s, 3H).

¹³C-NMR (101 MHz, $CDCl_3$) δ = 164.6 (C_q), 163.0 (C_q), 147.7 (CH), 143.7 (C_q), 143.4 (C_q), 139.3 (CH), 138.1 (C_q), 134.2 (CH), 133.2 (C_q), 130.6 (CH), 129.1 (C_q), 128.5 (CH), 128.3 (CH), 127.2 (CH), 125.5 (CH), 121.2 (CH), 118.2 (CH), 110.4 (CH), 21.3 (CH_3), 16.5 (CH_3).

IR (ATR): 2922, 1732, 1590, 1463, 1426, 1268, 1183, 1066, 883, 737 cm^{-1} .

MS (ESI) m/z (relative intensity): 320 (100) $[M+H]^+$, 342 (50) $[M+Na]^+$. **HR-MS** (ESI) m/z calcd. for $C_{20}H_{18}NO_3^+$ $[M+H]^+$ 320.1281, found 320.1282.



3-methyl-2-(pyridin-2-yloxy)phenyl 3-chlorobenzoate 62ah: The general procedure **C** was followed using **60a** (46.3 mg, 0.25 mmol) and **61h** (62.4 mg, 0.40 mmol). Isolation by column chromatography on silica gel (*n*hexane/EtOAc: 10:1→5:1) yielded **62ah** (62.9 mg, 74%) as a white solid.

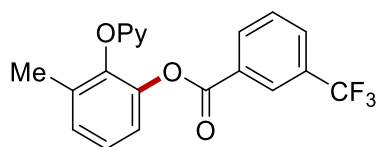
M. p. = 75–77 °C.

¹H-NMR (400 MHz, $CDCl_3$) δ = 8.13 (ddd, J = 4.9, 2.0, 0.8 Hz, 1H), 7.75 – 7.67 (m, 2H), 7.57 (ddd, J = 8.3, 7.2, 2.0 Hz, 1H), 7.49 (ddd, J = 7.9, 2.2, 1.1 Hz, 1H), 7.29 (dd, J = 7.9, 7.9 Hz, 1H), 7.24 – 7.17 (m, 3H), 6.92 (ddd, J = 7.2, 5.0, 0.9 Hz, 1H), 6.85 – 6.81 (m, 1H), 2.27 (s, 3H).

¹³C-NMR (101 MHz, CDCl₃) δ = 163.2 (C_q), 162.9 (C_q), 147.7 (CH), 143.5 (C_q), 143.1 (C_q), 139.5 (CH), 134.5 (C_q), 133.5 (CH), 133.3 (C_q), 131.0 (C_q), 130.0 (CH), 129.7 (CH), 128.8 (CH), 128.2 (CH), 125.5 (CH), 121.0 (CH), 118.4 (CH), 110.4 (CH), 16.5 (CH₃).

IR (ATR): 3017, 2924, 1744, 1572, 1464, 1425, 1231, 1188, 1059, 833 cm⁻¹.

MS (ESI) *m/z* (relative intensity): 340 (100) [M+H]⁺, 362 (50) [M+Na]⁺. **HR-MS** (ESI) *m/z* calcd. for C₁₉H₁₅³⁵ClNO₃⁺ [M+H]⁺ 340.0735, found 340.0739.



3-methyl-2-(pyridin-2-yloxy)phenyl 3-(trifluoromethyl)benzoate 62ai: The general procedure **C/D** was followed using **60a** (46.3 mg, 0.25 mmol) and **61i** (76.0 mg, 0.40 mmol). Isolation by column chromatography on silica gel (*n*hexane/EtOAc: 10:1→5:1) yielded **62ai** (75.6 mg, 81%) as a yellow oil.

¹H-NMR (400 MHz, CDCl₃) δ = 8.11 (ddd, *J* = 5.0, 2.0, 0.8 Hz, 1H), 8.07 – 8.03 (m, 1H), 7.99 – 7.96 (m, 1H), 7.80 – 7.76 (m, 1H), 7.57 – 7.48 (m, 2H), 7.25 – 7.21 (m, 3H), 6.90 (ddd, *J* = 7.2, 5.0, 0.9 Hz, 1H), 6.84 – 6.80 (m, 1H), 2.29 (s, 3H).

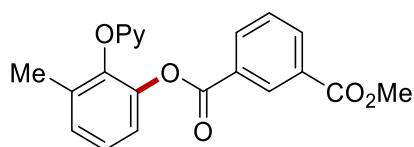
¹³C-NMR (101 MHz, CDCl₃) δ = 163.1 (C_q), 162.9 (C_q), 147.7 (CH), 143.5 (C_q), 143.1 (C_q), 139.5 (CH), 133.4 (C_q), 133.3 (CH), 131.1 (q, ²*J*_{C-F} = 33.0 Hz, C_q), 130.2 (C_q), 130.0 (q, ³*J*_{C-F} = 3.6 Hz, CH), 129.1 (CH), 128.9 (CH), 126.8 (q, ³*J*_{C-F} = 3.9 Hz, CH), 125.5 (CH), 123.6 (d, ¹*J*_{C-F} = 272.8 Hz, C_q), 121.0 (CH), 118.5 (CH), 110.3 (CH), 16.4 (CH₃).

¹⁹F-NMR (376 MHz, CDCl₃) δ = -62.81.

IR (ATR): 3076, 2925, 1747, 1595, 1465, 1428, 1335, 1230, 1129, 748 cm⁻¹.

MS (ESI) *m/z* (relative intensity): 374 (100) [M+H]⁺, 396 (50) [M+Na]⁺. **HR-MS** (ESI) *m/z* calcd. for C₂₀H₁₅F₃NO₃⁺ [M+H]⁺ 374.0999, found 374.1004.

The spectral data were in accordance with those reported in the literature.³



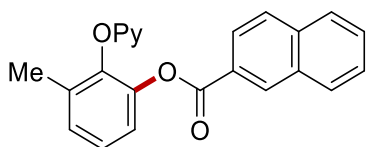
methyl (3-methyl-2-(pyridin-2-yloxy)phenyl) isophthalate 62aj: The general procedure **D** was followed using **60a** (46.3 mg, 0.25 mmol) and **61j** (72.1 mg, 0.40 mmol). Isolation by column chromatography on silica gel (*n*hexane/EtOAc: 10:1→5:1) yielded **62aj** (52.7 mg, 58%) as a yellow oil.

¹H-NMR (400 MHz, CDCl₃) δ = 8.47 (ddd, J = 1.8, 1.8, 0.6 Hz, 1H), 8.21 – 8.17 (m, 1H), 8.10 (ddd, J = 5.0, 2.1, 0.8 Hz, 1H), 8.03 – 7.96 (m, 1H), 7.54 – 7.50 (m, 1H), 7.45 – 7.41 (m, 1H), 7.25 – 7.17 (m, 3H), 6.87 (ddd, J = 7.2, 5.0, 0.9 Hz, 1H), 6.83 – 6.79 (m, 1H), 3.92 (s, 3H), 2.26 (s, 3H).

¹³C-NMR (101 MHz, CDCl₃) δ = 166.1 (C_q), 163.6 (C_q), 162.9 (C_q), 147.7 (CH), 143.6 (C_q), 143.3 (C_q), 139.4 (CH), 134.4 (CH), 134.2 (CH), 133.4 (C_q), 131.2 (CH), 130.7 (C_q), 129.7 (C_q), 128.8 (CH), 128.7 (CH), 125.5 (CH), 121.1 (CH), 118.3 (CH), 110.3 (CH), 52.4 (CH₃), 16.5 (CH₃).

IR (ATR): 3076, 2952, 1723, 1589, 1464, 1427, 1223, 1187, 1065, 774 cm⁻¹.

MS (ESI) m/z (relative intensity): 364 (100) [M+H]⁺, 386 (20) [M+Na]⁺. **HR-MS** (ESI) m/z calcd. for C₂₁H₁₈NO₅⁺ [M+H]⁺ 364.1179, found 364.1179.



3-methyl-2-(pyridin-2-yloxy)phenyl 2-naphthoate 62ak: The general procedure **C** was followed using **60a** (46.3 mg, 0.25 mmol) and **61k** (68.8 mg, 0.40 mmol). Isolation by column chromatography on silica gel (*n*hexane/EtOAc: 10:1→5:1) yielded **62ak** (48.8 mg, 55%) as a white solid.

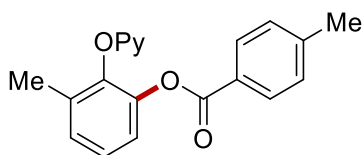
M. p. = 140–142 °C.

¹H-NMR (400 MHz, CDCl₃) δ = 8.30 (s, 1H), 8.19 – 8.14 (m, 1H), 7.90 – 7.83 (m, 2H), 7.82 – 7.77 (m, 2H), 7.59 (ddd, J = 8.2, 6.9, 1.3 Hz, 1H), 7.56 – 7.48 (m, 2H), 7.29 – 7.21 (m, 3H), 6.93 – 6.89 (m, 1H), 6.84 – 6.80 (m, 1H), 2.30 (s, 3H).

¹³C-NMR (101 MHz, CDCl₃) δ = 164.6 (C_q), 163.1 (C_q), 147.7 (CH), 143.7 (C_q), 143.5 (C_q), 139.4 (CH), 135.8 (C_q), 133.3 (C_q), 132.4 (C_q), 131.8 (CH), 129.5 (CH), 128.6 (CH), 128.6 (CH), 128.2 (CH), 127.9 (CH), 126.8 (CH), 126.4 (C_q), 125.5 (CH), 125.4 (CH), 121.2 (CH), 118.3 (CH), 110.5 (CH), 16.5 (CH₃).

IR (ATR): 3052, 2921, 1726, 1571, 1463, 1424, 1227, 1183, 1073, 762 cm⁻¹.

MS (ESI) m/z (relative intensity): 356 (100) [M+H]⁺, 378 (60) [M+Na]⁺. **HR-MS** (ESI) m/z calcd. for C₂₃H₁₈NO₃⁺ [M+H]⁺ 356.1281, found 356.1282.



3-methyl-2-(pyridin-2-yloxy)phenyl 4-methylbenzoate 62aI: The general procedure **C** was followed using **60a** (46.3 mg, 0.25 mmol) and **61I** (54.4 mg, 0.40 mmol). Isolation by column chromatography on silica gel (*n*hexane/EtOAc: 10:1→5:1) yielded **62aI** (50.3 mg, 63%) as a white solid.

M. p. = 107–109 °C.

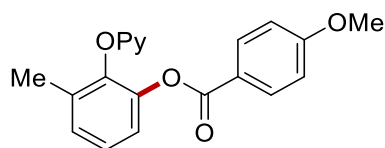
¹H-NMR (400 MHz, CDCl₃) δ = 8.13 (ddd, *J* = 5.0, 2.0, 0.8 Hz, 1H), 7.74 – 7.68 (m, 2H), 7.54 (ddd, *J* = 8.3, 7.2, 2.0 Hz, 1H), 7.23 – 7.17 (m, 3H), 7.16 – 7.12 (m, 2H), 6.90 (ddd, *J* = 7.2, 4.9, 0.9 Hz, 1H), 6.83 – 6.80 (m, 1H), 2.38 (s, 3H), 2.27 (s, 3H).

¹³C-NMR (101 MHz, CDCl₃) δ = 164.5 (C_q), 163.0 (C_q), 147.7 (CH), 144.3 (C_q), 143.7 (C_q), 143.5 (C_q), 139.3 (CH), 133.2 (C_q), 130.1 (CH), 129.1 (CH), 128.5 (CH), 126.4 (C_q), 125.5 (CH), 121.2 (CH), 118.2 (CH), 110.4 (CH), 21.8 (CH₃), 16.5 (CH₃).

IR (ATR): 2922, 2853, 1732, 1573, 1426, 1233, 1176, 1072, 881, 745 cm⁻¹.

MS (ESI) *m/z* (relative intensity): 320 (100) [M+H]⁺, 342 (60) [M+Na]⁺. **HR-MS** (ESI) *m/z* calcd. for C₂₀H₁₈NO₃⁺ [M+H]⁺ 320.1281, found 320.1283.

The spectral data were in accordance with those reported in the literature.^[180]



3-methyl-2-(pyridin-2-yloxy)phenyl 4-methoxybenzoate 62aM: The general procedure **C** was followed using **60a** (46.3 mg, 0.25 mmol) and **61m** (60.9 mg, 0.40 mmol). Isolation by column chromatography on silica gel (*n*hexane/EtOAc: 10:1→5:1) yielded **62aM** (48.6 mg, 58%) as a white solid.

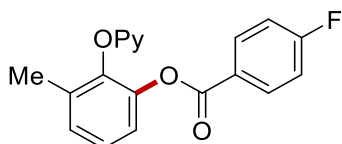
M. p. = 120–122 °C.

¹H-NMR (400 MHz, CDCl₃) δ = 8.12 (ddd, *J* = 5.0, 2.0, 0.8 Hz, 1H), 7.80 – 7.74 (m, 2H), 7.54 (ddd, *J* = 8.3, 7.2, 2.0 Hz, 1H), 7.23 – 7.15 (m, 3H), 6.89 (ddd, *J* = 7.2, 5.0, 0.9 Hz, 1H), 6.84 – 6.78 (m, 3H), 3.83 (s, 3H), 2.26 (s, 3H).

¹³C-NMR (101 MHz, CDCl₃) δ = 164.1 (C_q), 163.8 (C_q), 163.0 (C_q), 147.7 (CH), 143.8 (C_q), 143.5 (C_q), 139.3 (CH), 133.1 (C_q), 132.2 (CH), 128.4 (CH), 125.4 (CH), 121.5 (C_q), 121.3 (CH), 118.2 (CH), 113.6 (CH), 110.4 (CH), 55.5 (CH₃), 16.5 (CH₃).

IR (ATR): 2923, 2853, 1722, 1604, 1463, 1426, 1234, 1160, 1073, 760 cm⁻¹.

MS (ESI) *m/z* (relative intensity): 336 (100) [M+H]⁺, 358 (90) [M+Na]⁺. **HR-MS** (ESI) *m/z* calcd. for C₂₀H₁₈NO₄⁺ [M+H]⁺ 336.1230, found 336.1232. The spectral data were in accordance with those reported in the literature.^[180]



3-methyl-2-(pyridin-2-yloxy)phenyl 4-fluorobenzoate 62an: The general procedure **C** was followed using **60a** (46.3 mg, 0.25 mmol) and **61n** (56.0 mg, 0.40 mmol). Isolation by column chromatography on silica gel (*n*hexane/EtOAc: 10:1→5:1) yielded **62an** (55.0 mg, 68%) as a white solid.

M. p. = 110–112 °C.

¹H-NMR (400 MHz, CDCl₃) δ = 8.12 (ddd, *J* = 5.0, 2.0, 0.8 Hz, 1H), 7.86 – 7.80 (m, 2H), 7.55 (ddd, *J* = 8.3, 7.2, 2.0 Hz, 1H), 7.23 – 7.16 (m, 3H), 7.04 – 6.98 (m, 2H), 6.90 (ddd, *J* = 7.2, 5.0, 0.9 Hz, 1H), 6.82 – 6.80 (m, 1H), 2.26 (s, 3H).

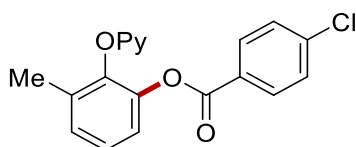
¹³C-NMR (101 MHz, CDCl₃) δ = 166.1 (d, ¹*J*_{C-F} = 254.8 Hz, C_q), 163.4 (C_q), 162.9 (C_q), 147.7 (CH), 143.6 (C_q), 143.3 (C_q), 139.4 (CH), 133.3 (C_q), 132.7 (d, ³*J*_{C-F} = 9.5 Hz, CH), 128.7 (CH), 125.5 (CH), 125.4 (d, ⁴*J*_{C-F} = 3.0 Hz, C_q), 121.1 (CH), 118.3 (CH), 115.6 (d, ²*J*_{C-F} = 22.1 Hz, CH), 110.3 (CH), 16.5 (CH₃).

¹⁹F-NMR (376 MHz, CDCl₃) δ = -104.63.

IR (ATR): 3065, 2926, 1732, 1572, 1427, 1235, 1187, 1072, 855, 756 cm⁻¹.

MS (ESI) *m/z* (relative intensity): 324 (100) [M+H]⁺, 346 (60) [M+Na]⁺. **HR-MS** (ESI) *m/z* calcd. for C₁₉H₁₅FNO₃⁺ [M+H]⁺ 324.1030, found 324.1034.

The spectral data were in accordance with those reported in the literature.^[180]



3-methyl-2-(pyridin-2-yloxy)phenyl 4-chlorobenzoate 62ao: The general procedure **C** was followed using **60a** (46.3 mg, 0.25 mmol) and **61o** (62.6 mg, 0.40 mmol). Isolation by column chromatography on silica gel (*n*hexane/EtOAc: 10:1→5:1) yielded **62ao** (50.9 mg, 60%) as a white solid.

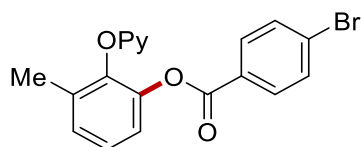
M. p. = 125–127 °C.

¹H-NMR (400 MHz, CDCl₃) δ = 8.11 (ddd, *J* = 5.0, 2.0, 0.8 Hz, 1H), 7.77 – 7.71 (m, 2H), 7.56 (ddd, *J* = 8.3, 7.2, 2.0 Hz, 1H), 7.34 – 7.28 (m, 2H), 7.24 – 7.15 (m, 3H), 6.91 (ddd, *J* = 7.2, 5.0, 0.9 Hz, 1H), 6.83 – 6.79 (m, 1H), 2.26 (s, 3H).

¹³C-NMR (101 MHz, CDCl₃) δ = 163.6 (C_q), 162.9 (C_q), 147.7 (CH), 143.6 (C_q), 143.2 (C_q), 140.0 (C_q), 139.4 (CH), 133.3 (C_q), 131.4 (CH), 128.8 (CH), 128.7 (CH), 127.7 (C_q), 125.5 (CH), 121.1 (CH), 118.3 (CH), 110.3 (CH), 16.5 (CH₃).

IR (ATR): 2923, 2852, 1733, 1590, 1465, 1428, 1266, 1067, 1011, 752 cm⁻¹.

MS (ESI) *m/z* (relative intensity): 340 (100) [M+H]⁺, 362 (65) [M+Na]⁺. **HR-MS** (ESI) *m/z* calcd. for C₁₉H₁₅³⁵ClNO₃⁺ [M+H]⁺ 340.0735, found 340.0737.



3-methyl-2-(pyridin-2-yloxy)phenyl 4-bromobenzoate 62ap: The general procedure **C** was followed using **60a** (46.3 mg, 0.25 mmol) and **61p** (80.4 mg, 0.40 mmol). Isolation by column chromatography on silica gel (*n*hexane/EtOAc: 10:1→5:1) yielded **62ap** (68.2 mg, 71%) as a white solid.

M. p. = 120–122 °C.

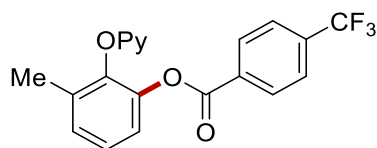
¹H-NMR (400 MHz, CDCl₃) δ = 8.11 (ddd, *J* = 5.0, 2.0, 0.8 Hz, 1H), 7.69 – 7.64 (m, 2H), 7.56 (ddd, *J* = 8.3, 7.2, 2.0 Hz, 1H), 7.51 – 7.45 (m, 2H), 7.24 – 7.16 (m, 3H), 6.91 (ddd, *J* = 7.2, 5.0, 0.9 Hz, 1H), 6.83 – 6.79 (m, 1H), 2.26 (s, 3H).

¹³C-NMR (101 MHz, CDCl₃) δ = 163.7 (C_q), 162.9 (C_q), 147.7 (CH), 143.5 (C_q), 143.2 (C_q), 139.4 (CH), 133.3 (C_q), 131.8 (CH), 131.5 (CH), 128.7 (CH), 128.7 (C_q), 128.1 (C_q), 125.5 (CH), 121.0 (CH), 118.3 (CH), 110.3 (CH), 16.5 (CH₃).

IR (ATR): 3200, 2957, 1648, 1511, 1247, 1178, 1035, 804 cm⁻¹.

MS (ESI) *m/z* (relative intensity): 384 (100) [M+H]⁺, 406 (80) [M+Na]⁺, 791 (30) [2M+Na]⁺.

HR-MS (ESI) *m/z* calcd. for C₁₉H₁₅⁷⁹BrNO₃⁺ [M+H]⁺ 384.0230, found 384.0227.



3-methyl-2-(pyridin-2-yloxy)phenyl 4-(trifluoromethyl)benzoate 62aq: The general procedure **C** was followed using **60a** (46.3 mg, 0.25 mmol) and **61q** (76.0 mg, 0.40 mmol). Isolation by column chromatography on silica gel (*n*hexane/EtOAc: 10:1→5:1) yielded **62aq** (71.9 mg, 77%) as a white solid.

M. p. = 90–92 °C.

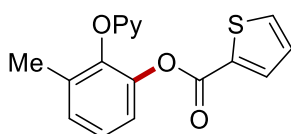
¹H-NMR (400 MHz, CDCl₃) δ = 8.12 (ddd, J = 5.0, 2.0, 0.8 Hz, 1H), 7.96 – 7.91 (m, 2H), 7.64 – 7.59 (m, 2H), 7.56 (ddd, J = 8.3, 7.2, 2.0 Hz, 1H), 7.25 – 7.19 (m, 3H), 6.91 (ddd, J = 7.2, 5.0, 1.0 Hz, 1H), 6.84 – 6.80 (m, 1H), 2.27 (s, 3H).

¹³C-NMR (101 MHz, CDCl₃) δ = 163.3 (C_q), 162.9 (C_q), 147.8 (CH), 143.5 (C_q), 143.2 (C_q), 139.5 (CH), 134.9 (q, $^2J_{C-F}$ = 32.7 Hz, C_q), 133.4 (C_q), 132.5 (C_q), 130.4 (CH), 128.9 (CH), 125.6 (CH), 125.5 (q, $^3J_{C-F}$ = 3.7 Hz, CH), 123.6 (d, $^1J_{C-F}$ = 272.6 Hz, C_q), 121.0 (CH), 118.4 (CH), 110.3 (CH), 16.5 (CH₃).

¹⁹F-NMR (376 MHz, CDCl₃) δ = -63.19.

IR (ATR): 2925, 2853, 1752, 1573, 1426, 1234, 1074, 1014, 857, 763 cm⁻¹.

MS (ESI) m/z (relative intensity): 374 (100) [M+H]⁺, 396 (75) [M+Na]⁺. **HR-MS** (ESI) m/z calcd. for C₂₀H₁₅F₃NO₃⁺ [M+H]⁺ 374.0999, found 374.0998.



3-methyl-2-(pyridin-2-yloxy)phenyl thiophene-2-carboxylate 62ar: The general procedure **C** was followed using **60a** (46.3 mg, 0.25 mmol) and **61r** (51.3 mg, 0.40 mmol). Isolation by column chromatography on silica gel (*n*hexane/EtOAc: 10:1→5:1) yielded **62ar** (45.5 mg, 59%) as a brown solid.

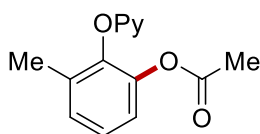
M. p. = 57–63 °C.

¹H-NMR (400 MHz, CDCl₃) δ = 8.11 (ddd, J = 5.0, 2.0, 0.8 Hz, 1H), 7.63 (dd, J = 3.8, 1.3 Hz, 1H), 7.56 (ddd, J = 8.3, 7.2, 2.0 Hz, 1H), 7.52 (dd, J = 5.0, 1.3 Hz, 1H), 7.23 – 7.18 (m, 3H), 7.02 (dd, J = 5.0, 3.8 Hz, 1H), 6.90 (ddd, J = 7.2, 5.0, 0.9 Hz, 1H), 6.85 – 6.83 (m, 1H), 2.26 (s, 3H).

¹³C-NMR (101 MHz, CDCl₃) δ = 162.9 (C_q), 159.8 (C_q), 147.7 (CH), 143.6 (C_q), 143.0 (C_q), 139.3 (CH), 134.5 (CH), 133.5 (CH), 133.3 (C_q), 132.5 (C_q), 128.7 (CH), 127.8 (CH), 125.4 (CH), 121.1 (CH), 118.3 (CH), 110.4 (CH), 16.5 (CH₃).

IR (ATR): 3082, 2924, 1724, 1593, 1465, 1424, 1231, 1186, 1056, 729 cm⁻¹.

MS (ESI) m/z (relative intensity): 312 (100) [M+H]⁺, 334 (20) [M+Na]⁺. **HR-MS** (ESI) m/z calcd. for C₁₇H₁₄NO₃S⁺ [M+H]⁺ 312.0689, found 312.0692.



3-methyl-2-(pyridin-2-yloxy)phenyl acetate 62as: The general procedure **C** was followed using **60a** (46.3 mg, 0.25 mmol) and **61s** (24.0 mg, 0.40 mmol). Isolation by column

chromatography on silica gel (*n*hexane/EtOAc: 10:1→5:1) yielded **62as** (51.7 mg, 85%) as a white solid.

M. p. = 95–97 °C.

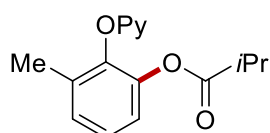
¹H-NMR (400 MHz, CDCl₃) δ = 8.14 (ddd, *J* = 5.0, 2.0, 0.8 Hz, 1H), 7.67 (ddd, *J* = 8.3, 7.2, 2.0 Hz, 1H), 7.19 – 7.13 (m, 2H), 7.07 – 7.01 (m, 1H), 6.96 (ddd, *J* = 7.2, 5.0, 0.9 Hz, 1H), 6.92 – 6.90 (m, 1H), 2.21 (s, 3H), 2.02 (s, 3H).

¹³C-NMR (101 MHz, CDCl₃) δ = 168.7 (C_q), 162.9 (C_q), 147.8 (CH), 143.6 (C_q), 143.2 (C_q), 139.5 (CH), 133.2 (C_q), 128.6 (CH), 125.5 (CH), 121.1 (CH), 118.3 (CH), 110.1 (CH), 20.6 (CH₃), 16.5 (CH₃).

IR (ATR): 2926, 1769, 1588, 1465, 1427, 1272, 1182, 1030, 883, 777 cm⁻¹.

MS (ESI) *m/z* (relative intensity): 244 (100) [M+H]⁺, 266 (65) [M+Na]⁺. **HR-MS** (ESI) *m/z* calcd. for C₁₄H₁₄NO₃⁺ [M+H]⁺ 244.0968, found 244.0986.

The spectral data were in accordance with those reported in the literature.^[180]



3-methyl-2-(pyridin-2-yloxy)phenyl isobutyrate 62at: The general procedure **C** was followed using **60a** (46.3 mg, 0.25 mmol) and **61t** (35.2 mg, 0.40 mmol). Isolation by column chromatography on silica gel (*n*hexane/EtOAc: 10:1→5:1) yielded **62at** (35.9 mg, 53%) as a white solid.

M. p. = 60–65 °C.

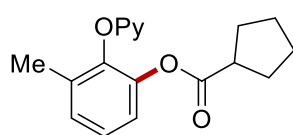
¹H-NMR (400 MHz, CDCl₃) δ = 8.13 (ddd, *J* = 5.0, 2.0, 0.8 Hz, 1H), 7.65 (ddd, *J* = 8.3, 7.1, 2.0 Hz, 1H), 7.19 – 7.12 (m, 2H), 7.07 – 7.00 (m, 1H), 6.95 (ddd, *J* = 7.2, 5.0, 0.9 Hz, 1H), 6.90 – 6.86 (m, 1H), 2.54 (hept, *J* = 7.0 Hz, 1H), 2.20 (s, 3H), 1.05 (d, *J* = 7.0 Hz, 6H).

¹³C-NMR (101 MHz, CDCl₃) δ = 174.7 (C_q), 163.0 (C_q), 147.8 (CH), 143.6 (C_q), 143.4 (C_q), 139.4 (CH), 133.2 (C_q), 128.4 (CH), 125.6 (CH), 121.1 (CH), 118.2 (CH), 110.1 (CH), 34.1 (CH), 18.8 (CH₃), 16.5 (CH₃).

IR (ATR): 2987, 1754, 1594, 1463, 1424, 1272, 1234, 1089, 882, 788 cm⁻¹.

MS (ESI) *m/z* (relative intensity): 272 (100) [2M+Na]⁺, 294 (20) [M+Na]⁺, 285 (90) [M+H]⁺.

HR-MS (ESI) *m/z* calcd. for C₁₆H₁₈NO₃⁺ [M+H]⁺ 272.1281, found 272.1275.



3-methyl-2-(pyridin-2-yloxy)phenyl cyclopentanecarboxylate 62au: The general procedure **C** was followed using **60a** (46.3 mg, 0.25 mmol) and **61u** (45.7 mg, 0.40 mmol). Isolation by column chromatography on silica gel (*n*hexane/EtOAc: 10:1→5:1) yielded **62au** (44.6 mg, 60%) as colorless oil.

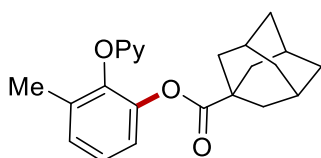
¹H-NMR (400 MHz, CDCl₃) δ = 8.14 (ddd, J = 5.0, 2.0, 0.8 Hz, 1H), 7.66 (ddd, J = 8.3, 7.2, 2.0 Hz, 1H), 7.19 – 7.12 (m, 2H), 7.07 – 7.01 (m, 1H), 6.95 (ddd, J = 7.2, 5.0, 1.0 Hz, 1H), 6.89 – 6.85 (m, 1H), 2.73 (tt, J = 8.5, 7.1 Hz, 1H), 2.19 (s, 3H), 1.82 – 1.42 (m, 8H).

¹³C-NMR (101 MHz, CDCl₃) δ = 174.4 (C_q), 162.9 (C_q), 147.8 (CH), 143.6 (C_q), 143.4 (C_q), 139.4 (CH), 133.2 (C_q), 128.4 (CH), 125.6 (CH), 121.2 (CH), 118.2 (CH), 110.0 (CH), 43.7 (CH), 29.9 (CH₂), 25.8 (CH₂), 16.4 (CH₃).

IR (ATR): 2955, 2870, 1757, 1589, 1465, 1428, 1273, 1240, 1125, 777 cm⁻¹.

MS (ESI) m/z (relative intensity): 298 (100) [M+H]⁺, 320 (80) [M+Na]⁺. **HR-MS** (ESI) m/z calcd. for C₁₈H₂₀NO₃⁺ [M+H]⁺ 298.1438, found 298.1453.

The spectral data were in accordance with those reported in the literature.^[180]



3-methyl-2-(pyridin-2-yloxy)phenyl adamantane-1-carboxylate 62av: The general procedure **C** was followed using **60a** (46.3 mg, 0.25 mmol) and **61v** (72.1 mg, 0.40 mmol). Isolation by column chromatography on silica gel (*n*hexane/EtOAc: 10:1→5:1) yielded **62av** (68.7 mg, 76%) as a white solid.

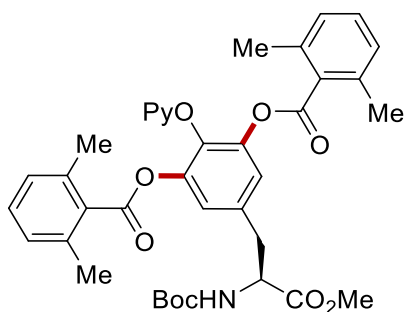
M. p. = 96–98 °C.

¹H-NMR (400 MHz, CDCl₃) δ = 8.14 (dd, J = 5.0, 1.9 Hz, 1H), 7.65 (ddd, J = 8.4, 7.2, 2.0 Hz, 1H), 7.18 – 7.10 (m, 2H), 7.05 – 7.00 (m, 1H), 6.95 (ddd, J = 7.2, 5.0, 0.9 Hz, 1H), 6.87 (dd, J = 8.4, 0.9 Hz, 1H), 2.20 (s, 3H), 1.94 – 1.90 (m, 3H), 1.76 – 1.73 (m, 6H), 1.70–1.57 (m, 6H).

¹³C-NMR (101 MHz, CDCl₃) δ = 175.2 (C_q), 162.9 (C_q), 147.8 (CH), 143.7 (C_q), 143.3 (C_q), 139.3 (CH), 133.1 (C_q), 128.2 (CH), 125.5 (CH), 121.1 (CH), 118.1 (CH), 110.1 (CH), 41.0 (C_q), 38.5 (CH₂), 36.4 (CH₂), 27.9 (CH), 16.4 (CH₃).

IR (ATR): 2906, 2853, 1741, 1590, 1463, 1422, 1269, 1213, 1049, 781 cm⁻¹.

MS (ESI) m/z (relative intensity): 364 (100) [M+H]⁺, 386 (20) [M+Na]⁺. **HR-MS** (ESI) m/z calcd. for C₂₃H₂₆NO₃⁺ [M+H]⁺ 364.1907, found 364.1905.



(S)-5-{2-[(*tert*-butoxycarbonyl)amino]-3-methoxy-3-oxopropyl}-2-(pyridin-2-yloxy)-1,3-phenylene bis(2,6-dimethylbenzoate) 88aa: The general procedure **E** was followed using **87a** (93.1 mg, 0.25 mmol) and **61a** (112.5 mg, 0.75 mmol). Isolation by column chromatography on silica gel (*n*hexane/EtOAc: 3:1→1:1) yielded **88aa** (121.9 mg, 73%) as a white solid.

M. p. = 60–68 °C.

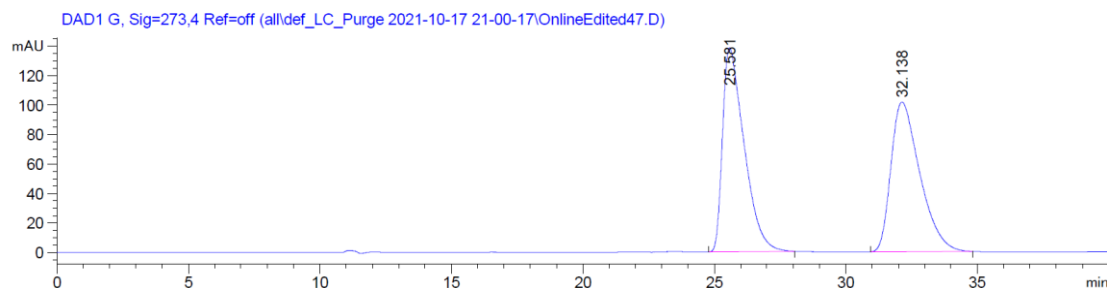
¹H-NMR (400 MHz, CDCl₃) δ = 8.07 (d, *J* = 4.9 Hz, 1H), 7.61 – 7.55 (m, 1H), 7.20 – 7.11 (m, 4H), 7.01 – 6.97 (m, 4H), 6.92 – 6.83 (m, 2H), 5.26 (brs, 1H), 4.70 (ddd, *J* = 7.6, 6.6, 6.6 Hz, 1H), 3.77 (s, 3H), 3.30 – 3.17 (m, 2H), 2.27 (s, 12H), 1.45 (s, 9H).

¹³C-NMR (101 MHz, CDCl₃) δ = 172.0 (C_q), 167.2 (C_q), 162.4 (C_q), 155.2 (C_q), 147.7 (CH), 144.7 (C_q), 139.4 (CH), 136.7 (C_q), 135.6 (C_q), 134.3 (C_q), 132.4 (C_q), 130.0 (CH), 127.8 (CH), 122.1 (CH), 118.8 (CH), 110.3 (CH), 80.2 (C_q), 54.3 (CH), 52.6 (CH₃), 37.9 (CH₂), 28.4 (CH₃), 19.9 (CH₃).

IR (ATR): 3318, 2970, 1740, 1592, 1489, 1420, 1222, 1167, 1040, 773 cm⁻¹.

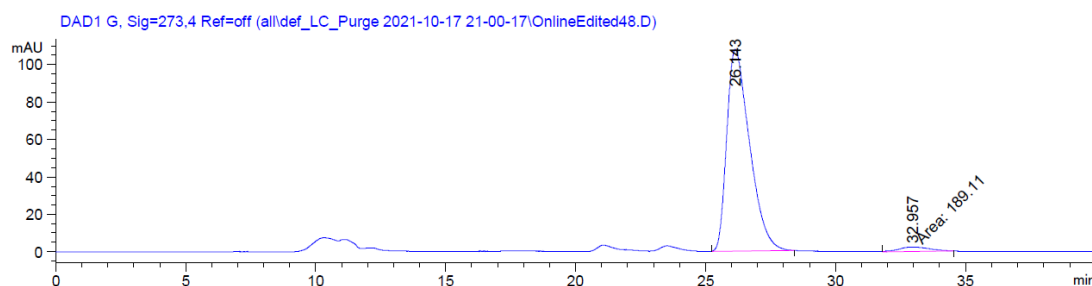
MS (ESI) *m/z* (relative intensity): 669 (100) [M+H]⁺, 691 (65) [M+Na]⁺. **HR-MS** (ESI) *m/z* calcd. for C₃₈H₄₁N₂O₉⁺ [M+H]⁺ 669.2807, found 669.2807.

HPLC separation (Chiralpak® IA-3, *n*hexane/ *i*PrOH 75:25, 1.0 mL/min, detection at 273 nm): *t_r* (major) = 26.1 min, *t_r* (minor) = 33.0 min, 98% ee.

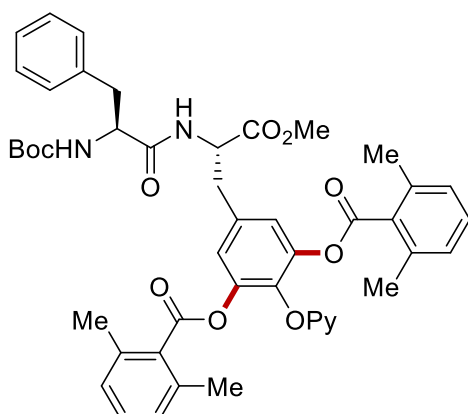


| Peak # | RetTime [min] | Type | Width [min] | Area [mAU*s] | Height [mAU] | Area % |
|--------|---------------|------|-------------|--------------|--------------|---------|
| 1 | 25.581 | BB | 0.7729 | 7880.91016 | 138.49452 | 50.3793 |
| 2 | 32.138 | BB | 0.9252 | 7762.22803 | 101.61554 | 49.6207 |

Experimental Data



| Peak # | RetTime [min] | Type | Width [min] | Area [mAU*s] | Height [mAU] | Area % |
|--------|---------------|------|-------------|--------------|--------------|---------|
| 1 | 26.143 | BB | 0.8051 | 6578.95313 | 107.78815 | 99.0214 |
| 2 | 32.957 | MM | 0.7057 | 65.01891 | 1.53551 | 0.9786 |



5-({S}-2-([S]-2-[(*tert*-butoxycarbonyl)amino]-3-phenylpropanamido)-3-methoxy-3-oxopropyl)-2-(pyridin-2-yloxy)-1,3-phenylene bis(2,6-dimethylbenzoate) **88ba:** The general procedure **E** was followed using **87b** (129.8 mg, 0.25 mmol) and **61a** (112.6 mg, 0.75 mmol). Isolation by column chromatography on silica gel (*n*hexane/EtOAc: 7:3→5:5) yielded **88ba** (152.5 mg, 75%) as a white solid.

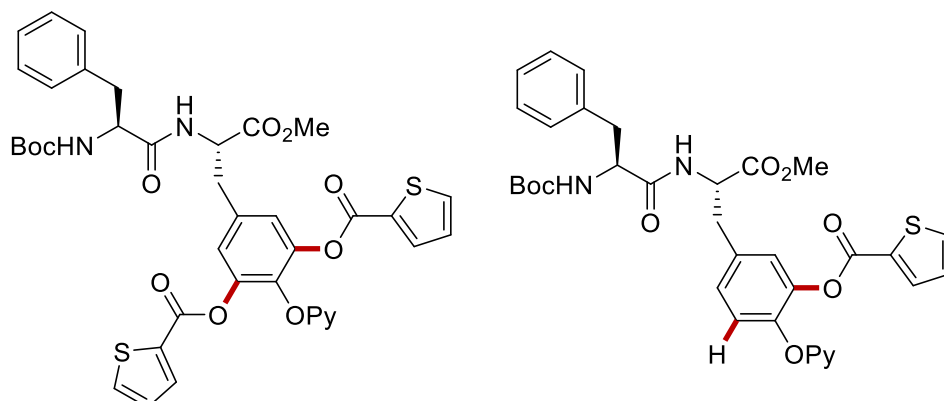
M. p. = 82–83 °C.

¹H-NMR (400 MHz, CDCl₃) δ = 8.03 (d, *J* = 4.9 Hz, 1H), 7.68 – 7.53 (m, 1H), 7.25 – 7.14 (m, 7H), 7.10 (s, 2H), 7.02 (d, *J* = 7.6 Hz, 4H), 6.96 – 6.83 (m, 3H), 5.36 (d, *J* = 8.3 Hz, 1H), 5.08 – 4.99 (m, 1H), 4.64 – 4.32 (m, 1H), 3.79 (s, 3H), 3.36 – 3.20 (m, 3H), 2.90 (dd, *J* = 11.6, 4.3 Hz, 1H), 2.30 (s, 12H), 1.32 (s, 9H).

¹³C-NMR (101 MHz, CDCl₃) δ = 171.5 (C_q), 171.2 (C_q), 167.4 (C_q), 162.5 (C_q), 155.8 (C_q), 147.6 (CH), 144.5 (C_q), 139.4 (CH), 137.1 (C_q), 136.5 (C_q), 135.9 (C_q), 133.8 (C_q), 132.1 (C_q), 130.1 (CH), 129.4 (CH), 128.6 (CH), 127.9 (CH), 126.8 (CH), 122.2 (CH), 118.8 (CH), 110.4 (CH), 80.1 (C_q), 56.2 (CH), 53.0 (CH), 52.7 (CH₃), 38.3 (CH₂), 37.5 (CH₂), 28.2 (CH₃), 20.0 (CH₃).

IR (ATR): 2964, 2926, 1755, 1716, 1674, 1499, 1429, 1225, 1101, 1060, 773 cm⁻¹.

MS (ESI) m/z (relative intensity): 816 (40) $[M+H]^+$, 838 (100) $[M+Na]^+$. **HR-MS** (ESI): m/z calcd. for $C_{47}H_{50}N_3O_{10}^+$ $[M+H]^+$ 816.3491, found 816.3492.



5-({S}-2-([S]-2-[(*tert*-butoxycarbonyl)amino]-3-phenylpropanamido)-3-methoxy-3-oxopropyl)-2-(pyridin-2-yloxy)-1,3-phenylene bis(thiophene-2-carboxylate) (88br) and **5-({S}-2-([S]-2-[(*tert*-butoxycarbonyl)amino]-3-phenylpropanamido)-3-methoxy-3-oxopropyl)-2-(pyridin-2-yloxy)phenyl thiophene-2-carboxylate 88br'**: The general procedure **E** was followed using **87b** (129.8 mg, 0.25 mmol) and **61r** (96.1 mg, 0.75 mmol). Isolation by column chromatography on silica gel (*n*hexane/EtOAc: 7:3→5:5) and recycling preparative HPLC yielded **88br** (73.1 mg, 38%) as a white solid and **88br'** (43.6 mg, 27%) as a white solid.

88br:

M. p. = 75–77 °C.

¹H-NMR (400 MHz, CDCl₃) δ = 8.04 (d, J = 4.9 Hz, 1H), 7.72 (s, 2H), 7.66 – 7.49 (m, 3H), 7.34 – 7.12 (m, 5H), 7.12 – 7.06 (m, 2H), 7.00 – 6.83 (m, 5H), 5.64 – 5.40 (m, 1H), 5.12 – 4.91 (m, 1H), 4.76 – 4.37 (m, 1H), 3.77 (s, 3H), 3.34 – 2.90 (m, 4H), 1.37 (s, 9H).

¹³C-NMR (101 MHz, CDCl₃) δ = 171.1 (C_q), 170.9 (C_q), 162.2 (C_q), 159.3 (C_q), 155.8 (C_q), 147.3 (CH), 143.5 (C_q), 139.3 (CH), 137.0 (C_q), 136.4 (C_q), 134.9 (CH), 133.9 (CH), 132.8 (C_q), 132.1 (C_q), 129.6 (CH), 128.5 (CH), 127.9 (CH), 126.8 (CH), 122.2 (CH), 118.7 (CH), 110.5 (CH), 79.9 (C_q), 55.8 (CH), 52.9 (CH), 52.7 (CH₃), 37.9 (CH₂), 37.5 (CH₂), 28.2 (CH₃).

IR (ATR): 2955, 2925, 1736, 1666, 1498, 1429, 1412, 1246, 1218, 1072, 736 cm⁻¹.

MS (ESI) m/z (relative intensity): 772 (50) $[M+H]^+$, 794 (100) $[M+Na]^+$. **HR-MS** (ESI): m/z calcd. for $C_{39}H_{38}N_3O_{10}S_2^+$ $[M+H]^+$ 772.1993, found 772.1999.

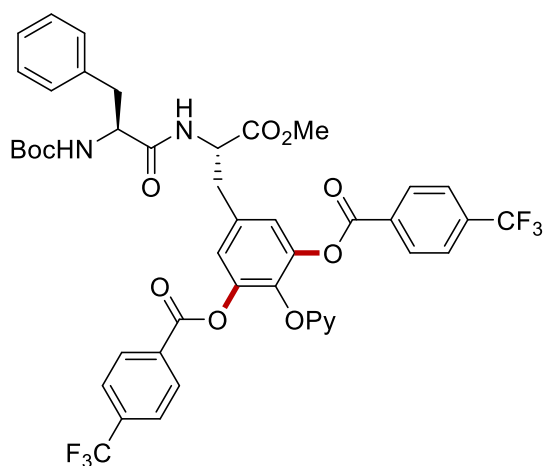
88br':

M. p. = 62–64 °C.

¹H-NMR (400 MHz, CDCl₃) δ = 8.10 (d, J = 4.9 Hz, 1H), 7.77 – 7.46 (m, 3H), 7.29 – 7.17 (m, 6H), 7.07 (t, J = 4.3 Hz, 1H), 7.03 – 6.84 (m, 4H), 6.74 (d, J = 7.8 Hz, 1H), 5.50 – 5.20 (m, 1H), 5.10 – 4.78 (m, 1H), 4.64 – 4.30 (m, 1H), 3.75 (s, 3H), 3.35 – 2.84 (m, 4H), 1.38 (s, 9H).
¹³C-NMR (101 MHz, CDCl₃) δ = 171.2 (C_q), 171.1 (C_q), 171.1 (C_q), 159.6 (C_q), 155.7 (C_q), 147.5 (CH), 144.1 (C_q), 142.0 (C_q), 139.4 (CH), 136.9 (C_q), 134.7 (CH), 133.8 (CH), 133.2 (C_q), 132.3 (C_q), 129.5 (CH), 128.6 (CH), 128.5 (CH), 127.9 (CH), 127.7 (CH), 125.2 (CH), 123.3 (CH), 118.6 (CH), 110.9 (CH), 80.0 (C_q), 55.7 (CH), 53.0 (CH), 52.5 (CH₃), 38.0 (CH₂), 37.3 (CH₂), 28.2 (CH₃).

IR (ATR): 2979, 2925, 1737, 1710, 1656, 1504, 1273, 1250, 1233, 1166, 737 cm⁻¹.

MS (ESI) m/z (relative intensity): 646 (65) [M+H]⁺, 668 (100) [M+Na]⁺. **HR-MS** (ESI): m/z calcd. for C₃₄H₃₆N₃O₈S⁺ [M+H]⁺ 646.2218, found 646.2218.



5-({S}-2-{{[S]-2-[(*tert*-butoxycarbonyl)amino]-3-phenylpropanamido]-3-methoxy-3-oxopropyl}-2-(pyridin-2-yloxy)-1,3-phenylene bis[4-(trifluoromethyl)benzoate] 88bq:
 The general procedure **E** was followed using **87b** (129.8 mg, 0.25 mmol) and **61q** (142.5 mg, 0.75 mmol). Isolation by column chromatography on silica gel (*n*hexane/EtOAc: 7:3→5:5) yielded **88bq** (129.9 mg, 58%) as a white solid.

M. p. = 156–158 °C.

¹H-NMR (600 MHz, CDCl₃) δ = 8.08 – 8.04 (m, 1H), 8.02 (d, J = 8.1 Hz, 4H), 7.68 (d, J = 8.1 Hz, 4H), 7.55 (ddd, J = 8.3, 7.2, 2.0 Hz, 1H), 7.25 – 7.20 (m, 2H), 7.20 – 7.10 (m, 3H), 6.98 (s, 2H), 6.90 (dd, J = 7.2, 5.0 Hz, 1H), 6.88 – 6.78 (m, 2H), 5.43 (d, J = 8.8 Hz, 1H), 5.07 – 4.92 (m, 1H), 4.66 – 4.43 (m, 1H), 3.77 (s, 3H), 3.42 – 2.91 (m, 4H), 1.37 (s, 9H).

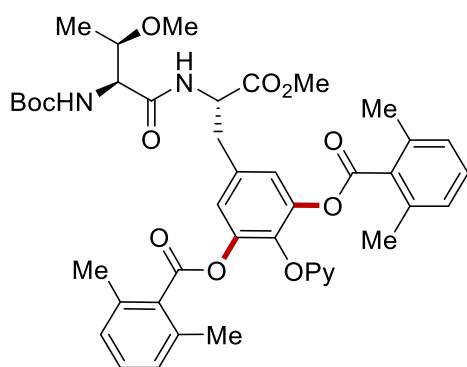
¹³C-NMR (151 MHz, CDCl₃) δ = 171.0 (C_q), 170.7 (C_q), 162.7 (C_q), 162.1 (C_q), 155.6 (C_q), 147.4 (CH), 143.6 (C_q), 139.5 (CH), 136.8 (C_q), 136.2 (C_q), 135.1 (q, ² J_{C-F} = 32.8 Hz, C_q), 133.1 (C_q), 132.0 (C_q), 130.4 (CH), 129.5 (CH), 128.5 (CH), 126.8 (CH), 125.5 (q, ³ J_{C-F} = 3.7

Hz, CH), 123.4 (q, $^1J_{C-F} = 272.9$ Hz, C_q), 122.3 (CH), 118.9 (CH), 110.3 (CH), 80.0 (C_q), 55.7 (CH), 52.9 (CH), 52.6 (CH₃), 37.9 (CH₂), 37.5 (CH₂), 28.2 (CH₃).

$^{19}\text{F-NMR}$ (565 MHz, CDCl₃) $\delta = -63.2$ (s).

IR (ATR): 3343, 2926, 1747, 1726, 1501, 1429, 1323, 1256, 1089, 767, 697 cm⁻¹.

MS (ESI) m/z (relative intensity): 896 (50) [M+H]⁺, 918 (100) [M+Na]⁺. **HR-MS** (ESI): m/z calcd. for C₄₅H₄₀F₆N₃O₁₀⁺ [M+H]⁺ 896.2612, found 896.2613.



5-({S}-2-{{[2S,3R]-2-[(tert-butoxycarbonyl)amino]-3-methoxybutanamido}-3-methoxy-3-oxopropyl)-2-(pyridin-2-yloxy)-1,3-phenylene bis(2,6-dimethylbenzoate) 88ca: The general procedure **E** was followed using **87c** (121.9 mg, 0.25 mmol) and **61a** (112.6 mg, 0.75 mmol). Isolation by column chromatography on silica gel (*n*-hexane/EtOAc: 7:3→5:5) yielded **88ca** (131.1 mg, 67%) as a white solid.

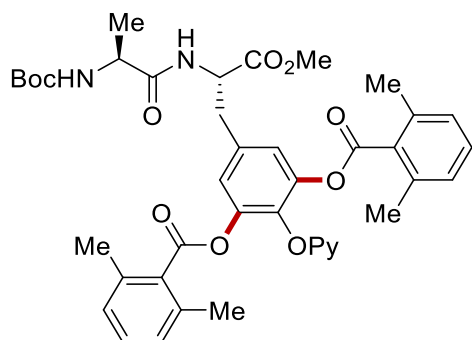
M. p.: 75–77 °C.

$^1\text{H-NMR}$ (400 MHz, CDCl₃) $\delta = 8.04$ (dd, $J = 5.1, 2.0$ Hz, 1H), 7.63 – 7.45 (m, 1H), 7.32 (d, $J = 7.7$ Hz, 1H), 7.23 – 7.11 (m, 4H), 6.99 (d, $J = 7.6$ Hz, 4H), 6.93 – 6.81 (m, 2H), 5.64 (d, $J = 7.5$ Hz, 1H), 5.11 – 4.92 (m, 1H), 4.27 (d, $J = 6.6$ Hz, 1H), 4.07 – 3.91 (m, 1H), 3.77 (s, 3H), 3.33 (s, 3H), 3.28 (dd, $J = 14.1, 5.5$ Hz, 1H), 3.22 (dd, $J = 14.1, 5.5$ Hz, 1H), 2.28 (s, 12H), 1.43 (s, 9H), 1.13 (d, $J = 6.3$ Hz, 3H).

$^{13}\text{C-NMR}$ (101 MHz, CDCl₃) $\delta = 171.2$ (C_q), 170.2 (C_q), 167.1 (C_q), 162.4 (C_q), 156.0 (C_q), 147.6 (CH), 144.6 (C_q), 139.3 (CH), 136.6 (C_q), 135.7 (C_q), 133.9 (C_q), 132.3 (C_q), 130.0 (CH), 127.8 (CH), 122.1 (CH), 118.7 (CH), 110.3 (CH), 80.1 (C_q), 76.4 (CH), 58.0 (CH), 57.0 (CH₃), 53.0 (CH), 52.6 (CH₃), 37.6 (CH₂), 28.3 (CH₃), 19.9 (CH₃), 14.5 (CH₃).

IR (ATR): 2979, 2924, 1748, 1679, 1467, 1428, 1223, 1162, 1048, 772 cm⁻¹.

MS (ESI) m/z (relative intensity): 784 (65) [M+H]⁺, 806 (100) [M+Na]⁺. **HR-MS** (ESI): m/z calcd. for C₄₃H₅₀N₃O₁₁⁺ [M+H]⁺ 784.3440, found 784.3443.



5-({S}-2-{{[S]-2-[(*tert*-butoxycarbonyl)amino]propanamido}-3-methoxy-3-oxopropyl)-2-(pyridin-2-yloxy)-1,3-phenylene bis(2,6-dimethylbenzoate) 88da: The general procedure **E** was followed using **87d** (110.9 mg, 0.25 mmol) and **61a** (112.6 mg, 0.75 mmol). Isolation by column chromatography on silica gel (*n*hexane/EtOAc: 7:3→5:5) yielded **88da** (99.6 mg, 54%) as a white solid.

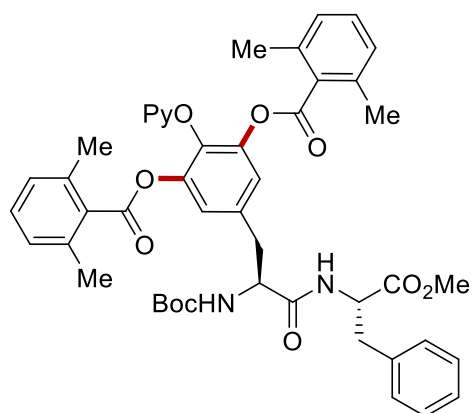
M. p. = 83–87 °C.

¹H-NMR (400 MHz, CDCl₃) δ = 8.06 (d, *J* = 5.0 Hz, 1H), 7.60 (dd, *J* = 7.7, 7.7 Hz, 1H), 7.30 – 7.16 (m, 2H), 7.12 (s, 2H), 7.07 – 6.84 (m, 7H), 5.37 (brs, 1H), 5.15 – 4.89 (m, 1H), 4.41 – 4.05 (m, 1H), 3.82 (s, 3H), 3.35 (dd, *J* = 13.9, 5.9 Hz, 1H), 3.31 (dd, *J* = 13.9, 6.2 Hz, 1H), 2.30 (s, 12H), 1.43 (s, 9H), 1.39 (d, *J* = 7.3 Hz, 3H).

¹³C-NMR (101 MHz, CDCl₃) δ = 172.8 (C_q), 171.4 (C_q), 167.4 (C_q), 162.5 (C_q), 155.7 (C_q), 147.6 (CH), 144.6 (C_q), 139.4 (CH), 136.5 (C_q), 135.7 (C_q), 133.9 (C_q), 132.3 (C_q), 130.1 (CH), 127.8 (CH), 122.2 (CH), 118.8 (CH), 110.4 (CH), 80.1 (C_q), 52.9 (CH), 52.7 (CH₃), 50.5 (CH), 37.4 (CH₂), 28.4 (CH₃), 19.9 (CH₃), 18.2 (CH₃).

IR (ATR): 2978, 2929, 1756, 1714, 1501, 1467, 1429, 1259, 1224, 1060, 773 cm⁻¹.

MS (ESI) *m/z* (relative intensity): 740 (85) [M+H]⁺, 762 (100) [M+Na]⁺. **HR-MS** (ESI): *m/z* calcd. for C₄₁H₄₆N₃O₁₀⁺ [M+H]⁺ 740.3178, found 740.3186.



5-{{(S)-2-[(*tert*-butoxycarbonyl)amino]-3-{{(S)-1-methoxy-1-oxo-3-phenylpropan-2-yl}amino}-3-oxopropyl}-2-(pyridin-2-yloxy)-1,3-phenylene bis(2,6-dimethylbenzoate)

88ea: The general procedure **E** was followed using **87e** (129.9 mg, 0.25 mmol) and **61a** (112.5 mg, 0.75 mmol). Isolation by column chromatography on silica gel (*n*hexane/EtOAc: 3:1→1:1) yielded **88ea** (132.6 mg, 65%) as a white solid.

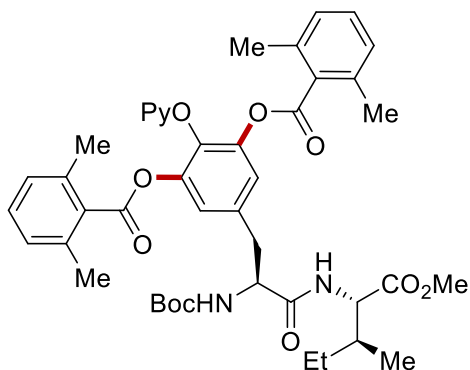
M. p. = 80–83 °C.

¹H-NMR (400 MHz, CDCl₃) δ = 8.01 (ddd, *J* = 4.9, 2.0, 0.9 Hz, 1H), 7.57 (ddd, *J* = 8.3, 7.2, 2.0 Hz, 1H), 7.29 – 7.21 (m, 5H), 7.20 – 7.15 (m, 2H), 7.10 – 7.04 (m, 2H), 6.99 (d, *J* = 7.6 Hz, 4H), 6.90 – 6.84 (m, 2H), 6.44 (d, *J* = 7.5 Hz, 1H), 5.20 (brs, 1H), 4.79 (ddd, *J* = 7.6, 6.1, 6.1 Hz, 1H), 4.52 – 4.34 (m, 1H), 3.65 (s, 3H), 3.33 – 3.17 (m, 1H), 3.17 – 3.03 (m, 3H), 2.27 (s, 12H), 1.44 (s, 9H).

¹³C-NMR (101 MHz, CDCl₃) δ = 171.3 (C_q), 170.3 (C_q), 167.1 (C_q), 162.3 (C_q), 155.3 (C_q), 147.5 (CH), 144.6 (C_q), 139.2 (CH), 136.6 (C_q), 135.8 (C_q), 135.6 (C_q), 134.7 (C_q), 132.2 (C_q), 129.9 (CH), 129.3 (CH), 128.7 (CH), 128.6 (CH), 127.7 (CH), 127.1 (CH), 122.2 (CH), 118.6 (CH), 110.2 (CH), 80.3 (C_q), 55.3 (CH), 53.5 (CH), 52.3 (CH₃), 37.7 (CH₂), 37.7 (CH₂), 28.3 (CH₃), 19.8 (CH₃).

IR (ATR): 3320, 2977, 1739, 1592, 1498, 1428, 1223, 1165, 1046, 772 cm⁻¹.

MS (ESI) *m/z* (relative intensity): 816 (100) [M+H]⁺, 838 (5) [M+Na]⁺. **HR-MS** (ESI) *m/z* calcd. for C₄₇H₅₀N₃O₁₀⁺ [M+H]⁺ 816.3491, found 816.3488.



5-{(S)-2-[(*tert*-butoxycarbonyl)amino]-3-[[2*S*,3*S*]-1-methoxy-3-methyl-1-oxopentan-2-yl]amino}-3-oxopropyl}-2-(pyridin-2-yloxy)-1,3-phenylene bis(2,6-dimethylbenzoate)

88fa: The general procedure **E** was followed using **87f** (121.4 mg, 0.25 mmol) and **61a** (112.5 mg, 0.75 mmol). Isolation by column chromatography on silica gel (*n*hexane/EtOAc: 3:1→1:1) yielded **88fa** (148.6 mg, 76%) as a white solid.

M. p. = 66–69 °C.

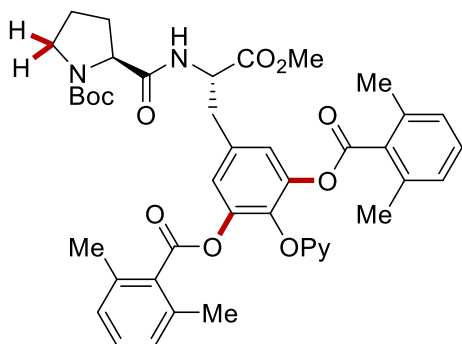
¹H-NMR (400 MHz, CDCl₃) δ = 8.06 (ddd, *J* = 5.0, 2.0, 0.8 Hz, 1H), 7.57 (ddd, *J* = 8.3, 7.2, 2.0 Hz, 1H), 7.21 (s, 2H), 7.17 (t, *J* = 7.6 Hz, 2H), 7.00 – 6.97 (m, 4H), 6.89 (ddd, *J* = 7.2, 5.0, 0.9 Hz, 1H), 6.86 (dt, *J* = 8.4, 0.9 Hz, 1H), 6.67 (d, *J* = 7.1 Hz, 1H), 5.26 (brs, 1H), 4.55

(dd, $J = 8.3, 4.9$ Hz, 1H), 4.46 (d, $J = 7.7$ Hz, 1H), 3.67 (s, 3H), 3.29 – 3.16 (m, 2H), 2.27 (s, 12H), 1.94 – 1.87 (m, 1H), 1.47 – 1.38 (m, 10H), 1.20 – 1.11 (m, 1H), 0.90 – 0.86 (m, 6H).

$^{13}\text{C-NMR}$ (101 MHz, CDCl_3) $\delta = 171.7$ (C_q), 170.5 (C_q), 167.0 (C_q), 162.3 (C_q), 155.5 (C_q), 147.5 (CH), 144.6 (C_q), 139.2 (CH), 136.5 (C_q), 135.6 (C_q), 134.9 (C_q), 132.2 (C_q), 129.8 (CH), 127.6 (CH), 122.0 (CH), 118.6 (CH), 110.2 (CH), 80.4 (C_q), 56.7 (CH), 55.3 (CH), 52.0 (CH_3), 37.8 (CH), 37.0 (CH_2), 28.2 (CH_3), 25.1 (CH_2), 19.8 (CH_3), 15.3 (CH_3), 11.5 (CH_3).

IR (ATR): 3345, 2967, 1740, 1681, 1592, 1466, 1428, 1223, 1046, 772 cm^{-1} .

MS (ESI) m/z (relative intensity): 782 (100) $[\text{M}+\text{H}]^+$, 804 (90) $[\text{M}+\text{Na}]^+$. **HR-MS** (ESI) m/z calcd. for $\text{C}_{44}\text{H}_{52}\text{N}_3\text{O}_{10}^+$ $[\text{M}+\text{H}]^+$ 782.3647, found 782.3631.



5-({S}-2-([S]-1-[tert-butoxycarbonyl]pyrrolidine-2-carboxamido)-3-methoxy-3-oxopropyl)-2-(pyridin-2-yloxy)-1,3-phenylene bis(2,6-dimethylbenzoate) 88ga:

The general procedure **E** was followed using **87g** (117.4 mg, 0.25 mmol) and **61a** (112.6 mg, 0.75 mmol). Isolation by column chromatography on silica gel (*n*hexane/EtOAc: 5:5) yielded **88ga** (137.5 mg, 72%) as a white solid.

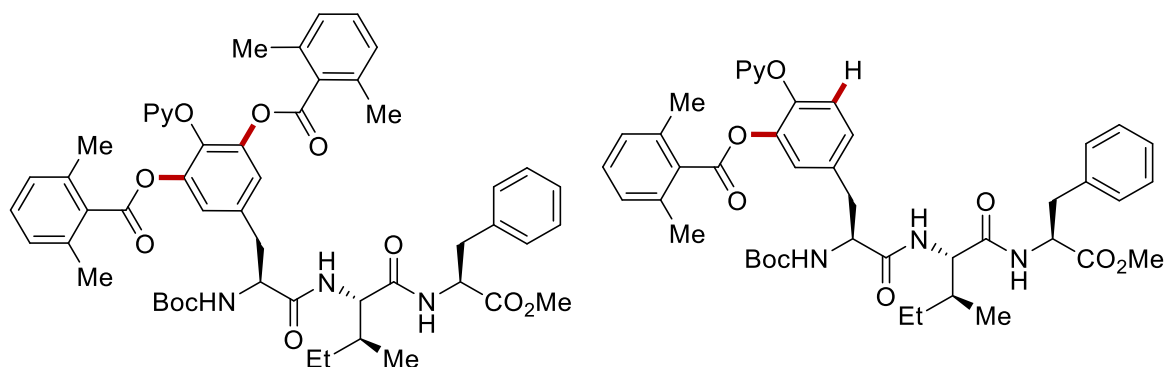
M. p. = 61–65 °C.

$^1\text{H-NMR}$ (600 MHz, $\text{DMSO-}d_6$, 80 °C) $\delta = 8.06$ – 7.97 (m, 2H), 7.74 (ddd, $J = 8.3, 7.2, 2.0$ Hz, 1H), 7.34 (s, 2H), 7.25 (t, $J = 7.6$ Hz, 2H), 7.08 (d, $J = 7.6$ Hz, 4H), 7.02 (ddd, $J = 7.2, 4.9, 0.9$ Hz, 1H), 6.92 (dt, $J = 8.3, 0.9$ Hz, 1H), 4.75 (ddd, $J = 9.0, 8.5, 5.6$ Hz, 1H), 4.19 – 4.07 (m, 1H), 3.69 (s, 3H), 3.39 (ddd, $J = 10.3, 7.5, 5.0$ Hz, 1H), 3.33 – 3.24 (m, 2H), 3.19 (dd, $J = 14.2, 9.0$ Hz, 1H), 2.24 (s, 12H), 2.12 – 2.01 (m, 1H), 1.83–1.65 (m, 3H), 1.34 (s, 9H).

$^{13}\text{C-NMR}$ (101 MHz, $\text{DMSO-}d_6$) $\delta = 172.8$ (C_q), 171.9 (C_q), 166.5 (C_q), 161.7 (C_q), 153.4 (C_q), 147.1 (CH), 143.7 (C_q), 140.1 (CH), 136.1 (C_q), 135.8 (C_q), 134.7 (C_q), 132.0 (C_q), 130.1 (CH), 127.6 (CH), 122.2 (CH), 119.2 (CH), 110.0 (CH), 78.5 (C_q), 59.9 (CH), 52.7 (CH), 51.9 (CH_3), 46.4 (CH_2), 35.4 (CH_2), 30.9 (CH_2), 27.8 (CH_3), 23.0 (CH_2), 19.1 (CH_3).

IR (ATR): 2979, 2929, 1756, 1748, 1696, 1428, 1224, 1101, 1061, 1050, 772 cm^{-1} .

MS (ESI) m/z (relative intensity): 766 (60) $[M+H]^+$, 788 (100) $[M+Na]^+$. **HR-MS** (ESI): m/z calcd. for $C_{44}H_{48}N_3O_{10}^+$ $[M+H]^+$ 766.3334, found 766.3337.



5-([S]-2-[(*tert*-butoxycarbonyl)amino]-3-[(2*S*,3*S*)-1-[(*S*)-1-methoxy-1-oxo-3-phenylpropan-2-yl]amino]-3-methyl-1-oxopentan-2-yl)amino]-3-oxopropyl)-2-(pyridin-2-yloxy)-1,3-phenylene bis(2,6-dimethylbenzoate) 88ha and methyl (6*S*,9*S*,12*S*)-12-benzyl-9-[(*S*)-*sec*-butyl]-6-{3-[(2,6-dimethylbenzoyl)oxy]-4-[pyridin-2-yloxy]benzyl}-2,2-dimethyl-4,7,10-trioxo-3-oxa-5,8,11-triazatriodecan-13-oate 88ha':

The general procedure **E** was followed using **87h** (158.2 mg, 0.25 mmol) and **61a** (112.6 mg, 0.75 mmol). Isolation by column chromatography on silica gel (*n*hexane/EtOAc: 1:1) and recycling preparative HPLC yielded **88ha** (104.5 mg, 45%) as a white solid and **88ha'** (50.7 mg, 26%) as a white solid.

88ha:

M. p. = 104–105 °C.

¹H-NMR (600 MHz, CDCl₃) δ = 8.02 (dd, J = 5.0, 2.0 Hz, 1H), 7.54 (ddd, J = 8.4, 7.2, 2.0 Hz, 1H), 7.25 – 7.22 (m, 2H), 7.21 – 7.17 (m, 3H), 7.15 (t, J = 7.6 Hz, 2H), 7.09 – 7.03 (m, 2H), 6.97 (d, J = 7.6 Hz, 4H), 6.86 (dd, J = 7.2, 4.9 Hz, 1H), 6.83 (d, J = 8.4 Hz, 1H), 6.78 (d, J = 8.2 Hz, 1H), 6.39 (d, J = 7.8 Hz, 1H), 5.21 (d, J = 7.8 Hz, 1H), 4.81 (ddd, J = 7.8, 6.2, 6.2 Hz, 1H), 4.45 – 4.38 (m, 1H), 4.26 (dd, J = 8.3, 6.4 Hz, 1H), 3.65 (s, 3H), 3.25 – 3.17 (m, 2H), 3.06 (dd, J = 14.0, 6.2, 1H), 3.02 (dd, J = 14.0, 6.4 Hz, 1H), 2.25 (s, 12H), 1.91 – 1.82 (m, 1H), 1.42 (s, 9H), 1.39 – 1.34 (m, 1H), 1.05 (ddd, J = 13.5, 9.6, 7.2 Hz, 1H), 0.84 (d, J = 6.8 Hz, 3H), 0.81 (t, J = 7.4 Hz, 3H).

¹³C-NMR (151 MHz, CDCl₃) δ = 171.6 (C_q), 170.8 (C_q), 170.2 (C_q), 167.0 (C_q), 162.3 (C_q), 155.6 (C_q), 147.4 (CH), 144.6 (C_q), 139.2 (CH), 136.5 (C_q), 135.7 (C_q), 135.6 (C_q), 134.9 (C_q), 132.2 (C_q), 129.8 (CH), 129.2 (CH), 128.5 (CH), 127.6 (CH), 127.1 (CH), 122.0 (CH), 118.6 (CH), 110.2 (CH), 80.5 (C_q), 57.9 (CH), 55.2 (CH), 53.1 (CH), 52.2 (CH₃), 37.7 (CH₂), 37.0 (CH₂), 36.5 (CH₂), 28.2 (CH₃), 24.7 (CH), 19.8 (CH₃), 15.2 (CH₃), 11.3 (CH₃).

IR (ATR): 3063, 2963, 1757, 1746, 1641, 1520, 1428, 1265, 1222, 1048, 772, cm⁻¹.

MS (ESI) m/z (relative intensity): 929 (50) $[M+H]^+$, 951 (100) $[M+Na]^+$. **HR-MS** (ESI): m/z calcd. for $C_{53}H_{61}N_4O_{11}^+$ $[M+H]^+$ 929.4331, found 929.4326.

88ha':

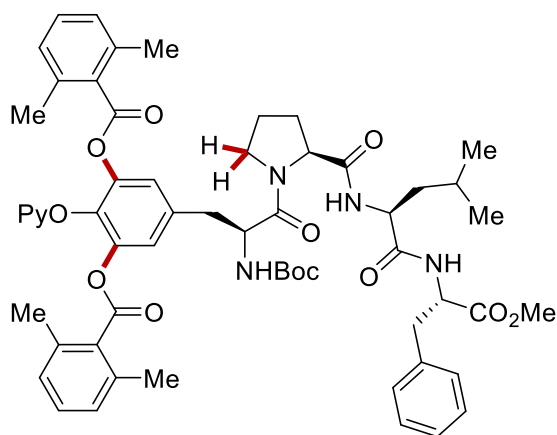
M. p. = 100–102 °C.

1H -NMR (600 MHz, $CDCl_3$) δ = 8.11 (dd, J = 5.0, 2.0 Hz, 1H), 7.62 (ddd, J = 8.3, 7.2, 2.0 Hz, 1H), 7.25 – 7.21 (m, 2H), 7.21 – 7.13 (m, 4H), 7.13 – 7.05 (m, 3H), 6.99 (d, J = 7.7 Hz, 2H), 6.94 (ddd, J = 7.2, 5.0, 1.0 Hz, 1H), 6.88 (ddd, J = 8.3, 1.0, 1.0 Hz, 1H), 6.71 (d, J = 8.4 Hz, 1H), 6.44 (d, J = 8.0 Hz, 1H), 5.13 (d, J = 7.9 Hz, 1H), 4.80 (ddd, J = 7.9, 6.2, 6.2 Hz, 1H), 4.41 – 4.32 (m, 1H), 4.25 (dd, J = 8.4, 6.4 Hz, 1H), 3.66 (s, 3H), 3.16 – 2.98 (m, 4H), 2.34 (s, 6H), 1.87 – 1.76 (m, 1H), 1.40 (s, 9H), 1.37 – 1.30 (m, 1H), 1.09 – 0.99 (m, 1H), 0.88 – 0.76 (m, 6H).

^{13}C -NMR (151 MHz, $CDCl_3$) δ = 171.6 (C_q), 171.0 (C_q), 170.3 (C_q), 167.4 (C_q), 162.9 (C_q), 155.5 (C_q), 147.6 (CH), 144.5 (C_q), 142.5 (C_q), 139.4 (CH), 135.7 (C_q), 135.5 (C_q), 134.4 (C_q), 132.5 (C_q), 129.7 (CH), 129.2 (CH), 128.6 (CH), 127.8 (CH), 127.6 (CH), 127.1 (CH), 124.5 (CH), 123.5 (CH), 118.7 (CH), 111.2 (CH), 80.4 (C_q), 57.8 (CH), 55.5 (CH), 53.1 (CH), 52.2 (CH_3), 37.7 (CH_2), 37.0 (CH_2), 36.7 (CH_2), 28.2 (CH_3), 24.6 (CH), 19.8 (CH_3), 15.2 (CH_3), 11.3 (CH_3).

IR (ATR): 3272, 2962, 2932, 1746, 1687, 1641, 1467, 1428, 1228, 1049, 771 cm^{-1} .

MS (ESI) m/z (relative intensity): 781 (60) $[M+H]^+$, 803 (100) $[M+Na]^+$. **HR-MS** (ESI): m/z calcd. for $C_{44}H_{53}N_4O_9^+$ $[M+H]^+$ 781.3807, found 781.3809.



5-({S}-2-{{tert-butoxycarbonyl}amino}-3-{{[S]-2-[[{S]-1-{{(S)-1-methoxy-1-oxo-3-phenylpropan-2-yl}amino}-4-methyl-1-oxopentan-2-yl]carbamoyl]pyrrolidin-1-yl}-3-oxopropyl)-2-(pyridin-2-yloxy)-1,3-phenylene bis(2,6-dimethylbenzoate) 88ia: The general procedure **E** was followed using **87i** (182.5 mg, 0.25 mmol) and **61a** (112.6 mg, 0.75

mmol). Isolation by column chromatography on silica gel (CH₂Cl₂/EtOAc: 4:1→2:1) yielded **88ia** (133.3 mg, 52%) as a white solid.

M. p. = 75–79 °C.

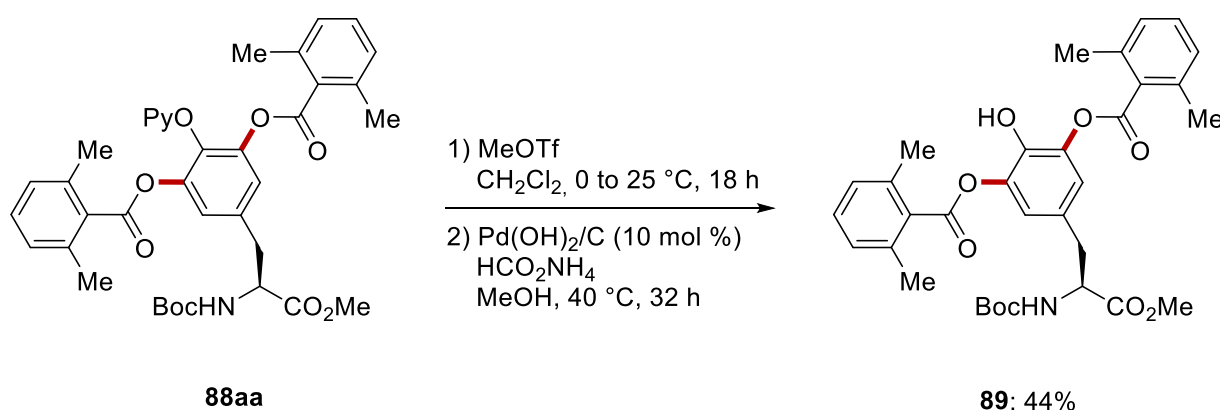
¹H-NMR (600 MHz, DMSO-*d*₆, 100 °C) δ = 8.06 – 7.98 (m, 1H), 7.78 – 7.67 (m, 2H), 7.59 (brs, 1H), 7.39 (s, 2H), 7.29 – 7.16 (m, 8H), 7.07 (d, *J* = 7.6 Hz, 4H), 7.01 (dd, *J* = 7.2, 4.9 Hz, 1H), 6.90 (d, *J* = 8.3 Hz, 1H), 4.63 – 4.51 (m, 2H), 4.48 – 4.37 (m, 1H), 4.30 (ddd, *J* = 8.4, 8.4, 5.8 Hz, 1H), 3.77 – 3.61 (m, 2H), 3.60 (s, 3H), 3.20 – 2.97 (m, 4H), 2.25 (s, 12H), 2.10 – 1.81 (m, 4H), 1.72 – 1.58 (m, 1H), 1.59 – 1.45 (m, 2H), 1.36 (s, 9H), 0.89 (d, *J* = 6.6 Hz, 3H), 0.85 (d, *J* = 6.6 Hz, 3H).

¹³C-NMR (151 MHz, DMSO-*d*₆, 100 °C) δ = 171.2 (C_q), 170.9 (C_q), 170.5 (C_q), 169.8 (C_q), 165.8 (C_q), 161.4 (C_q), 154.5 (C_q), 146.6 (CH), 143.4 (C_q), 139.1 (CH), 136.6 (C_q), 135.9 (C_q), 135.4 (C_q), 134.4 (C_q), 131.6 (C_q), 129.3 (CH), 128.4 (CH), 127.6 (CH), 127.1 (CH), 125.8 (CH), 121.4 (CH), 118.4 (CH), 109.3 (CH), 77.9 (C_q), 59.3 (CH), 52.8 (CH), 51.0 (CH₃), 50.9 (CH), 46.3 (CH₂), 40.2 (CH₂), 36.5 (CH₂), 35.8 (CH₂), 28.1 (CH₂), 27.8 (CH₃), 24.0 (CH₂), 23.7 (CH), 22.2 (CH₃), 21.3 (CH₃), 18.5 (CH₃). One aliphatic CH is missing due to overlap, the overlap was verified by HSQC analysis showing that the peak at 52.8 ppm corresponds to two carbons.

IR (ATR): 2953, 2869, 1749, 1671, 1650, 1537, 1467, 1224, 1051, 774 cm⁻¹.

MS (ESI) *m/z* (relative intensity): 1026 (40) [M+H]⁺, 1048 (100) [M+Na]⁺. **HR-MS** (ESI): *m/z* calcd. for C₅₈H₆₈N₅O₁₂⁺ [M+H]⁺ 1026.4859, found 1026.4864.

5.4.2 Removal of Pyridyl Group



To a stirred solution of **88aa** (100.3 mg, 0.15 mmol) in CH₂Cl₂ (1.0 mL) methyl trifluoromethanesulfonate (73.8 mg, 0.45 mmol) was added at 0 °C. After 30 min, the mixture was allowed to warm up to 25 °C and stirred for 18 h. The crude mixture was concentrated under reduced pressure to afford a white solid. In a sealed-tube, the crude product, Pd(OH)₂/C (20 wt%, containing 50% water) (9.2 mg, 5.0 mol %), and ammonium formate

(141.9 mg, 15.0 equiv.) were dissolved in methanol (2.0 mL), and stirred at 40 °C for 32 hours. The mixture was filtered through a short plug of celite, concentrated under reduced pressure and purified by column chromatography on silica gel (*n*Hexane/EtOAc: 8/2 → 7/3), yielding **89** (39.1 mg, 44%) as a white solid.

(S)-5-{2-[(*tert*-butoxycarbonyl)amino]-3-methoxy-3-oxopropyl}-2-hydroxy-1,3-phenylene bis(2,6-dimethylbenzoate) **89:**

M. p. = 63–70 °C.

¹H-NMR (400 MHz, CDCl₃) δ = 7.26 (t, *J* = 7.6 Hz, 2H), 7.06 (d, *J* = 7.7 Hz, 4H), 6.89 – 6.79 (m, 2H), 6.47 (brs, 1H), 5.20 (brs, 1H), 4.66 (ddd, *J* = 7.7, 6.8, 6.8 Hz, 1H), 3.79 (s, 3H), 3.11 – 3.17 (m, 2H), 2.27 (s, 6H), 2.24 (s, 6H), 1.49 (s, 9H).

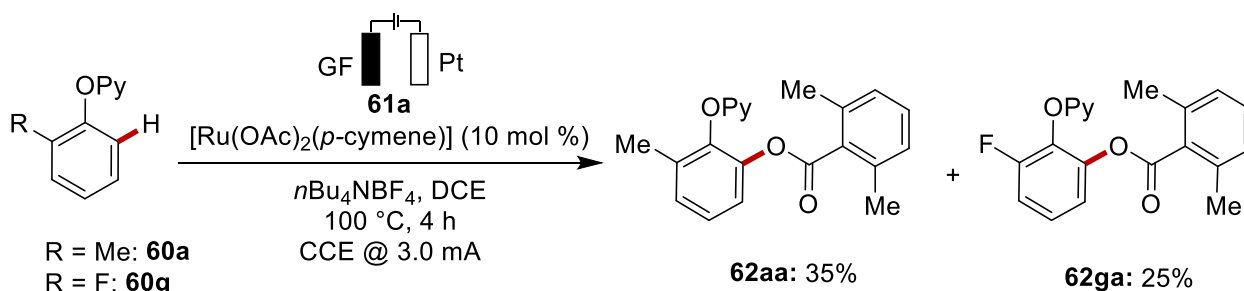
¹³C-NMR (101 MHz, CDCl₃) δ = 172.1 (C_q), 167.0 (C_q), 155.3 (C_q), 143.1 (C_q), 136.4 (C_q), 135.8 (C_q), 135.2 (C_q), 132.2 (C_q), 131.7 (CH), 127.8 (CH), 116.2 (CH), 80.4 (C_q), 54.3 (CH), 52.5 (CH₃), 38.0 (CH₂), 28.3 (CH₃), 19.8 (CH₃).

IR (ATR): 3352, 2928, 1683, 1618, 1440, 1367, 1238, 1160, 1050, 772 cm⁻¹.

MS (ESI) *m/z* (relative intensity): 614 (100) [M+Na]⁺. **HR-MS** (ESI): *m/z* calcd. for C₃₃H₃₇N₁O₉Na⁺ [M+Na]⁺ 614.2361, found 614.2353.

5.4.3 Mechanistic Study

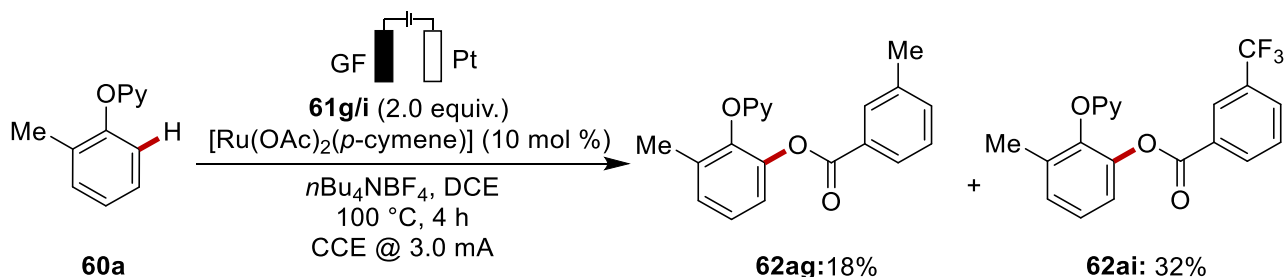
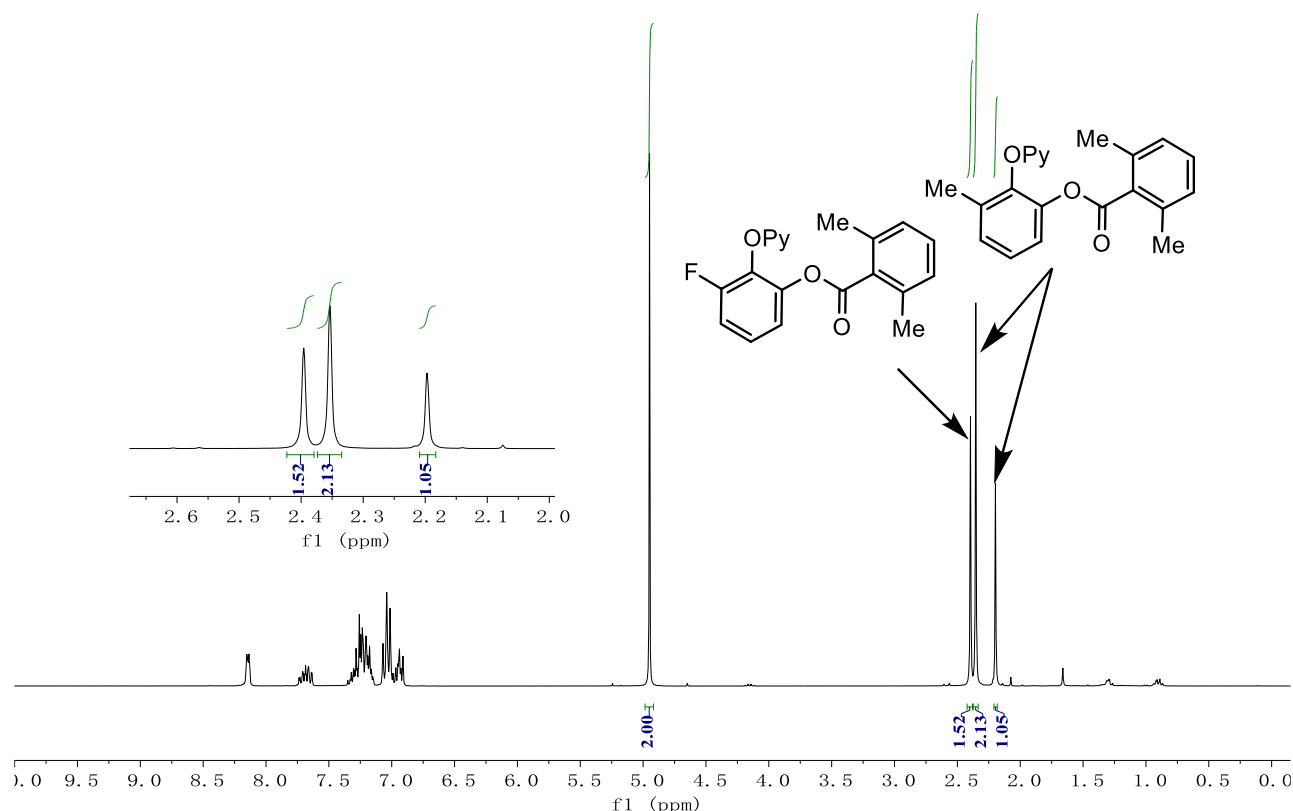
5.4.3.1 Competition Experiments



A solution of **60a** (46.3 mg, 0.25 mmol), **60g** (47.3 mg, 0.25 mmol), **61a** (37.5 mg, 0.25 mmol), [Ru(OAc)₂(*p*-cymene)] (8.8 mg, 10 mol %) and *n*Bu₄NBF₄ (82.3 mg, 0.25 mmol) in DCE (4.0 mL) was placed in a 25 mL Schlenk tube. The tube was sealed with a septum equipped with a Pt electrode (10 mm × 15 mm × 0.25 mm) and a GF electrode (10 mm × 15 mm × 6 mm). An oil bulb was attached to the system by using a needle. The tube was placed in an oil bath and stirred at 100 °C. After 4 h at 3.0 mA, the mixture was cooled to ambient temperature and the solvent was removed under vacuum. The residue was purified by column chromatography on silica gel (*n*hexane/EtOAc: 20:1→10:1). The products **62aa**

Experimental Data

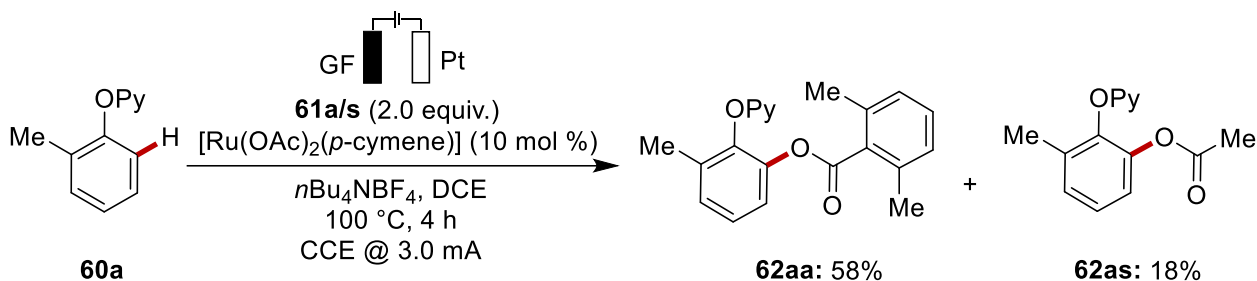
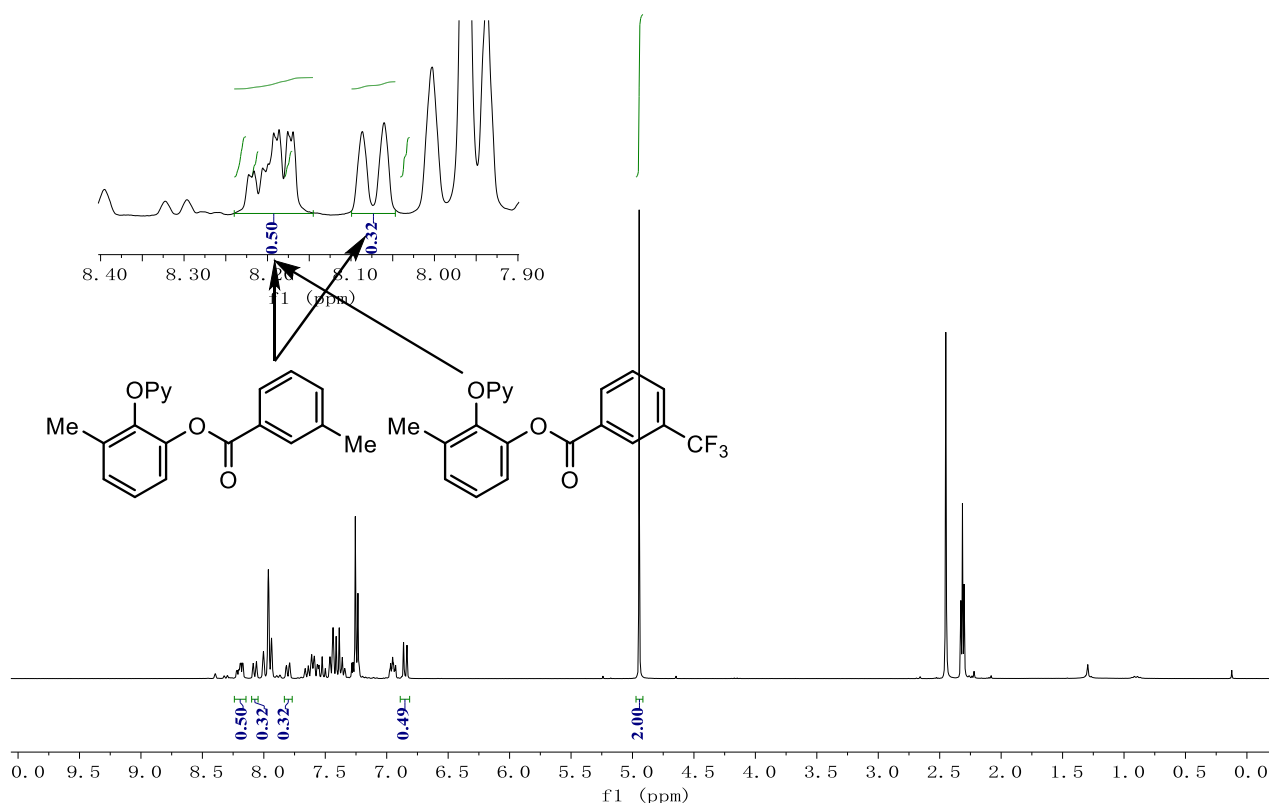
(35%) and **62ga** (25%) were obtained as a mixture and the conversion was determined by ¹H-NMR spectroscopy with CH₂Br₂ (43.5 mg, 0.25 mmol) as internal standard.



A solution of **60a** (46.3 mg, 0.25 mmol), **61g** (34.0 mg, 0.25 mmol), **61i** (47.5 mg, 0.25 mmol), [Ru(OAc)₂(*p*-cymene)] (8.8 mg, 10 mol %) and *n*Bu₄NBF₄ (82.3 mg, 0.25 mmol) in DCE (4.0 mL) was placed in a 25 mL Schlenk tube. The tube was sealed with a septum equipped with a Pt electrode (10 mm × 15 mm × 0.25 mm) and a GF electrode (10 mm × 15 mm × 6 mm). An oil bulb was attached to the system by using a needle. The tube was placed in an oil bath and stirred at 100 °C. After 4 h at 3.0 mA, the mixture was cooled to ambient temperature and the solvent was removed *in vacuo*. The residue was purified by column chromatography on silica gel (*n*hexane/EtOAc: 20:1→10:1). The products **62ag** (18%) and **62ai** (32%) were obtained as a mixture and the conversion was determined by ¹H-NMR spectroscopy with CH₂Br₂ (43.5 mg, 0.25 mmol) as internal standard.

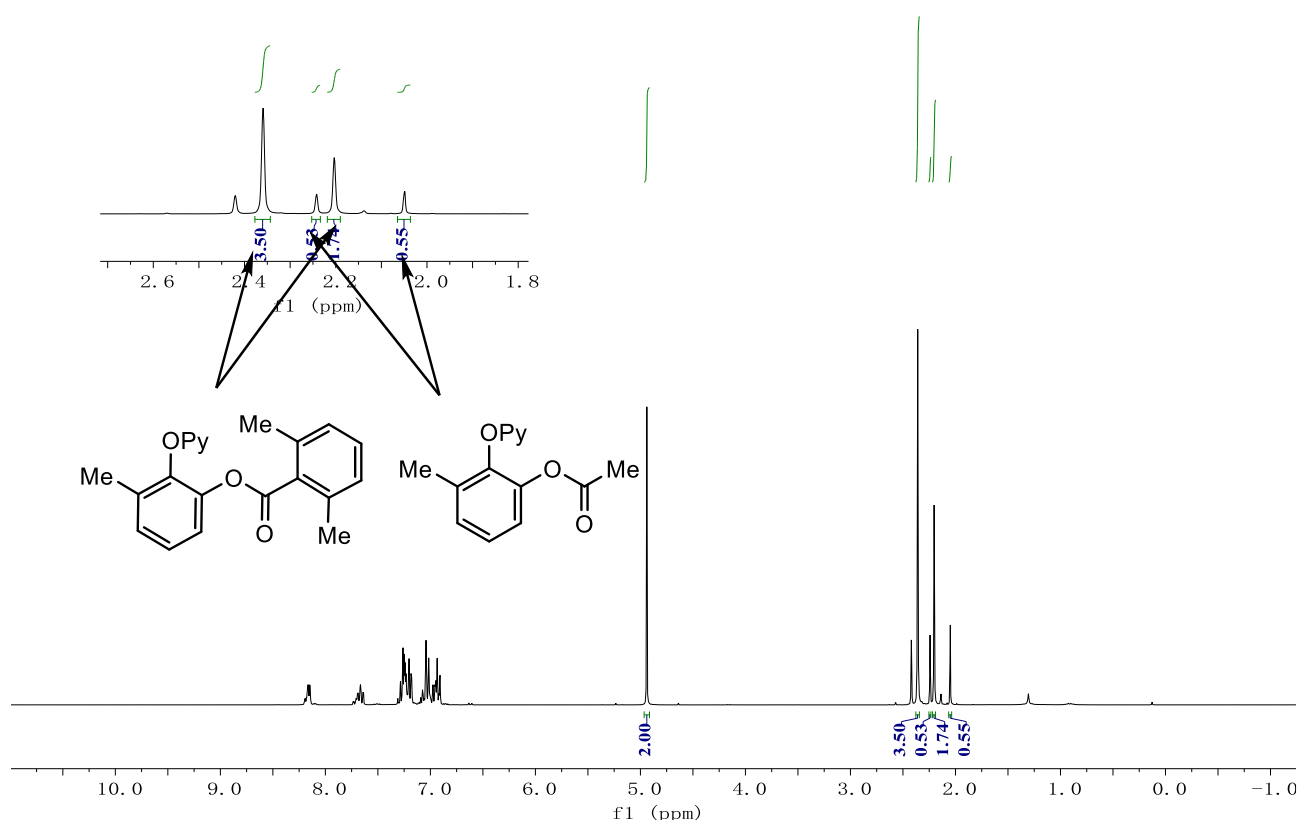
Experimental Data

xhc-013. 1. fid

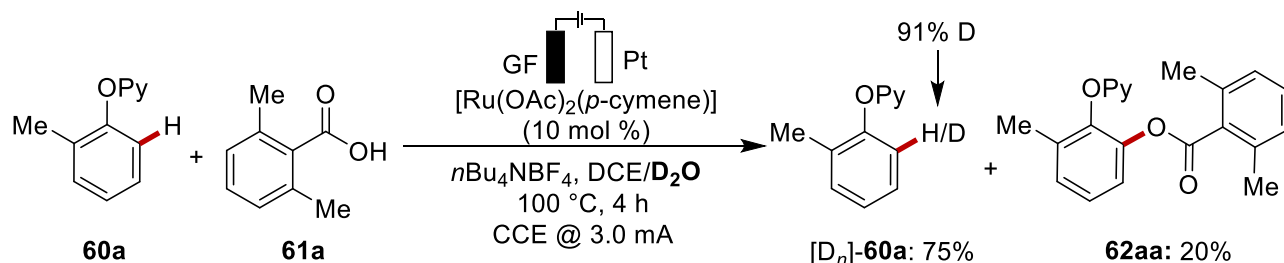


A solution of **60a** (46.3 mg, 0.25 mmol), **61a** (37.5 mg, 0.25 mmol), **61s** (15.0 mg, 0.25 mmol), $[\text{Ru}(\text{OAc})_2(p\text{-cymene})]$ (8.8 mg, 10 mol %) and $n\text{Bu}_4\text{NBF}_4$ (82.3 mg, 0.25 mmol) in DCE (4.0 mL) was placed in a 25 mL Schlenk tube. The tube was sealed with a septum equipped with a Pt electrode (10 mm × 15 mm × 0.25 mm) and a GF electrode (10 mm × 15 mm × 6 mm). An oil bulb was attached to the system by using a needle. The tube was placed in an oil bath and stirred at 100 °C. After 4 h at 3.0 mA, the mixture was cooled to ambient temperature and the solvent was removed *in vacuo*. The residue was purified by column chromatography on silica gel (*n*hexane/EtOAc: 20:1 → 10:1). The products **62aa** (58%) and **62as** (18%) were obtained as a mixture and the conversion was determined by $^1\text{H-NMR}$ spectroscopy with CH_2Br_2 (43.5 mg, 0.25 mmol) as internal standard.

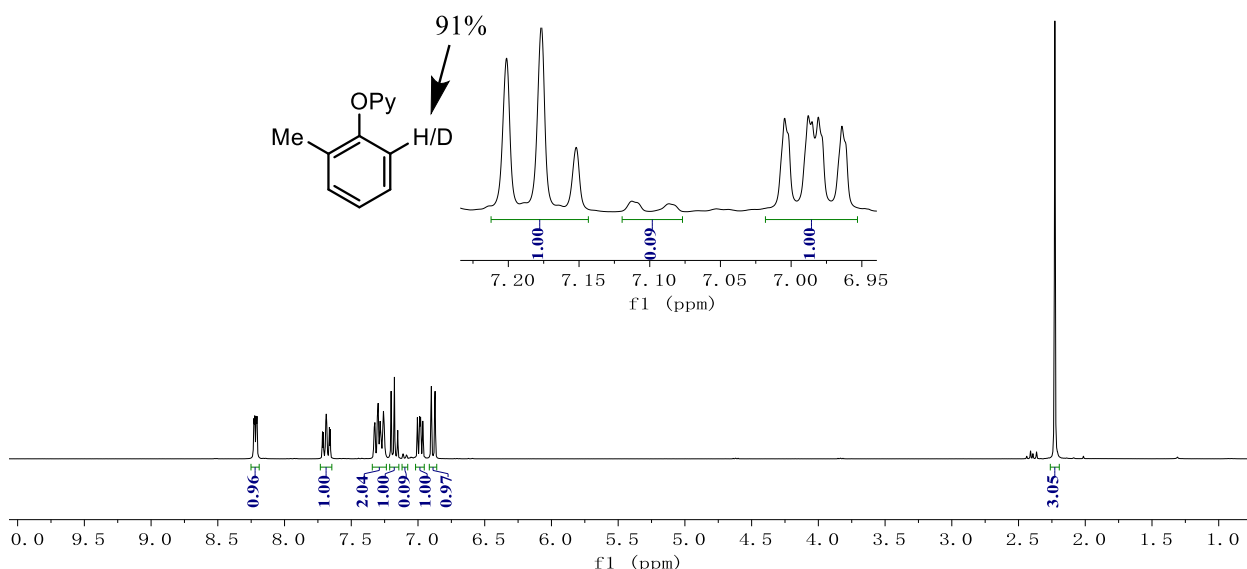
xhb-209.1.fid



5.4.3.2 H/D Exchange Experiments

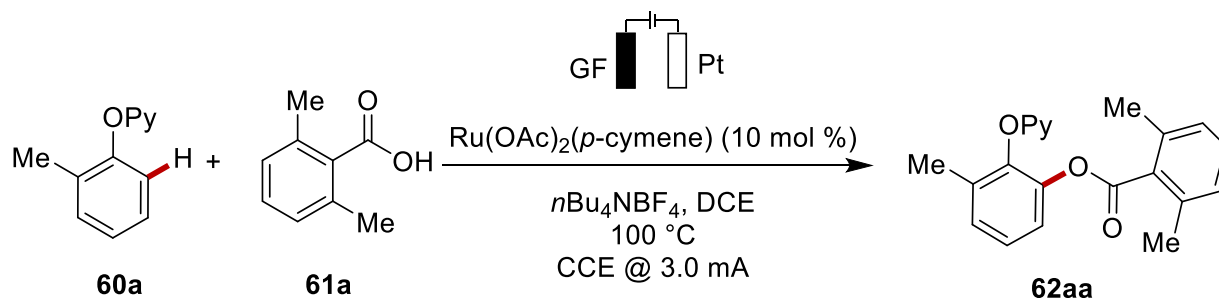


To a 25 mL Schlenk tube equipped with a magnetic stirring bar were added **60a** (46.3 mg, 0.25 mmol), **61a** (60.0 mg, 0.40 mmol), $[\text{Ru}(\text{OAc})_2(\textit{p}\text{-cymene})]$ (8.8 mg, 10 mol %) and $n\text{Bu}_4\text{NBF}_4$ (82.3 mg, 0.25 mmol) in DCE (3.8 mL) and D_2O (0.2 mL). The tube was sealed with a septum equipped with a Pt electrode (10 mm \times 15 mm \times 0.25 mm) and a GF electrode (10 mm \times 15 mm \times 6 mm). An oil bulb was attached to the system by using a needle. The tube was placed in an oil bath and stirred at 100 $^\circ\text{C}$. After 4 h at 3.0 mA, the mixture was cooled to ambient temperature and the solvent was removed *in vacuo*. The residue was purified by column chromatography on silica gel (*n*hexane/EtOAc: 20:1 \rightarrow 10:1) affording **62aa** (16.6 mg, 20%) and unreacted $[\text{D}_n]\text{-60a}$ (34.7 mg, 75%). The deuterium-incorporation was estimated by $^1\text{H-NMR}$ spectroscopy.



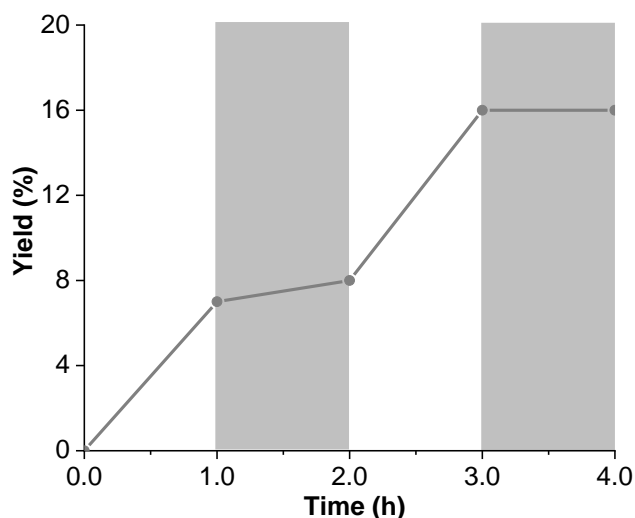
5.4.3.3 On/off Electricity Experiment

On/off electricity reaction was carried out in a 25 mL Schlenk tube, with a GF anode (10 mm × 15 mm × 6 mm) and a Pt cathode (10 mm × 15 mm × 0.25 mm). **60a** (55.5 mg, 0.30 mmol), **61a** (60.0 mg, 0.40 mmol), [Ru(OAc)₂(*p*-cymene)] (10.6 mg, 10 mol %) and *n*Bu₄NBF₄ (99.0 mg, 0.30 mmol) were placed in the tube and dissolved in DCE (5.0 mL). Electrocatalysis was performed at 100 °C with a constant current of 3.0 mA. Aliquots of 0.20 mL were taken from the cell every 1.0 h, and separately mixed with an aliquot (0.20 mL) of a solution of 1,3,5-trimethoxybenzene (0.30 mmol in 5.0 mL of DCE). The mixture was diluted with H₂O (3.0 mL) and extracted with EtOAc (2 X 3.0 mL). After evaporation of solvent, the crude mixture was analyzed by ¹H-NMR spectroscopy.



Experimental Data

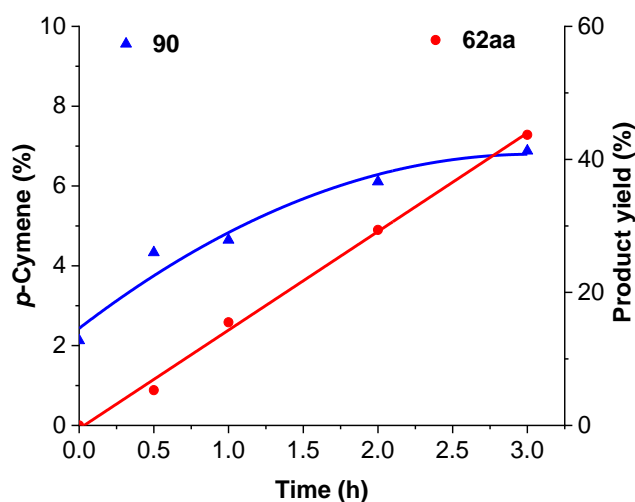
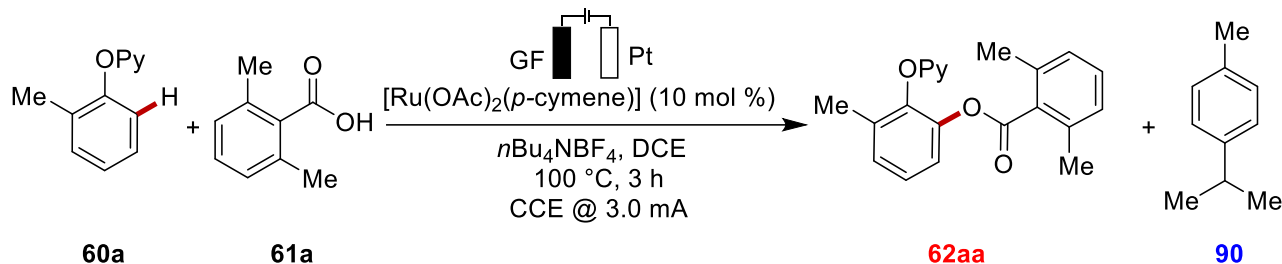
| Time [h] | 0 | 1.0 | 2.0 | 3.0 | 4.0 |
|--------------------------|---|-----|-----|-----|-----|
| Yield of 62aa [%] | 0 | 7 | 8 | 16 | 16 |



Scheme 5-3 On/off electricity experiment.

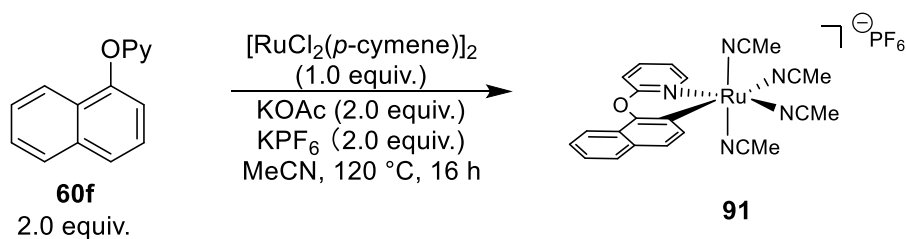
5.4.3.4 Detection of Free *p*-Cymene

A 25 mL Schlenk-tube was charged with **60a** (46.3 mg, 0.25 mmol), **61a** (60.0 mg, 0.40 mmol), [Ru(OAc)₂(*p*-cymene)] (8.8 mg, 10 mol %) and *n*Bu₄NBF₄ (82.3 mg, 0.25 mmol). *n*Dodecane (10 μL) and DCE (4.0 mL) were added and the mixture was stirred at 100 °C with a constant current of 3.0 mA. During the course of the reaction, aliquots of 100 μL were taken via syringe after 0 h, 0.5 h, 1 h, 2 h and 3 h, respectively. The sample was diluted with EtOAc, filtered through a short plug of silica gel and analyzed by gas chromatography.



Scheme 5-4 Release of *p*-cymene (90) in the reaction of 60a and 61a.

5.4.3.5 Synthesis of Cyclometalated Ruthenium Complex



An oven-dried pressure tube was charged with 2-(naphthalen-1-yloxy)pyridine **60f** (221 mg, 1.00 mmol), $[\text{RuCl}_2(\textit{p}\text{-cymene})]_2$ (306 mg, 0.50 mmol), KOAc (196 mg, 2.00 mmol) and KPF_6 (368 mg, 2.00 mmol). After evacuation and refilling with N_2 for three times, MeCN (6.5 mL) was added and the tube was sealed. The reaction mixture was stirred at 120 °C. After 16 h, the reaction was cooled down to the ambient temperature. The crude mixture was loaded on an aluminium oxide (Al_2O_3 , neutral, conditioned with CH_2Cl_2) column and eluted with MeCN/ CH_2Cl_2 (2:1) using N_2 instead of air. The yellow band was collected and the solvent was removed under reduced pressure. The complex was dissolved in MeCN (4 mL) and precipitated with Et_2O , affording the desired complex **91** (378 mg, 60%) as a yellow solid. The complex **91** was transferred to the glovebox subsequently.

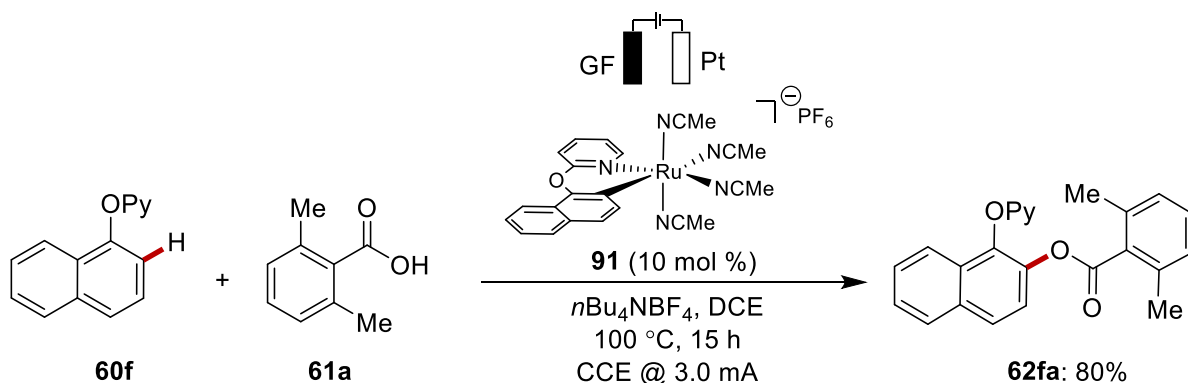
M. p. = >170 °C (decomp.).

¹H-NMR (400 MHz, MeCN-*d*₃) δ = 8.66 (ddd, *J* = 5.9, 1.9, 0.6 Hz, 1H), 8.26 (dq, *J* = 8.5, 0.9 Hz, 1H), 7.91 (d, *J* = 8.2 Hz, 1H), 7.87 – 7.78 (m, 2H), 7.50 – 7.43 (m, 2H), 7.40 (ddd, *J* = 8.2, 1.4, 0.6 Hz, 1H), 7.30 (ddd, *J* = 8.1, 6.8, 1.2 Hz, 1H), 7.11 (ddd, *J* = 7.2, 5.9, 1.4 Hz, 1H), 2.49 (s, 3H), 2.18 (s, 6H), 1.96 (s, 3H). **¹³C-NMR** (101 MHz, MeCN-*d*₃) δ = 165.4 (C_q), 154.9 (CH), 152.7 (C_q), 152.5 (C_q), 140.9 (CH), 140.4 (CH), 132.8 (C_q), 128.4 (CH), 126.1 (CH), 124.9 (C_q), 124.5 (C_q), 123.9 (CH), 123.5 (C_q), 122.4 (CH), 120.2 (CH), 119.7 (CH), 115.6 (CH), 4.4 (CH₃), 4.0 (CH₃). **¹⁹F-NMR** (376 MHz, MeCN-*d*₃) δ = -72.8 (d, *J* = 706 Hz). **³¹P-NMR** (162 MHz, MeCN-*d*₃) δ = -144.6 (hept, *J* = 706 Hz).

IR (ATR): 2270, 1568, 1472, 1390, 1258, 1155, 1039, 833, 772, 556 cm⁻¹.

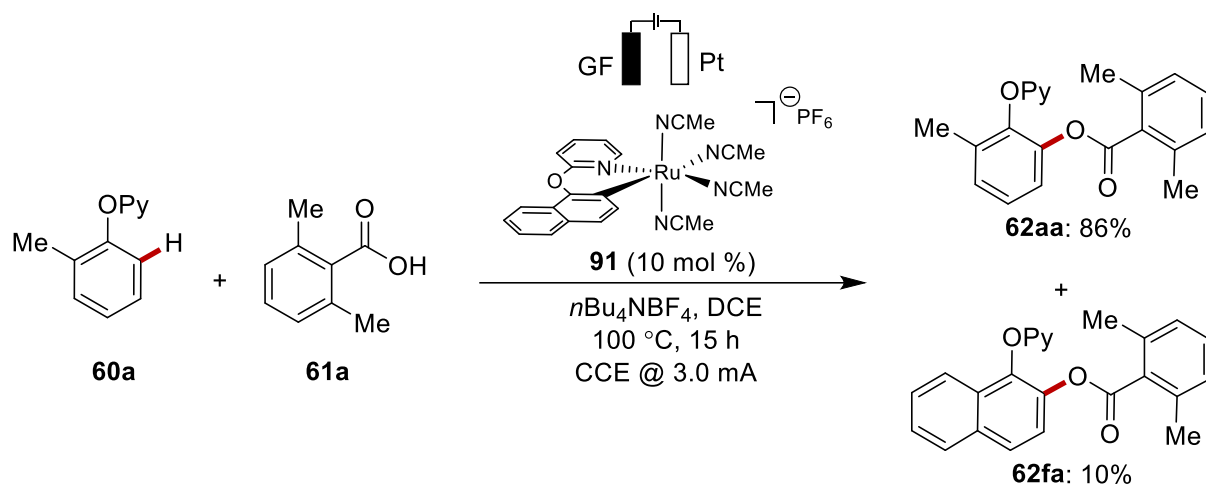
MS (ESI) *m/z* (relative intensity): 445 (100) [M–MeCN–PF₆]⁺. **HR-MS** (ESI) *m/z* calcd. for C₂₁H₁₉N₄ORu⁺ [M–MeCN–PF₆]⁺ 445.0602, found 445.0596.

5.4.3.6 Reactions with Cyclometalated Complex

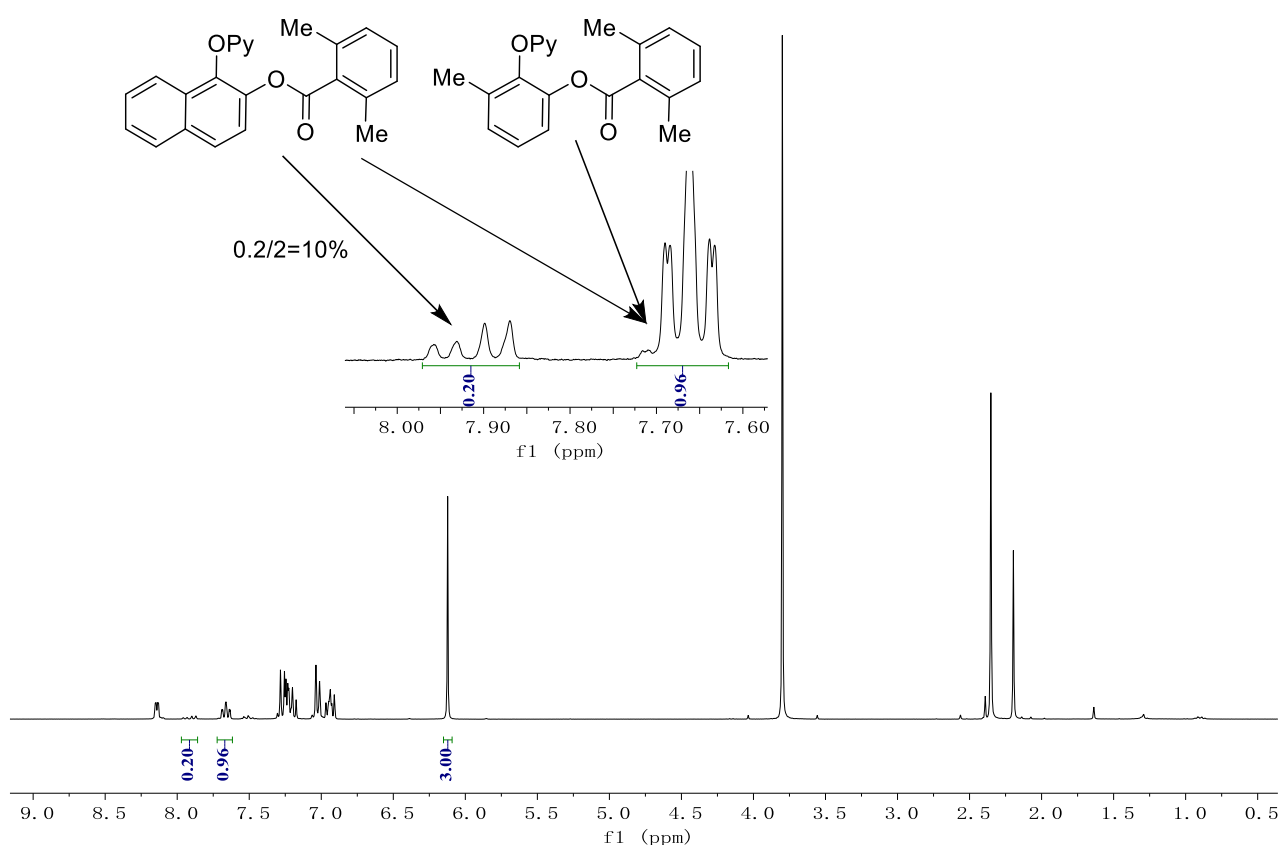


To a 25 mL Schlenk tube equipped with a magnetic stirring bar, **60f** (55.3 mg, 0.25 mmol), **61a** (60.0 mg, 0.40 mmol), **91** (15.8 mg, 10 mol %) and *n*Bu₄NBF₄ (82.3 mg, 0.25 mmol) were added. The tube was sealed with a septum equipped with a Pt plate electrode (10 mm × 15 mm × 0.25 mm) and a GF electrode (10 mm × 15 mm × 6 mm). Then the DCE (4.0 mL) was successively added. An oil bulb was attached to the system by using a needle. The tube was placed in an oil bath and stirred at 100 °C. After 15 h at 3.0 mA, the tube was cooled to ambient temperature and the solvent was removed under vacuum. Purification of the residue by column chromatography on silica gel (*n*hexane/EtOAc: 10:1→5:1) yielded product **62fa** (73.9 mg, 80%) as a white solid.

Experimental Data



To a 25 mL Schlenk tube equipped with a magnetic stirring bar, **60a** (46.3 mg, 0.25 mmol), **61a** (60.0 mg, 0.40 mmol), **91** (15.8 mg, 10 mol %) and $n\text{Bu}_4\text{NBF}_4$ (82.3 mg, 0.25 mmol) were added. The tube was sealed with a septum equipped with a Pt plate electrode (10 mm × 15 mm × 0.25 mm) and a GF electrode (10 mm × 15 mm × 6 mm). Then the DCE (4.0 mL) was successively added. An oil bulb was attached to the system by using a needle. The tube was placed in an oil bath and stirred at 100 °C. After 15 h at 3.0 mA, the tube was cooled to ambient temperature and the solvent was removed under vacuum. The residue was purified by column chromatography on silica gel ($n\text{hexane}/\text{EtOAc}$: 10:1→5:1). The products **62aa** (86%) and **62fa** (10%) were obtained as a mixture and the conversion was determined by $^1\text{H-NMR}$ spectroscopy with 1,3,5-trimethoxybenzene (42.0 mg, 0.25 mmol) as internal standard.



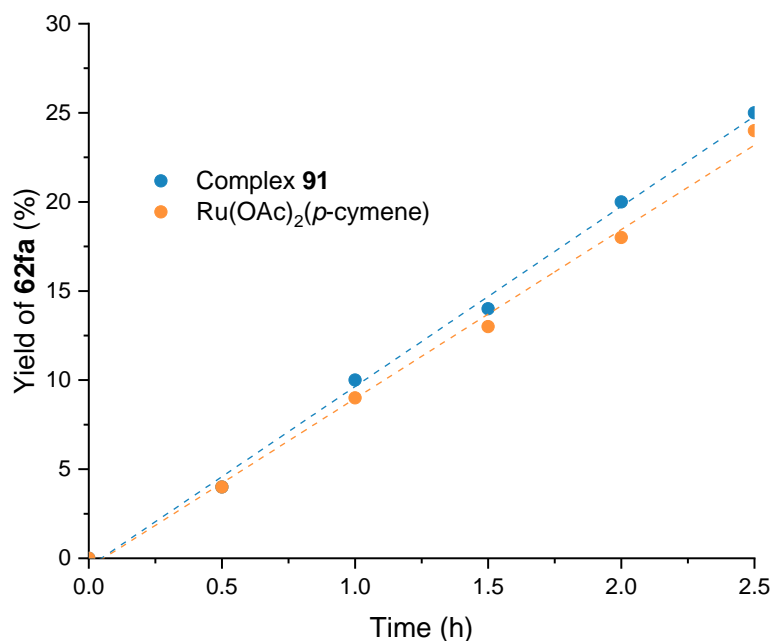
5.4.3.7 Reaction Rate Comparison of Complex **91** and $\text{Ru}(\text{OAc})_2(p\text{-cymene})$

a) A 25 mL Schlenk-tube was charged with **60f** (66.3 mg, 0.30 mmol), **61a** (60.0 mg, 0.40 mmol), $[\text{Ru}(\text{OAc})_2(p\text{-cymene})]$ (10.6 mg, 10 mol %), $n\text{Bu}_4\text{NBF}_4$ (99.0 mg, 0.30 mmol) and DCE (5.0 mL). Electrocatalysis was performed at 100 °C with a constant current of 3.0 mA. Aliquots of 0.20 mL were collected from the cell every 1.0 h, and separately mixed with an aliquot (0.20 mL) of a solution of 1,3,5-trimethoxybenzene (0.30 mmol in 5.0 mL of DCE). The mixture was diluted with H_2O (3.0 mL) and extracted with EtOAc (2 X 3.0 mL). After evaporation of solvent, the crude mixture was analyzed by $^1\text{H-NMR}$ spectroscopy.

b) A 25 mL Schlenk-tube was charged with **60f** (64.1 mg, 0.29 mmol), **61a** (60.0 mg, 0.40 mmol), complex **91** (19.0 mg, 10 mol %), $n\text{Bu}_4\text{NBF}_4$ (99.0 mg, 0.30 mmol) and DCE (5.0 mL). Electrocatalysis was performed at 100 °C with a constant current of 3.0 mA. Aliquots of 0.20 mL were collected from the cell every 1.0 h, and separately mixed with an aliquot (0.20 mL) of a solution of 1,3,5-trimethoxybenzene (0.30 mmol in 5.0 mL of DCE). The mixture was diluted with H_2O (3.0 mL) and extracted with EtOAc (2 X 3.0 mL). After evaporation of solvent, the crude mixture was analyzed by $^1\text{H-NMR}$ spectroscopy.

Experimental Data

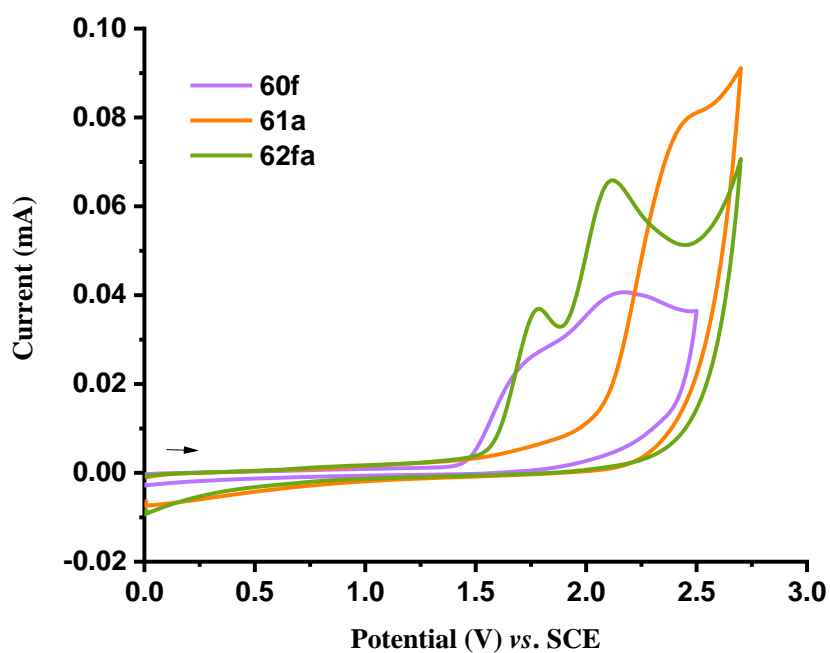
| Time [h] | 0 | 0.5 | 1.0 | 1.5 | 2.0 | 2.5 |
|---|---|-----|-----|-----|-----|-----|
| Yield with complex 91 [%] | 0 | 4 | 10 | 14 | 20 | 25 |
| Yield with [Ru(OAc) ₂ (<i>p</i> -cymene)] [%] | 0 | 4 | 9 | 13 | 18 | 24 |



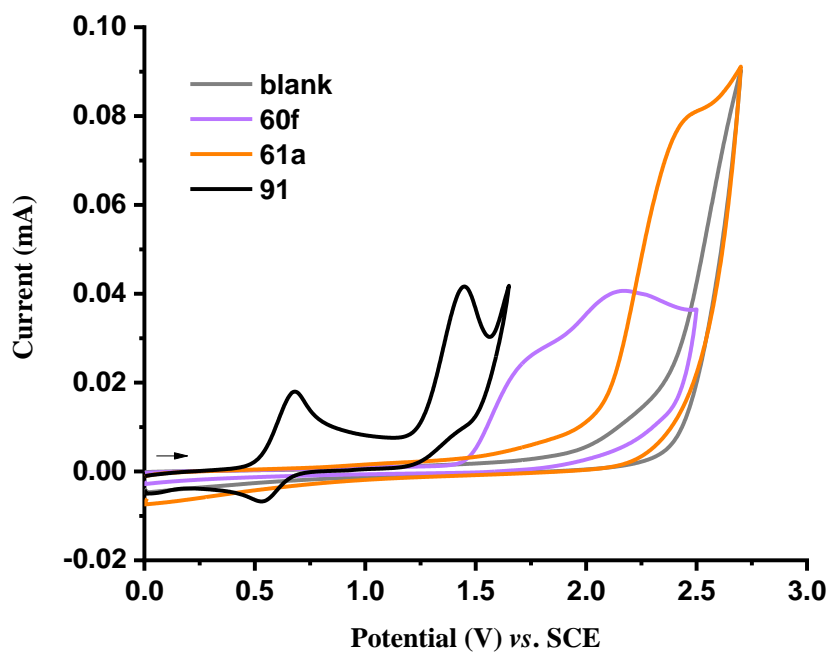
Scheme 5-5 Rate comparison of complex **91** and [Ru(OAc)₂(*p*-cymene)].

5.4.3.8 Cyclic Voltammetry Studies

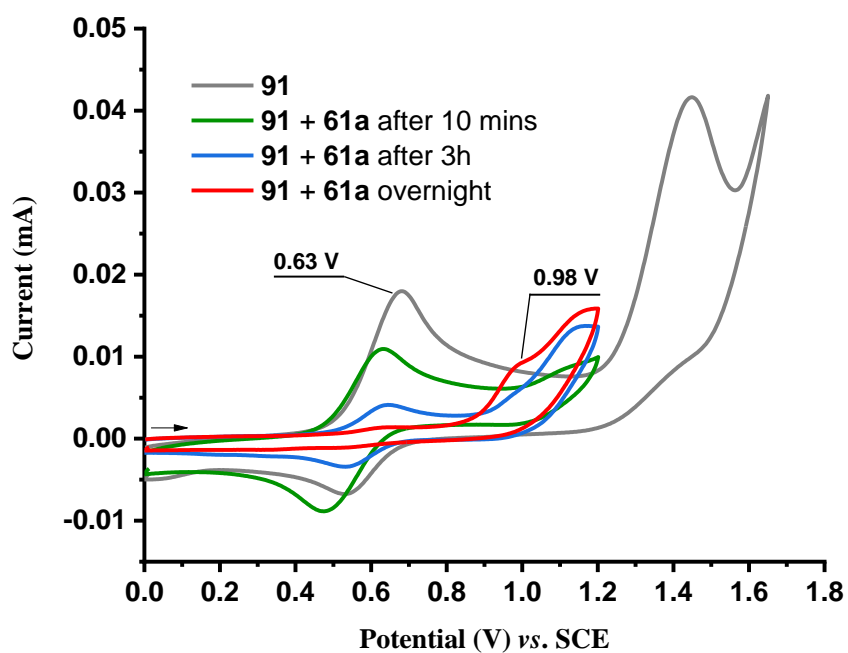
The cyclic voltammetry was carried out with a Metrohm Autolab PGSTAT204 workstation and the following analysis was performed with Nova 2.1 software. A glassy-carbon electrode (3 mm diameter, disc-electrode) was used as the working electrode, a Pt wire was employed as the counter electrode and a saturated calomel electrode (SCE) electrode was used as a reference electrode. The voltammograms were recorded at room temperature in DCE at a substrate concentration of 5 mmol/L and with 100 mmol/L *n*Bu₄NPF₆ as supporting electrolyte. The scan rate is 100 mV/s. Deviations from the general experimental conditions are indicated in the respective figures and descriptions.



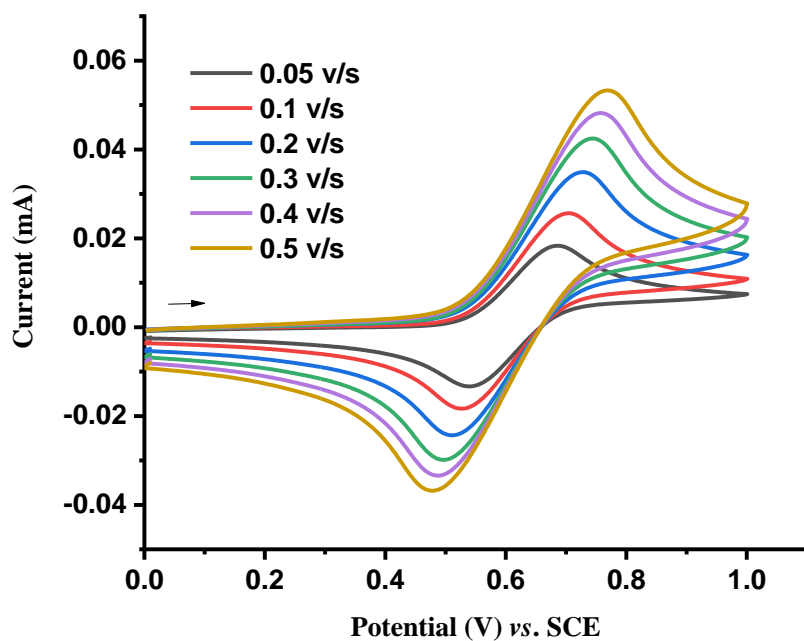
Scheme 5-6 Cyclic voltammogram of 60f, 61a and 62fa in DCE with $n\text{Bu}_4\text{NPF}_6$ (100 mmol/L) at 100 mV/s.



Scheme 5-7 Cyclic voltammogram of 60f, 61a and 91 in DCE with $n\text{Bu}_4\text{NPF}_6$ (100 mmol/L) at 100 mV/s.



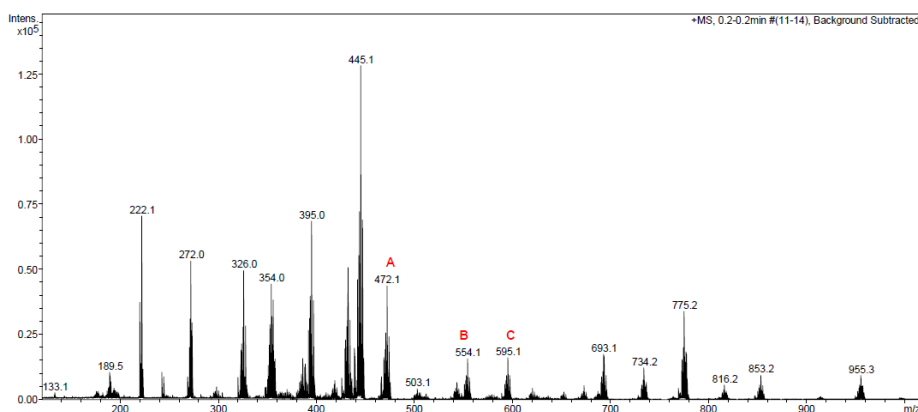
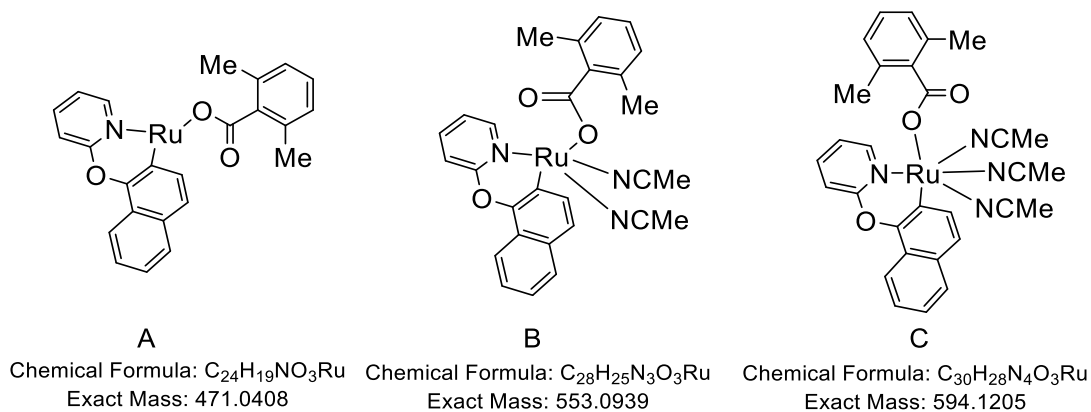
Scheme 5-8 Cyclic voltammogram of complex 91 with 61a as additive in DCE with $n\text{Bu}_4\text{NPF}_6$ (100 mmol/L) at 100 mV/s.



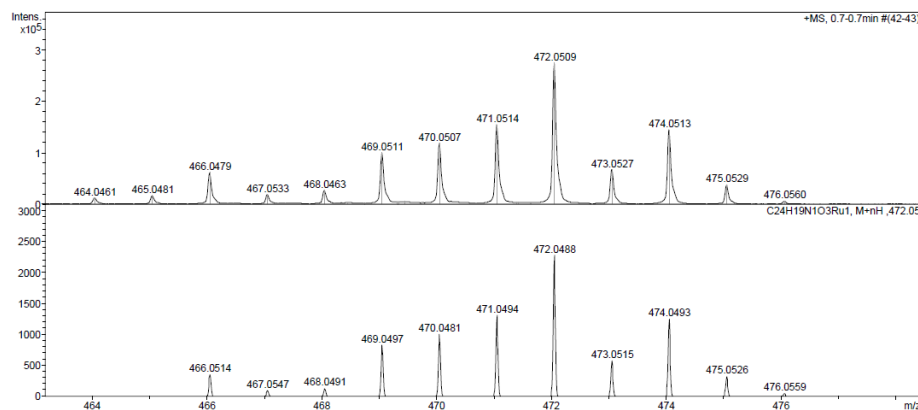
Scheme 5-9 Cyclic voltammogram of complex 91 in DCE with $n\text{Bu}_4\text{NPF}_6$ (100 mmol/L) at different scan rates.

5.4.3.9 ESI–HRMS Analysis of Complex **91** with **61a**

The mixture solution of complex **91** (9.5 mg, 0.015 mmol), **61a** (22.5 mg, 0.15 mmol) and *n*-Bu₄NPF₆ (116.2 mg, 0.3 mmol) in DCE (3 mL) was tested by ESI–HRMS after stirring overnight under room temperature.

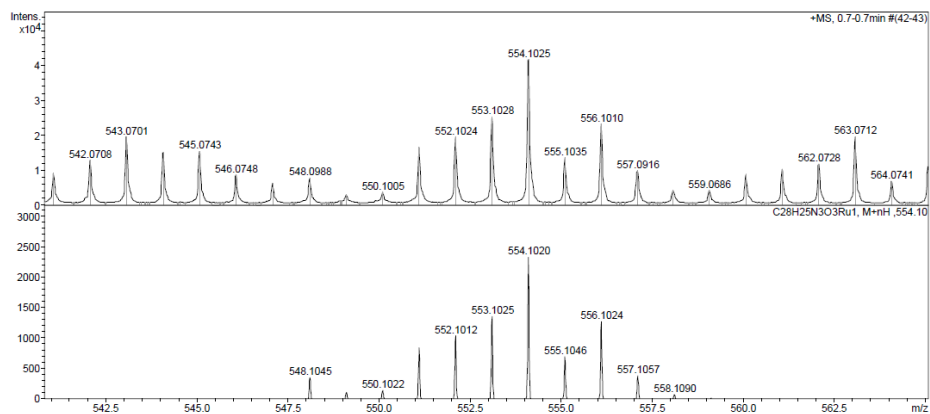


ESI–HRMS analysis- A:

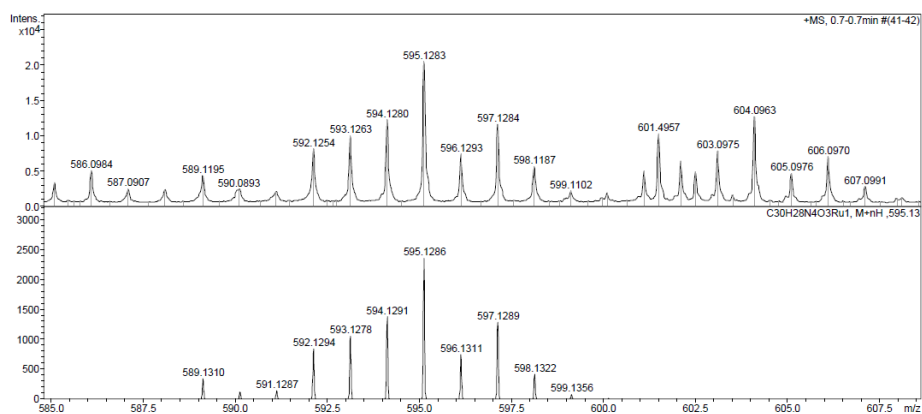


ESI–HRMS analysis- B:

Experimental Data



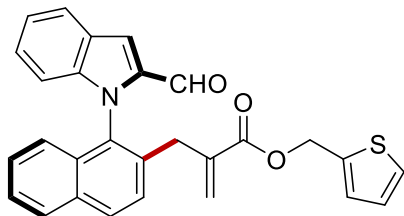
ESI-HRMS analysis- C:



Scheme 5-10 Monitoring of the mixture solution of 91 and 61a in DCE after CV studies using high resolution ESI-HRMS.

5.5 Palladaelectro-Catalyzed C–H Olefination for N–C Axial Chirality via Chiral Transient Directing Group Strategy

5.5.1 Characterization Data



Thiophen-2-ylmethyl-2-[(1-(2-formyl-1H-indol-1-yl) naphthalen-2-yl] methyl acrylate **67ab:** The general procedure **F** was followed using 1-(naphthalen-1-yl)-1H-indole-2-carbaldehyde **63a** (54.2 mg, 0.20 mmol) and thiophen-2-ylmethyl methacrylate **66b** (109.4 mg, 0.60 mmol). Isolation by column chromatography (*n*hexane/EtOAc = 5:1) yielded **67ab** (27.1 mg, 30%) as a yellow oil and **63a** (22.5 mg, 41%) as yellow solid.

¹H-NMR (400 MHz, CDCl₃): δ = 9.65 (s, 1H), 7.95 (d, *J* = 8.6 Hz, 1H), 7.93–7.90 (m, 1H), 7.87–7.83 (m, 1H), 7.54 (d, *J* = 0.9 Hz, 1H), 7.51 (d, *J* = 8.5 Hz, 1H), 7.46 (ddd, *J* = 8.1, 6.8, 1.2 Hz, 1H), 7.32–7.27 (m, 2H), 7.26–7.22 (m, 2H), 6.99 (dd, *J* = 3.5, 1.2 Hz, 1H), 6.94 (dd, *J* = 5.1, 3.5 Hz, 1H), 6.81 (dd, *J* = 8.5, 1.0 Hz, 1H), 6.76–6.72 (m, 1H), 6.09 (d, *J* = 1.0 Hz, 1H), 5.20–5.18 (m, 3H), 3.44 (ABq, *J* = 16.1 Hz, Δ*v* = 28.9 Hz, 2H).

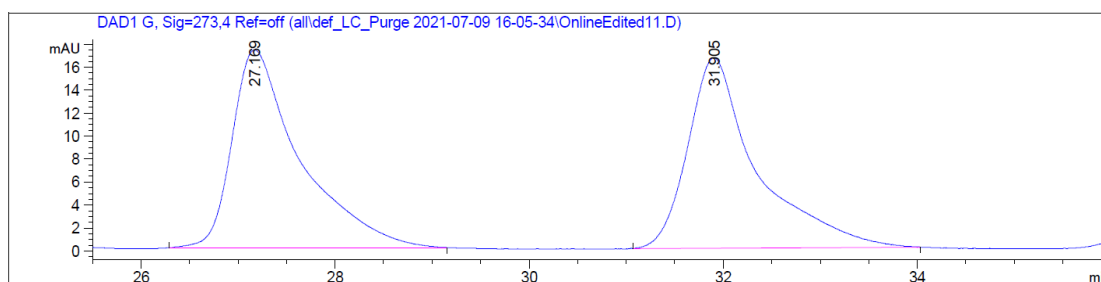
¹³C-NMR (75 MHz, CDCl₃): δ = 181.4 (C_q), 166.0 (CH), 140.8 (CH), 137.7 (CH), 137.6 (CH), 137.0 (CH), 135.5 (CH), 133.1 (CH), 131.8 (CH), 131.7 (CH), 129.3 (C_q), 128.1 (C_q), 128.1 (C_q), 128.0 (CH), 127.7 (C_q), 127.4 (C_q), 127.2 (C_q), 126.7 (C_q), 126.4 (CH), 126.2 (C_q), 123.3 (C_q), 122.3 (C_q), 121.8 (C_q), 114.8 (C_q), 111.8 (C_q), 60.8 (CH), 33.9 (CH).

IR (ATR): 2957, 1714, 1673, 1405, 1314, 1106, 752 cm⁻¹.

MS (ESI) *m/z* (relative intensity): 474 (100) [M + Na]⁺, 452 (75) [M + H]⁺. **HR-MS (ESI): *m/z*** calcd. for [C₂₈H₂₁NO₃S + H]⁺ 452.1315 found 452.1314.

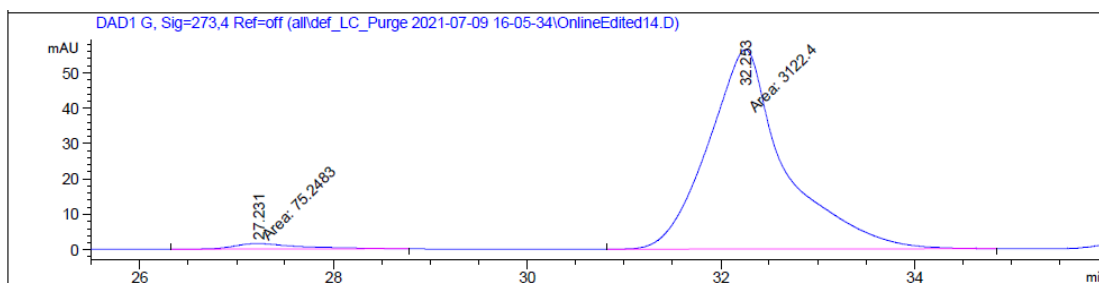
[α]_D²⁰ = –37.0 (c = 1.0, CHCl₃).

HPLC separation (Chiralpak[®] IA-3, *n*hexane/*i*PrOH 98/2, 1.0 mL/min, detection at 273 nm): *t_r* (major) = 32.3 min, *t_r* (minor) = 27.2 min, 95% ee.

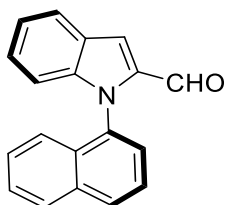


Experimental Data

| Peak # | RetTime [min] | Type | Width [min] | Area [mAU*s] | Height [mAU] | Area % |
|--------|---------------|------|-------------|--------------|--------------|---------|
| 1 | 27.169 | BB | 0.6123 | 836.53931 | 17.23328 | 50.5299 |
| 2 | 31.905 | BB | 0.5987 | 818.99341 | 16.56907 | 49.4701 |



| Peak # | RetTime [min] | Type | Width [min] | Area [mAU*s] | Height [mAU] | Area % |
|--------|---------------|------|-------------|--------------|--------------|---------|
| 1 | 27.231 | MM | 0.7978 | 75.24831 | 1.57200 | 2.3532 |
| 2 | 32.253 | MM | 0.9225 | 3122.40063 | 56.41489 | 97.6468 |



1-(naphthalen-1-yl)-1H-indole-2-carbaldehyde 63a:

M.p.: 90–92 °C (racemic sample).

¹H-NMR (400 MHz, CDCl₃): δ = 9.75 (s, 1H), 8.04 (d, *J* = 8.2 Hz, 1H), 7.99 (d, *J* = 8.3 Hz, 1H), 7.87 (d, *J* = 8.2 Hz, 1H), 7.63 (t, *J* = 7.7 Hz, 1H), 7.59–7.48 (m, 3H), 7.36 (t, *J* = 7.6 Hz, 1H), 7.33–7.18 (m, 2H), 7.09 (d, *J* = 8.5 Hz, 1H), 6.94–6.88 (m, 1H).

¹³C-NMR (101 MHz, CDCl₃) (one carbon is missing due to overlap): δ = 181.6 (CH), 141.6 (C_q), 137.4 (C_q), 134.3 (C_q), 133.8 (C_q), 131.3 (C_q), 129.4 (CH), 128.4 (CH), 127.4 (CH), 127.1 (CH), 126.7 (CH), 126.4 (CH), 125.4 (CH), 123.3 (CH), 122.5 (CH), 121.8 (CH), 114.5 (CH), 111.8 (CH).

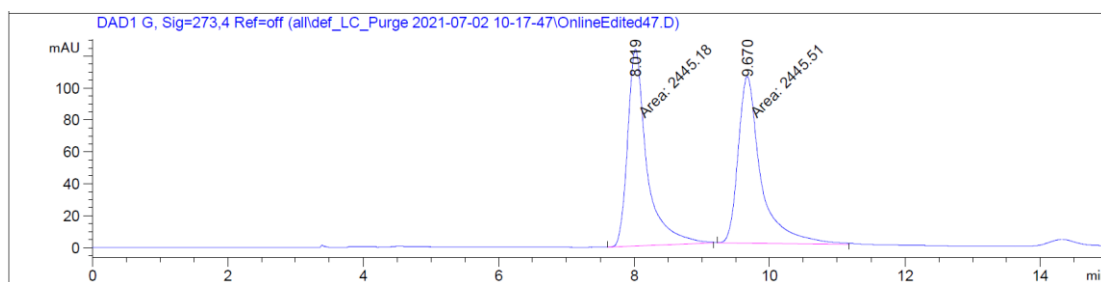
IR (ATR): 2817, 1673, 798, 772, 752, 734, 484 cm⁻¹.

MS (ESI) *m/z* (relative intensity): 294 (100) [M+Na]⁺, 272 (70) [M+H]⁺. **HR-MS** (ESI) *m/z* calc. for [C₁₉H₁₃NO + H]⁺ 272.1070, found 272.1071.

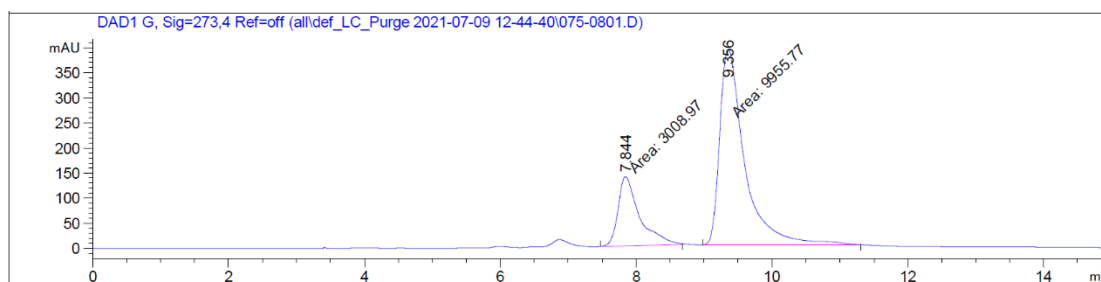
[α]_D²⁰ = +60.7 (c = 1.0, CHCl₃).

Experimental Data

HPLC separation (Chiralpak® IB-3, *n*hexane/*i*PrOH 95:5, 1.0 mL/min, detection at 273 nm):
 t_r (major) = 9.4 min, t_r (minor) = 7.8 min, 54% ee.



| Peak # | RetTime [min] | Type | Width [min] | Area [mAU*s] | Height [mAU] | Area % |
|--------|---------------|------|-------------|--------------|--------------|---------|
| 1 | 8.019 | MM | 0.3301 | 2445.17529 | 123.43890 | 49.9965 |
| 2 | 9.670 | MM | 0.3899 | 2445.51367 | 104.54658 | 50.0035 |

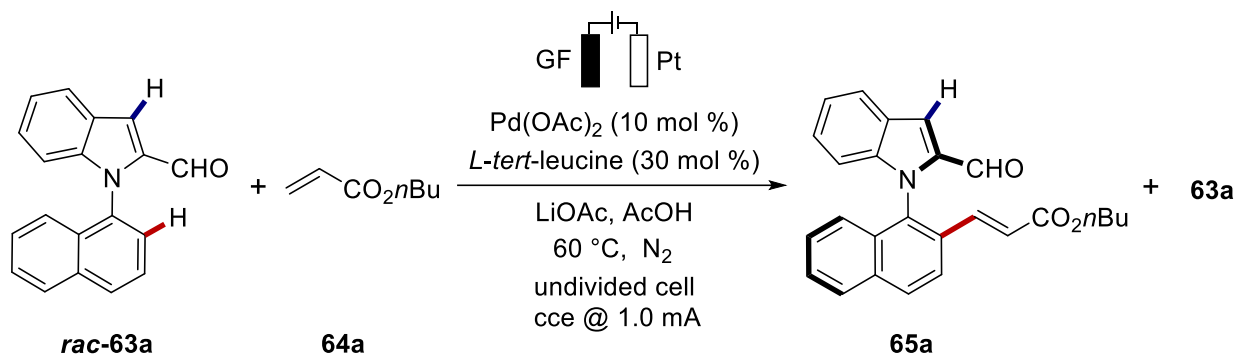


| Peak # | RetTime [min] | Type | Width [min] | Area [mAU*s] | Height [mAU] | Area % |
|--------|---------------|------|-------------|--------------|--------------|---------|
| 1 | 7.844 | MM | 0.3650 | 3008.97314 | 137.39168 | 23.2089 |
| 2 | 9.356 | MM | 0.4261 | 9955.76563 | 389.42172 | 76.7911 |

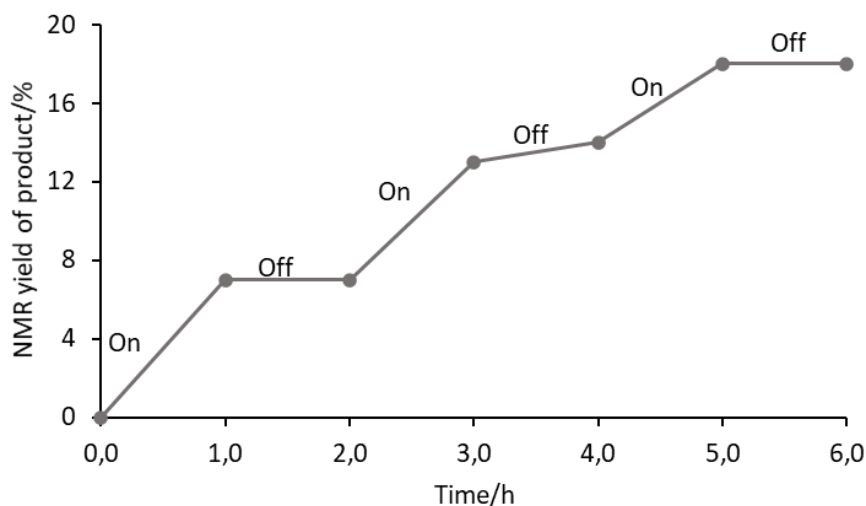
5.5.2 On/off Experiment

On/off electricity reaction was carried out in an undivided cell, with a GF anode (10 mm × 15 mm × 6 mm) and a Pt cathode (10 mm × 15 mm × 0.25 mm). **rac-63a** (81.4 mg, 0.30 mmol, 1.0 equiv.), **64a** (115.5 mg, 0.90 mmol, 3.0 equiv.), Pd(OAc)₂ (6.7 mg, 10 mol %), *L*-tert-leucine (11.7 mg, 30 mol %) and LiOAc (40.5 mg, 2.0 equiv.) were placed in a 10 mL cell and dissolved in AcOH (6.0 mL) under nitrogen atmosphere. Electrocatalysis was performed at 60 °C with a constant current of 1.0 mA. Aliquots of 0.20 mL were collected from the cell every 1.0 h, and separately mixed with an aliquot (0.20 mL) of a solution of 1,3,5-trimethoxybenzene (0.30 mmol in 6.0 mL of AcOH). The mixture was extracted with

EtOAc/H₂O. After evaporation of solvent, the crude mixture was analyzed by ¹H-NMR spectroscopy.



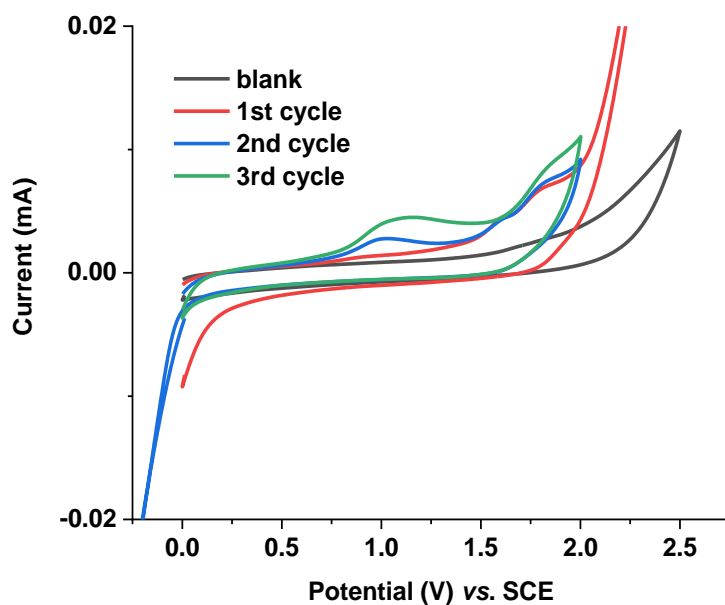
| Time (h) | 0 | 1.0 | 2.0 | 3.0 | 4.0 | 5.0 | 6.0 |
|----------------------|---|-----|-----|-----|-----|-----|-----|
| Yield 65a (%) | 0 | 7 | 7 | 13 | 14 | 18 | 18 |



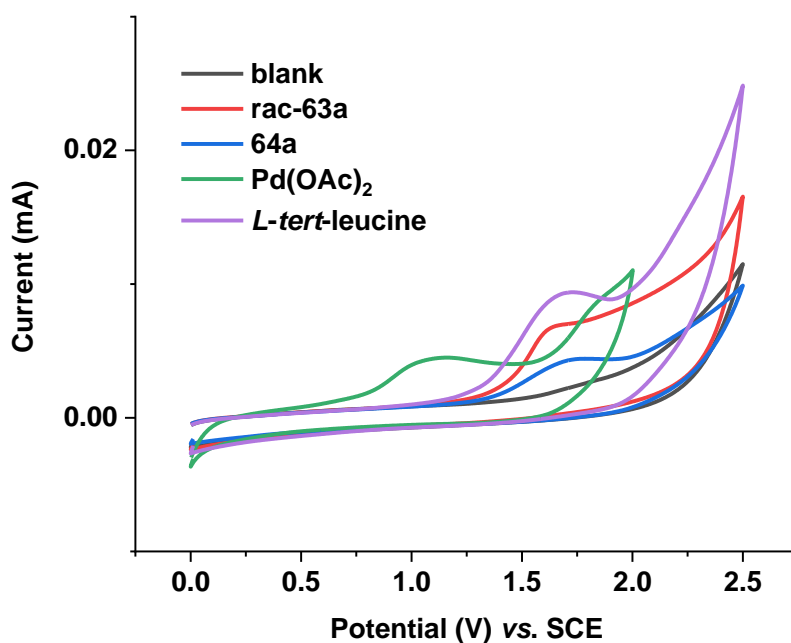
Scheme 5-11 On/off electricity experiment.

5.5.3 Cyclic Voltammetry Study

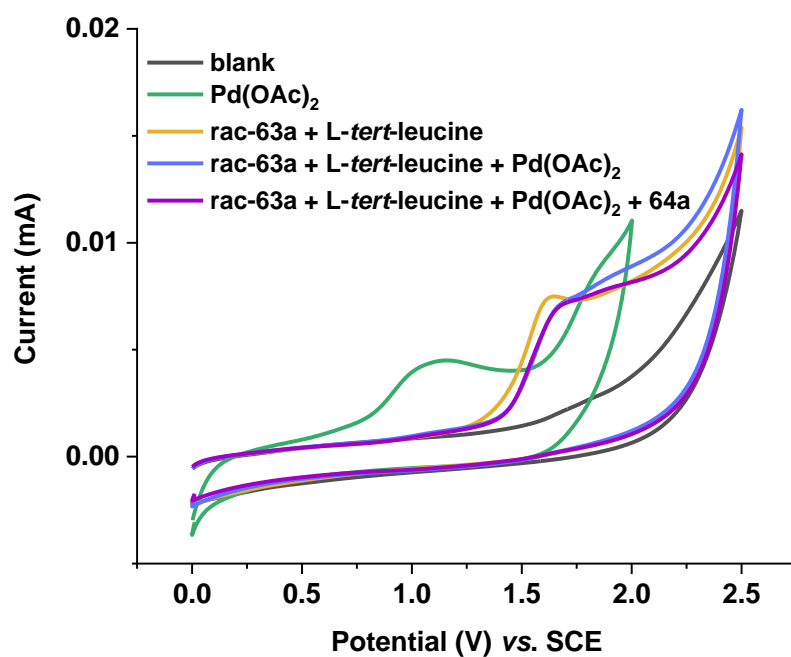
CV measurements were conducted with a Metrohm Autolab PGSTAT204 potentiostat and Nova 2.1 software. A glassy carbon working electrode (disk, diameter: 3 mm), a coiled Pt wire counter electrode and a saturated calomel (SCE) reference electrode were employed. The voltammograms were recorded at room temperature in AcOH at a substrate concentration of 5.0 mmol/L and with 0.1 M *n*Bu₄NPF₆ as supporting electrolyte. The scan rate is 100 mV/s. Deviations from the general experimental conditions are indicated in the respective figures and descriptions.



Scheme 5-12 Cyclic voltammogram of different scan cycles for Pd(OAc)₂ in AcOH with *n*Bu₄NPF₆ (0.1 M) at 100 mV/s.



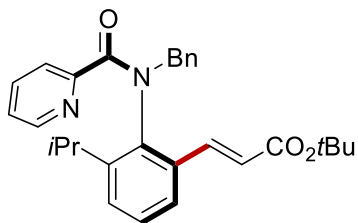
Scheme 5-13 Cyclic voltammogram of several reactants in AcOH with *n*Bu₄NPF₆ (0.1 M) at 100 mV/s.



Scheme 5-14 Cyclic voltammogram of several reaction mixtures in AcOH with $n\text{Bu}_4\text{NPF}_6$ (0.1 M) at 100 mV/s.

5.6 Palladaelectro-Catalyzed C–H Olefinations for Axially Chiral Anilides Mediated by the Mono-*N*-Protected Amino Acid

5.6.1 Characterization Data



tert-butyl 3-(3-(*N*-benzylpicolinamido)-3-isopropylphenyl)acrylate 70aa: Prepared according to general procedure **H** on a 0.5 mmol scale, column chromatography (*n*hexane/acetone = 9:1) afforded the title compound as a pale yellow foam (205 mg, 0.45 mmol, 90%).

¹H-NMR (400 MHz, CDCl₃) δ 8.11 – 8.08 (m, 1H), 7.66 (dt, *J* = 7.9, 1.1 Hz, 1H), 7.54 (td, *J* = 7.8, 1.8 Hz, 1H), 7.32 (d, *J* = 15.9 Hz, 1H), 7.25 – 7.16 (m, 8H), 7.06 – 7.01 (m, 1H), 5.90 (d, *J* = 15.9 Hz, 1H), 5.20 (d, *J* = 13.6 Hz, 1H), 4.75 (d, *J* = 13.6 Hz, 1H), 2.98 (hept, *J* = 6.8 Hz, 1H), 1.50 (s, 9H), 0.84 (d, *J* = 6.8 Hz, 3H), 0.81 (d, *J* = 6.8 Hz, 3H).

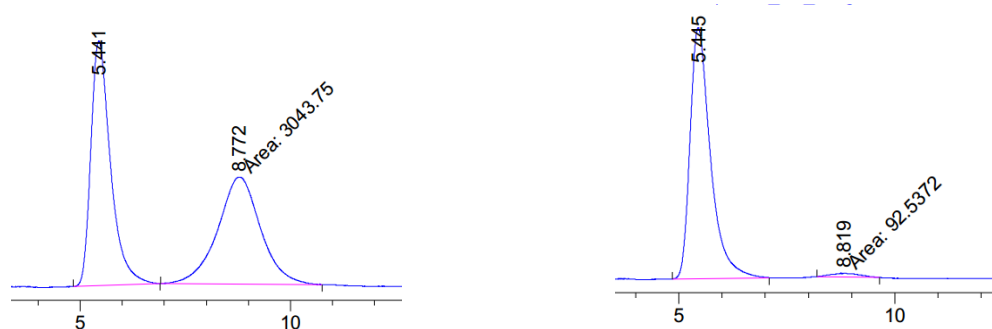
¹³C-NMR (101 MHz, CDCl₃) δ 168.4 (C_q), 165.7 (C_q), 153.3 (C_q), 147.6 (CH), 147.1, (C_q) 140.5 (CH), 139.0 (C_q), 136.0 (CH), 135.9 (C_q), 133.4 (C_q), 130.6 (CH), 128.4 (CH), 128.3 (CH), 128.1 (CH), 127.9 (CH), 124.4 (CH), 124.3 (CH), 124.2 (CH), 121.7 (CH), 80.3 (C_q), 54.5 (CH₂), 28.3 (CH₃), 28.2 (CH), 24.2 (CH₃), 23.6 (CH₃).

HRMS (ESI) calcd. for C₂₉H₃₃N₂O₃⁺ [M+H]⁺: 457.2486. Found: 457.2488.

[α]_D²⁰ = -88.9 (*c* = 1.00, CH₂Cl₂).

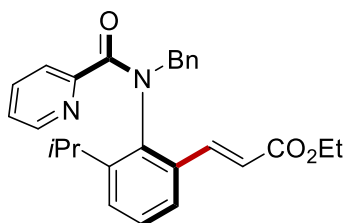
ν_{max} (thin film/cm⁻¹): 1049, 1078, 1147, 1233, 1257, 1287, 1316, 1367, 1390, 1445, 1472, 1568, 1585, 1639, 1704, 2869, 2931, 2967, 3007.

HPLC separation (AS-3 column, *n*hexane/*i*PrOH 95/5, 1.2 mL/min, 273 nm): *t_r*(major) = 5.4 min, *t_r*(minor) = 8.8 min, 98% ee.



Experimental Data

| Peak # | RetTime [min] | Type | Width [min] | Area [mAU*s] | Height [mAU] | Area % | Peak # | RetTime [min] | Type | Width [min] | Area [mAU*s] | Height [mAU] | Area % |
|--------|---------------|------|-------------|--------------|--------------|---------|--------|---------------|------|-------------|--------------|--------------|---------|
| 1 | 5.441 | BB | 0.4660 | 3175.45264 | 97.49440 | 51.0588 | 1 | 5.445 | BV R | 0.4726 | 4323.95996 | 131.51231 | 99.0395 |
| 2 | 8.772 | MM | 1.1871 | 3043.75049 | 42.73253 | 48.9412 | 2 | 8.819 | MM | 0.5617 | 41.93618 | 1.24432 | 0.9605 |



ethyl (E)-3-(2-(N-benzylpicolinamido)-3-isopropylphenyl)acrylate 70ab: Prepared according to general procedure **H** on a 0.5 mmol scale, column chromatography (*n*hexane/EtOAc = 7:3) afforded the title compound as yellow oil (186 mg, 0.43 mmol, 87%). **¹H-NMR** (400 MHz, CDCl₃) δ 8.11 – 8.07 (m, 1H), 7.67 (dt, *J* = 7.9, 1.1 Hz, 1H), 7.58 – 7.52 (m, 1H), 7.48 – 7.42 (m, 1H), 7.27 – 7.21 (m, 3H), 7.21 – 7.15 (m, 5H), 7.06 – 7.02 (m, 1H), 6.01 (d, *J* = 15.9 Hz, 1H), 5.17 (d, *J* = 13.6 Hz, 1H), 4.78 (d, *J* = 13.6 Hz, 1H), 4.25 – 4.14 (m, 2H), 2.93 (hept, *J* = 6.7 Hz, 1H), 1.30 (t, *J* = 7.1 Hz, 3H), 0.81 (d, *J* = 6.7 Hz, 3H), 0.75 (d, *J* = 6.7 Hz, 3H).

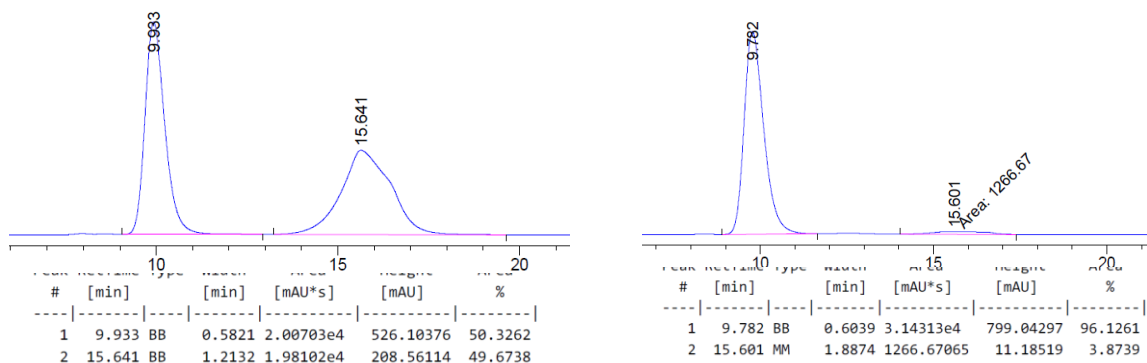
¹³C-NMR (101 MHz, CDCl₃) δ 168.4 (C_q), 166.5 (C_q), 153.3 (C_q), 147.6 (CH), 147.1 (C_q), 141.7 (CH), 139.2 (C_q), 136.1 (CH), 135.9 (C_q), 133.4 (C_q), 130.6 (CH), 128.6 (CH), 128.4 (CH), 128.2 (CH), 128.0 (CH), 124.4 (CH), 124.3 (CH), 119.8 (CH), 60.4 (CH₂), 54.6 (CH₂), 28.2 (CH), 24.2 (CH₃), 23.5 (CH₃), 14.4 (CH₃).

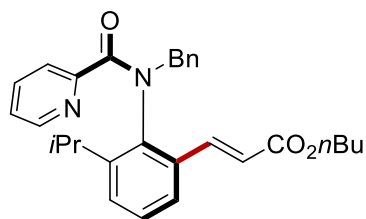
HRMS (ESI) calcd. for C₂₇H₂₉N₂O₃⁺ [M+H]⁺: 429.2173. Found: 429.2173.

[α]_D²⁰ = -120.2 (*c* = 1.02, CHCl₃).

ν_{max} (thin film/cm⁻¹): 1044, 1078, 1166, 1260, 1308, 1365, 1390, 1444, 1495, 1567, 1585, 1638, 1709, 2869, 2929, 2964, 3061.

HPLC separation (AS-3 column, *n*hexane/*i*PrOH 95/5, 1.2 mL/min, 273 nm): *t*_r(major) = 9.8 min, *t*_r(minor) = 15.6 min, 92% ee.





butyl (E)-3-(2-(N-benzylpicolinamido)-3-isopropylphenyl)acrylate 70ac: Prepared according to general procedure **H** on a 0.5 mmol scale, column chromatography (*n*hexane/EtOAc = 7:3) afforded the title compound as yellow oil (178 mg, 0.39 mmol, 78%).

¹H-NMR (400 MHz, CDCl₃) δ 8.06 – 8.02 (m, 1H), 7.64 (dt, *J* = 7.8, 1.1 Hz, 1H), 7.50 (td, *J* = 7.8, 1.8 Hz, 1H), 7.43 (d, *J* = 16.0 Hz, 1H), 7.23 – 7.18 (m, 3H), 7.17 – 7.11 (m, 5H), 7.01 – 6.95 (m, 1H), 5.98 (d, *J* = 15.9 Hz, 1H), 5.15 (d, *J* = 13.6 Hz, 1H), 4.75 (d, *J* = 13.6 Hz, 1H), 4.15 – 4.06 (m, 2H), 2.93 (hept, *J* = 6.8 Hz, 1H), 1.68 – 1.58 (m, 2H), 1.45 – 1.34 (m, 2H), 0.94 (t, *J* = 7.3 Hz, 3H), 0.79 (d, *J* = 6.8 Hz, 3H), 0.75 (d, *J* = 6.8 Hz, 3H).

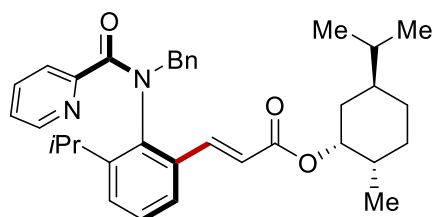
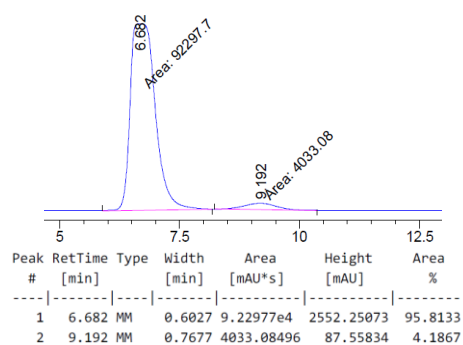
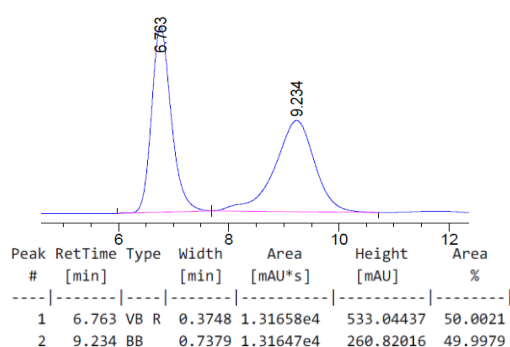
¹³C-NMR (101 MHz, CDCl₃) δ 168.2 (C_q), 166.3 (C_q), 153.0 (C_q), 147.3 (CH), 146.9 (C_q), 141.3 (CH), 138.9 (C_q), 135.8 (CH), 135.7 (C_q), 133.1 (C_q), 130.3 (CH), 128.5 (CH), 128.3 (CH), 128.1 (CH), 127.7 (CH), 124.3 (CH), 124.1 (CH), 124.0 (CH), 119.6 (CH), 64.2 (CH₂), 54.4 (CH₂), 30.6 (CH₂), 28.0 (CH), 24.1 (CH₃), 23.3 (CH₃), 19.1 (CH₂), 13.7 (CH₃).

HRMS (ESI) calcd. for C₂₉H₃₃N₂O₃⁺ [M+H]⁺: 457.2486. Found: 457.2487.

[α]_D²⁰ = -49.9 (*c* = 0.95, CHCl₃).

ν_{max} (thin film/cm⁻¹): 1064, 1166, 1260, 1307, 1388, 1445, 1470, 1567, 1585, 1640, 1709, 2870, 2932, 2961, 3030, 3063.

HPLC separation (AS-3 column, *n*hexane/*i*PrOH 90/10, 1.0 mL/min, 273 nm): *t_r*(major) = 6.7 min, *t_r*(minor) = 9.2 min, 92% ee.



(2R,5R)-5-isopropyl-2-methylcyclohexyl (E)-3-(2-(N-benzylpicolinamido)-3-isopropylphenyl)acrylate 70ad: Prepared according to general procedure H on a 0.5 mmol scale, column chromatography (*n*hexane/acetone = 9:1) afforded the title compound as a colorless foam (197 mg, 0.37 mmol, 73%).

¹H-NMR (400 MHz, CDCl₃) δ 8.17 – 8.05 (m, 1H), 7.75 – 7.65 (m, 1H), 7.59 – 7.35 (m, 2H), 7.30 – 7.10 (m, 9H), 7.10 – 7.01 (m, 1H), 6.07 – 5.89 (m, 1H), 5.45 – 5.08 (m, 1H), 4.93 – 4.57 (m, 2H), 3.19 – 2.87 (m, 1H), 2.04 (td, *J* = 14.5, 3.8 Hz, 1H), 1.91 (hept, *J* = 3.4 Hz, 1H), 1.79 – 1.66 (m, 2H), 1.62 – 1.36 (m, 2H), 1.03 – 0.88 (m, 11H), 0.84 – 0.76 (m, 6H).

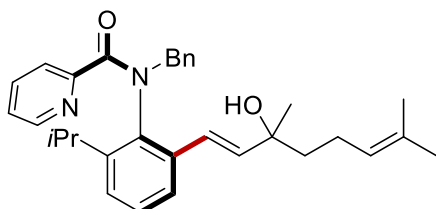
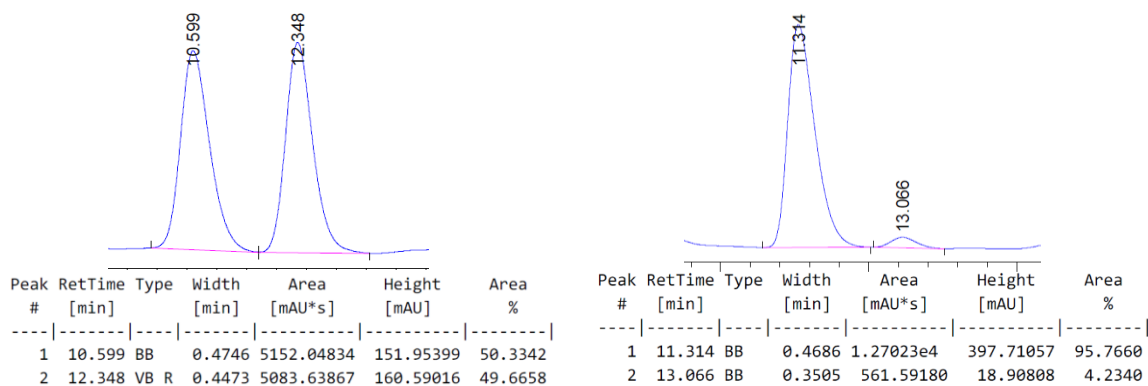
¹³C-NMR (101 MHz, CDCl₃) δ 168.3 (C_q), 165.9 (C_q), 153.3 (C_q), 147.4 (CH), 147.1 (C_q), 141.2 (CH), 139.1 (C_q), 135.9 (CH), 135.8 (C_q), 133.3 (C_q), 130.5 (CH), 128.6 (CH), 128.4 (CH), 128.1 (CH), 127.9 (CH), 124.4 (CH), 124.3 (CH), 124.1 (CH), 120.2 (CH), 74.1 (CH), 54.4 (CH₂), 47.1 (CH), 41.0 (CH₂), 34.3 (CH₂), 31.4 (CH), 28.2 (CH), 26.3 (CH), 24.1 (CH₃), 23.6 (CH₂), 23.5 (CH₃), 22.1 (CH₃), 20.9 (CH₃), 16.5 (CH₃).

HRMS (ESI) calcd. for C₃₅H₄₃N₂O₃⁺ [M+H]⁺: 539.3268. Found: 539.3272.

[α]_D²⁰ = -58.5 (*c* = 1.00, CH₂Cl₂).

ν_{max} (thin film/cm⁻¹): 1078, 1168, 1260, 1306, 1388, 1445, 1585, 1643, 1704, 2869, 2928, 2957.

HPLC separation (AD-3 column, *n*hexane/*i*PrOH 90/10, 1.0 mL/min, 273 nm): *t_r*(major) = 11.3 min, *t_r*(minor) = 13.1 min, 92% ee.



(E)-N-benzyl-N-(2-(3-hydroxy-3,7-dimethylocta-1,6-dien-1-yl)-6-isopropylphenyl)picolinamide 70ae

Prepared according to general procedure **H** on a 0.5 mmol scale, column chromatography (*n*-hexane/acetone = 9:1) afforded the title compound as a colorless oil (73 mg, 0.15 mmol, 30%). The two diastereoisomers were separated by column chromatography.

Diastereoisomer 1:

¹H-NMR (400 MHz, CDCl₃) δ 8.18 (d, *J* = 4.8, 1H), 7.52 – 7.43 (m, 2H), 7.37 – 7.31 (m, 2H), 7.27 – 7.21 (m, 3H), 7.16 – 7.11 (m, 2H), 7.10 – 7.05 (m, 1H), 7.06 – 7.01 (m, 1H), 6.14 (d, *J* = 16.1 Hz, 1H), 5.90 (d, *J* = 16.1 Hz, 1H), 5.29 (d, *J* = 13.7 Hz, 1H), 5.10 – 5.03 (m, 1H), 4.66 (d, *J* = 13.7 Hz, 1H), 3.03 (hept, *J* = 6.8 Hz, 1H), 1.99 – 1.81 (m, 2H), 1.66 (q, *J* = 1.3 Hz, 3H), 1.55 (d, *J* = 1.4 Hz, 3H), 1.53 – 1.39 (m, 2H), 1.15 (s, 3H), 0.91 (d, *J* = 6.6 Hz, 3H), 0.90 (d, *J* = 6.6 Hz, 3H).

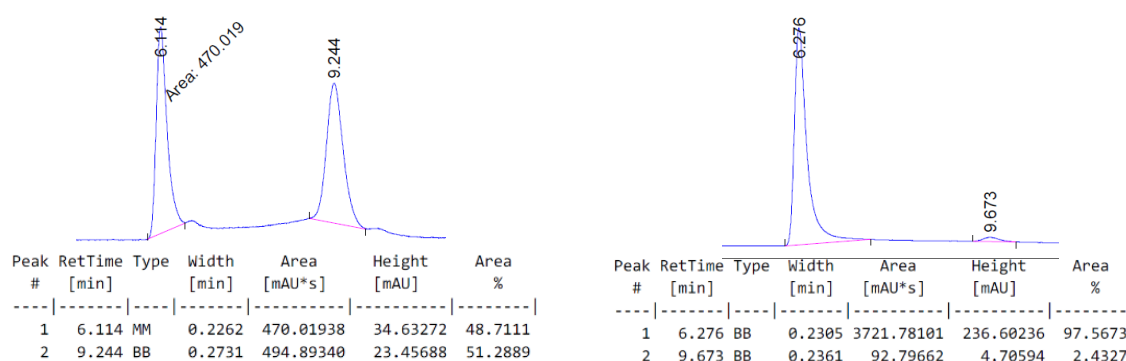
¹³C-NMR (101 MHz, CDCl₃) δ 168.9 (C_q), 153.6 (C_q), 147.9 (CH), 146.8 (C_q), 138.5 (CH), 137.9 (C_q), 136.6 (C_q), 135.8 (CH), 135.5 (C_q), 131.7 (C_q), 130.8 (CH), 128.5 (CH), 128.1 (CH), 127.9 (CH), 126.1 (CH), 124.5 (CH), 124.2 (CH), 124.1 (CH), 123.7 (CH), 123.4 (CH), 73.1 (C_q), 54.3 (CH₂), 42.3 (CH₂), 28.3 (CH), 28.1 (CH₃), 25.8 (CH₃), 24.5 (CH₃), 23.6 (CH₃), 23.0 (CH₂), 17.8 (CH₃).

HRMS (ESI) calcd. for C₃₂H₃₉N₂O₂⁺ [M+H]⁺: 483.3006. Found: 483.2994.

[α]_D²⁰ = -204 (*c* = 0.50, CH₂Cl₂).

ν_{max} (thin film/cm⁻¹): 1078, 1167, 1238, 1286, 1336, 1396, 1441, 1473, 1567, 1585, 1637, 2868, 2926, 2963, 3059, 3440.

HPLC separation (AD-3 column, *n*hexane/*i*PrOH 80/20, 1.0 mL/min, 273 nm): *t_r*(major) = 6.3 min, *t_r*(minor) = 9.7 min, 95% ee.



Diastereoisomer 2:

¹H-NMR (400 MHz, CDCl₃) δ 8.20 – 8.16 (m, 1H), 7.52 – 7.44 (m, 2H), 7.35 – 7.31 (m, 2H), 7.26 – 7.21 (m, 3H), 7.15 – 7.12 (m, 2H), 7.09 – 7.05 (m, 1H), 7.03 (ddd, *J* = 6.9, 4.8, 1.8 Hz, 1H), 6.18 (d, *J* = 16.1 Hz, 1H), 5.92 (d, *J* = 16.1 Hz, 1H), 5.26 (d, *J* = 13.6 Hz, 1H), 5.09 – 5.03 (m, 1H), 4.70 (d, *J* = 13.6 Hz, 1H), 3.02 (hept, *J* = 6.8 Hz, 1H), 1.96 – 1.81 (m, 2H),

1.66 (s, 3H), 1.56 (s, 3H), 1.50 – 1.41 (m, 2H), 1.16 (s, 3H), 0.88 (d, $J = 6.7$ Hz, 3H), 0.88 (d, $J = 6.7$ Hz, 3H).

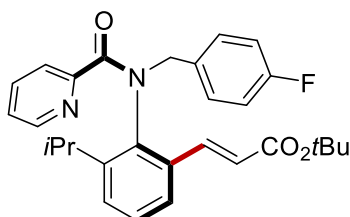
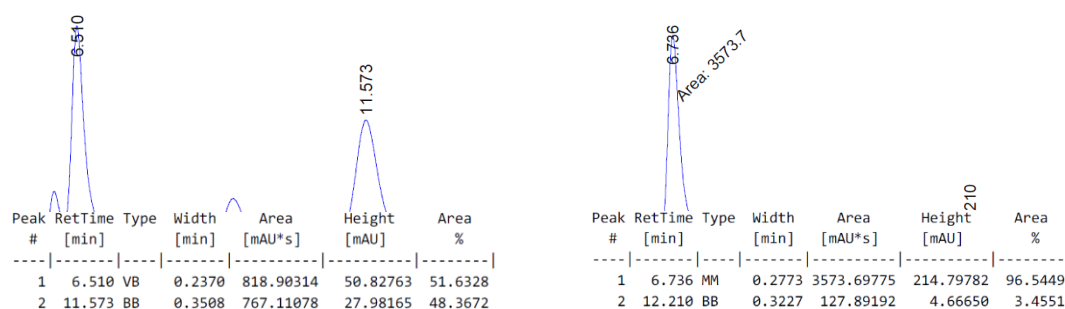
$^{13}\text{C-NMR}$ (101 MHz, CDCl_3) δ 168.9 (C_q), 153.6 (C_q), 147.9 (CH), 146.8 (C_q), 138.7 (CH), 137.8 (C_q), 136.6 (C_q), 135.7 (CH), 135.4 (C_q), 131.8 (C_q), 130.7 (CH), 128.5 (CH), 128.1 (CH), 127.8 (CH), 126.1 (CH), 124.4 (CH), 124.2 (CH), 124.1 (CH), 123.7 (CH), 123.5 (CH), 73.0 (C_q), 54.3 (CH_2), 42.6 (CH_2), 28.3 (CH), 27.5 (CH_3), 25.8 (CH_3), 24.5 (CH_3), 23.6 (CH_3), 22.9 (CH_2), 17.8 (CH_3).

HRMS (ESI) calcd. for $\text{C}_{32}\text{H}_{39}\text{N}_2\text{O}_2^+$ $[\text{M}+\text{H}]^+$: 483.3006. Found: 483.2995.

$[\alpha]_D^{20} = -88.8$ ($c = 1.00$, CH_2Cl_2).

ν_{max} (thin film/ cm^{-1}): 1078, 1167, 1240, 1286, 1336, 1394, 1442, 1472, 1568, 1585, 1637, 2868, 2926, 2964, 3061, 3454.

HPLC separation (AD-3 column, *n*hexane/*i*PrOH 80/20, 1.0 mL/min, 273 nm): t_r (major) = 6.7 min, t_r (minor) = 12.2 min, 93% ee.



tert-butyl (E)-3-(2-(N-(4-fluorobenzyl)picolinamido)-3-isopropylphenyl)acrylate 70ba:

Prepared according to general procedure **H** on a 0.5 mmol scale, column chromatography (*n*hexane/EtOAc = 7:3) afforded the title compound as yellow oil (156 mg, 0.33 mmol, 66%).

$^1\text{H-NMR}$ (400 MHz, CDCl_3) δ 8.07 – 8.03 (m, 1H), 7.66 -7.62 (m, 1H), 7.54 – 7.48 (m, 1H), 7.24 (d, $J = 15.9$ Hz, 1H), 7.21 – 7.13 (m, 5H), 7.03 – 6.97 (m, 1H), 6.87 – 6.81 (m, 2H), 5.87 (d, $J = 15.8$ Hz, 1H), 5.26 (d, $J = 13.7$ Hz, 1H), 4.55 (d, $J = 13.7$ Hz, 1H), 2.97 (hept, $J = 6.8$ Hz, 1H), 1.46 (s, 9H), 0.90 (d, $J = 6.8$ Hz, 3H), 0.82 (d, $J = 6.8$ Hz, 3H).

$^{13}\text{C-NMR}$ (101 MHz, CDCl_3) δ 168.4 (C_q), 165.6 (C_q), 162.6 (d, $J = 246.4$ Hz, C_q), 153.1 (C_q), 147.5 (CH), 147.0 (C_q), 140.3 (CH), 138.9 (C_q), 136.0 (CH), 133.3 (C_q), 132.2 (d, $J = 8.2$ Hz, CH), 131.8 (d, $J = 3.2$ Hz, C_q), 128.5 (CH), 128.2 (CH), 124.4 (CH), 124.2 (CH), 124.1 (CH),

Experimental Data

115.2 (d, $J = 21.3$ Hz, CH), 80.3 (C_q), 53.7 (CH₂), 29.3 (CH), 28.2 (CH₃), 24.3 (CH₃), 23.5 (CH₃).

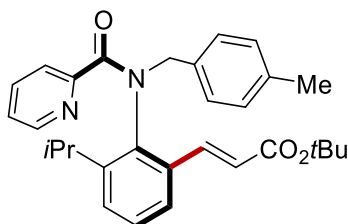
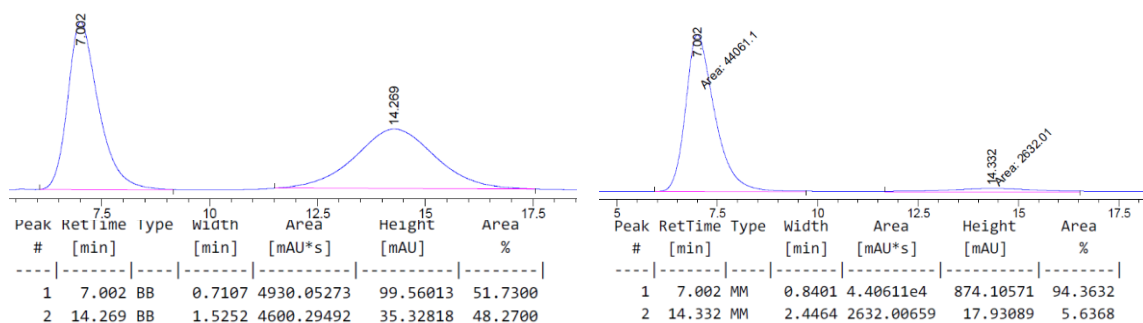
¹⁹F-NMR (376 MHz, CDCl₃) δ -114.31.

HRMS (ESI) calcd. for C₂₉H₃₂FN₂O₃⁺ [M+H]⁺: 475.2391. Found: 475.2389.

[α]_D²⁰ = -92.4 ($c = 1.12$, CHCl₃).

ν_{\max} (thin film/cm⁻¹): 1048, 1094, 1144, 1220, 1284, 13165, 1390, 1446, 1509, 1568, 1586, 1642, 1704, 2870, 2931, 2968, 3062.

HPLC separation (AS-3 column, *n*hexane/*i*PrOH 95/5, 1.0 mL/min, 273 nm): t_r (major) = 7.0 min, t_r (minor) = 14.3 min, 88% ee.



tert-butyl (E)-3-(3-isopropyl-2-(N-(4-methylbenzyl)picolinamido)phenyl)acrylate 70ca:

Prepared according to general procedure H on a 0.5 mmol scale, column chromatography (*n*hexane/EtOAc = 7:3) afforded the title compound as yellow oil (207 mg, 0.44 mmol, 88%).

¹H-NMR (400 MHz, CDCl₃) δ 8.11 – 8.08 (m, 1H), 7.64 (dt, $J = 7.9, 1.1$ Hz, 1H), 7.53 (td, $J = 7.7, 1.8$ Hz, 1H), 7.30 – 7.24 (m, 1H), 7.21 – 7.15 (m, 3H), 7.11 – 7.08 (m, 2H), 7.05 – 7.02 (m, 1H), 7.00 – 6.96 (m, 2H), 5.87 (d, $J = 15.9$ Hz, 1H), 5.22 (d, $J = 13.7$ Hz, 1H), 4.64 (d, $J = 13.7$ Hz, 1H), 3.01 (hept, $J = 6.7$ Hz, 1H), 2.25 (s, 3H), 1.49 (s, 9H), 0.89 (d, $J = 6.7$ Hz, 3H), 0.84 (d, $J = 6.7$ Hz, 3H).

¹³C-NMR (101 MHz, CDCl₃) δ 168.4 (C_q), 165.7 (C_q), 153.4 (C_q), 147.5 (CH), 147.2 (C_q), 140.5 (CH), 139.0 (C_q), 137.5 (C_q), 136.0 (CH), 133.4 (C_q), 132.8 (C_q), 130.5 (CH), 129.0 (CH), 128.4 (CH), 128.1 (CH), 124.3 (CH), 124.2 (CH), 124.0 (CH), 121.5 (CH), 80.3 (C_q), 54.1 (CH₂), 28.3 (CH), 28.2 (CH₃), 24.2 (CH₃), 23.6 (CH₃), 21.2 (CH₃).

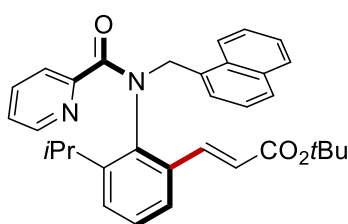
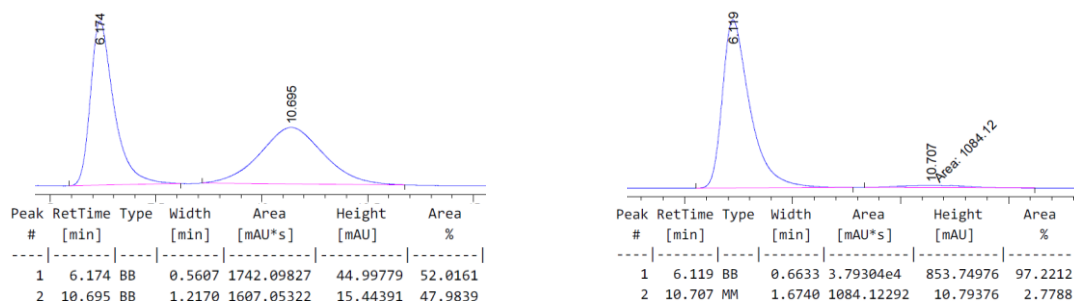
HRMS (ESI) calcd. for C₃₀H₃₅N₂O₃⁺ [M+H]⁺: 471.2642. Found: 471.2641.

[α]_D²⁰ = -70.4 ($c = 1.00$, CHCl₃).

Experimental Data

ν_{\max} (thin film/cm⁻¹): 1050, 1144, 1232, 1258, 1366, 1390, 1446, 1472, 1514, 1567, 1586, 1643, 1703, 2869, 2929, 2967, 3057.

HPLC separation (AS-3 column, *n*hexane/*i*PrOH 95/5, 1.0 mL/min, 273 nm): t_r (major) = 6.2 min, t_r (minor) = 10.7 min, 94% ee.



tert-butyl (E)-3-(3-isopropyl-2-(N-(4-methylbenzyl)picolinamido)phenyl)acrylate 70da:

Prepared according to general procedure **H** on a 0.5 mmol scale, column chromatography (*n*hexane/EtOAc = 7:3) afforded the title compound as white solid (202 mg, 0.40 mmol, 80%).

¹H-NMR (400 MHz, CDCl₃) δ 8.13 – 8.11 (m, 1H), 7.77 – 7.73 (m, 1H), 7.73 – 7.66 (m, 3H), 7.59 (s, 1H), 7.56 – 7.50 (m, 2H), 7.43 – 7.37 (m, 3H), 7.24 – 7.22 (m, 1H), 7.19 (t, J = 7.5 Hz, 1H), 7.16 (dd, J = 7.7, 1.9 Hz, 1H), 7.06 – 7.03 (m, 1H), 5.88 (d, J = 15.9 Hz, 1H), 5.29 (d, J = 13.7 Hz, 1H), 4.99 (d, J = 13.7 Hz, 1H), 2.99 (hept, J = 6.8 Hz, 1H), 1.39 (s, 9H), 0.78 (d, J = 6.8 Hz, 3H), 0.73 (d, J = 6.8 Hz, 3H).

¹³C-NMR (101 MHz, CDCl₃) δ 168.6 (C_q), 165.7 (C_q), 153.4 (C_q), 147.7 (CH), 147.2 (C_q), 140.5 (CH), 139.3 (C_q), 136.1 (CH), 133.5 (C_q), 133.3 (C_q), 133.3 (C_q), 133.1 (C_q), 129.6 (CH), 128.6 (CH), 128.5 (CH), 128.2 (CH), 128.1 (CH), 127.7 (CH), 126.0 (CH), 126.0 (CH), 124.4 (CH), 124.4 (CH), 124.3 (CH), 121.8 (CH), 80.3 (C_q), 54.9 (CH₂), 28.3 (CH), 28.2 (CH₃), 24.2 (CH₃), 23.6 (CH₃).

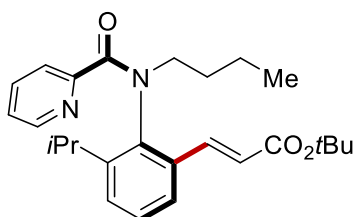
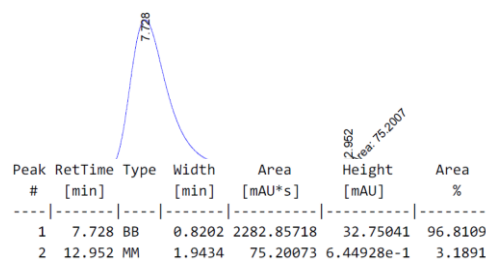
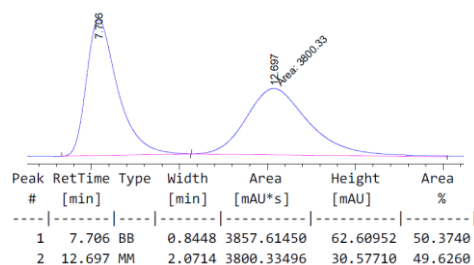
HRMS (ESI) calcd. for C₃₃H₃₅N₂O₃⁺ [M+H]⁺: 507.2642. Found: 507.2644.

[α]_D²⁰ = -54.5 (c = 1.05, CHCl₃).

ν_{\max} (thin film/cm⁻¹): 1050, 11487, 1233, 1258, 1289, 1365, 1393, 1445, 1472, 1568, 1585, 1638, 1704, 2869, 2931, 2967, 3060.

Experimental Data

HPLC separation (AS-3 column, *n*hexane/*i*PrOH 95/5, 1.0 mL/min, 273 nm): t_r (major) = 7.7 min, t_r (minor) = 12.9 min, 94% ee.



tert-butyl (E)-3-(2-(*N*-butylpicolinamido)-3-isopropylphenyl)acrylate 70ea: Prepared according to general procedure **H** on a 0.5 mmol scale, column chromatography (*n*hexane/EtOAc = 7:3) afforded the title compound as yellow oil (192 mg, 0.45 mmol, 91%).

¹H-NMR (400 MHz, CDCl₃) δ 8.08 – 8.05 (m, 1H), 7.84 – 7.78 (m, 1H), 7.61 (dt, $J = 7.8, 1.1$ Hz, 1H), 7.57 – 7.49 (m, 1H), 7.32 – 7.28 (m, 1H), 7.23 – 7.14 (m, 2H), 7.04 – 6.99 (m, 1H), 6.13 (d, $J = 15.9$ Hz, 1H), 3.94 (ddd, $J = 13.1, 11.1, 5.3$ Hz, 1H), 3.54 – 3.42 (m, 1H), 3.08 (hept, $J = 6.8$ Hz, 1H), 1.78 – 1.55 (m, 2H), 1.51 (s, 9H), 1.40 – 1.30 (m, 2H), 1.19 (d, $J = 6.8$ Hz, 3H), 0.89 (t, $J = 7.4$ Hz, 3H), 0.86 (d, $J = 6.8$ Hz, 3H).

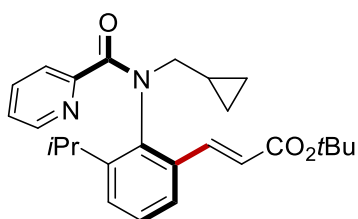
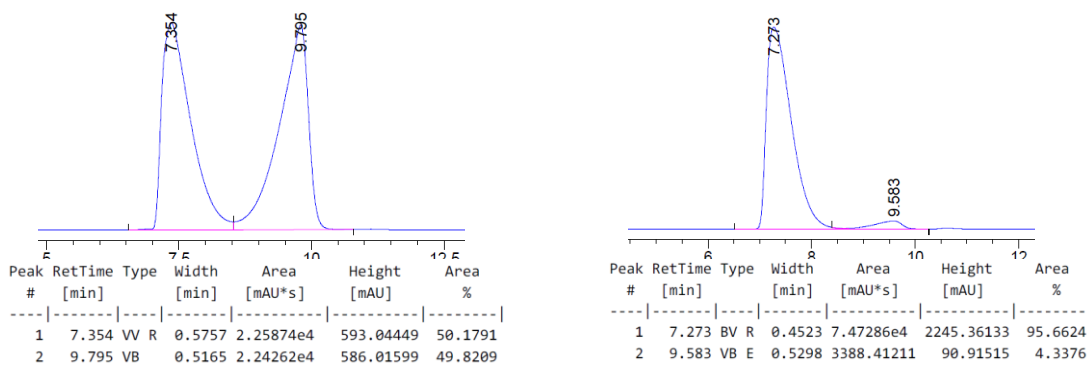
¹³C-NMR (101 MHz, CDCl₃) δ 168.4 (C_q), 165.9 (C_q), 153.6 (C_q), 147.5 (CH), 147.1 (C_q), 141.0 (CH), 140.5 (C_q), 136.0 (CH), 133.2 (C_q), 128.5 (CH), 127.9 (CH), 124.2 (CH), 124.1 (CH), 123.9 (CH), 122.1 (CH), 80.6 (C_q), 52.0 (CH₂), 29.1 (CH₂), 28.3 (CH₃), 28.1 (CH), 24.8 (CH₃), 23.4 (CH₃), 20.7 (CH₂), 13.9 (CH₃).

HRMS (ESI) calcd. for C₂₆H₃₅N₂O₃⁺ [M+H]⁺: 423.2642. Found: 423.2643.

[α]_D²⁰ = -159.6 ($c = 1.08$, CHCl₃).

ν_{max} (thin film/cm⁻¹): 1046, 1099, 1149, 1231, 1258, 1321, 1367, 1393, 1446, 1473, 1567, 1586, 1649, 1705, 2870, 2963, 3065.

HPLC separation (AD-3 column, *n*hexane/*i*PrOH 90/10, 1.0 mL/min, 273 nm): t_r (major) = 7.2 min, t_r (minor) = 9.6 min, 92% ee.



tert-butyl (E)-3-(2-(N-(cyclopropylmethyl)picolinamido)-3-isopropylphenyl)acrylate

70fa: Prepared according to general procedure **H** on a 0.5 mmol scale, column chromatography (*n*hexane/EtOAc = 7:3) afforded the title compound as yellow oil (176 mg, 0.42 mmol, 84%).

¹H-NMR (400 MHz, CDCl₃) δ 8.11 – 8.07 (m, 1H), 7.99 (d, *J* = 16.0 Hz, 1H), 7.63 (dt, *J* = 7.9, 1.1 Hz, 1H), 7.54 (td, *J* = 7.7, 1.8 Hz, 1H), 7.33 – 7.28 (m, 1H), 7.25 – 7.16 (m, 2H), 7.06 – 7.02 (m, 1H), 6.10 (d, *J* = 16.0 Hz, 1H), 4.22 (dd, *J* = 13.7, 7.1 Hz, 1H), 3.11 – 3.23 (m, 2H), 1.53 (s, 9H), 1.22 (d, *J* = 6.8 Hz, 3H), 1.12 – 1.03 (m, 1H), 0.98 (d, *J* = 6.8 Hz, 3H), 0.56 – 0.39 (m, 2H), 0.38 – 0.30 (m, 1H), 0.15 (dtd, *J* = 9.3, 5.4, 4.2 Hz, 1H).

¹³C-NMR (101 MHz, CDCl₃) δ 168.7 (C_q), 166.1 (C_q), 153.8 (C_q), 147.5 (CH), 147.3 (C_q), 141.3 (CH), 140.2 (C_q), 136.0 (CH), 133.5 (C_q), 128.6 (CH), 128.1 (CH), 124.2 (CH), 124.1 (CH), 123.9 (CH), 121.7 (CH), 80.6 (C_q), 55.8 (CH₂), 28.4 (CH₃), 28.3 (CH₃), 24.7 (CH), 23.7 (CH₃), 9.3 (CH), 4.6 (CH₂), 4.5 (CH₂).

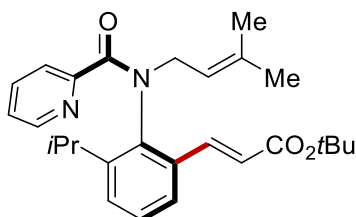
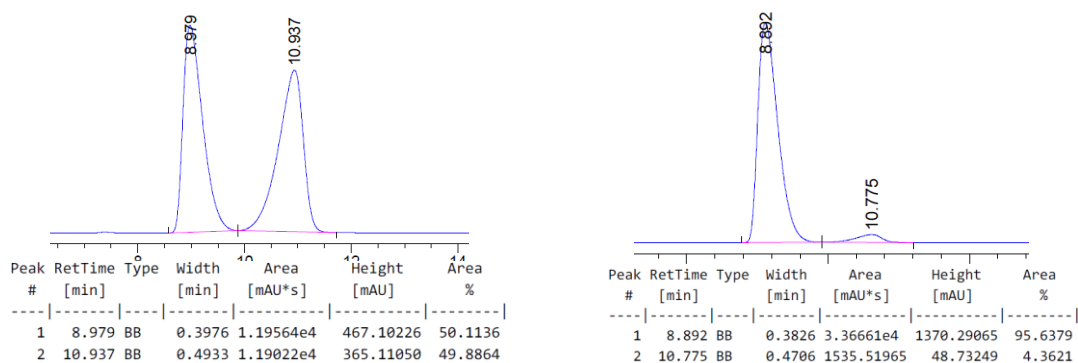
HRMS (ESI) calcd. for C₂₆H₃₃N₂O₃⁺ [M+H]⁺: 421.2486. Found: 421.2480.

[α]_D²⁰ = -97.7 (*c* = 0.90, CHCl₃).

ν_{max} (thin film/cm⁻¹): 1023, 1052, 1141, 1247, 1296, 1317, 1367, 1392, 1446, 1472, 1567, 1586, 1631, 1704, 2872, 2977, 3062.

HPLC separation (AD-3 column, *n*hexane/*i*PrOH 90/10, 1.0 mL/min, 273 nm): *t_r*(major) = 8.9 min, *t_r*(minor) = 10.8 min, 91% ee.

Experimental Data



tert-butyl (E)-3-(3-isopropyl-2-(N-(3-methylbut-2-en-1-yl)picolinamido)phenyl)acrylate

70ga: Prepared according to general procedure **H** on a 0.5 mmol scale, column chromatography (*n*hexane/EtOAc = 7:3) afforded the title compound as yellow oil (139 mg, 0.32 mmol, 64%).

¹H-NMR (400 MHz, CDCl₃) δ 8.10 – 8.07 (m, 1H), 7.77 (d, *J* = 16.0 Hz, 1H), 7.61 (dt, *J* = 7.9, 1.1 Hz, 1H), 7.53 (td, *J* = 7.7, 1.8 Hz, 1H), 7.32 – 7.27 (m, 1H), 7.20 – 7.16 (m, 2H), 7.04 – 7.00 (m, 1H), 6.12 (d, *J* = 15.9 Hz, 1H), 5.46 – 5.39 (m, 1H), 4.62 – 4.52 (m, 1H), 4.18 – 4.08 (m, 1H), 3.10 (hept, *J* = 6.8 Hz, 1H), 1.61 (d, *J* = 1.3 Hz, 3H), 1.51 (s, 9H), 1.50 (s, 3H), 1.16 (d, *J* = 6.8 Hz, 3H), 0.84 (d, *J* = 6.8 Hz, 3H).

¹³C-NMR (101 MHz, CDCl₃) δ 168.2 (C_q), 166.2 (C_q), 153.4 (C_q), 147.6 (CH), 147.1 (C_q), 141.2 (CH), 139.9 (C_q), 137.5 (C_q), 136.0 (CH), 133.3 (C_q), 128.3 (CH), 128.1 (CH), 124.2 (CH), 124.0 (CH), 124.0 (CH), 121.3 (CH), 118.2 (CH), 80.4 (C_q), 49.0 (CH₂), 28.3 (CH₃), 28.2 (CH), 25.9 (CH₃), 24.7 (CH₃), 23.4 (CH₃), 17.7 (CH₃).

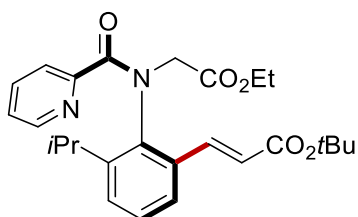
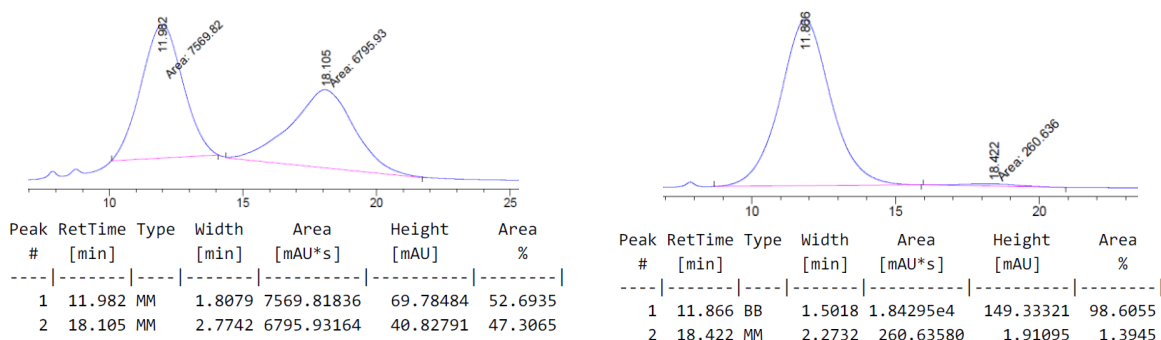
HRMS (ESI) calcd. for C₂₇H₃₅N₂O₃⁺ [M+H]⁺: 435.2642. Found: 435.2638.

[α]_D²⁰ = -85.6 (*c* = 1.00, CHCl₃).

ν_{max} (thin film/cm⁻¹): 1038, 1148, 1240, 1258, 1289, 1316, 1366, 1392, 1446, 1472, 1567, 1586, 1638, 1704, 2931, 2965, 3067.

HPLC separation (AS-3 column, *n*hexane/*i*PrOH 98/2, 1.0 mL/min, 273 nm): *t_r*(major) = 11.9 min, *t_r*(minor) = 18.1 min, 97% ee.

Experimental Data



tert-butyl (E)-3-(2-(N-(2-ethoxy-2-oxoethyl)picolinamido)-3-isopropylphenyl)acrylate 70ha: Prepared according to general procedure **H** on a 0.5 mmol scale, column chromatography (*n*hexane/EtOAc = 7:3) afforded the title compound as yellow oil (86 mg, 0.19 mmol, 38%).

¹H-NMR (400 MHz, CDCl₃) δ 8.14 – 8.07 (m, 2H), 7.75 (dt, *J* = 7.9, 1.0 Hz, 1H), 7.59 (td, *J* = 7.7, 1.7 Hz, 1H), 7.32 – 7.29 (m, 1H), 7.24 – 7.18 (m, 2H), 7.12 – 7.06 (m, 1H), 6.08 (d, *J* = 15.9 Hz, 1H), 4.37 (d, *J* = 16.4 Hz, 1H), 4.30 – 4.21 (m, 3H), 3.32 (hept, *J* = 6.8 Hz, 1H), 1.53 (s, 9H), 1.31 – 1.27 (m, 3H), 1.18 (d, *J* = 6.7 Hz, 3H), 0.88 (d, *J* = 6.7 Hz, 3H).

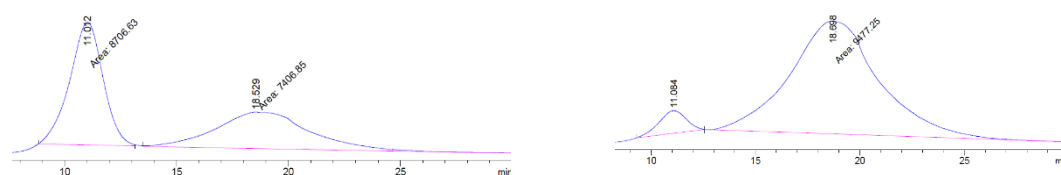
¹³C-NMR (101 MHz, CDCl₃) δ 168.8 (C_q), 168.0 (C_q), 165.9 (C_q), 152.4 (C_q), 147.6 (CH), 147.1 (C_q), 141.0 (CH), 140.8 (C_q), 136.1 (CH), 133.4 (C_q), 128.5 (CH), 128.4 (CH), 124.7 (CH), 124.5 (CH), 122.8 (CH), 80.4 (C_q), 61.4 (CH₂), 54.1 (CH₂), 28.4 (CH₃), 28.3 (CH), 25.0 (CH₃), 23.2 (CH₃), 14.3 (CH₃).

HRMS (ESI) calcd. for C₂₆H₃₃N₂O₅⁺ [M+H]⁺: 453.2384. Found: 453.2384.

[α]_D²⁰ = -94.2 (*c* = 1.00, CHCl₃).

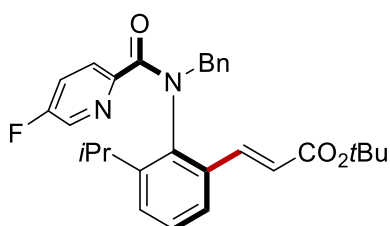
ν_{max} (thin film/cm⁻¹): 1039, 1146, 1196, 1238, 1258, 1320, 1367, 1442, 1473, 1568, 1586, 1650, 1704, 2870, 2932, 2971, 3063.

HPLC separation (AS-3 column, *n*hexane/*i*PrOH 95/5, 1.2 mL/min, 273 nm): *t_r*(major) = 11.0 min, *t_r*(minor) = 18.7 min, 88% ee.



Experimental Data

| Peak # | RetTime [min] | Type | Width [min] | Area [mAU*s] | Height [mAU] | Area % | Peak # | RetTime [min] | Type | Width [min] | Area [mAU*s] | Height [mAU] | Area % |
|--------|---------------|------|-------------|--------------|--------------|---------|--------|---------------|------|-------------|--------------|--------------|---------|
| 1 | 11.012 | MM | 1.7245 | 8706.63086 | 84.14453 | 54.0332 | 1 | 11.084 | BB | 1.0559 | 572.49786 | 6.36179 | 5.6966 |
| 2 | 18.529 | MM | 4.9100 | 7406.84912 | 25.14221 | 45.9668 | 2 | 18.698 | MM | 4.9601 | 9477.24707 | 31.84527 | 94.3034 |



tert-butyl (E)-3-(2-(N-benzyl-5-fluoropicolinamido)-3-isopropylphenyl)acrylate 70ia:

Prepared according to general procedure H on a 0.5 mmol scale, column chromatography (*n*hexane/acetone = 9:1) afforded the title compound as a colorless foam (121 mg, 0.26 mmol, 51%).

¹H-NMR (400 MHz, CDCl₃) δ 7.84 (dd, *J* = 2.9, 0.6 Hz, 1H), 7.72 (ddd, *J* = 8.7, 4.4, 0.6 Hz, 1H), 7.21 – 7.16 (m, 2H), 7.16 – 7.09 (m, 8H), 5.82 (d, *J* = 15.9 Hz, 1H), 5.16 (d, *J* = 13.6 Hz, 1H), 4.62 (d, *J* = 13.6 Hz, 1H), 2.90 (hept, *J* = 6.8 Hz, 1H), 1.42 (s, 9H), 0.80 (d, *J* = 6.8 Hz, 3H), 0.76 (d, *J* = 6.8 Hz, 3H).

¹³C-NMR (101 MHz, CDCl₃) δ 167.3 (C_q), 165.7 (C_q), 159.4 (d, *J* = 261.0 Hz, C_q), 149.5 (d, *J* = 4.4 Hz, C_q), 147.0 (C_q), 140.3 (CH), 139.0 (C_q), 135.7 (d, *J* = 23.6 Hz, CH), 135.7 (C_q), 133.4 (C_q), 130.6 (CH), 128.5 (CH), 128.5 (CH), 128.2 (CH), 128.0 (CH), 126.2 (d, *J* = 4.9 Hz, CH), 124.2 (CH), 122.9 (d, *J* = 18.5 Hz, CH), 121.7 (CH), 80.3 (C_q), 54.6 (CH₂), 28.3 (CH₃), 24.1 (CH), 23.6 (CH₃).

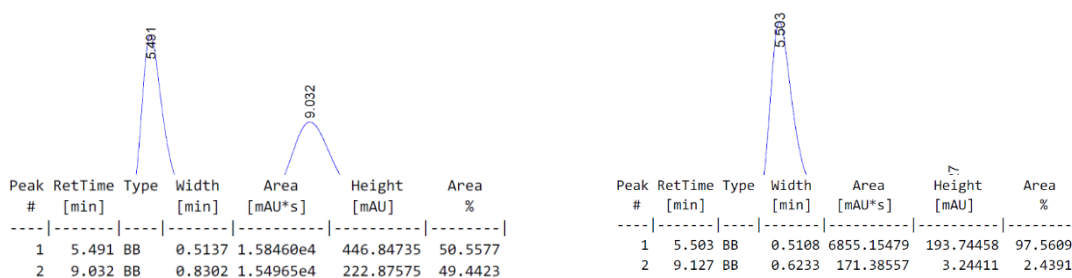
¹⁹F-NMR (376 MHz) δ -123.58.

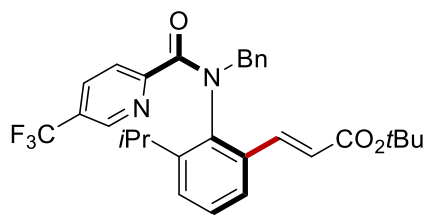
HRMS (ESI) calcd. for C₂₉H₃₂N₂O₃F⁺ [M+H]⁺: 475.2391. Found: 475.2383.

[α]_D²⁰ = -63.0 (*c* = 0.67, CH₂Cl₂).

ν_{max} (thin film/cm⁻¹): 981, 1147, 1228, 1287, 1315, 1367, 1404, 1446, 1481, 1583, 1643, 1705, 2967.

HPLC separation (AS-3 column, *n*hexane/*i*PrOH 95/5, 1.0 mL/min, 273 nm): *t_r*(major) = 5.5 min, *t_r*(minor) = 9.1 min, 95% ee.





tert-butyl (E)-3-(2-(N-benzyl-5-(trifluoromethyl)picolinamido)-3-isopropylphenyl)acrylate 70ja: Prepared according to general procedure H on a 0.5 mmol scale, column chromatography (*n*hexane/acetone = 9:1) afforded the title compound as a white solid (110 mg, 0.21 mmol, 42%).

¹H-NMR (400 MHz, CDCl₃) δ 8.32 – 8.27 (m, 1H), 7.82 – 7.71 (m, 2H), 7.18 – 7.09 (m, 9H), 5.80 (d, *J* = 15.9 Hz, 1H), 5.26 (d, *J* = 13.6 Hz, 1H), 4.58 (d, *J* = 13.6 Hz, 1H), 2.96 (hept, *J* = 6.8 Hz, 1H), 1.43 (s, 9H), 0.87 (d, *J* = 6.8 Hz, 3H), 0.83 (d, *J* = 6.8 Hz, 3H).

¹³C-NMR (101 MHz, CDCl₃) δ 167.2 (C_q), 165.6 (C_q), 147.2 (C_q), 147.2 (C_q), 144.44 (q, *J* = 4.0 Hz, CH), 139.9 (CH), 138.4 (C_q), 134.41 (d, *J* = 248.3 Hz, C_q), 133.52 (q, *J* = 3.5 Hz, CH), 130.6 (CH), 128.7 (CH), 128.6 (CH), 128.6 (CH), 128.2 (CH), 126.9 (q, *J* = 33.2 Hz, C_q), 124.3 (CH), 124.2 (CH), 122.1 (C_q), 122.0 (CH), 80.5 (C_q), 54.6 (CH₂), 28.3 (CH₃), 24.3 (CH), 23.7 (CH₃).

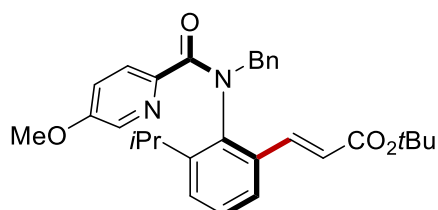
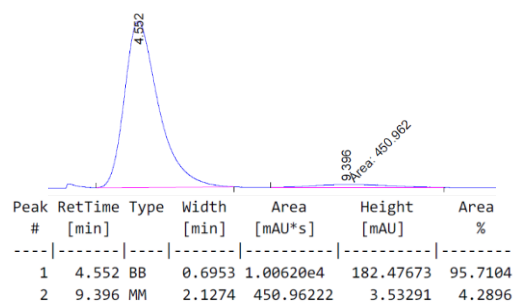
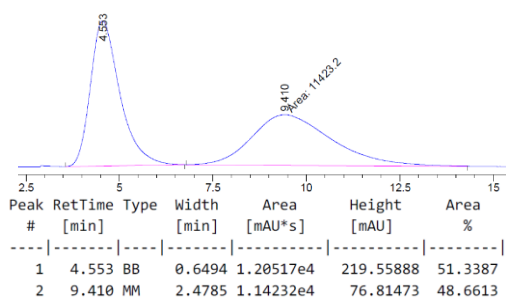
¹⁹F-NMR (376 MHz) δ -62.65.

HRMS (ESI) calcd. for C₃₀H₃₂N₂O₃F₃⁺ [M+H]⁺: 525.2360. Found: 525.2356.

[α]_D²⁰ = -55.9 (*c* = 0.95, CH₂Cl₂).

ν_{max} (thin film/cm⁻¹): 1017, 1076, 1134, 1290, 1322, 1367, 1407, 1446, 1571, 1647, 1707, 1871, 2932, 2969.

HPLC separation (AS-3 column, *n*hexane/*i*PrOH 98/2, 1.2 mL/min, 273 nm): *t_r*(major) = 4.6 min, *t_r*(minor) = 9.4 min, 91% ee.



tert-butyl (E)-3-(2-(N-benzyl-5-methoxypicolinamido)-3-isopropylphenyl)acrylate 70ka:

Prepared according to general procedure H on a 0.5 mmol scale, column chromatography (*n*hexane/acetone = 9:1) afforded the title compound as a colorless foam (228 mg, 0.47 mmol, 94%).

¹H-NMR (400 MHz, CDCl₃) δ 7.77 – 7.70 (m, 2H), 7.33 (d, *J* = 15.9 Hz, 1H), 7.25 – 7.09 (m, 8H), 7.02 (dd, *J* = 8.7, 2.9 Hz, 1H), 5.92 (d, *J* = 15.9 Hz, 1H), 5.14 (d, *J* = 13.6 Hz, 1H), 4.76 (d, *J* = 13.6 Hz, 1H), 3.73 (s, 3H), 2.93 (hept, *J* = 6.8 Hz, 1H), 1.49 (s, 9H), 0.81 (d, *J* = 6.8 Hz, 3H), 0.76 (d, *J* = 6.8 Hz, 3H).

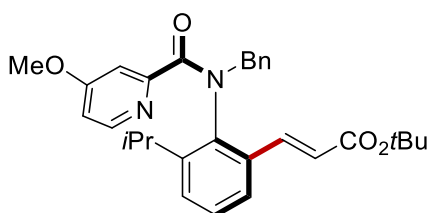
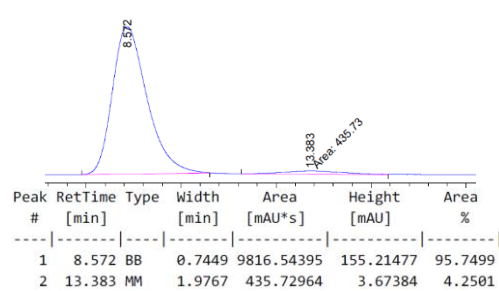
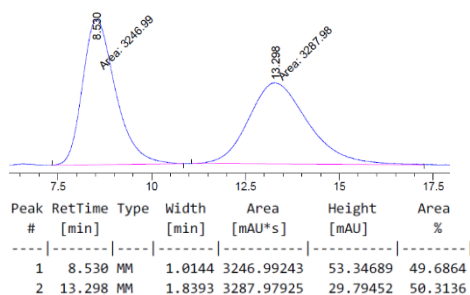
¹³C-NMR (101 MHz, CDCl₃) δ 168.0 (C_q), 165.8 (C_q), 156.2 (C_q), 146.9 (C_q), 145.4 (C_q), 140.7 (CH), 139.7 (C_q), 136.1 (C_q), 135.2 (CH), 133.3 (C_q), 130.6 (CH), 128.4 (CH), 128.2 (CH), 127.9 (CH), 127.9 (CH), 125.7 (CH), 124.2 (CH), 121.5 (CH), 119.7 (CH), 80.3 (C_q), 55.6 (CH), 54.6 (CH₂), 28.3 (CH₃), 24.0 (CH₃), 23.6 (CH₃).

HRMS (ESI) calcd. for C₃₀H₃₅N₂O₄⁺ [M+H]⁺: 487.2591. Found: 487.2582.

[α]_D²⁰ = -113.4 (*c* = 0.76, CH₂Cl₂).

ν_{max} (thin film/cm⁻¹): 1028, 1146, 1228, 1268, 1294, 1315, 1385, 1445, 1572, 1585, 1635, 1704, 2870, 2934, 2966.

HPLC separation (AS-3 column, *n*hexane/*i*PrOH 95/5, 1.0 mL/min, 273 nm): *t_r*(major) = 8.6 min, *t_r*(minor) = 13.4 min, 92% ee.

**Tert-butyl (E)-3-(2-(N-benzyl-4-methoxypicolinamido)-3-isopropylphenyl)acrylate 70la:**

Prepared according to general procedure H on a 0.5 mmol scale, column chromatography (*n*hexane/acetone = 9:1) afforded the title compound as a brown foam (236 mg, 0.48 mmol, 97%).

¹H-NMR (400 MHz, CDCl₃) δ 7.90 (d, *J* = 5.7 Hz, 1H), 7.28 (d, *J* = 15.9 Hz, 1H), 7.24 – 7.15 (m, 9H), 6.55 (dd, *J* = 5.7, 2.6 Hz, 1H), 5.91 (d, *J* = 15.9 Hz, 1H), 5.25 (d, *J* = 13.5 Hz, 1H), 4.68 (d, *J* = 13.5 Hz, 1H), 3.72 (s, 3H), 3.03 (hept, *J* = 6.8 Hz, 1H), 1.49 (s, 9H), 0.90 (d, *J* = 6.8 Hz, 3H), 0.89 (d, *J* = 6.8 Hz, 3H).

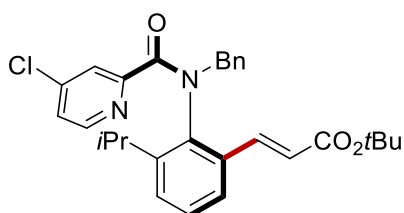
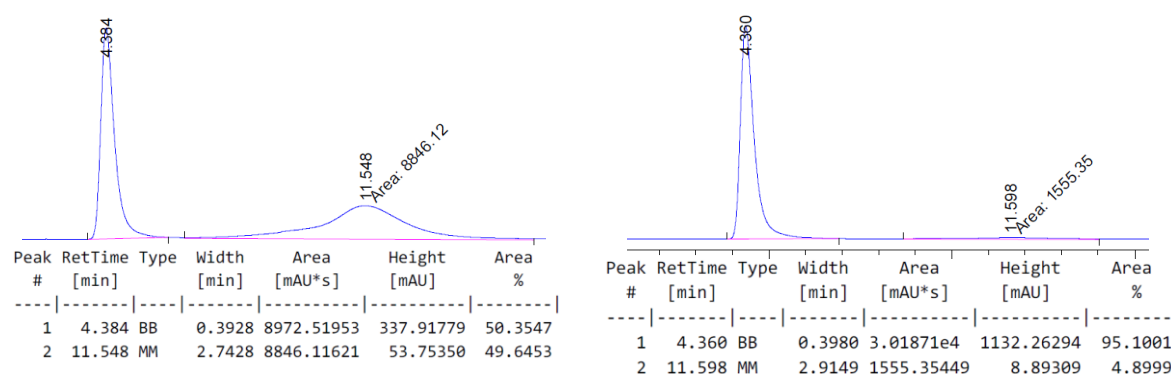
¹³C-NMR (101 MHz, CDCl₃) δ 168.5 (C_q), 165.8 (C_q), 165.6 (C_q), 155.1 (C_q), 148.8 (CH), 147.3 (C_q), 140.5 (CH), 139.1 (C_q), 135.8 (C_q), 133.2 (C_q), 130.6 (CH), 128.5 (CH), 128.4 (CH), 128.1 (CH), 127.9 (CH), 124.0 (CH), 121.5 (CH), 111.4 (CH), 109.5 (CH), 80.3 (C_q), 55.2 (CH), 54.5 (CH₂), 28.3 (CH₃), 24.2 (CH₃), 23.7 (CH₃).

HRMS (ESI) calcd. for C₃₀H₃₅N₂O₄⁺ [M+H]⁺: 487.2591. Found: 487.2589.

[α]_D²⁰ = -53.8 (*c* = 1.00, CH₂Cl₂).

*v*_{max} (thin film/cm⁻¹): 1036, 1146, 1258, 1303, 1430, 1448, 1566, 1591, 1638, 1703, 2870, 2967.

HPLC separation (AS-3 column, *n*hexane/*i*PrOH 90/10, 1.2 mL/min, 273 nm): *t*_r(major) = 4.4 min, *t*_r(minor) = 11.6 min, 90% ee.



tert-butyl (E)-3-(2-(N-benzyl-4-chloropicolinamido)-3-isopropylphenyl)acrylate 70ma:

Prepared according to general procedure **H** on a 0.5 mmol scale, column chromatography (*n*hexane/acetone = 9:1) afforded the title compound as a brown foam (160 mg, 0.33 mmol, 65%).

¹H-NMR (400 MHz, CDCl₃) δ 7.97 – 7.93 (m, 1H), 7.74 (dd, *J* = 2.0, 0.6 Hz, 1H), 7.25 – 7.14 (m, 9H), 7.07 – 7.02 (m, 1H), 5.85 (d, *J* = 15.9 Hz, 1H), 5.33 (d, *J* = 13.5 Hz, 1H), 4.60 (d, *J* = 13.5 Hz, 1H), 3.03 (hept, *J* = 6.8 Hz, 1H), 1.50 (s, 9H), 0.95 (d, *J* = 6.8, 3H), 0.94 (d, *J* = 6.8, 3H).

Experimental Data

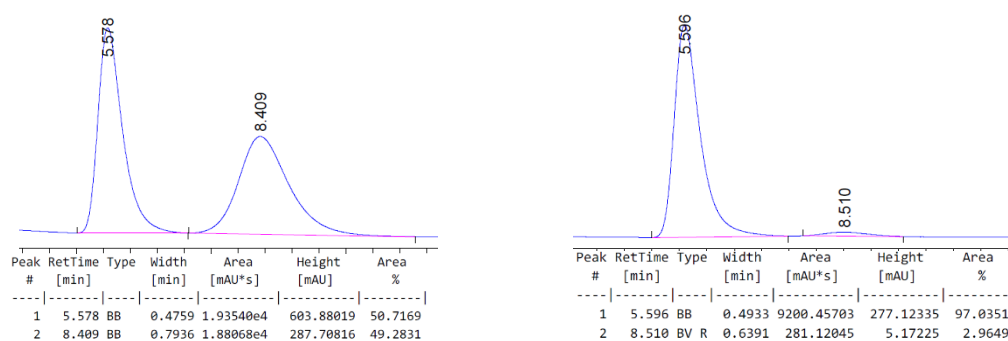
$^{13}\text{C-NMR}$ (101 MHz, CDCl_3) δ 167.4 (C_q), 165.6 (C_q), 154.8 (C_q), 148.3 (CH), 147.1 (C_q), 144.2 (C_q), 140.1 (CH), 138.6 (C_q), 135.5 (C_q), 133.3 (C_q), 130.5 (CH), 128.5 (CH), 128.5 (CH), 128.4 (CH), 128.1 (CH), 125.0 (CH), 124.6 (CH), 124.0 (CH), 121.8 (CH), 80.4 (C_q), 54.6 (CH_2), 28.3 (CH_3), 24.2 (CH), 23.7 (CH_3).

HRMS (ESI) calcd. for $\text{C}_{29}\text{H}_{32}\text{N}_2\text{O}_3\text{Cl}^+$ $[\text{M}+\text{H}]^+$: 491.2096. Found: 491.2079.

$[\alpha]_{\text{D}}^{20} = -29.4$ ($c = 0.82$, CH_2Cl_2).

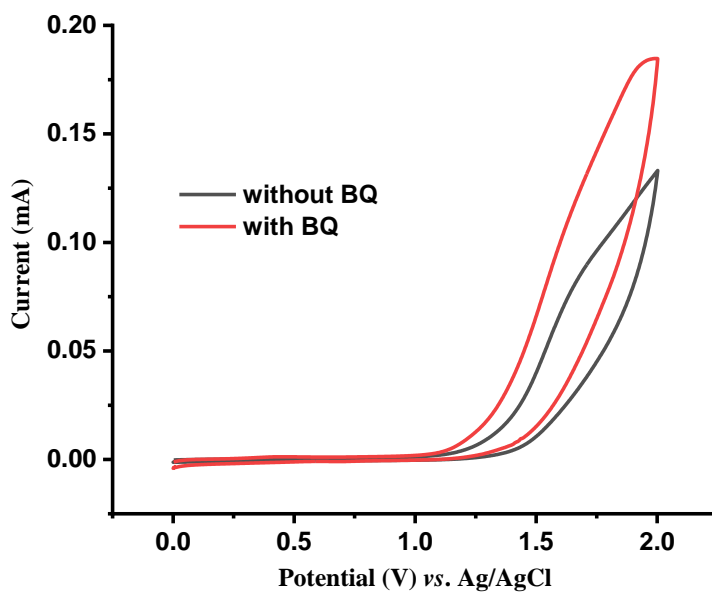
ν_{max} (thin film/ cm^{-1}): 1012, 1051, 1078, 1095, 1146, 1232, 1258, 1286, 1320, 1367, 1413, 1446, 1474, 1554, 1573, 1639, 1704, 2870, 1965.

HPLC separation (AS-3 column, *n*hexane/*i*PrOH 95/5, 1.0 mL/min, 273 nm): $t_{\text{r}}(\text{major}) = 5.6$ min, $t_{\text{r}}(\text{minor}) = 8.5$ min, 93% ee.

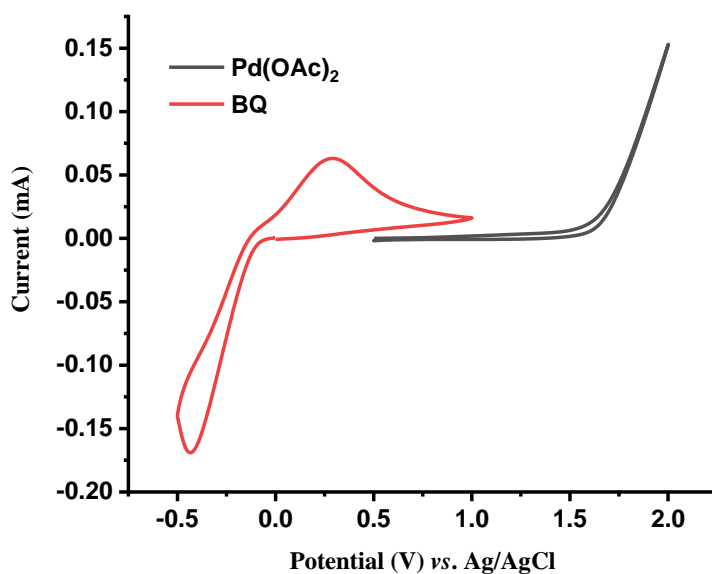


5.6.2 Cyclic Voltammetry Study

CV measurements were conducted with a Metrohm Autolab PGSTAT204 potentiostat and Nova 2.1 software. A glassy carbon working electrode (disk, diameter: 3mm), a coiled Pt wire counter electrode and a silver-silver chloride electrode (Ag/AgCl) were employed. The voltammograms were recorded at room temperature in TFE/DME (1/1) at a substrate concentration of 5.0 mM and with 0.1 M *n*Bu₄NPF₆ as supporting electrolyte. The scan rate is 100 mV/s. Deviations from the general experimental conditions are indicated in the respective figures and descriptions.



Scheme 5-15 Cyclic voltammogram of the mixture of 68a, 69a, Pd(OAc)₂, S-5-oxoproline and NaOAc, with or without BQ.



Scheme 5-16 Cyclic voltammogram of Pd(OAc)₂ and BQ separately.

5.7 Yield Optimization for Palladaelectro-Catalyzed C–H Annulation using Machine Learning

5.7.1 Details of Dataset

We focused on four key reaction parameters that are closely related to electrochemistry: electrode materials (anode/cathode), solvents, supporting electrolytes, and current/potential). A comprehensive overview of all the parameters can be found in Scheme 5-17.

| Electrode materials (anode/cathode): 16 | | | | Supporting electrolytes: 9 | | |
|---|-----------------|-----------------|--------|--|---|-------------------------------|
| Pt/Pt | Pt/GF | Pt/BDD | Pt/Fe | NaOAc | KOAc | LiOAc |
| GF/Pt | GF/GF | GF/BDD | GF/Fe | NaOPiv | K ₃ PO ₄ | NaO ₂ CAd |
| BDD/Pt | BDD/GF | BDD/BDD | BDD/Fe | LiClO ₄ | <i>n</i> Bu ₄ NPF ₆ | <i>n</i> Bu ₄ NOAc |
| Fe/Pt | Fe/GF | Fe/BDD | Fe/Fe | | | |
| Solvent: 10 | | | | Current/Potential: 6 | | |
| AcOH | TFE | EtOH | MeCN | 0.3 mA | 0.6 mA | 0.9 mA |
| AcOH:TFE (1:1) | AcOH:EtOH (1:1) | AcOH:MeCN (1:1) | | 1.2 mA | 1.0 V | 1.5 V |
| TFE:EtOH (1:1) | TFE:MeCN (1:1) | EtOH:MeCN (1:1) | | (total discharge into the reaction is 38.8 C, minimum amount of electricity required for the reaction) | | |

Scheme 5-17 Details of key reaction parameters.

Our combination of the four key reaction dimensions resulted in 8,640 reaction conditions. During the process of ML guided optimization, we experimentally tested 74 of these combinations, the outcomes of which are displayed in Table 5-2.

Table 5-2 Experimental dataset.

| Entry | Stage | Round | Anode/ Cathode | Solvent | Electrolyte | Current/ Potential | Yield (%) |
|-------|-------|-------|-------------------|-----------------|---|-----------------------|-----------|
| 1 | 0 | 0 | Pt/Pt | AcOH | K ₃ PO ₄ | 0.3 mA | 17 |
| 2 | 0 | 0 | GF/Pt | AcOH: TFE(1:1) | <i>n</i> Bu ₄ NOAc | 0.3 mA | 0 |
| 3 | 0 | 0 | BDD/Pt | AcOH: TFE(1:1) | LiClO ₄ | 0.9 mA | 13 |
| 4 | 0 | 0 | Fe/Pt | AcOH: MeCN(1:1) | LiOAc | 1.2 mA | 0 |
| 5 | 0 | 0 | Pt/GF | TFE | NaO ₂ CAd | 1.0 V | 0 |
| 6 | 0 | 0 | GF/GF | TFE: EtOH(1:1) | NaOAc | 1.5 V | 0 |
| 7 | 0 | 0 | BDD/GF | TFE: MeCN(1:1) | NaOPiv | 0.3 mA | 3 |
| 8 | 0 | 0 | Fe/GF | EtOH | <i>n</i> Bu ₄ NOAc | 0.6 mA | 0 |
| 9 | 0 | 0 | Pt/BDD | EtOH: MeCN(1:1) | <i>n</i> Bu ₄ NPF ₆ | 0.9 mA | 0 |
| 10 | 0 | 0 | GF/BDD | MeCN | K ₃ PO ₄ | 1.2 mA | 0 |
| 11 | 0 | 0 | BDD/BDD | AcOH | KOAc | 1.0 V | 5 |
| 12 | 0 | 0 | Fe/BDD | AcOH: TFE(1:1) | LiClO ₄ | 1.5 V | 3 |

Experimental Data

| | | | | | | | |
|----|---|----|---------|-----------------|--------------------------------|--------|----|
| 13 | 0 | 0 | Pt/Fe | AcOH: EtOH(1:1) | LiOAc | 0.3 mA | 3 |
| 14 | 0 | 0 | GF/Fe | AcOH: MeCN(1:1) | NaO ₂ CAd | 0.6 mA | 7 |
| 15 | 0 | 0 | BDD/Fe | TFE | NaOAc | 0.9 mA | 0 |
| 16 | 0 | 0 | Fe/Fe | TFE: EtOH(1:1) | NaOPiv | 1.2 mA | 0 |
| 17 | 1 | 1 | GF/Pt | AcOH | NaOPiv | 0.9 mA | 25 |
| 18 | 1 | 1 | GF/Pt | AcOH: EtOH(1:1) | K ₃ PO ₄ | 1.0 V | 2 |
| 19 | 1 | 1 | GF/Pt | AcOH: MeCN(1:1) | KOAc | 1.5 V | 1 |
| 20 | 1 | 1 | BDD/BDD | AcOH: TFE(1:1) | NaOPiv | 0.6 mA | 36 |
| 21 | 1 | 2 | BDD/GF | AcOH | LiOAc | 0.6 mA | 20 |
| 22 | 1 | 2 | BDD/Pt | AcOH: EtOH(1:1) | KOAc | 0.6 mA | 3 |
| 23 | 1 | 2 | GF/GF | TFE | K ₃ PO ₄ | 0.6 mA | 0 |
| 24 | 2 | 3 | BDD/GF | AcOH | K ₃ PO ₄ | 0.9 mA | 19 |
| 25 | 2 | 3 | GF/GF | AcOH | NaO ₂ CAd | 0.9 mA | 2 |
| 26 | 2 | 3 | BDD/GF | AcOH: TFE(1:1) | NaOPiv | 0.9 mA | 29 |
| 27 | 2 | 3 | GF/GF | AcOH: TFE(1:1) | K ₃ PO ₄ | 0.9 mA | 26 |
| 28 | 2 | 4 | Pt/BDD | AcOH: TFE(1:1) | NaOPiv | 1.0 V | 48 |
| 29 | 2 | 4 | Pt/BDD | AcOH: TFE(1:1) | K ₃ PO ₄ | 1.5 V | 12 |
| 30 | 2 | 4 | Pt/GF | AcOH: TFE(1:1) | NaOPiv | 1.5 V | 35 |
| 31 | 2 | 4 | Pt/GF | AcOH: TFE(1:1) | K ₃ PO ₄ | 1.0 V | 29 |
| 32 | 2 | 5 | GF/Pt | AcOH: TFE(1:1) | NaOPiv | 1.2 mA | 37 |
| 33 | 2 | 5 | GF/Pt | AcOH: TFE(1:1) | K ₃ PO ₄ | 0.6 mA | 35 |
| 34 | 2 | 5 | GF/Pt | AcOH: TFE(1:1) | KOAc | 0.9 mA | 37 |
| 35 | 2 | 5 | BDD/BDD | AcOH: TFE(1:1) | K ₃ PO ₄ | 0.3 mA | 40 |
| 36 | 2 | 6 | BDD/BDD | AcOH: TFE(1:1) | KOAc | 1.2 mA | 21 |
| 37 | 2 | 6 | BDD/GF | AcOH: TFE(1:1) | KOAc | 0.3 mA | 29 |
| 38 | 2 | 6 | BDD/Pt | AcOH: TFE(1:1) | KOAc | 1.0 V | 48 |
| 39 | 2 | 6 | BDD/Fe | AcOH: TFE(1:1) | KOAc | 1.5 V | 18 |
| 40 | 2 | 7 | Fe/Pt | AcOH: TFE(1:1) | NaOPiv | 0.3 mA | 55 |
| 41 | 2 | 7 | GF/BDD | AcOH: TFE(1:1) | KOAc | 0.6 mA | 45 |
| 42 | 2 | 7 | BDD/Pt | AcOH: TFE(1:1) | K ₃ PO ₄ | 1.2 mA | 26 |
| 43 | 2 | 7 | BDD/Pt | AcOH: TFE(1:1) | LiOAc | 0.3 mA | 49 |
| 44 | 2 | 8 | GF/Pt | AcOH: TFE(1:1) | LiOAc | 1.0 V | 46 |
| 45 | 2 | 8 | BDD/BDD | AcOH: TFE(1:1) | LiOAc | 0.9 mA | 18 |
| 46 | 2 | 8 | BDD/GF | AcOH: TFE(1:1) | LiOAc | 1.2 mA | 17 |
| 47 | 2 | 8 | BDD/Fe | AcOH: TFE(1:1) | LiOAc | 0.6 mA | 29 |
| 48 | 2 | 9 | BDD/Pt | AcOH: TFE(1:1) | NaO ₂ CAd | 1.5 V | 21 |
| 49 | 2 | 9 | Fe/Pt | AcOH: TFE(1:1) | LiOAc | 1.5 V | 55 |
| 50 | 2 | 9 | Fe/Pt | AcOH: TFE(1:1) | NaO ₂ CAd | 0.9 mA | 33 |
| 51 | 2 | 9 | Fe/Pt | AcOH: TFE(1:1) | NaOAc | 1.0 V | 53 |
| 52 | 2 | 10 | GF/Pt | AcOH: TFE(1:1) | NaOAc | 1.5 V | 25 |

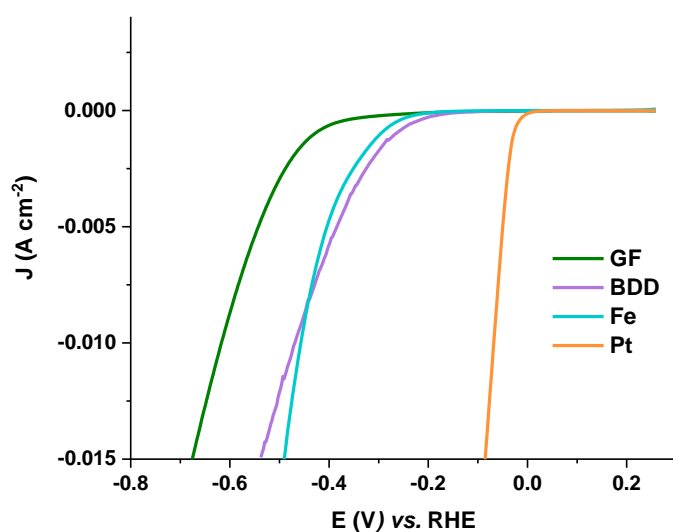
Experimental Data

| | | | | | | | |
|----|---|----|--------|----------------|--------------------------------|--------|----|
| 53 | 2 | 10 | BDD/Pt | AcOH: TFE(1:1) | NaOAc | 0.6 mA | 36 |
| 54 | 2 | 10 | Pt/Pt | AcOH: TFE(1:1) | NaOAc | 0.3 mA | 64 |
| 55 | 3 | 11 | Fe/Pt | AcOH: TFE(1:1) | LiOAc | 0.3 mA | 48 |
| 56 | 3 | 11 | GF/Pt | AcOH: TFE(1:1) | LiOAc | 0.3 mA | 58 |
| 57 | 3 | 11 | Fe/Pt | AcOH: TFE(1:1) | KOAc | 0.3 mA | 45 |
| 58 | 3 | 11 | BDD/Pt | AcOH: TFE(1:1) | KOAc | 0.3 mA | 47 |
| 59 | 3 | 11 | GF/Pt | AcOH: TFE(1:1) | KOAc | 0.3 mA | 63 |
| 60 | 3 | 11 | Pt/Pt | AcOH: TFE(1:1) | LiOAc | 0.3 mA | 62 |
| 61 | 3 | 11 | Pt/Pt | AcOH: TFE(1:1) | KOAc | 0.3 mA | 60 |
| 62 | 3 | 11 | BDD/Pt | AcOH: TFE(1:1) | K ₃ PO ₄ | 0.3 mA | 47 |
| 63 | 3 | 11 | Fe/Pt | AcOH: TFE(1:1) | K ₃ PO ₄ | 0.3 mA | 0 |
| 64 | 3 | 11 | GF/Pt | AcOH: TFE(1:1) | K ₃ PO ₄ | 0.3 mA | 51 |
| 65 | 3 | 11 | Fe/Pt | AcOH: TFE(1:1) | NaOAc | 0.3 mA | 45 |
| 66 | 3 | 11 | BDD/Pt | AcOH: TFE(1:1) | NaOAc | 0.3 mA | 34 |
| 67 | 3 | 11 | Pt/Pt | AcOH: TFE(1:1) | K ₃ PO ₄ | 0.3 mA | 58 |
| 68 | 3 | 11 | GF/Pt | AcOH: TFE(1:1) | NaOAc | 0.3 mA | 60 |
| 69 | 3 | 11 | BDD/Pt | AcOH: TFE(1:1) | NaOPiv | 0.3 mA | 33 |
| 70 | 3 | 11 | GF/Pt | AcOH: TFE(1:1) | NaOPiv | 0.3 mA | 70 |
| 71 | 3 | 11 | Pt/Pt | AcOH: TFE(1:1) | NaOPiv | 0.3 mA | 61 |
| 72 | 3 | 11 | GF/BDD | AcOH: TFE(1:1) | KOAc | 0.3 mA | 60 |
| 73 | 3 | 11 | GF/Pt | AcOH: TFE(1:1) | LiOAc | 0.9 mA | 41 |
| 74 | 3 | 11 | GF/Pt | AcOH: TFE(1:1) | LiOAc | 1.2 mA | 27 |

5.7.2 Details of Descriptors

5.7.2.1 Descriptors of Electrode Material Combinations

Linear sweep voltammetry (LSV) was utilized to determine the onset potentials of hydrogen evolution reactions (HER) for four electrode materials. This process was conducted in a standard three-electrode system using a Metrohm Autolab PGSTAT204 potentiostat. The setup consisted of a working electrode, a Pt wire as counter electrode, and a saturated calomel electrode (SCE) as reference electrode. The polarization curves were obtained in an N₂-purged 0.5 M H₂SO₄ aqueous solution at room temperature, with a scan rate of 5 mV/s. Scheme 5-18 shows the curves of HER for 4 electrode materials. All potentials were referenced to a reversible hydrogen electrode (RHE).



Scheme 5-18 Linear sweep voltammogram of four electrode materials.

For each of the 16 anode/cathode combinations, we used descriptors such as the onset potential of the anode material, onset potential of the cathode material, and their difference to characterize them. Details of descriptors were presented in Table 5-3.

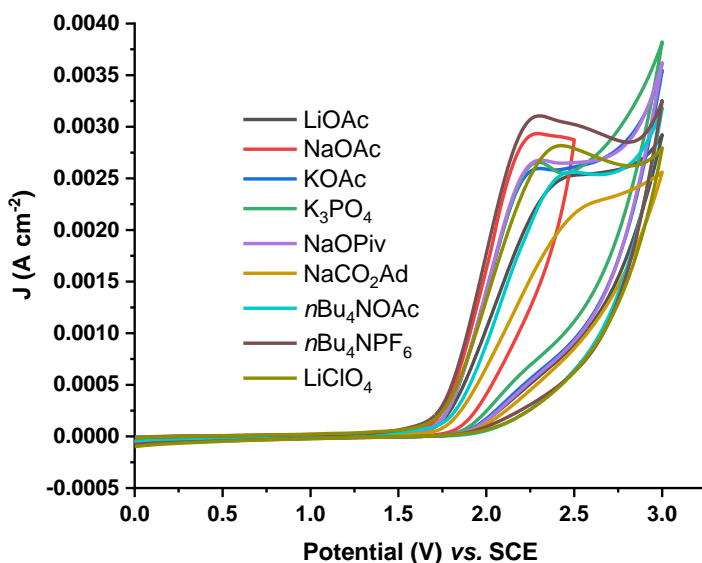
Table 5-3 Descriptors of electrode material combinations.

| Anode/Cathode | U(Anode)/ V | U(Cathode)/ V | U(Cathode)-U(Anode)/ V |
|---------------|-------------|---------------|------------------------|
| Pt/Pt | -0.02 | -0.02 | 0.00 |
| GF/Pt | -0.38 | -0.02 | 0.36 |
| BDD/Pt | -0.23 | -0.02 | 0.21 |
| Fe/Pt | -0.26 | -0.02 | 0.24 |
| Pt/GF | -0.02 | -0.38 | -0.36 |
| GF/GF | -0.38 | -0.38 | 0.00 |
| BDD/GF | -0.23 | -0.38 | -0.15 |
| Fe/GF | -0.26 | -0.38 | -0.12 |
| Pt/BDD | -0.02 | -0.23 | -0.21 |
| GF/BDD | -0.38 | -0.23 | 0.15 |
| BDD/BDD | -0.23 | -0.23 | 0.00 |
| Fe/BDD | -0.26 | -0.23 | 0.03 |
| Pt/Fe | -0.02 | -0.26 | -0.24 |
| GF/Fe | -0.38 | -0.26 | 0.12 |
| BDD/Fe | -0.23 | -0.26 | -0.03 |
| Fe/Fe | -0.26 | -0.26 | 0.00 |

5.7.2.2 Descriptors of Supporting Electrolytes

9 different bases are used as supporting electrolytes for our study. Using cyclic voltammetry, we separately measured the oxidation curves of substrate **71a** with each of the 9 bases, and obtained the onset potential and Tafel slope as their descriptors.

CV measurements were conducted with a Metrohm Autolab PGSTAT204 potentiostat and Nova 2.1 software. A glassy carbon working electrode (disk, diameter: 3mm), a coiled Pt wire counter electrode and a SCE were employed. The voltammograms were recorded at room temperature in a substrate concentration of 5.0 mmol/L. 3 mL AcOH/TFE (1/1) solution with 100 mmol/L $n\text{Bu}_4\text{NPF}_6$ as supporting electrolyte was stirred for several minutes and kept still for 1 minute before CV test (blank test). Then 5.0 mmol/L bases and 5.0 mmol/L biaryl **71a** were then dissolved into the solution. The CV tests were typically conducted between the range of 0 V to 3 V (vs. SCE) and scan rate was set as 100 mV/s. Scheme 5-19 shows the CV curves of substrate **71a** with different supporting electrolytes.



Scheme 5-19 Cyclic voltammogram of substrate **71a** with different supporting electrolytes.

Determination of Tafel slope: Remove a segment from the CV, leaving only a linear sweep voltammogram and convert the graph into E-log(|i|) relationship. Find out the linear region in the E-log(|i|) diagram and fit the curve to get Tafel slope.

Based on the curves in Scheme 5-19, Onset potential and Tafel slope were obtained and chosen as the descriptors for the nine supporting electrolytes, which is listed in Table 5-4.

Table 5-4 Descriptors of supporting electrolytes.

| Electrolytes | Onset potential / V | Tafel slope / mV / dec |
|---|---------------------|------------------------|
| <i>n</i> Bu ₄ NOAc | 1.82 | 261 |
| <i>n</i> Bu ₄ NPF ₆ | 1.75 | 245 |
| NaCO ₂ Ad | 1.79 | 200 |
| K ₃ PO ₄ | 1.78 | 177 |
| NaOAc | 1.75 | 220 |
| KOAc | 1.75 | 190 |
| LiOAc | 1.72 | 200 |
| LiClO ₄ | 1.76 | 273 |
| NaOPiv | 1.79 | 177 |

5.7.2.3 Descriptors of Solvent

In our study, ten selections of solvents are categorized into two groups: four pure solvents and six solvent mixtures created from combining pure solvents in a 1:1 ratio. To generate descriptors for the mixed solvents, we utilized 16 molecular properties from the PubChem database for both components, resulting in 32-dimensional descriptors. To maintain consistency in solvent descriptors, we also treated pure solvents as 1:1 ratio with themselves, which also resulted in 32-dimensional descriptors. This was done by Chen-Hang Chao and Shu-Wen Li.

5.7.2.4 Descriptors of Electrochemical Conditions

Six different rates of discharge into the reaction (current/potential) are employed in our study and One-Hot encoding is used as the descriptor for electrochemical conditions. This was done by Chen-Hang Chao and Shu-Wen Li.

5.7.3 Results of Yield Optimization

5.7.3.1 First Stage

For round 1, Table 5-2 (Entry 1-16) was chosen as the reaction dataset. The Ridge model with feature selection, yield prediction and orthogonal rule selection was applied, resulting in four selected reaction condition combinations that were experimentally tested. Details of reactions were presented in Table 5-5. The Pearson correlation coefficient between the predicted values and the true values is 0.407.

Table 5-5 The predicted and experimental yields of the selected reaction conditions in round 1.

| Anode/ Cathode | Solvent | Electrolyte | Current/ Potential | Predicted yield (%) | Experimental yield (%) |
|-------------------|---------------------|--------------------------------|-----------------------|------------------------|---------------------------|
| GF/Pt | AcOH | NaOPiv | 0.9 mA | 6 | 25 |
| GF/Pt | AcOH: EtOH (1:1) | K ₃ PO ₄ | 1.0 V | 6 | 2 |
| GF/Pt | AcOH: MeCN (1:1) | KOAc | 1.5 V | 6 | 1 |
| BDD/BDD | AcOH: TFE (1:1) | NaOPiv | 0.6 mA | 6 | 36 |

For round 2, Table 5-2 (Entry 1-20) was used as the reaction dataset. The Ridge model with feature selection, yield prediction and orthogonal rule selection was applied, which resulted in the identification of three promising reaction condition combinations that were experimentally tested. Details of reactions were presented in Table 5-6. The next round will proceed to the second stage. The Pearson correlation coefficient between the predicted values and the true values is 0.573.

Table 5-6 The predicted and experimental yields of the selected reaction conditions in round 2.

| Anode/ Cathode | Solvent | Electrolyte | Current/ Potential | Predicted yield (%) | Experimental yield (%) |
|-------------------|---------------------|--------------------------------|-----------------------|------------------------|---------------------------|
| BDD/GF | AcOH | LiOAc | 0.6 mA | 24 | 20 |
| BDD/Pt | AcOH: EtOH (1:1) | KOAc | 0.6 mA | 24 | 3 |
| GF/GF | TFE | K ₃ PO ₄ | 0.6 mA | 24 | 0 |

5.7.3.2 Second Stage

For round 3, Table 5-2 (Entry 1-23) was chosen as the reaction dataset. The Ridge model with feature selection, yield prediction and orthogonal rule selection was applied, resulting in four selected reaction condition combinations that were experimentally tested. Details of reactions were presented in Table 5-7. The Pearson correlation coefficient between the predicted values and the true values is 0.600.

Table 5-7 The predicted and experimental yields of the selected reaction conditions in round 3.

| Anode/ Cathode | Solvent | Electrolyte | Current/ Potential | Predicted yield (%) | Experimental yield (%) |
|---------------------------|--------------------|--------------------------------|-------------------------------|--------------------------------|-----------------------------------|
| BDD/GF | AcOH | K ₃ PO ₄ | 0.9 mA | 26 | 19 |
| GF/GF | AcOH | NaO ₂ CAd | 0.9 mA | 25 | 2 |
| BDD/GF | AcOH: TFE (1:1) | NaOPiv | 0.9 mA | 24 | 29 |
| GF/GF | AcOH: TFE (1:1) | K ₃ PO ₄ | 0.9 mA | 24 | 26 |

For round 4, Table 5-2 (Entry 1-27) was chosen as the reaction dataset. The Support Vector Regression model with feature selection, yield prediction and orthogonal rule selection was used, resulting in four selected reaction condition combinations that were experimentally tested. Details of reactions were presented in Table 5-8. The Pearson correlation coefficient between the predicted values and the true values is 0.810.

Table 5-8 The predicted and experimental yields of the selected reaction conditions in round 4.

| Anode/ Cathode | Solvent | Electrolyte | Current/ Potential | Predicted yield (%) | Experimental yield (%) |
|---------------------------|--------------------|--------------------------------|-------------------------------|--------------------------------|-----------------------------------|
| Pt/BDD | AcOH: TFE (1:1) | NaOPiv | 1.0 V | 27 | 48 |
| Pt/BDD | AcOH: TFE (1:1) | K ₃ PO ₄ | 1.5 V | 27 | 12 |
| Pt/GF | AcOH: TFE (1:1) | NaOPiv | 1.5 V | 27 | 35 |
| Pt/GF | AcOH: TFE (1:1) | K ₃ PO ₄ | 1.0 V | 27 | 29 |

For round 5, Table 5-2 (Entry 1-31) was chosen as the reaction dataset. The k-Nearest Neighbors Regression model with feature selection, yield prediction and orthogonal rule selection was used, resulting in four selected reaction condition combinations that were experimentally tested. Details of reactions were presented in Table 5-9. The Pearson correlation coefficient between the predicted values and the true values is 0.836.

Table 5-9 The predicted and experimental yields of the selected reaction conditions in round 5.

| Anode/ Cathode | Solvent | Electrolyte | Current/ Potential | Predicted yield (%) | Experimental yield (%) |
|-------------------|--------------------|--------------------------------|-----------------------|------------------------|---------------------------|
| GF/Pt | AcOH: TFE (1:1) | NaOPiv | 1.2 mA | 30 | 37 |
| GF/Pt | AcOH: TFE (1:1) | K ₃ PO ₄ | 0.6 mA | 30 | 35 |
| GF/Pt | AcOH: TFE (1:1) | KOAc | 0.9 mA | 30 | 37 |
| BDD/BDD | AcOH: TFE (1:1) | K ₃ PO ₄ | 0.3 mA | 30 | 40 |

For round 6, Table 5-2 (Entry 1-35) was chosen as the reaction dataset. The k-Nearest Neighbors Regression model with feature selection, yield prediction and orthogonal rule selection was applied, resulting in four selected reaction condition combinations that were experimentally tested. Details of reactions were presented in Table 5-10. The Pearson correlation coefficient between the predicted values and the true values is 0.879.

Table 5-10 The predicted and experimental yields of the selected reaction conditions in round 6.

| Anode/ Cathode | Solvent | Electrolyte | Current/ Potential | Predicted yield (%) | Experimental yield (%) |
|-------------------|--------------------|-------------|-----------------------|------------------------|---------------------------|
| BDD/BDD | AcOH: TFE (1:1) | KOAc | 1.2 mA | 35 | 21 |
| BDD/GF | AcOH: TFE (1:1) | KOAc | 0.3 mA | 35 | 29 |
| BDD/Pt | AcOH: TFE (1:1) | KOAc | 1.0 V | 35 | 48 |
| BDD/Fe | AcOH: TFE (1:1) | KOAc | 1.5 V | 35 | 18 |

For round 7, Table 5-2 (Entry 1-39) was chosen as the reaction dataset. The k-Nearest Neighbors Regression model with feature selection, yield prediction and orthogonal rule selection was applied, resulting in four selected reaction condition combinations that were experimentally tested. Details of reactions were presented in Table 5-11. The Pearson correlation coefficient between the predicted values and the true values is 0.794.

Table 5-11 The predicted and experimental yields of the selected reaction conditions in round 7.

| Anode/ Cathode | Solvent | Electrolyte | Current/ Potential | Predicted yield (%) | Experimental yield (%) |
|-------------------|--------------------|--------------------------------|-----------------------|------------------------|---------------------------|
| Fe/Pt | AcOH: TFE (1:1) | NaOPiv | 0.3 mA | 39 | 55 |
| GF/BDD | AcOH: TFE (1:1) | KOAc | 0.6 mA | 37 | 45 |
| BDD/Pt | AcOH: TFE (1:1) | K ₃ PO ₄ | 1.2 mA | 36 | 26 |
| BDD/Pt | AcOH: TFE (1:1) | LiOAc | 0.3 mA | 36 | 49 |

For round 8, Table 5-2 (Entry 1-43) was chosen as the reaction dataset. The Extra-Trees model with feature selection, yield prediction and orthogonal rule selection was applied, resulting in four selected reaction condition combinations that were experimentally tested. Details of reactions were presented in Table 5-12. The Pearson correlation coefficient between the predicted values and the true values is 0.819.

Table 5-12 The predicted and experimental yields of the selected reaction conditions in round 8.

| Anode/ Cathode | Solvent | Electrolyte | Current/ Potential | Predicted yield (%) | Experimental yield (%) |
|-------------------|--------------------|-------------|-----------------------|------------------------|---------------------------|
| GF/Pt | AcOH: TFE (1:1) | LiOAc | 1.0 V | 49 | 46 |
| BDD/BDD | AcOH: TFE (1:1) | LiOAc | 0.9 mA | 49 | 18 |
| BDD/GF | AcOH: TFE (1:1) | LiOAc | 1.2 mA | 49 | 17 |
| BDD/Fe | AcOH: TFE (1:1) | LiOAc | 0.6 mA | 49 | 29 |

For round 9, Table 5-2 (Entry 1-47) was chosen as the reaction dataset. The k-Nearest Neighbors Regression model with feature selection, yield prediction and orthogonal rule selection was applied, resulting in four selected reaction condition combinations that were experimentally tested. Details of reactions were presented in Table 5-13. The Pearson correlation coefficient between the predicted values and the true values is 0.833.

Table 5-13 The predicted and experimental yields of the selected reaction conditions in round 9.

| Anode/ Cathode | Solvent | Electrolyte | Current/ Potential | Predicted yield (%) | Experimental yield (%) |
|-------------------|--------------------|----------------------|-----------------------|------------------------|---------------------------|
| BDD/Pt | AcOH: TFE (1:1) | NaO ₂ CAd | 1.5 V | 45 | 21 |
| Fe/Pt | AcOH: TFE (1:1) | LiOAc | 1.5 V | 45 | 55 |
| Fe/Pt | AcOH: TFE (1:1) | NaO ₂ CAd | 0.9 mA | 45 | 33 |
| Fe/Pt | AcOH: TFE (1:1) | NaOAc | 1.0 V | 45 | 53 |

For round 10, Table 5-2 (Entry 1-51) was chosen as the reaction dataset. The Support Vector Regression model with feature selection, yield prediction and orthogonal rule selection was applied, resulting in three selected reaction condition combinations that were experimentally tested. Details of reactions were presented in Table 5-14. The next round will proceed to the third stage. The Pearson correlation coefficient between the predicted values and the true values is 0.827.

Table 5-14 The predicted and experimental yields of the selected reaction conditions in round 10.

| Anode/ Cathode | Solvent | Electrolyte | Current/ Potential | Predicted yield (%) | Experimental yield (%) |
|-------------------|--------------------|-------------|-----------------------|------------------------|---------------------------|
| GF/Pt | AcOH: TFE (1:1) | NaOAc | 1.5 V | 37 | 25 |
| BDD/Pt | AcOH: TFE (1:1) | NaOAc | 0.6 mA | 37 | 36 |
| Pt/Pt | AcOH: TFE (1:1) | NaOAc | 0.3 mA | 37 | 64 |

5.7.3.3 Third Stage

For round 11, Table 5-2 (Entry 1-54) was chosen as the reaction dataset. The Support Vector Regression model with hyperparameter optimization, feature selection, yield prediction and orthogonal rule selection was applied. The top 20 predicted reaction condition combinations

with the highest yield were selected for experimental testing. Details of reactions were presented in Table 5-15. The Pearson correlation coefficient between the predicted values and the true values is 0.833.

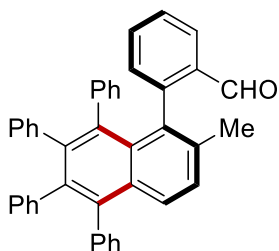
Table 5-15 The predicted and experimental yields of the selected reaction conditions in round 11.

| Anode/ Cathode | Solvent | Electrolyte | Current/ Potential | Predicted yield (%) | Experimental yield (%) |
|---------------------------|--------------------|--------------------------------|-------------------------------|--------------------------------|-----------------------------------|
| Fe/Pt | AcOH: TFE (1:1) | LiOAc | 0.3 mA | 42 | 48 |
| GF/Pt | AcOH: TFE (1:1) | LiOAc | 0.3 mA | 42 | 58 |
| Fe/Pt | AcOH: TFE (1:1) | KOAc | 0.3 mA | 41 | 45 |
| BDD/Pt | AcOH: TFE (1:1) | KOAc | 0.3 mA | 41 | 47 |
| GF/Pt | AcOH: TFE (1:1) | KOAc | 0.3 mA | 41 | 63 |
| Pt/Pt | AcOH: TFE (1:1) | LiOAc | 0.3 mA | 40 | 62 |
| Pt/Pt | AcOH: TFE (1:1) | KOAc | 0.3 mA | 40 | 60 |
| BDD/Pt | AcOH: TFE (1:1) | K ₃ PO ₄ | 0.3 mA | 39 | 47 |
| Fe/Pt | AcOH: TFE (1:1) | K ₃ PO ₄ | 0.3 mA | 39 | 0 |
| GF/Pt | AcOH: TFE (1:1) | K ₃ PO ₄ | 0.3 mA | 38 | 51 |
| Fe/Pt | AcOH: TFE (1:1) | NaOAc | 0.3 mA | 38 | 45 |
| BDD/Pt | AcOH: TFE (1:1) | NaOAc | 0.3 mA | 38 | 34 |
| Pt/Pt | AcOH: TFE (1:1) | K ₃ PO ₄ | 0.3 mA | 38 | 58 |

Experimental Data

| | | | | | |
|--------|--------------------|--------|--------|----|----|
| GF/Pt | AcOH: TFE (1:1) | NaOAc | 0.3 mA | 38 | 60 |
| BDD/Pt | AcOH: TFE (1:1) | NaOPiv | 0.3 mA | 37 | 33 |
| GF/Pt | AcOH: TFE (1:1) | NaOPiv | 0.3 mA | 37 | 70 |
| Pt/Pt | AcOH: TFE (1:1) | NaOPiv | 0.3 mA | 36 | 61 |
| GF/BDD | AcOH: TFE (1:1) | KOAc | 0.3 mA | 35 | 60 |
| GF/Pt | AcOH: TFE (1:1) | LiOAc | 0.9 mA | 35 | 41 |
| GF/Pt | AcOH: TFE (1:1) | LiOAc | 1.2 mA | 35 | 27 |

5.7.4 Characterization Data



(R)-2-(2-methyl-5,6,7,8-tetraphenyl-naphthalen-1-yl) benzaldehyde 73aa: The general procedure **K** was followed using 2'-methyl-[1,1'-biphenyl]-2-carbaldehyde **71a** (39.3 mg, 0.20 mmol) and 1,2-diphenylethyne **72a** (106.9 mg, 0.60 mmol). Isolation by column chromatography (*n*hexane/EtOAc = 20:1) yielded **73aa** (99.1 mg, 90%) as a yellow solid.

¹H-NMR (300 MHz, CDCl₃) δ 9.65 (s, 1H), 7.67 (d, *J* = 8.7 Hz, 1H), 7.49 (dd, *J* = 7.8, 1.5 Hz, 1H), 7.32 (d, *J* = 8.7 Hz, 1H), 7.29 – 7.18 (m, 6H), 7.14 – 7.06 (m, 1H), 6.91 – 6.77 (m, 6H), 6.75 – 6.63 (m, 6H), 6.63 – 6.54 (m, 2H), 6.53 – 6.42 (m, 2H), 1.90 (s, 3H).

¹³C-NMR (75 MHz, CDCl₃) δ 192.7 (CH), 146.6 (C_q), 141.9 (C_q), 141.4 (C_q), 140.5 (C_q, overlapped, 2C), 139.9 (C_q), 138.6 (C_q), 138.5 (C_q), 138.3 (C_q), 136.6 (C_q), 134.5 (C_q), 133.6 (C_q), 133.0 (CH), 132.5 (CH), 132.0 (CH), 131.8 (C_q), 131.7 (C_q), 131.5 (CH), 131.5 (CH), 131.3 (CH), 131.3 (CH), 131.2 (CH, overlapped, 2C), 131.1 (CH), 128.5 (CH), 127.8 (CH), 127.7 (CH), 127.6 (CH), 127.0 (CH), 126.8 (CH), 126.8 (CH, overlapped, 2C), 126.6 (CH),

Experimental Data

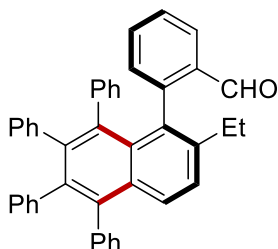
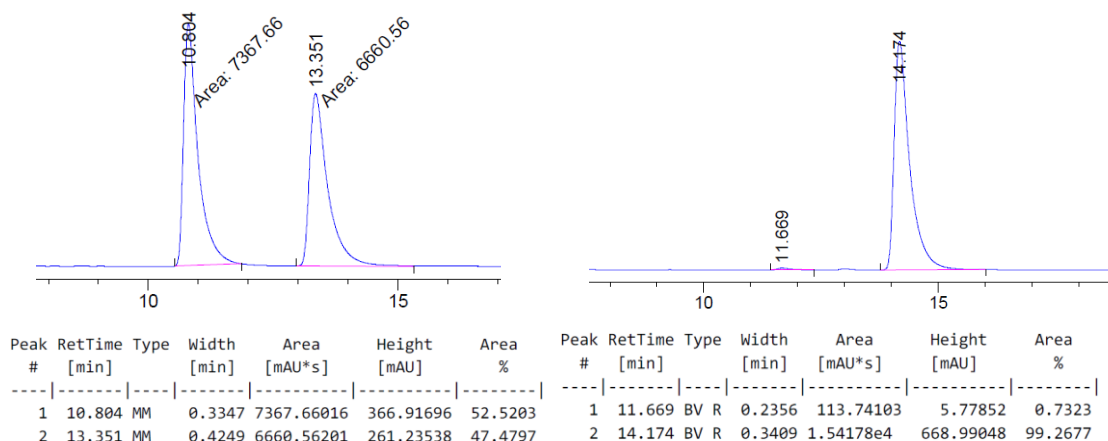
126.6 (CH), 126.6 (CH), 126.3 (CH), 126.2 (CH), 125.4 (CH), 125.3 (CH), 125.1 (CH), 21.7 (CH₃).

HRMS (ESI) calcd. for C₄₂H₃₀ONa⁺: 573.2189. Found: 573.2186.

[α]_D²⁰ = -111.2 (c = 1.00, CHCl₃).

v_{max} (thin film/cm⁻¹): 3056, 3023, 2830, 2740, 1696, 1595, 1440, 1194, 1071, 1028.

HPLC separation (IF-3 column, *n*hexane/*i*PrOH 99.5/0.5, 1.0 mL/min, 250.4 nm): tr(major) = 14.2 min, tr(minor) = 11.7 min, 99% ee.



(R)-2-(2-ethyl-5,6,7,8-tetraphenyl)naphthalen-1-yl)benzaldehyde 73ba: The general procedure **K** was followed using 2'-ethyl-[1,1'-biphenyl]-2-carbaldehyde **71b** (42.1 mg, 0.20 mmol) and 1,2-diphenylethyne **72a** (106.9 mg, 0.60 mmol). Isolation by column chromatography (*n*hexane/EtOAc = 20:1) yielded **73ba** (102.8 mg, 91%) as a yellow solid.

¹H-NMR (400 MHz, CDCl₃) δ 9.64 (s, 1H), 7.73 (d, *J* = 8.8 Hz, 1H), 7.49 (dd, *J* = 7.8, 1.5 Hz, 1H), 7.38 (d, *J* = 8.8 Hz, 1H), 7.30 – 7.26 (m, 4H), 7.24 – 7.18 (m, 2H), 7.13 – 7.07 (m, 1H), 6.92 (dd, *J* = 7.6, 1.3 Hz, 1H), 6.86 – 6.79 (m, 5H), 6.74 – 6.63 (m, 6H), 6.60 – 6.50 (m, 3H), 6.49 – 6.44 (m, 1H), 2.27 – 2.09 (m, 2H), 0.93 (t, *J* = 7.5 Hz, 3H).

¹³C-NMR (101 MHz, CDCl₃) δ 192.8 (CH), 145.9 (C_q), 142.5 (C_q), 142.0 (C_q), 141.5 (C_q), 140.6 (C_q), 140.5 (C_q), 139.9 (C_q), 138.6 (C_q), 138.6 (C_q, overlapped, 2C), 134.0 (C_q), 133.4 (C_q), 132.6 (CH, overlapped, 2C), 132.3 (CH), 131.7 (C_q), 131.6 (C_q), 131.5 (CH), 131.5 (CH), 131.3 (CH, overlapped, 2C), 131.2 (CH), 131.1 (CH, overlapped, 2C), 128.2 (CH), 127.7 (CH), 127.6 (CH), 127.0 (CH), 126.8 (CH), 126.8 (CH), 126.8 (CH), 126.6 (CH), 126.6

Experimental Data

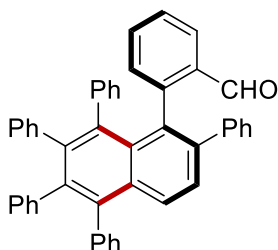
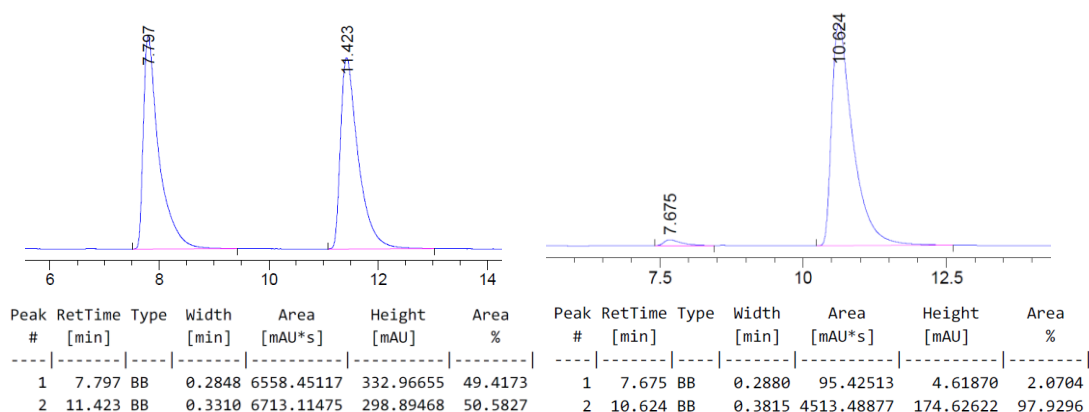
(CH), 126.6 (CH), 126.5 (CH), 126.3 (CH), 126.2 (CH), 125.4 (CH), 125.2 (CH), 125.1 (CH₂), 27.1 (CH₃), 15.2 (CH₃).

HRMS (ESI) calcd. for C₄₃H₃₂ONa⁺: 587.2345. Found: 587.2339.

[α]_D²⁰ = -84.0 (c = 1.00, CHCl₃).

ν_{max} (thin film/cm⁻¹): 3057, 3023, 2968, 2740, 1695, 1596, 1440, 1194, 1027, 748.

HPLC separation (IA-3 column, *n*hexane/*i*PrOH 99.5/0.5, 1.0 mL/min, 250.4 nm): tr(major) = 10.6 min, tr(minor) = 7.7 min, 96% ee.



(R)-2-(2,5,6,7,8-pentaphenylnaphthalen-1-yl)benzaldehyde 73ca: The general procedure **K** was followed using [1,1':2,1''-terphenyl]-2-carbaldehyde **71c** (51.6 mg, 0.20 mmol) and 1,2-diphenylethyne **72a** (106.9 mg, 0.60 mmol). Isolation by column chromatography (*n*hexane/EtOAc = 20:1) yielded **73ca** (67.4 mg, 55%) as a yellow solid.

¹H-NMR (300 MHz, CDCl₃) δ 9.63 (s, 1H), 7.79 (d, *J* = 8.7 Hz, 1H), 7.40 (d, *J* = 8.7 Hz, 1H), 7.37 – 7.27 (m, 4H), 7.26 – 7.20 (m, 1H), 7.16 (dd, *J* = 7.7, 1.5 Hz, 1H), 7.12 – 7.05 (m, 1H), 7.05 – 6.97 (m, 4H), 6.96 – 6.87 (m, 3H), 6.86 – 6.76 (m, 7H), 6.75 – 6.51 (m, 6H), 6.46 – 6.41 (m, 2H).

¹³C-NMR (101 MHz, CDCl₃) δ 191.9 (CH), 145.2 (C_q), 142.2 (C_q), 142.0 (C_q), 141.6 (C_q), 141.3 (C_q), 140.5 (C_q), 140.3 (C_q), 139.7 (C_q), 139.4 (C_q), 139.0 (C_q), 138.6 (C_q), 134.0 (C_q), 133.8 (CH), 133.3 (C_q), 132.7 (C_q), 132.6 (CH), 131.8 (CH), 131.6 (C_q), 131.6 (CH), 131.4 (CH), 131.3 (CH), 131.2 (CH), 131.2 (CH), 131.1 (CH), 131.0 (CH), 129.4 (CH, overlapped, 2C), 127.9 (CH), 127.9 (CH), 127.7 (CH), 127.7 (CH), 127.7 (CH, overlapped, 2C), 126.9

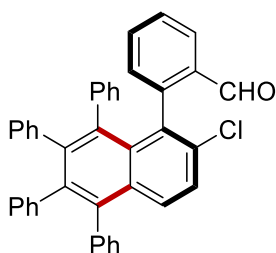
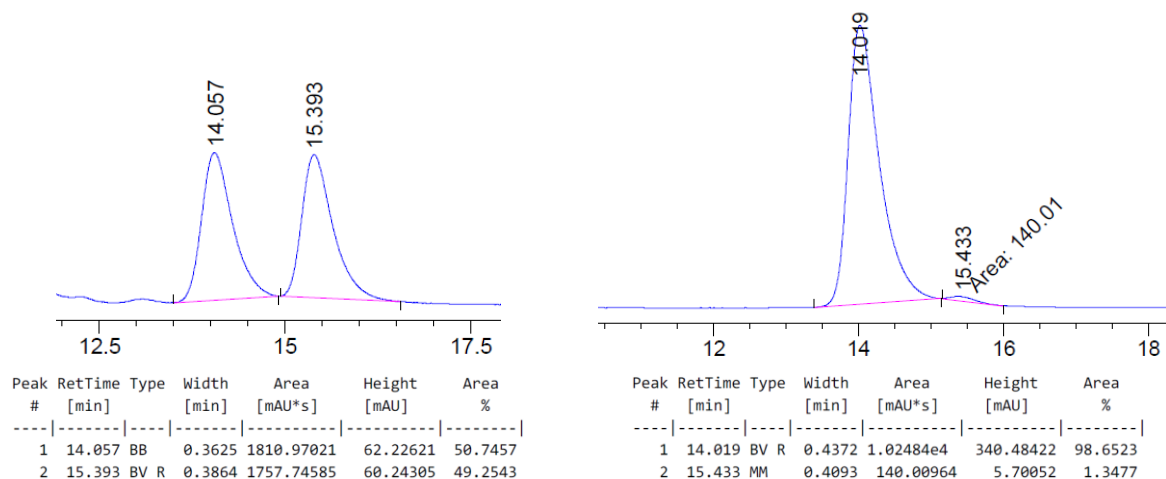
(CH), 126.8 (CH), 126.7 (CH), 126.7 (CH), 126.7 (CH, overlapped, 2C), 126.4 (CH), 126.4 (CH), 126.4 (CH), 126.3 (CH), 125.5 (CH), 125.3 (CH), 125.2 (CH).

HRMS (ESI) calcd. for $C_{47}H_{32}ONa^+$: 635.2345. Found: 635.2339.

$[\alpha]_D^{20} = -246.5$ ($c = 0.20$, $CHCl_3$).

ν_{max} (thin film/ cm^{-1}): 3060, 3023, 2924, 1670, 1596, 1442, 1194, 1072, 1023.

HPLC separation (ID-3 column, *n*hexane/*i*PrOH 99/1, 1.0 mL/min, 250.4 nm): $tr(\text{major}) = 14.0$ min, $tr(\text{minor}) = 15.4$ min, 97% ee.



(S)-2-(2-chloro-5,6,7,8-tetraphenylnaphthalen-1-yl)benzaldehyde 73da: The general procedure **K** was followed using 2'-chloro-[1,1'-biphenyl]-2-carbaldehyde **71d** (43.2 mg, 0.20 mmol) and 1,2-diphenylethyne **72a** (106.9 mg, 0.60 mmol). Isolation by column chromatography (*n*hexane/EtOAc = 20:1) yielded **73da** (59.4 mg, 52%) as a yellow solid.

1H -NMR (600 MHz, $CDCl_3$) δ 9.70 (s, 1H), 7.70 (d, $J = 9.1$ Hz, 1H), 7.48 (dd, $J = 7.7, 1.0$ Hz, 1H), 7.46 (d, $J = 9.1$ Hz, 1H), 7.31 – 7.21 (m, 6H), 7.16 – 7.12 (m, 1H), 6.91 – 6.88 (m, 1H), 6.88 – 6.84 (m, 2H), 6.83 – 6.62 (m, 10H), 6.53 – 6.50 (m, 1H), 6.49 – 6.45 (m, 1H), 6.40 – 6.37 (m, 1H).

^{13}C -NMR (126 MHz, $CDCl_3$) δ 192.0 (CH), 144.1 (C_q), 142.9 (C_q), 140.7 (C_q), 140.1 (C_q), 140.0 (C_q), 139.7 (C_q), 139.3 (C_q), 138.9 (C_q), 138.5 (C_q), 134.6 (C_q), 134.1 (C_q), 133.8 (C_q), 132.9 (CH), 132.7 (C_q), 132.4 (CH), 132.0 (C_q), 132.0 (CH), 131.4 (CH), 131.3 (CH), 131.1 (CH), 131.1 (CH), 131.1 (CH), 131.0 (CH), 130.9 (CH), 129.4 (CH), 127.9 (CH), 127.8 (CH),

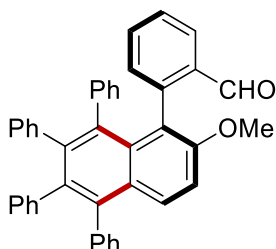
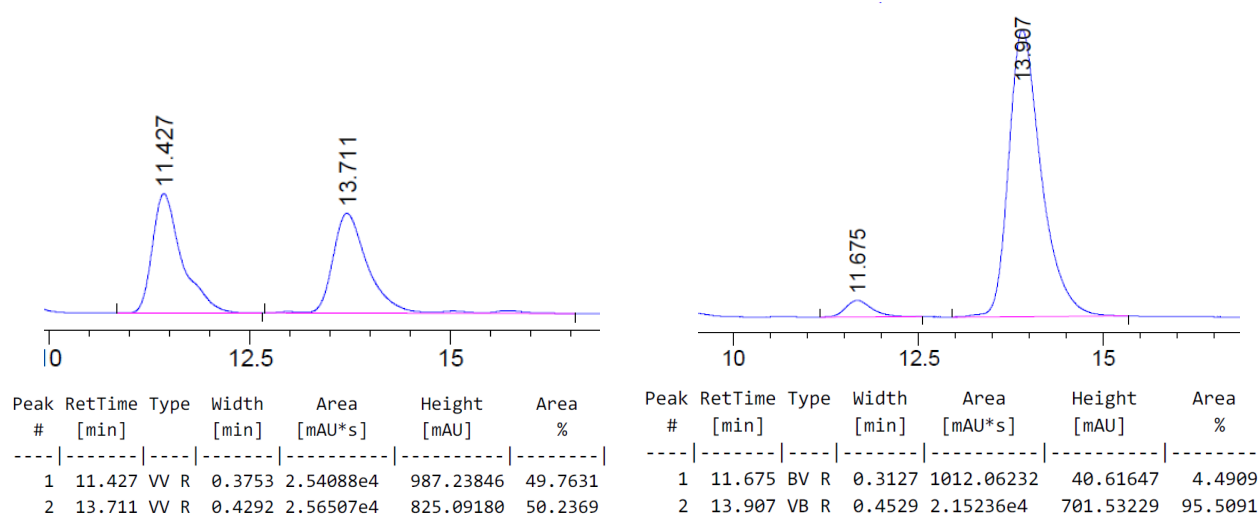
127.6 (CH), 127.2 (CH), 127.0 (CH), 126.9 (CH), 126.9 (CH), 126.8 (CH), 126.8 (CH), 126.7 (CH), 126.4 (CH), 126.3 (CH), 125.6 (CH, overlapped, 2C), 125.3 (CH).

HRMS (ESI) calcd. for $C_{41}H_{27}ClONa^+$: 593.1643. Found: 593.1649.

$[\alpha]_D^{20} = -102.5$ ($c = 1.00$, $CHCl_3$).

ν_{max} (thin film/ cm^{-1}): 3057, 3025, 2927, 2851, 2743, 1698, 1586, 1494, 1442, 1196, 1027.

HPLC separation (IC-3 column, *n*hexane/*i*PrOH 98/2, 1.0 mL/min, 250.4 nm): $tr(\text{major}) = 13.9$ min, $tr(\text{minor}) = 11.7$ min, 91% ee.



(S)-2-(2-methoxy-5,6,7,8-tetraphenyl-naphthalen-1-yl)benzaldehyde 73ea: The general procedure **K** was followed using 2'-methoxy-[1,1'-biphenyl]-2-carbaldehyde **71e** (42.4 mg, 0.20 mmol) and 1,2-diphenylethyne **72a** (106.9 mg, 0.60 mmol). Isolation by column chromatography (*n*hexane/EtOAc = 10:1) yielded **73ea** (79.3 mg, 70%) as a yellow solid.

1H -NMR (300 MHz, $CDCl_3$) δ 9.75 (s, 1H), 7.77 (d, $J = 9.4$ Hz, 1H), 7.48 (dd, $J = 7.7, 1.5$ Hz, 1H), 7.33 – 7.17 (m, 7H), 7.11 – 7.03 (m, 1H), 6.95 – 6.58 (m, 13H), 6.52 – 6.35 (m, 3H), 3.67 (s, 3H).

^{13}C -NMR (126 MHz, $CDCl_3$) δ 193.5 (CH), 155.6 (C_q), 143.1 (C_q), 142.2 (C_q), 141.2 (C_q), 140.5 (C_q), 140.5 (C_q), 139.9 (C_q), 138.6 (C_q), 137.7 (C_q), 137.3 (C_q), 134.1 (C_q), 132.8 (CH), 132.8 (C_q), 132.7 (CH), 132.6 (CH), 131.6 (CH), 131.4 (CH), 131.4 (CH), 131.3 (CH), 131.3 (CH), 131.2 (CH), 130.9 (CH), 130.0 (CH), 128.9 (C_q), 127.8 (CH), 127.6 (CH), 126.9 (CH,

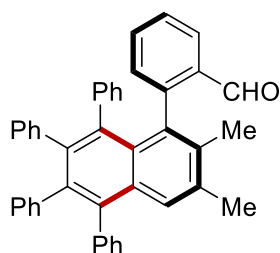
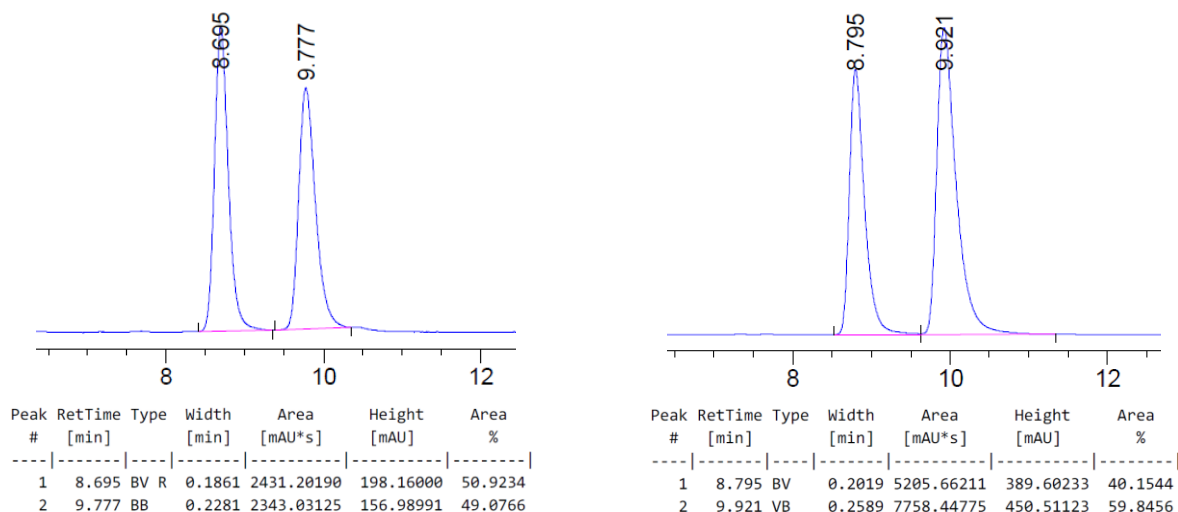
overlapped, 2C), 126.7 (CH), 126.7 (CH, overlapped, 2C), 126.6 (CH), 126.3 (CH), 126.2 (CH), 126.1 (CH), 125.4 (CH), 125.3 (CH), 125.2 (CH), 121.4 (C_q), 112.3 (CH), 56.4 (CH₃).

HRMS (ESI) calcd. for C₄₂H₃₀O₂Na⁺: 589.2138. Found: 589.2133.

[α]_D²⁰ = +0.5 (c = 0.54, CHCl₃).

ν_{max} (thin film/cm⁻¹): 3055, 3022, 2923, 2852, 1696, 1596, 1440, 1348, 1273, 1110, 1027.

HPLC separation (IE-3 column, *n*hexane/*i*PrOH 95/5, 1.0 mL/min, 250.4 nm): tr(major) = 9.9 min, tr(minor) = 8.8 min, 20% ee.



(R)-2-(2,3-dimethyl-5,6,7,8-tetraphenylnaphthalen-1-yl)benzaldehyde 73fa: The general procedure **K** was followed using 2',3'-dimethyl-[1,1'-biphenyl]-2-carbaldehyde **71f** (42.0 mg, 0.20 mmol) and 1,2-diphenylethyne **72a** (106.9 mg, 0.60 mmol). Isolation by column chromatography (*n*hexane/EtOAc = 20:1) yielded **73fa** (95.9 mg, 85%) as a yellow solid.

¹H-NMR (600 MHz, CDCl₃) δ 9.63 (s, 1H), 7.56 – 7.52 (m, 1H), 7.48 (dd, *J* = 7.7, 1.4 Hz, 1H), 7.28 – 7.26 (m, 4H), 7.24 – 7.19 (m, 2H), 7.11 – 7.07 (m, 1H), 6.87 (dd, *J* = 7.8, 1.2 Hz, 1H), 6.86 – 6.76 (m, 5H), 6.75 – 6.70 (m, 2H), 6.70 – 6.62 (m, 4H), 6.58 – 6.52 (m, 2H), 6.51 – 6.48 (m, 1H), 6.44 – 6.40 (m, 1H), 2.35 (s, 3H), 1.81 (s, 3H).

¹³C-NMR (151 MHz, CDCl₃) δ 192.7 (CH), 146.9 (C_q), 141.5 (C_q), 140.8 (C_q), 140.5 (C_q), 140.5 (C_q), 139.8 (C_q), 138.4 (C_q), 138.0 (C_q), 137.7 (C_q), 136.2 (C_q), 134.8 (C_q), 134.2 (C_q), 133.8 (C_q), 132.8 (CH), 132.2 (CH), 132.1 (CH), 131.4 (C_q), 131.4 (CH), 131.3 (CH), 131.1

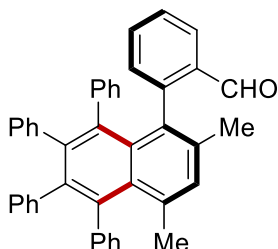
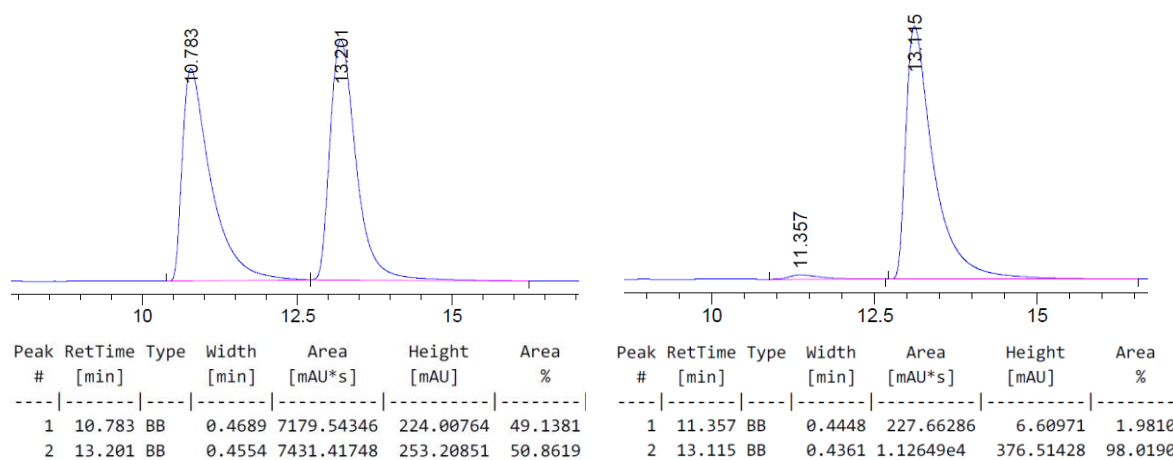
(CH), 131.1 (CH, overlapped, 2C), 131.0 (CH, overlapped, 2C), 130.3 (C_q), 127.5 (CH), 127.5 (CH), 127.4 (CH), 126.8 (CH), 126.6 (CH), 126.5 (CH), 126.4 (CH), 126.4 (CH), 126.3 (CH), 126.3 (CH), 126.0 (CH), 125.9 (CH), 125.1 (CH), 124.9 (CH), 124.8 (CH), 21.4 (CH₃), 17.6 (CH₃).

HRMS (ESI) calcd. for C₄₃H₃₂ONa⁺: 587.2345. Found: 587.2341.

[α]_D²⁰ = -112.4 (c = 1.00, CHCl₃).

ν_{max} (thin film/cm⁻¹): 3011, 2924, 2853, 1693, 1597, 1440, 1222, 1025, 814.

HPLC separation (IA-3 column, *n*hexane/*i*PrOH 99.7/0.3, 1.0 mL/min, 250.4 nm): tr(major) = 13.1 min, tr(minor) = 11.4 min, 96% ee.



(R)-2-(2,4-dimethyl-5,6,7,8-tetraphenyl-naphthalen-1-yl)benzaldehyde 73ga: The general procedure **K** was followed using 2',4'-dimethyl-[1,1'-biphenyl]-2-carbaldehyde **71g** (42.0 mg, 0.20 mmol) and 1,2-diphenylethyne **72a** (106.9 mg, 0.60 mmol). Isolation by column chromatography (*n*hexane/EtOAc = 20:1) yielded **73ga** (101.6 mg, 90%) as a yellow solid.

¹H-NMR (400 MHz, CDCl₃) δ 9.65 (s, 1H), 7.48 (dd, *J* = 7.8, 1.4 Hz, 1H), 7.25 – 7.17 (m, 4H), 7.17 – 7.06 (m, 4H), 6.84 (dd, *J* = 7.8, 1.2 Hz, 1H), 6.83 – 6.76 (m, 3H), 6.76 – 6.62 (m, 8H), 6.58 – 6.54 (m, 1H), 6.52 – 6.48 (m, 1H), 6.46 (td, *J* = 7.5, 1.4 Hz, 1H), 6.28 (dt, *J* = 7.7, 1.5 Hz, 1H), 1.96 (s, 3H), 1.90 (s, 3H).

¹³C-NMR (101 MHz, CDCl₃) δ 193.0 (CH), 146.8 (C_q), 142.9 (C_q), 142.2 (C_q), 140.7 (C_q), 140.6 (C_q), 140.5 (C_q), 139.4 (C_q), 138.6 (C_q), 137.7 (C_q), 135.9 (C_q), 135.7 (C_q), 134.0 (C_q),

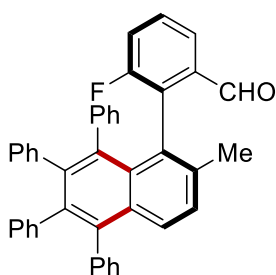
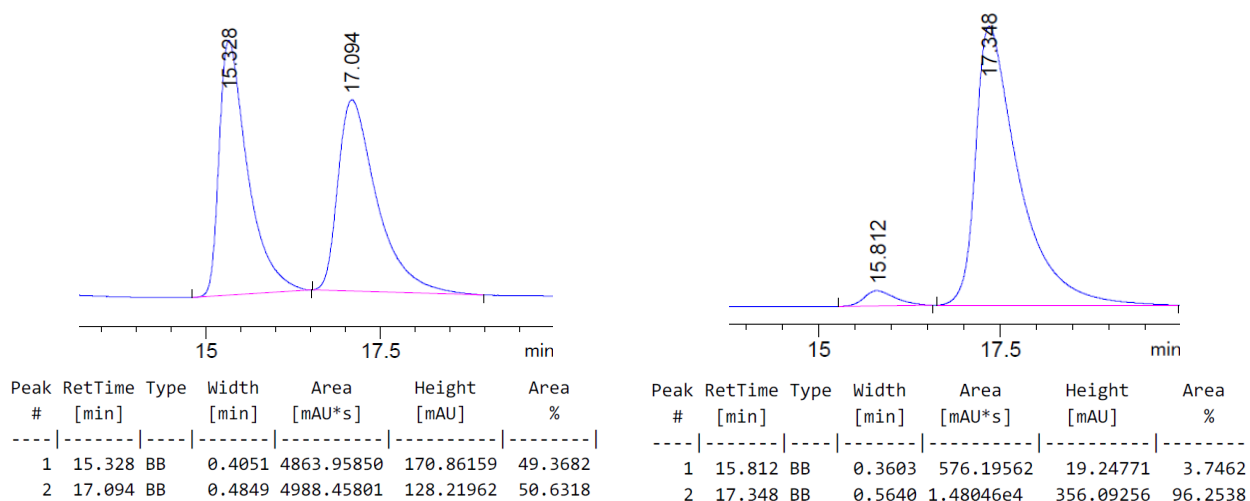
133.2 (C_q), 132.9 (CH), 132.8 (C_q), 132.7 (CH), 132.4 (CH), 132.2 (CH), 131.9 (CH), 131.8 (CH), 131.6 (CH, overlapped, 2C), 131.2 (CH), 131.1 (CH), 131.0 (CH), 131.0 (CH), 127.1 (CH), 127.1 (CH), 126.8 (CH, overlapped, 2C), 126.7 (CH), 126.4 (CH), 126.4 (CH, overlapped, 2C), 126.3 (CH), 126.3 (CH), 126.2 (CH), 125.1 (CH), 125.1 (CH), 125.0 (CH), 25.1 (CH₃), 20.9 (CH₃).

HRMS (ESI) calcd. for C₄₃H₃₂ONa⁺: 587.2345. Found: 587.2345.

[α]_D²⁰ = -306.5 (*c* = 0.83, CHCl₃).

ν_{max} (thin film/cm⁻¹): 3050, 3022, 2928, 2829, 1695, 1594, 1492, 1442, 1249, 1194, 1071.

HPLC separation (IE-3 column, *n*hexane/*i*PrOH 99.5/0.5, 1.0 mL/min, 250.4 nm): tr(major) = 17.3 min, tr(minor) = 15.8 min, 93% ee.



(S)-3-fluoro-2-(2-methyl-5,6,7,8-tetraphenylnaphthalen-1-yl)benzaldehyde 73ha: The general procedure **K** was followed using 6-fluoro-2'-methyl-[1,1'-biphenyl]-2-carbaldehyde **71h** (42.8 mg, 0.20 mmol) and 1,2-diphenylethyne **72a** (106.9 mg, 0.60 mmol). Isolation by column chromatography (*n*hexane/EtOAc = 20:1) yielded **73ha** (88.6 mg, 78%) as a yellow solid.

¹H-NMR (600 MHz, CDCl₃) δ 9.43 (s, 1H), 7.72 (d, *J* = 8.7 Hz, 1H), 7.42 (dd, *J* = 7.8, 1.2 Hz, 1H), 7.36 (d, *J* = 8.7 Hz, 1H), 7.31 – 7.28 (m, 2H), 7.27 – 7.24 (m, 2H), 7.23 – 7.20 (m, 1H), 7.10 – 7.05 (m, 1H), 6.95 – 6.92 (m, 1H), 6.90 – 6.84 (m, 3H), 6.83 – 6.77 (m, 3H), 6.75 –

6.71 (m, 2H), 6.71 – 6.64 (m, 4H), 6.64 – 6.60 (m, 1H), 6.58 – 6.55 (m, 1H), 6.49 – 6.46 (m, 1H), 1.95 (s, 3H).

¹³C-NMR (126 MHz, CDCl₃) δ 191.5 (d, *J* = 3.8 Hz, CH), 158.9 (d, *J* = 244.6 Hz, C_q), 142.2 (C_q), 140.7 (C_q), 140.6 (C_q), 140.5 (C_q), 139.9 (C_q), 139.0 (C_q), 138.7 (C_q), 137.7 (C_q), 137.3 (C_q), 135.6 (d, *J* = 3.0 Hz, C_q), 133.9 (d, *J* = 18.5 Hz, C_q), 131.8 (C_q), 131.7 (CH), 131.6 (C_q), 131.5 (CH), 131.4 (CH), 131.2 (CH), 131.2 (CH, overlapped, 2C), 131.2 (CH), 131.0 (CH), 129.0 (d, *J* = 8.1 Hz, CH), 128.7 (CH), 128.5 (CH), 127.7 (CH), 127.7 (CH), 127.0 (C_q), 126.8 (CH), 126.7 (CH), 126.6 (CH, overlapped, 2C), 126.6 (CH), 126.3 (CH), 126.2 (CH), 125.9 (CH), 125.4 (CH), 125.1 (CH), 122.7 (d, *J* = 2.9 Hz, CH), 120.8 (d, *J* = 22.9 Hz, CH), 21.4 (CH₃).

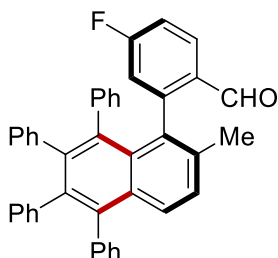
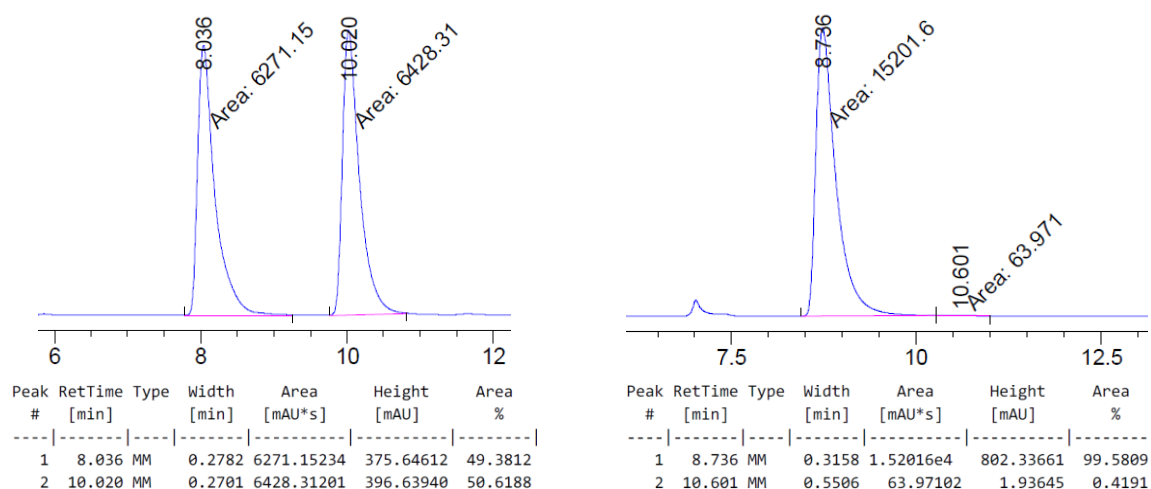
¹⁹F-NMR (471 MHz, CDCl₃) δ -110.38.

HRMS (ESI) calcd. for C₄₂H₂₉FONa⁺: 591.2095. Found: 591.2100.

[α]_D²⁰ = +31.7 (*c* = 0.93, CHCl₃).

ν_{max} (thin film/cm⁻¹): 3057, 3024, 2851, 1690, 1603, 1493, 1441, 1368, 1236, 1072, 1027.

HPLC separation (IA-3 column, *n*hexane/*i*PrOH 99.5/0.5, 1.0 mL/min, 250.4 nm): tr(major) = 8.7 min, tr(minor) = 10.6 min, 99% ee.



(*R*)-4-fluoro-2-(2-methyl-5,6,7,8-tetraphenylnaphthalen-1-yl)benzaldehyde 73ia: The general procedure **K** was followed using 5-fluoro-2'-methyl-[1,1'-biphenyl]-2-carbaldehyde **71i** (42.8 mg, 0.20 mmol) and 1,2-diphenylethyne **2a** (106.9 mg, 0.60 mmol). Isolation by

column chromatography (*n*hexane/EtOAc = 20:1) yielded **73ia** (71.6 mg, 63%) as a yellow solid.

¹H-NMR (600 MHz, CDCl₃) δ 9.53 (s, 1H), 7.68 (d, *J* = 8.7 Hz, 1H), 7.54 (dd, *J* = 8.7, 6.0 Hz, 1H), 7.34 – 7.30 (m, 1H), 7.29 – 7.25 (m, 4H), 7.23 – 7.20 (m, 1H), 6.87 – 6.83 (m, 2H), 6.83 – 6.72 (m, 6H), 6.71 – 6.64 (m, 5H), 6.61 – 6.56 (m, 4H), 1.93 (s, 3H).

¹³C-NMR (126 MHz, CDCl₃) δ 191.1 (CH), 165.3 (d, *J* = 255.6 Hz, C_q), 149.4 (d, *J* = 9.6 Hz, C_q), 142.2 (C_q), 141.3 (C_q), 140.4 (C_q, overlapped, 2C), 139.8 (C_q), 138.8 (C_q), 138.8 (C_q), 138.0 (C_q), 136.4 (C_q), 133.0 (C_q), 132.5 (CH), 131.8 (C_q), 131.5 (CH), 131.5 (CH), 131.4 (CH), 131.4 (C_q), 131.2 (CH), 131.2 (CH), 131.1 (CH), 131.1 (CH), 130.6 (d, *J* = 2.5 Hz, C_q), 129.5 (d, *J* = 10.1 Hz, CH), 128.4 (CH), 128.3 (CH), 127.8 (CH), 127.7 (CH), 126.9 (CH), 126.7 (CH), 126.7 (CH), 126.7 (CH), 126.6 (CH), 126.3 (CH), 126.3 (CH), 125.6 (CH), 125.5 (CH), 125.2 (CH), 119.0 (d, *J* = 21.5 Hz, CH), 114.5 (d, *J* = 21.9 Hz, CH), 21.6 (CH₃).

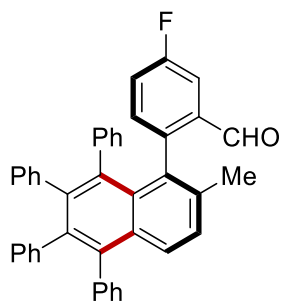
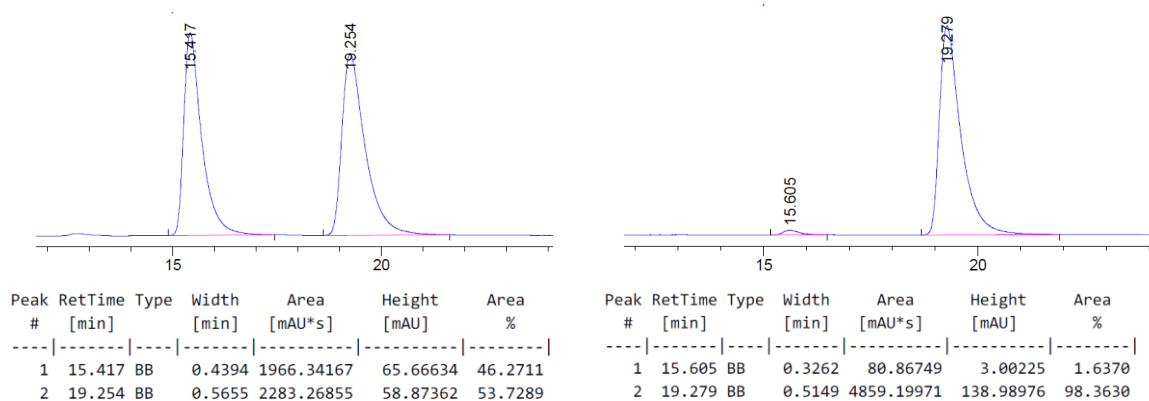
¹⁹F-NMR (376 MHz, CDCl₃) δ -105.70.

HRMS (ESI) calcd. for C₄₂H₂₉FONa⁺: 591.2095. Found: 591.2093.

[α]_D²⁰ = -118.0 (*c* = 0.60, CHCl₃).

ν_{max} (thin film/cm⁻¹): 3056, 3023, 2924, 2852, 1695, 1601, 1576, 1440, 1182, 1027.

HPLC separation (IF-3 column, *n*hexane/*i*PrOH 99.7/0.3, 1.0 mL/min, 250.4 nm): tr(major) = 19.3 min, tr(minor) = 15.6 min, 97% ee.



(*R*)-5-fluoro-2-(2-methyl-5,6,7,8-tetraphenylnaphthalen-1-yl)benzaldehyde 73ja: The general procedure **K** was followed using 4-fluoro-2'-methyl-[1,1'-biphenyl]-2-carbaldehyde

71j (42.8 mg, 0.20 mmol) and 1,2-diphenylethyne **72a** (106.9 mg, 0.60 mmol). Isolation by column chromatography (*n*hexane/EtOAc = 20:1) yielded **73ja** (61.4 mg, 54%) as a yellow solid.

¹H-NMR (600 MHz, CDCl₃) δ 9.58 (s, 1H), 7.69 (d, *J* = 8.7 Hz, 1H), 7.33 (d, *J* = 8.8 Hz, 1H), 7.28 – 7.26 (m, 4H), 7.25 – 7.19 (m, 1H), 7.15 (dd, *J* = 9.0, 2.8 Hz, 1H), 6.95 – 6.91 (m, 1H), 6.88 – 6.77 (m, 6H), 6.77 – 6.68 (m, 6H), 6.62 – 6.59 (m, 1H), 6.58 – 6.55 (m, 2H), 6.50 – 6.47 (m, 1H), 1.92 (s, 3H).

¹³C-NMR (126 MHz, CDCl₃) δ 191.5 (d, *J* = 2.0 Hz, CH), 161.5 (d, *J* = 247.8 Hz, C_q), 142.5 (d, *J* = 3.5 Hz, C_q), 142.1 (C_q), 141.6 (C_q), 140.4 (C_q), 140.4 (C_q), 139.8 (C_q), 138.8 (C_q), 138.7 (C_q), 138.1 (C_q), 136.9 (C_q), 135.3 (d, *J* = 6.4 Hz, C_q), 133.8 (d, *J* = 7.0 Hz, CH), 133.3 (C_q), 132.4 (CH), 131.9 (C_q, overlapped, 2C), 131.4 (CH), 131.4 (CH), 131.3 (CH), 131.2 (CH), 131.1 (CH), 131.1 (CH), 131.1 (CH), 128.4 (CH), 128.1 (CH), 127.8 (CH), 127.7 (CH), 127.0 (CH), 126.9 (CH), 126.7 (CH, overlapped, 2C), 126.6 (CH), 126.3 (CH), 126.2 (CH), 125.5 (CH), 125.4 (CH), 125.2 (CH), 120.2 (d, *J* = 22.1 Hz, CH), 112.7 (d, *J* = 22.2 Hz, CH), 21.7 (CH₃).

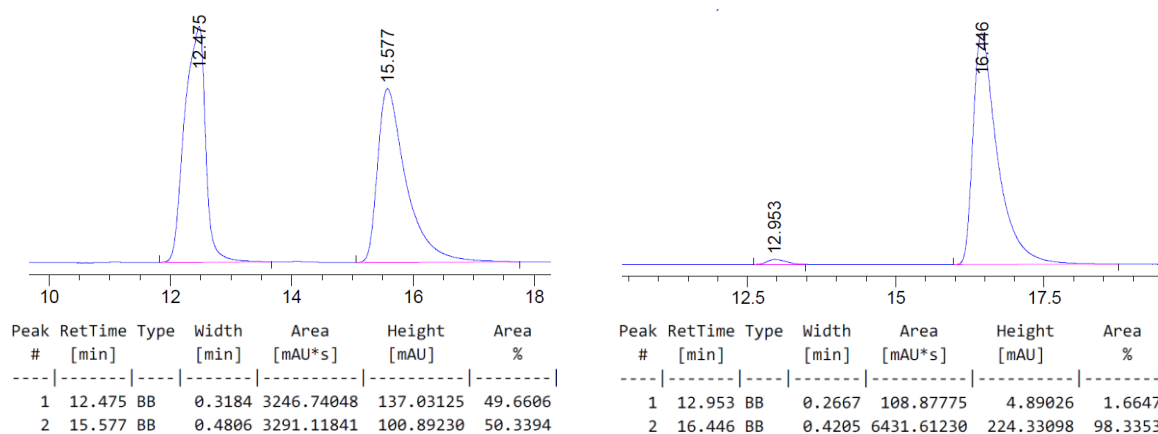
¹⁹F-NMR (376 MHz, CDCl₃) δ -114.80.

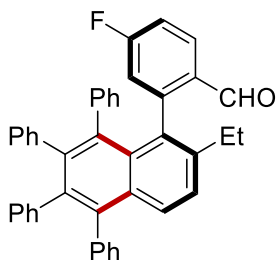
HRMS (ESI) calcd. for C₄₂H₂₉FONa⁺: 591.2095. Found: 591.2088.

[α]_D²⁰ = -123.3 (*c* = 1.00, CHCl₃).

ν_{max} (thin film/cm⁻¹): 3057, 3023, 2838, 1692, 1601, 1488, 1370, 1262, 1146, 1027.

HPLC separation (IF-3 column, *n*hexane/*i*PrOH 99.7/0.3, 1.0 mL/min, 250.4 nm): tr(major) = 16.4 min, tr(minor) = 13.0 min, 97% ee.





(R)-2-(2-ethyl-5,6,7,8-tetraphenyl-naphthalen-1-yl)-4-fluorobenzaldehyde 73ka: The general procedure **K** was followed using 2'-ethyl-5-fluoro-[1,1'-biphenyl]-2-carbaldehyde **71k** (45.6 mg, 0.20 mmol) and 1,2-diphenylethyne **72a** (106.9 mg, 0.60 mmol). Isolation by column chromatography (*n*hexane/EtOAc = 20:1) yielded **73ka** (87.3 mg, 75%) as a yellow solid.

¹H-NMR (600 MHz, CDCl₃) δ 9.53 (s, 1H), 7.75 (d, *J* = 8.8 Hz, 1H), 7.55 (dd, *J* = 8.7, 6.0 Hz, 1H), 7.38 (d, *J* = 8.9 Hz, 1H), 7.30 – 7.26 (m, 4H), 7.25 – 7.19 (m, 1H), 6.87 – 6.82 (m, 4H), 6.82 – 6.72 (m, 3H), 6.72 – 6.63 (m, 6H), 6.64 – 6.58 (m, 3H), 6.58 – 6.53 (m, 1H), 2.30 – 2.13 (m, 2H), 0.97 (t, *J* = 7.6 Hz, 3H).

¹³C-NMR (126 MHz, CDCl₃) δ 191.1 (CH), 165.0 (d, *J* = 255.6 Hz, C_q), 148.8 (d, *J* = 9.5 Hz, C_q), 142.3 (C_q), 142.2 (C_q), 141.4 (C_q), 140.4 (C_q, overlapped, 2C), 139.8 (C_q), 138.8 (C_q), 138.8 (C_q), 138.3 (C_q), 132.4 (CH), 131.9 (d, *J* = 2.5 Hz, C_q), 131.6 (C_q), 131.4 (CH, overlapped, 2C), 131.4 (CH), 131.4 (C_q), 131.2 (CH), 131.1 (CH), 131.1 (CH, overlapped, 2C), 131.0 (C_q), 129.2 (d, *J* = 10.2 Hz, CH), 128.6 (CH), 127.7 (CH), 127.7 (CH), 127.0 (CH), 126.8 (CH), 126.7 (CH, overlapped, 2C), 126.7 (CH), 126.6 (CH), 126.3 (CH), 126.2 (CH), 125.6 (CH), 125.4 (CH), 125.2 (CH), 119.4 (d, *J* = 21.7 Hz, CH), 114.6 (d, *J* = 22.1 Hz, CH), 27.1 (CH₂), 15.3 (CH₃).

¹⁹F-NMR (376 MHz, CDCl₃) δ -105.95.

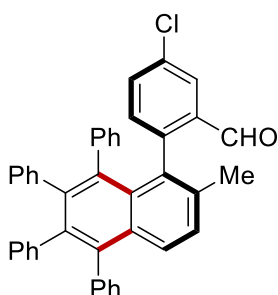
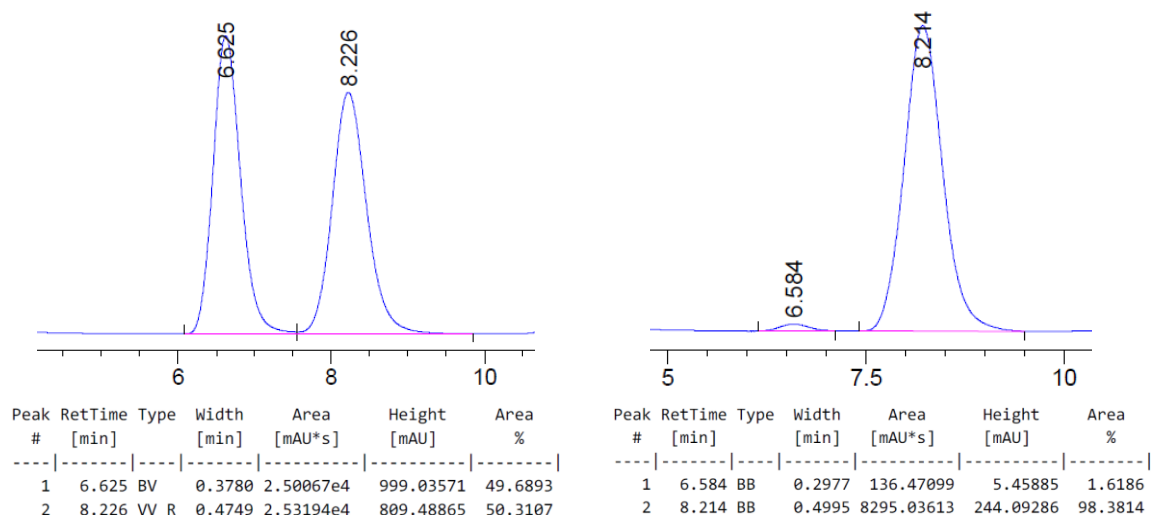
HRMS (ESI) calcd. for C₄₃H₃₁FONa⁺: 605.2251. Found: 605.2251.

[α]_D²⁰ = -76.1 (*c* = 1.00, CHCl₃).

ν_{max} (thin film/cm⁻¹): 3058, 3023, 2970, 1695, 1601, 1577, 1441, 1370, 1269, 1220, 1181.

HPLC separation (IC-3 column, *n*hexane/*i*PrOH 99/1, 1.0 mL/min, 250.4 nm): tr(major) = 8.2 min, tr(minor) = 6.6 min, 97% ee.

Experimental Data



(R)-5-chloro-2-(2-methyl-5,6,7,8-tetraphenyl-naphthalen-1-yl)benzaldehyde 73la: The general procedure **K** was followed using 4-chloro-2'-methyl-[1,1'-biphenyl]-2-carbaldehyde **71I** (46.0 mg, 0.20 mmol) and 1,2-diphenylethyne **72a** (106.9 mg, 0.60 mmol). Isolation by column chromatography (*n*hexane/EtOAc = 20:1) yielded **73la** (51.4 mg, 44%) as a yellow solid.

¹H-NMR (400 MHz, CDCl₃) δ 9.58 (s, 1H), 7.69 (d, *J* = 8.7 Hz, 1H), 7.43 (d, *J* = 2.3 Hz, 1H), 7.33 (d, *J* = 8.7 Hz, 1H), 7.29 – 7.26 (m, 4H), 7.24 – 7.20 (m, 1H), 7.18 (dd, *J* = 8.2, 2.3 Hz, 1H), 6.87 – 6.68 (m, 12H), 6.64 – 6.56 (m, 3H), 6.48 (dt, *J* = 7.7, 1.5 Hz, 1H), 1.93 (s, 3H).

¹³C-NMR (101 MHz, CDCl₃) δ 191.3 (CH), 144.7 (C_q), 142.1 (C_q), 141.5 (C_q), 140.4 (C_q), 140.4 (C_q), 139.8 (C_q), 138.8 (C_q), 138.7 (C_q), 138.0 (C_q), 136.5 (C_q), 134.7 (C_q), 133.5 (CH), 133.2 (C_q), 133.1 (C_q), 132.8 (CH), 132.5 (CH), 131.9 (C_q), 131.8 (C_q), 131.4 (CH), 131.4 (CH), 131.3 (CH), 131.2 (CH), 131.1 (CH), 131.1 (CH), 131.0 (CH), 128.4 (CH), 128.2 (CH), 127.8 (CH), 127.7 (CH), 127.0 (CH), 126.9 (CH), 126.7 (CH, overlapped, 2C), 126.6 (CH), 126.5 (CH), 126.3 (CH), 126.3 (CH), 125.5 (CH), 125.3 (CH), 125.2 (CH), 21.7 (CH₃).

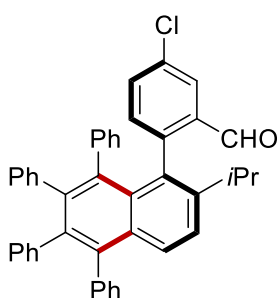
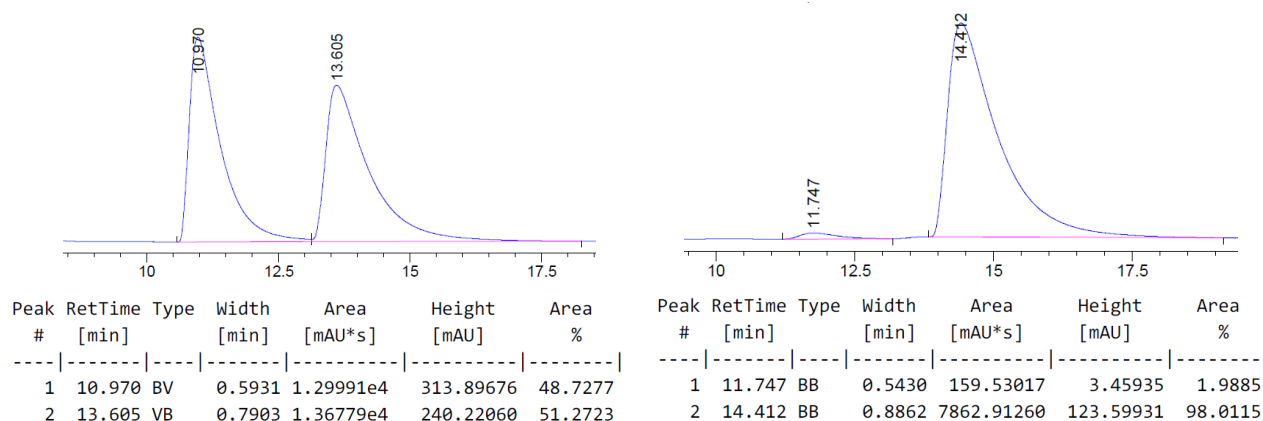
HRMS (ESI) calcd. for C₄₂H₂₉ClONa⁺: 607.1799. Found: 607.1794.

[α]_D²⁰ = -92.4 (*c* = 1.00, CHCl₃).

ν_{max} (thin film/cm⁻¹): 3057, 3024, 2834, 1695, 1600, 1441, 1382, 1179, 1072, 1027.

Experimental Data

HPLC separation (IB-3 column, *n*hexane/*i*PrOH 99.9/0.1, 1.0 mL/min, 250.4 nm): *tr*(major) = 14.4 min, *tr*(minor) = 11.7 min, 96% ee.



(*R*)-5-chloro-2-(2-isopropyl-5,6,7,8-tetraphenylnaphthalen-1-yl)benzaldehyde 73ma:

The general procedure **K** was followed using 4-chloro-2'-isopropyl-[1,1'-biphenyl]-2-carbaldehyde **71m** (51.6 mg, 0.20 mmol) and 1,2-diphenylethyne **72a** (106.9 mg, 0.60 mmol). Isolation by column chromatography (*n*hexane/EtOAc = 20:1) yielded **73ma** (57.5 mg, 47%) as a yellow solid.

¹H-NMR (400 MHz, CDCl₃) δ 9.57 (s, 1H), 7.78 (d, *J* = 9.0 Hz, 1H), 7.46 (d, *J* = 9.0 Hz, 1H), 7.40 (d, *J* = 2.3 Hz, 1H), 7.29 – 7.25 (m, 4H), 7.24 – 7.18 (m, 1H), 7.14 (dd, *J* = 8.2, 2.3 Hz, 1H), 6.87 – 6.66 (m, 12H), 6.62 (td, *J* = 7.5, 1.5 Hz, 1H), 6.58 – 6.54 (m, 1H), 6.52 (dt, *J* = 7.5, 1.5 Hz, 1H), 6.44 (dt, *J* = 7.7, 1.6 Hz, 1H), 2.39 (hept, *J* = 6.8 Hz, 1H), 1.05 (d, *J* = 6.9 Hz, 3H), 0.99 (d, *J* = 6.8 Hz, 3H).

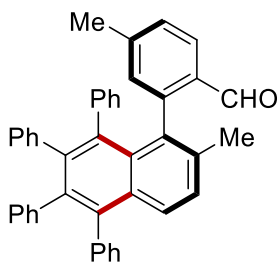
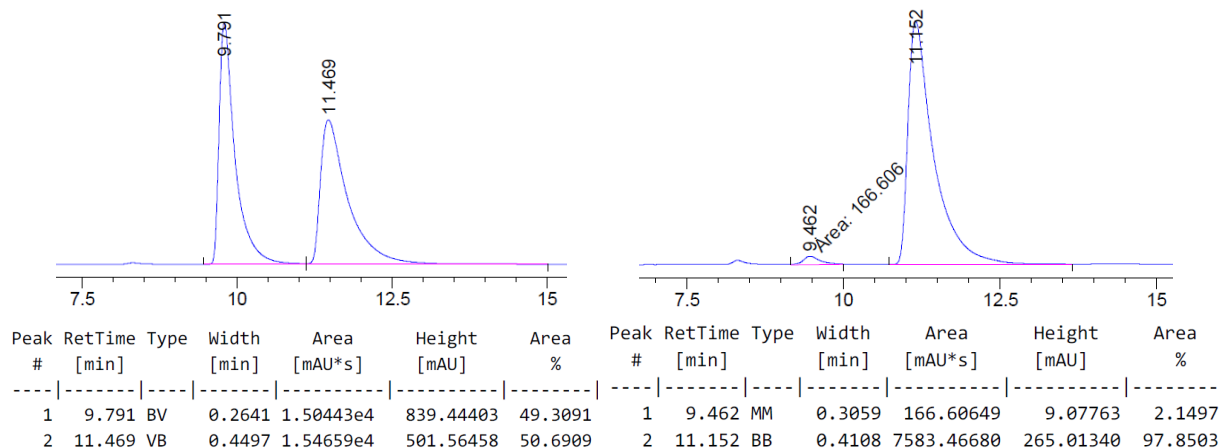
¹³C-NMR (101 MHz, CDCl₃) δ 191.2 (CH), 146.8 (C_q), 144.0 (C_q), 142.3 (C_q), 141.8 (C_q), 140.4 (C_q, overlapped, 2C), 139.8 (C_q), 138.9 (C_q), 138.7 (C_q), 138.5 (C_q), 135.3 (C_q), 133.8 (CH), 133.3 (C_q), 132.4 (CH), 132.3 (CH), 131.6 (C_q), 131.6 (C_q), 131.4 (CH), 131.4 (CH), 131.2 (CH), 131.2 (CH), 131.1 (CH), 131.1 (CH), 131.1 (CH), 131.1 (CH), 128.9 (CH), 127.8 (CH), 127.7 (CH), 127.0 (CH), 126.9 (CH), 126.7 (CH), 126.7 (CH), 126.6 (CH), 126.3 (CH), 126.2 (CH, overlapped, 2C), 125.5 (CH), 125.2 (CH, overlapped, 2C), 123.5 (CH), 30.2 (CH), 24.1 (CH₃), 22.9 (CH₃).

HRMS (ESI) calcd. for C₄₄H₃₃ClONa⁺: 635.2112. Found: 635.2108.

$[\alpha]_D^{20} = -55.1$ ($c = 1.00$, CHCl_3).

ν_{max} (thin film/ cm^{-1}): 3059, 2966, 2927, 2845, 1695, 1590, 1440, 1383, 1179, 1108, 1027.

HPLC separation (IF-3 column, *n*hexane/*i*PrOH 99.7/0.3, 1.0 mL/min, 250.4 nm): tr(major) = 11.2 min, tr(minor) = 9.5 min, 96% ee.



(R)-4-methyl-2-(2-methyl-5,6,7,8-tetraphenylnaphthalen-1-yl)benzaldehyde 73na: The general procedure **K** was followed using 2',5-dimethyl-[1,1'-biphenyl]-2-carbaldehyde **71n** (42.0 mg, 0.20 mmol) and 1,2-diphenylethyne **72a** (106.9 mg, 0.60 mmol). Isolation by column chromatography (*n*hexane/EtOAc = 20:1) yielded **73na** (81.3 mg, 72%) as a yellow solid.

¹H-NMR (600 MHz, CDCl_3) δ 9.54 (s, 1H), 7.67 (dd, $J = 8.8, 0.5$ Hz, 1H), 7.44 (d, $J = 7.9$ Hz, 1H), 7.32 (dd, $J = 8.7, 0.5$ Hz, 1H), 7.29 – 7.26 (m, 4H), 7.23 – 7.19 (m, 1H), 6.90 – 6.87 (m, 1H), 6.87 – 6.81 (m, 4H), 6.81 – 6.77 (m, 1H), 6.76 – 6.67 (m, 4H), 6.67 – 6.59 (m, 5H), 6.58 – 6.56 (m, 1H), 6.55 – 6.52 (m, 1H), 2.22 (s, 3H), 1.93 (s, 3H).

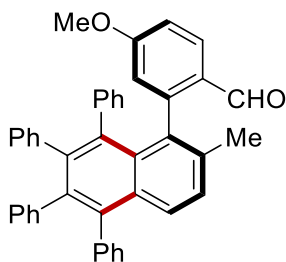
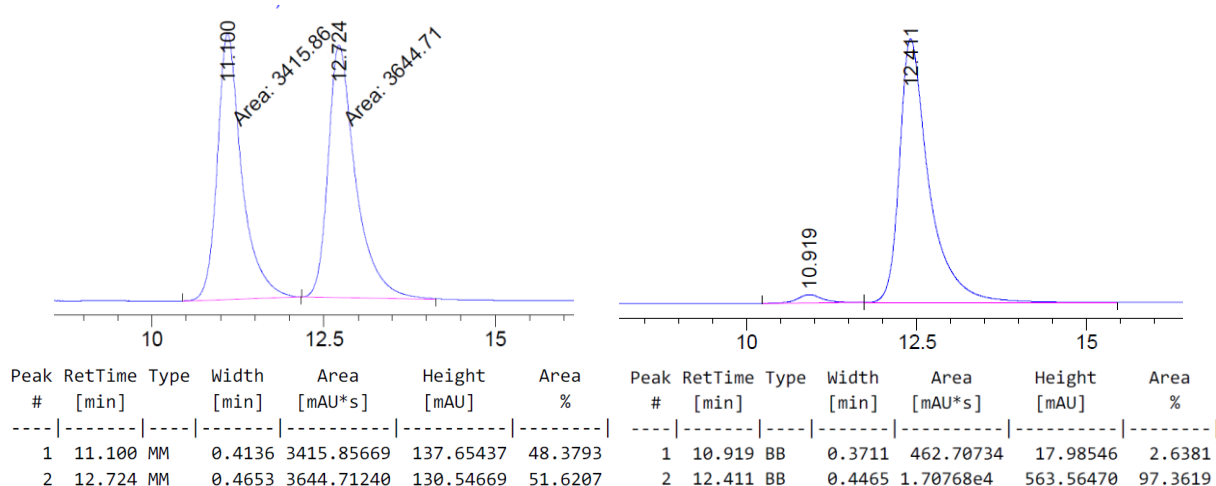
¹³C-NMR (101 MHz, CDCl_3) δ 192.5 (CH), 146.5 (C_q), 143.7 (C_q), 141.9 (C_q), 141.3 (C_q), 140.6 (C_q), 140.6 (C_q), 140.0 (C_q), 138.7 (C_q), 138.5 (C_q), 138.3 (C_q), 136.5 (C_q), 134.5 (C_q), 132.9 (CH), 132.4 (CH), 131.8 (C_q), 131.7 (C_q), 131.7 (C_q), 131.5 (CH), 131.4 (CH), 131.4 (CH), 131.3 (CH), 131.2 (CH, overlapped, 2C), 131.1 (CH), 128.4 (CH), 127.9 (CH), 127.7 (CH), 127.7 (CH), 127.6 (CH), 126.9 (CH), 126.7 (CH), 126.6 (CH), 126.6 (CH), 126.5 (CH), 126.3 (CH), 126.1 (CH), 126.0 (CH), 125.4 (CH), 125.3 (CH), 125.1 (CH), 21.7 (CH_3), 21.6 (CH_3).

HRMS (ESI) calcd. for $C_{43}H_{32}ONa^+$: 587.2345. Found: 587.2343.

$[\alpha]_D^{20} = -30.3$ ($c = 1.00$, $CHCl_3$).

ν_{max} (thin film/ cm^{-1}): 3055, 3022, 2829, 1687, 1600, 1492, 1440, 1253, 1072, 1027.

HPLC separation (ID-3 column, *n*hexane/*i*PrOH 99/1, 1.0 mL/min, 250.4 nm): $tr(\text{major}) = 12.4$ min, $tr(\text{minor}) = 10.9$ min, 95% ee.



(R)-4-methoxy-2-(2-methyl-5,6,7,8-tetraphenylnaphthalen-1-yl)benzaldehyde 73oa:

The general procedure **K** was followed using 5-methoxy-2'-methyl-[1,1'-biphenyl]-2-carbaldehyde **71o** (45.2 mg, 0.20 mmol) and 1,2-diphenylethyne **72a** (106.9 mg, 0.60 mmol). Isolation by column chromatography (*n*hexane/EtOAc = 10:1) yielded **73oa** (62.7 mg, 54%) as a yellow solid.

¹H-NMR (600 MHz, $CDCl_3$) δ 9.42 (s, 1H), 7.67 (d, $J = 8.5$ Hz, 1H), 7.52 (d, $J = 8.7$ Hz, 1H), 7.32 (dd, $J = 8.7, 0.5$ Hz, 1H), 7.28 – 7.25 (m, 4H), 7.23 – 7.19 (m, 1H), 6.86 – 6.76 (m, 5H), 6.74 – 6.70 (m, 1H), 6.70 – 6.55 (m, 10H), 6.33 (d, $J = 2.5$ Hz, 1H), 3.74 (s, 3H), 1.96 (s, 3H).

¹³C-NMR (126 MHz, $CDCl_3$) δ 191.4 (CH), 163.1 (C_q), 148.8 (C_q), 142.0 (C_q), 141.3 (C_q), 140.6 (C_q), 140.5 (C_q), 139.9 (C_q), 138.7 (C_q), 138.5 (C_q), 138.2 (C_q), 136.4 (C_q), 134.2 (C_q), 132.4 (CH), 131.7 (CH, C_q , overlapped, 2C), 131.5 (C_q), 131.5 (CH), 131.4 (CH), 131.2 (CH), 131.2 (CH, overlapped, 2C), 131.1 (CH), 129.1 (CH), 128.4 (CH), 128.1 (C_q), 127.8 (CH), 127.8 (CH), 127.6 (CH), 126.7 (CH), 126.7 (CH), 126.6 (CH), 126.5 (CH), 126.3 (CH,

Experimental Data

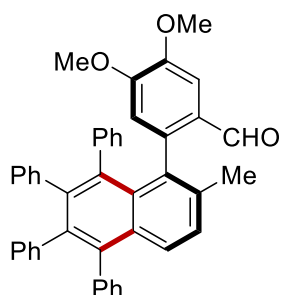
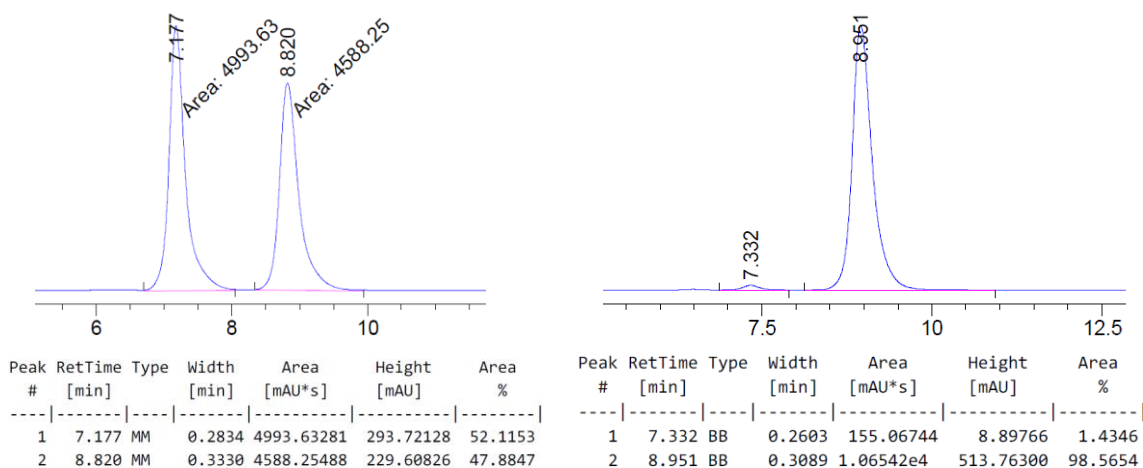
overlapped, 2C), 126.2 (CH), 125.4 (CH), 125.3 (CH), 125.1 (CH), 117.0 (CH), 113.3 (CH), 55.5 (CH₃), 21.6 (CH₃).

HRMS (ESI) calcd. for C₄₃H₃₂O₂Na⁺: 603.2295. Found: 603.2287.

[α]_D²⁰ = -23.1 (c = 0.83, CHCl₃).

ν_{max} (thin film/cm⁻¹): 3022, 2920, 2836, 1683, 1591, 1492, 1440, 1250, 1175, 1028.

HPLC separation (IA-3 column, *n*hexane/*i*PrOH 98/2, 1.0 mL/min, 250.4 nm): tr(major) = 9.0 min, tr(minor) = 7.3 min, 97% ee.



(R)-4,5-dimethoxy-2-(2-methyl-5,6,7,8-tetraphenylnaphthalen-1-yl)benzaldehyde 73pa:

The general procedure **K** was followed using 4,5-dimethoxy-2'-methyl-[1,1'-biphenyl]-2-carbaldehyde **71p** (51.2 mg, 0.20 mmol) and 1,2-diphenylethyne **72a** (106.9 mg, 0.60 mmol). Isolation by column chromatography (*n*hexane/EtOAc = 5:1) yielded **73pa** (108.6 mg, 89%) as a yellow solid.

¹H-NMR (400 MHz, CDCl₃) δ 9.36 (s, 1H), 7.68 (d, *J* = 8.7 Hz, 1H), 7.33 (d, *J* = 8.8 Hz, 1H), 7.29 – 7.24 (m, 4H), 7.24 – 7.18 (m, 1H), 7.05 (s, 1H), 6.86 – 6.75 (m, 5H), 6.74 – 6.61 (m, 9H), 6.54 – 6.49 (m, 1H), 6.28 (s, 1H), 3.85 (s, 3H), 3.78 (s, 3H), 1.99 (s, 3H).

¹³C-NMR (101 MHz, CDCl₃) δ 191.4 (CH), 152.8 (C_q), 147.9 (C_q), 142.1 (C_q), 141.8 (C_q), 141.5 (C_q), 140.6 (C_q), 140.5 (C_q), 139.9 (C_q), 138.8 (C_q), 138.6 (C_q), 138.2 (C_q), 136.9 (C_q), 133.8 (C_q), 132.1 (CH), 132.0 (C_q), 131.9 (CH), 131.7 (C_q), 131.5 (CH), 131.4 (CH), 131.2 (CH), 131.2 (CH, overlapped, 2C), 131.0 (CH), 128.4 (CH), 127.9 (CH), 127.8 (C_q), 127.8

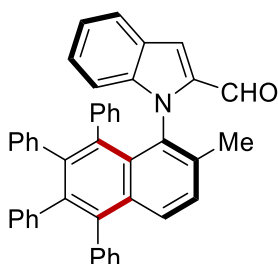
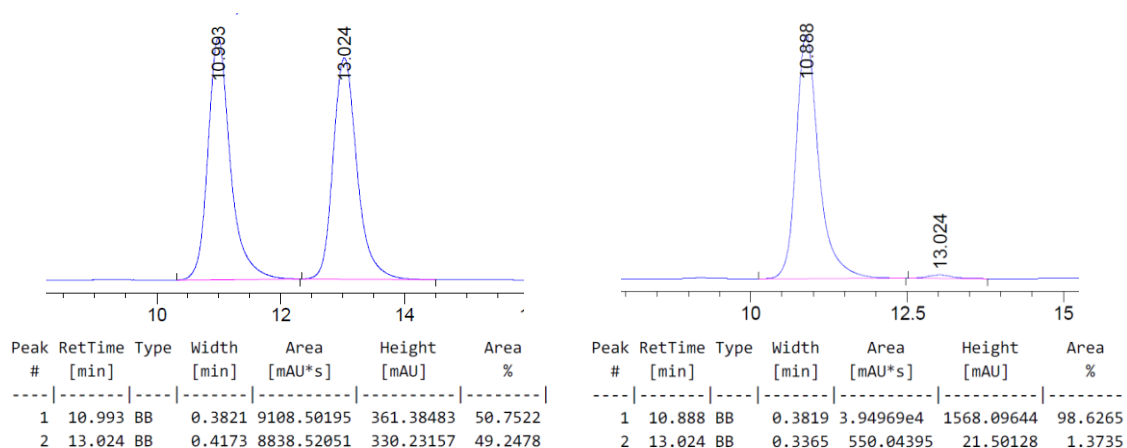
(CH), 127.6 (CH), 126.7 (CH), 126.6 (CH), 126.6 (CH), 126.5 (CH), 126.3 (CH), 126.2 (CH), 126.0 (CH), 125.4 (CH), 125.2 (CH), 125.1 (CH), 114.2 (CH), 108.1 (CH), 56.1 (CH₃), 56.0 (CH₃), 21.7 (CH₃).

HRMS (ESI) calcd. for C₄₄H₃₄O₃Na⁺: 633.2400. Found: 633.2397.

[α]_D²⁰ = -16.8 (c = 1.00, CHCl₃).

ν_{max} (thin film/cm⁻¹): 3020, 2924, 1675, 1596, 1507, 1441, 1337, 1263, 1214, 1141, 1022.

HPLC separation (ID-3 column, *n*hexane/*i*PrOH 90/10, 1.0 mL/min, 250.4 nm): tr(major) = 10.9 min, tr(minor) = 13.0 min, 97% ee.



1-(2-methyl-5,6,7,8-tetraphenylindole-1-yl)-1H-indole-2-carbaldehyde 73qa: The general procedure **K** was followed using 1-(*o*-tolyl)-1H-indole-2-carbaldehyde **71q** (47.0 mg, 0.20 mmol) and 1,2-diphenylethyne **72a** (106.9 mg, 0.60 mmol). Isolation by column chromatography (*n*hexane/EtOAc = 20:1) yielded **73qa** (53.0 mg, 45%) as a yellow solid.

¹H-NMR (600 MHz, CDCl₃) δ 9.55 (s, 1H), 7.78 (d, *J* = 8.8 Hz, 1H), 7.48 (dt, *J* = 8.0, 1.0 Hz, 1H), 7.37 (dd, *J* = 8.8, 0.6 Hz, 1H), 7.34 – 7.30 (m, 1H), 7.29 – 7.24 (m, 4H), 7.23 – 7.19 (m, 1H), 7.11 – 7.07 (m, 1H), 6.84 – 6.74 (m, 8H), 6.72 – 6.68 (m, 1H), 6.66 – 6.58 (m, 4H), 6.56 – 6.52 (m, 1H), 6.52 – 6.47 (m, 1H), 6.10 – 6.03 (m, 2H), 1.71 (s, 3H).

¹³C-NMR (126 MHz, CDCl₃) δ 182.3 (CH), 142.7 (C_q), 141.1 (C_q), 140.5 (C_q), 140.5 (C_q), 139.9 (C_q), 139.2 (C_q), 139.1 (C_q), 138.9 (C_q), 137.2 (C_q), 136.8 (C_q), 136.1 (C_q), 132.7 (C_q), 131.9 (C_q), 131.5 (CH), 131.3 (CH), 131.3 (CH), 131.1 (CH, overlapped, 3C), 130.4 (CH), 129.4 (C_q), 128.9 (CH), 128.9 (CH), 128.7 (CH), 127.7 (CH), 127.6 (CH), 126.8 (C_q), 126.7

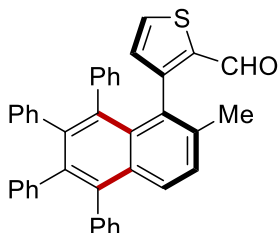
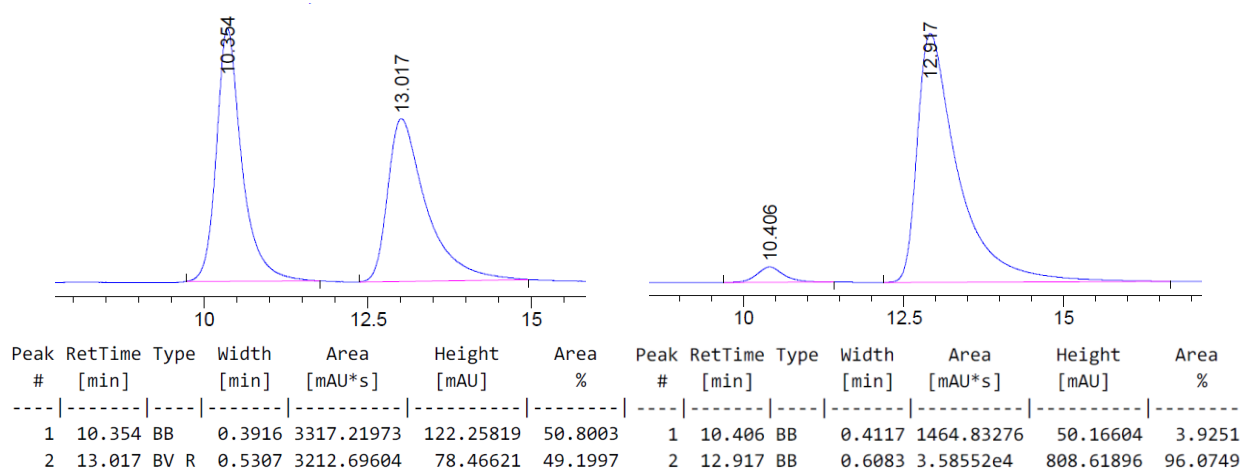
(CH), 126.6 (CH), 126.6 (CH), 126.5 (CH), 126.2 (CH), 126.0 (CH), 125.7 (CH), 125.4 (CH), 125.0 (CH, overlapped, 2C), 125.0 (CH), 124.9 (CH), 122.9 (CH), 121.1 (CH), 115.8 (CH), 112.3 (CH), 17.7 (CH₃).

HRMS (ESI) calcd. for C₄₄H₃₁NONa⁺: 612.2298. Found: 612.2294.

[α]_D²⁰ = +153.8 (*c* = 0.37, CHCl₃).

ν_{max} (thin film/cm⁻¹): 3056, 3023, 1670, 1614, 1522, 1456, 1397, 1217, 1125, 1072, 1027.

HPLC separation (ID-3 column, *n*hexane/*i*PrOH 99/1, 1.0 mL/min, 250.4 nm): tr(major) = 12.9 min, tr(minor) = 10.4 min, 92% ee.



3-(2-methyl-5,6,7,8-tetraphenyl-naphthalen-1-yl)thiophene-2-carbaldehyde 73ra: The general procedure **K** was followed using 3-(*o*-tolyl)thiophene-2-carbaldehyde **71r** (40.4 mg, 0.20 mmol) and 1,2-diphenylethyne **72a** (106.9 mg, 0.60 mmol). Isolation by column chromatography (*n*hexane/EtOAc = 20:1) yielded **73ra** (57.8 mg, 52%) as a yellow solid.

¹H-NMR (600 MHz, CDCl₃) δ 9.22 (s, 1H), 7.69 (d, *J* = 8.7 Hz, 1H), 7.33 (dd, *J* = 8.7, 0.5 Hz, 1H), 7.30 – 7.25 (m, 4H), 7.24 (dd, *J* = 4.9, 1.3 Hz, 1H), 7.23 – 7.20 (m, 1H), 6.86 (dd, *J* = 3.5, 2.1 Hz, 2H), 6.85 – 6.78 (m, 5H), 6.78 – 6.73 (m, 3H), 6.73 – 6.69 (m, 3H), 6.65 – 6.61 (m, 1H), 6.60 – 6.58 (m, 1H), 6.50 (d, *J* = 4.9 Hz, 1H), 2.03 (s, 3H).

¹³C-NMR (126 MHz, CDCl₃) δ 184.4 (CH), 152.9 (C_q), 142.1 (C_q), 141.3 (C_q), 140.4 (C_q), 140.4 (C_q), 139.7 (C_q), 138.7 (C_q, overlapped, 3C), 138.3 (C_q), 137.9 (C_q), 137.0 (C_q), 133.0 (CH), 132.4 (CH), 132.2 (C_q), 131.7 (CH), 131.7 (CH), 131.6 (C_q), 131.5 (CH), 131.3 (CH), 131.2 (CH), 131.2 (CH), 131.2 (CH), 130.9 (CH), 130.1 (C_q), 128.4 (CH), 128.2 (CH), 127.7

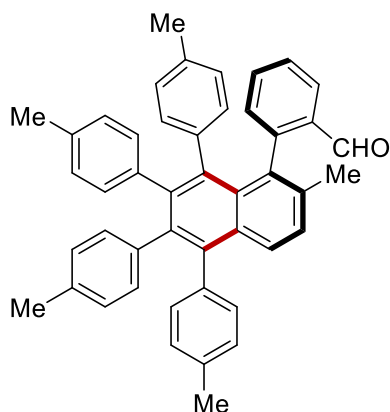
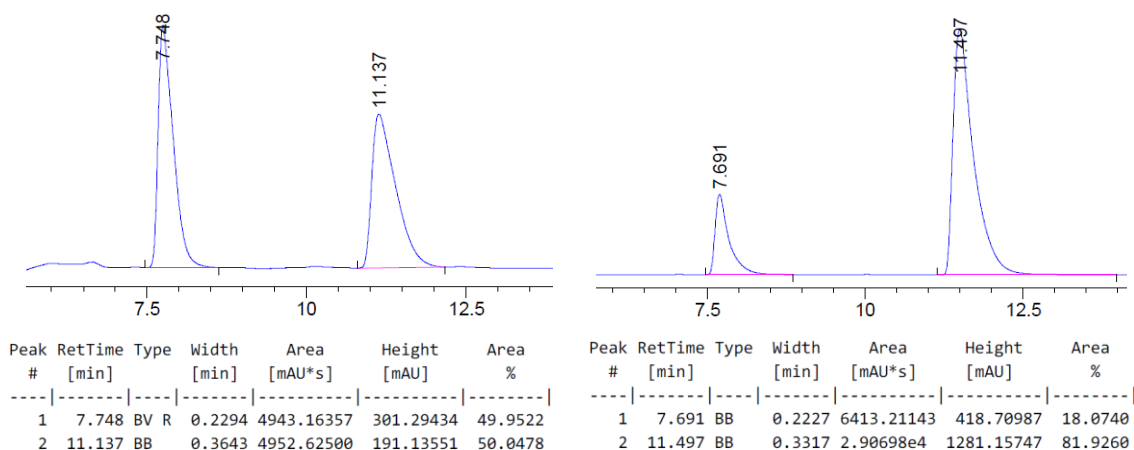
(CH), 127.7 (CH), 127.3 (CH), 126.7 (CH, overlapped, 2C), 126.7 (CH), 126.6 (CH), 126.4 (CH), 126.2 (CH), 125.5 (CH), 125.4 (CH), 125.2 (CH), 21.3 (CH₃).

HRMS (ESI) calcd. for C₄₀H₂₈OSNa⁺: 579.1753. Found: 579.1753.

[α]_D²⁰ = -82.7 (c = 1.06, CHCl₃).

v_{max} (thin film/cm⁻¹): 3055, 3023, 1656, 1601, 1493, 1440, 1414, 1362, 1072, 1026.

HPLC separation (IA-3 column, *n*hexane/*i*PrOH 99/1, 1.0 mL/min, 250.4 nm): tr(major) = 11.5 min, tr(minor) = 7.7 min, 64% ee.



(R)-2-(2-methyl-5,6,7,8-tetra-*p*-tolynaphthalen-1-yl)benzaldehyde 73ab: The general procedure **K** was followed using 2'-methyl-[1,1'-biphenyl]-2-carbaldehyde **71a** (39.3 mg, 0.20 mmol) and 1,2-di-*p*-tolylethyne **72b** (123.7 mg, 0.60 mmol). Isolation by column chromatography (*n*hexane/EtOAc = 20:1) yielded **73ab** (100.6 mg, 83%) as a yellow solid.

¹H-NMR (400 MHz, CDCl₃) δ 9.59 (s, 1H), 7.62 (d, *J* = 8.6 Hz, 1H), 7.48 (dd, *J* = 7.7, 1.6 Hz, 1H), 7.26 – 7.23 (m, 1H), 7.19 (td, *J* = 7.5, 1.5 Hz, 1H), 7.14 – 7.09 (m, 3H), 7.09 – 7.05 (m, 2H), 6.82 (dd, *J* = 7.6, 1.4 Hz, 1H), 6.73 – 6.57 (m, 5H), 6.57 – 6.40 (m, 5H), 6.31 – 6.20 (m, 2H), 2.33 (s, 3H), 2.07 (s, 3H), 2.02 (s, 3H), 2.00 (s, 3H), 1.85 (s, 3H).

¹³C-NMR (101 MHz, CDCl₃) δ 192.9 (CH), 147.0 (C_q), 142.1 (C_q), 138.7 (C_q), 138.5 (C_q, overlapped, 2C), 138.3 (C_q), 137.8 (C_q), 137.7 (C_q), 137.2 (C_q), 136.2 (C_q), 135.8 (C_q), 134.3

Experimental Data

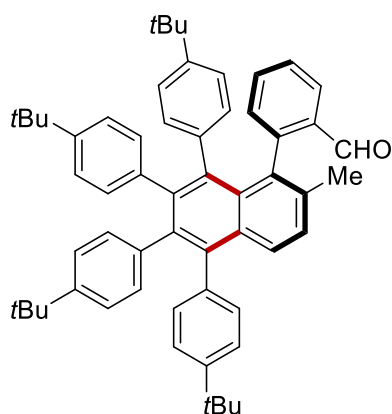
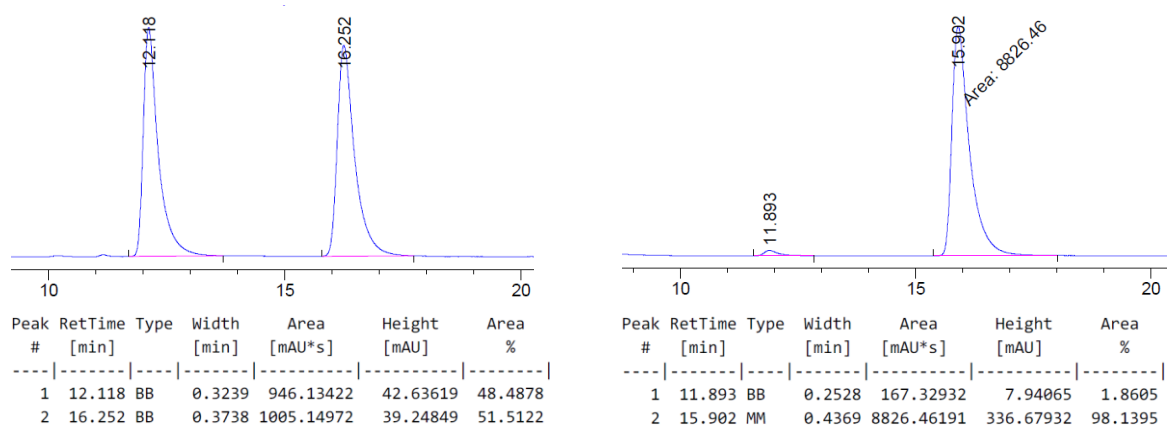
(C_q), 134.3 (C_q), 134.3 (C_q), 134.1 (C_q), 133.4 (C_q), 132.8 (CH), 132.5 (CH), 132.1 (C_q), 132.0 (CH, C_q, overlapped, 2C), 131.4 (CH), 131.3 (CH), 131.2 (CH), 131.1 (CH, overlapped, 2C), 131.0 (CH), 130.9 (CH), 128.4 (CH), 128.3 (CH), 128.1 (CH), 127.8 (CH), 127.5 (CH), 127.5 (CH), 127.3 (CH, overlapped, 2C), 127.0 (CH), 126.9 (CH), 126.3 (CH), 126.3 (CH), 21.7 (CH₃), 21.4 (CH₃), 21.2 (CH₃), 21.1 (CH₃), 21.0 (CH₃).

HRMS (ESI) calcd. for C₄₆H₃₈ONa⁺: 629.2815. Found: 629.2805.

[α]_D²⁰ = -142.7 (c = 1.00, CHCl₃).

v_{max} (thin film/cm⁻¹): 3016, 2921, 2852, 1688, 1594, 1515, 1446, 1383, 1245, 1110, 1020.

HPLC separation (IF-3 column, *n*hexane/*i*PrOH 99.5/0.5, 1.0 mL/min, 250.4 nm): tr(major) = 15.9 min, tr(minor) = 11.9 min, 96% ee.



(R)-2-(5,6,7,8-tetrakis(4-(tert-butyl)phenyl)-2-methylnaphthalen-1-yl)benzaldehyde

73ac: The general procedure **K** was followed using 2'-methyl-[1,1'-biphenyl]-2-carbaldehyde **71a** (39.3 mg, 0.20 mmol) and 1,2-bis(4-(tert-butyl)phenyl)ethyne **72c** (174.1 mg, 0.60 mmol). Isolation by column chromatography (*n*hexane/EtOAc = 20:1) yielded **73ac** (140.9 mg, 91%) as a yellow solid. Crystals suitable for X-ray structure analysis could be obtained from saturated solution of CH₂Cl₂/*n*hexane.

¹H-NMR (600 MHz, CDCl₃) δ 9.68 (s, 1H), 7.80 (d, *J* = 8.7 Hz, 1H), 7.49 – 7.46 (m, 1H), 7.30 (d, *J* = 8.7 Hz, 1H), 7.26 – 7.22 (m, 2H), 7.21 – 7.14 (m, 3H), 7.07 – 7.03 (m, 1H), 6.91 –

Experimental Data

6.88 (m, 1H), 6.84 – 6.76 (m, 2H), 6.72 – 6.63 (m, 5H), 6.58 (dd, $J = 8.1, 2.0$ Hz, 1H), 6.50 – 6.45 (m, 2H), 6.42 (dd, $J = 8.2, 2.0$ Hz, 1H), 6.35 (dd, $J = 8.0, 2.0$ Hz, 1H), 1.89 (s, 3H), 1.30 (s, 9H), 1.10 (s, 9H), 1.07 (s, 9H), 1.01 (s, 9H).

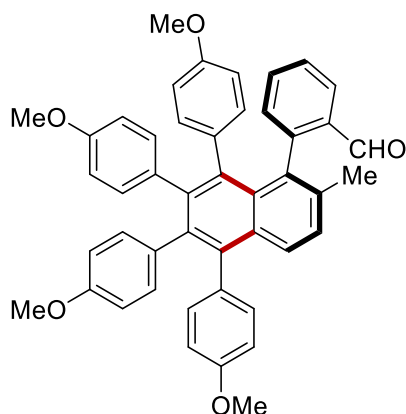
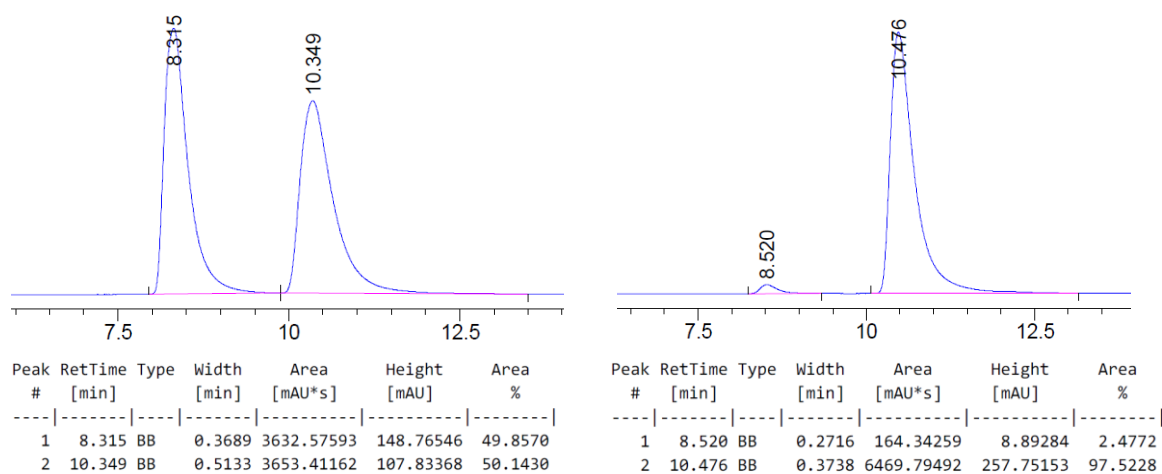
$^{13}\text{C-NMR}$ (126 MHz, CDCl_3) δ 192.9 (CH), 149.1 (C_q), 147.5 (C_q), 147.3 (C_q), 147.0 (C_q), 147.0 (C_q), 142.5 (C_q), 139.0 (C_q), 138.6 (C_q), 138.6 (C_q), 138.4 (C_q), 137.8 (C_q , overlapped, 2C), 137.1 (C_q), 136.1 (C_q), 134.4 (C_q), 133.7 (C_q), 132.9 (CH), 132.4 (CH), 132.2 (CH), 131.7 (C_q), 131.6 (C_q), 131.2 (CH, overlapped, 2C), 131.1 (CH), 131.0 (CH), 130.9 (CH), 130.7 (CH, overlapped, 2C), 128.1 (CH), 128.0 (CH), 126.8 (CH), 126.5 (CH), 124.4 (CH), 124.2 (CH), 123.4 (CH), 123.3 (CH), 123.1 (CH), 123.0 (CH), 122.8 (CH), 122.6 (CH), 34.5 (C_q), 34.1 (C_q), 34.1 (C_q), 34.0 (C_q), 31.5 (CH_3 , overlapped, 3C), 31.3 (CH_3 , overlapped, 3C), 31.2 (CH_3 , overlapped, 3C), 21.8 (CH_3).

HRMS (ESI) calcd. for $\text{C}_{58}\text{H}_{62}\text{ONa}^+$: 797.4693. Found: 797.4681.

$[\alpha]_D^{20} = -115.2$ ($c = 1.00$, CHCl_3).

ν_{max} (thin film/ cm^{-1}): 2964, 2902, 2865, 2696, 2595, 1509, 1361, 1268, 1194, 1117, 1018.

HPLC separation (IE-3 column, *n*hexane/*i*PrOH 99.5/0.5, 1.0 mL/min, 250.4 nm): t_r (major) = 10.5 min, t_r (minor) = 8.5 min, 95% ee.



(R)-2-(5,6,7,8-tetrakis(4-methoxyphenyl)-2-methylnaphthalen-1-yl)benzaldehyde 73ad:

The general procedure **K** was followed using 2'-methyl-[1,1'-biphenyl]-2-carbaldehyde **71a** (39.3 mg, 0.20 mmol) and 1,2-bis(4-methoxyphenyl)ethyne **72d** (142.8 mg, 0.60 mmol). Isolation by column chromatography (*n*hexane/EtOAc = 10:1) yielded **73ad** (120.6 mg, 90%) as a yellow solid.

¹H-NMR (400 MHz, CDCl₃) δ 9.61 (s, 1H), 7.66 (d, *J* = 8.7 Hz, 1H), 7.58 – 7.52 (m, 1H), 7.29 – 7.21 (m, 2H), 7.18 – 7.09 (m, 3H), 6.86 – 6.79 (m, 3H), 6.75 – 6.65 (m, 2H), 6.60 (dd, *J* = 8.4, 2.2 Hz, 1H), 6.48 – 6.43 (m, 2H), 6.43 – 6.37 (m, 2H), 6.36 – 6.29 (m, 2H), 6.26 (dd, *J* = 8.5, 2.7 Hz, 1H), 6.21 (dd, *J* = 8.4, 2.7 Hz, 1H), 6.04 (dd, *J* = 8.4, 2.7 Hz, 1H), 3.80 (s, 3H), 3.61 (s, 3H), 3.60 (s, 3H), 3.54 (s, 3H), 1.86 (s, 3H).

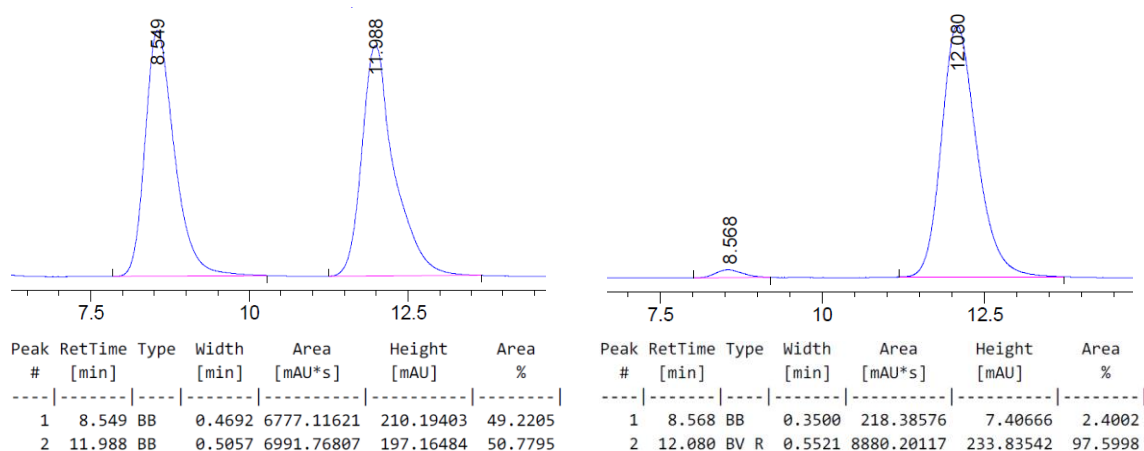
¹³C-NMR (101 MHz, CDCl₃) δ 192.9 (CH), 158.1 (C_q), 156.9 (C_q), 156.8 (C_q), 156.7 (C_q), 147.1 (C_q), 142.2 (C_q), 138.8 (C_q), 138.5 (C_q), 138.2 (C_q), 136.3 (C_q), 134.3 (C_q), 134.3 (C_q), 133.5 (CH), 133.4 (C_q, overlapped, 2C), 133.3 (C_q), 133.0 (CH), 132.5 (CH), 132.5 (C_q, overlapped, 2C), 132.3 (C_q), 132.2 (CH), 132.2 (C_q), 132.2 (CH), 132.1 (CH), 132.0 (CH), 132.0 (CH), 131.9 (CH), 128.2 (CH), 127.7 (CH), 126.7 (CH), 126.5 (CH), 113.5 (CH), 113.2 (CH), 113.2 (CH), 112.2 (CH, overlapped, 2C), 111.9 (CH), 111.9 (CH), 111.8 (CH), 55.2 (CH₃), 55.2 (CH₃), 55.0 (CH₃), 54.9 (CH₃), 21.7 (CH₃).

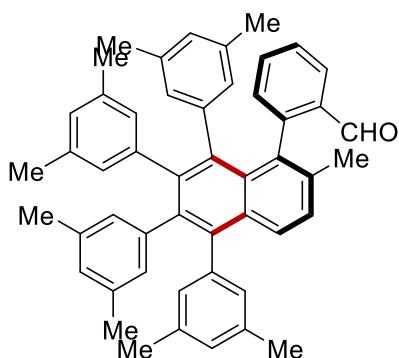
HRMS (ESI) calcd. for C₄₆H₃₈O₅Na⁺: 693.2611. Found: 693.2603.

[α]_D²⁰ = -125.5 (*c* = 1.03, CHCl₃).

ν_{max} (thin film/cm⁻¹): 2955, 2931, 2835, 1694, 1609, 1514, 1463, 1285, 1242, 1171, 1106, 1030.

HPLC separation (AD-3 column, *n*hexane/*i*PrOH 95/5, 1.0 mL/min, 250.4 nm): tr(major) = 12.1 min, tr(minor) = 8.6 min, 95% ee.



**(R)-2-(5,6,7,8-tetrakis(3,5-dimethylphenyl)-2-methylnaphthalen-1-yl)benzaldehyde**

73ae: The general procedure **K** was followed using 2'-methyl-[1,1'-biphenyl]-2-carbaldehyde **71a** (39.3 mg, 0.20 mmol) and 1,2-bis(3,5-dimethylphenyl)ethyne **72e** (140.5 mg, 0.60 mmol). Isolation by column chromatography (*n*hexane/EtOAc = 20:1) yielded **73ae** (109.9 mg, 83%) as a yellow solid.

¹H-NMR (600 MHz, CDCl₃) δ 9.67 (s, 1H), 7.67 (d, *J* = 8.7 Hz, 1H), 7.47 (dd, *J* = 7.8, 1.4 Hz, 1H), 7.31 – 7.26 (m, 2H), 7.12 – 7.07 (m, 1H), 6.94 – 6.91 (m, 1H), 6.87 (dd, *J* = 7.6, 1.2 Hz, 1H), 6.86 – 6.81 (m, 2H), 6.47 (d, *J* = 8.7 Hz, 2H), 6.41 – 6.38 (m, 2H), 6.30 – 6.26 (m, 1H), 6.22 – 6.17 (m, 3H), 6.01 – 5.98 (m, 1H), 2.26 (s, 3H), 2.24 (s, 3H), 2.00 – 1.94 (m, 6H), 1.93 (s, 3H), 1.91 (s, 3H), 1.88 (s, 3H), 1.85 (s, 3H), 1.78 (s, 3H).

¹³C-NMR (126 MHz, CDCl₃) δ 192.0 (CH), 146.9 (C_q), 142.1 (C_q), 141.1 (C_q), 140.3 (C_q), 140.2 (C_q), 139.9 (C_q), 138.7 (C_q), 138.3 (C_q), 138.0 (C_q), 136.6 (C_q), 136.6 (C_q), 135.9 (C_q), 135.5 (C_q), 135.3 (C_q), 135.1 (C_q, overlapped, 2C), 134.8 (C_q), 134.6 (C_q), 134.4 (C_q), 133.4 (C_q), 132.1 (CH), 131.8 (CH), 131.6 (C_q), 131.3 (C_q), 131.2 (CH), 129.3 (CH), 129.3 (CH), 129.3 (CH, overlapped, 3C), 129.2 (CH, overlapped, 2C), 127.9 (CH), 127.9 (CH, overlapped, 2C), 126.9 (CH), 126.5 (CH), 126.5 (CH), 126.2 (CH), 125.8 (CH), 21.7 (CH₃), 21.4 (CH₃), 21.4 (CH₃), 21.1 (CH₃, overlapped, 2C), 21.0 (CH₃), 20.9 (CH₃), 20.8 (CH₃), 20.7 (CH₃).

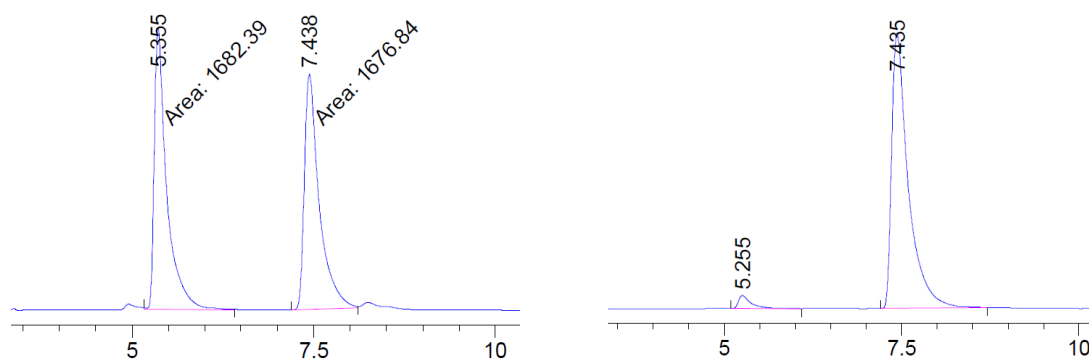
HRMS (ESI) calcd. for C₅₀H₄₆ONa⁺: 685.3441. Found: 685.3439.

[α]_D²⁰ = -109.8 (*c* = 0.83, CHCl₃).

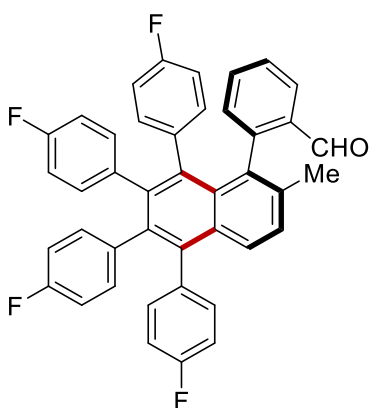
ν_{max} (thin film/cm⁻¹): 3002, 2914, 2861, 1691, 1599, 1447, 1373, 1194, 1037, 846.

HPLC separation (IA-3 column, *n*hexane/*i*PrOH 99.7/0.3, 1.0 mL/min, 250.4 nm): tr(major) = 7.4 min, tr(minor) = 5.3 min, 93% ee.

Experimental Data



| Peak # | RetTime [min] | Type | Width [min] | Area [mAU*s] | Height [mAU] | Area % | Peak # | RetTime [min] | Type | Width [min] | Area [mAU*s] | Height [mAU] | Area % |
|--------|---------------|------|-------------|--------------|--------------|---------|--------|---------------|------|-------------|--------------|--------------|---------|
| 1 | 5.355 | MM | 0.1990 | 1682.38806 | 140.92331 | 50.0826 | 1 | 5.255 | BB | 0.1785 | 253.11084 | 20.43827 | 3.4658 |
| 2 | 7.438 | MM | 0.2377 | 1676.83801 | 117.59368 | 49.9174 | 2 | 7.435 | BB | 0.2377 | 7050.03076 | 431.20215 | 96.5342 |



(R)-2-(5,6,7,8-tetrakis(4-fluorophenyl)-2-methylnaphthalen-1-yl)benzaldehyde 73af:

The general procedure **K** was followed using 2'-methyl-[1,1'-biphenyl]-2-carbaldehyde **71a** (39.3 mg, 0.20 mmol) and 1,2-bis(4-fluorophenyl)ethyne **72f** (128.5 mg, 0.60 mmol). Isolation by column chromatography (*n*hexane/EtOAc = 20:1) yielded **73af** (77.2 mg, 62%) as a yellow solid.

¹H-NMR (600 MHz, CDCl₃) δ 9.57 (s, 1H), 7.62 (d, *J* = 8.7 Hz, 1H), 7.57 (dd, *J* = 7.7, 1.4 Hz, 1H), 7.35 (d, *J* = 8.8 Hz, 1H), 7.29 – 7.26 (m, 1H), 7.23 – 7.15 (m, 3H), 7.02 – 6.96 (m, 2H), 6.88 – 6.84 (m, 1H), 6.77 – 6.71 (m, 2H), 6.63 – 6.55 (m, 3H), 6.53 – 6.40 (m, 5H), 6.36 (td, *J* = 8.6, 2.7 Hz, 1H), 6.25 (td, *J* = 8.6, 2.7 Hz, 1H), 1.91 (s, 3H).

¹³C-NMR (101 MHz, CDCl₃) δ 192.4 (CH), 161.8 (d, *J* = 246.2 Hz, C_q), 160.8 (d, *J* = 245.3 Hz, C_q), 160.6 (d, *J* = 245.2 Hz, C_q), 160.5 (d, *J* = 245.8 Hz, C_q), 146.2 (C_q), 141.2 (C_q), 138.3 (C_q), 137.8 (C_q, overlapped, 2C), 137.1 (C_q), 137.1 (d, *J* = 3.6 Hz, C_q), 136.2 (d, *J* = 3.6 Hz, C_q, overlapped, 2C), 135.5 (d, *J* = 3.6 Hz, C_q), 134.5 (C_q), 133.8 (d, *J* = 8.2 Hz, CH), 133.7 (C_q), 133.3 (CH), 132.8 (d, *J* = 7.9 Hz, CH), 132.8 (d, *J* = 8.0 Hz, CH), 132.6 (d, *J* = 7.9 Hz, CH), 132.5 (d, *J* = 8.1 Hz, CH), 132.4 (d, *J* = 8.3 Hz, CH), 132.4 (d, *J* = 8.2 Hz, CH), 132.3 (d, *J* = 7.9 Hz, CH), 132.1 (CH), 131.9 (C_q), 131.9 (C_q), 129.0 (CH), 127.6 (CH), 127.2 (CH, overlapped, 2C), 115.1 (d, *J* = 21.4 Hz, CH), 114.9 (d, *J* = 21.3 Hz, CH), 114.2 (d, *J* =

Experimental Data

21.3 Hz, CH), 114.0 (d, $J = 21.3$ Hz, CH), 113.9 (d, $J = 21.4$ Hz, CH), 113.8 (d, $J = 21.4$ Hz, CH), 113.7 (d, $J = 21.4$ Hz, CH), 113.6 (d, $J = 21.4$ Hz, CH), 21.7 (CH₃).

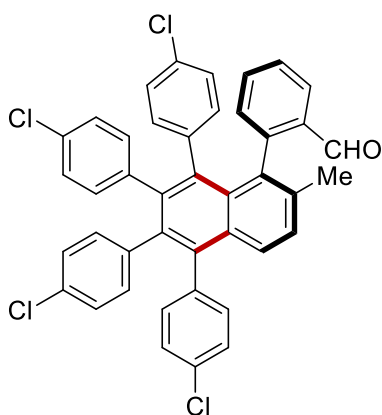
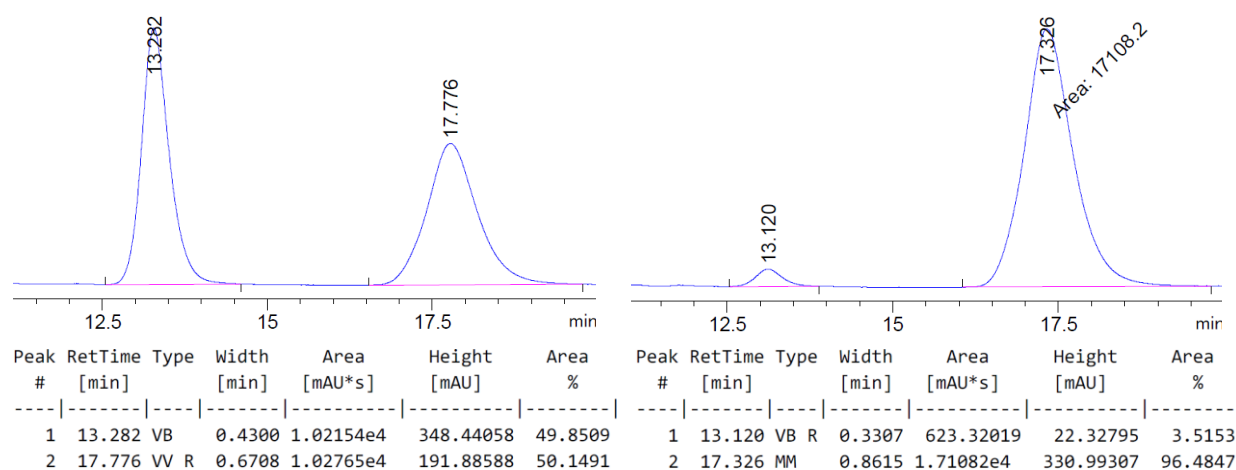
¹⁹F-NMR (471 MHz, CDCl₃) δ -115.29, -116.43, -116.68, -116.73.

HRMS (ESI) calcd. for C₄₂H₂₆F₄ONa⁺: 645.1812. Found: 645.1823.

$[\alpha]_D^{20} = -70.3$ ($c = 0.35$, CHCl₃).

ν_{\max} (thin film/cm⁻¹): 3044, 2927, 2736, 1695, 1595, 1511, 1374, 1217, 1156, 1093, 1015.

HPLC separation (IC-3 column, *n*hexane/*i*PrOH 99/1, 1.0 mL/min, 250.4 nm): tr(major) = 17.3 min, tr(minor) = 13.1 min, 93% ee.



(R)-2-(5,6,7,8-tetrakis(4-chlorophenyl)-2-methylnaphthalen-1-yl)benzaldehyde 73ag:

The general procedure **K** was followed using 2'-methyl-[1,1'-biphenyl]-2-carbaldehyde **71a** (39.3 mg, 0.20 mmol) and 1,2-bis(4-chlorophenyl)ethyne **72g** (147.6 mg, 0.60 mmol). Isolation by column chromatography (*n*hexane/EtOAc = 20:1) yielded **73ag** (43.9 mg, 32%) as a yellow solid.

¹H-NMR (600 MHz, CDCl₃) δ 9.53 (s, 1H), 7.60 – 7.56 (m, 2H), 7.37 – 7.34 (m, 1H), 7.30 – 7.22 (m, 4H), 7.17 – 7.12 (m, 2H), 6.89 – 6.86 (m, 2H), 6.84 – 6.81 (m, 1H), 6.77 (dd, $J = 8.2, 2.2$ Hz, 1H), 6.74 (dd, $J = 8.2, 2.2$ Hz, 1H), 6.73 – 6.69 (m, 2H), 6.62 (dd, $J = 8.2, 2.2$

Experimental Data

Hz, 1H), 6.59 (dd, $J = 8.2, 2.2$ Hz, 1H), 6.53 – 6.48 (m, 2H), 6.42 (dd, $J = 8.2, 2.2$ Hz, 1H), 6.38 (dd, $J = 8.2, 2.2$ Hz, 1H), 1.90 (s, 3H).

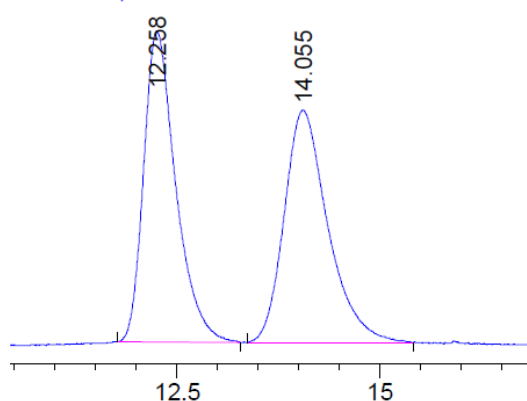
$^{13}\text{C-NMR}$ (126 MHz, CDCl_3) δ 192.3 (CH), 145.9 (C_q), 140.4 (C_q), 139.3 (C_q), 138.4 (C_q), 138.4 (C_q), 138.1 (C_q), 137.8 (C_q), 137.5 (C_q), 137.3 (C_q), 137.1 (C_q), 134.5 (C_q), 133.8 (C_q), 133.4 (CH), 133.3 (CH), 133.1 (C_q), 132.5 (CH), 132.5 (CH), 132.3 (CH), 132.2 (CH), 132.2 (CH), 132.1 (CH), 132.1 (CH), 132.1 (CH), 132.0 (C_q), 131.8 (C_q), 131.8 (C_q , overlapped, 2C), 131.7 (C_q), 129.2 (CH), 128.4 (CH), 128.3 (CH), 127.5 (CH), 127.5 (CH), 127.4 (CH, overlapped, 2C), 127.2 (CH), 127.1 (CH), 127.1 (CH, overlapped, 2C), 127.0 (CH), 21.8 (CH_3).

HRMS (ESI) calcd. for $\text{C}_{42}\text{H}_{26}\text{Cl}_4\text{ONa}^+$: 709.0630. Found: 709.0616.

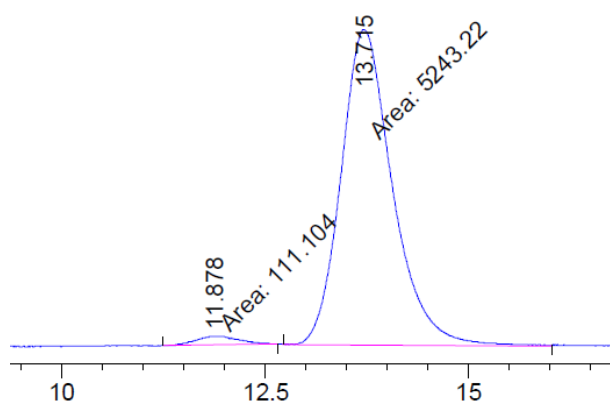
$[\alpha]_{\text{D}}^{20} = -91.1$ ($c = 0.83$, CHCl_3).

ν_{max} (thin film/ cm^{-1}): 2962, 2842, 1687, 1595, 1491, 1392, 1262, 1195, 1088, 1013.

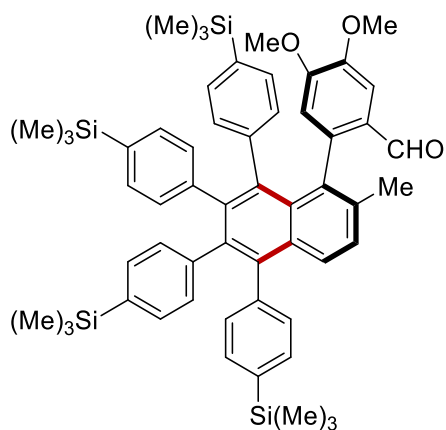
HPLC separation (IC-3 column, *n*hexane/*i*PrOH 99/1, 1.0 mL/min, 250.4 nm): $t_{\text{r}}(\text{major}) = 13.7$ min, $t_{\text{r}}(\text{minor}) = 11.9$ min, 96% ee.



| Peak # | RetTime [min] | Type | Width [min] | Area [mAU*s] | Height [mAU] | Area % |
|--------|---------------|------|-------------|--------------|--------------|---------|
| 1 | 12.258 | BV R | 0.3690 | 1969.95422 | 71.60642 | 49.6683 |
| 2 | 14.055 | BV R | 0.4500 | 1996.26404 | 53.41977 | 50.3317 |



| Peak # | RetTime [min] | Type | Width [min] | Area [mAU*s] | Height [mAU] | Area % |
|--------|---------------|------|-------------|--------------|--------------|---------|
| 1 | 11.878 | MM | 0.5998 | 111.10446 | 3.08723 | 2.0750 |
| 2 | 13.715 | MM | 0.7347 | 5243.21533 | 118.93991 | 97.9250 |



(R)-2-(2-methyl-5,6,7,8-tetrakis(4-(trimethylsilyl)phenyl)naphthalen-1-

yl)benzaldehyde 73ph: The general procedure **K** was followed using 4,5-dimethoxy-2'-methyl-[1,1'-biphenyl]-2-carbaldehyde **71p** (51.2 mg, 0.20 mmol) and 1,2-bis(4-(trimethylsilyl)phenyl)ethyne **72h** (193.3 mg, 0.60 mmol). Isolation by column chromatography (*n*hexane/EtOAc = 10:1) yielded **73ph** (64.7 mg, 36%) as a yellow solid.

¹H-NMR (400 MHz, CDCl₃) δ 9.34 (s, 1H), 7.74 (d, *J* = 8.7 Hz, 1H), 7.42 – 7.35 (m, 2H), 7.31 (d, *J* = 8.7 Hz, 1H), 7.25 – 7.22 (m, 1H), 7.21 – 7.16 (m, 1H), 7.03 (s, 1H), 6.93 (d, *J* = 8.1 Hz, 2H), 6.81 – 6.73 (m, 5H), 6.70 (dd, *J* = 7.5, 1.2 Hz, 1H), 6.60 (dd, *J* = 7.5, 1.7 Hz, 1H), 6.56 – 6.53 (m, 2H), 6.44 (dd, *J* = 7.5, 1.6 Hz, 1H), 6.27 (s, 1H), 3.82 (s, 3H), 3.75 (s, 3H), 1.97 (s, 3H), 0.24 (s, 9H), 0.10 (s, 9H), 0.04 (s, 9H), -0.01 (s, 9H).

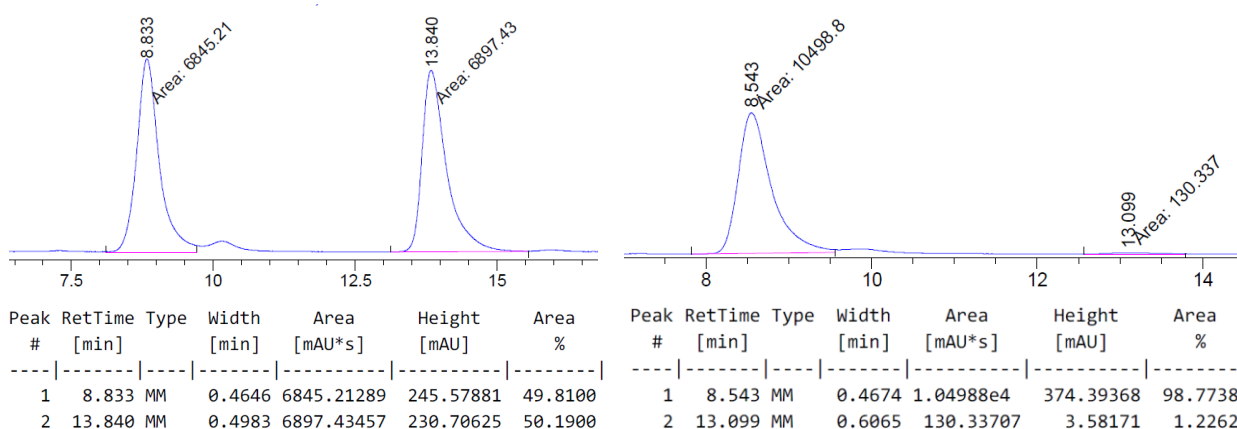
¹³C-NMR (101 MHz, CDCl₃) δ 191.5 (CH), 152.6 (C_q), 147.9 (C_q), 142.2(C_q), 141.9 (C_q), 141.8 (C_q), 140.9 (C_q), 140.9 (C_q), 140.3 (C_q), 138.8 (C_q), 138.6 (C_q), 138.3 (C_q), 138.2 (C_q), 136.8 (C_q), 136.5 (C_q), 136.4 (C_q), 136.1 (C_q), 133.7 (C_q), 132.6 (CH), 132.4 (CH), 131.8 (C_q), 131.6 (CH), 131.5 (C_q), 131.5 (CH, overlapped, 2C), 131.3 (CH), 131.2 (CH), 131.0 (CH), 130.9 (CH), 130.8 (CH), 130.8 (CH), 130.6 (CH), 130.6 (CH, overlapped, 2C), 130.5 (CH), 130.3 (CH), 128.3 (CH), 128.0 (CH), 128.0 (C_q), 114.5 (CH), 107.6 (CH), 55.8 (CH₃), 55.8 (CH₃), 21.8 (CH₃), -1.0 (CH₃, overlapped, 3C), -1.2 (CH₃, overlapped, 3C), -1.2 (CH₃, overlapped, 6C).

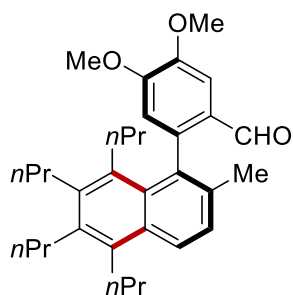
HRMS (ESI) calcd. for C₅₆H₆₆O₃Si₄Na⁺: 921.3981. Found: 921.3979.

[α]_D²⁰ = -15.0 (*c* = 0.33, CHCl₃).

ν_{max} (thin film/cm⁻¹): 2954, 1680, 1597, 1509, 1389, 1246, 1216, 1112, 1088, 1020.

HPLC separation (ID-3 column, *n*hexane/*i*PrOH 98/2, 1.0 mL/min, 250.4 nm): tr(major) = 8.5 min, tr(minor) = 13.1 min, 98% ee.





(R)-4,5-dimethoxy-2-(2-methyl-5,6,7,8-tetrapropyl)naphthalen-1-yl)benzaldehyde 73pi:

The general procedure **K** was followed using 4,5-dimethoxy-2'-methyl-[1,1'-biphenyl]-2-carbaldehyde **71p** (51.2 mg, 0.20 mmol) and oct-4-yne **72i** (66.1 mg, 0.60 mmol). Isolation by column chromatography (*n*hexane/EtOAc = 10:1) yielded **73pi** (39.8 mg, 42%) as a yellow oil.

¹H-NMR (400 MHz, CDCl₃) δ 9.46 (s, 1H), 8.02 (d, *J* = 8.8 Hz, 1H), 7.59 (s, 1H), 7.31 (d, *J* = 8.8 Hz, 1H), 6.73 (s, 1H), 4.03 (s, 3H), 3.87 (s, 3H), 3.08 – 2.98 (m, 2H), 2.75 – 2.66 (m, 2H), 2.67 – 2.60 (m, 2H), 2.27 – 2.19 (m, 2H), 2.03 (s, 3H), 1.79 – 1.69 (m, 2H), 1.68 – 1.57 (m, 2H), 1.56 – 1.45 (m, 2H), 1.16 (t, *J* = 7.3 Hz, 3H), 1.11 (t, *J* = 7.3 Hz, 3H), 1.02 (t, *J* = 7.3 Hz, 3H), 1.00 – 0.80 (m, 2H), 0.50 (t, *J* = 7.3 Hz, 3H).

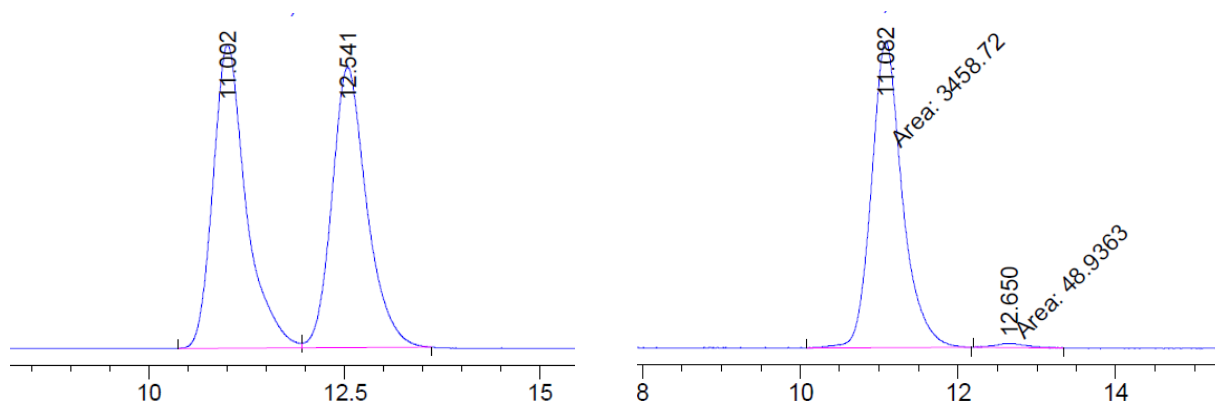
¹³C-NMR (126 MHz, CDCl₃) δ 191.1 (CH), 154.1 (C_q), 148.7 (C_q), 144.1 (C_q), 140.2 (C_q), 136.9 (C_q), 135.2 (C_q), 134.7 (C_q), 134.6 (C_q), 132.2 (C_q), 131.7 (C_q), 131.1 (C_q), 127.5 (C_q), 127.0 (CH), 125.3 (CH), 112.8 (CH), 108.2 (CH), 56.3 (CH₃), 56.3 (CH₃), 33.0 (CH₂), 32.6 (CH₂), 32.1 (CH₂), 32.0 (CH₂), 26.4 (CH₂), 25.3 (CH₂), 24.9 (CH₂), 24.7 (CH₂), 22.2 (CH₃), 15.2 (CH₃), 15.1 (CH₃), 15.1 (CH₃), 14.2 (CH₃).

HRMS (ESI) calcd. for C₃₂H₄₂O₃Na⁺: 497.3026. Found: 497.3020.

[α]_D²⁰ = +38.8 (*c* = 0.50, CHCl₃).

ν_{max} (thin film/cm⁻¹): 2956, 2928, 2868, 1678, 1596, 1507, 1342, 1266, 1206, 1134, 1027.

HPLC separation (IC-3 column, *n*hexane/*i*PrOH 98/2, 1.0 mL/min, 250.4 nm): tr(major) = 11.1 min, tr(minor) = 12.7 min, 97% ee.

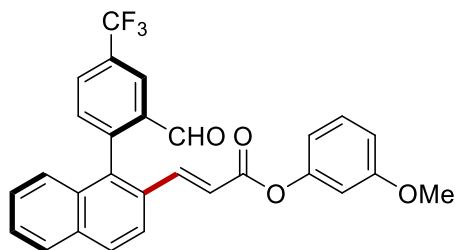


Experimental Data

| Peak # | RetTime [min] | Type | Width [min] | Area [mAU*s] | Height [mAU] | Area % | Peak # | RetTime [min] | Type | Width [min] | Area [mAU*s] | Height [mAU] | Area % |
|--------|---------------|------|-------------|--------------|--------------|---------|--------|---------------|------|-------------|--------------|--------------|---------|
| 1 | 11.002 | BV | 0.4169 | 5119.51904 | 173.18506 | 50.6908 | 1 | 11.082 | MM | 0.4546 | 3458.72217 | 126.81260 | 98.6049 |
| 2 | 12.541 | VV R | 0.4420 | 4979.99316 | 160.04778 | 49.3092 | 2 | 12.650 | MM | 0.4818 | 48.93633 | 1.69289 | 1.3951 |

5.8 Enantioselectivity Prediction of Palladaelectro-Catalyzed C–H Olefination using Machine Learning

5.8.1 Characterization Data



3-methoxyphenyl (E)-3-(1-(2-formyl-4-(trifluoromethyl)phenyl)naphthalen-2-yl)acrylate 76fe: Prepared according to general procedure **M** on a 0.20 mmol scale, with *L*-tert-leucine (5.3 mg, 20 mol %) as the transient directing group, LiOAc (26.4 mg, 2 equiv.) as the additive and AcOH as the solvent. Column chromatography (*n*hexane/EtOAc = 5:1) afforded the title compound as a white solid (58.2 mg, 61%).

¹H-NMR (600 MHz, CDCl₃) δ 9.51 (s, 1H), 8.47 – 8.40 (m, 1H), 8.06 – 7.99 (m, 2H), 7.98 – 7.91 (m, 2H), 7.62 – 7.41 (m, 4H), 7.30 – 7.15 (m, 2H), 6.81 – 6.63 (m, 4H), 3.78 (s, 3H).

¹³C-NMR (126 MHz, CDCl₃) δ 189.8 (CH), 164.9 (C_q), 160.6 (C_q), 151.7 (C_q), 144.6 (C_q), 143.3 (CH), 135.8 (C_q), 135.6 (C_q), 134.1 (C_q), 133.0 (C_q), 133.0 (CH), 131.8 (q, *J* = 33.6 Hz, C_q), 131.1 (C_q), 130.5 (q, *J* = 3.3 Hz, CH), 130.0 (CH), 129.9 (CH), 128.6 (CH), 128.0 (CH), 128.0 (CH), 126.7 (CH), 125.2 (q, *J* = 3.8 Hz, CH), 123.4 (d, *J* = 274.3 Hz, C_q), 122.9 (CH), 120.1 (CH), 113.8 (CH), 112.0 (CH), 107.5 (CH), 55.6 (CH₃).

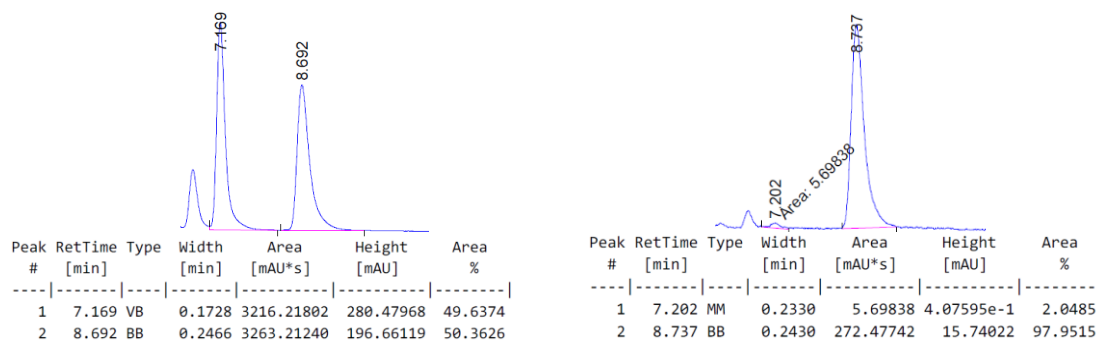
¹⁹F-NMR (376 MHz, CDCl₃) δ -62.87.

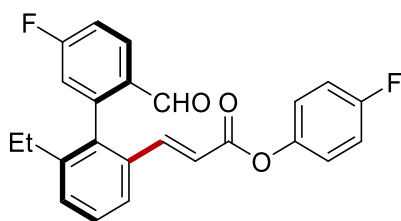
HRMS (ESI) calcd. for C₂₈H₁₉O₄F₃Na⁺: 499.1128. Found: 499.1123.

[α]_D²⁰ = -30.8 (*c* = 0.50, CHCl₃).

ν_{max} (thin film/cm⁻¹): 1043, 1069, 1102, 1129, 1164, 1252, 1295, 1332, 1387, 1441, 1489, 1592, 1612, 1628, 1698, 1725, 2774, 2847, 2920, 3066.

HPLC separation (IF-3 column, *n*hexane/*i*PrOH 80/20, 1.0 mL/min, 273 nm): *t_r*(major) = 8.7 min, *t_r*(minor) = 7.2 min, 96% ee.





4-fluorophenyl (E)-3-(6-ethyl-5'-fluoro-2'-formyl-[1,1'-biphenyl]-2-yl)acrylate 76gf:

Prepared according to general procedure **M** on a 0.20 mmol scale, with *L-tert*-leucine (5.3 mg, 20 mol %) as the transient directing group, BQ (43.2 mg, 2 equiv.) as the additive and AcOH as the solvent. Column chromatography (*n*hexane/EtOAc = 10:1) afforded the title compound as colorless oil (55.3 mg, 70%).

¹H-NMR (600 MHz, CDCl₃) δ 9.55 (s, 1H), 8.11 (dd, *J* = 8.7, 5.9 Hz, 1H), 7.67 (dd, *J* = 7.9, 1.3 Hz, 1H), 7.50 – 7.46 (m, 1H), 7.44 (dd, *J* = 7.7, 1.3 Hz, 1H), 7.36 (d, *J* = 15 Hz, 1H), 7.28 – 7.24 (m, 1H), 7.03 (d, *J* = 6.4 Hz, 4H), 6.98 (dd, *J* = 8.7, 2.6 Hz, 1H), 6.48 (d, *J* = 15.8 Hz, 1H), 2.41 – 2.28 (d, *J* = 7.5 Hz, 2H), 1.05 (t, *J* = 7.5 Hz, 3H).

¹³C-NMR (126 MHz, CDCl₃) δ 189.8 (CH), 165.9 (d, *J* = 259.0 Hz, C_q), 164.9 (C_q), 160.3 (d, *J* = 244.2 Hz, C_q), 146.5 (d, *J* = 3.0 Hz, C_q), 145.1 (d, *J* = 9.1 Hz, C_q), 144.4 (CH), 143.3 (C_q), 136.5 (C_q), 133.6 (C_q), 131.3 (d, *J* = 2.9 Hz, C_q), 131.1 (d, *J* = 10.2 Hz, CH), 130.7 (CH), 129.4 (CH), 124.3 (CH), 123.0 (d, *J* = 8.6 Hz, CH), 119.1 (CH), 118.2 (d, *J* = 21.7 Hz, CH), 116.4 (d, *J* = 21.8 Hz), 116.1 (d, *J* = 23.4 Hz, CH), 26.7 (CH₂), 15.0 (CH₃).

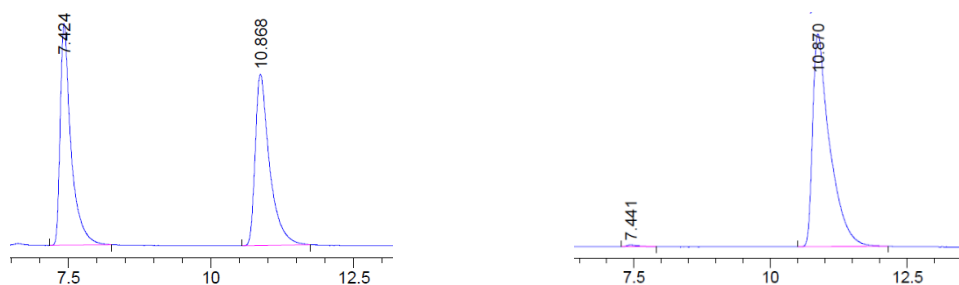
¹⁹F-NMR (376 MHz, CDCl₃) δ -102.14, -117.01.

HRMS (ESI) calcd. for C₂₄H₁₈F₂O₃Na⁺: 415.1116. Found: 415.1115.

[α]_D²⁰ = -20.13 (*c* = 0.77, CHCl₃).

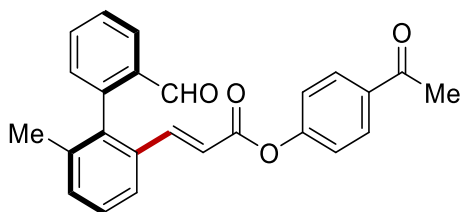
ν_{max} (thin film/cm⁻¹): 1013, 1064, 1093, 1182, 1220, 1236, 1272, 1311, 1392, 1452, 1501, 1579, 1603, 1632, 1691, 1728, 2751, 2845, 2969, 3069.

HPLC separation (IB-3 column, *n*hexane/*i*PrOH 80/20, 1.0 mL/min, 273 nm): *t_r*(major) = 10.9 min, *t_r*(minor) = 7.4 min, 99% ee.



| Peak # | RetTime [min] | Type | Width [min] | Area [mAU*s] | Height [mAU] | Area % |
|--------|---------------|------|-------------|--------------|--------------|---------|
| 1 | 7.424 | BB | 0.1906 | 1633.84314 | 124.10645 | 49.3175 |
| 2 | 10.868 | BB | 0.2520 | 1679.06189 | 96.02110 | 50.6825 |

| Peak # | RetTime [min] | Type | Width [min] | Area [mAU*s] | Height [mAU] | Area % |
|--------|---------------|------|-------------|--------------|--------------|---------|
| 1 | 7.441 | BB | 0.1811 | 52.11143 | 3.61574 | 0.6373 |
| 2 | 10.870 | BB | 0.3129 | 8124.25391 | 371.77307 | 99.3627 |



acetylphenyl (E)-3-(2'-formyl-6-methyl-[1,1'-biphenyl]-2-yl)acrylate 76hg: Prepared according to general procedure **M** on a 0.20 mmol scale, with *L-tert-leucine* (5.3 mg, 20 mol %) as the transient directing group, **BQ** (43.2 mg, 2 equiv.) as the additive and AcOH as the solvent. Column chromatography (*n*hexane/EtOAc = 10:1) afforded the title compound as colorless oil (50.4 mg, 66%).

¹H-NMR (300 MHz, CDCl₃) δ 9.58 (s, 1H), 8.04 – 7.95 (m, 1H), 7.89 (d, *J* = 8.7 Hz, 2H), 7.69 – 7.56 (m, 2H), 7.55 – 7.43 (m, 1H), 7.41 – 7.27 (m, 3H), 7.22 – 7.12 (m, 1H), 7.09 (d, *J* = 8.7 Hz, 2H), 6.39 (d, *J* = 15.9 Hz, 1H), 2.51 (s, 3H), 1.95 (s, 3H).

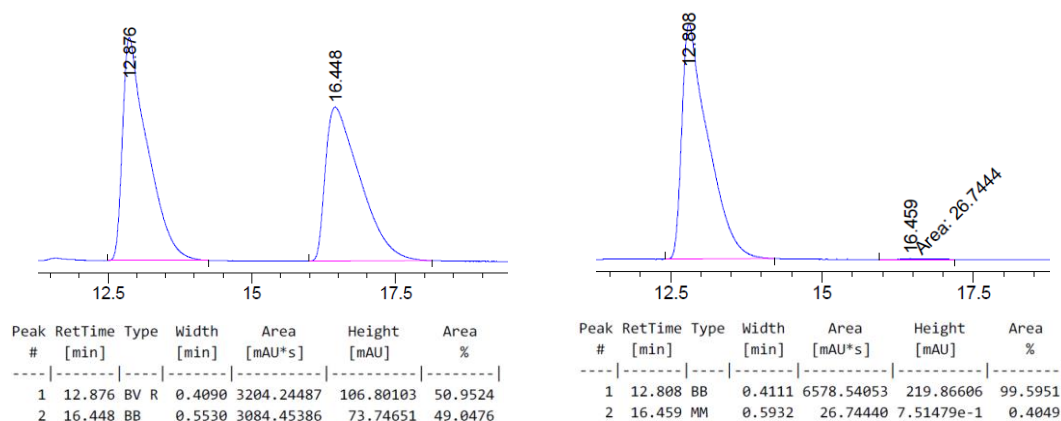
¹³C-NMR (75 MHz, CDCl₃) δ 197.0 (C_q), 191.5 (CH), 164.4 (C_q), 154.5 (C_q), 145.3 (CH), 142.4 (C_q), 138.8 (C_q), 137.7 (C_q), 134.7 (C_q), 134.5 (CH), 134.3 (C_q), 133.6 (C_q), 132.3 (CH), 131.0 (CH), 130.0 (CH), 128.9 (CH), 128.7 (CH), 128.4 (CH), 124.4 (CH), 121.8 (CH), 118.4 (CH), 26.7 (CH₃), 20.9 (CH₃).

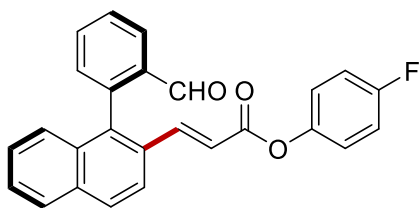
HRMS (ESI) calcd. for C₂₅H₂₀O₄Na⁺: 407.1254. Found: 407.1258.

[α]_D²⁰ = -46.2 (*c* = 1.00, CHCl₃).

ν_{max} (thin film/cm⁻¹): 1013, 1163, 1195, 1263, 1310, 1357, 1408, 1502, 1595, 1630, 1682, 1732, 2745, 2837, 2922, 3064.

HPLC separation (IA-3 column, *n*hexane/*i*PrOH 80/20, 1.0 mL/min, 273 nm): *t_r*(major) = 12.8 min, *t_r*(minor) = 16.5 min, 99% ee.





4-fluorophenyl (E)-3-(1-(2-formylphenyl)naphthalen-2-yl)acrylate 76ef: Prepared according to general procedure **M** on a 0.20 mmol scale, with *L*-*tert*-leucine (5.3 mg, 20 mol %) as the transient directing group, KH_2PO_4 (54.4 mg, 2 equiv.) as the additive and AcOH as the solvent. Column chromatography (*n*hexane/EtOAc = 10:1) afforded the title compound as colorless oil (53.5 mg, 67%).

$^1\text{H-NMR}$ (600 MHz, CDCl_3) δ 9.50 (s, 1H), 8.16 (dd, $J = 7.8, 1.4$, 1H), 8.01 – 7.98 (m, 1H), 7.95 – 7.92 (m, 1H), 7.90 (d, $J = 8.7$ Hz, 1H), 7.81 – 7.72 (m, 1H), 7.70 – 7.52 (m, 3H), 7.45 – 7.25 (m, 3H), 7.06 – 7.04 (m, 2H), 7.04 (d, $J = 1.5$ Hz, 2H), 6.65 (d, $J = 15.9$ Hz, 1H).

$^{13}\text{C-NMR}$ (126 MHz, CDCl_3) δ 191.4 (CH), 165.1 (C_q), 160.3 (d, $J = 244.3$ Hz, C_q), 146.6 (d, $J = 2.9$ Hz, C_q), 144.4 (CH), 141.1 (C_q), 137.6 (C_q), 135.4 (C_q), 134.3 (CH), 134.1 (C_q), 133.4 (C_q), 132.1 (CH), 130.9 (C_q), 129.4 (CH), 129.3 (CH), 128.4 (CH), 128.2 (CH), 127.8 (CH), 127.6 (CH), 127.3 (CH), 123.1 (d, $J = 8.4$ Hz, CH), 122.8 (CH), 118.9 (CH), 116.1 (d, $J = 23.5$ Hz, CH).

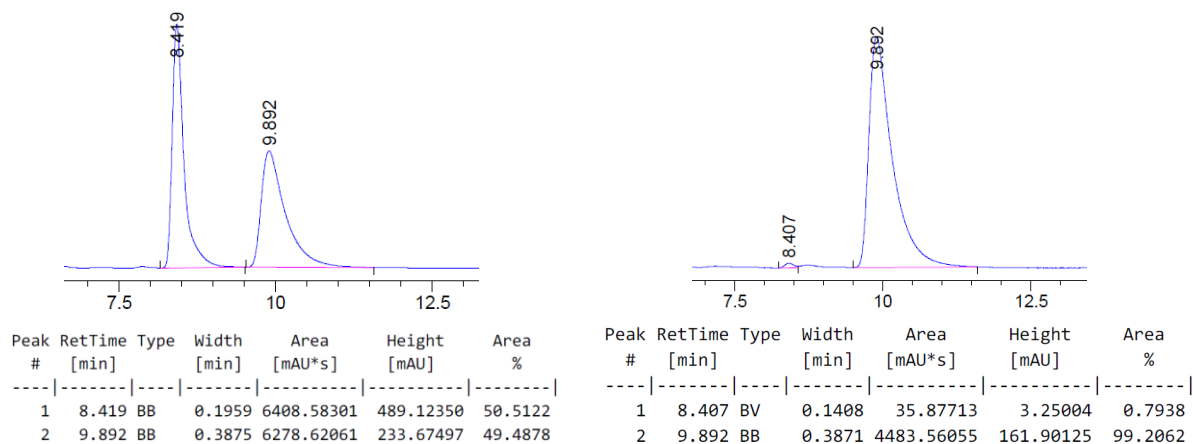
$^{19}\text{F-NMR}$ (376 MHz, CDCl_3) δ -117.07.

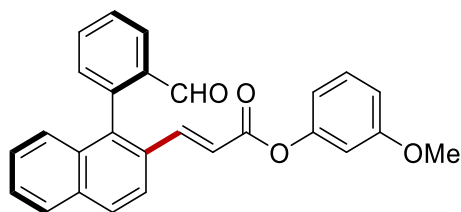
HRMS (ESI) calcd. for $\text{C}_{26}\text{H}_{17}\text{FO}_3\text{Na}^+$: 419.1054. Found: 419.1056.

$[\alpha]_{\text{D}}^{20}$ = -40.9 ($c = 1.00$, CHCl_3).

ν_{max} (thin film/ cm^{-1}): 1045, 1089, 1130, 1182, 1251, 1295, 1372, 1501, 1595, 1626, 1695, 1728, 2745, 2837, 3061.

HPLC separation (IF-3 column, *n*hexane/*i*PrOH 80/20, 1.0 mL/min, 273 nm): t_{r} (major) = 9.9 min, t_{r} (minor) = 8.4 min, 98% ee.





3-methoxyphenyl (E)-3-(1-(2-formylphenyl)naphthalen-2-yl)acrylate 76ee: Prepared according to general procedure **M** on a 0.20 mmol scale, with L-tryptophen (8.2 mg, 20 mol %) as the transient directing group and AcOH as the solvent. Column chromatography (*n*hexane/EtOAc = 10:1) afforded the title compound as colorless oil (14.5 mg, 18%).

¹H-NMR (300 MHz, CDCl₃) δ 9.49 (s, 1H), 8.14 (dd, *J* = 7.7, 1.5 Hz, 1H), 7.97 (d, *J* = 8.8 Hz, 1H), 7.93 – 7.85 (m, 2H), 7.80 – 7.72 (m, 1H), 7.67 – 7.49 (m, 3H), 7.42 – 7.33 (m, 2H), 7.29 – 7.20 (m, 2H), 6.82 – 6.74 (m, 1H), 6.70 – 6.61 (m, 3H), 3.76 (s, 3H).

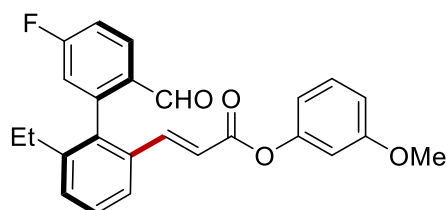
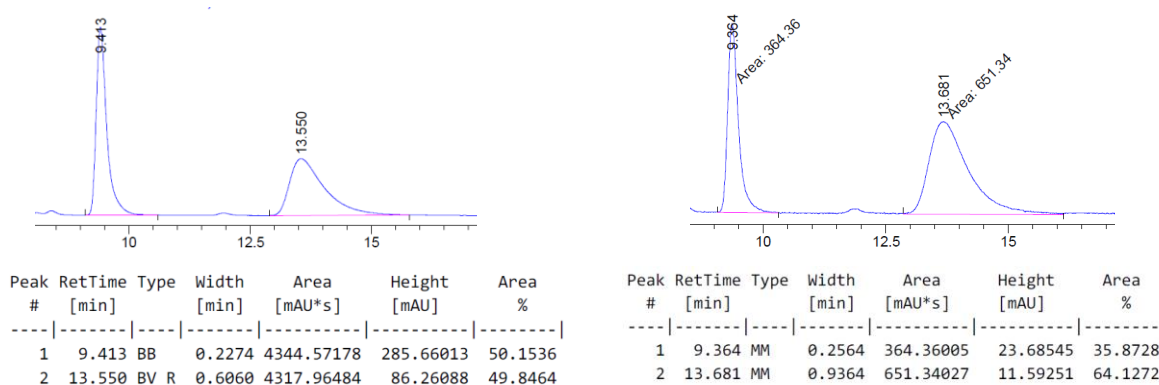
¹³C-NMR (75 MHz, CDCl₃) δ 191.3 (CH), 165.0 (C_q), 160.5 (C_q), 151.8 (C_q), 144.1 (CH), 141.1 (C_q), 137.5 (C_q), 135.4 (C_q), 134.2 (CH), 134.1 (C_q), 133.4 (C_q), 132.1 (CH), 131.0 (C_q), 129.8 (CH), 129.3 (CH), 129.2 (CH), 128.3 (CH), 128.1 (CH), 127.7 (CH), 127.6 (CH), 127.2 (CH), 122.8 (CH), 119.2 (CH), 113.8 (CH), 111.9 (CH), 107.6 (CH), 55.5 (CH₃).

HRMS (ESI) calcd. for C₂₇H₂₀O₄Na⁺: 431.1254. Found: 431.1244.

[α]_D²⁰ = -1.0 (*c* = 0.50, CHCl₃).

ν_{max} (thin film/cm⁻¹): 1019, 1045, 1136, 1192, 1262, 1296, 1368, 1387, 1450, 1489, 1509, 1594, 1693, 1733, 1762, 2749, 2839, 2926, 3063.

HPLC separation (IF-3 column, *n*hexane/*i*PrOH 70/30, 1.0 mL/min, 273 nm): *t_r*(major) = 13.7 min, *t_r*(minor) = 9.4 min, 28% ee.



3-methoxyphenyl (E)-3-(6-ethyl-5'-fluoro-2'-formyl-[1,1'-biphenyl]2-yl)acrylate 76g:

Prepared according to general procedure **M** on a 0.20 mmol scale, with with L-tryptophen (8.2 mg, 20 mol %) as the transient directing group, sodium benzoate (57.6 mg, 2 equiv.) as the additive and AcOH as the solvent. Column chromatography (*n*hexane/EtOAc = 10:1) afforded the title compound as brown foam (28 mg, 34%).

¹H-NMR (400 MHz, CDCl₃) δ 9.55 (s, 1H), 8.10 (dd, *J* = 8.7, 5.9 Hz, 1H), 7.67 (dd, *J* = 7.7, 1.5 Hz, 1H), 7.51 – 7.45 (m, 1H), 7.43 (dd, *J* = 7.7, 1.4 Hz, 1H), 7.35 (d, *J* = 15.8 Hz, 1H), 7.29 – 7.22 (m, 2H), 6.98 (dd, *J* = 8.8, 2.6 Hz, 1H), 6.79 – 6.74 (m, 1H), 6.69 – 6.65 (m, 1H), 6.64 – 6.61 (m, 1H), 6.48 (d, *J* = 15.8 Hz, 1H), 3.78 (s, 3H), 2.34 (qd, *J* = 7.5, 3.6 Hz, 2H), 1.05 (t, *J* = 7.6 Hz, 3H).

¹³C-NMR (101 MHz, CDCl₃) δ 189.9 (CH), 165.9 (d, *J* = 258.9 Hz, C_q), 164.8 (C_q), 160.6 (C_q), 151.7 (C_q), 145.2 (d, *J* = 9.2 Hz, C_q), 144.1 (CH), 143.3 (C_q), 136.5 (C_q), 133.7 (C_q), 131.3 (d, *J* = 2.8 Hz, C_q), 131.1 (d, *J* = 10.1 Hz, CH), 130.7 (CH), 129.9 (CH), 129.4 (CH), 124.3 (CH), 119.4 (CH), 118.2 (d, *J* = 21.8 Hz, CH), 116.5 (d, *J* = 21.9 Hz, CH), 113.8 (CH), 112.0 (CH), 107.5 (CH), 55.5 (CH₃), 26.7 (CH₂), 15.0 (CH₃).

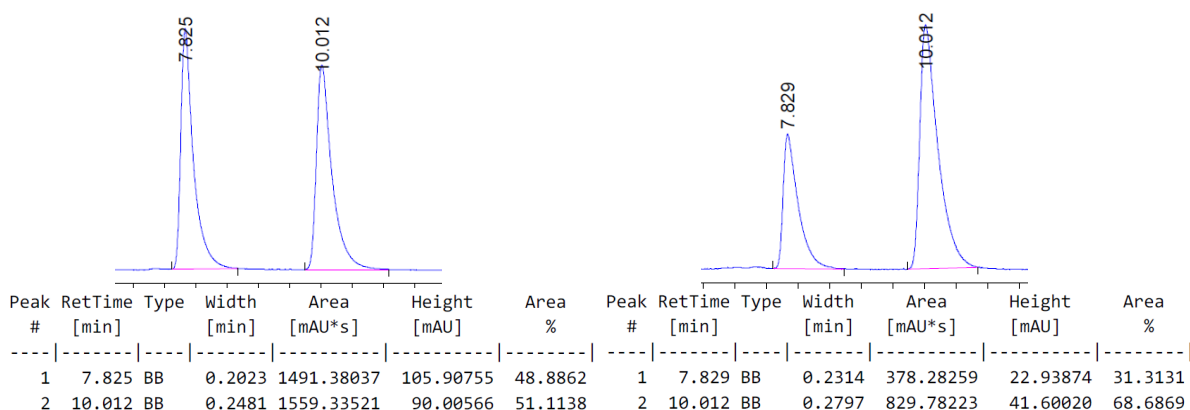
¹⁹F-NMR (282 MHz, CDCl₃) δ -102.18.

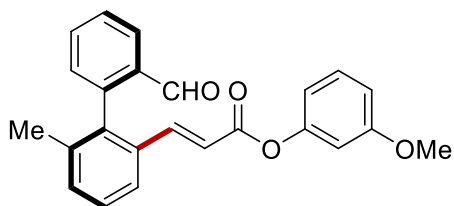
HRMS (ESI) calcd. for C₂₅H₂₁O₄FNa⁺: 427.1316. Found: 427.1319.

[α]_D²⁰ = -12.5 (*c* = 1.0, CHCl₃).

v_{max} (thin film/cm⁻¹): 1042, 1143, 1188, 1271, 1312, 1452, 1490, 1589, 1605, 1633, 1694, 1732, 2838, 2934, 2967.

HPLC separation (IB-3 column, *n*hexane/*i*PrOH 80/20, 1.0 mL/min, 273 nm): *t_r*(major) = 10.0 min, *t_r*(minor) = 7.8 min, 37% ee.




3-methoxyphenyl (E)-3-(2'-formyl-6-methyl-[1,1'-biphenyl]-2-yl)acrylate 76he:

Prepared according to general procedure **M** on a 0.20 mmol scale, with L-isoleucine (5.3 mg, 20 mol %) as the transient directing group, K_2CO_3 (55.3 mg, 2 equiv.) as the additive and AcOH as the solvent. Column chromatography (*n*hexane/EtOAc = 10:1) afforded the title compound as colorless oil (38.7 mg, 52%).

1H -NMR (400 MHz, $CDCl_3$) δ 9.65 (s, 1H), 8.07 (dd, J = 7.8, 1.5 Hz, 1H), 7.73 – 7.66 (m, 2H), 7.59 – 7.54 (m, 1H), 7.42 (d, J = 7.4 Hz, 1H), 7.40 – 7.36 (m, 2H), 7.26 – 7.21 (m, 2H), 6.76 (dd, J = 8.4, 2.5, 1H), 6.66 (dd, J = 8.1, 2.2, 1H), 6.64 – 6.61 (m, 1H), 6.47 (d, J = 15.9 Hz, 1H), 3.77 (s, 3H), 2.02 (s, 3H).

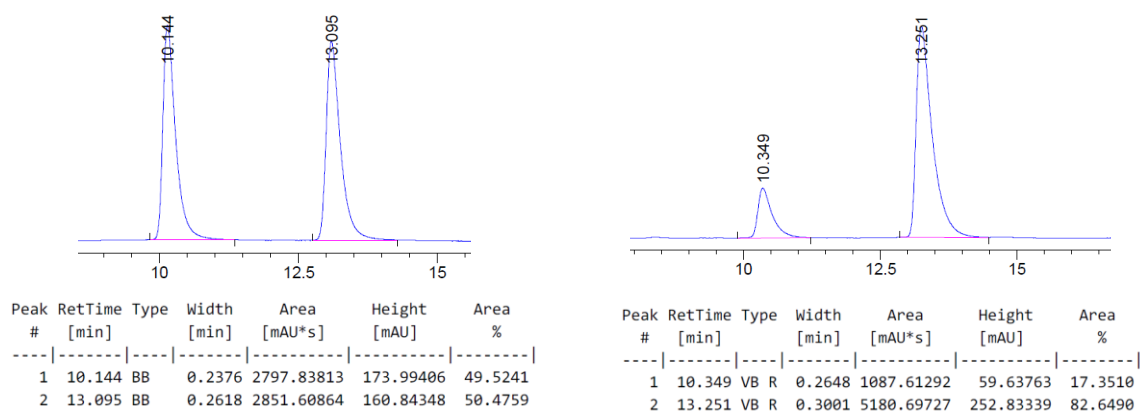
^{13}C -NMR (101 MHz, $CDCl_3$) δ 191.6 (CH), 164.9 (C_q), 160.5 (C_q), 151.8 (C_q), 144.6 (CH), 142.5 (C_q), 138.6 (C_q), 137.6 (C_q), 134.5 (CH), 134.3 (C_q), 133.8 (C_q), 132.1 (CH), 131.0 (CH), 129.8 (CH), 128.8 (CH), 128.7 (CH), 128.3 (CH), 124.3 (CH), 118.9 (CH), 113.8 (CH), 111.8 (CH), 107.6 (CH), 55.5 (CH_3), 20.9 (CH_3).

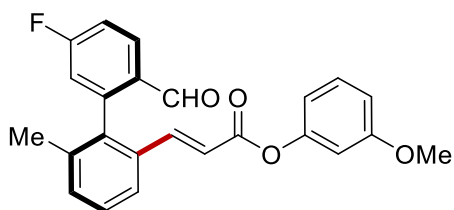
HRMS (ESI) calcd. for $C_{24}H_{20}O_4Na^+$: 395.1254. Found: 395.1256.

$[\alpha]_D^{20}$ = -19.5 (c = 1.00, $CHCl_3$).

ν_{max} (thin film/ cm^{-1}): 1039, 1133, 1191, 1220, 1253, 1309, 1391, 1451, 1489, 1591, 1607, 1631, 1693, 1728, 2745, 2837, 2957, 3064.

HPLC separation (IB-3 column, *n*hexane/*i*PrOH 90/10, 1.0 mL/min, 273 nm): t_r (major) = 13.3 min, t_r (minor) = 10.3 min, 66% ee.





3-methoxyphenyl (*E*)-3-(5'-fluoro-2'-formyl-6-methyl-[1,1'-biphenyl]-2-yl)acrylate 76ie:

Prepared according to general procedure **M** on a 0.20 mmol scale, with L-isoleucine (5.3 mg, 20 mol %) as the transient directing group and AcOH as the solvent. Column chromatography (*n*hexane/EtOAc = 10:1) afforded the title compound as colorless oil (33.1 mg, 42%).

¹H-NMR (400 MHz, CDCl₃) δ 9.55 (s, 1H), 8.11 (dd, *J* = 8.7, 5.8 Hz, 1H), 7.67 (dd, *J* = 7.7, 1.3 Hz, 1H), 7.47 – 7.36 (m, 3H), 7.28 – 7.22 (m, 2H), 6.96 (dd, *J* = 8.7, 2.5 Hz, 1H), 6.76 (dd, *J* = 8.3, 2.4 Hz, 1H), 6.67 (dd, *J* = 8.1, 2.2 Hz, 1H), 6.64 – 6.62 (m, 1H), 6.49 (d, *J* = 15.8 Hz, 1H), 3.78 (s, 3H), 2.04 (s, 3H).

¹³C-NMR (101 MHz, CDCl₃) δ 189.9 (CH), 166.1 (d, *J* = 258.3 Hz, C_q), 164.8 (C_q), 160.6 (C_q), 151.7 (C_q), 145.5 (d, *J* = 9.1 Hz, C_q), 144.0 (CH), 137.4 (C_q), 137.2 (C_q), 133.7 (C_q), 132.3 (CH), 131.3 (d, *J* = 10.1 Hz, CH), 131.0 (d, *J* = 2.9 Hz, C_q), 129.9 (CH), 129.1 (CH), 124.4 (CH), 119.5 (CH), 118.0 (d, *J* = 21.8 Hz, CH), 116.4 (d, *J* = 21.9 Hz, CH), 113.8 (CH), 112.0 (CH), 107.6 (CH), 55.6 (CH₃), 20.8 (CH₃).

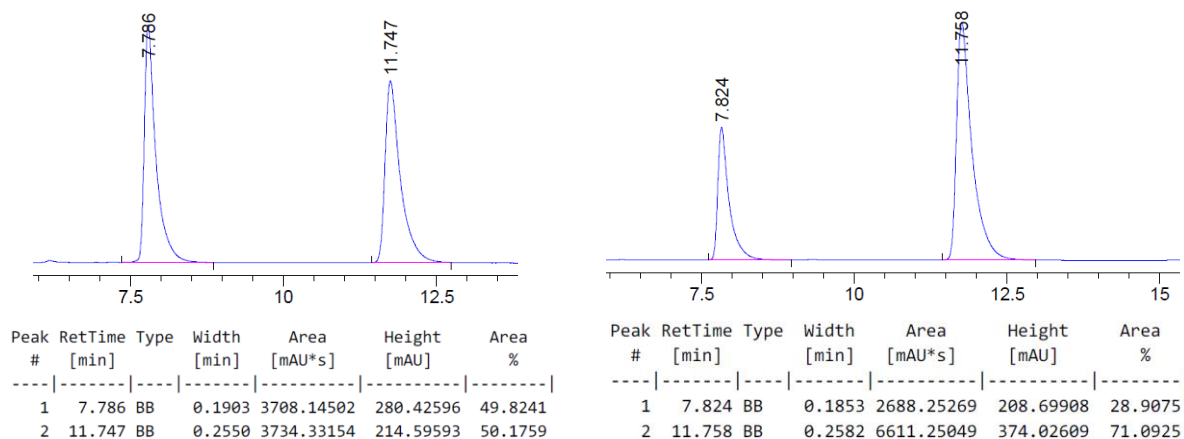
¹⁹F-NMR (376 MHz, CDCl₃) δ -102.03.

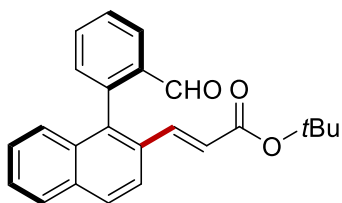
HRMS (ESI) calcd. for C₂₄H₁₉O₄FNa⁺: 413.1160. Found: 413.1158.

[α]_D²⁰ = -11.7 (*c* = 1.00, CHCl₃).

ν_{max} (thin film/cm⁻¹): 1039, 1133, 1187, 1212, 1225, 1246, 1268, 1309, 1391, 1455, 1489, 1581, 1603, 1633, 1690, 1730, 2751, 2838, 2959, 3068.

HPLC separation (IB-3 column, *n*hexane/*i*PrOH 80/20, 1.0 mL/min, 273 nm): *t_r*(major) = 11.8 min, *t_r*(minor) = 7.8 min, 42% ee.





(E)-(tert-butyl carbonic) (E)-3-(1-(2-formylphenyl)naphthalen-2-yl)acrylic anhydride

76ea: Prepared according to general procedure **M** on a 0.20 mmol scale, with *L*-tert-leucine (5.3 mg, 20 mol %) as the transient directing group, LiOAc (26.4 mg, 2 equiv.) as the additive and AcOH as the solvent. Column chromatography (*n*hexane/EtOAc = 10:1) afforded the title compound as colorless oil (45.6 mg, 57%).

¹H-NMR (400 MHz, CDCl₃) δ 9.46 (s, 1H), 8.16 (dd, *J* = 7.8, 1.5, 1H), 7.96 – 7.91 (m, 1H), 7.91 – 7.88 (m, 1H), 7.84 (d, *J* = 8.8 Hz, 1H), 7.78 – 7.73 (m, 1H), 7.68 – 7.62 (m, 1H), 7.54 – 7.49 (m, 1H), 7.42 – 7.35 (m, 2H), 7.34 – 7.32 (m, 1H), 7.26 – 7.23 (m, 1H), 6.43 (d, *J* = 15.9 Hz, 1H), 1.44 (s, 9H).

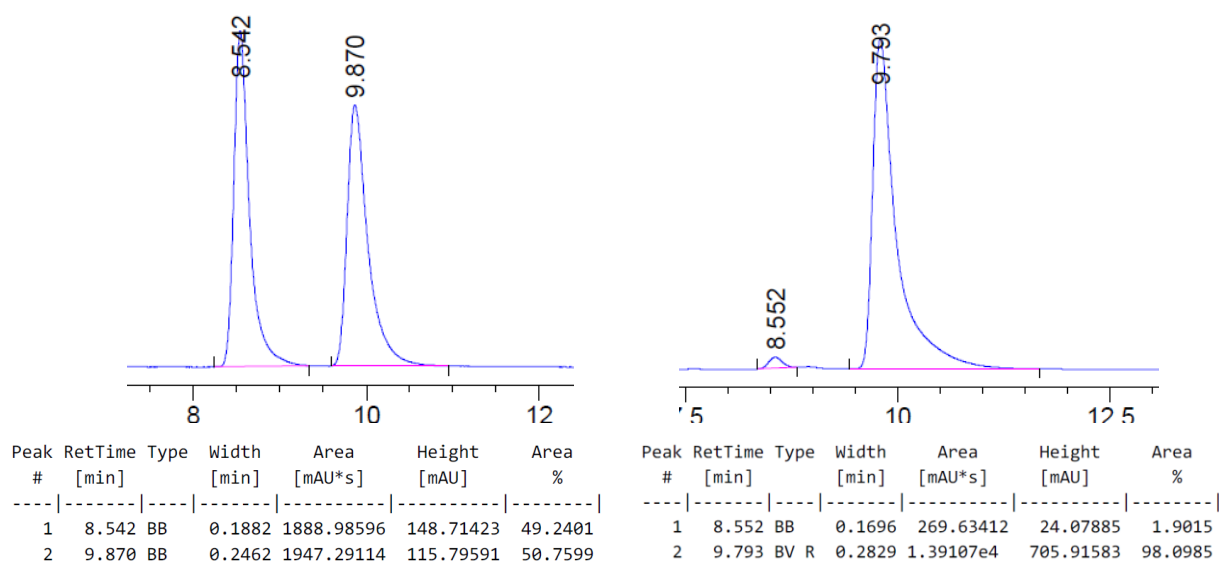
¹³C-NMR (126 MHz, CDCl₃) δ 191.5 (CH), 165.9 (C_q), 141.5 (C_q), 141.1 (CH), 136.7 (C_q), 135.4 (C_q), 134.2 (CH), 133.8 (C_q), 133.5 (C_q), 132.1 (CH), 131.4 (C_q), 129.1 (CH), 129.0 (CH), 128.3 (CH), 127.9 (CH), 127.4 (CH), 127.3 (CH), 127.1 (CH), 122.8 (CH), 122.1 (CH), 80.7 (C_q), 28.2 (CH₃).

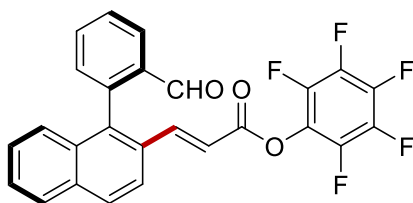
HRMS (ESI) calcd. for C₂₄H₂₂O₃Na⁺: 381.1461. Found: 381.1464.

[α]_D²⁰ = -13.9 (*c* = 1.00, CHCl₃).

ν_{max} (thin film/cm⁻¹): 1043, 1144, 1194, 1249, 1297, 1367, 1390, 1596, 1628, 1695, 2745, 2836, 2931, 2977, 3060.

HPLC separation (ID-3 column, *n*hexane/*i*PrOH 90/10, 1.0 mL/min, 273 nm): *t_r*(major) = 9.8 min, *t_r*(minor) = 8.6 min, 96% ee.





perfluorophenyl (E)-3-(1-(2-formylphenyl)naphthalen-2-yl)acrylate 76eb: Prepared according to general procedure **M** on a 0.20 mmol scale, with *L-tert*-leucine (5.3 mg, 20 mol %) as the transient directing group, LiOAc (26.4 mg, 2 equiv.) as the additive and AcOH as the solvent. Column chromatography (*n*hexane/EtOAc = 10:1) afforded the title compound as colorless oil (23.8 mg, 25%).

¹H-NMR (600 MHz, CDCl₃) δ 9.51 (s, 1H), 8.17 (dd, *J* = 7.8, 1.4 Hz, 1H), 8.00 (d, *J* = 8.8 Hz, 1H), 7.96 – 7.90 (m, 2H), 7.80 – 7.76 (m, 1H), 7.71 – 7.67 (m, 2H), 7.60 – 7.55 (m, 1H), 7.45 – 7.41 (m, 1H), 7.38 – 7.36 (m, 1H), 7.30 – 7.27 (m, 1H), 6.69 (d, *J* = 15.9 Hz, 1H).

¹³C-NMR (126 MHz, CDCl₃) δ 191.2 (CH), 162.4 (C_q), 146.9 (CH), 142.6 – 142.2 (m, C_q), 140.7 (C_q), 140.6 – 140.5 (m, C_q), 140.5 – 140.3 (m, C_q), 139.2 – 138.8 (m, C_q), 138.5 (C_q), 137.2 – 136.8 (m, C_q), 135.5 (C_q), 134.4 (C_q), 134.3 (CH), 133.4 (C_q), 132.2 (CH), 130.4 (C_q), 129.5 (CH), 129.4 (CH), 128.4 (CH), 128.4 (CH), 128.1 (CH), 127.8 (CH), 127.4 (CH), 125.5 – 124.9 (m, C_q), 122.6 (CH), 116.0 (CH).

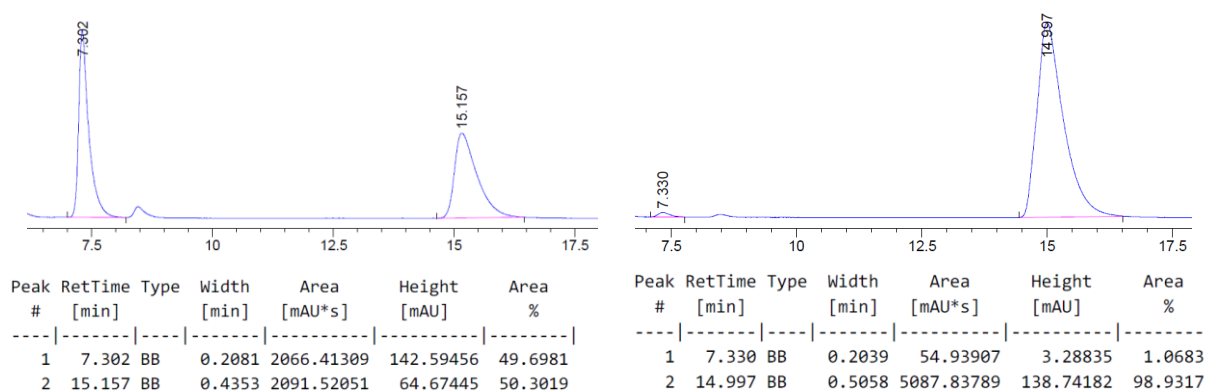
¹⁹F-NMR (376 MHz, CDCl₃) δ -152.39, -158.19, -162.51.

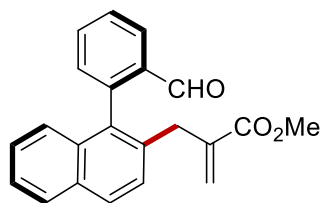
HRMS (ESI) calcd. for C₂₆H₁₃F₅O₃Na⁺: 491.0677. Found: 491.0674.

[α]_D²⁰ = -46.364 (*c* = 0.33, CHCl₃).

ν_{max} (thin film/cm⁻¹): 1104, 1193, 1252, 1293, 1385, 1471, 1516, 1596, 1623, 1696, 1755, 2745, 2845, 3059.

HPLC separation (IB-3 column, *n*hexane/*i*PrOH 90/10, 1.0 mL/min, 273 nm): *t_r*(major) = 15.0 min, *t_r*(minor) = 7.3 min, 98% ee.





methyl 2-((1-(2-formylphenyl)naphthalen-2-yl)methyl)acrylate 76ec: Prepared according to general procedure **M** on a 0.20 mmol scale, with *L-tert*-leucine (5.3 mg, 20 mol %) as the transient directing group, LiOAc (26.4 mg, 2 equiv.) as the additive and AcOH as the solvent. Column chromatography (*n*hexane/EtOAc = 10:1) afforded the title compound as white foam (40 mg, 54%).

¹H-NMR (400 MHz, CDCl₃) δ 9.47 (s, 1H), 8.13 (dd, *J* = 7.6, 1.4 Hz, 1H), 7.93 – 7.85 (m, 2H), 7.74 – 7.69 (m, 1H), 7.64 – 7.57 (m, 1H), 7.50 – 7.40 (m, 2H), 7.38 – 7.30 (m, 2H), 7.18 (d, *J* = 8.5 Hz, 1H), 6.19 (d, *J* = 1.2 Hz, 1H), 5.24 (q, *J* = 1.5 Hz, 1H), 3.64 (s, 3H), 3.61 – 3.43 (m, 2H).

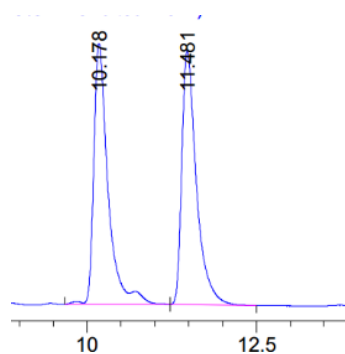
¹³C-NMR (101 MHz, CDCl₃) δ 192.0 (CH), 167.1 (C_q), 142.9 (C_q), 139.4 (C_q), 135.0 (C_q), 134.8 (C_q), 134.2 (C_q), 134.2 (CH), 133.6 (C_q), 132.2 (C_q), 131.7 (CH), 128.7 (CH), 128.6 (CH), 128.1 (CH), 127.5 (CH), 127.4 (CH), 127.2 (CH₂), 126.9 (CH), 126.2 (CH), 125.9 (CH), 52.0 (CH₃), 36.2 (CH₂).

HRMS (ESI) calcd. for C₂₂H₁₈O₃Na⁺: 353.1148. Found: 353.1137.

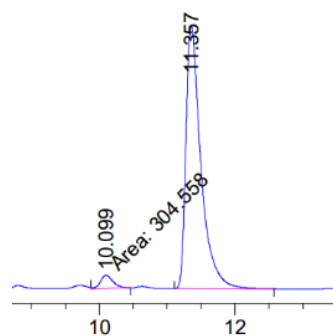
[α]_D²⁰ = +2.5 (*c* = 1.17, CHCl₃).

ν_{max} (thin film/cm⁻¹): 1136, 1195, 1263, 1281, 1332, 1384, 1437, 1508, 1596, 1632, 1695, 1719, 2749, 2847, 2925, 2950, 3057.

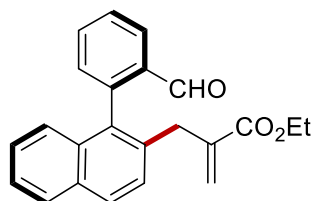
HPLC separation (ID-3 column, *n*hexane/*i*PrOH 90/10, 1.0 mL/min, 273 nm): *t_r*(major) = 11.4 min, *t_r*(minor) = 10.1 min, 92% ee.



| Peak # | RetTime [min] | Type | Width [min] | Area [mAU*s] | Height [mAU] | Area % |
|--------|---------------|------|-------------|--------------|--------------|---------|
| 1 | 10.178 | VV R | 0.2104 | 4367.02734 | 296.04617 | 50.2820 |
| 2 | 11.481 | BB | 0.2225 | 4318.03711 | 288.76123 | 49.7180 |



| Peak # | RetTime [min] | Type | Width [min] | Area [mAU*s] | Height [mAU] | Area % |
|--------|---------------|------|-------------|--------------|--------------|---------|
| 1 | 10.099 | MM | 0.2141 | 304.55798 | 23.71046 | 4.0665 |
| 2 | 11.357 | BV R | 0.2286 | 7184.95850 | 466.69745 | 95.9335 |



ethyl 2-((1-(2-formylphenyl)naphthalen-2-yl)methyl)acrylate 76ed: Prepared according to general procedure **A** on a 0.20 mmol scale, with *L-tert*-leucine (5.3 mg, 20 mol %) as the transient directing group, LiOAc (26.4 mg, 2 equiv.) as the additive and AcOH as the solvent. Column chromatography (*n*hexane/EtOAc = 10:1) afforded the title compound as white foam (25 mg, 37%).

¹H-NMR (400 MHz, CDCl₃) δ 9.46 (s, 1H), 8.19 – 8.08 (m, 1H), 7.93 – 7.85 (m, 2H), 7.74 – 7.68 (m, 1H), 7.63 – 7.58 (m, 1H), 7.50 – 7.42 (m, 2H), 7.38 – 7.31 (m, 2H), 7.20 – 7.14 (m, 1H), 6.18 (q, *J* = 1.2 Hz, 1H), 5.19 (q, *J* = 1.5 Hz, 1H), 4.11 (q, *J* = 7.1 Hz, 2H), 3.67 – 3.36 (m, 2H), 1.20 (t, *J* = 7.1 Hz, 3H).

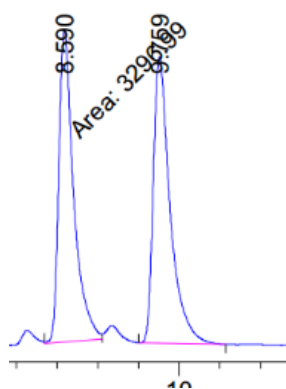
¹³C-NMR (101 MHz, CDCl₃) δ 191.8 (CH), 166.5 (C_q), 142.8 (C_q), 139.6 (C_q), 134.9 (C_q), 134.8 (C_q), 134.1 (C_q), 134.0 (CH), 133.5 (C_q), 132.0 (C_q), 131.6 (CH), 128.5 (CH), 128.4 (CH), 128.0 (CH), 127.5 (CH), 127.2 (CH), 126.7 (CH), 126.7 (CH₂), 126.0 (CH), 125.7 (CH), 60.8 (CH₂), 36.1 (CH₂), 14.1 (CH₃).

HRMS (ESI) calcd. for C₂₃H₂₀O₃Na⁺: 367.1305. Found: 367.1309.

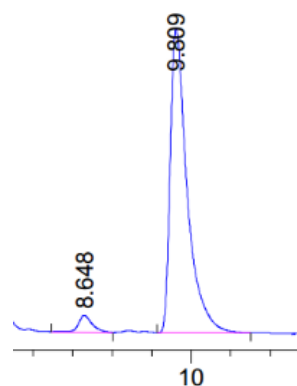
[α]_D²⁰ = +3.8 (*c* = 0.91, CHCl₃).

ν_{max} (thin film/cm⁻¹): 1027, 1134, 1206, 1250, 1263, 1299, 1326, 1369, 1384, 1447, 1508, 1596, 1632, 1696, 2748, 2842, 2933, 2981, 3059.

HPLC separation (ID-3 column, *n*hexane/*i*PrOH 90/10, 1.0 mL/min, 273 nm): *t_r*(major) = 9.8 min, *t_r*(minor) = 8.6 min, 91% ee.



| Peak # | RetTime [min] | Type | Width [min] | Area [mAU*s] | Height [mAU] | Area % |
|--------|---------------|------|-------------|--------------|--------------|---------|
| 1 | 8.590 | MM | 0.2110 | 3296.99268 | 260.37784 | 48.9986 |
| 2 | 9.759 | BB | 0.2149 | 3431.75366 | 238.41435 | 51.0014 |



| Peak # | RetTime [min] | Type | Width [min] | Area [mAU*s] | Height [mAU] | Area % |
|--------|---------------|------|-------------|--------------|--------------|---------|
| 1 | 8.648 | VB R | 0.1733 | 342.19162 | 27.85601 | 4.3157 |
| 2 | 9.809 | BB | 0.2222 | 7586.87891 | 508.14691 | 95.6843 |

6 References

- [1] F. Wöhler, *Ann. Phys.* **1828**, *88*, 253-256.
- [2] a) L. F. Tietze, T. Eicher, U. Diederichsen, A. Speicher, N. Schützenmeister, *Reactions and syntheses: in the organic chemistry laboratory*, John Wiley & Sons, **2015**; b) K. C. Nicolaou, *Proc. Math. Phys. Eng. Sci.* **2014**, *470*, 20130690.
- [3] a) B. M. Trost, *Science* **1991**, *254*, 1471-1477; b) B. M. Trost, *Angew. Chem. Int. Ed.* **1995**, *34*, 259-281.
- [4] P. T. Anastas, J. C. Warner, *Green chemistry: Theory and practice* **1998**, *29*.
- [5] T. Dalton, T. Faber, F. Glorius, *ACS Cent. Sci.* **2021**, *7*, 245-261.
- [6] a) U. Dhawa, N. Kaplaneris, L. Ackermann, *Org. Chem. Front.* **2021**, *8*, 4886-4913; b) F. Kakiuchi, T. Kochi, *Chem. Lett.* **2020**, *49*, 1256-1269; c) J. Chen, S. Lv, S. Tian, *ChemSusChem* **2019**, *12*, 115-132; d) T. H. Meyer, L. H. Finger, P. Gandeepan, L. Ackermann, *Trends Chem.* **2019**, *1*, 63-76.
- [7] A. De Meijere, S. Bräse, M. Oestreich, *Metal catalyzed cross-coupling reactions and more*, John Wiley & Sons, **2013**.
- [8] C. Glaser, *Ber. Dtsch. Chem. Ges.* **1869**, *2*, 422-424.
- [9] F. Ullmann, J. Bielecki, *Ber. Dtsch. Chem. Ges.* **1901**, *34*, 2174-2185.
- [10] R. F. Heck, J. Nolley Jr, *J. Org. Chem.* **1972**, *37*, 2320-2322.
- [11] K. Tamao, K. Sumitani, M. Kumada, *J. Am. Chem. Soc.* **1972**, *94*, 4374-4376.
- [12] a) S. Baba, E. Negishi, *J. Am. Chem. Soc.* **1976**, *98*, 6729-6731; b) E.-i. Negishi, S. Baba, *J. Chem. Soc., Chem. Commun.* **1976**, 596b-597b.
- [13] D. Milstein, J. Stille, *J. Am. Chem. Soc.* **1978**, *100*, 3636-3638.
- [14] Y. Hatanaka, T. Hiayama, *J. Org. Chem.* **1988**, *53*, 918-920.
- [15] N. Miyaura, A. Suzuki, *Chem. Rev.* **1995**, *95*, 2457-2483.
- [16] K. Sonogashira, *J. Organomet. Chem.* **2002**, *653*, 46-49.
- [17] The nobel prize in chemistry 2010 - press release: https://www.nobelprize.org/nobel_prizes/chemistry/laureates/2010/press.html (accessed on 2007.2002.2021).
- [18] T. Rogge, N. Kaplaneris, N. Chatani, J. Kim, S. Chang, B. Punji, L. L. Schafer, D. G. Musaev, J. Wencel-Delord, C. A. Roberts, R. Sarpong, Z. E. Wilson, M. A. Brimble, M. J. Johansson, L. Ackermann, *Nat. Rev. Methods Primers* **2021**, *1*, 43.
- [19] a) P. Gandeepan, T. Müller, D. Zell, G. Cera, S. Warratz, L. Ackermann, *Chem. Rev.* **2019**, *119*, 2192-2452; b) Z. Dong, Z. Ren, S. J. Thompson, Y. Xu, G. Dong, *Chem. Rev.* **2017**, *117*, 9333-9403; c) D.-S. Kim, W.-J. Park, C.-H. Jun, *Chem. Rev.* **2017**, *117*, 8977-9015; d) O. Daugulis, J. Roane, L. D. Tran, *Acc. Chem. Res.* **2015**, *48*, 1053-1064; e) G. Rouquet, N. Chatani, *Angew. Chem. Int. Ed.* **2013**, *52*, 11726-11743; f) R. Giri, B.-F. Shi, K. M. Engle, N. Maugel, J.-Q. Yu, *Chem. Soc. Rev.* **2009**, *38*, 3242-3272.
- [20] a) A. K. Bagdi, M. Rahman, D. Bhattacharjee, G. V. Zyryanov, S. Ghosh, O. N. Chupakhin, A. Hajra, *Green Chem.* **2020**, *22*, 6632-6681; b) S. H. Cho, J. Y. Kim, J. Kwak, S. Chang, *Chem. Soc. Rev.* **2011**, *40*, 5068-5083.
- [21] a) L. Ackermann, R. Vicente, **2009**, pp. 311-333; b) S. J. Blanksby, G. B. Ellison, *Acc. Chem. Res.* **2003**, *36*, 255-263.
- [22] a) L. Ackermann, *Chem. Rev.* **2011**, *111*, 1315-1345; b) D. Balcells, E. Clot, O. Eisenstein, *Chem. Rev.* **2010**, *110*, 749-823.
- [23] a) D. Lapointe, K. Fagnou, *Chem. Lett.* **2010**, *39*, 1118-1126; b) S. I. Gorelsky, D. Lapointe, K. Fagnou, *J. Am. Chem. Soc.* **2008**, *130*, 10848-10849.
- [24] Y. Boutadla, D. L. Davies, S. A. Macgregor, A. I. Poblador-Bahamonde, *Dalton Trans.* **2009**, 5820-5831.

References

- [25] T. Rogge, J. C. A. Oliveira, R. Kuniyil, L. Hu, L. Ackermann, *ACS Catal.* **2020**, *10*, 10551-10558.
- [26] a) D. Zell, M. Bursch, V. Müller, S. Grimme, L. Ackermann, *Angew. Chem. Int. Ed.* **2017**, *56*, 10378-10382; b) H. Wang, M. Moselage, M. J. González, L. Ackermann, *ACS Catal.* **2016**, *6*, 2705-2709.
- [27] a) J. Ye, M. Lautens, *Nat. Chem.* **2015**, *7*, 863-870; b) X.-C. Wang, W. Gong, L.-Z. Fang, R.-Y. Zhu, S. Li, K. M. Engle, J.-Q. Yu, *Nature* **2015**, *519*, 334-338; c) L. Jiao, E. Herdtweck, T. Bach, *J. Am. Chem. Soc.* **2012**, *134*, 14563-14572; d) M. Catellani, E. Motti, N. Della Ca', *Acc. Chem. Res.* **2008**, *41*, 1512-1522.
- [28] a) S. Bag, T. Patra, A. Modak, A. Deb, S. Maity, U. Dutta, A. Dey, R. Kancharla, A. Maji, A. Hazra, M. Bera, D. Maiti, *J. Am. Chem. Soc.* **2015**, *137*, 11888-11891; b) D. Leow, G. Li, T.-S. Mei, J.-Q. Yu, *Nature* **2012**, *486*, 518-522; c) S. Das, C. D. Incarvito, R. H. Crabtree, G. W. Brudvig, *Science* **2006**, *312*, 1941-1943; d) R. Breslow, *Acc. Chem. Res.* **1980**, *13*, 170-177.
- [29] L. Ackermann, N. Hofmann, R. Vicente, *Org. Lett.* **2011**, *13*, 1875-1877.
- [30] a) G. Duarah, P. P. Kaishap, T. Begum, S. Gogoi, *Adv. Synth. Catal.* **2019**, *361*, 654-672; b) S. I. Kozhushkov, L. Ackermann, *Chem. Sci.* **2013**, *4*, 886-896; c) P. B. Arockiam, C. Bruneau, P. H. Dixneuf, *Chem. Rev.* **2012**, *112*, 5879-5918.
- [31] J. Chatt, J. Davidson, *J. Chem. Soc.* **1965**, 843-855.
- [32] L. N. Lewis, J. F. Smith, *J. Am. Chem. Soc.* **1986**, *108*, 2728-2735.
- [33] S. Murai, F. Kakiuchi, S. Sekine, Y. Tanaka, A. Kamatani, M. Sonoda, N. Chatani, *Nature* **1993**, *366*, 529-531.
- [34] a) K. Korvorapun, J. Struwe, R. Kuniyil, A. Zangarelli, A. Casnati, M. Waeterschoot, L. Ackermann, *Angew. Chem. Int. Ed.* **2020**, *59*, 18103-18109; b) S. R. Yetra, T. Rogge, S. Warratz, J. Struwe, W. Peng, P. Vana, L. Ackermann, *Angew. Chem. Int. Ed.* **2019**, *58*, 7490-7494; c) T. Rogge, L. Ackermann, *Angew. Chem. Int. Ed.* **2019**, *58*, 15640-15645; d) M. Simonetti, D. M. Cannas, X. Just-Baringo, I. J. Vitorica-Yrezabal, I. Larrosa, *Nat. Chem.* **2018**, *10*, 724-731; e) J. Hubrich, T. Himmler, L. Rodefeld, L. Ackermann, *ACS Catal.* **2015**, *5*, 4089-4093; f) L. Ackermann, E. Diers, A. Manvar, *Org. Lett.* **2012**, *14*, 1154-1157; g) I. Özdemir, S. Demir, B. Çetinkaya, C. Gourlaouen, F. Maseras, C. Bruneau, P. H. Dixneuf, *J. Am. Chem. Soc.* **2008**, *130*, 1156-1157; h) L. Ackermann, A. Althammer, R. Born, *Angew. Chem. Int. Ed.* **2006**, *45*, 2619-2622.
- [35] a) G.-W. Wang, M. Wheatley, M. Simonetti, D. M. Cannas, I. Larrosa, *Chem* **2020**, *6*, 1459-1468; b) L. Ackermann, P. Novák, R. Vicente, N. Hofmann, *Angew. Chem. Int. Ed.* **2009**, *48*, 6045-6048; c) L. Ackermann, P. Novák, *Org. Lett.* **2009**, *11*, 4966-4969.
- [36] a) K. Raghuvanshi, D. Zell, K. Rauch, L. Ackermann, *ACS Catal.* **2016**, *6*, 3172-3175; b) J. Kim, J. Kim, S. Chang, *Chem. Eur. J.* **2013**, *19*, 7328-7333.
- [37] a) L. Massignan, X. Tan, T. H. Meyer, R. Kuniyil, A. M. Messinis, L. Ackermann, *Angew. Chem. Int. Ed.* **2020**, *59*, 3184-3189; b) Q. Bu, R. Kuniyil, Z. Shen, E. Gońka, L. Ackermann, *Chem. Eur. J.* **2020**, *26*, 16450-16454; c) G. G. Dias, T. Rogge, R. Kuniyil, C. Jacob, R. F. S. Menna-Barreto, E. N. da Silva Júnior, L. Ackermann, *Chem. Commun.* **2018**, *54*, 12840-12843; d) Y.-H. Sun, T.-Y. Sun, Y.-D. Wu, X. Zhang, Y. Rao, *Chem. Sci.* **2016**, *7*, 2229-2238; e) F. Yang, K. Rauch, K. Kettelhoit, L. Ackermann, *Angew. Chem. Int. Ed.* **2014**, *53*, 11285-11288; f) X. Yang, G. Shan, Y. Rao, *Org. Lett.* **2013**, *15*, 2334-2337; g) F. Yang, L. Ackermann, *Org. Lett.* **2013**, *15*, 718-720.
- [38] L. Ackermann, *Org. Lett.* **2005**, *7*, 3123-3125.
- [39] L. Ackermann, R. Vicente, A. Althammer, *Org. Lett.* **2008**, *10*, 2299-2302.

- [40] a) L. Ackermann, *Acc. Chem. Res.* **2014**, *47*, 281-295; b) L. Ackermann, *Org. Process Res. Dev.* **2015**, *19*, 260-269; c) L. Wang, L. Ackermann, *Chem. Commun.* **2014**, *50*, 1083-1085; d) W. Liu, L. Ackermann, *Chem. Commun.* **2014**, *50*, 1878-1881; e) A. Gray, A. Tsybizova, J. Roithova, *Chem. Sci.* **2015**, *6*, 5544-5553.
- [41] a) X.-X. Guo, *J. Org. Chem.* **2013**, *78*, 1660-1664; b) Y. Yu, L. Huang, W. Wu, H. Jiang, *Org. Lett.* **2014**, *16*, 2146-2149; c) P. Zhao, D. Chen, G. Song, K. Han, X. Li, *J. Org. Chem.* **2012**, *77*, 1579-1584; d) S. P. Midya, M. K. Sahoo, V. G. Landge, P. R. Rajamohan, E. Balaraman, *Nat. Commun.* **2015**, *6*, 8591; e) M. Nagamoto, D. Yamauchi, T. Nishimura, *Chem. Commun.* **2016**, *52*, 5876-5879.
- [42] a) G. Song, F. Wang, X. Li, *Chem. Soc. Rev.* **2012**, *41*, 3651-3678; b) S. M. Abu Sohel, R.-S. Liu, *Chem. Soc. Rev.* **2009**, *38*, 2269-2281; c) M. Gulías, J. L. Mascareñas, *Angew. Chem. Int. Ed.* **2016**, *55*, 11000-11019; d) Y. Yang, K. Li, Y. Cheng, D. Wan, M. Li, J. You, *Chem. Commun.* **2016**, *52*, 2872-2884; e) S. Prakash, R. Kuppusamy, C.-H. Cheng, *ChemCatChem* **2018**, *10*, 683-705.
- [43] a) T. Satoh, M. Miura, *Chem. Eur. J.* **2010**, *16*, 11212-11222; b) K. Fagnou, M. Lautens, *Chem. Rev.* **2003**, *103*, 169-196.
- [44] L. Ackermann, A. V. Lygin, N. Hofmann, *Angew. Chem. Int. Ed.* **2011**, *50*, 6379-6382.
- [45] a) L. Wang, L. Ackermann, *Org. Lett.* **2013**, *15*, 176-179; b) B. Li, N. Wang, Y. Liang, S. Xu, B. Wang, *Org. Lett.* **2013**, *15*, 136-139; c) L. Ackermann, L. Wang, A. V. Lygin, *Chem. Sci.* **2012**, *3*, 177-180.
- [46] H. Lin, S.-S. Li, L. Dong, *Org. Biomol. Chem.* **2015**, *13*, 11228-11234.
- [47] a) P. Villuendas, E. P. Urriolabeitia, *J. Org. Chem.* **2013**, *78*, 5254-5263; b) B. Li, H. Feng, N. Wang, J. Ma, H. Song, S. Xu, B. Wang, *Chem. Eur. J.* **2012**, *18*, 12873-12879.
- [48] a) P. P. Kaishap, B. Sarma, S. Gogoi, *Chem. Commun.* **2016**, *52*, 9809-9812; b) M. Deponti, S. I. Kozhushkov, D. S. Yufit, L. Ackermann, *Org. Biomol. Chem.* **2013**, *11*, 142-148; c) R. K. Chinnagolla, M. Jeganmohan, *Chem. Commun.* **2012**, *48*, 2030-2032; d) L. Ackermann, J. Pospech, K. Graczyk, K. Rauch, *Org. Lett.* **2012**, *14*, 930-933.
- [49] a) W. Ma, K. Graczyk, L. Ackermann, *Org. Lett.* **2012**, *14*, 6318-6321; b) V. S. Thirunavukkarasu, M. Donati, L. Ackermann, *Org. Lett.* **2012**, *14*, 3416-3419; c) L. Ackermann, A. V. Lygin, N. Hofmann, *Org. Lett.* **2011**, *13*, 3278-3281.
- [50] a) G. L. Galiana, A. C. Gauthier, R. H. Mattson, *Drugs in R&D* **2017**, *17*, 329-339; b) W. Sneader, *Drug discovery: a history*, John Wiley & Sons, **2005**; c) J. A. May, H. Ratan, J. R. Glenn, W. Losche, P. Spangenberg, S. Heptinstall, *Platelets* **1998**, *9*, 227-232.
- [51] a) A. A. Antonov, K. P. Bryliakov, *Appl. Organomet. Chem.* **2022**, *36*, e6499; b) S. Moghimi, M. Mahdavi, A. Shafiee, A. Foroumadi, *Eur. J. Org. Chem.* **2016**, *2016*, 3282-3299.
- [52] K. Padala, M. Jeganmohan, *Chem. Commun.* **2013**, *49*, 9651-9653.
- [53] K. Padala, M. Jeganmohan, *Chem. Eur. J.* **2014**, *20*, 4092-4097.
- [54] K. Raghuvanshi, D. Zell, L. Ackermann, *Org. Lett.* **2017**, *19*, 1278-1281.
- [55] T. Sarkar, S. Pradhan, T. Punniyamurthy, *J. Org. Chem.* **2018**, *83*, 6444-6453.
- [56] E. Kianmehr, S. B. Nasab, *Eur. J. Org. Chem.* **2019**, *2019*, 1038-1044.
- [57] M. S. Taylor, E. N. Jacobsen, *India* **2004**, *101*, 5368-5373.
- [58] a) C. G. Newton, S.-G. Wang, C. C. Oliveira, N. Cramer, *Chem. Rev.* **2017**, *117*, 8908-8976; b) A. R. Dick, M. S. Sanford, *Tetrahedron* **2006**, *62*, 2439-2463.
- [59] C. J. Flynn, C. J. Elcoate, S. E. Lawrence, A. R. Maguire, *J. Am. Chem. Soc.* **2010**, *132*, 1184-1185.
- [60] J. T. Groves, P. Viski, *J. Org. Chem.* **1990**, *55*, 3628-3634.

References

- [61] W. Zhang, F. Wang, S. D. McCann, D. Wang, P. Chen, S. S. Stahl, G. Liu, *Science* **2016**, *353*, 1014-1018.
- [62] V. I. Sokolov, L. L. Troitskaya, O. A. Reutov, *J. Organomet. Chem.* **1977**, *133*, C28-C30.
- [63] K. M. Engle, J.-Q. Yu, *J. Org. Chem.* **2013**, *78*, 8927-8955.
- [64] T. G. Saint-Denis, R.-Y. Zhu, G. Chen, Q.-F. Wu, J.-Q. Yu, *Science* **2018**, *359*, eaao4798.
- [65] Q. Shao, K. Wu, Z. Zhuang, S. Qian, J.-Q. Yu, *Acc. Chem. Res.* **2020**, *53*, 833-851.
- [66] X. F. ZHANG Zhen-Feng, YANG Bo, YU Han, ZHANG Wan-Bin, *Chin. J. Org. Chem.* **2011**, *31*, 429-442.
- [67] a) T. Akiyama, J. Itoh, K. Yokota, K. Fuchibe, *Angew. Chem. Int. Ed.* **2004**, *43*, 1566-1568; b) D. Uraguchi, M. Terada, *J. Am. Chem. Soc.* **2004**, *126*, 5356-5357; c) J. Yu, F. Shi, L.-Z. Gong, *Acc. Chem. Res.* **2011**, *44*, 1156-1171; d) H. Wu, Y.-P. He, F. Shi, *Synthesis* **2015**, *47*, 1990-2016; e) P.-S. Wang, L.-Z. Gong, *Synthesis* **2021**, *54*, 4795-4801.
- [68] a) B. Zu, Y. Guo, J. Ke, C. He, *Synthesis* **2021**, *53*, 2029-2042; b) M. Zhang, Z. Zhong, L. Liao, A. Q. Zhang, *Org. Chem. Front.* **2022**, *9*, 3882-3896; c) D. Bag, P. K. Verma, S. D. Sawant, *Chem. Asian J.* **2020**, *15*, 3225-3238; d) G. Liao, T. Zhang, Z.-K. Lin, B.-F. Shi, *Angew. Chem. Int. Ed.* **2020**, *59*, 19773-19786; e) T. Bhattacharya, S. Pimparkar, D. Maiti, *RSC Advances* **2018**, *8*, 19456-19464; f) S. St John-Campbell, J. A. Bull, *Org. Biomol. Chem.* **2018**, *16*, 4582-4595.
- [69] B.-F. Shi, N. Maugel, Y.-H. Zhang, J.-Q. Yu, *Angew. Chem. Int. Ed.* **2008**, *47*, 4882-4886.
- [70] B.-F. Shi, Y.-H. Zhang, J. K. Lam, D.-H. Wang, J.-Q. Yu, *J. Am. Chem. Soc.* **2010**, *132*, 460-461.
- [71] L. Chu, X.-C. Wang, C. E. Moore, A. L. Rheingold, J.-Q. Yu, *J. Am. Chem. Soc.* **2013**, *135*, 16344-16347.
- [72] L. Chu, K.-J. Xiao, J.-Q. Yu, *Science* **2014**, *346*, 451-455.
- [73] K.-J. Xiao, L. Chu, J.-Q. Yu, *Angew. Chem. Int. Ed.* **2016**, *55*, 2856-2860.
- [74] K.-J. Xiao, L. Chu, G. Chen, J.-Q. Yu, *J. Am. Chem. Soc.* **2016**, *138*, 7796-7800.
- [75] D.-W. Gao, Y.-C. Shi, Q. Gu, Z.-L. Zhao, S.-L. You, *J. Am. Chem. Soc.* **2013**, *135*, 86-89.
- [76] C. Pi, Y. Li, X. Cui, H. Zhang, Y. Han, Y. Wu, *Chem. Sci.* **2013**, *4*, 2675-2679.
- [77] Y.-C. Shi, R.-F. Yang, D.-W. Gao, S.-L. You, *Beilstein J. Org. Chem.* **2013**, *9*, 1891-1896.
- [78] C. Pi, X. Cui, X. Liu, M. Guo, H. Zhang, Y. Wu, *Org. Lett.* **2014**, *16*, 5164-5167.
- [79] D.-W. Gao, Q. Gu, S.-L. You, *J. Am. Chem. Soc.* **2016**, *138*, 2544-2547.
- [80] Z.-J. Cai, C.-X. Liu, Q. Gu, C. Zheng, S.-L. You, *Angew. Chem. Int. Ed.* **2019**, *58*, 2149-2153.
- [81] Y. Huang, C. Pi, X. Cui, Y. Wu, *Adv. Synth. Catal.* **2020**, *362*, 1385-1390.
- [82] D.-W. Gao, Q. Gu, S.-L. You, *ACS Catal.* **2014**, *4*, 2741-2745.
- [83] S.-X. Li, Y.-N. Ma, S.-D. Yang, *Org. Lett.* **2017**, *19*, 1842-1845.
- [84] L. Jin, Q.-J. Yao, P.-P. Xie, Y. Li, B.-B. Zhan, Y.-Q. Han, X. Hong, B.-F. Shi, *Chem* **2020**, *6*, 497-511.
- [85] Q.-J. Yao, P.-P. Xie, Y.-J. Wu, Y.-L. Feng, M.-Y. Teng, X. Hong, B.-F. Shi, *J. Am. Chem. Soc.* **2020**, *142*, 18266-18276.
- [86] a) Q. Zhao, T. Poisson, X. Pannecoucke, T. Besset, *Synthesis* **2017**, *49*, 4808-4826; b) P. Gandeepan, L. Ackermann, *Chem* **2018**, *4*, 199-222; c) B. Niu, K. Yang, B. Lawrence, H. Ge, *ChemSusChem* **2019**, *12*, 2955-2969; d) S. B. Wu Yongjie, *Chin. J. Org. Chem.* **2020**, *40*, 3517-3535.

References

- [87] F. L. Zhang, K. Hong, T. J. Li, H. Park, J. Q. Yu, *Science* **2016**, *351*, 252-256.
- [88] H. Park, P. Verma, K. Hong, J.-Q. Yu, *Nat. Chem.* **2018**, *10*, 755-762.
- [89] L.-J. Xiao, K. Hong, F. Luo, L. Hu, W. R. Ewing, K.-S. Yeung, J.-Q. Yu, *Angew. Chem. Int. Ed.* **2020**, *59*, 9594-9600.
- [90] Q.-J. Yao, S. Zhang, B.-B. Zhan, B.-F. Shi, *Angew. Chem. Int. Ed.* **2017**, *56*, 6617-6621.
- [91] G. Liao, Q.-J. Yao, Z.-Z. Zhang, Y.-J. Wu, D.-Y. Huang, B.-F. Shi, *Angew. Chem. Int. Ed.* **2018**, *57*, 3661-3665.
- [92] G. Liao, B. Li, H.-M. Chen, Q.-J. Yao, Y.-N. Xia, J. Luo, B.-F. Shi, *Angew. Chem. Int. Ed.* **2018**, *57*, 17151-17155.
- [93] G. Liao, H.-M. Chen, Y.-N. Xia, B. Li, Q.-J. Yao, B.-F. Shi, *Angew. Chem. Int. Ed.* **2019**, *58*, 11464-11468.
- [94] J. Zhang, J. Fan, Y. Wu, Z. Guo, J. Wu, M. Xie, *Org. Lett.* **2022**, *24*, 5143-5148.
- [95] a) S. Zhang, Q.-J. Yao, G. Liao, X. Li, H. Li, H.-M. Chen, X. Hong, B.-F. Shi, *ACS Catal.* **2019**, *9*, 1956-1961; b) H.-M. Chen, S. Zhang, G. Liao, Q.-J. Yao, X.-T. Xu, K. Zhang, B.-F. Shi, *Organometallics* **2019**, *38*, 4022-4028.
- [96] J. Zhang, Q. Xu, J. Wu, J. Fan, M. Xie, *Org. Lett.* **2019**, *21*, 6361-6365.
- [97] H. Song, Y. Li, Q.-J. Yao, L. Jin, L. Liu, Y.-H. Liu, B.-F. Shi, *Angew. Chem. Int. Ed.* **2020**, *59*, 6576-6580.
- [98] J. Xu, Y. Liu, J. Zhang, X. Xu, Z. Jin, *Chem. Commun.* **2018**, *54*, 689-692.
- [99] a) C. A. Malapit, M. B. Prater, J. R. Cabrera-Pardo, M. Li, T. D. Pham, T. P. McFadden, S. Blank, S. D. Minter, *Chem. Rev.* **2022**, *122*, 3180-3218; b) L. Ackermann, *Acc. Chem. Res.* **2020**, *53*, 84-104; c) W. Leitner, E. A. Quadrelli, R. Schlögl, *Green Chem.* **2017**, *19*, 2307-2308.
- [100] K. J. Lee, B. D. McCarthy, J. L. Dempsey, *Chem. Soc. Rev.* **2019**, *48*, 2927-2945.
- [101] a) N. Sauermann, T. H. Meyer, Y. Qiu, L. Ackermann, *ACS Catal.* **2018**, *8*, 7086-7103; b) T. H. Meyer, I. Choi, C. Tian, L. Ackermann, *Chem* **2020**, *6*, 2484-2496.
- [102] H. Kolbe, *Justus Liebigs Ann. Chem.* **1849**, *69*, 257-294.
- [103] M. Faraday, *Pogg. Ann. Phys. Chem* **1834**, *33*, 433-451.
- [104] T. Shono, *Tetrahedron* **1984**, *40*, 811-850.
- [105] J. H. Simons, *J. Electrochem. Soc.* **1949**, *95*, 47.
- [106] M. M. Baizer, *J. Electrochem. Soc.* **1964**, *111*, 215.
- [107] C. Amatore, C. Cammoun, A. Jutand, *Adv. Synth. Catal.* **2007**, *349*, 292-296.
- [108] F. Kakiuchi, T. Kochi, H. Mutsutani, N. Kobayashi, S. Urano, M. Sato, S. Nishiyama, T. Tanabe, *J. Am. Chem. Soc.* **2009**, *131*, 11310-11311.
- [109] H. Aiso, T. Kochi, H. Mutsutani, T. Tanabe, S. Nishiyama, F. Kakiuchi, *J. Org. Chem.* **2012**, *77*, 7718-7724.
- [110] T. V. Grayaznova, Y. B. Dudkina, D. R. Islamov, O. N. Kataeva, O. G. Sinyashin, D. A. Vicic, Y. H. Budnikova, *J. Organomet. Chem.* **2015**, *785*, 68-71.
- [111] Z. Duan, L. Zhang, W. Zhang, L. Lu, L. Zeng, R. Shi, A. Lei, *ACS Catal.* **2020**, *10*, 3828-3831.
- [112] Q.-L. Yang, Y.-Q. Li, C. Ma, P. Fang, X.-J. Zhang, T.-S. Mei, *J. Am. Chem. Soc.* **2017**, *139*, 3293-3298.
- [113] Y.-Q. Li, Q.-L. Yang, P. Fang, T.-S. Mei, D. Zhang, *Org. Lett.* **2017**, *19*, 2905-2908.
- [114] C. Ma, C.-Q. Zhao, Y.-Q. Li, L.-P. Zhang, X.-T. Xu, K. Zhang, T.-S. Mei, *Chem. Commun.* **2017**, *53*, 12189-12192.
- [115] Q.-L. Yang, C.-Z. Li, L.-W. Zhang, Y.-Y. Li, X. Tong, X.-Y. Wu, T.-S. Mei, *Organometallics* **2019**, *38*, 1208-1212.
- [116] Z. Lin, U. Dhawa, X. Hou, M. Surke, B. Yuan, S.-W. Li, Y.-C. Liou, M. J. Johansson, L.-C. Xu, C.-H. Chao, X. Hong, L. Ackermann, *Nat. Commun.* **2023**, *14*, 4224.

- [117] U. Dhawa, C. Tian, T. Wdowik, J. C. A. Oliveira, J. Hao, L. Ackermann, *Angew. Chem. Int. Ed.* **2020**, *59*, 13451-13457.
- [118] Y. Qiu, C. Tian, L. Massignan, T. Rogge, L. Ackermann, *Angew. Chem. Int. Ed.* **2018**, *57*, 5818-5822.
- [119] F. Xu, Y.-J. Li, C. Huang, H.-C. Xu, *ACS Catal.* **2018**, *8*, 3820-3824.
- [120] M.-J. Luo, M. Hu, R.-J. Song, D.-L. He, J.-H. Li, *Chem. Commun.* **2019**, *55*, 1124-1127.
- [121] M.-J. Luo, T.-T. Zhang, F.-J. Cai, J.-H. Li, D.-L. He, *Chem. Commun.* **2019**, *55*, 7251-7254.
- [122] Z.-Q. Wang, C. Hou, Y.-F. Zhong, Y.-X. Lu, Z.-Y. Mo, Y.-M. Pan, H.-T. Tang, *Org. Lett.* **2019**, *21*, 9841-9845.
- [123] R. Mei, J. Koeller, L. Ackermann, *Chem. Commun.* **2018**, *54*, 12879-12882.
- [124] L. Yang, R. Steinbock, A. Scheremetjew, R. Kuniyil, L. H. Finger, A. M. Messinis, L. Ackermann, *Angew. Chem. Int. Ed.* **2020**, *59*, 11130-11135.
- [125] X. Tan, X. Hou, T. Rogge, L. Ackermann, *Angew. Chem. Int. Ed.* **2021**, *60*, 4619-4624.
- [126] Y. Wang, H. Simon, X. Chen, Z. Lin, S. Chen, L. Ackermann, *Angew. Chem. Int. Ed.* **2022**, *61*, e202201595.
- [127] G. Bonaccorso, *Mastering machine learning algorithms: expert techniques to implement popular machine learning algorithms and fine-tune your models*, Packt Publishing Ltd, **2018**.
- [128] D. T. Ahneman, J. G. Estrada, S. Lin, S. D. Dreher, A. G. Doyle, *Science* **2018**, *360*, 186-190.
- [129] S. Jaeger, S. Fulle, S. Turk, *J. Chem. Inf. Model.* **2018**, *58*, 27-35.
- [130] a) T. Lan, Q. An, *J. Am. Chem. Soc.* **2021**, *143*, 16804-16812; b) Z. Zhou, S. Kearnes, L. Li, R. N. Zare, P. Riley, *Sci. Rep.* **2019**, *9*, 10752.
- [131] J. M. Granda, L. Donina, V. Dragone, D.-L. Long, L. Cronin, *Nature* **2018**, *559*, 377-381.
- [132] B. J. Shields, J. Stevens, J. Li, M. Parasram, F. Damani, J. I. M. Alvarado, J. M. Janey, R. P. Adams, A. G. Doyle, *Nature* **2021**, *590*, 89-96.
- [133] Z. Zhou, X. Li, R. N. Zare, *ACS Cent. Sci.* **2017**, *3*, 1337-1344.
- [134] a) K. Yamamoto, M. Kuriyama, O. Onomura, *Acc. Chem. Res.* **2020**, *53*, 105-120; b) F. Wang, S. S. Stahl, *Acc. Chem. Res.* **2020**, *53*, 561-574; c) P. Xiong, H.-C. Xu, *Acc. Chem. Res.* **2019**, *52*, 3339-3350; d) M. Yan, Y. Kawamata, P. S. Baran, *Chem. Rev.* **2017**, *117*, 13230-13319.
- [135] a) L. Ackermann, Z. Lin, U. Dhawa, B. Yuan, Y.-C. Liou, M. Johansson, **2022**; b) D. M. Heard, A. J. J. Lennox, *Angew. Chem. Int. Ed.* **2020**, *59*, 18866-18884; c) B. A. Frontana-Uribe, R. D. Little, J. G. Ibanez, A. Palma, R. Vasquez-Medrano, *Green Chem.* **2010**, *12*, 2099-2119.
- [136] N. Kerru, L. Gummidi, S. Maddila, K. K. Gangu, S. B. Jonnalagadda, *Molecules* **2020**, *25*, 1909.
- [137] a) Y. Zhang, M. Li, X. Li, T. Zhang, M. Qin, L. Ren, *Front. pharmacol.* **2018**, *9*; b) M. C. Sharma, S. Sharma, P. Sharma, A. Kumar, *Med. Chem. Res.* **2013**, *22*, 5772-5788; c) T.-Y. Jin, S.-Q. Li, C.-R. Jin, H. Shan, R.-M. Wang, M.-X. Zhou, A.-L. Li, L.-Y. Li, S.-Y. Hu, T. Shen, L. Xiang, *J. Nat. Prod.* **2018**, *81*, 768-777; d) Y. Nishiyama, K. Iwasa, S. Okada, S. Takeuchi, M. Moriyasu, M. Kamigauchi, J. Koyama, A. Takeuchi, H. Tokuda, H. S. Kim, *Heterocycles* **2010**, *81*, 1193-1229.
- [138] a) R. Gujjarappa, N. Vodnala, C. C. Malakar, *Adv. Synth. Catal.* **2020**, *362*, 4896-4990; b) J. S. S. Neto, G. Zeni, *Tetrahedron* **2020**, *76*, 130876.
- [139] a) N. Guimond, K. Fagnou, *J. Am. Chem. Soc.* **2009**, *131*, 12050-12051; b) Y.-F. Wang, K. K. Toh, J.-Y. Lee, S. Chiba, *Angew. Chem. Int. Ed.* **2011**, *50*, 5927-5931.

- [140] Y. A. Hajam, R. Lone, R. Kumar, in *Plant Phenolics in Abiotic Stress Management* (Eds.: R. Lone, S. Khan, A. Mohammed Al-Sadi), Springer Nature Singapore, Singapore, **2023**, pp. 125-147.
- [141] Z. Qiu, C.-J. Li, *Chem. Rev.* **2020**, *120*, 10454-10515.
- [142] J. Nešvera, L. Rucká, M. Pátek, in *Adv. Appl. Microbiol.*, Vol. 93 (Eds.: S. Sariaslani, G. M. Gadd), Academic Press, **2015**, pp. 107-160.
- [143] F. Yang, H. Zhang, X. Liu, B. Wang, L. Ackermann, *Chin. J. Org. Chem.* **2019**, *39*, 59-73.
- [144] H. Wang, X. Gao, Z. Lv, T. Abdelilah, A. Lei, *Chem. Rev.* **2019**, *119*, 6769-6787.
- [145] G. Bringmann, T. Gulder, T. A. M. Gulder, M. Breuning, *Chem. Rev.* **2011**, *111*, 563-639.
- [146] a) J. Clayden, W. J. Moran, P. J. Edwards, S. R. LaPlante, *Angew. Chem. Int. Ed.* **2009**, *48*, 6398-6401; b) S. R. LaPlante, L. D. Fader, K. R. Fandrick, D. R. Fandrick, O. Hucke, R. Kemper, S. P. F. Miller, P. J. Edwards, *J. Med. Chem.* **2011**, *54*, 7005-7022; c) S. R. LaPlante, P. J. Edwards, L. D. Fader, A. Jakalian, O. Hucke, *Chemmedchem* **2011**, *6*, 505-513.
- [147] a) W. Fu, W. Tang, *ACS Catal.* **2016**, *6*, 4814-4858; b) J.-H. Xie, Q.-L. Zhou, *Acc. Chem. Res.* **2008**, *41*, 581-593; c) M. P. Carroll, P. J. Guiry, *Chem. Soc. Rev.* **2014**, *43*, 819-833.
- [148] G. Bringmann, A. J. Price Mortimer, P. A. Keller, M. J. Gresser, J. Garner, M. Breuning, *Angew. Chem. Int. Ed.* **2005**, *44*, 5384-5427.
- [149] J. Frey, A. Malekafzali, I. Delso, S. Choppin, F. Colobert, J. Wencel-Delord, *Angew. Chem. Int. Ed.* **2020**, *59*, 8844-8848.
- [150] Y.-J. Wu, P.-P. Xie, G. Zhou, Q.-J. Yao, X. Hong, B.-F. Shi, *Chem. Sci.* **2021**, *12*, 9391-9397.
- [151] M. Maddani, J. Fiaud, H. Kagan, M. Todd, Wiley-VCH, Weinheim, **2014**.
- [152] E. M. Sletten, C. R. Bertozzi, *Angew. Chem. Int. Ed.* **2009**, *48*, 6974-6998.
- [153] a) T. Furuya, A. S. Kamlet, T. Ritter, *Nature* **2011**, *473*, 470-477; b) K. Müller, C. Faeh, F. Diederich, *Science* **2007**, *317*, 1881-1886.
- [154] B.-B. Zhan, Z.-S. Jia, J. Luo, L. Jin, X.-F. Lin, B.-F. Shi, *Org. Lett.* **2020**, *22*, 9693-9698.
- [155] a) O. Kitagawa, M. Kohriyama, T. Taguchi, *J. Org. Chem.* **2002**, *67*, 8682-8684; b) J. Terauchi, D. P. Curran, *Tetrahedron: Asymmetry* **2003**, *14*, 587-592.
- [156] a) C. J. Taylor, A. Pomberger, K. C. Felton, R. Grainger, M. Barecka, T. W. Chamberlain, R. A. Bourne, C. N. Johnson, A. A. Lapkin, *Chem. Rev.* **2023**, *123*, 3089-3126; b) J. C. A. Oliveira, J. Frey, S.-Q. Zhang, L.-C. Xu, X. Li, S.-W. Li, X. Hong, L. Ackermann, *Trends Chem.* **2022**, *4*, 863-885.
- [157] J. I. Martínez Alvarado, J. M. Meinhardt, S. Lin, *Tetrahedron Chem* **2022**, *1*, 100012.
- [158] L. Breiman, *Mach. Learn.* **1996**, *24*, 123-140.
- [159] B. Kamiński, M. Jakubczyk, P. Szufel, *Cent. Eur. J. Oper. Res.* **2018**, *26*, 135-159.
- [160] P. Geurts, D. Ernst, L. Wehenkel, *Mach. Learn.* **2006**, *63*, 3-42.
- [161] J. H. Friedman, *Ann. Stat.* **2001**, *29*, 1189-1232.
- [162] E. Fix, J. L. Hodges, *Int. Stat. Rev.* **1989**, *57*, 238-247.
- [163] G. C. Cawley, N. L. C. Talbot, *Neural Process. Lett.* **2002**, *16*, 293-302.
- [164] C. Cortes, V. Vapnik, *Mach. Learn.* **1995**, *20*, 273-297.
- [165] G. Biau, *J. Mach. Learn. Res.* **2012**, *13*, 1063-1095.
- [166] C. García, J. García, M. López Martín, R. Salmerón, *J. Appl. Stat.* **2015**, *42*, 648-661.
- [167] Y. Zhang, L. Chen, *Theor. Econ. Lett.* **2021**, *11*, 258.

References

- [168] a) S. S. Woodard, M. G. Finn, K. B. Sharpless, *J. Am. Chem. Soc.* **1991**, *113*, 106-113; b) P. H.-Y. Cheong, C. Y. Legault, J. M. Um, N. Çelebi-Ölçüm, K. N. Houk, *Chem. Rev.* **2011**, *111*, 5042-5137.
- [169] R. R. Knowles, E. N. Jacobsen, *India* **2010**, *107*, 20678-20685.
- [170] a) J. M. Crawford, C. Kingston, F. D. Toste, M. S. Sigman, *Acc. Chem. Res.* **2021**, *54*, 3136-3148; b) A. F. Zahrt, S. V. Athavale, S. E. Denmark, *Chem. Rev.* **2020**, *120*, 1620-1689; c) A. C. Mater, M. L. Coote, *J. Chem. Inf. Model.* **2019**, *59*, 2545-2559.
- [171] M. J. Mio, L. C. Kopel, J. B. Braun, T. L. Gadzikwa, K. L. Hull, R. G. Brisbois, C. J. Markworth, P. A. Grieco, *Org. Lett.* **2002**, *4*, 3199-3202.
- [172] D. Maiti, S. L. Buchwald, *J. Org. Chem.* **2010**, *75*, 1791-1794.
- [173] M. San Segundo, A. Correa, *Chem. Sci.* **2020**, *11*, 11531-11538.
- [174] K. Grudzień, B. Trzaskowski, M. Smoleń, R. Gajda, K. Woźniak, K. Grela, *Dalton Trans.* **2017**, *46*, 11790-11799.
- [175] J. Zhang, S. Zhang, H. Zou, *Org. Lett.* **2021**, *23*, 3466-3471.
- [176] J. Zhang, Q. Xu, J. Fan, L. Zhou, N. Liu, L. Zhu, J. Wu, M. Xie, *Org. Chem. Front.* **2021**, *8*, 3404-3412.
- [177] B. Qi, L. Fang, Q. Wang, S. Guo, P. Shi, B. Chu, J. Zhu, *Tetrahedron Lett.* **2020**, *61*, 151771.
- [178] M. Sen, D. Kalsi, B. Sundararaju, *Chem. Eur. J.* **2015**, *21*, 15529-15533.
- [179] S.-C. Chuang, P. Gandeepan, C.-H. Cheng, *Org. Lett.* **2013**, *15*, 5750-5753.
- [180] K. Raghuvanshi, K. Rauch, L. Ackermann, *Chem. Eur. J.* **2015**, *21*, 1790-1794.

7 Acknowledgements

I extend my sincere gratitude to all those who have contributed to the completion of my doctoral journey, directly or indirectly.

Foremost, I express my deepest appreciation to Professor Dr. Lutz Ackermann, my doctoral supervisor, for his unwavering support, exceptional guidance, and trust in my abilities. Professor Ackermann's scientific creativity and dedication have been a constant source of inspiration. Besides him, I would like to thank Prof. Dr. Konrad Koszinowski and Prof. Dr. Dietmar Stalke for their willingness to serve as my second and third supervisors. Valuable suggestions from them have helped significantly to assess my work and improve further. I also would like to thank the members of the examination committee, Jun.-Prof. Dr. Nadja A. Simeth, Dr. Holm Frauendorf and Dr. Michael John for their participation.

Financial support from the Chinese Scholarship Council and Prof. Dr. Lutz Ackermann has been crucial in facilitating my research endeavors, and I am sincerely grateful for their generosity.

Furthermore, I would like to extend special thanks to the analytical departments at the IOBC for measuring my samples. I would like to highlight Dr. Golz for conducting measurements and solving crystal structures.

I gratefully acknowledge Ms. Gabriele Keil-Knepel, Bianca Spitalieri, Sabine Schacht, Vanessa Bergmann and Svenja Warratz for their kind assistance for the administrative works. I sincerely thank Mr. Stefan Beußhausen and Mr. Karsten Rauch for their kind support in ensuring the smooth running of the laboratory.

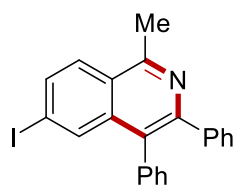
My sincere thanks also go to all the members of our group, past and present, for great work atmosphere, teamwork and companionship. I sincerely thank Dr. Leonardo Massignan, Dr. Joao Carlos Agostinho de Oliveira, Dr. Johanna Frey, Dr. Xuefeng Tan, Dr. Uttam Dhawa, Dr. Nikolaos Kaplaneris, Binbin Yuan, Tsuyoshi Ohyama, Max Surke, Zhipeng Lin, Dr. Antonis M. Messinis, Dr. Tomasz Wdowik, Dr. Isaac Choi, Dr. Cuiju Zhu, Aude Salamé, Masoom Nasuha Hussain, Chenhang Chao, Shu-Wen Li and Prof. Dr. Hong for their help on my projects. Many thanks to Dr. Alexej Scheremetjew, Tsuyoshi Ohyama, Ye Lin, Zhipeng Lin, Hendrik Simon, Yang Xu, and Tristan von Münchow for their time to correct this thesis. I particularly thank my lab mates during my PhD namely, Leonardo, Tjark, Lin, Agnese, Beckey, Bin, Alexej, Cuiju, Simon, Hendrik, Rong, Takuya and Triston for the fun atmosphere and chats about all different topics. Of course, I want to thank all the other group members who made the work and leisure activities in the Ackermann group so enjoyable. Special

Acknowledgements

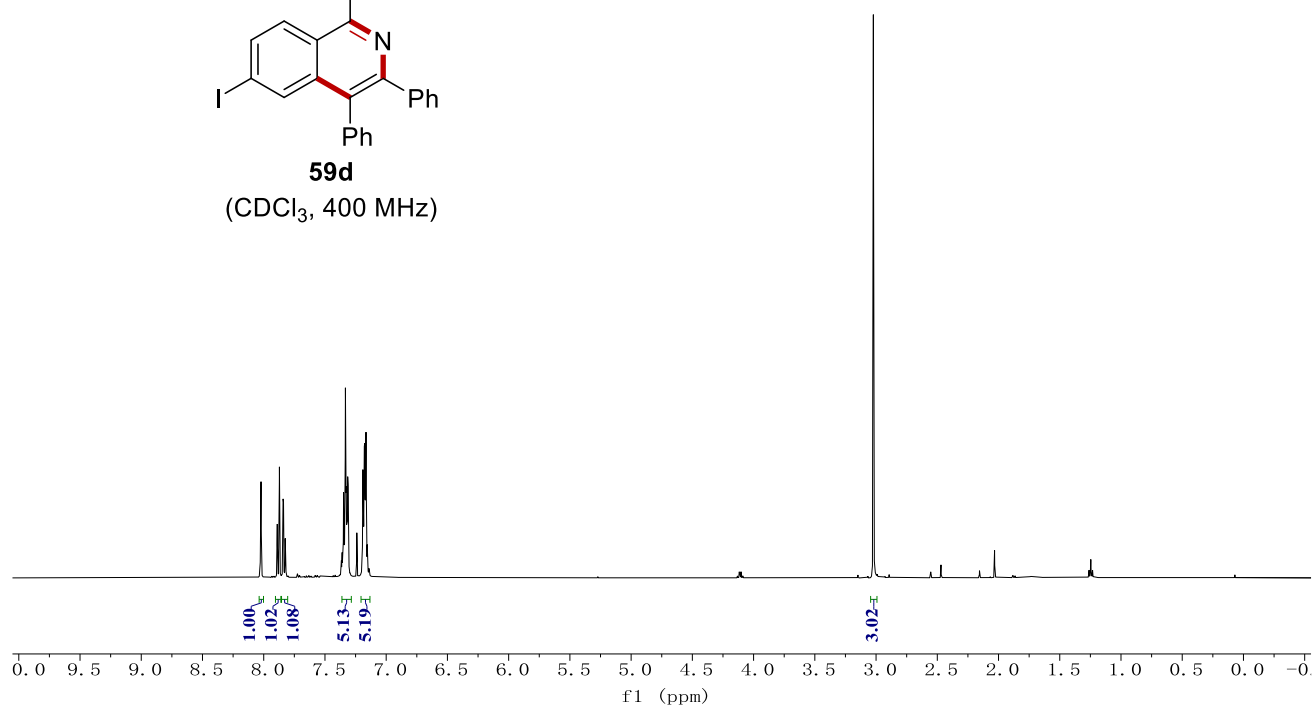
moments during the trips to Köln, Goslar, Königssee, and Basel, BBQs, PhD parties, flunky ball games and many more will keep you in my memories. Especially, I really enjoyed the football games with Tsuyoshi, Alexej, Maximilian, Takuya, Isaac, Max, Rong, Valentina, Sven, Simon, Philipp, Felix, Hendrik, Ye, Tristan, Can, Yulei, Matthias, Neeraj, Yanjun, Antonis, Matthew, Leonardo, Rajeshwaran, Oliver and others. I also treasure the wonderful girls' times and interesting chats with Lina, Julia Pöhlmann, Julia Struwe, Binbin, Xuexue, Xinran and Rong.

Last but not the least, I would like to express my deepest gratitude to my family for their unconditional support and encouragement.

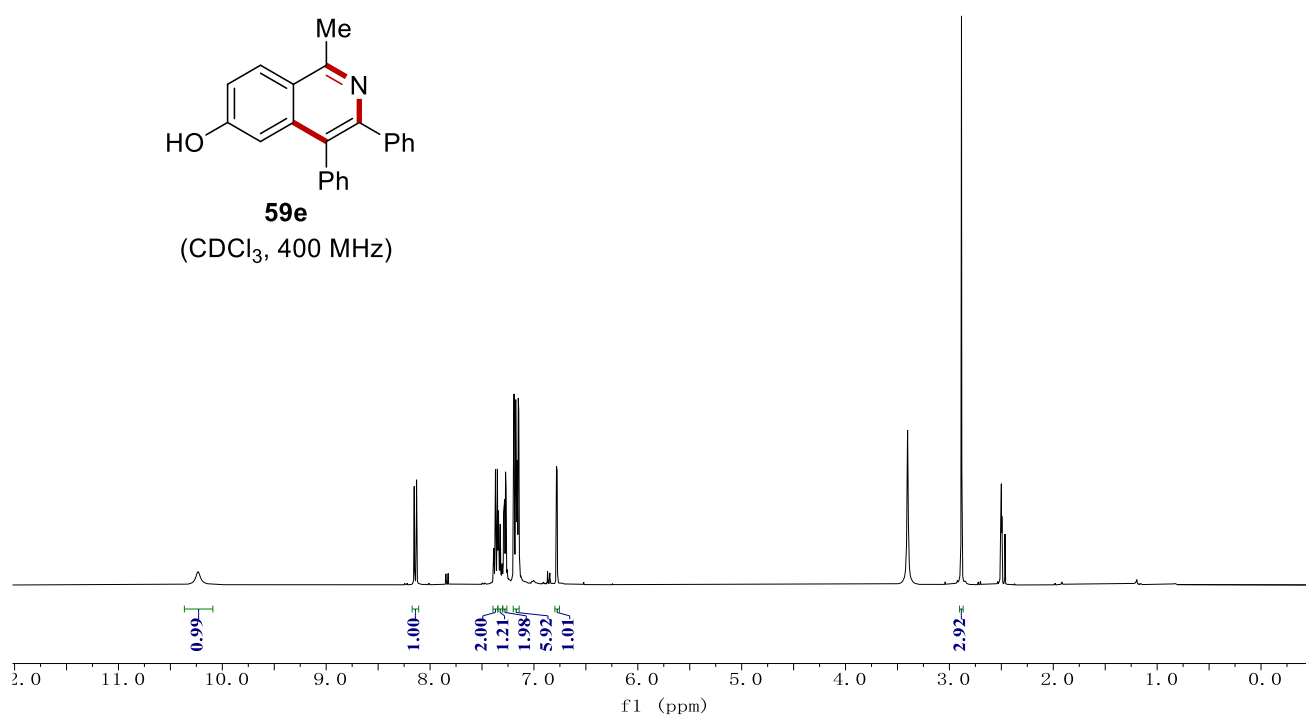
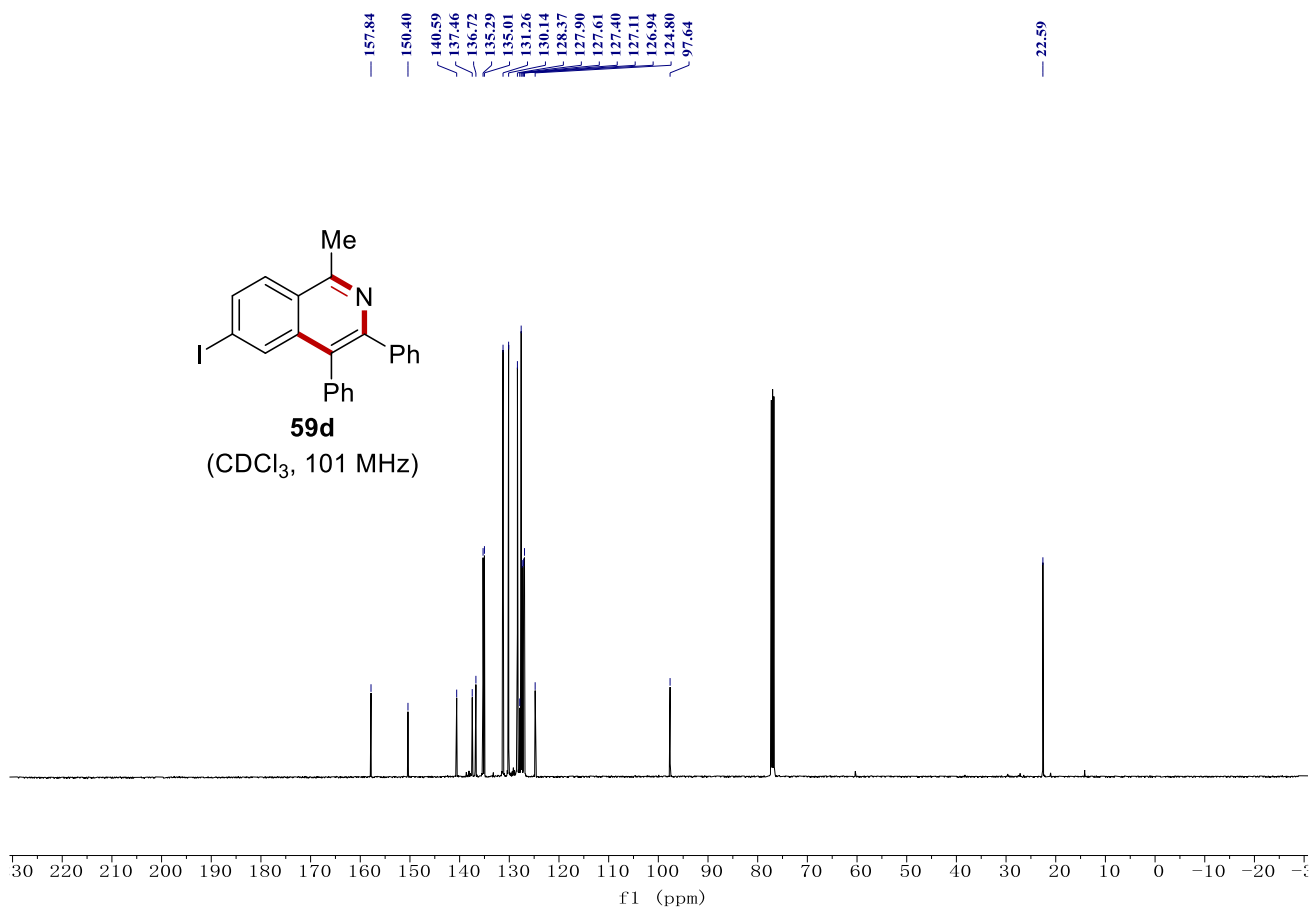
8 NMR Spectra



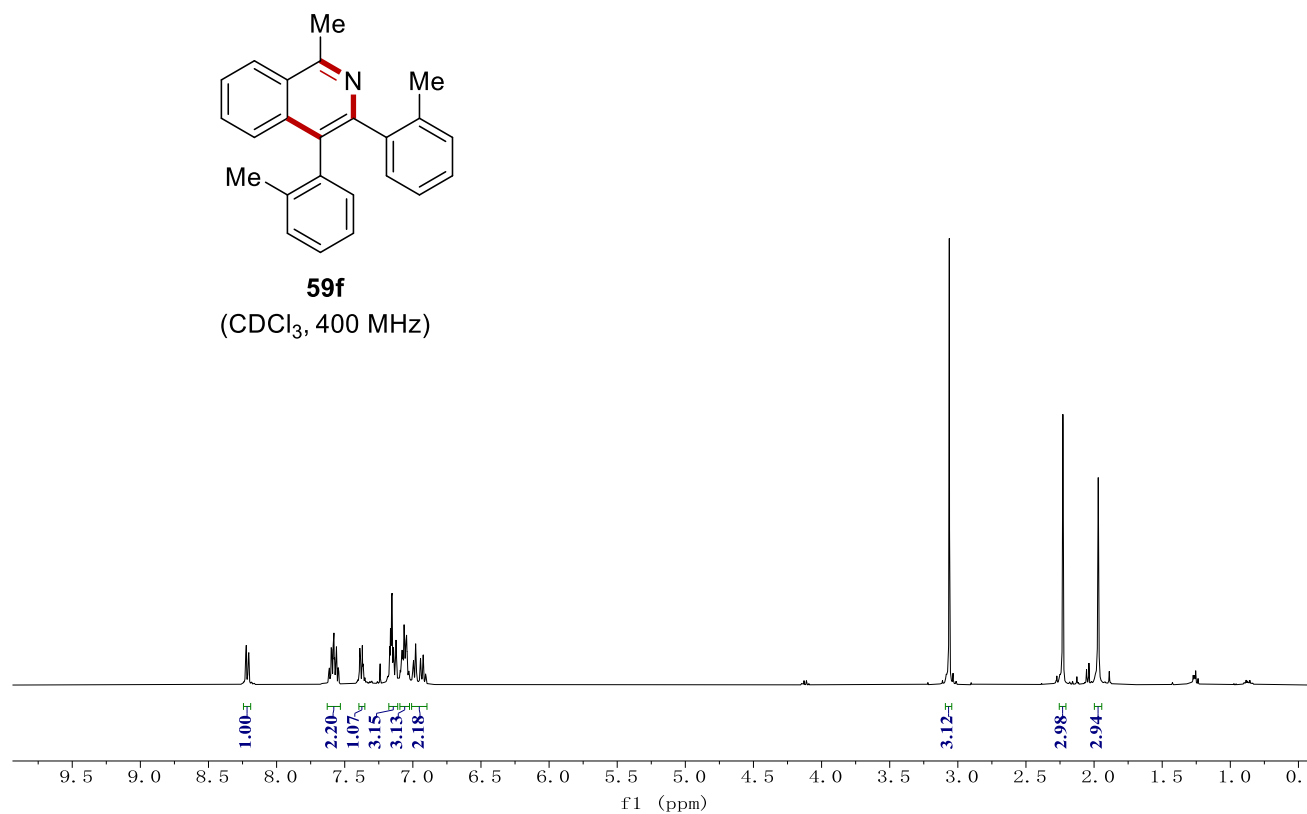
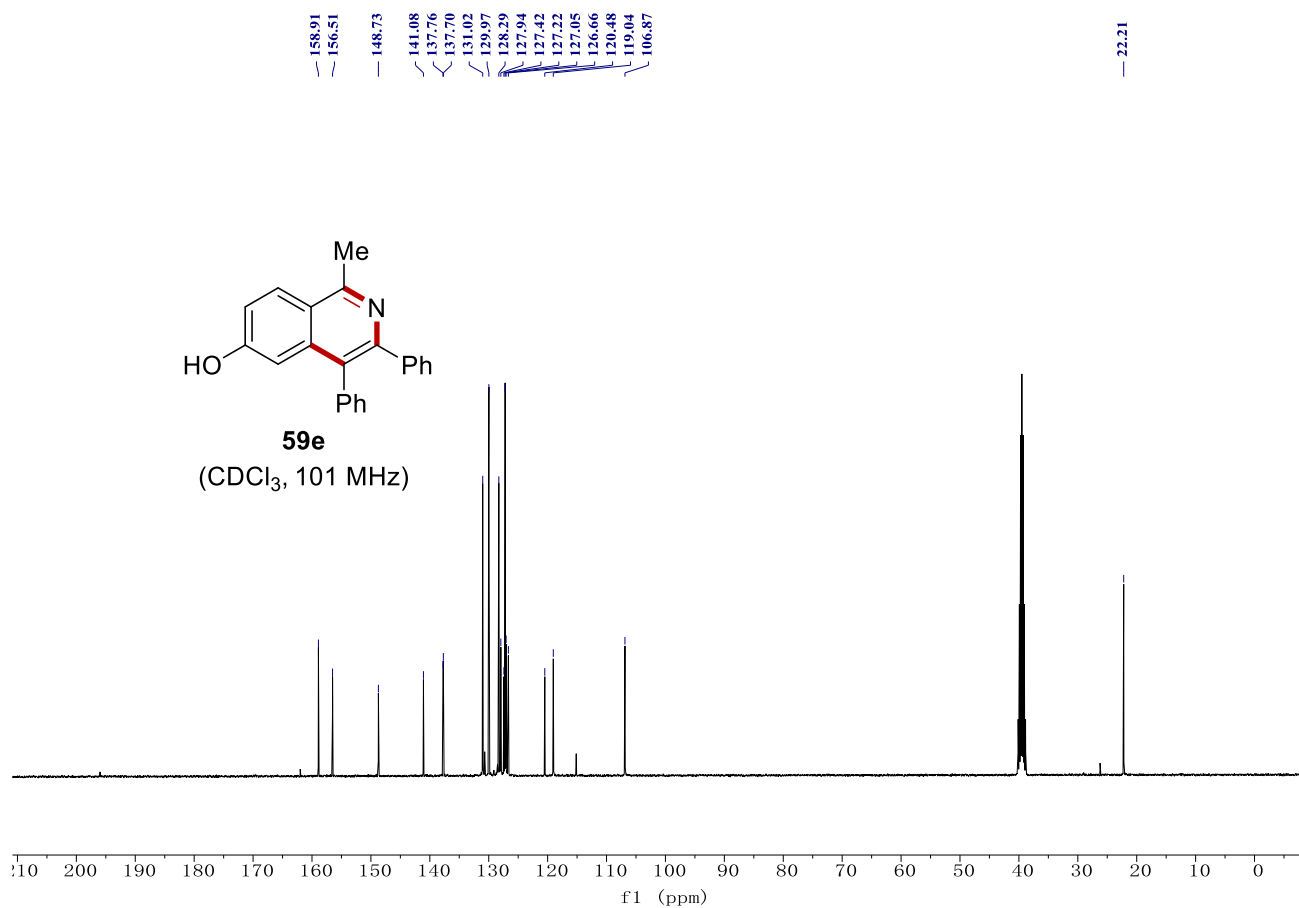
59d
(CDCl₃, 400 MHz)



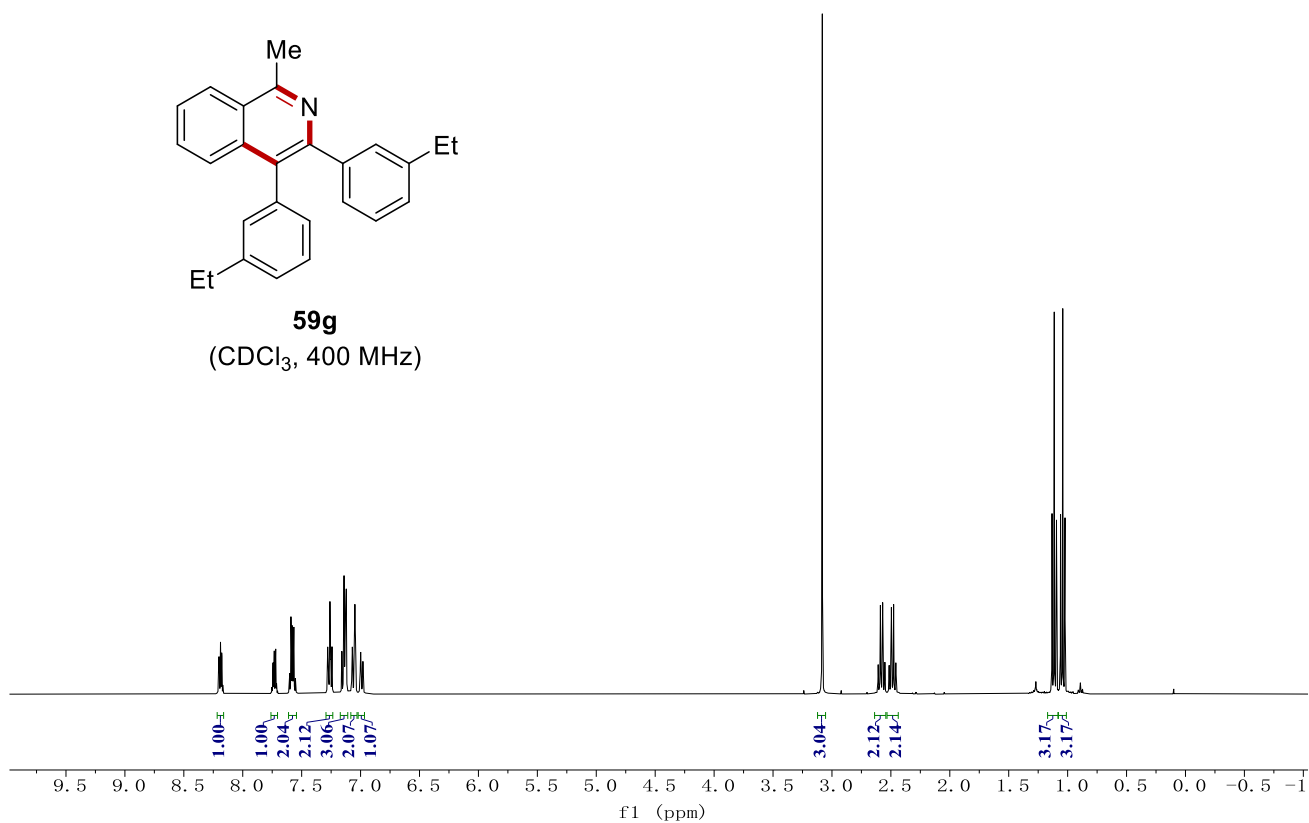
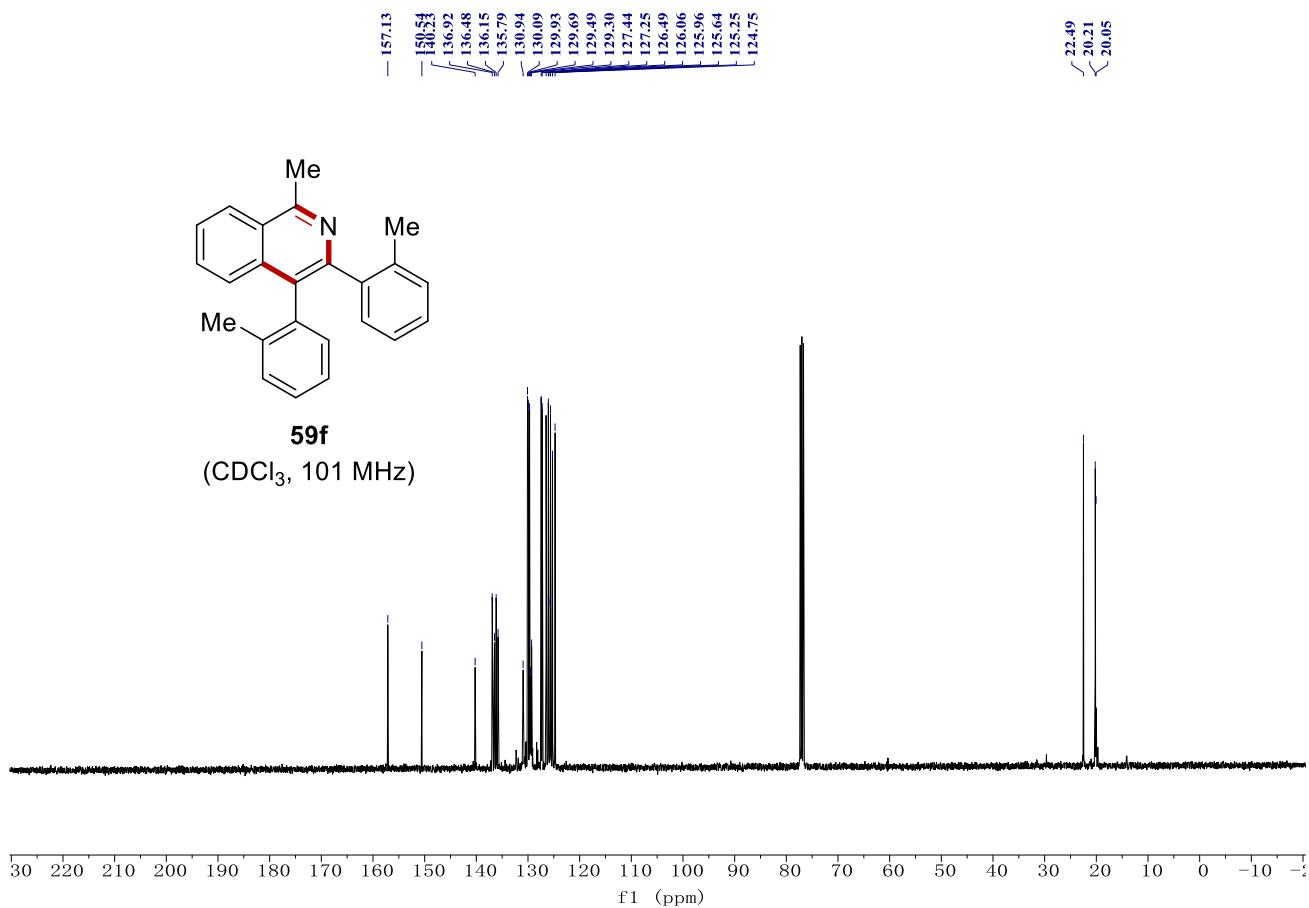
NMR Spectra



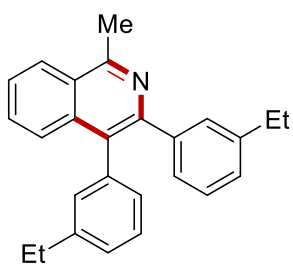
NMR Spectra



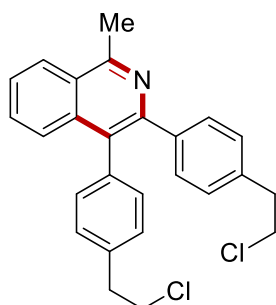
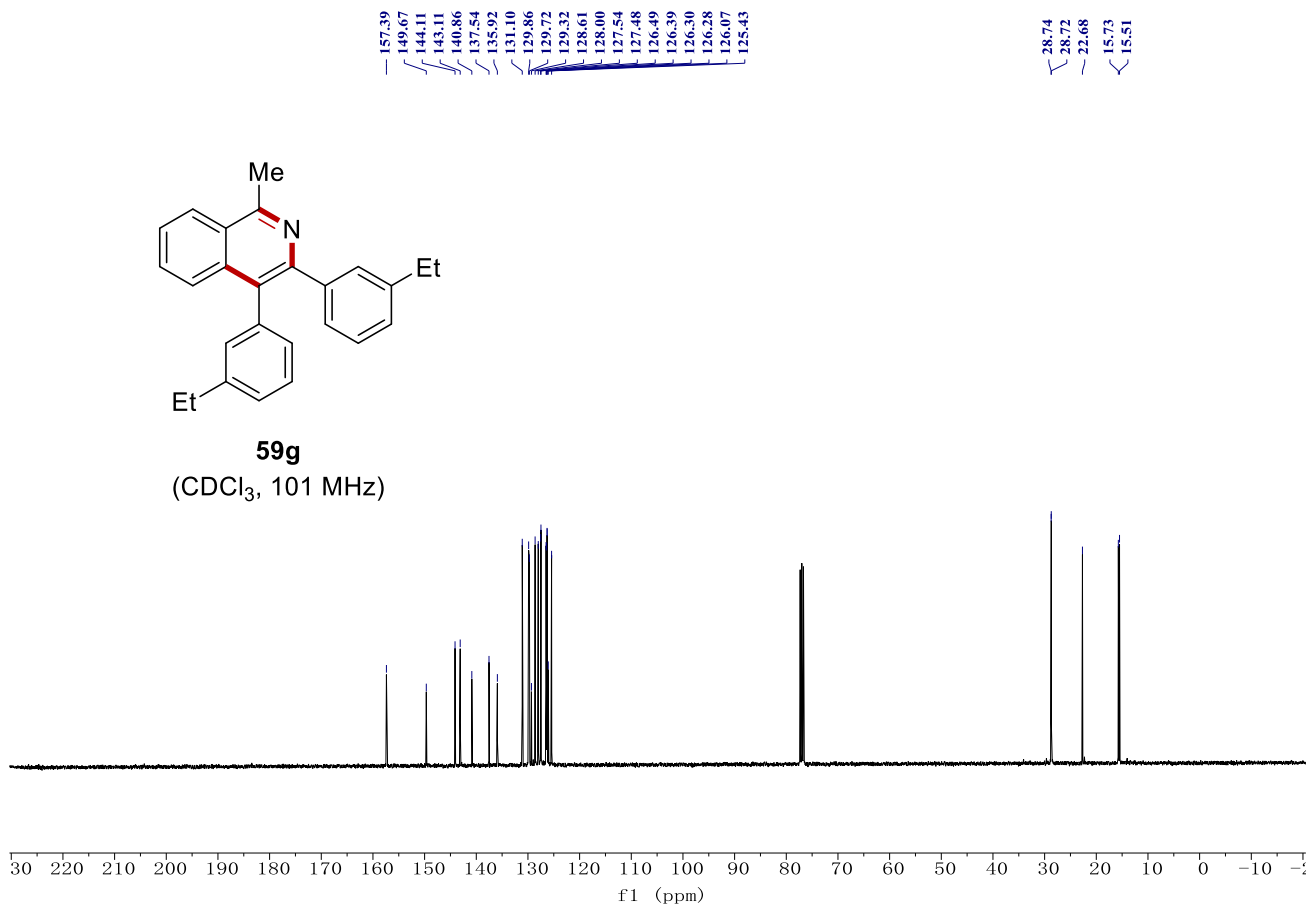
NMR Spectra



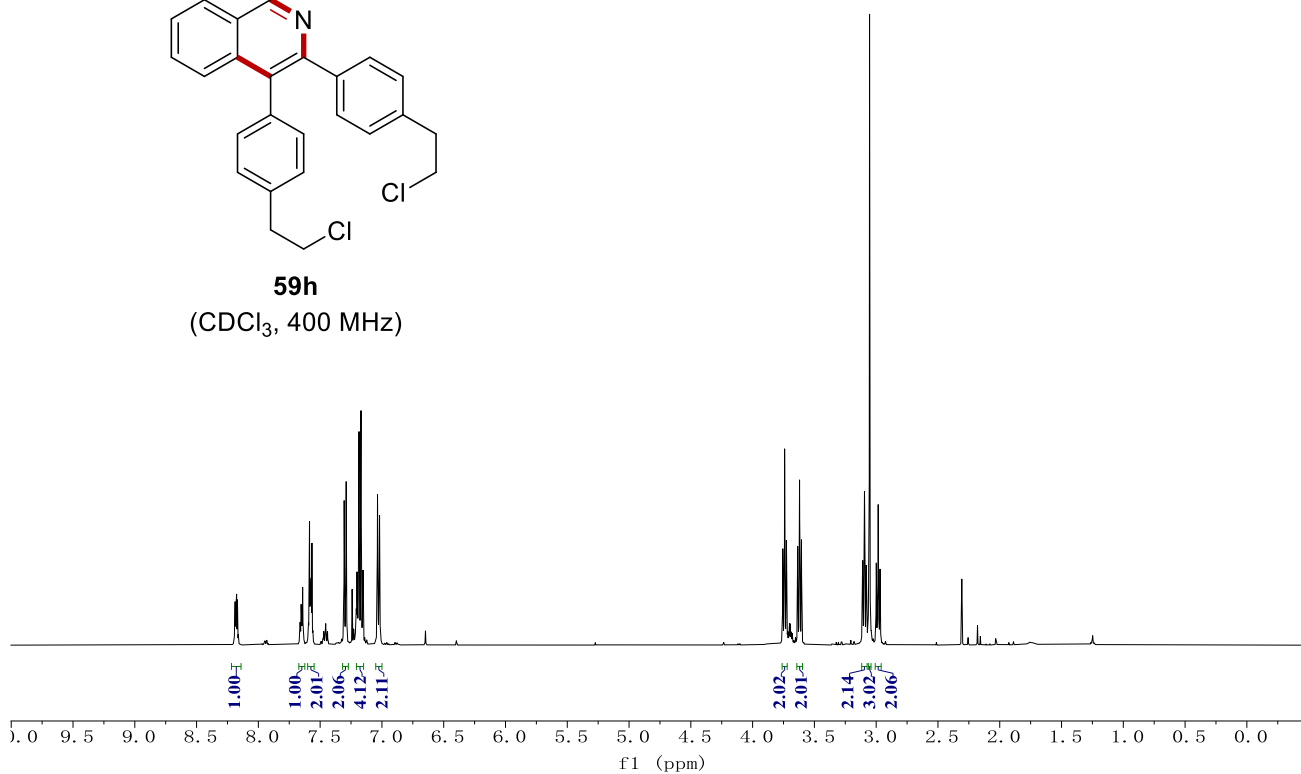
NMR Spectra



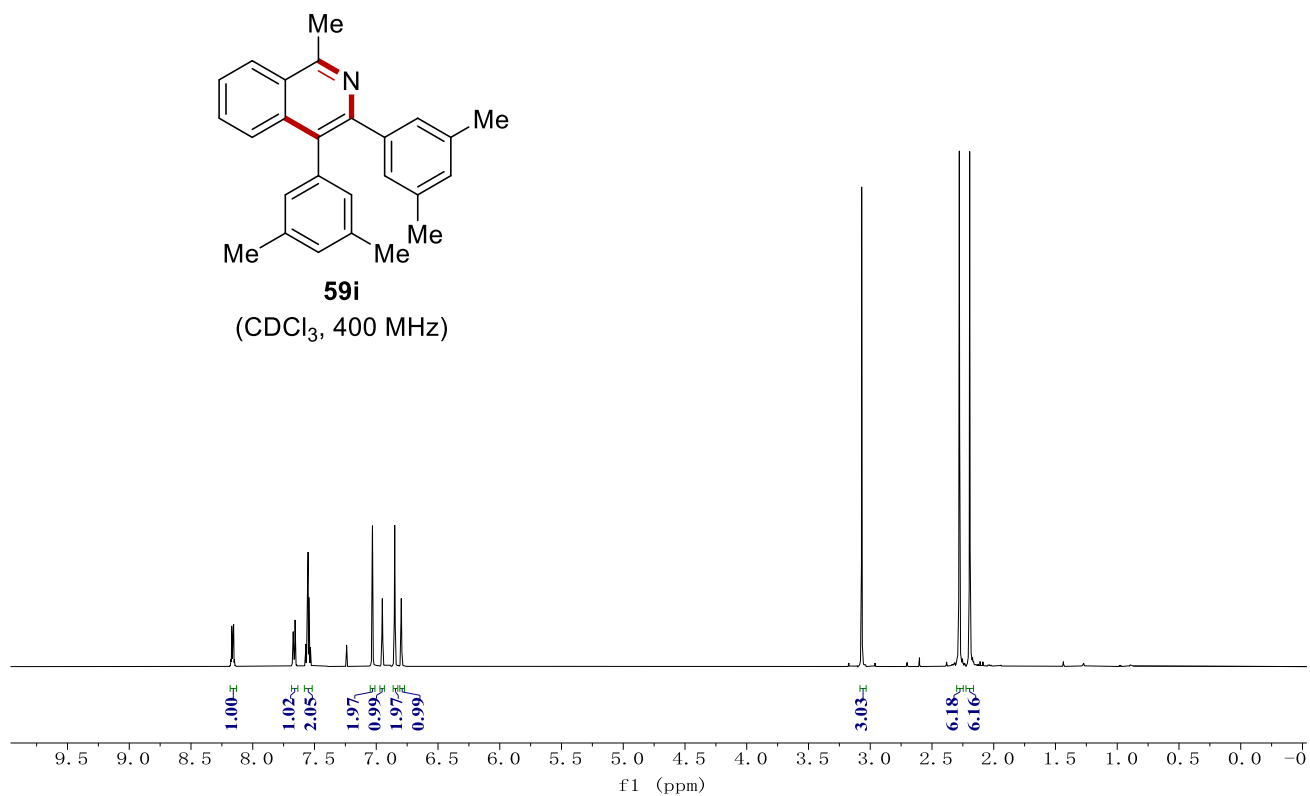
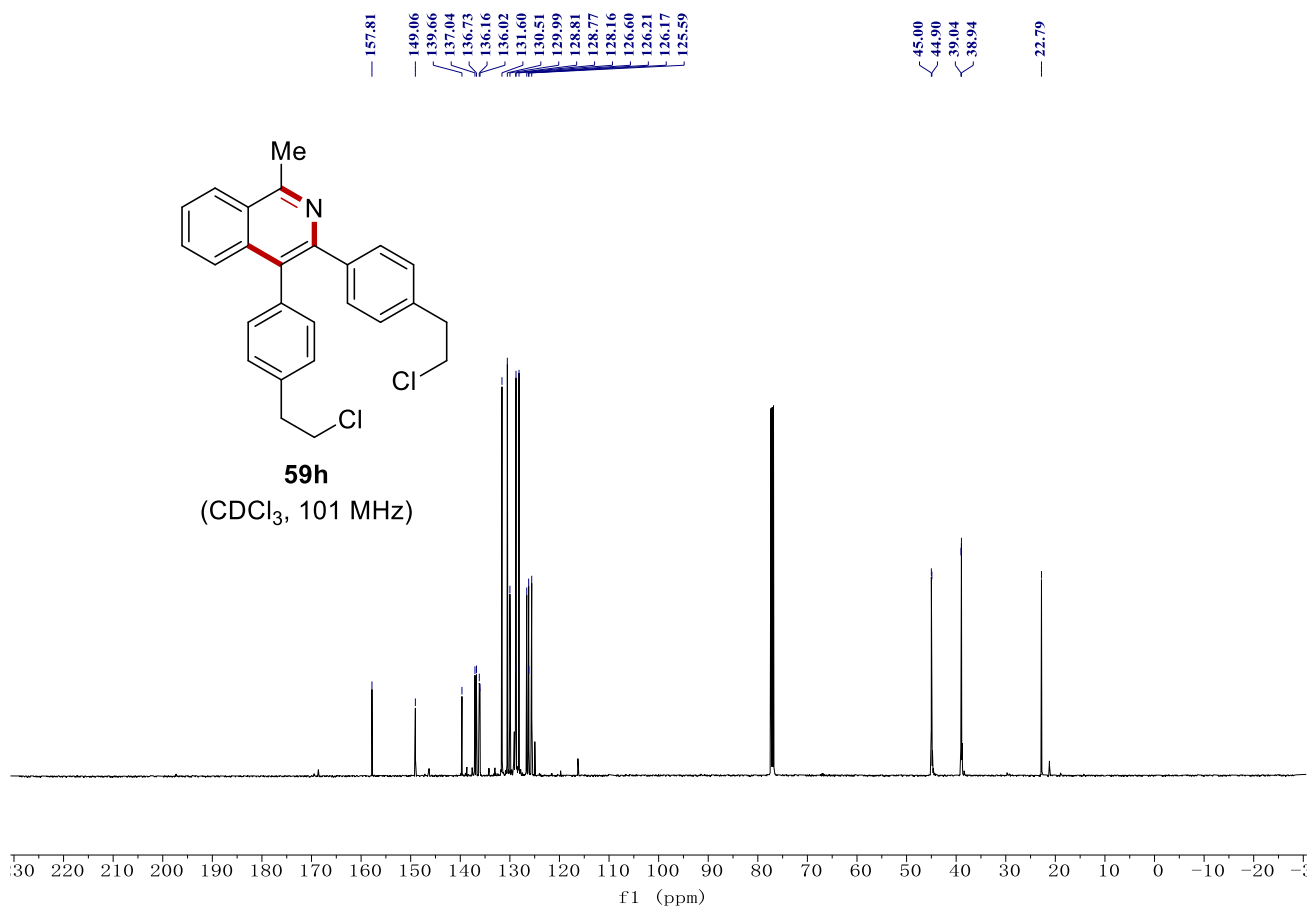
59g
(CDCl₃, 101 MHz)



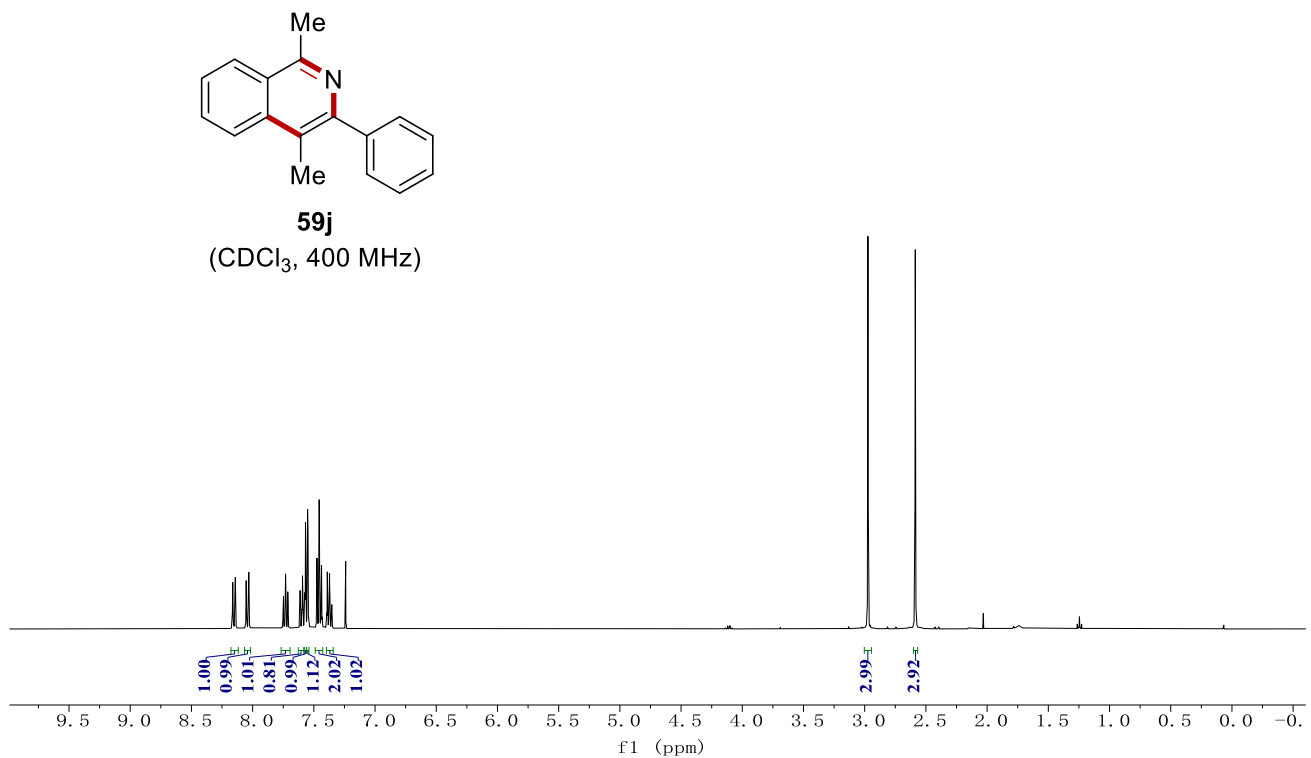
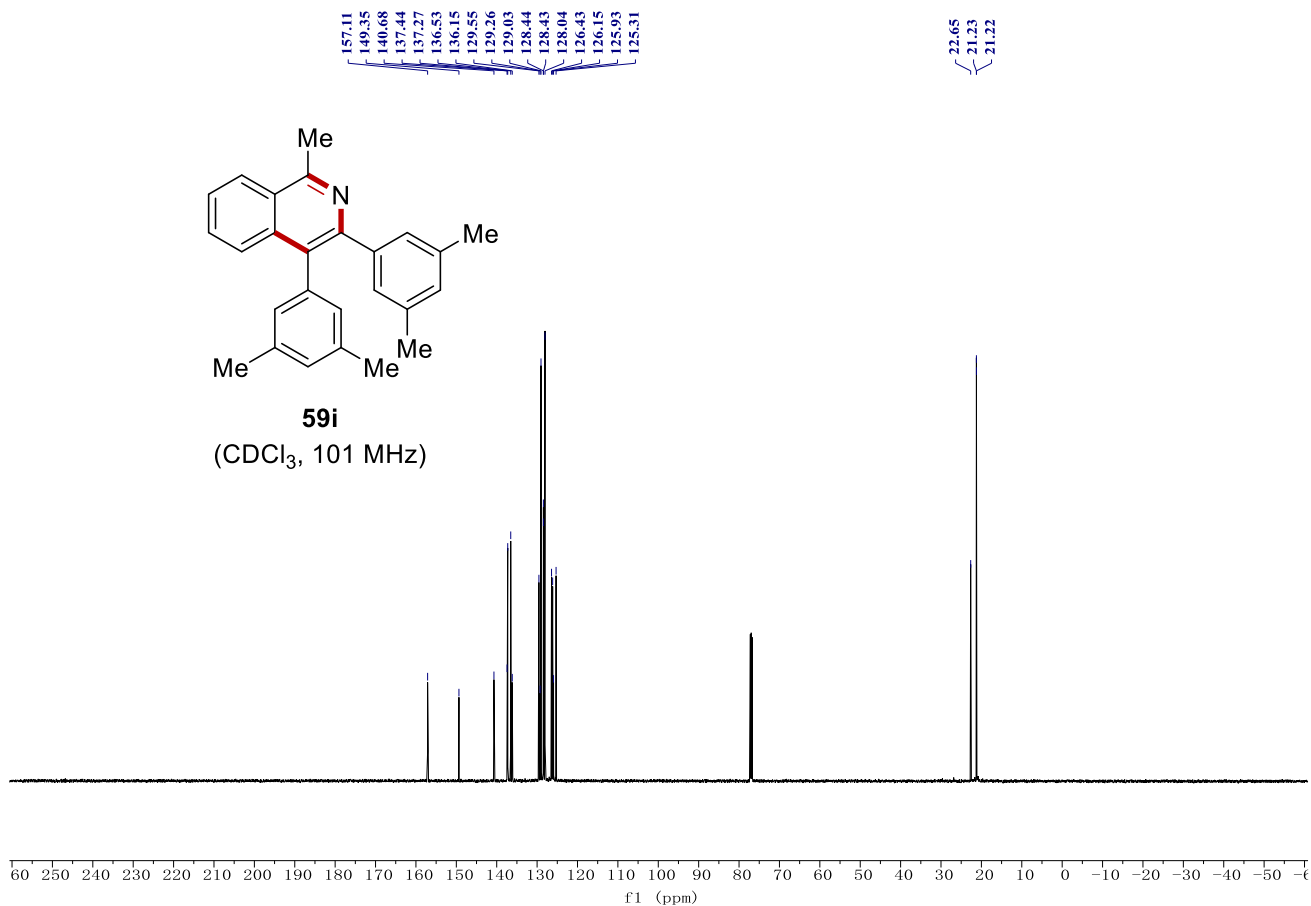
59h
(CDCl₃, 400 MHz)



NMR Spectra



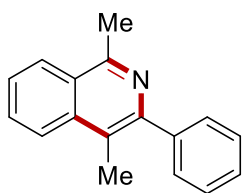
NMR Spectra



NMR Spectra

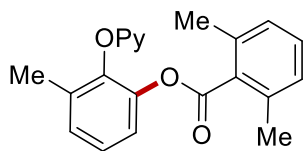
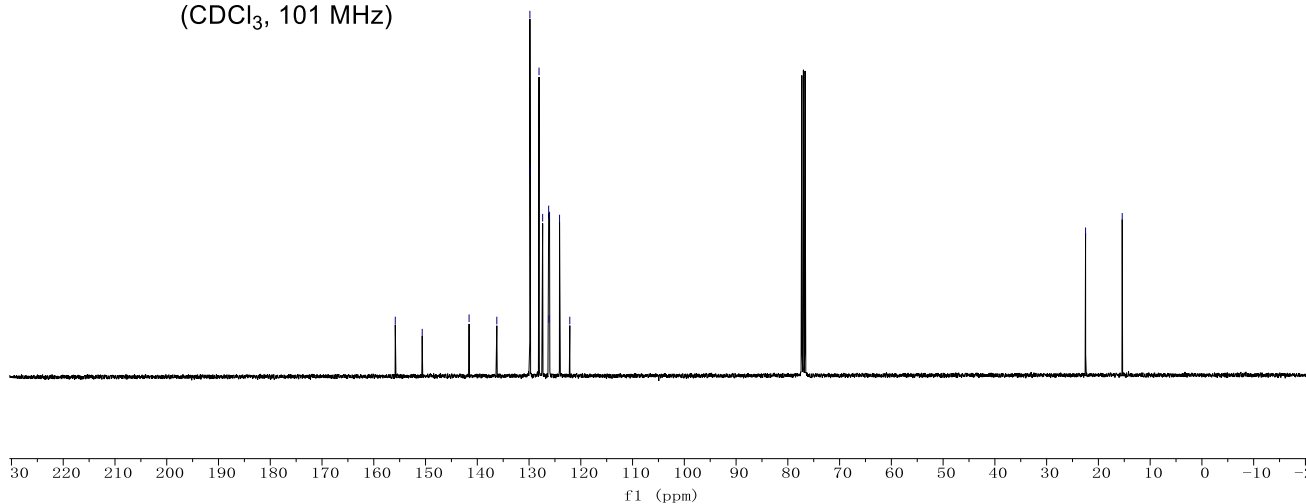
155.85
150.64
141.59
136.23
129.84
129.82
128.07
127.37
126.21
126.15
126.04
124.11
122.13

22.48
15.40



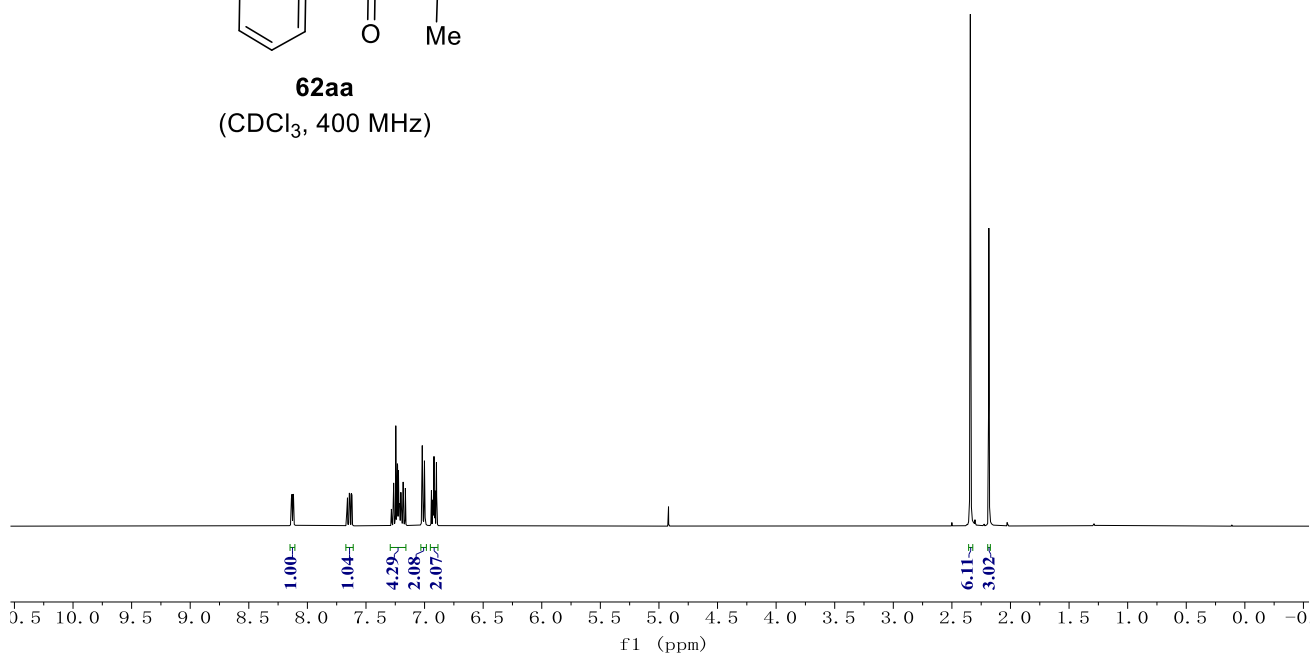
59j

(CDCl₃, 101 MHz)



62aa

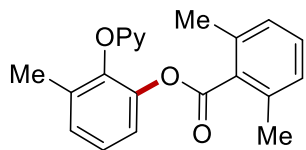
(CDCl₃, 400 MHz)



NMR Spectra

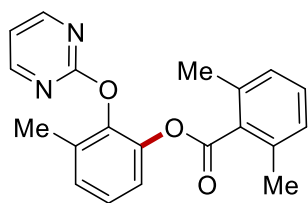
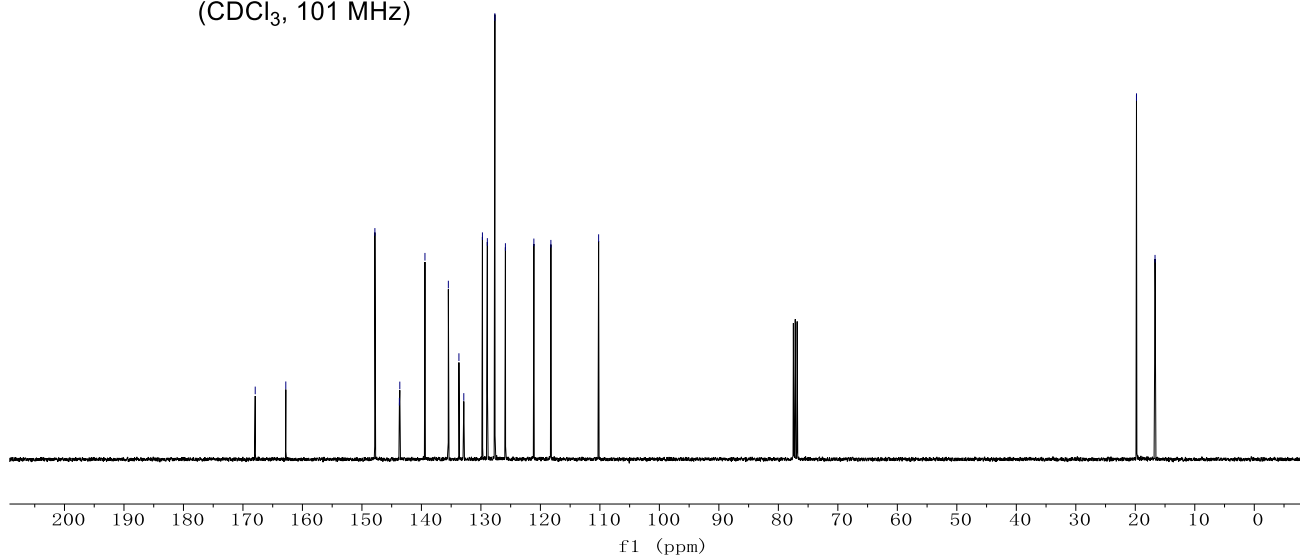
167.94
162.80
147.82
143.71
143.63
139.41
135.47
133.70
132.88
129.74
128.92
127.65
125.88
121.10
118.24
110.21

19.80
16.68



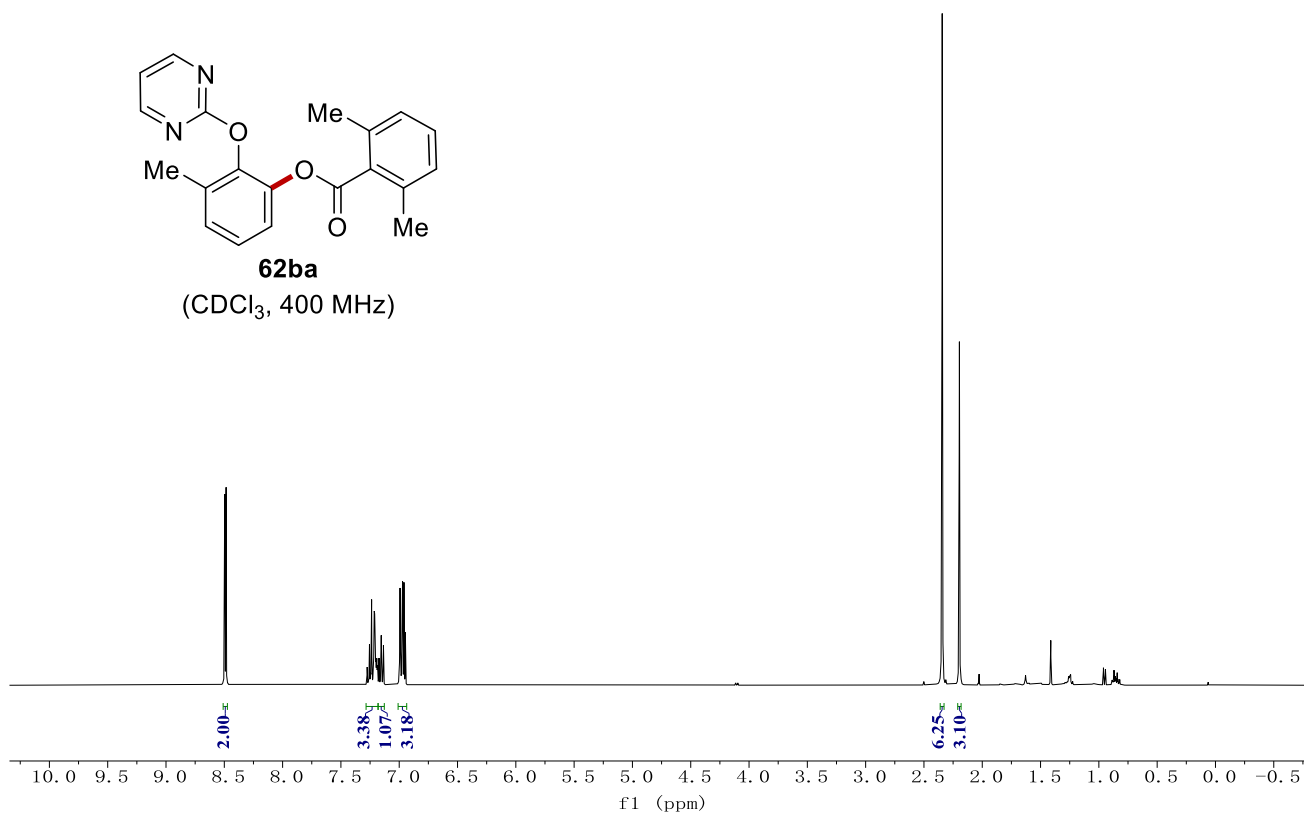
62aa

(CDCl₃, 101 MHz)

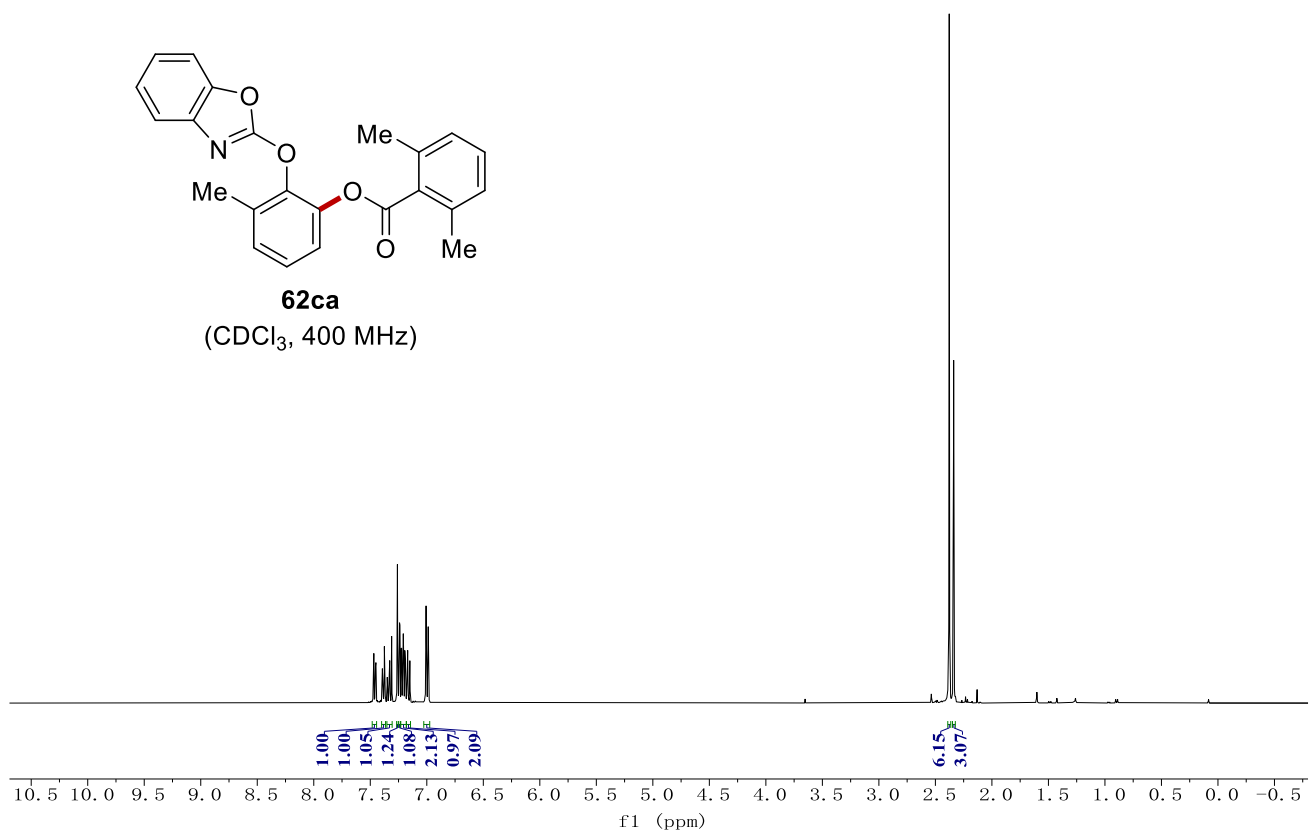
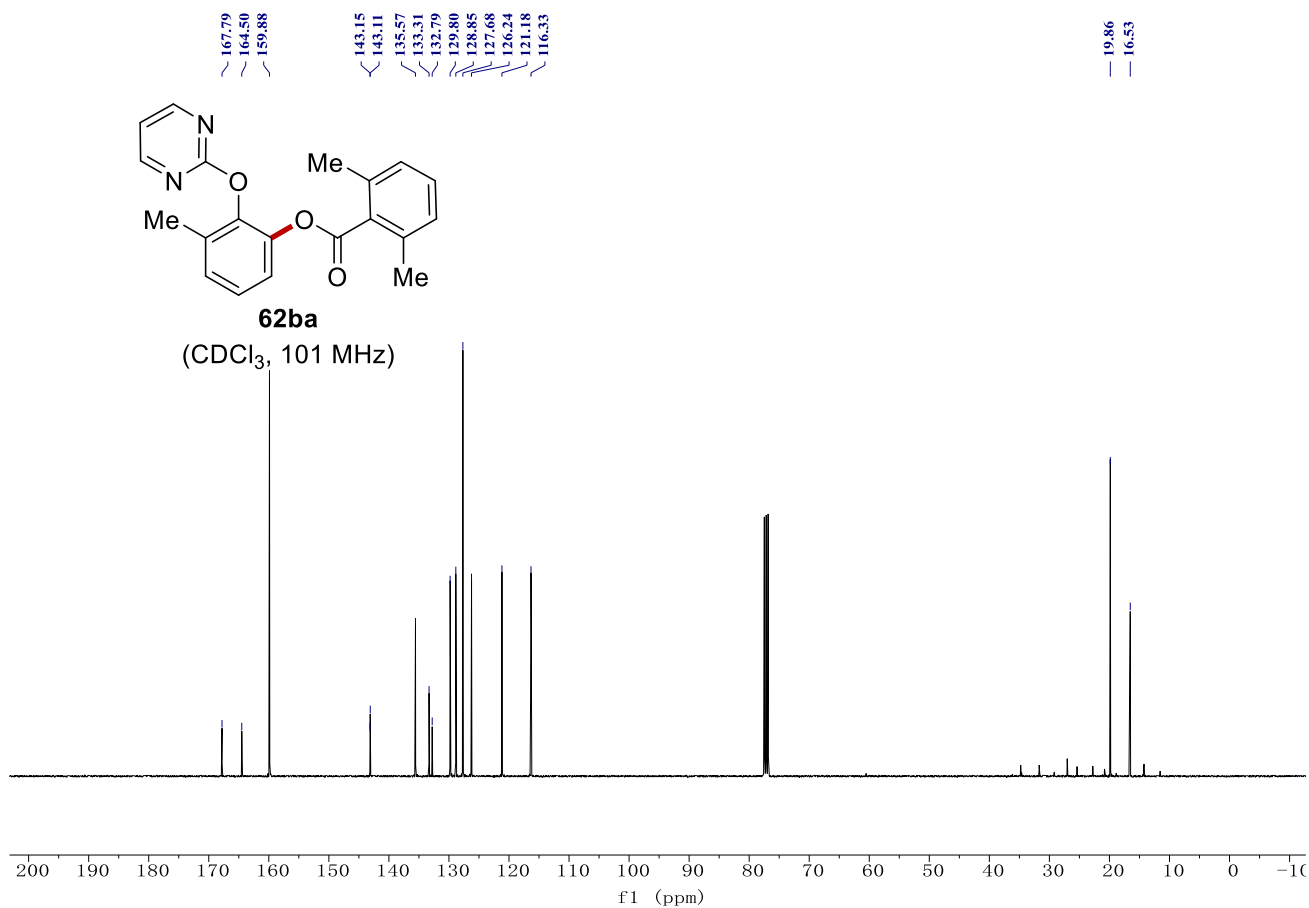


62ba

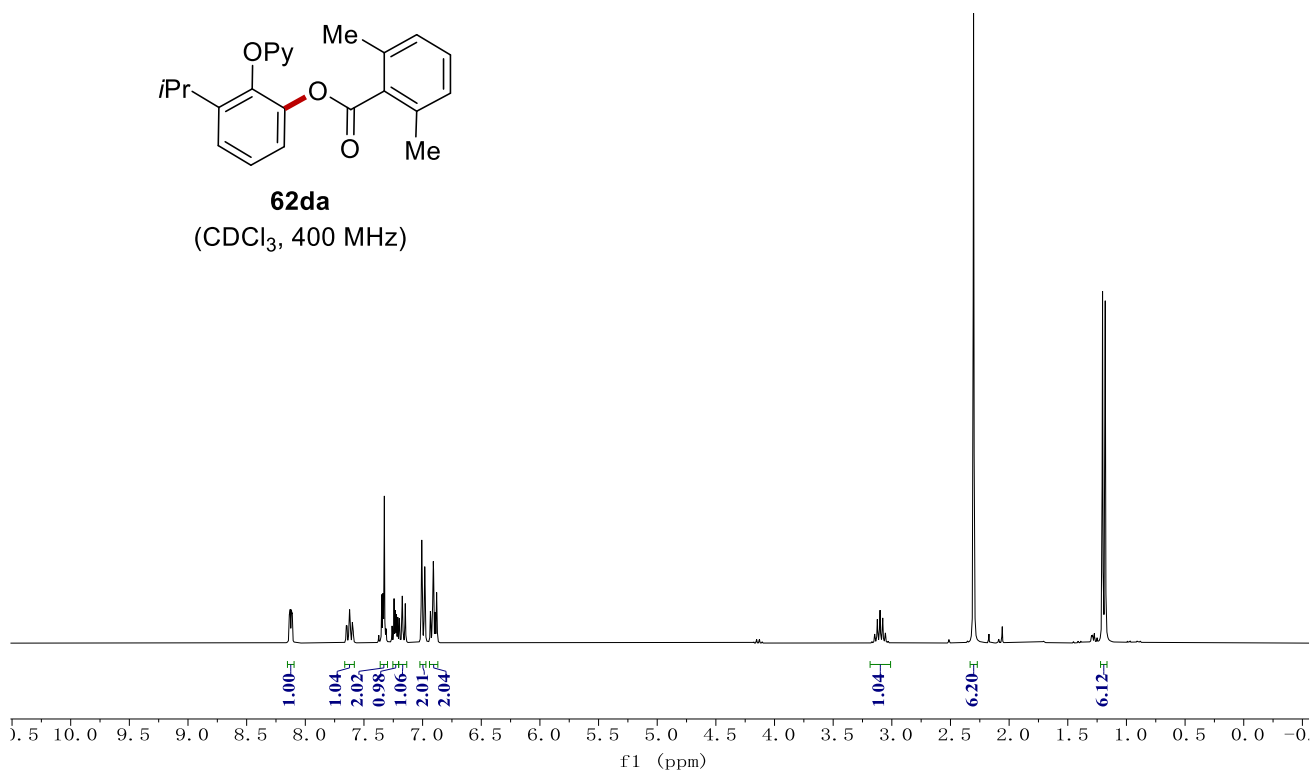
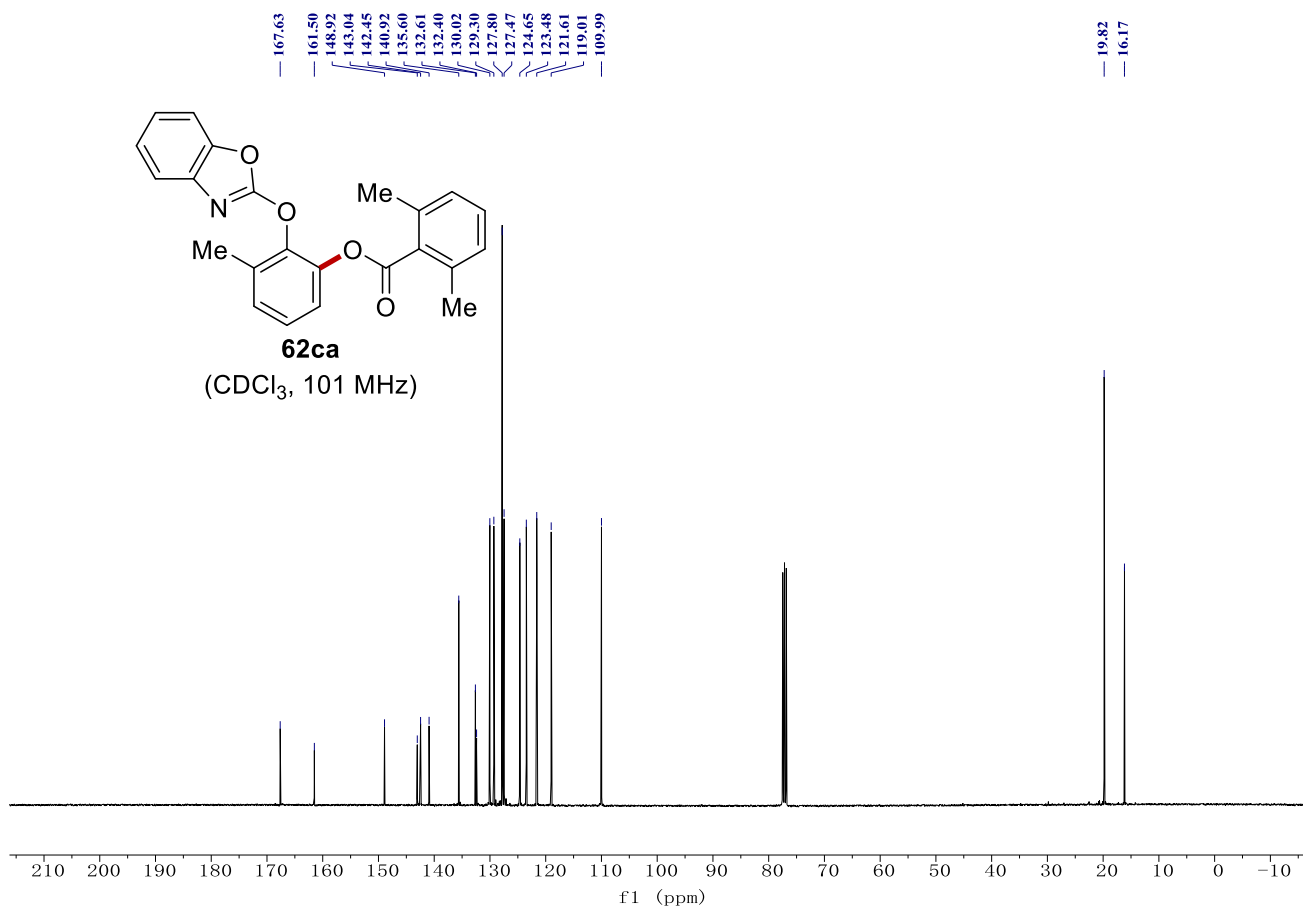
(CDCl₃, 400 MHz)



NMR Spectra



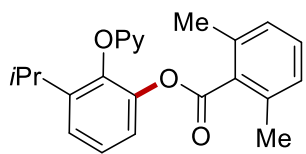
NMR Spectra



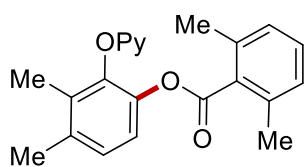
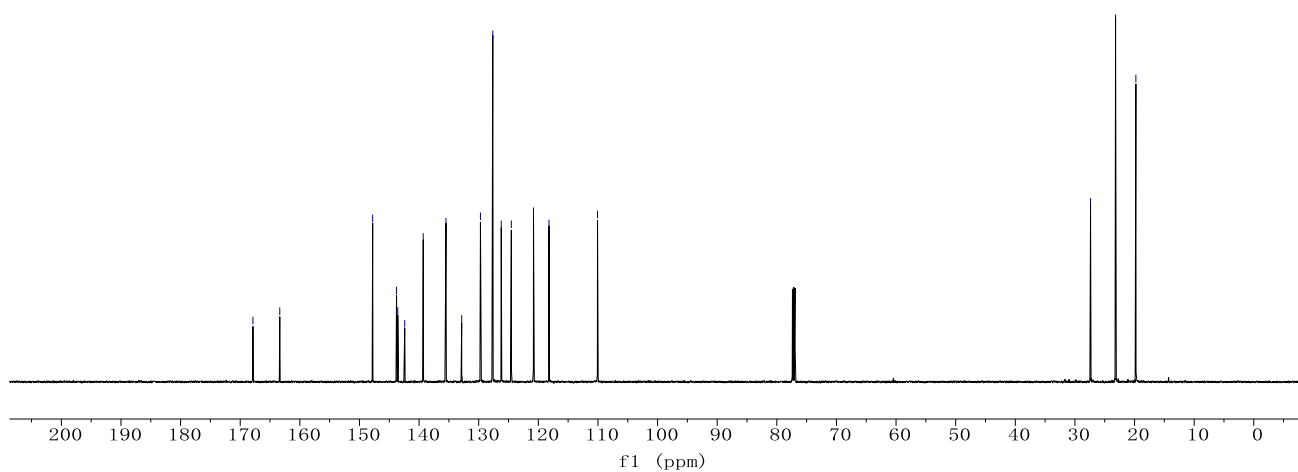
NMR Spectra

167.87
163.37
147.78
143.78
142.41
139.31
135.49
132.85
129.71
127.64
126.22
124.53
120.81
118.21
110.07

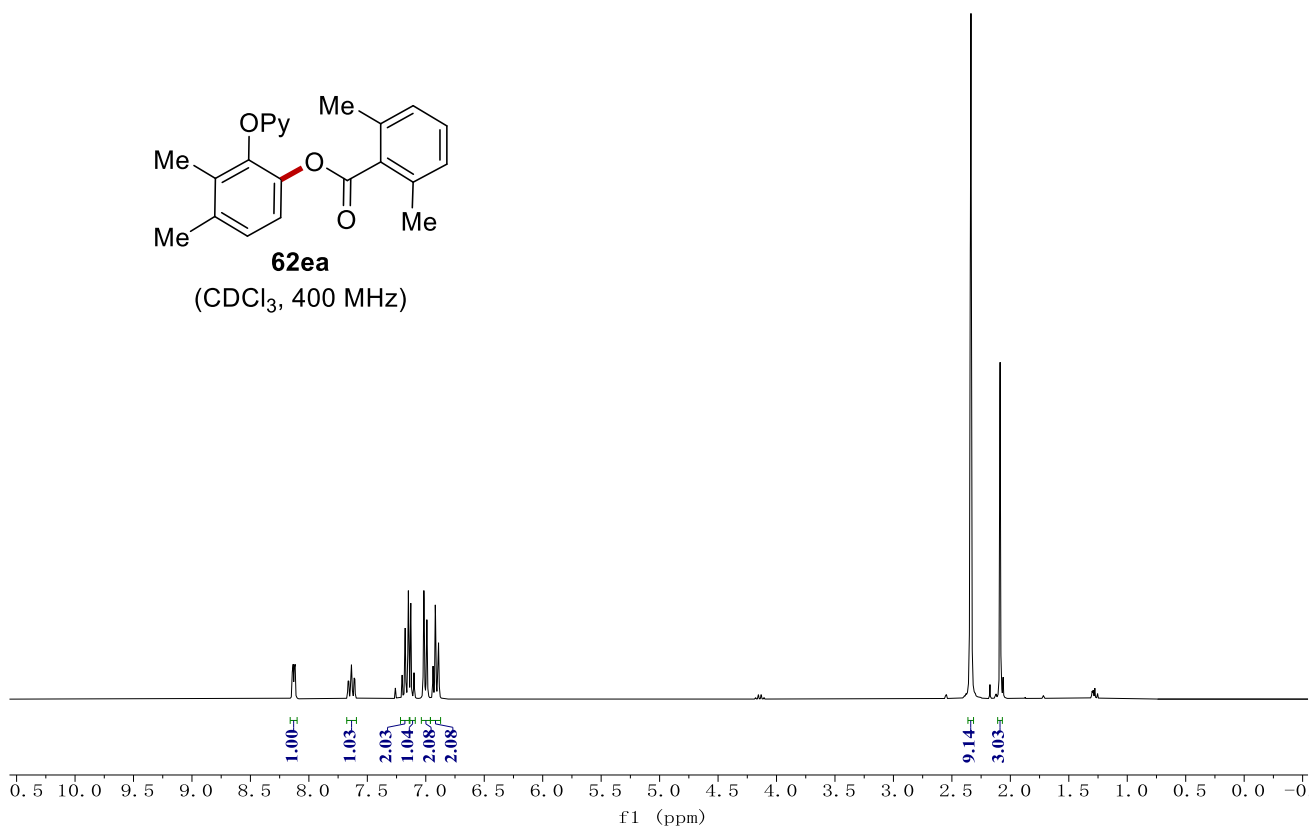
27.38
23.18
19.78



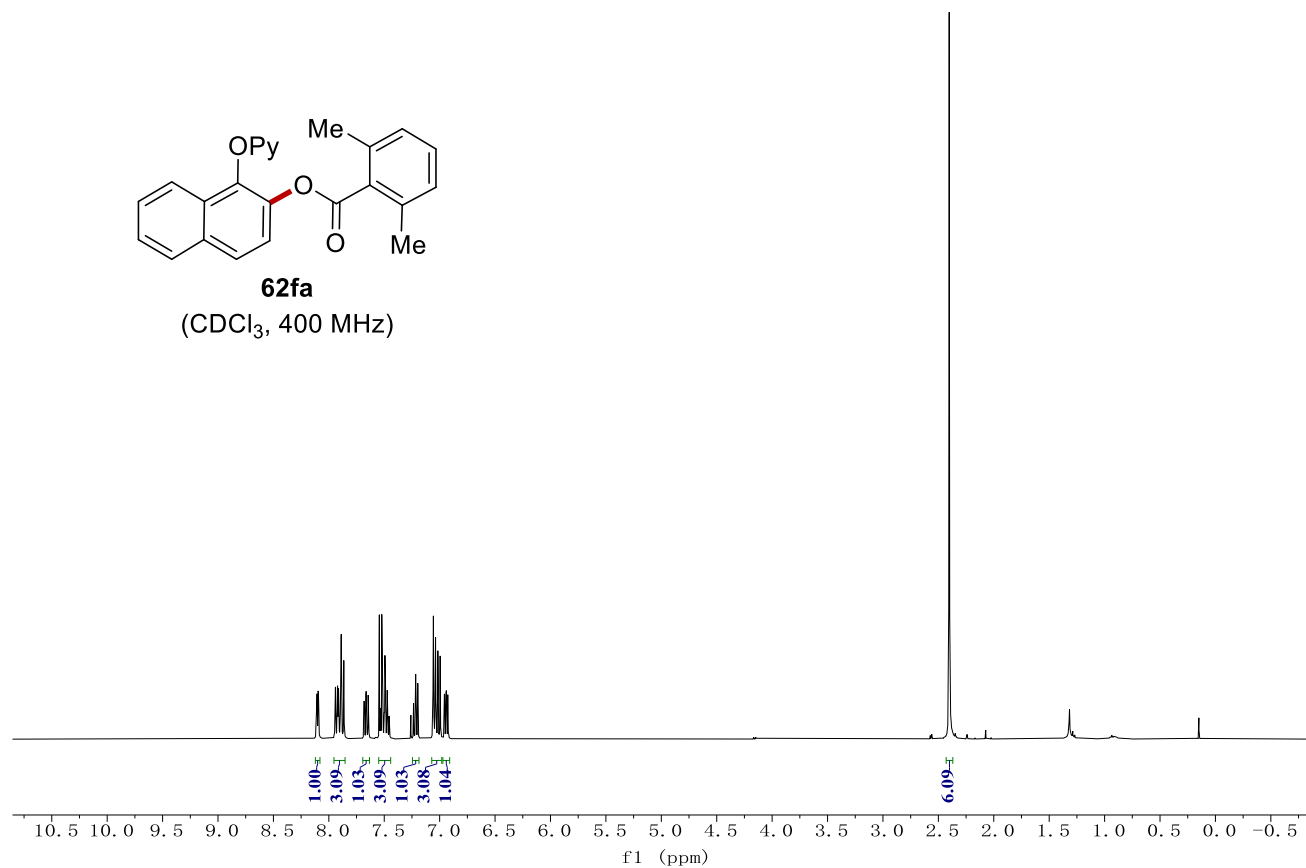
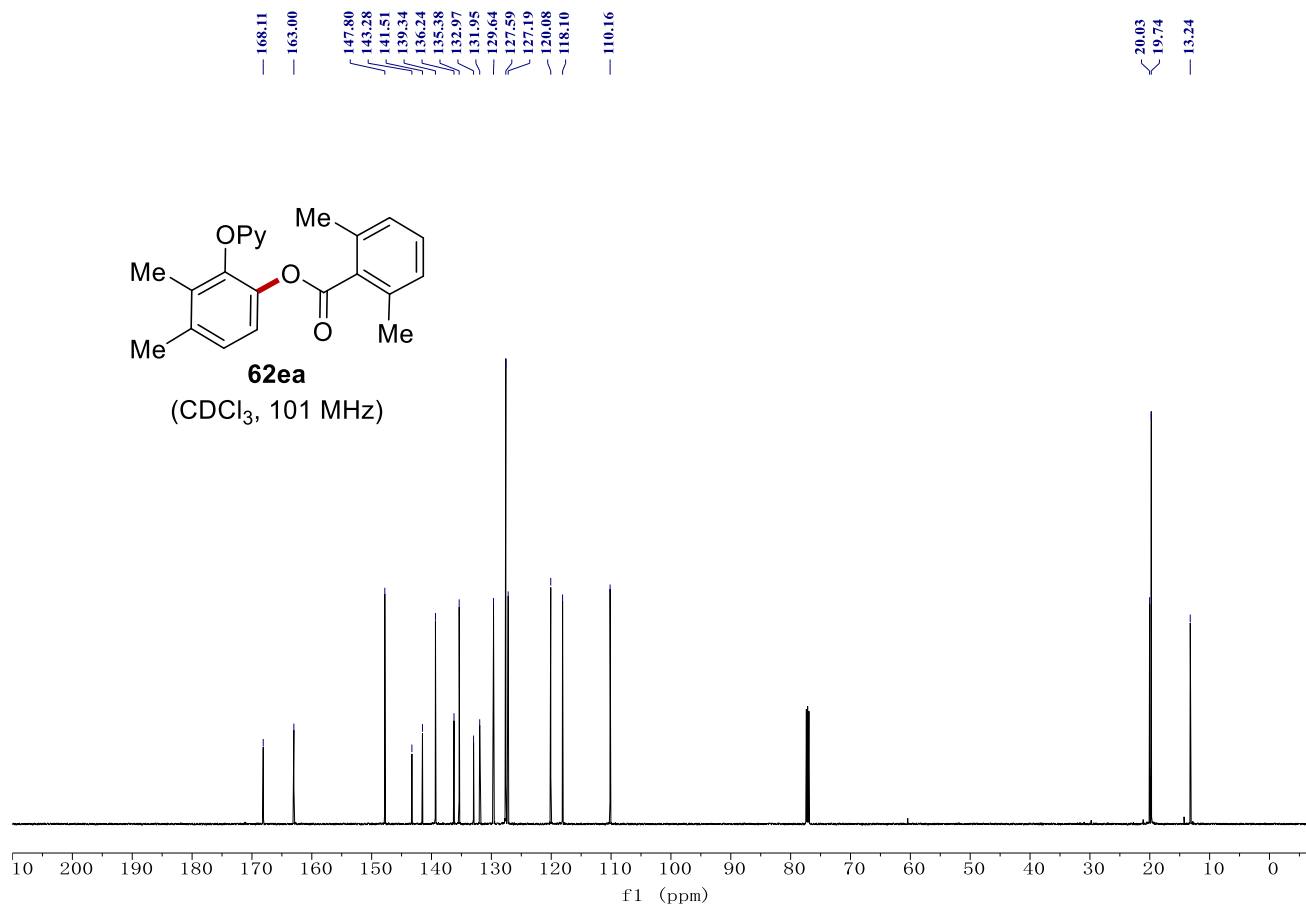
62da
(CDCl₃, 101 MHz)



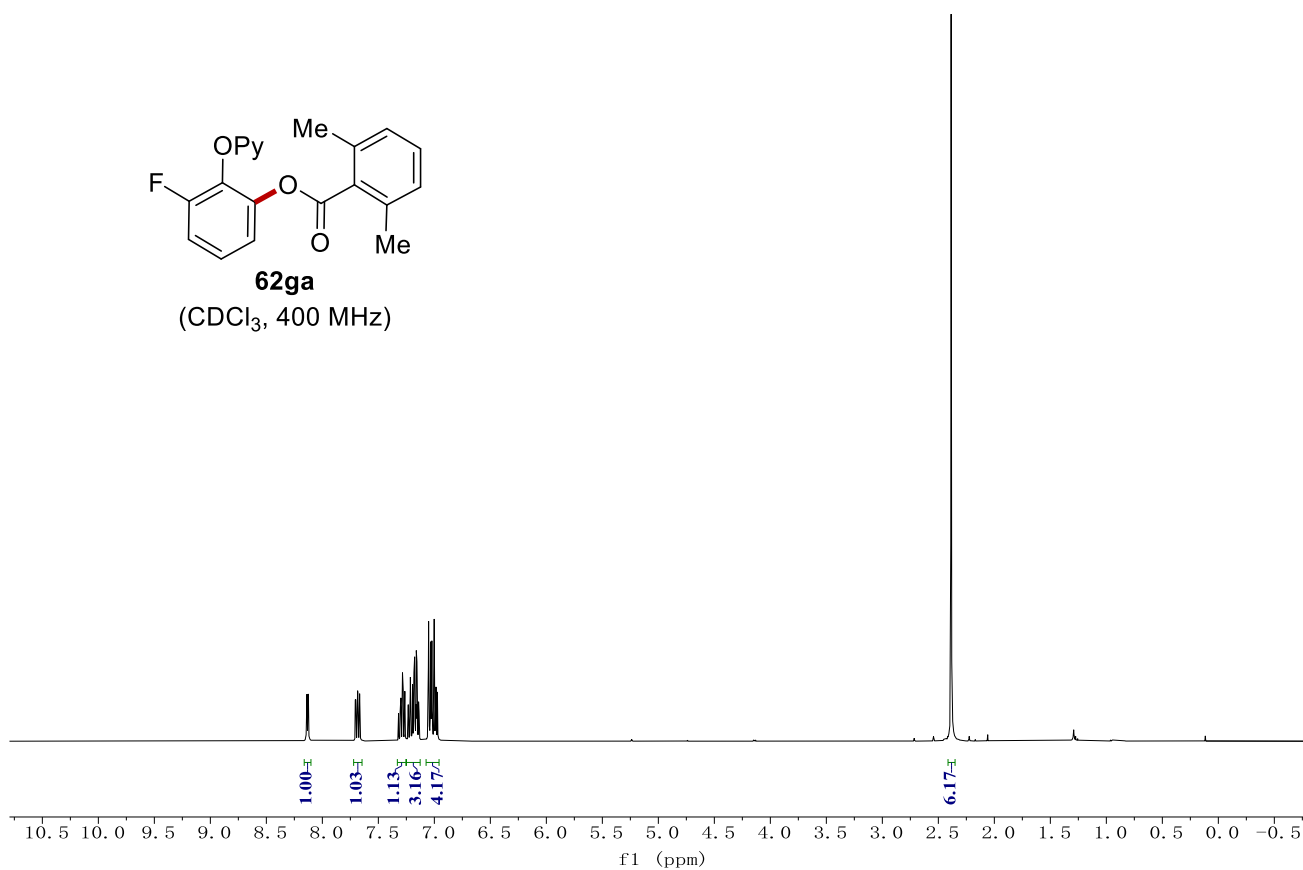
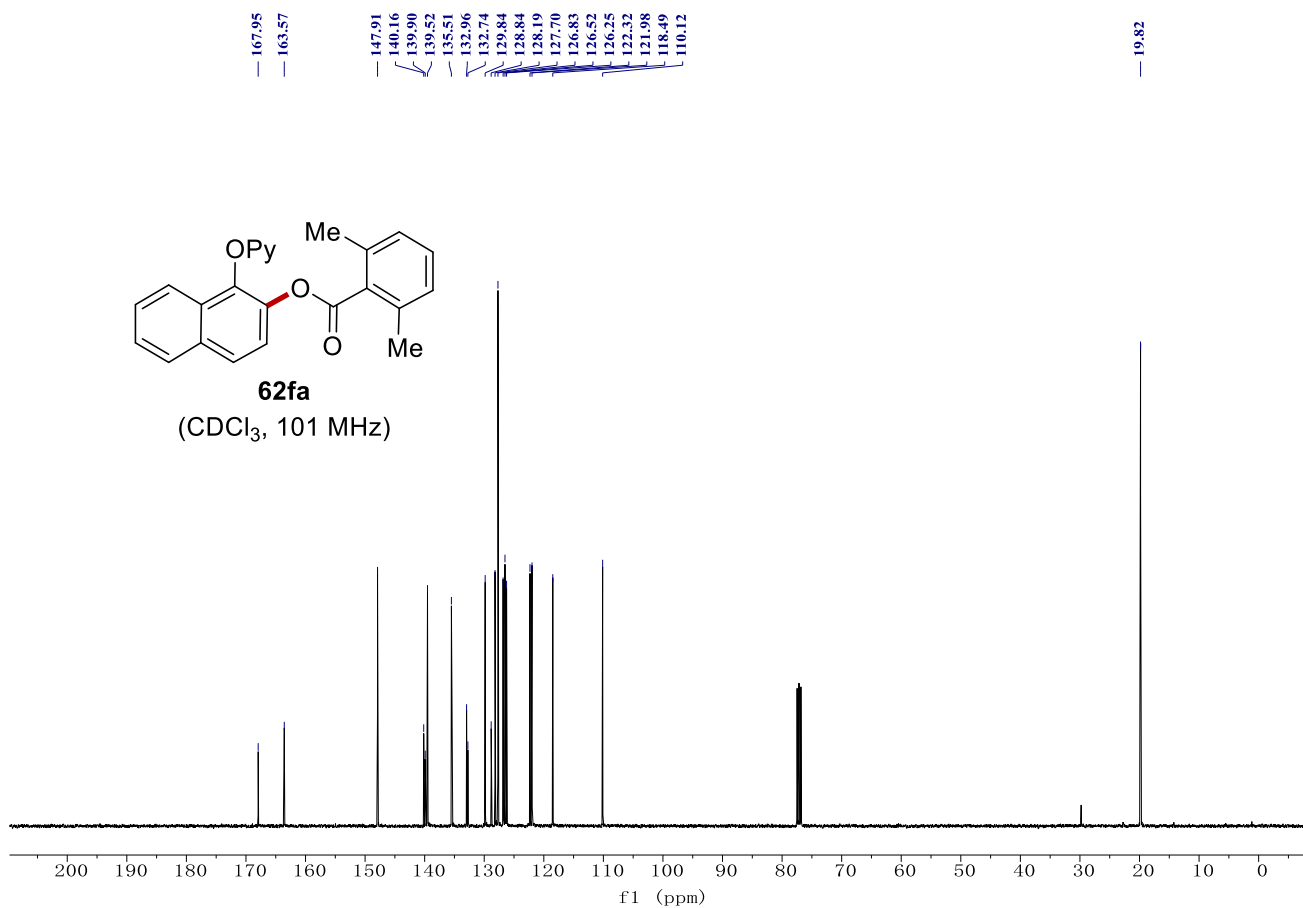
62ea
(CDCl₃, 400 MHz)



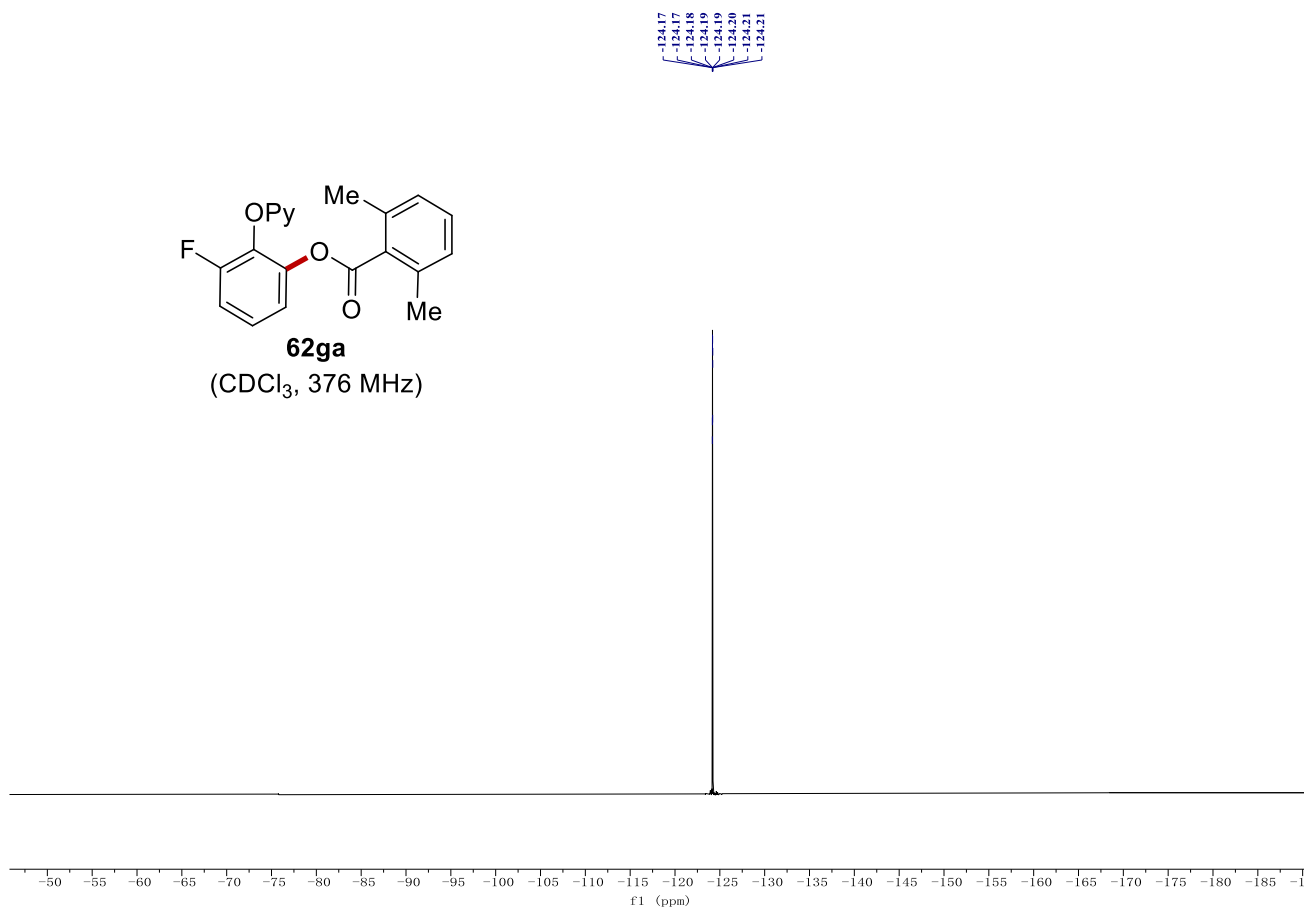
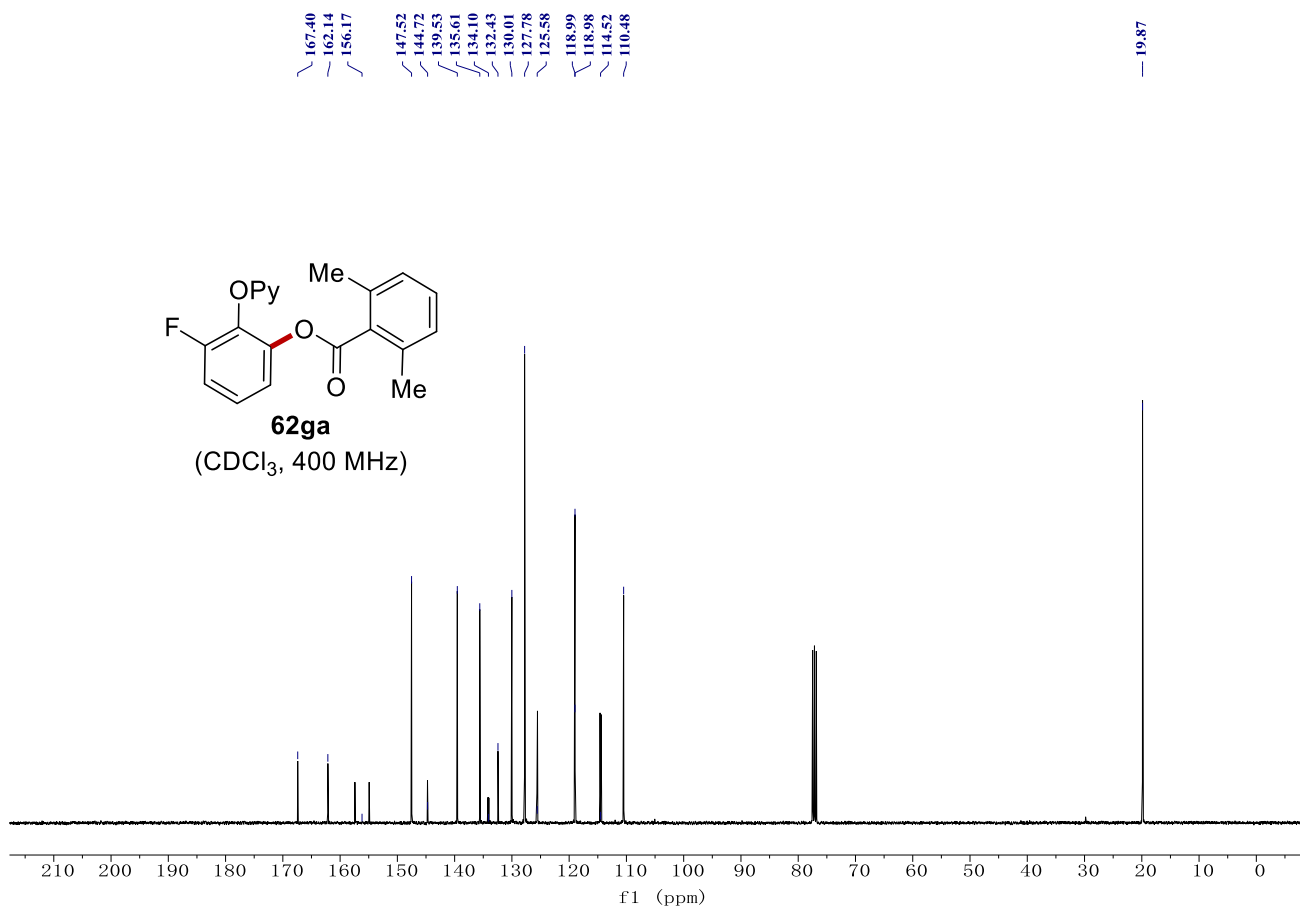
NMR Spectra



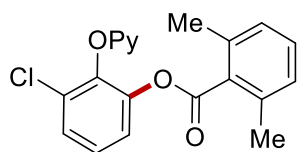
NMR Spectra



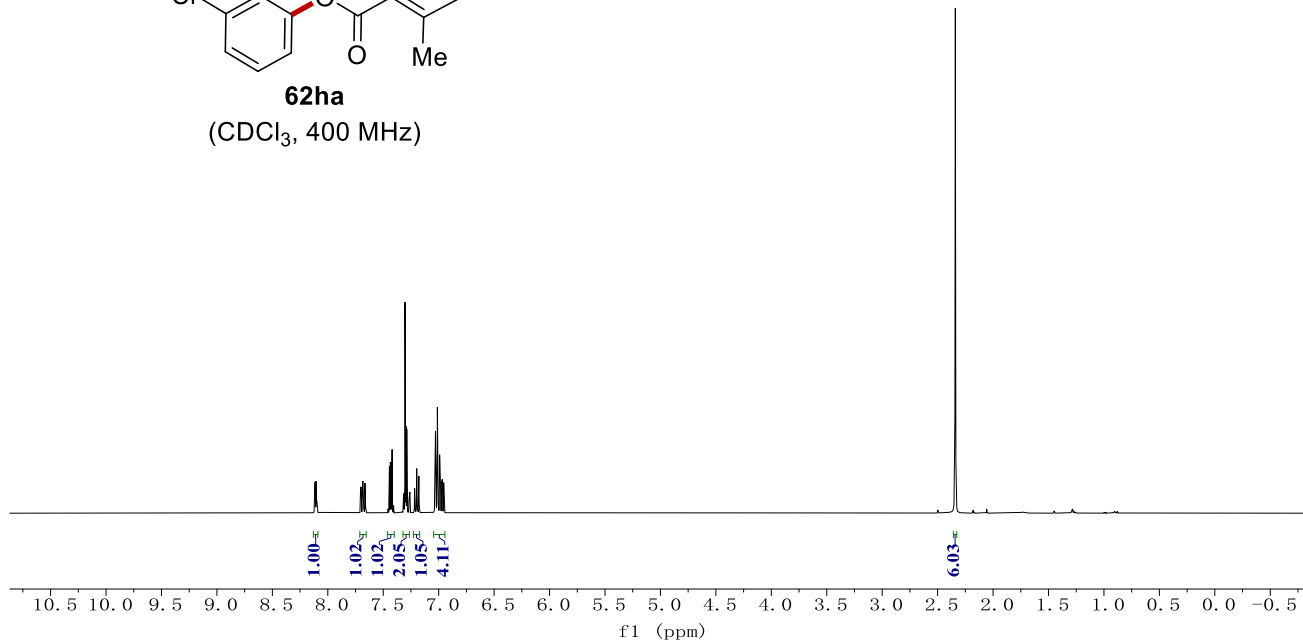
NMR Spectra



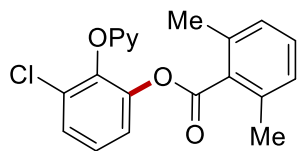
NMR Spectra



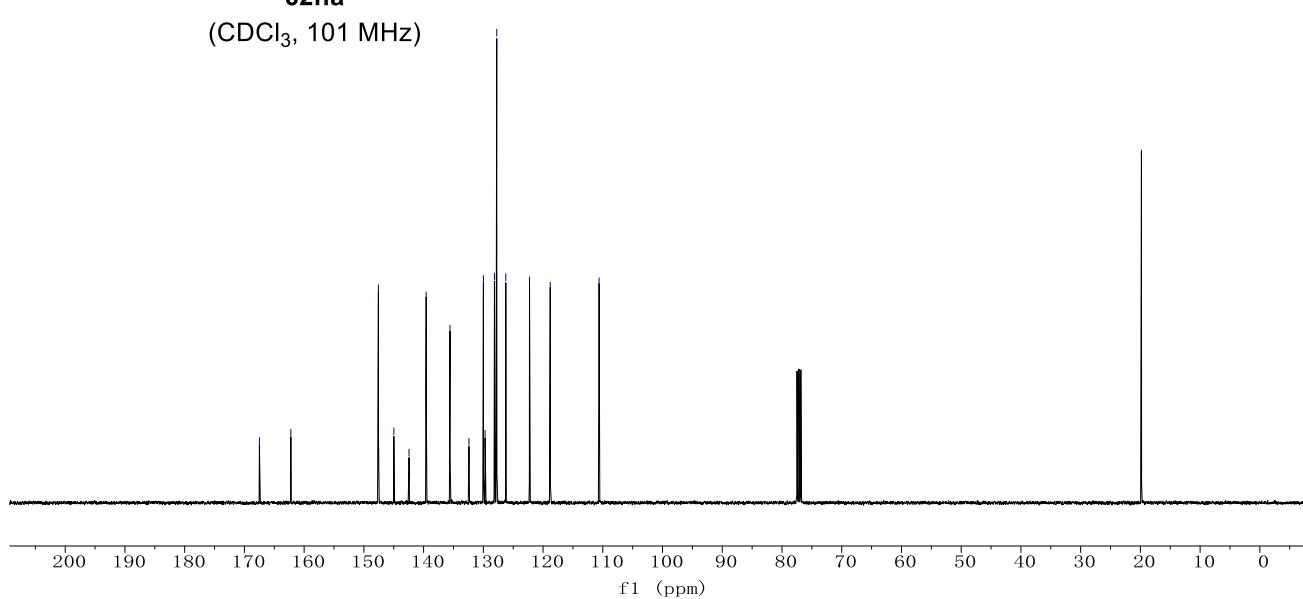
62ha
(CDCl₃, 400 MHz)



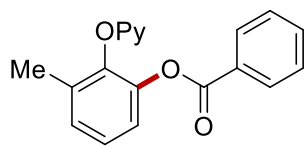
167.49, 162.22, 147.57, 144.98, 142.44, 139.57, 135.57, 132.41, 129.99, 129.70, 128.14, 127.75, 126.24, 122.27, 118.80, 110.62, 19.83



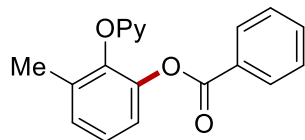
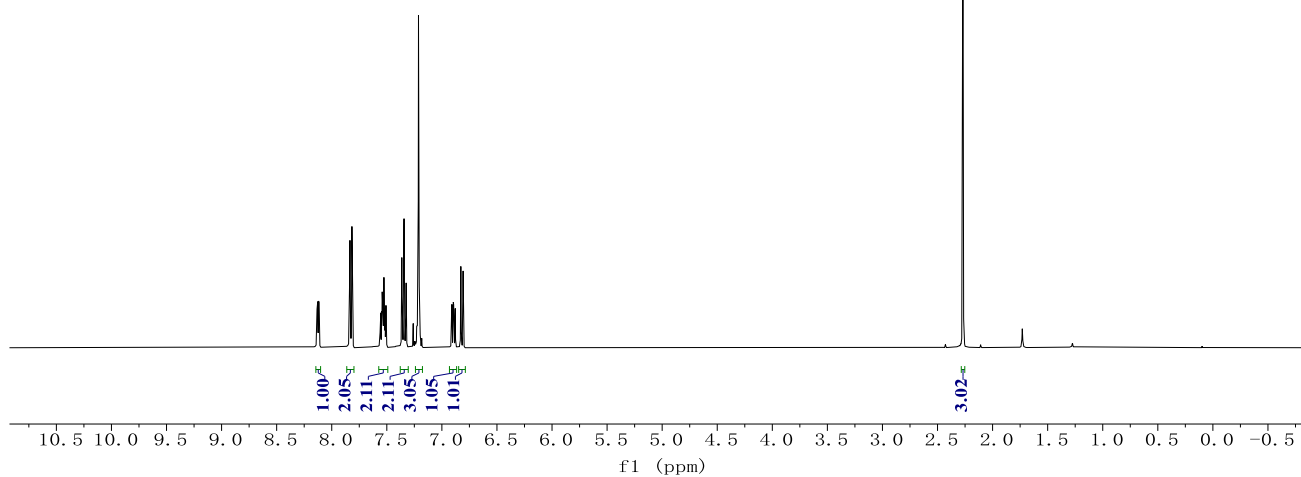
62ha
(CDCl₃, 101 MHz)



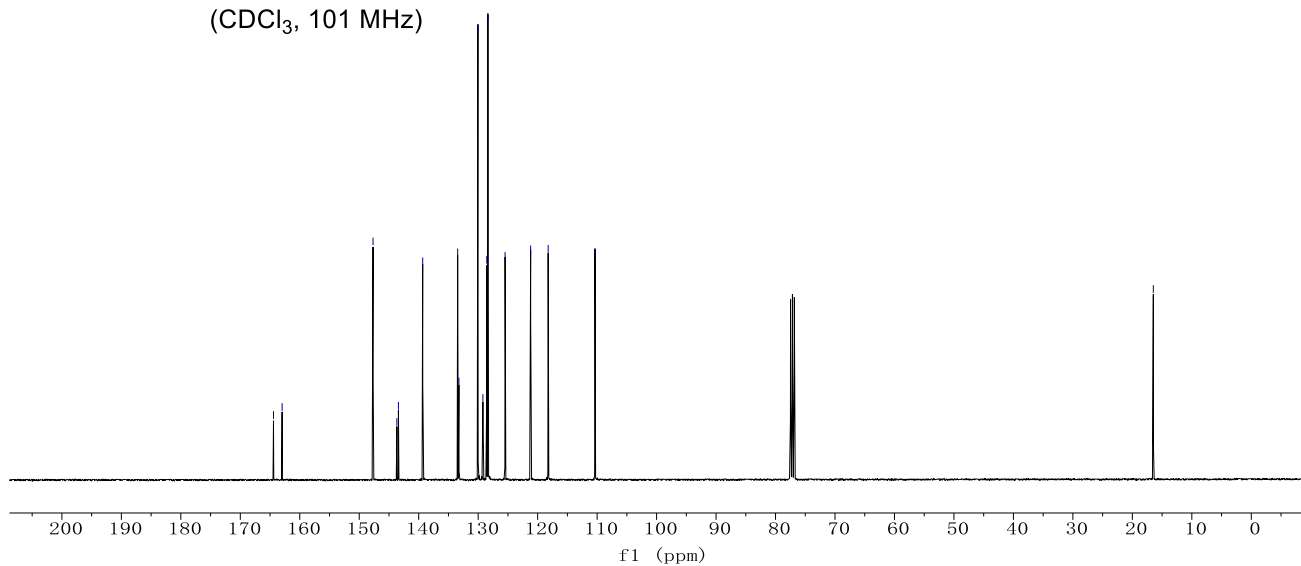
NMR Spectra



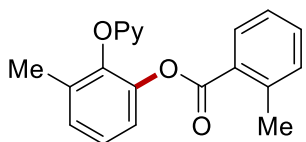
62ab
(CDCl₃, 400 MHz)



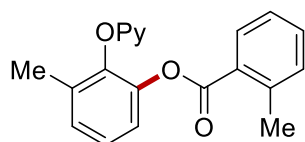
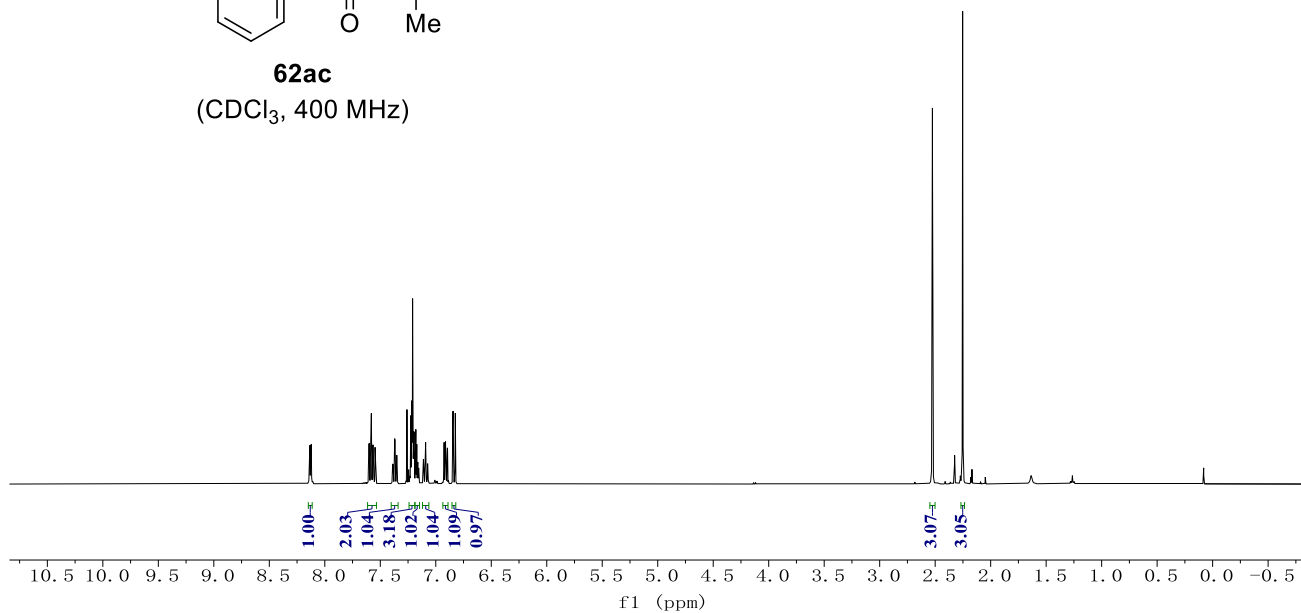
62ab
(CDCl₃, 101 MHz)



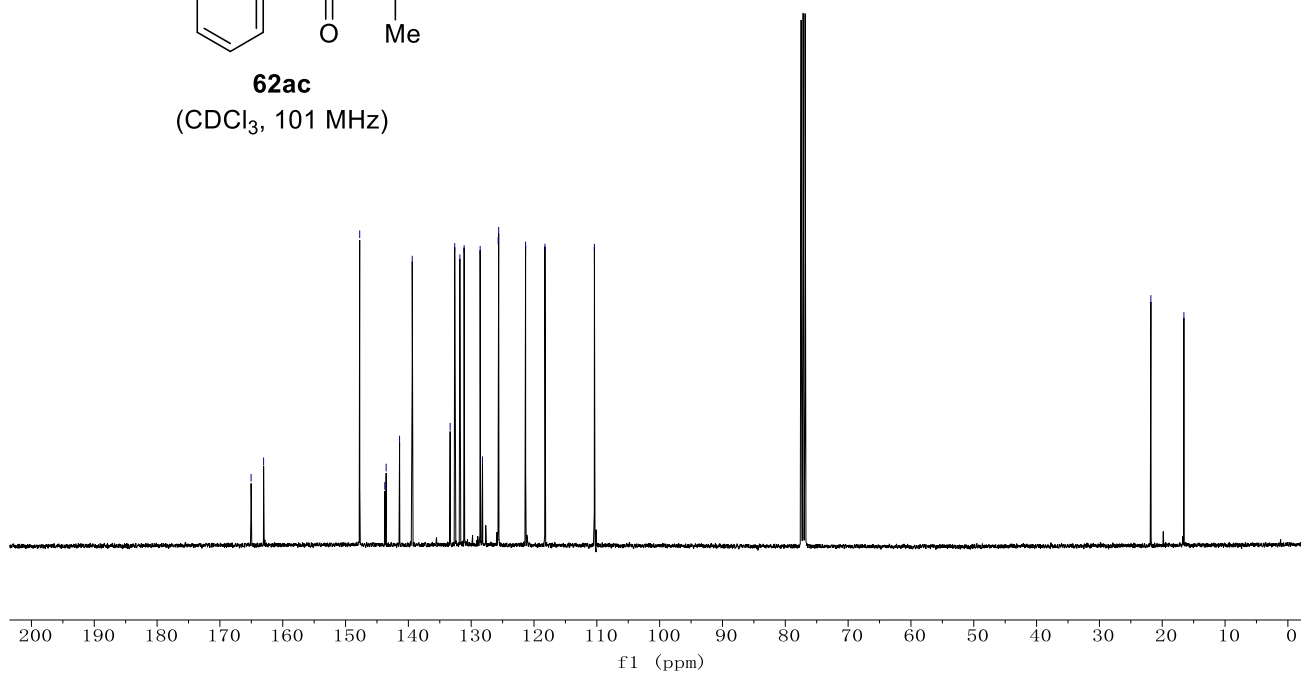
NMR Spectra



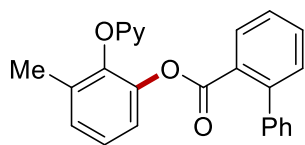
62ac
(CDCl₃, 400 MHz)



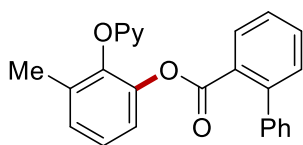
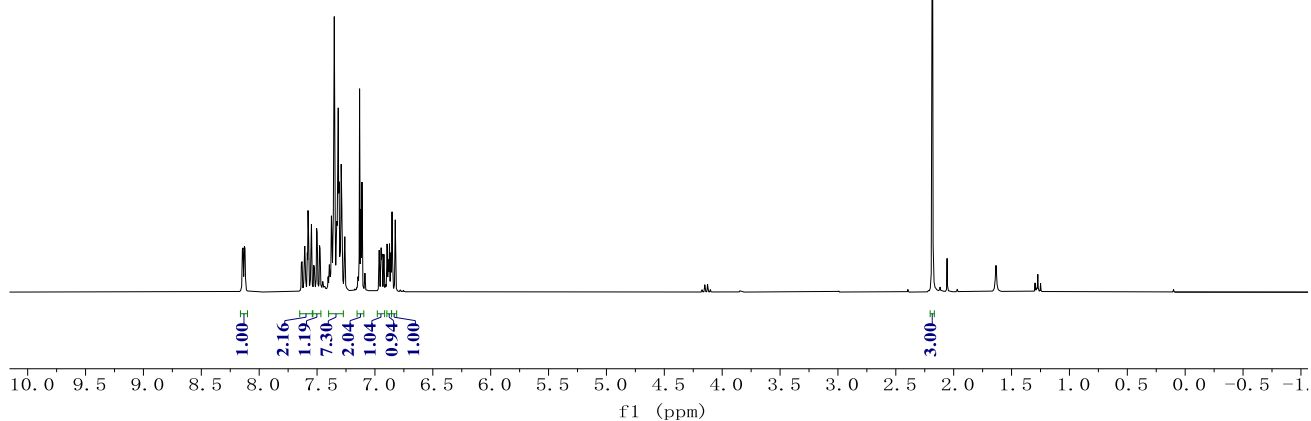
62ac
(CDCl₃, 101 MHz)



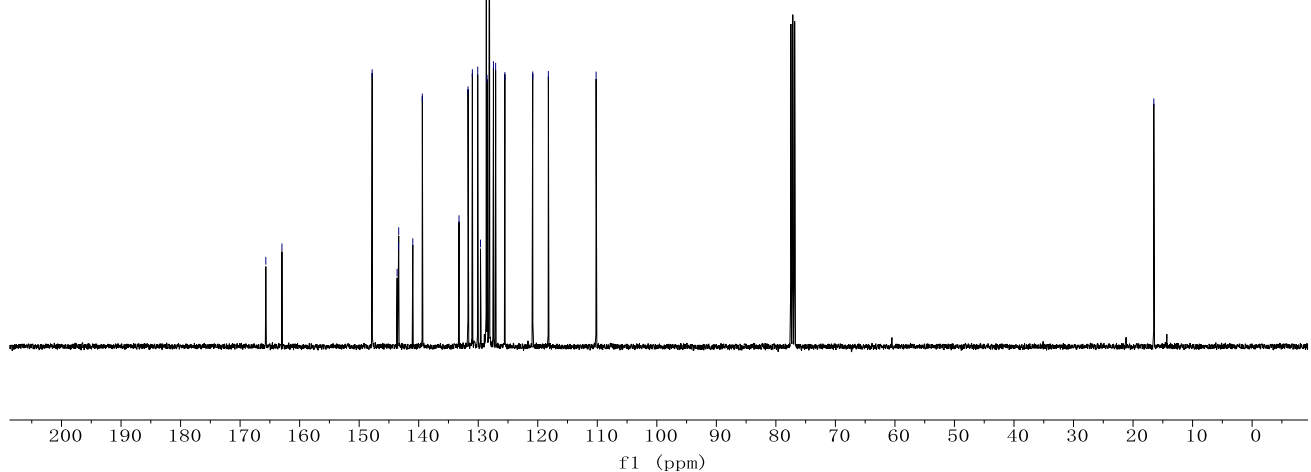
NMR Spectra



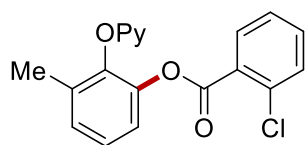
62ad
(CDCl₃, 400 MHz)



62ad
(CDCl₃, 101 MHz)

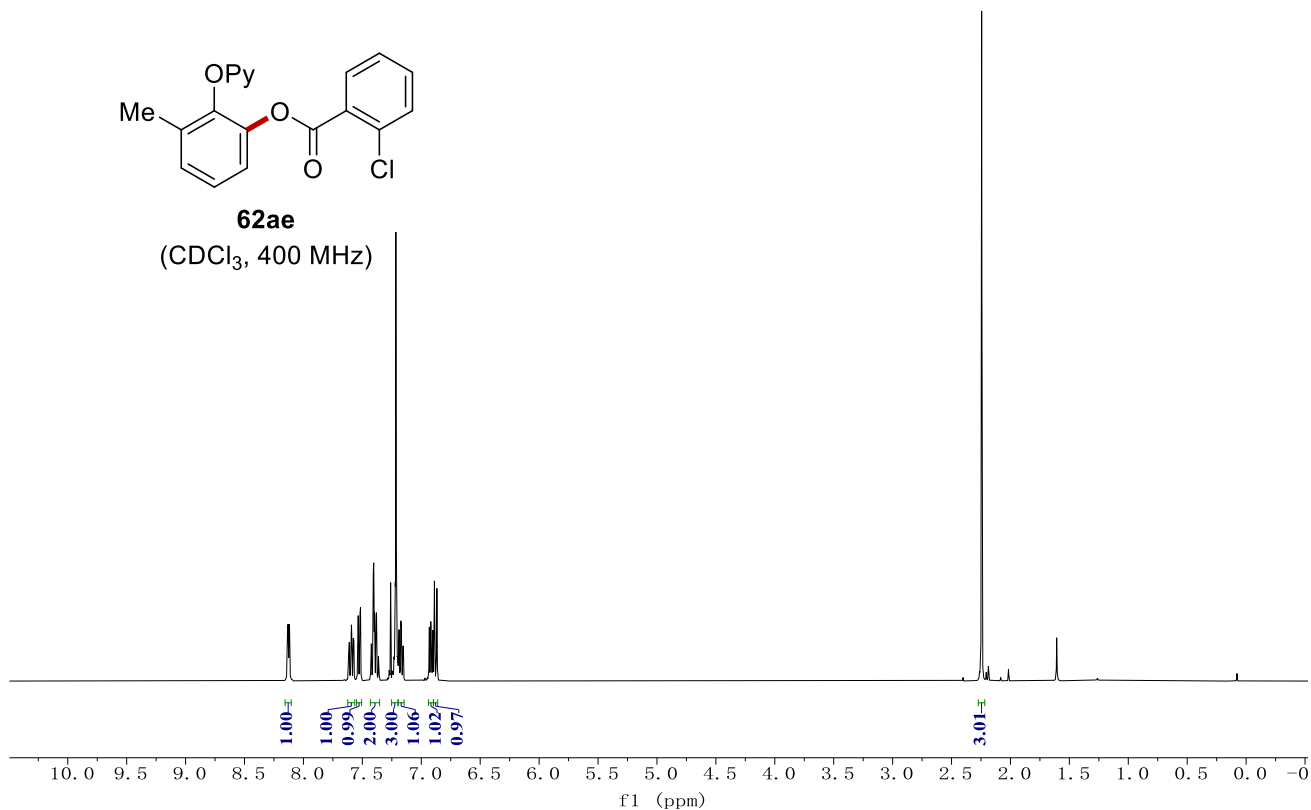


NMR Spectra



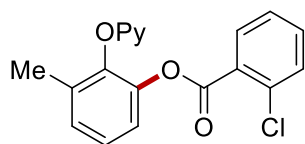
62ae

(CDCl₃, 400 MHz)



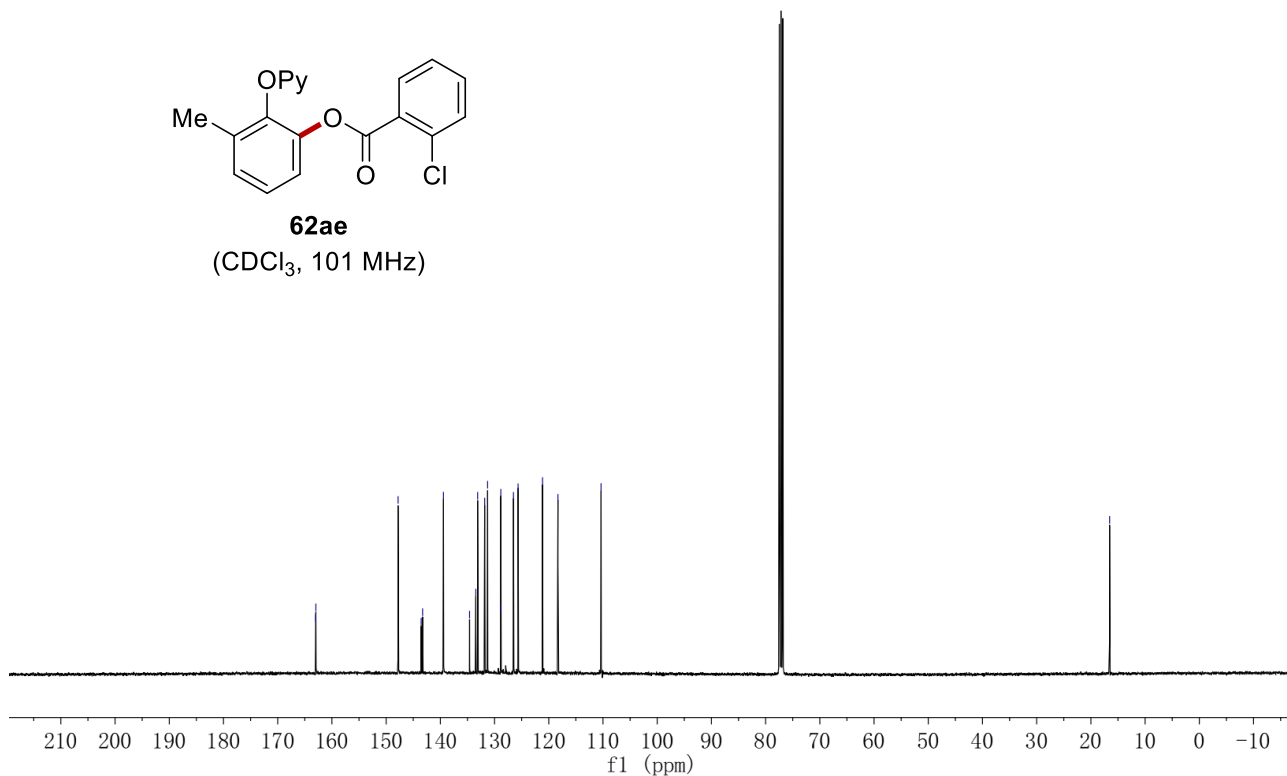
163.00
162.96
147.79
143.54
143.27
139.43
134.61
133.45
133.12
131.82
131.28
128.84
128.81
126.51
125.66
121.15
118.31
110.35

16.55

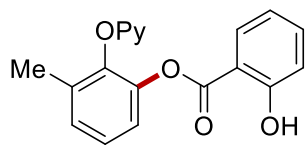


62ae

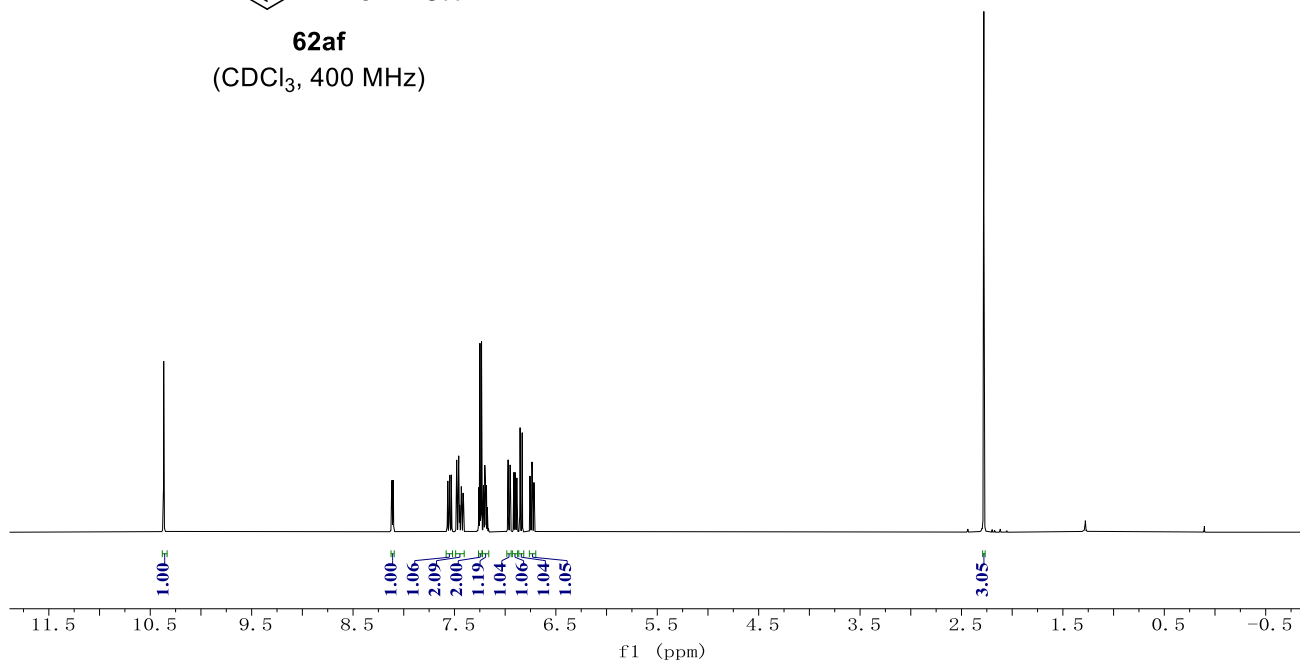
(CDCl₃, 101 MHz)



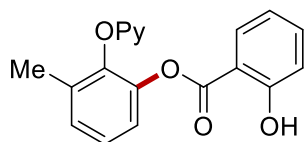
NMR Spectra



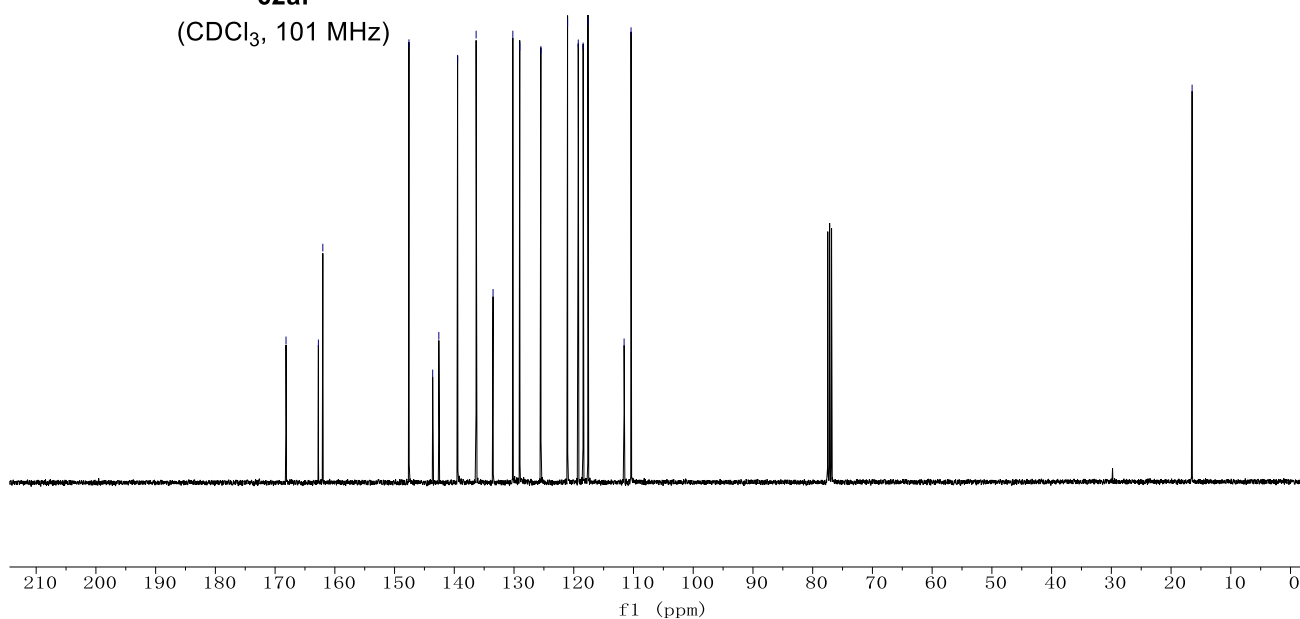
62af
(CDCl₃, 400 MHz)



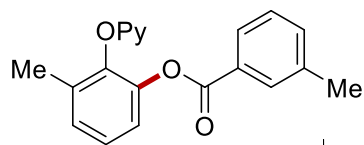
- 168.17
- 162.75
- 162.01
- 147.59
- 143.62
- 142.59
- 139.45
- 136.35
- 133.51
- 130.20
- 129.04
- 125.51
- 121.04
- 119.25
- 118.43
- 117.62
- 111.57
- 110.41
- 16.48



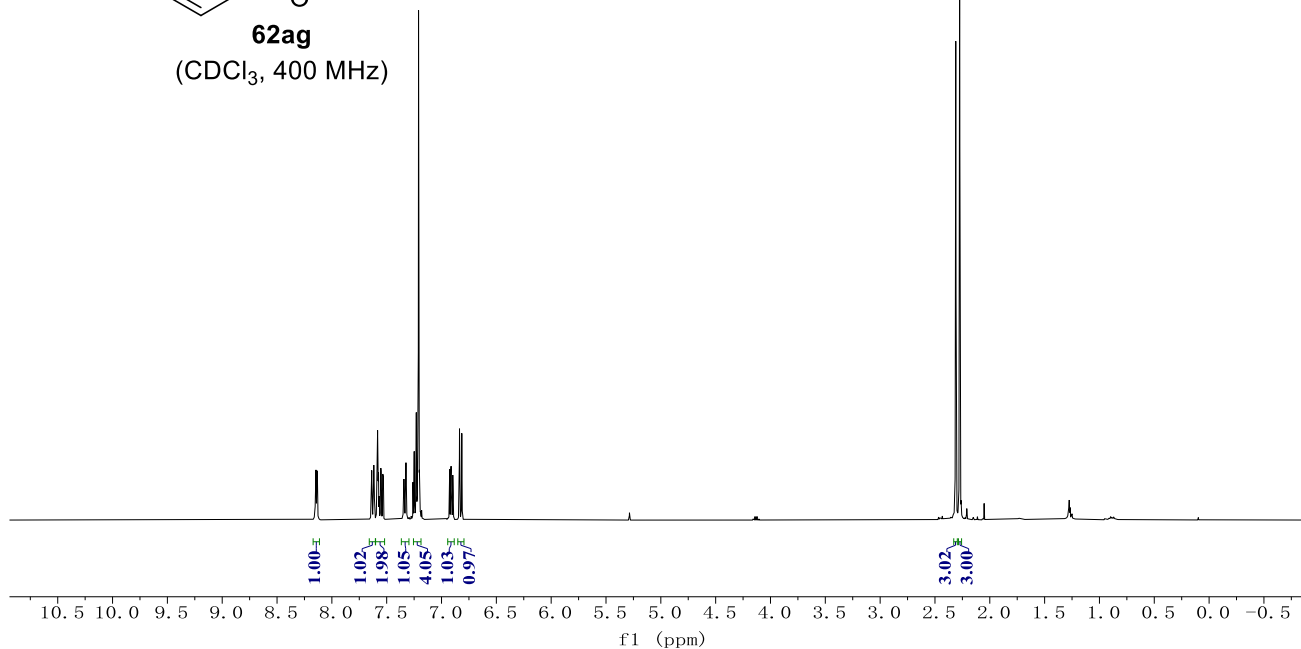
62af
(CDCl₃, 101 MHz)



NMR Spectra

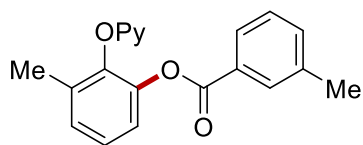


62ag
(CDCl₃, 400 MHz)

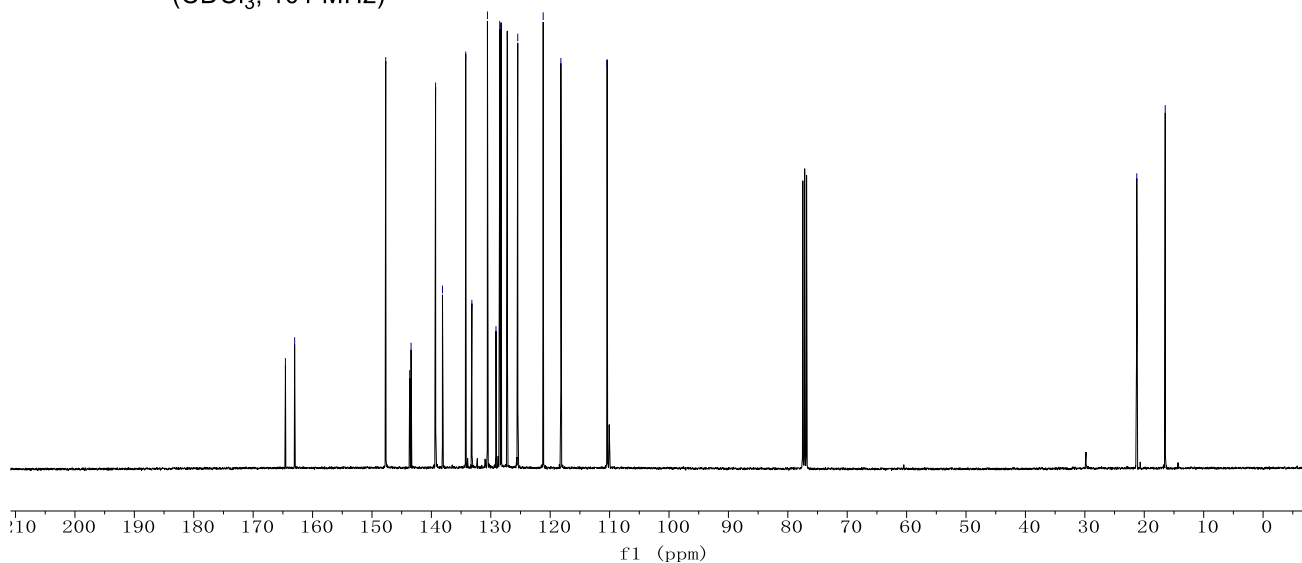


164.57
163.02
147.69
143.65
143.42
139.29
138.13
134.22
133.18
130.56
129.13
128.50
128.26
127.22
125.46
121.18
118.20
110.42

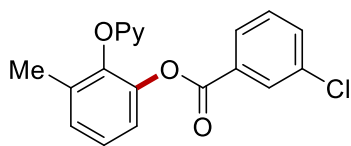
21.26
16.47



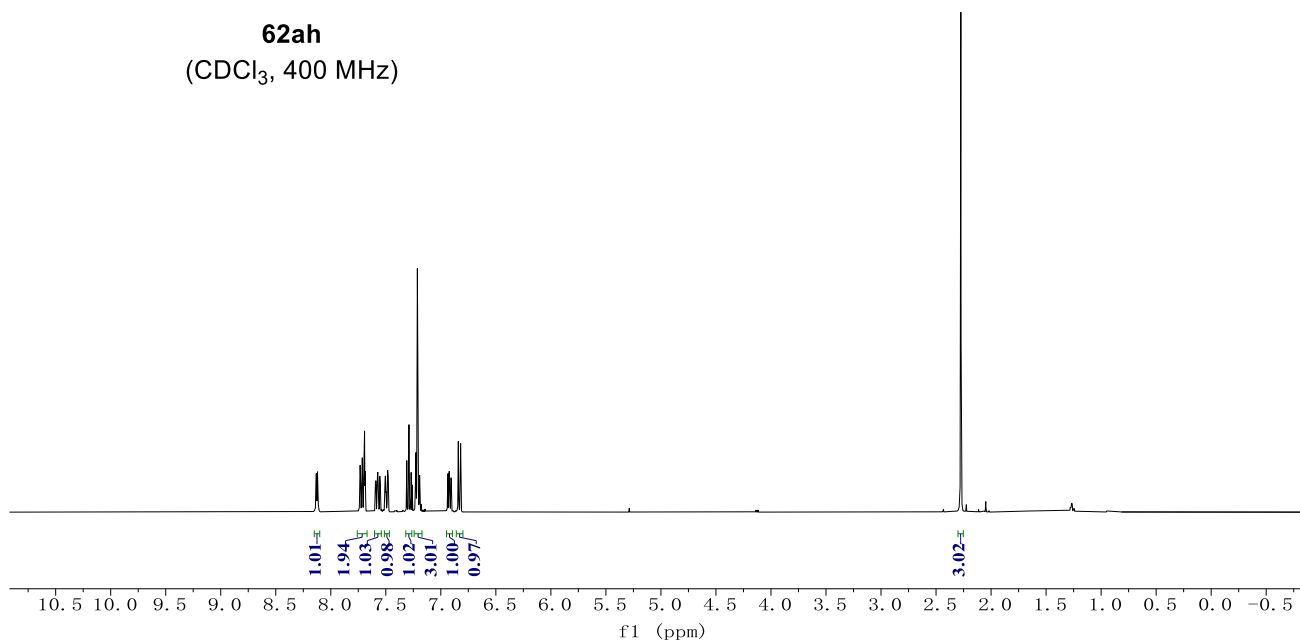
62ag
(CDCl₃, 101 MHz)



NMR Spectra

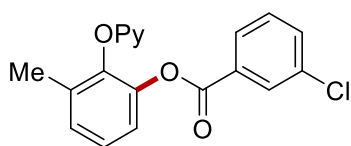


62ah
(CDCl₃, 400 MHz)

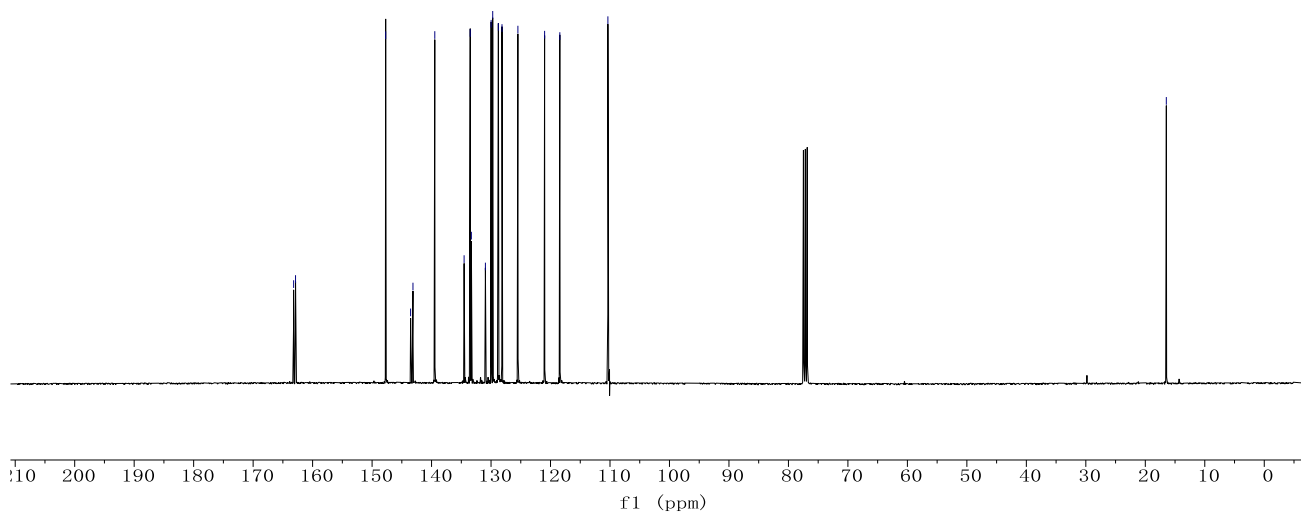


163.19
162.87
147.72
143.52
143.13
139.46
134.53
133.50
133.31
130.95
129.99
129.72
128.77
128.16
125.48
120.99
118.43
110.35

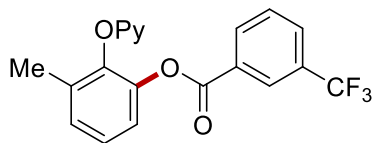
16.47



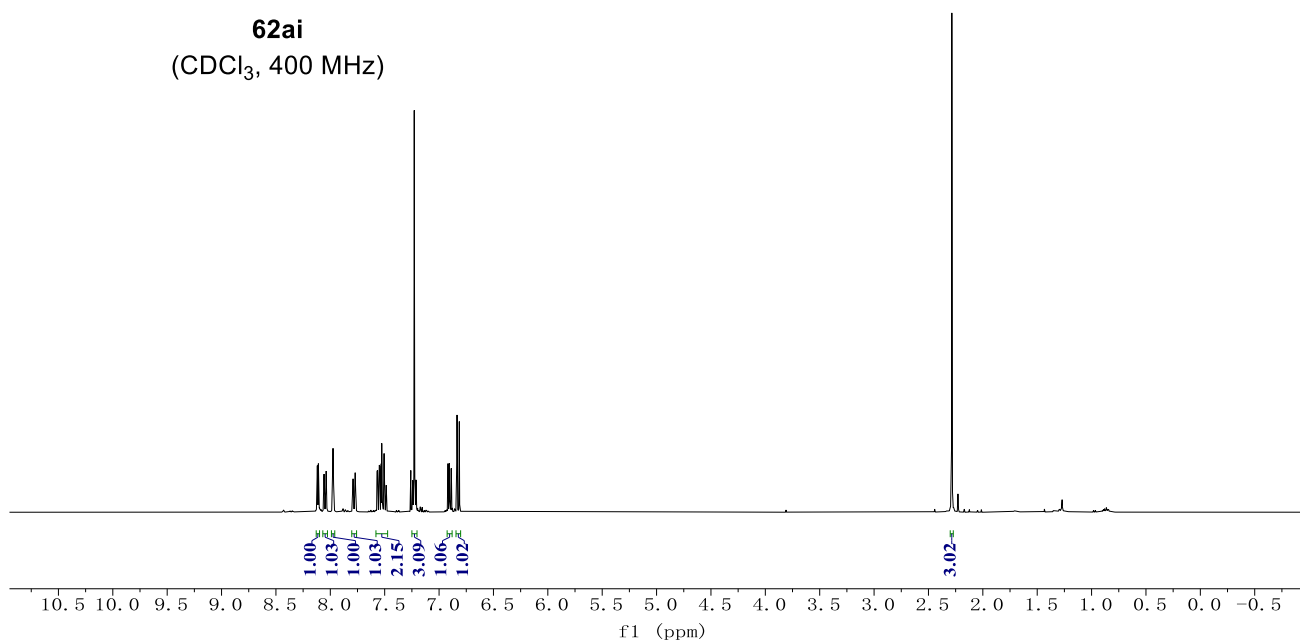
62ah
(CDCl₃, 101 MHz)



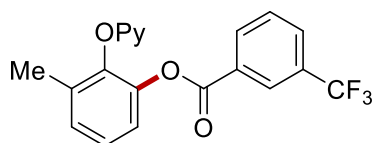
NMR Spectra



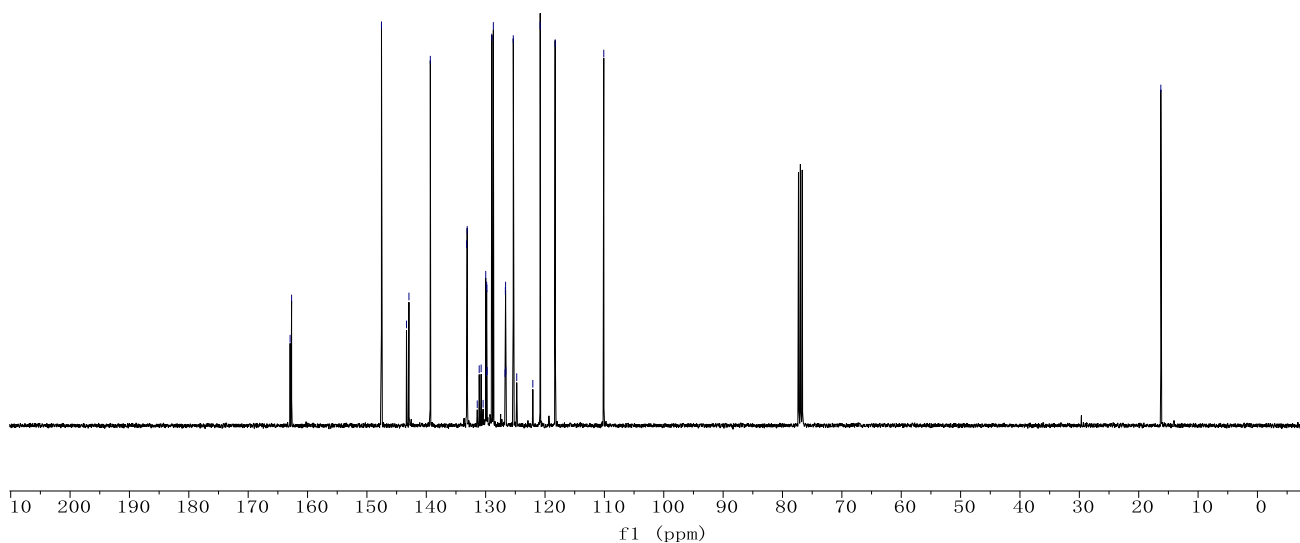
62ai
(CDCl₃, 400 MHz)



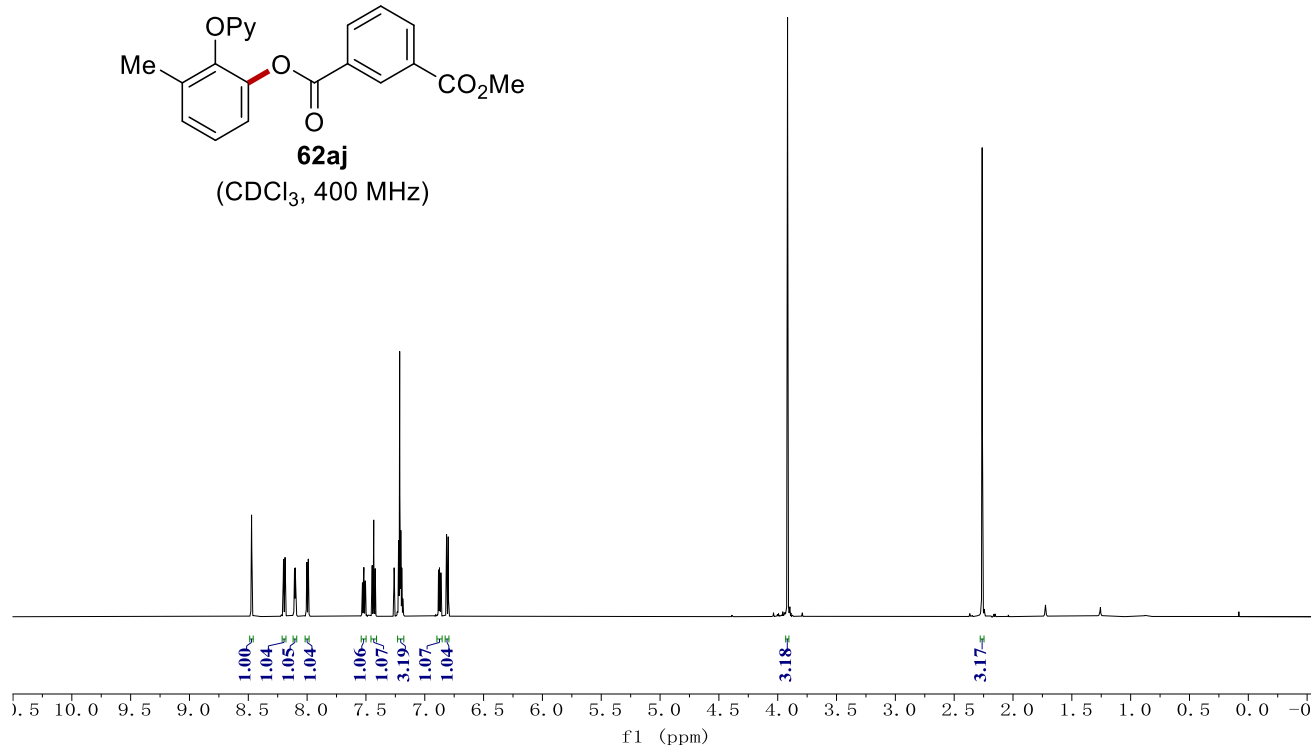
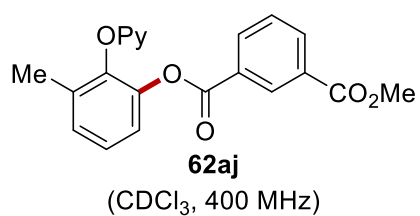
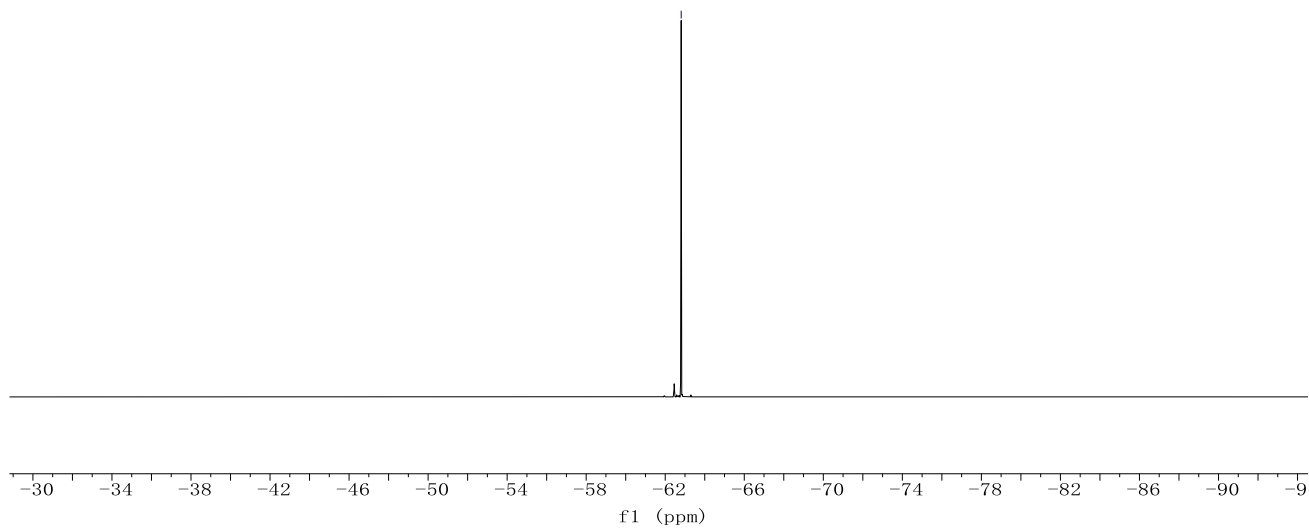
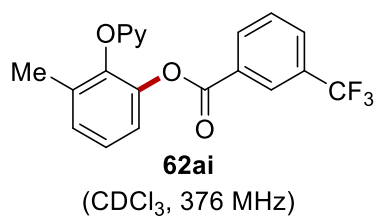
162.94
162.69
147.55
143.33
142.92
139.32
133.21
133.11
131.42
131.09
130.76
130.43
129.99
129.87
129.83
129.79
129.76
128.97
128.70
126.72
126.68
126.64
126.60
125.35
124.77
122.05
120.81
118.29
110.10
16.27



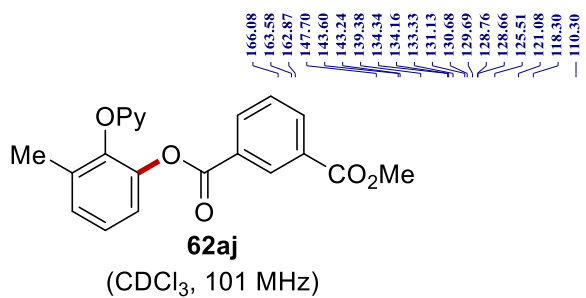
62ai
(CDCl₃, 101 MHz)



NMR Spectra



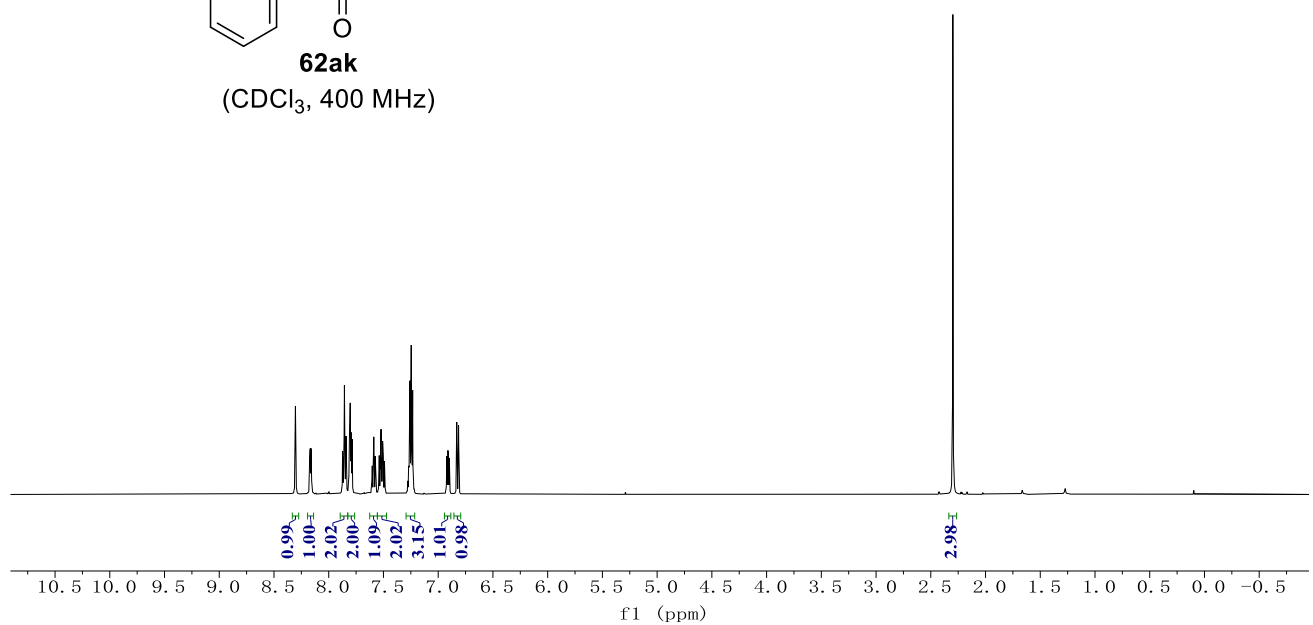
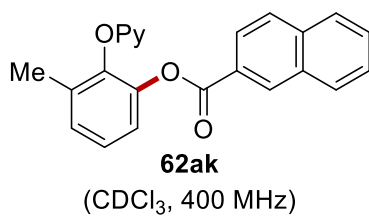
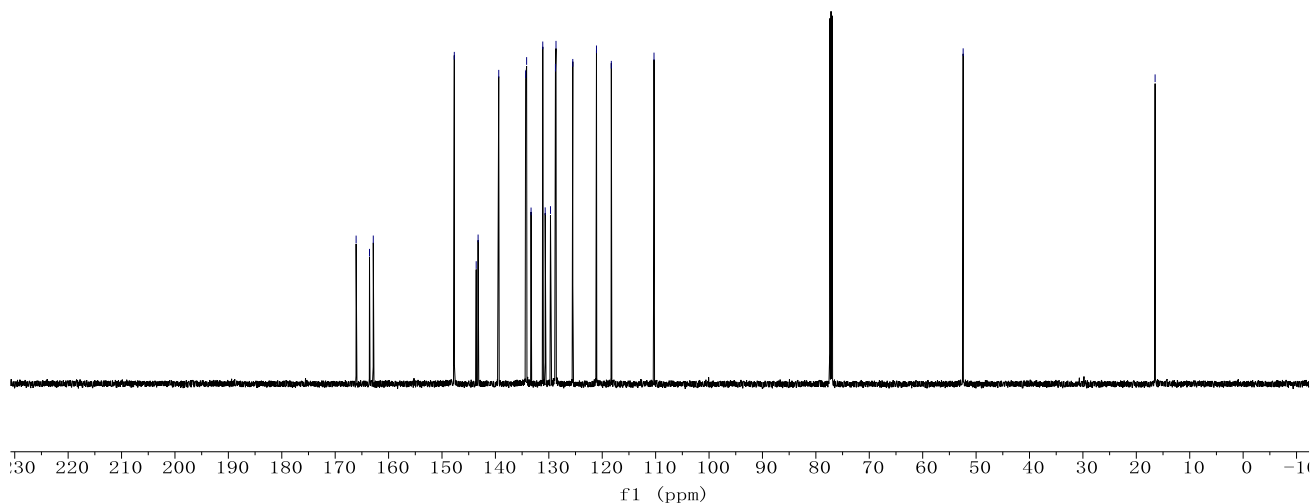
NMR Spectra



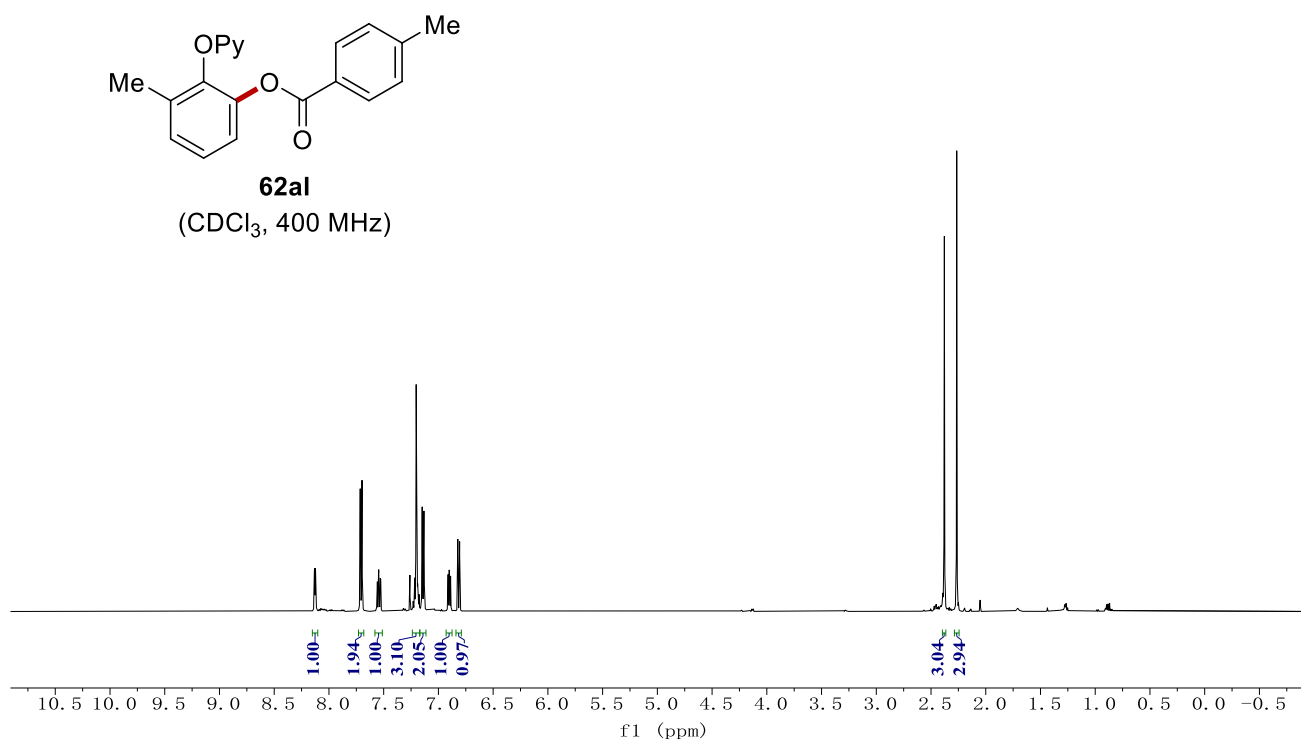
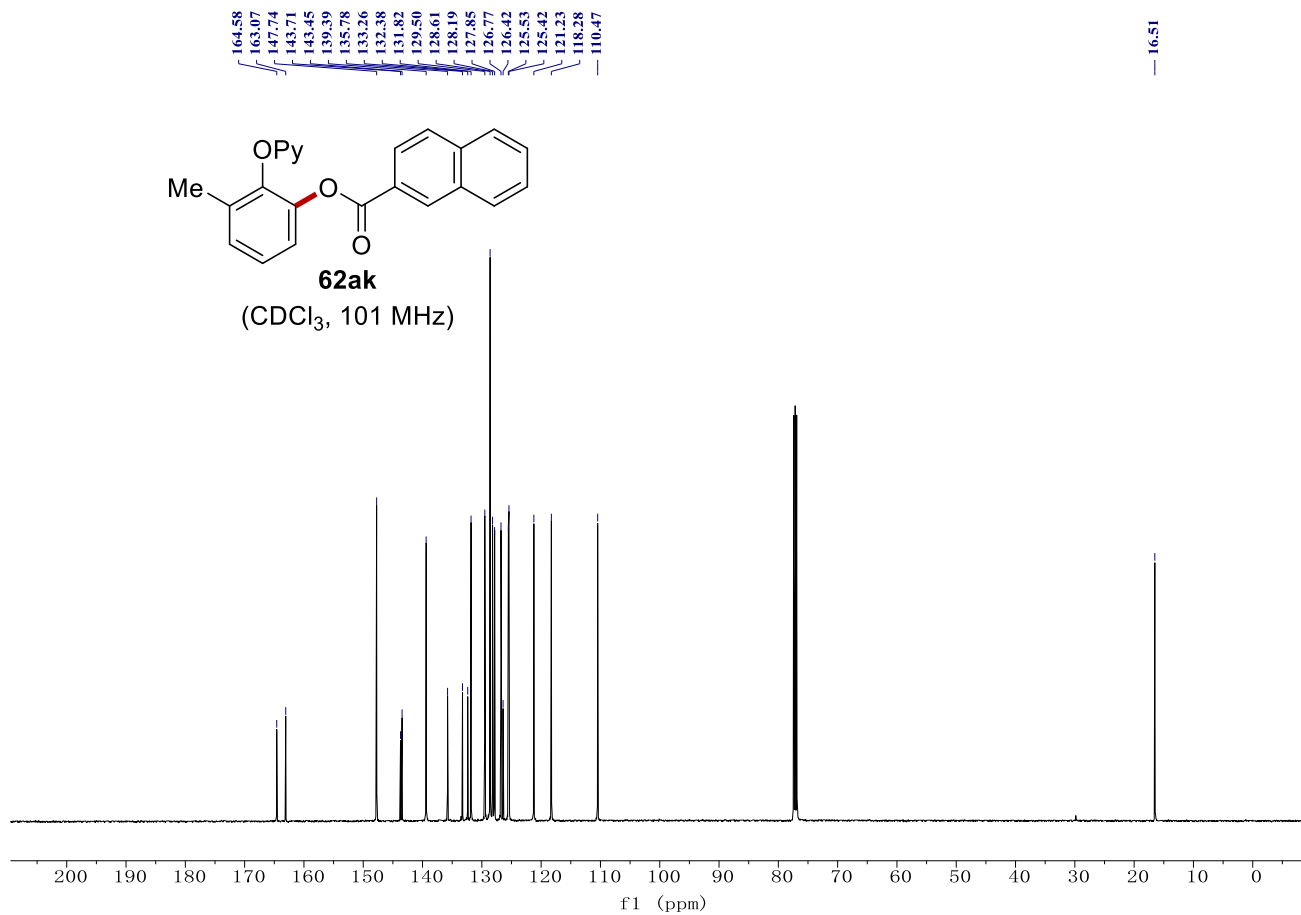
166.08
 163.58
 162.87
 147.70
 143.60
 139.38
 134.34
 134.16
 133.33
 131.13
 130.68
 129.69
 128.76
 128.66
 125.51
 121.08
 118.30
 110.30

52.42

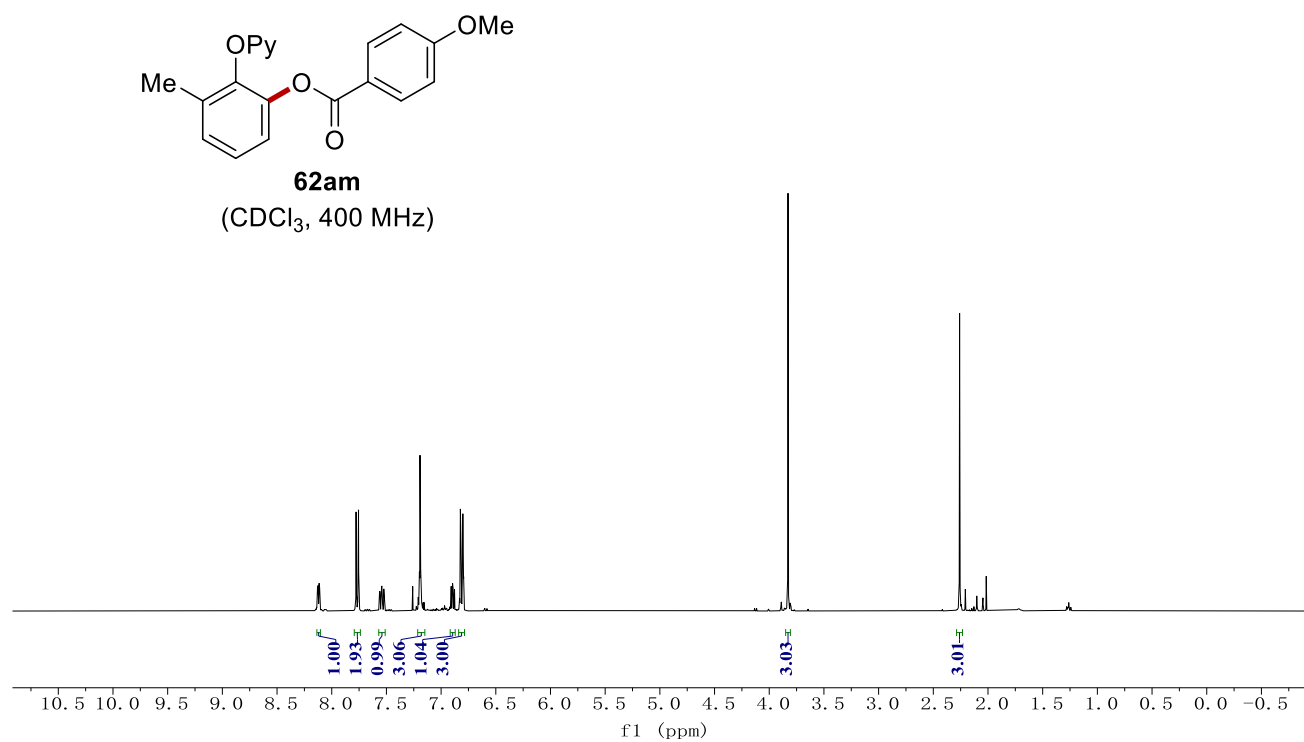
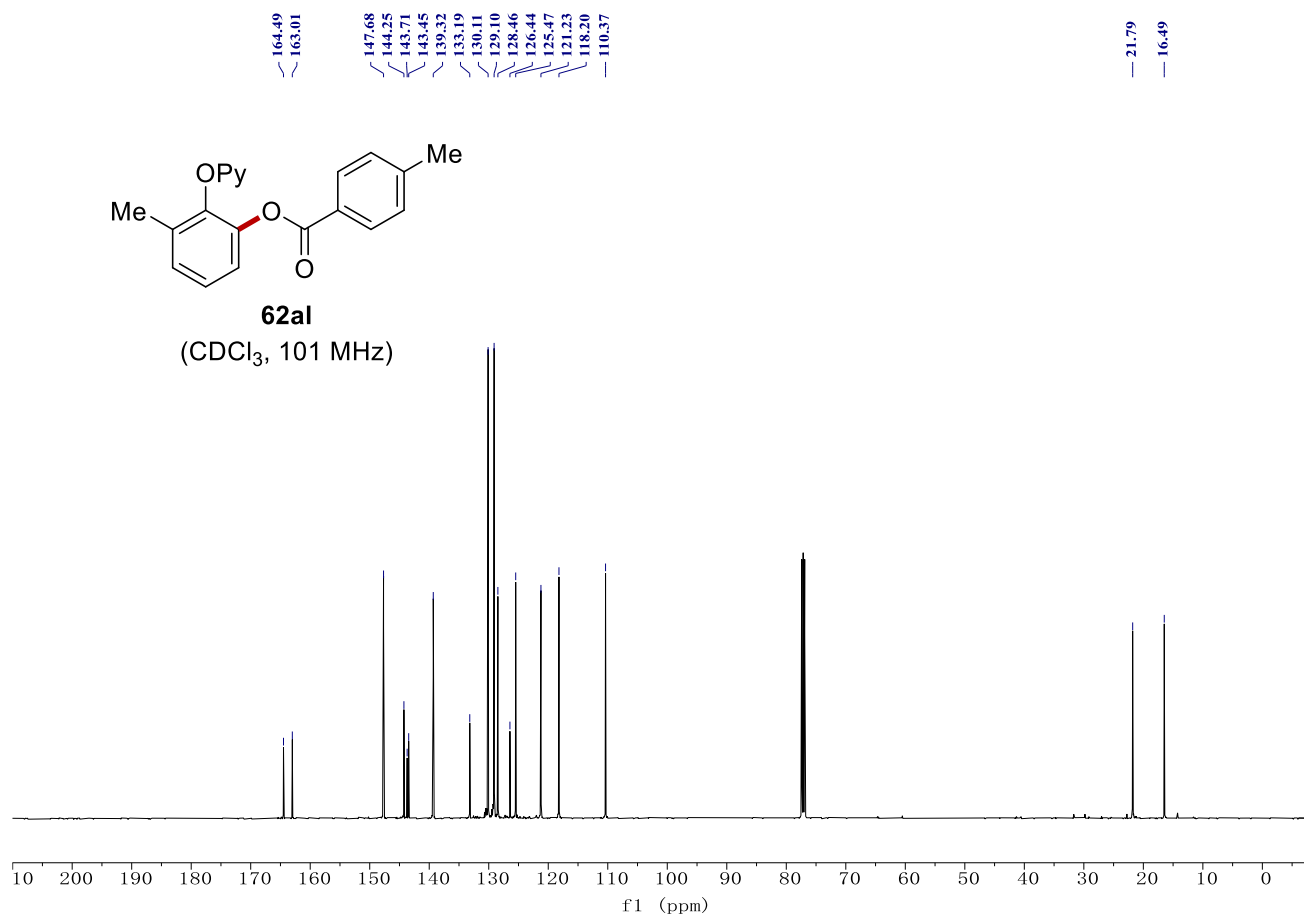
16.48



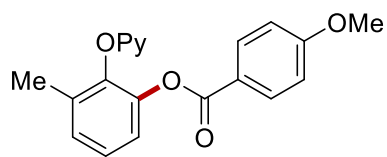
NMR Spectra



NMR Spectra



NMR Spectra

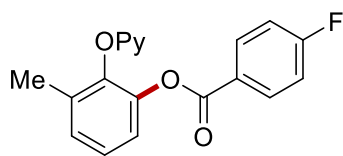
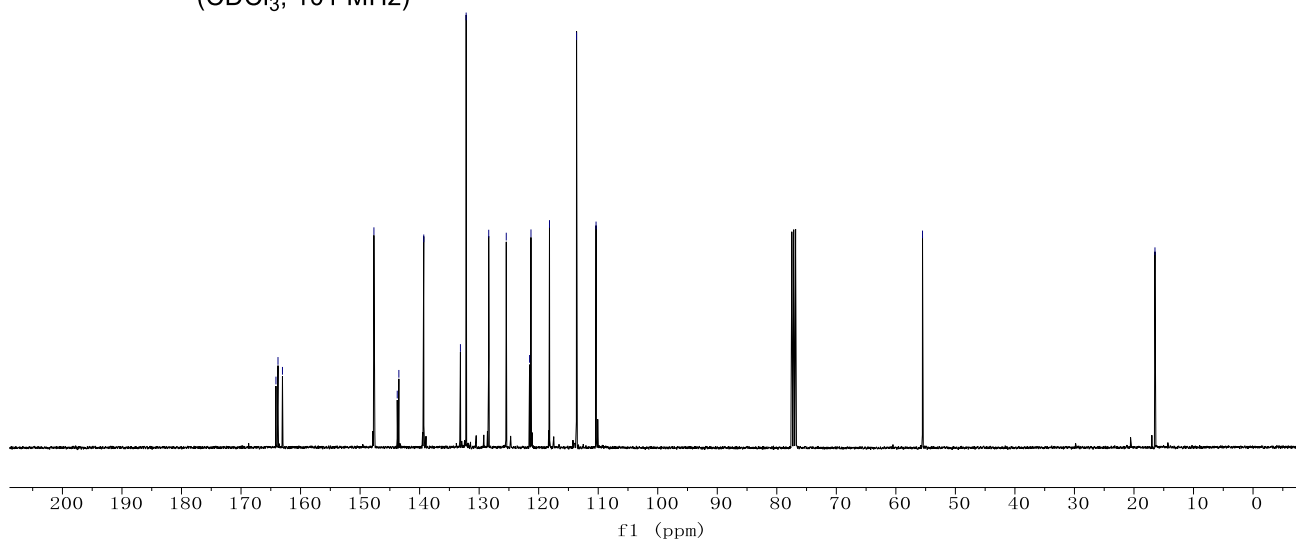


62am
(CDCl₃, 101 MHz)

164.13
163.79
163.04
147.68
143.76
143.49
139.30
133.14
132.18
128.39
125.44
121.53
121.29
118.18
113.64
110.36

— 55.52

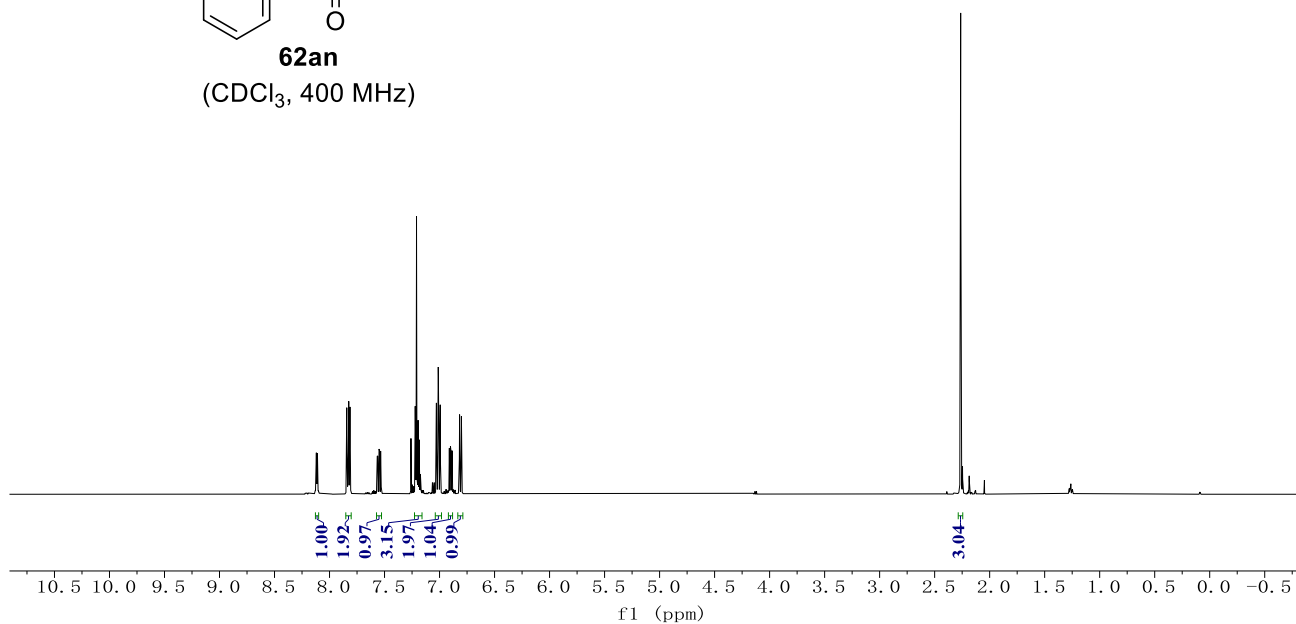
— 16.47



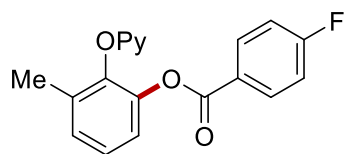
62an
(CDCl₃, 400 MHz)

1.00#
1.92#
0.97#
3.15#
1.97#
1.04#
0.98#

3.04#



NMR Spectra

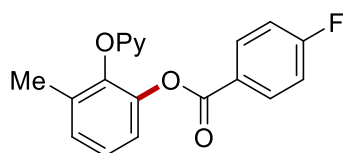
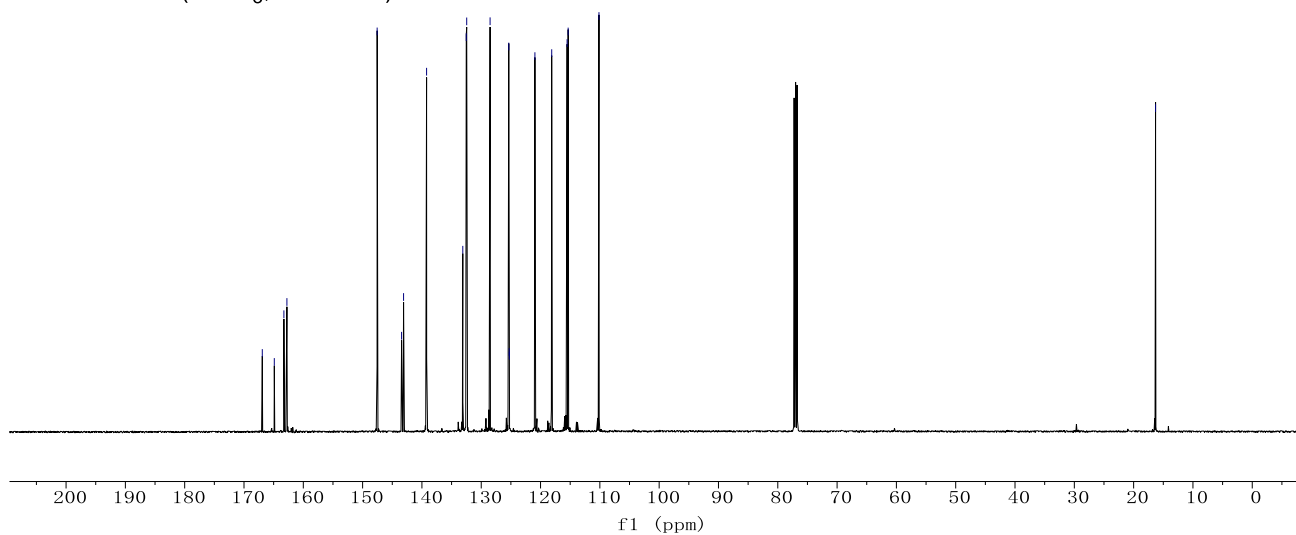


62an

(CDCl₃, 101 MHz)

166.92
164.89
163.27
162.76
147.55
143.43
143.10
139.21
133.11
132.53
132.45
128.51
125.36
125.28
125.26
120.95
118.12
115.52
115.34
110.15

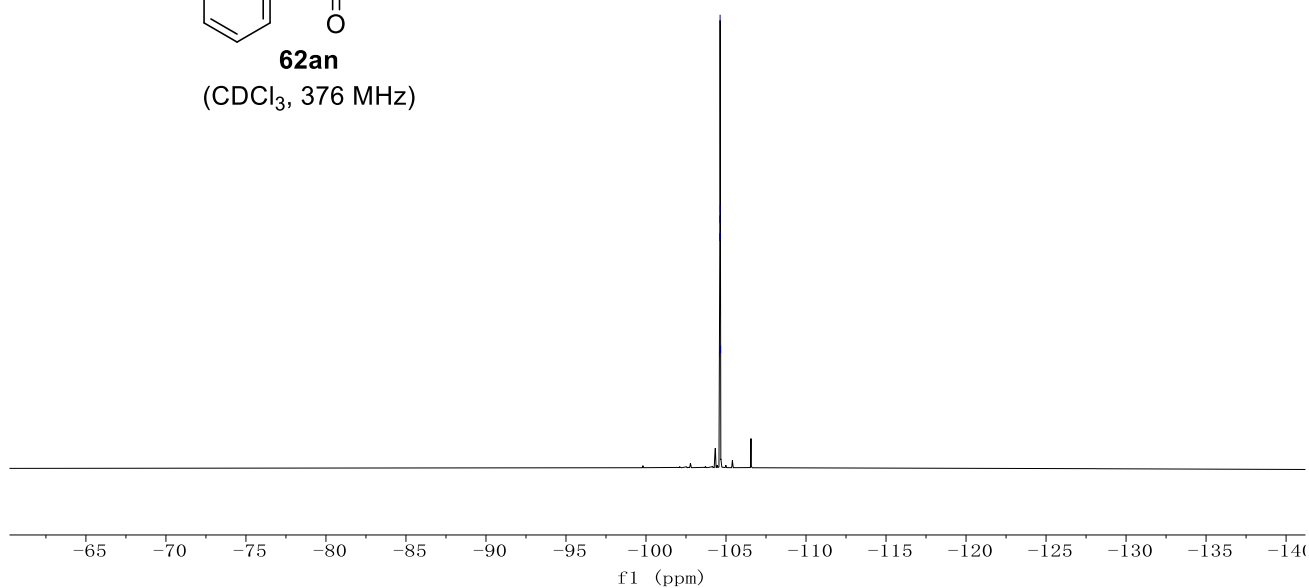
16.31



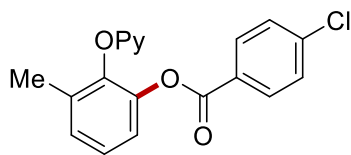
62an

(CDCl₃, 376 MHz)

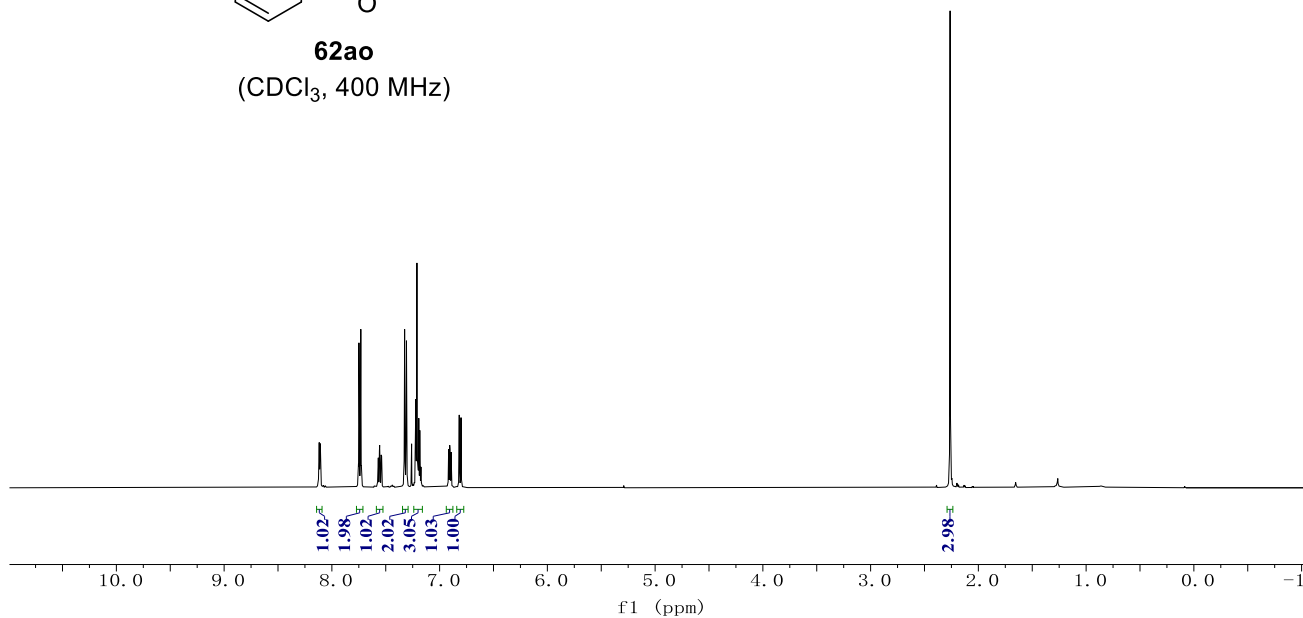
-104.60
-104.61
-104.62
-104.63
-104.64
-104.65
-104.66



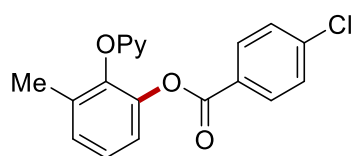
NMR Spectra



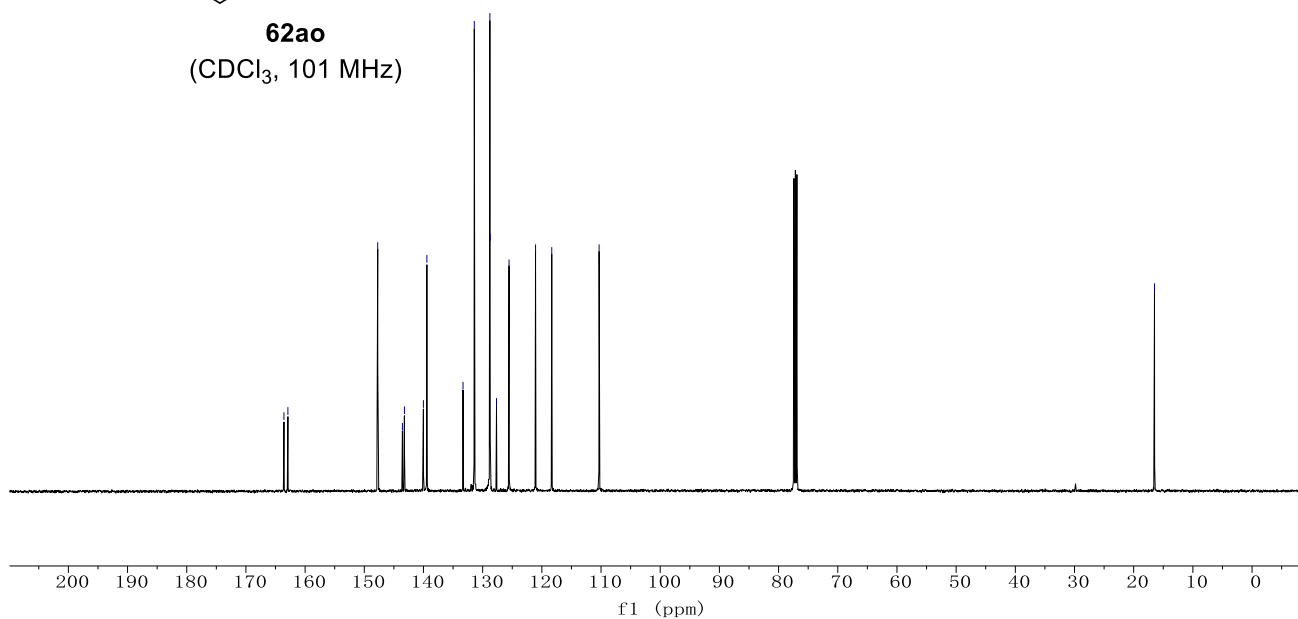
62ao
(CDCl₃, 400 MHz)



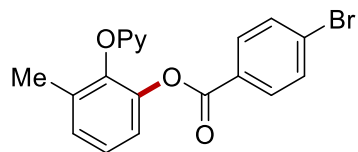
163.58
162.91
147.73
143.56
143.22
140.01
139.43
133.32
131.42
128.78
128.74
127.66
125.54
121.06
118.32
110.32
16.49



62ao
(CDCl₃, 101 MHz)

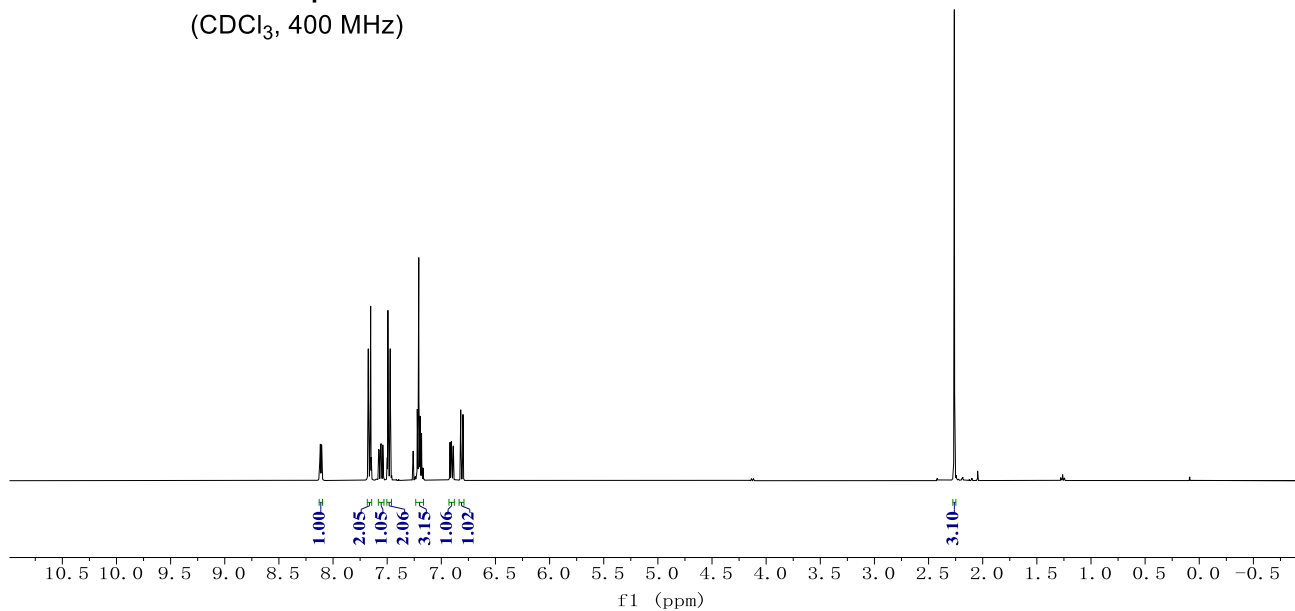


NMR Spectra



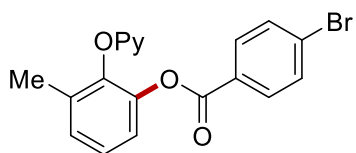
62ap

(CDCl₃, 400 MHz)



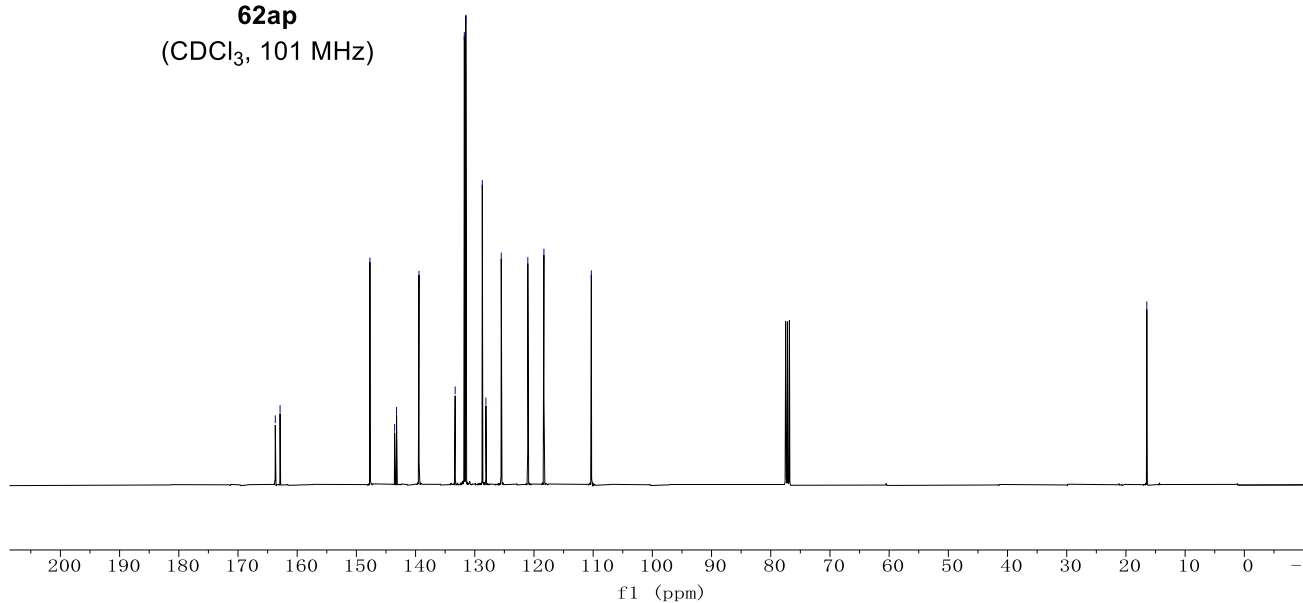
163.70
162.89
147.71
145.54
143.21
139.43
133.31
131.77
131.51
128.73
128.12
125.53
121.04
118.32
110.31

16.47

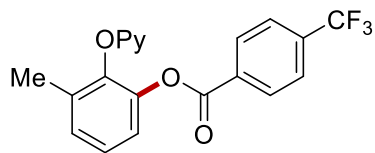


62ap

(CDCl₃, 101 MHz)

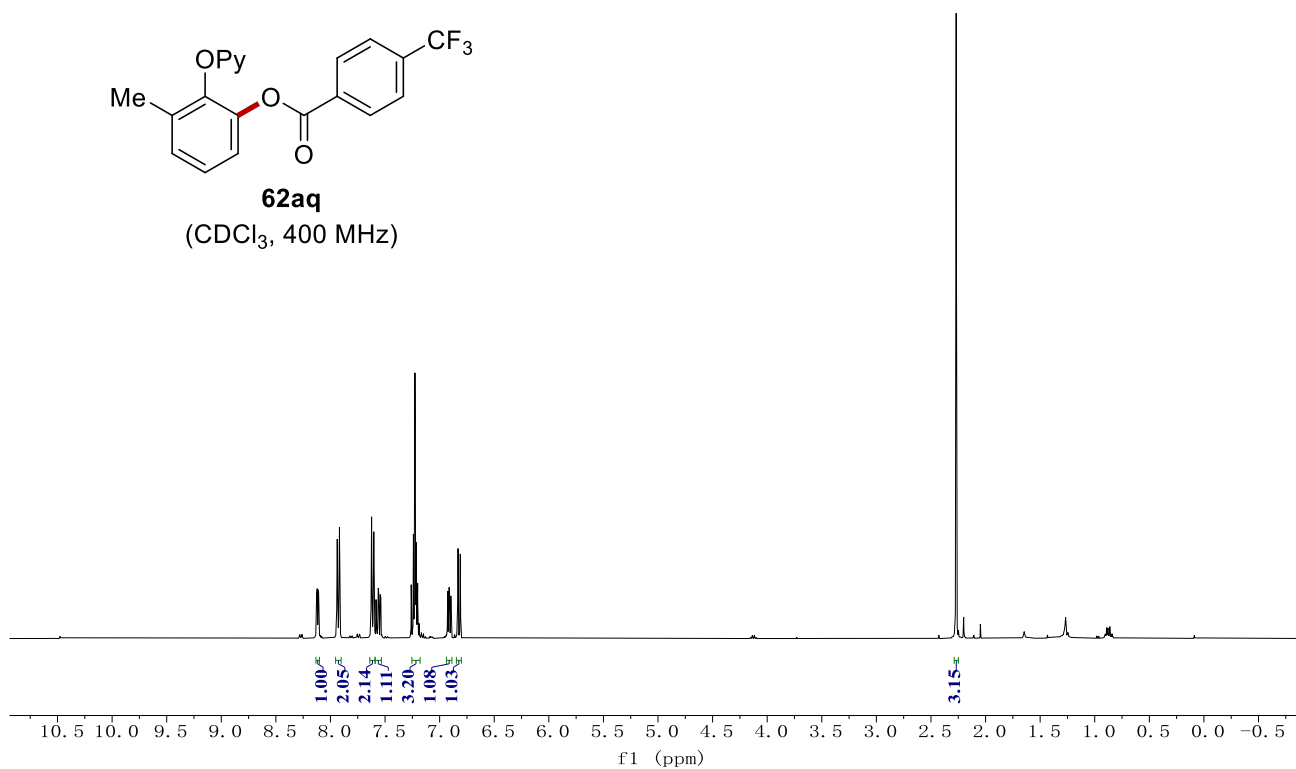


NMR Spectra



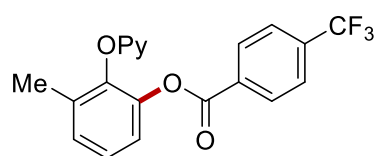
62aq

(CDCl₃, 400 MHz)



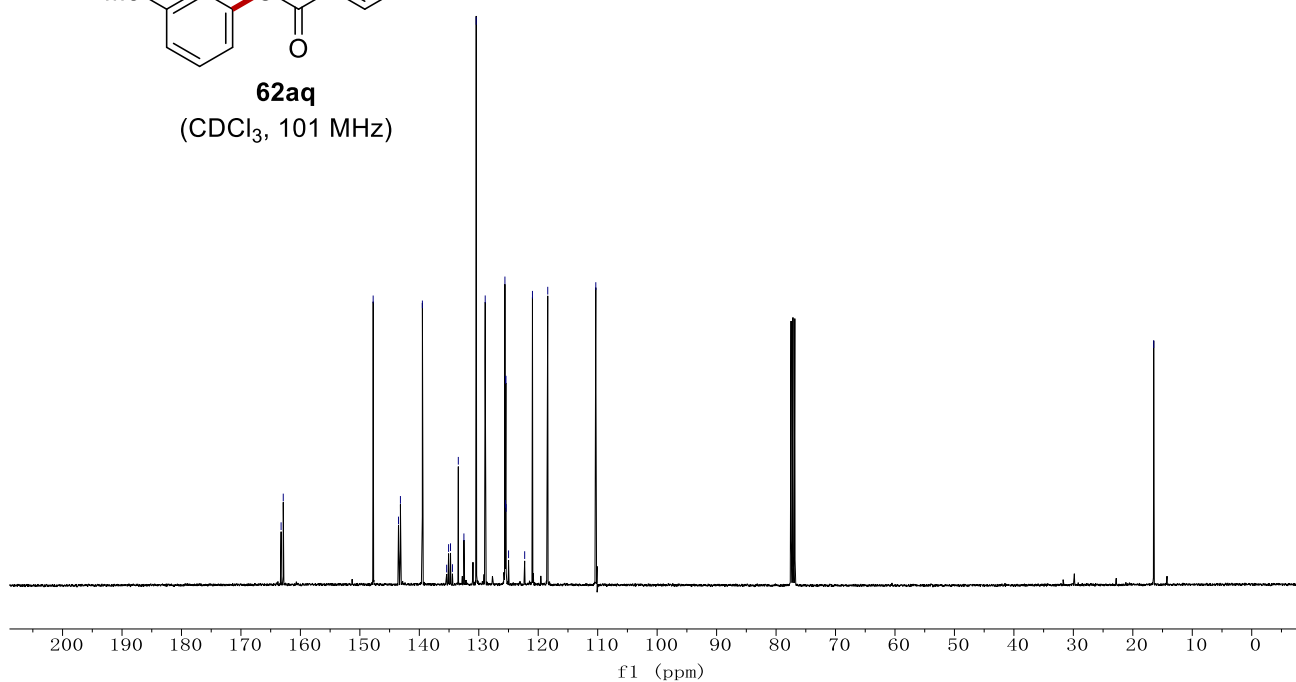
163.25
162.88
147.76
143.50
143.18
139.48
135.40
135.08
134.75
134.43
133.44
132.50
130.43
128.92
125.60
125.51
125.48
125.44
125.40
124.99
122.28
120.97
118.40
110.32

16.49

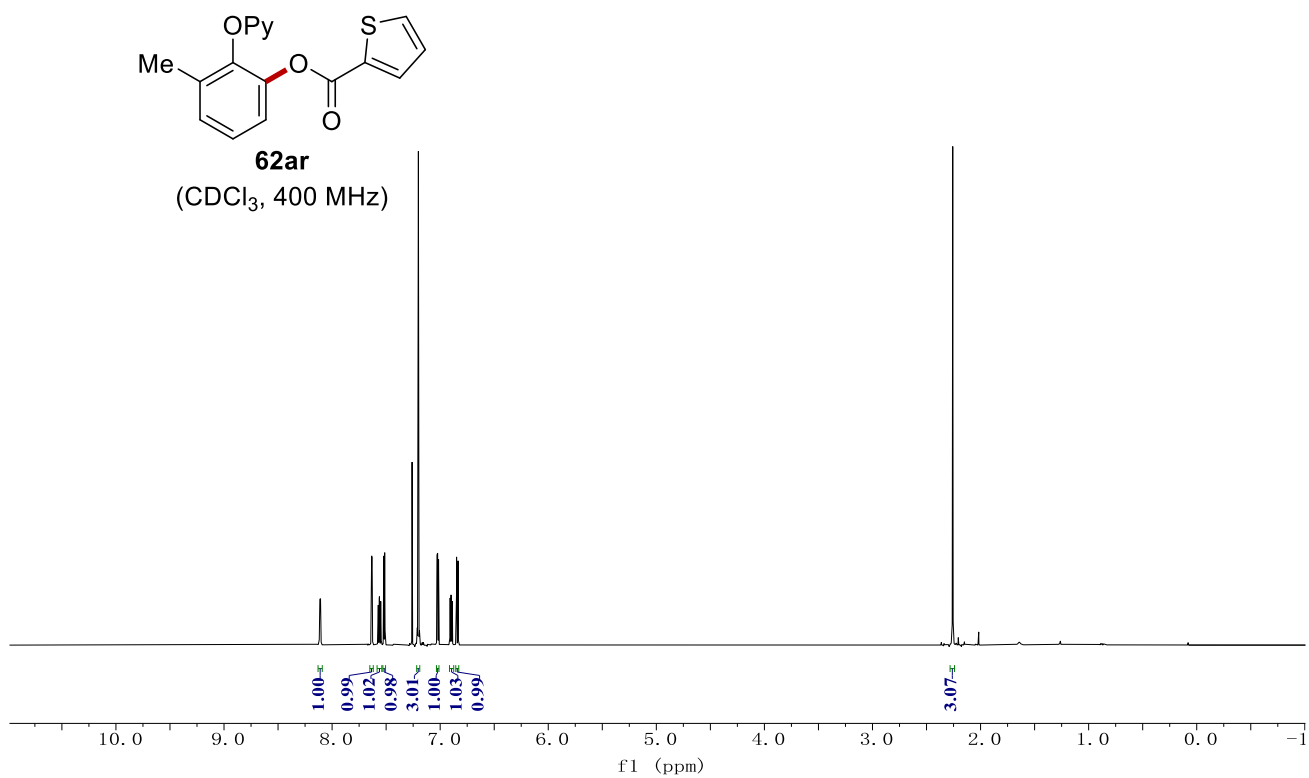
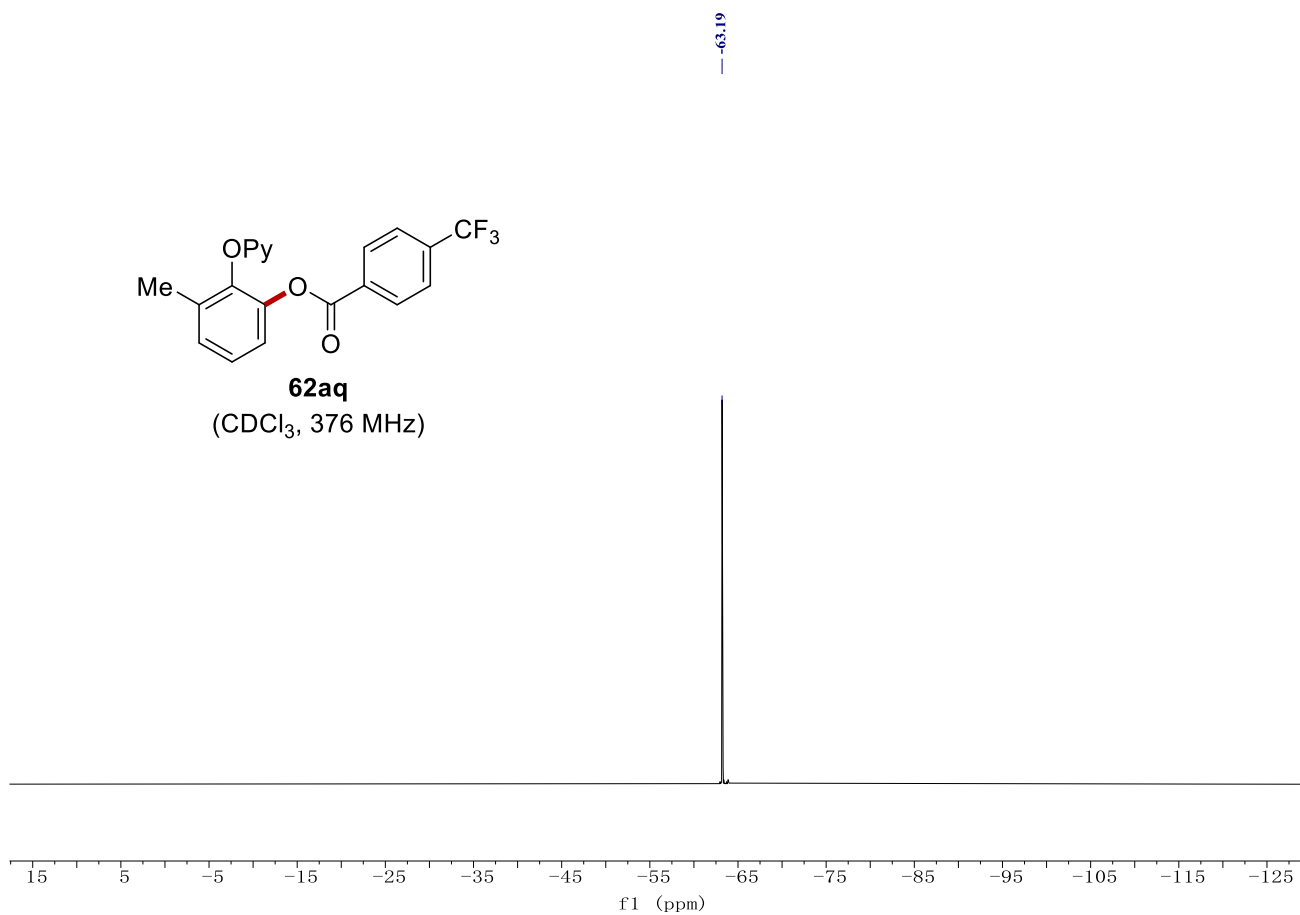


62aq

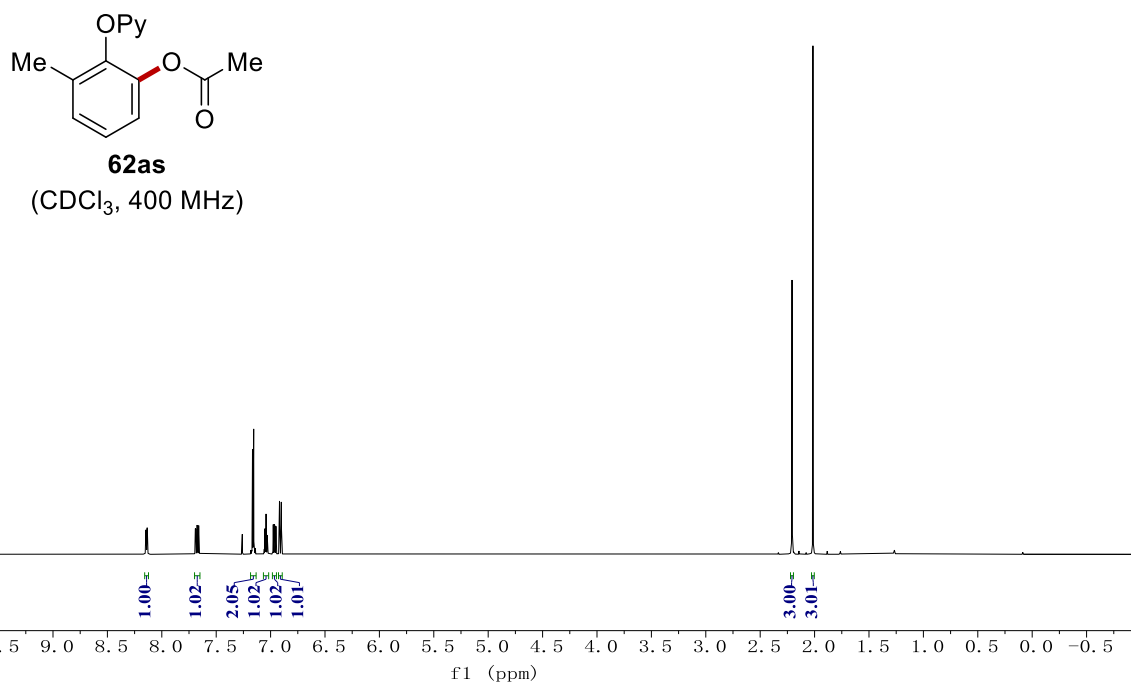
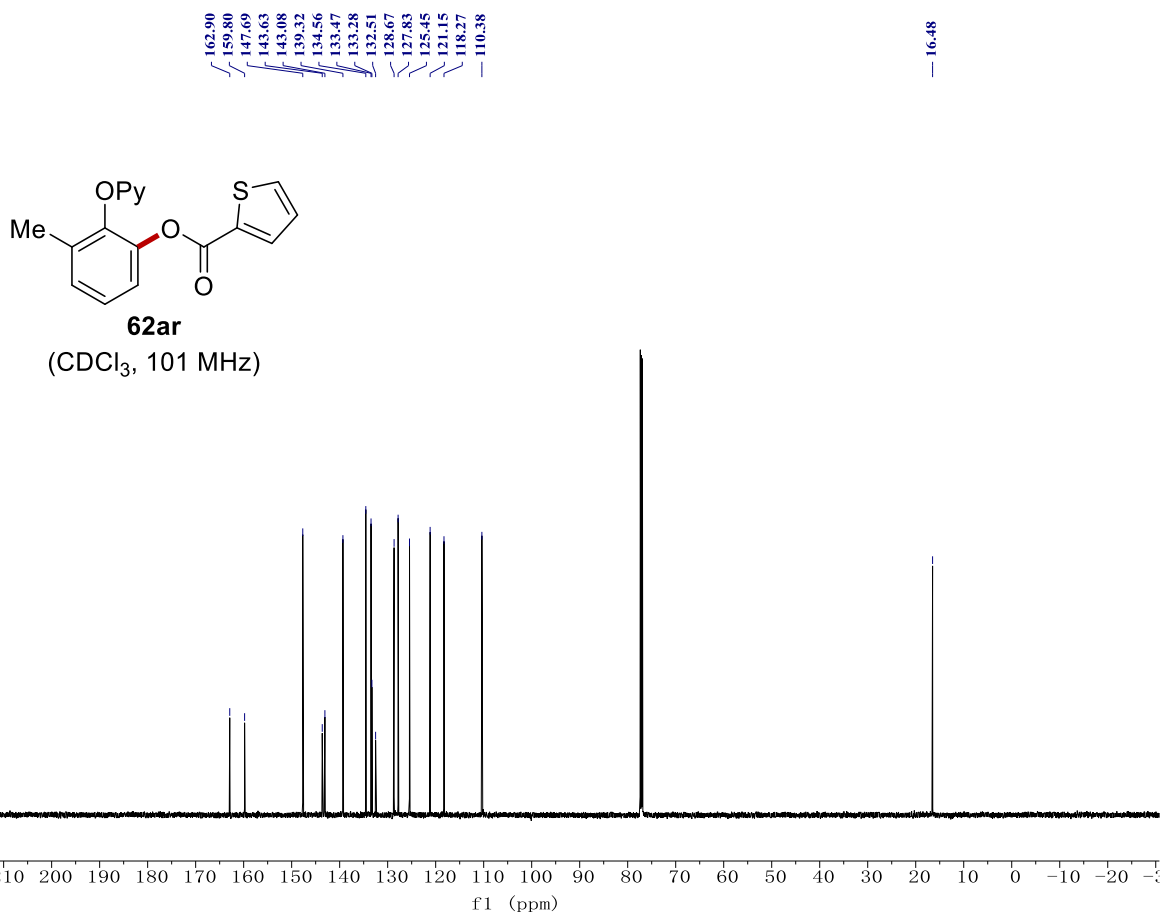
(CDCl₃, 101 MHz)



NMR Spectra

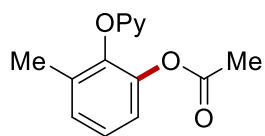


NMR Spectra



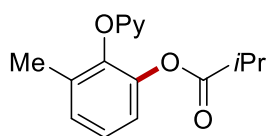
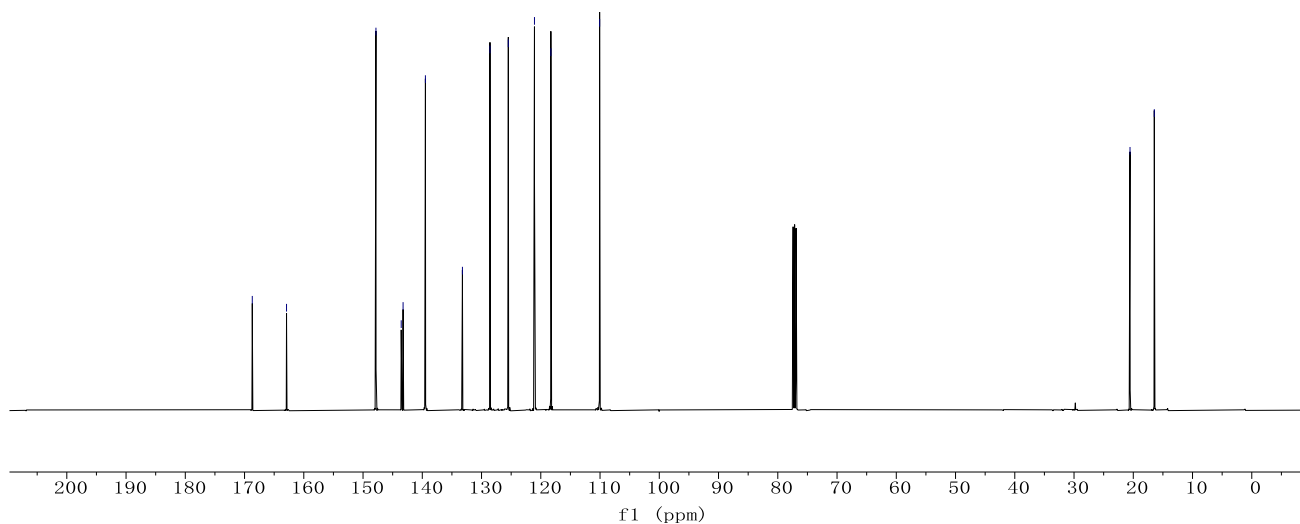
NMR Spectra

168.69
162.91
147.82
143.56
143.24
139.48
133.23
128.58
125.48
121.07
118.30
110.07
20.55
16.45



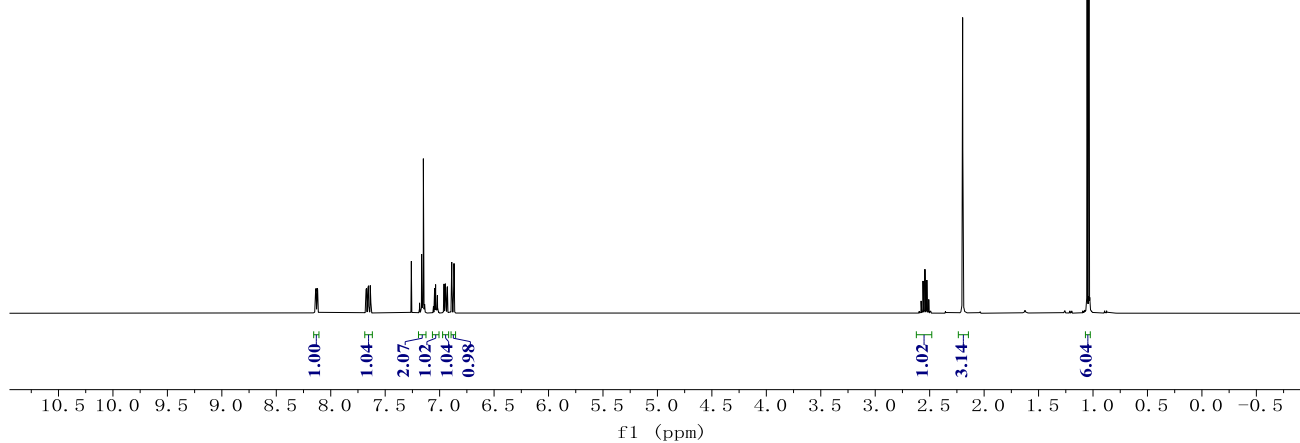
62as

(CDCl₃, 101 MHz)



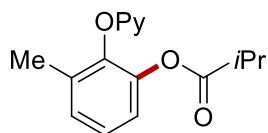
62at

(CDCl₃, 400 MHz)

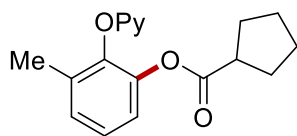
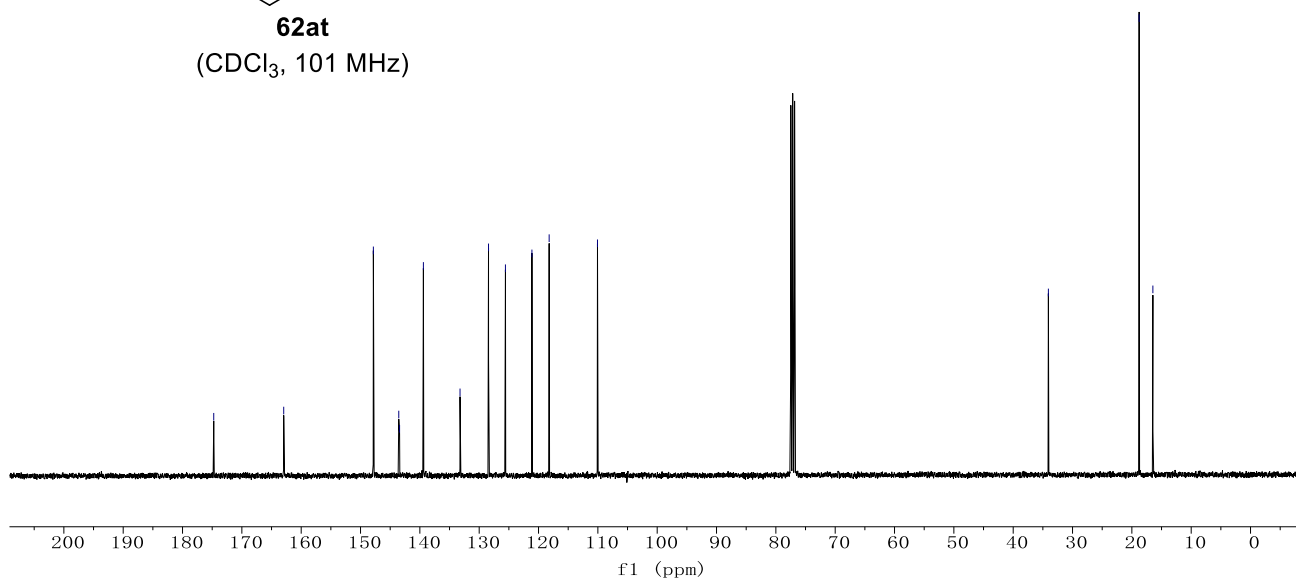


NMR Spectra

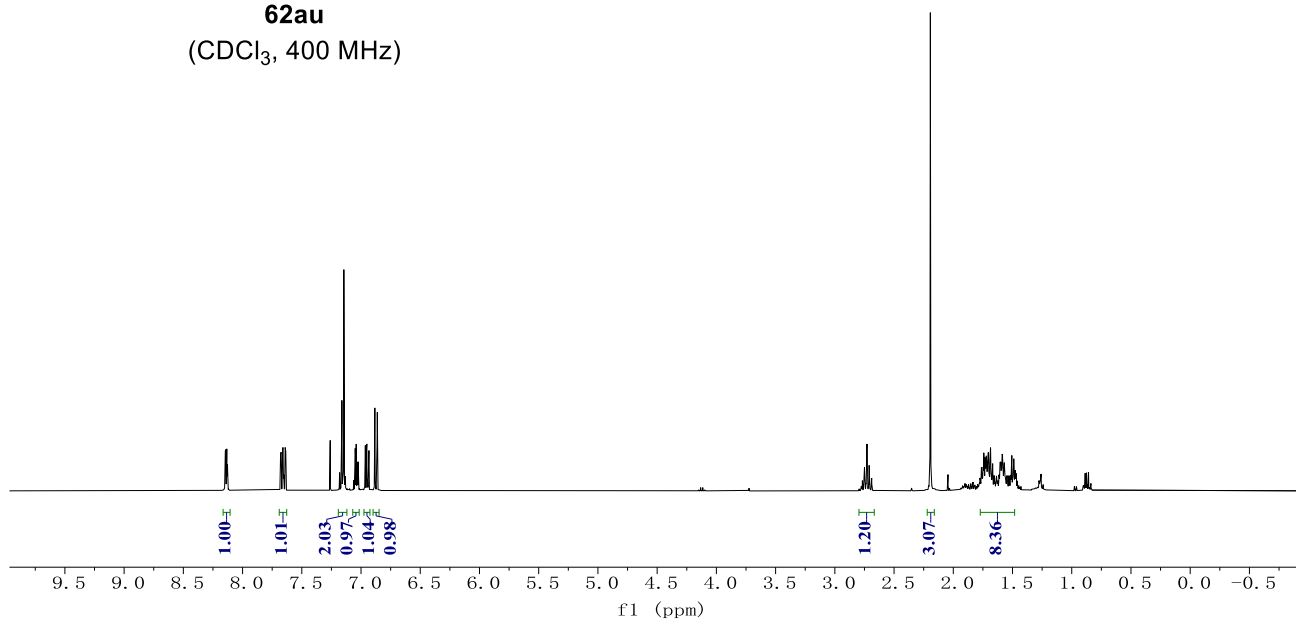
174.74
162.95
147.83
143.55
143.42
139.40
133.23
128.43
125.58
121.11
118.21
110.06
34.07
18.78
16.46



62at
(CDCl₃, 101 MHz)

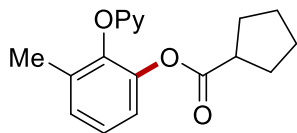


62au
(CDCl₃, 400 MHz)

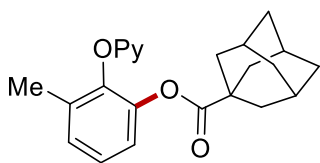
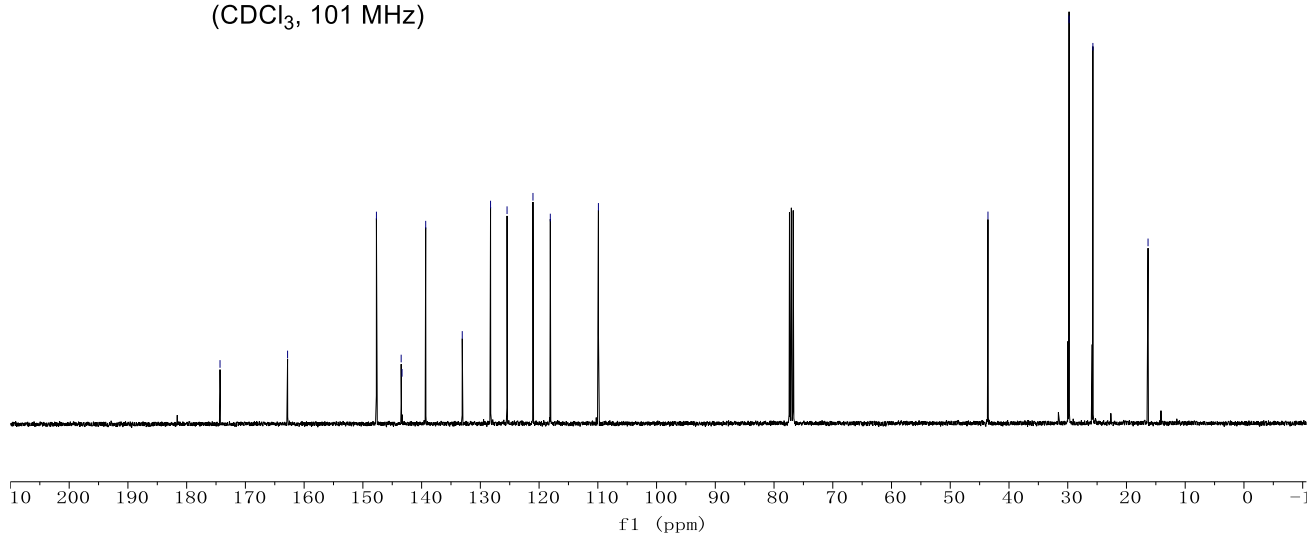


NMR Spectra

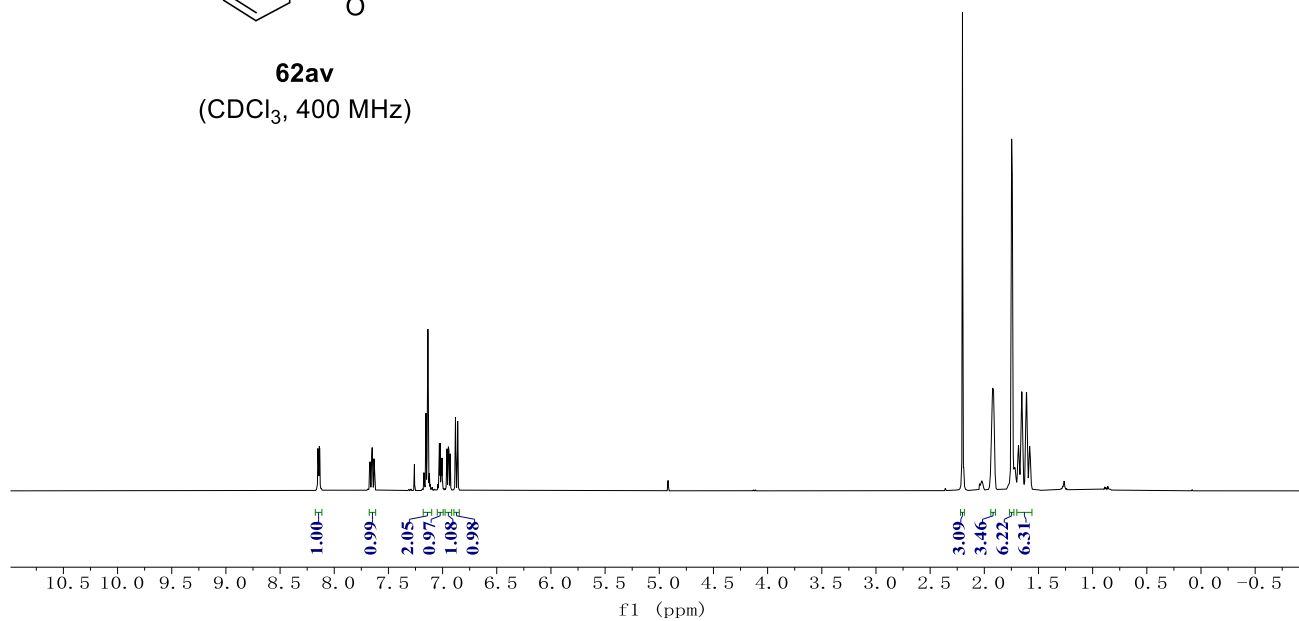
174.32 162.82 147.69 143.48 143.33 139.30 133.08 128.26 125.45 121.04 118.09 109.90 43.58 29.77 25.72 16.33



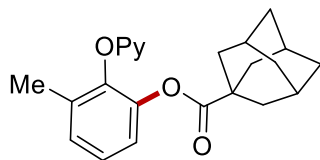
62au
(CDCl₃, 101 MHz)



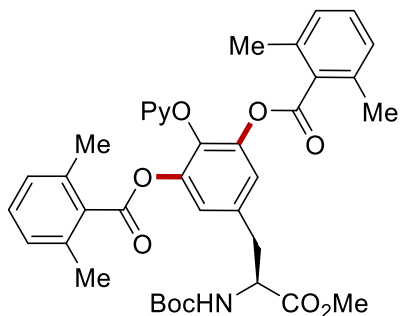
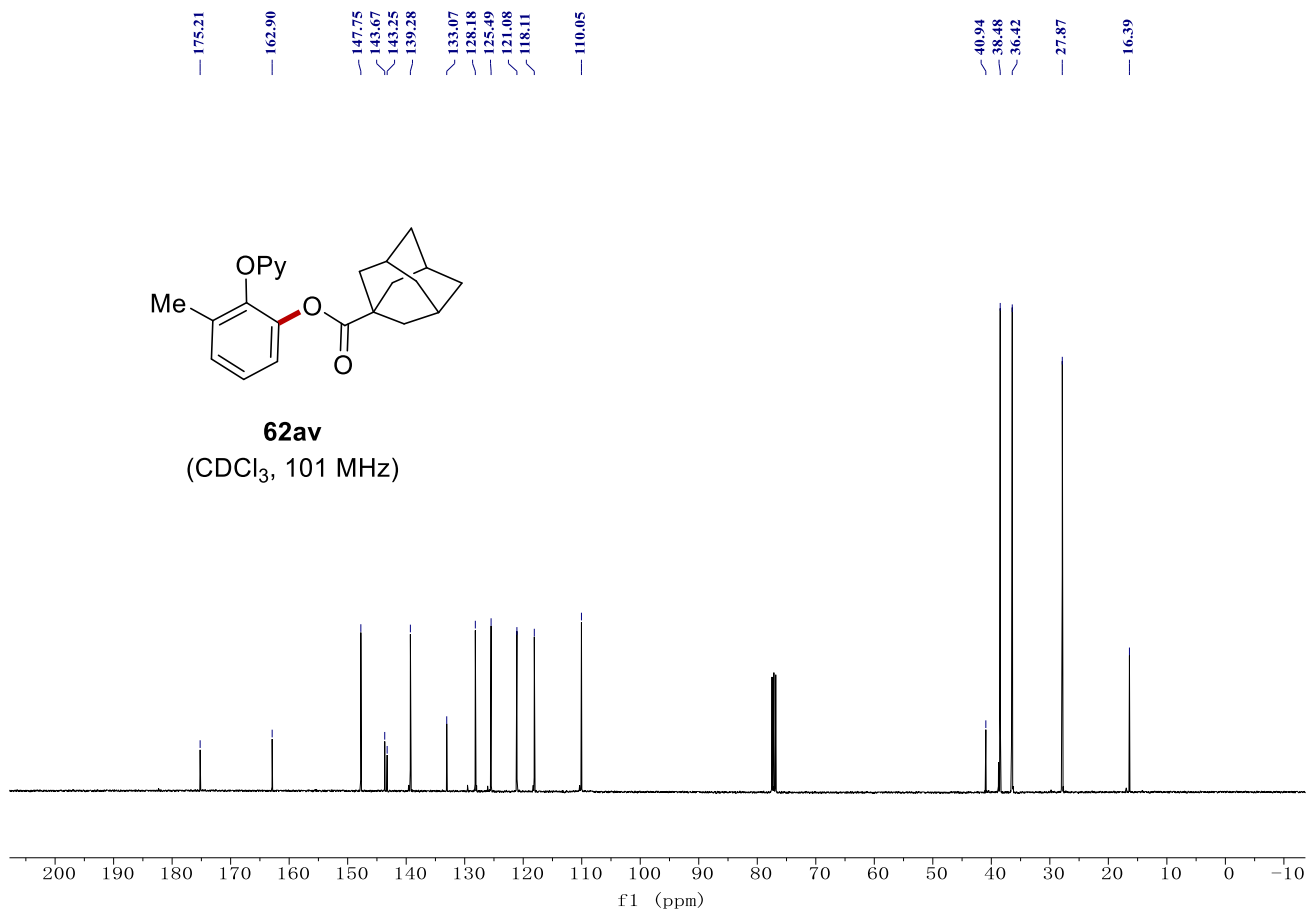
62av
(CDCl₃, 400 MHz)



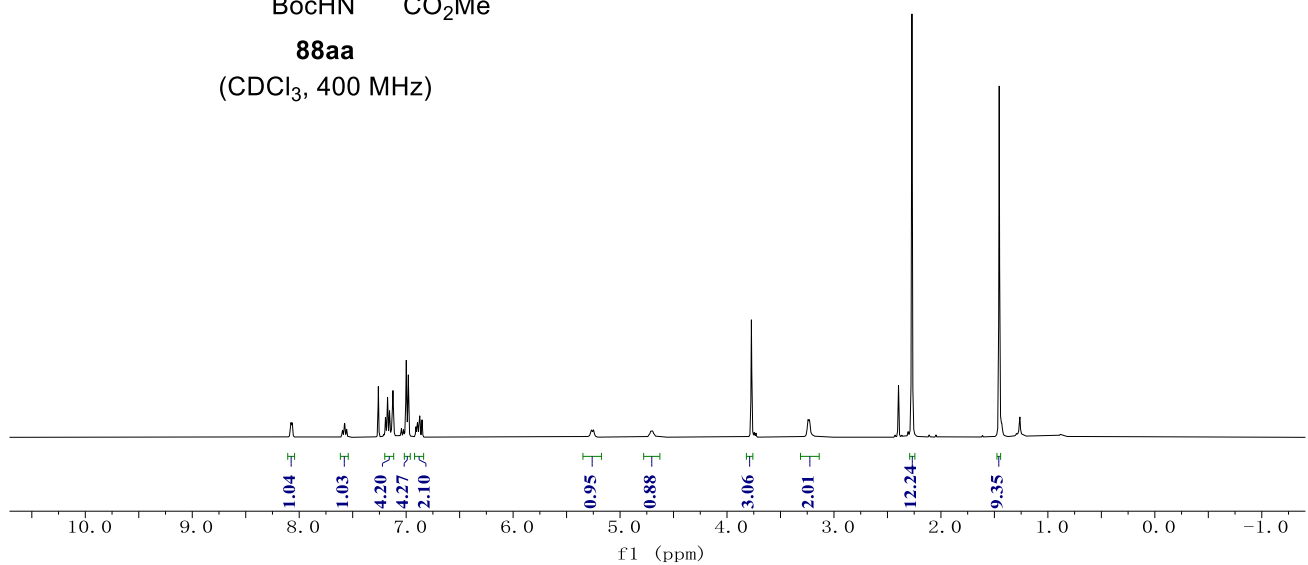
NMR Spectra



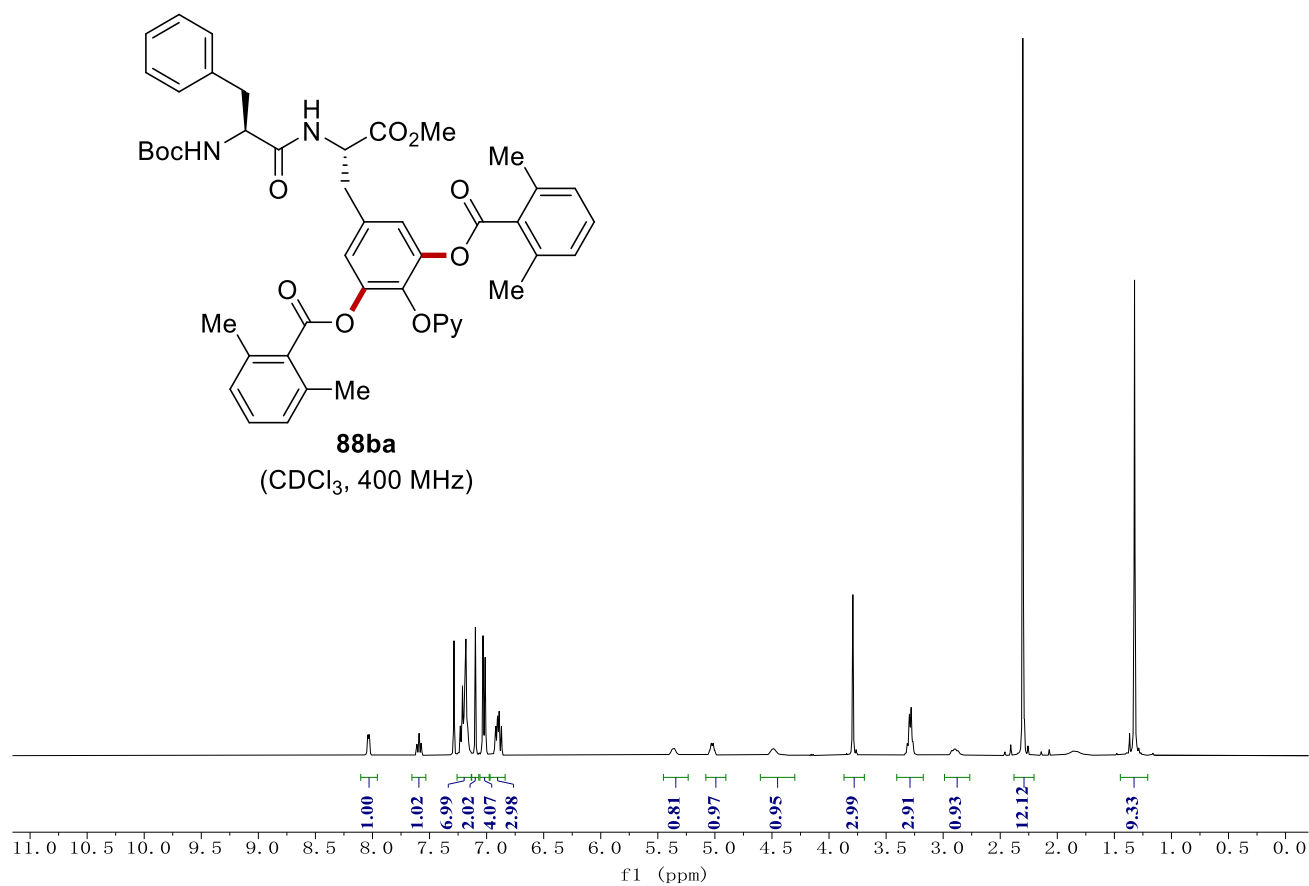
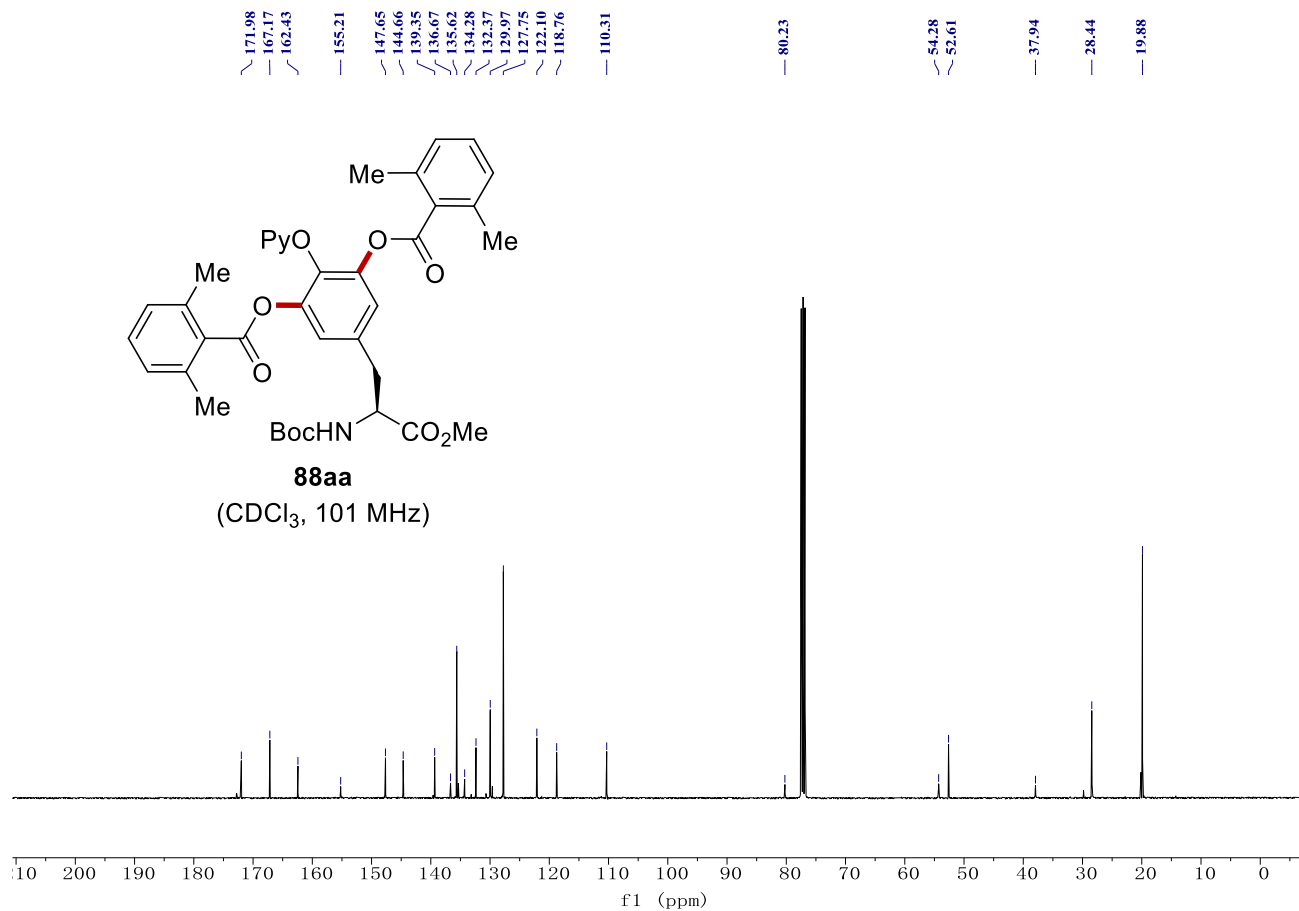
62av
(CDCl₃, 101 MHz)



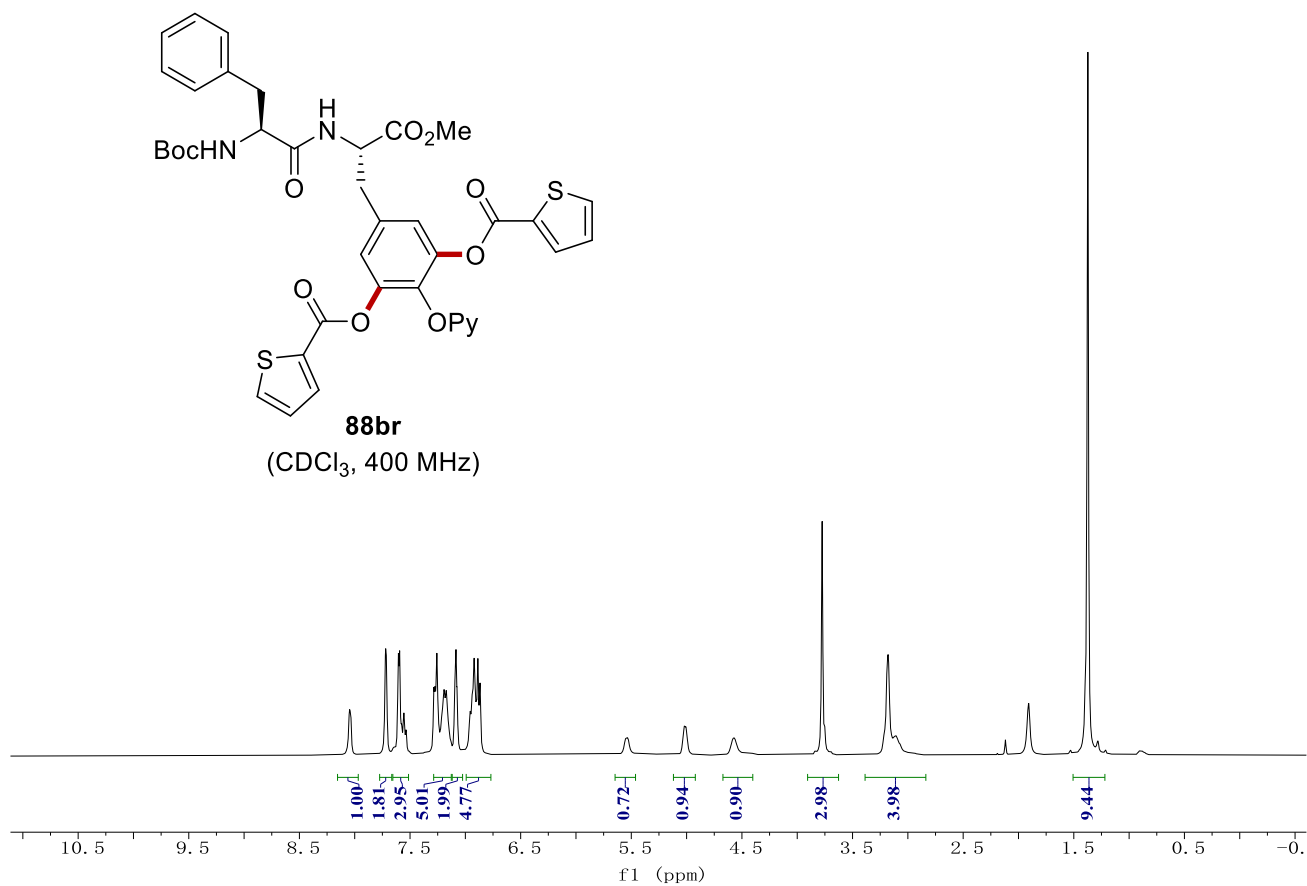
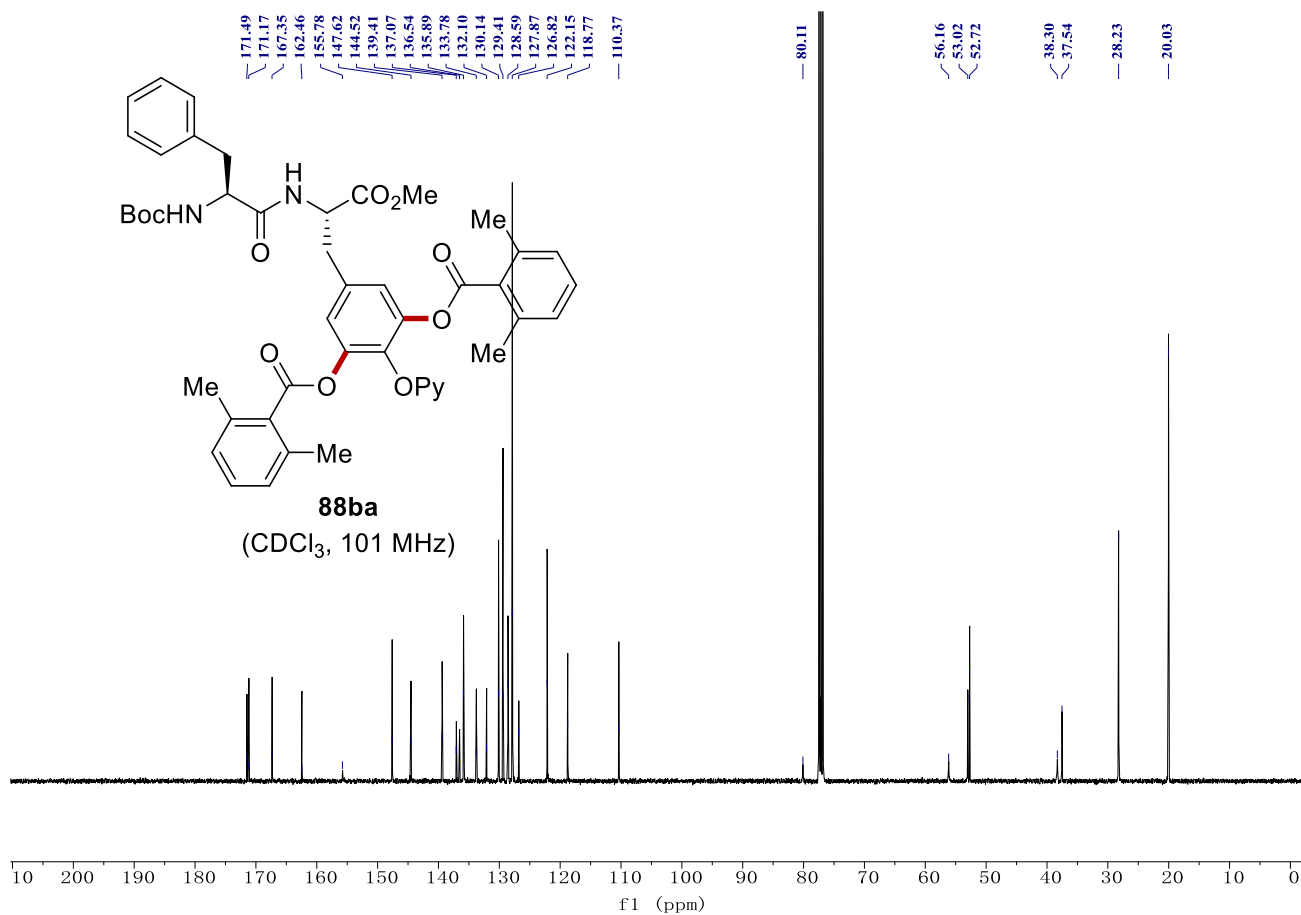
88aa
(CDCl₃, 400 MHz)



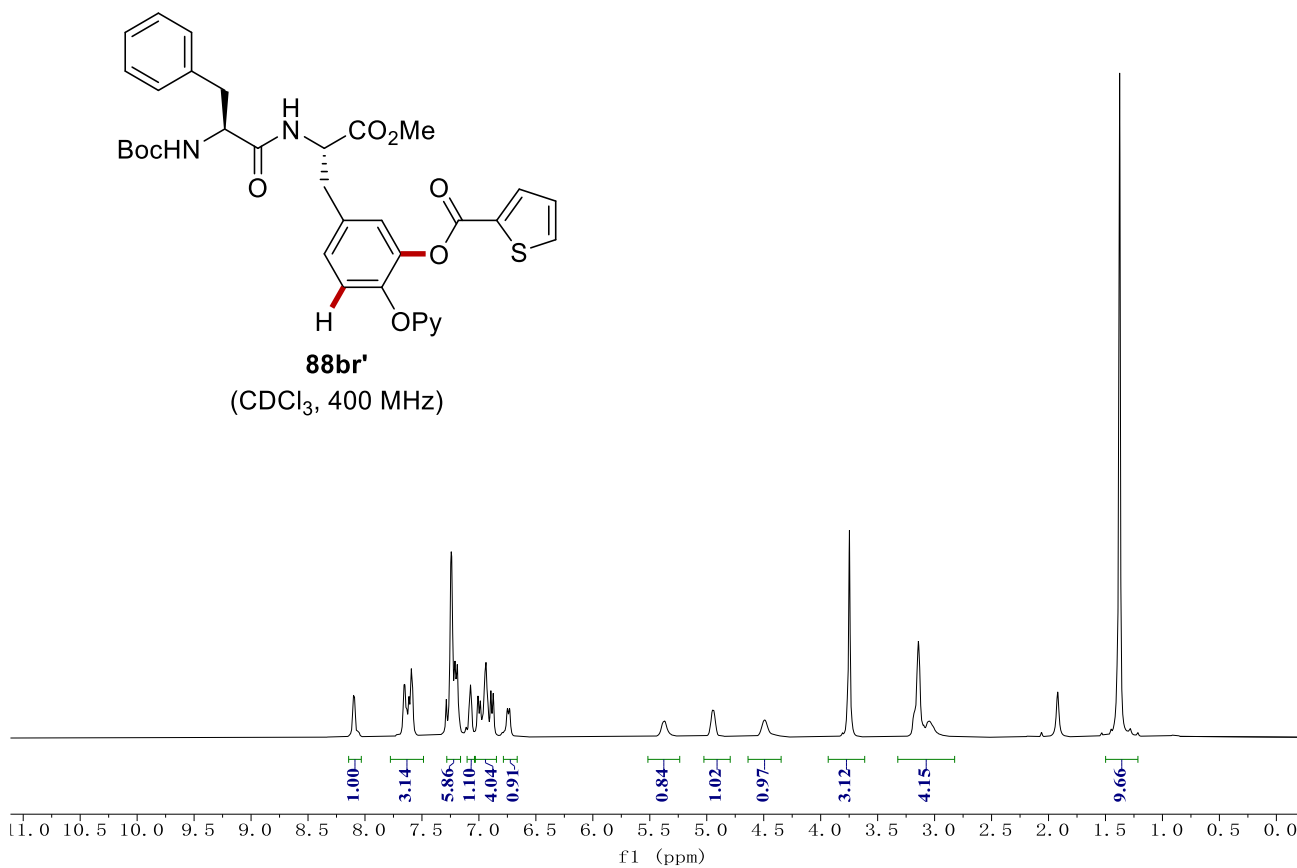
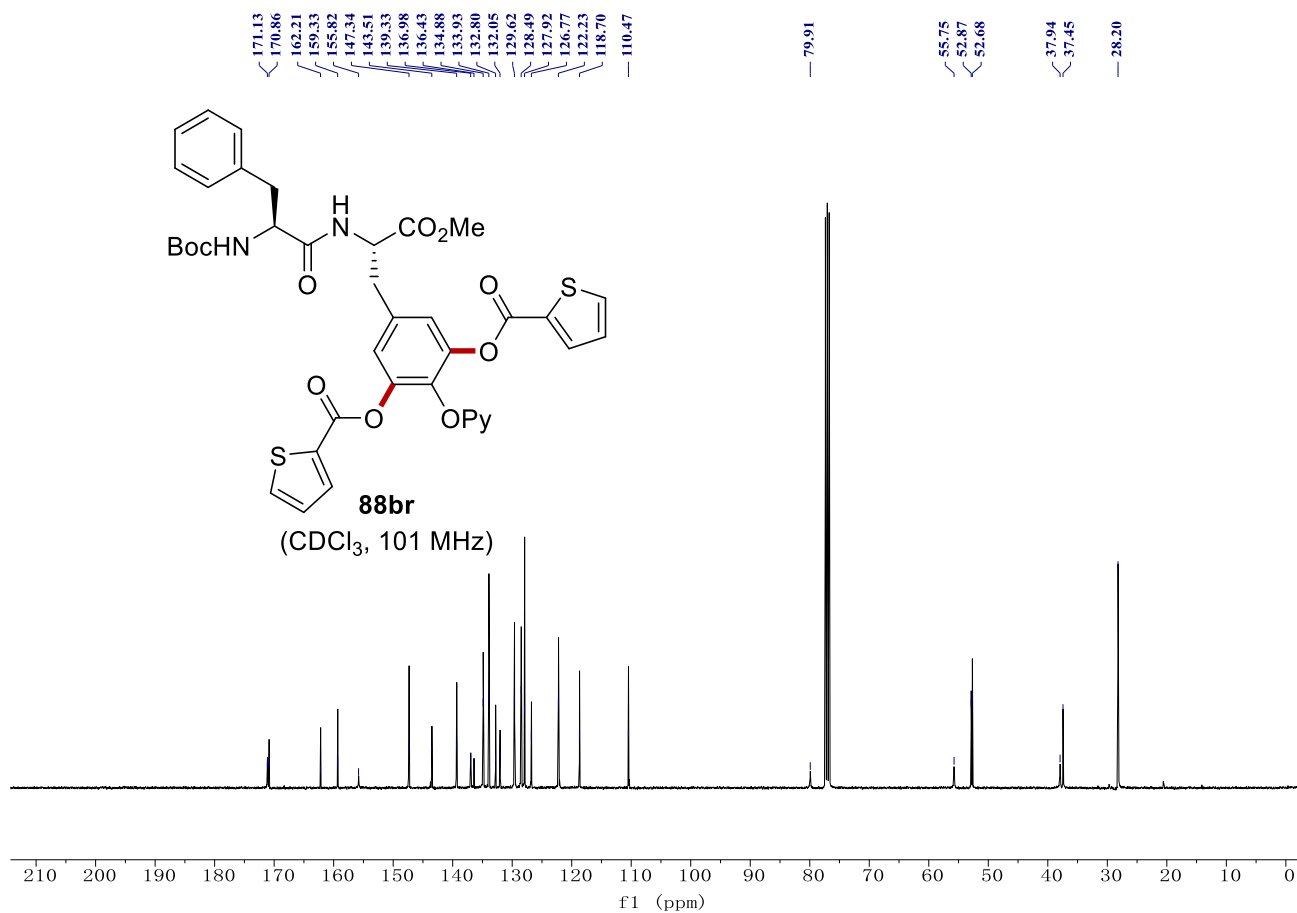
NMR Spectra



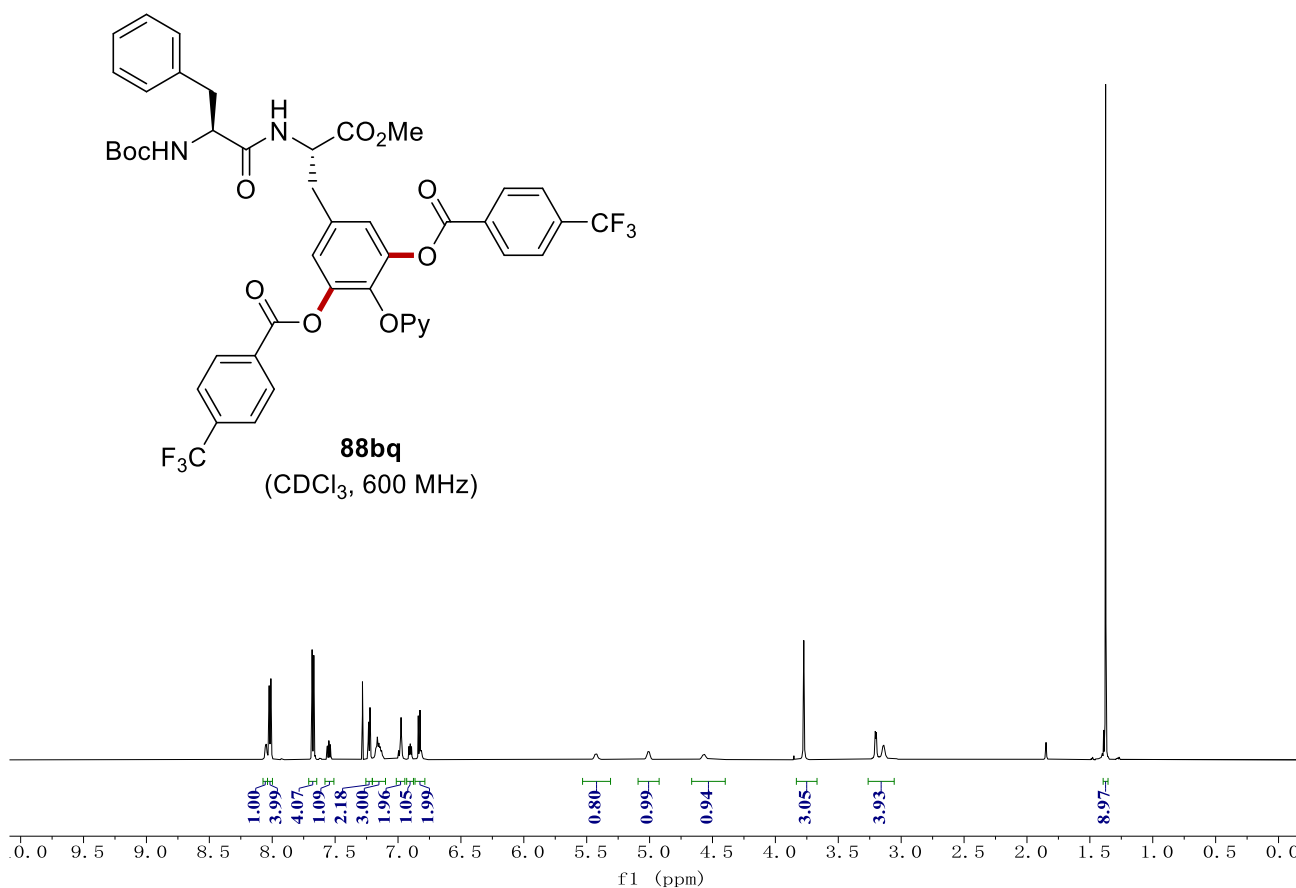
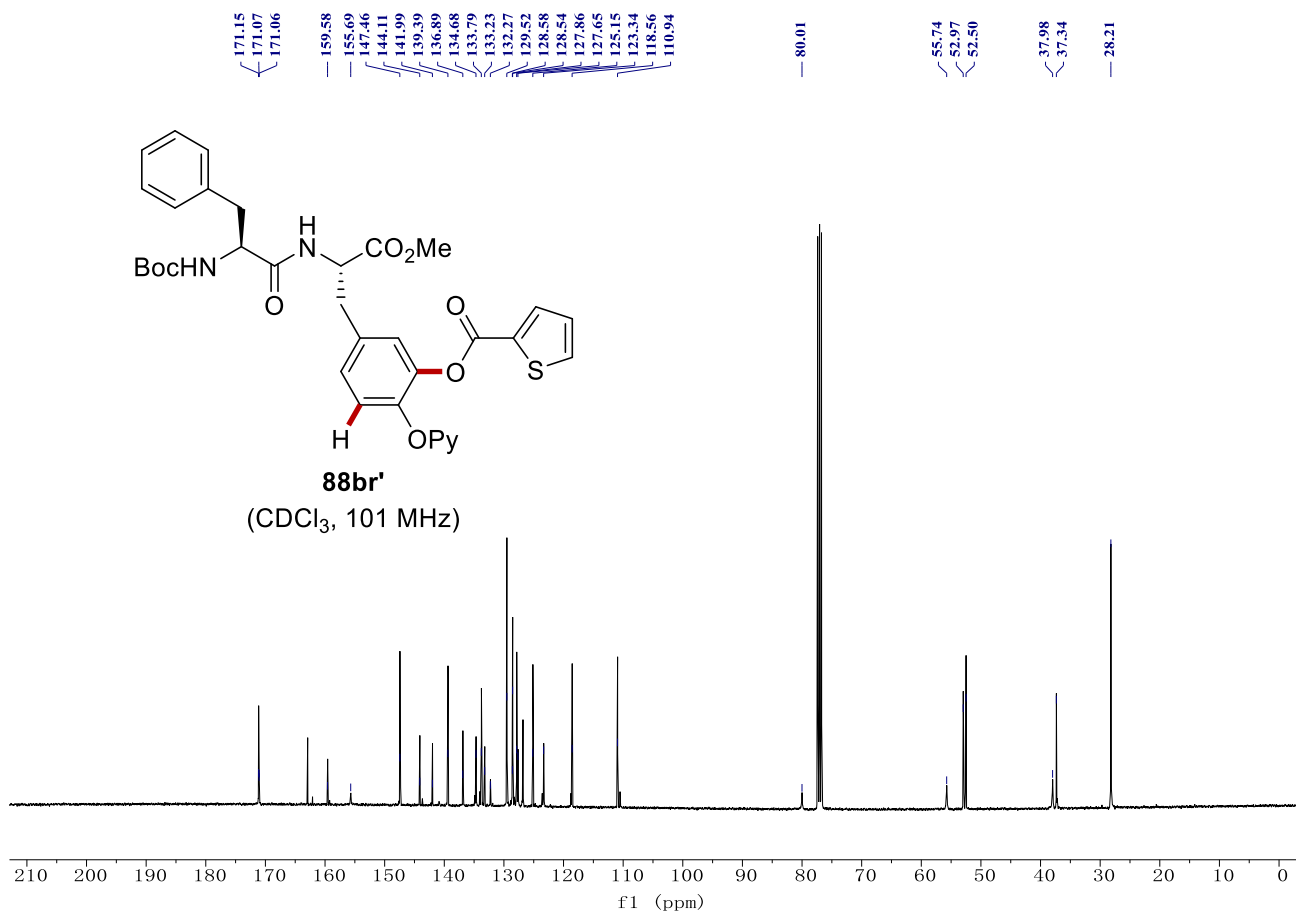
NMR Spectra



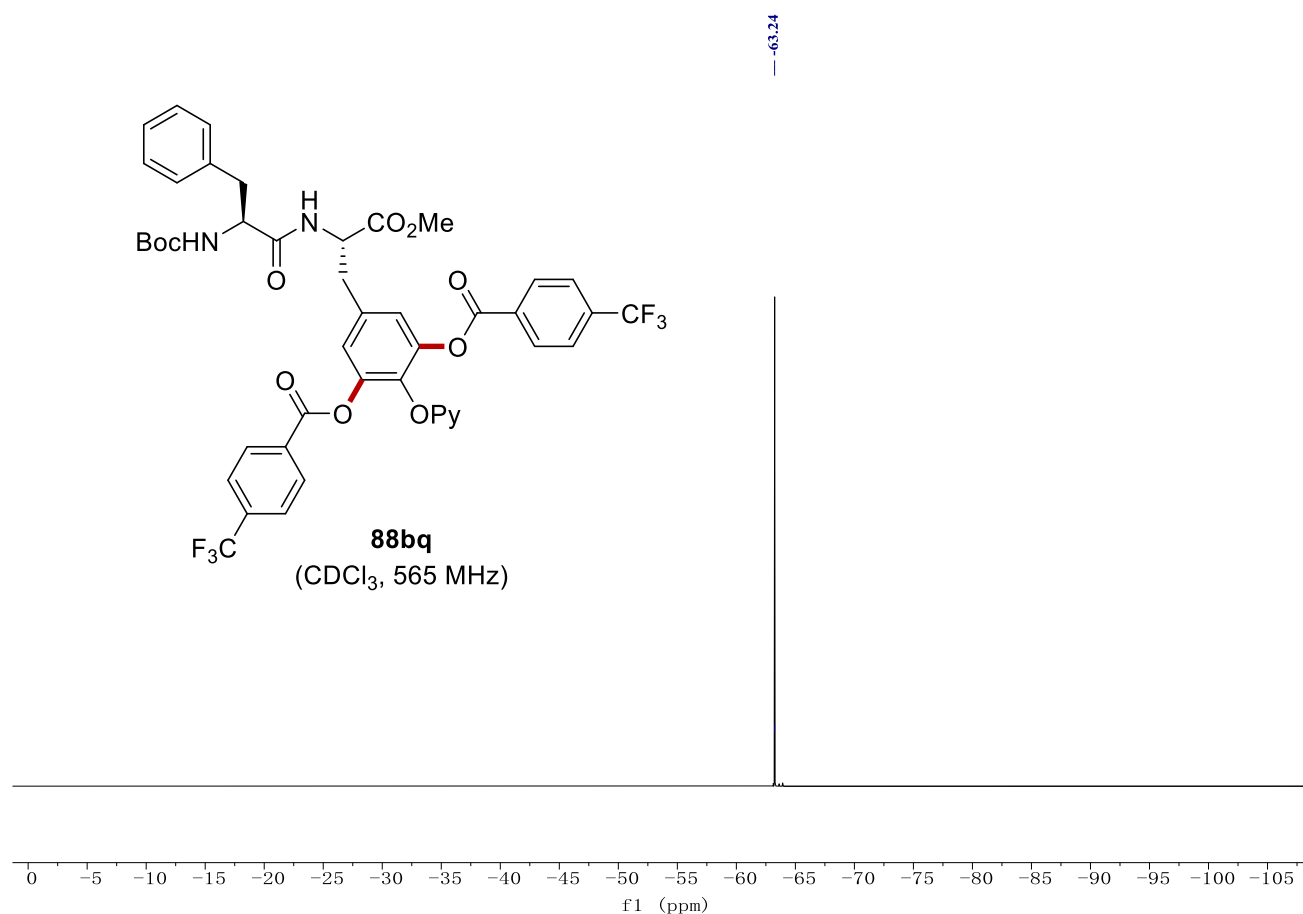
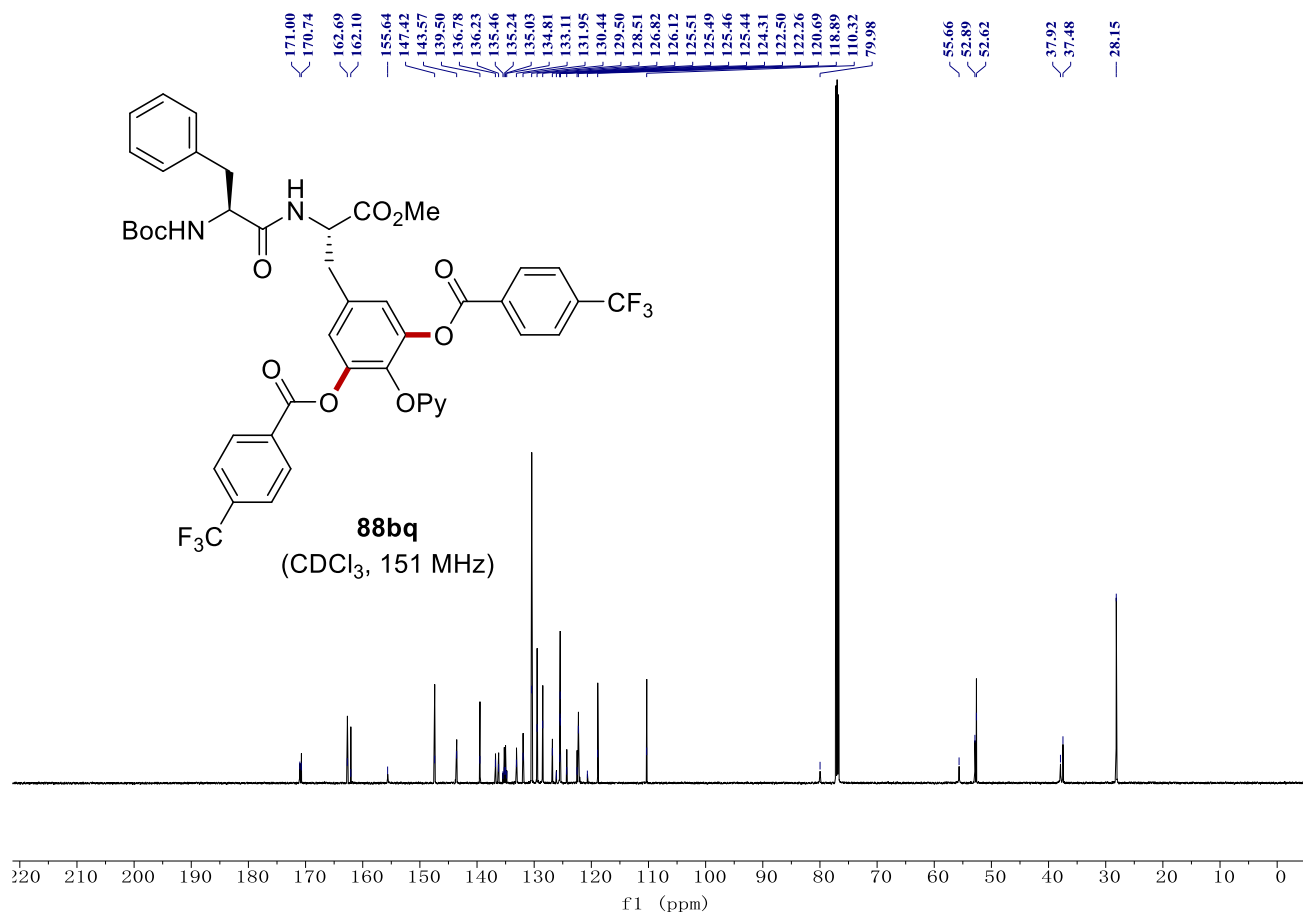
NMR Spectra



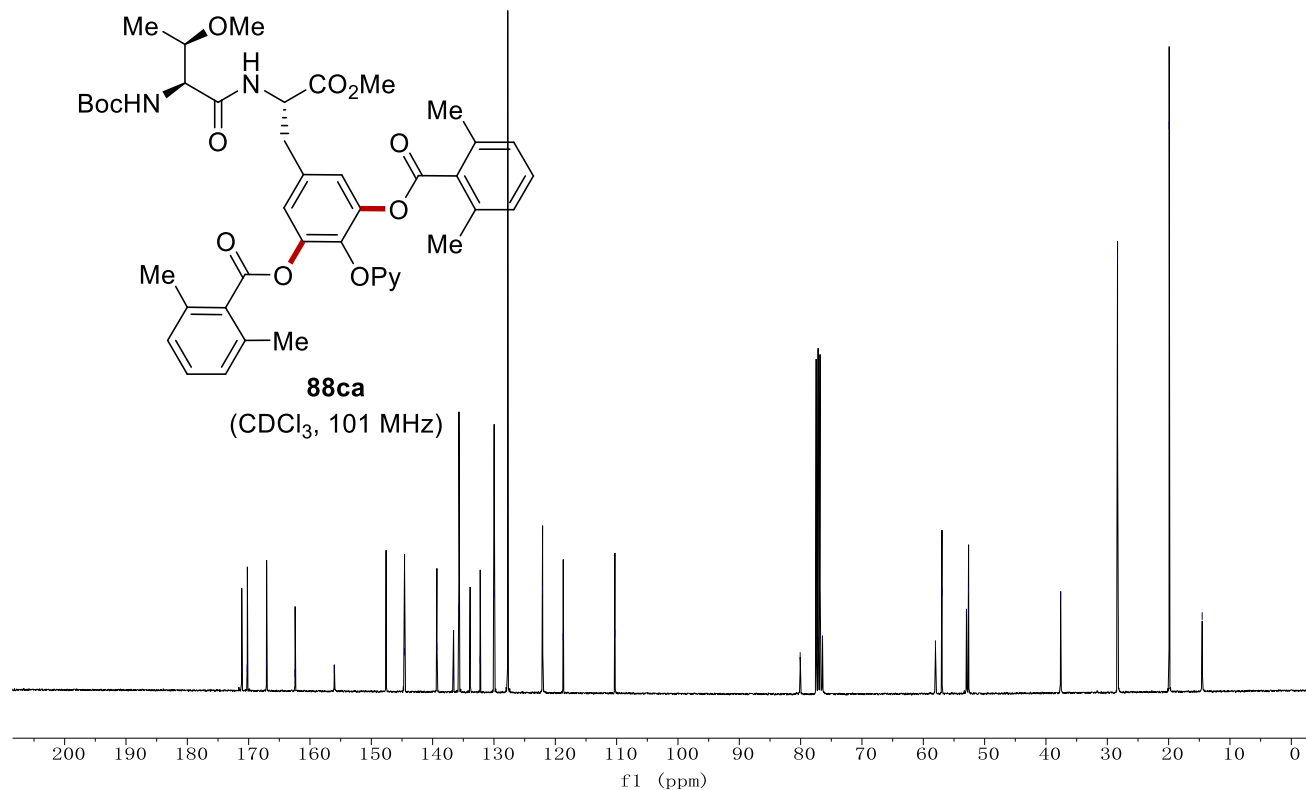
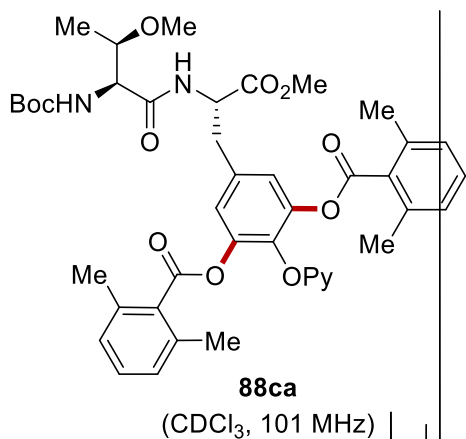
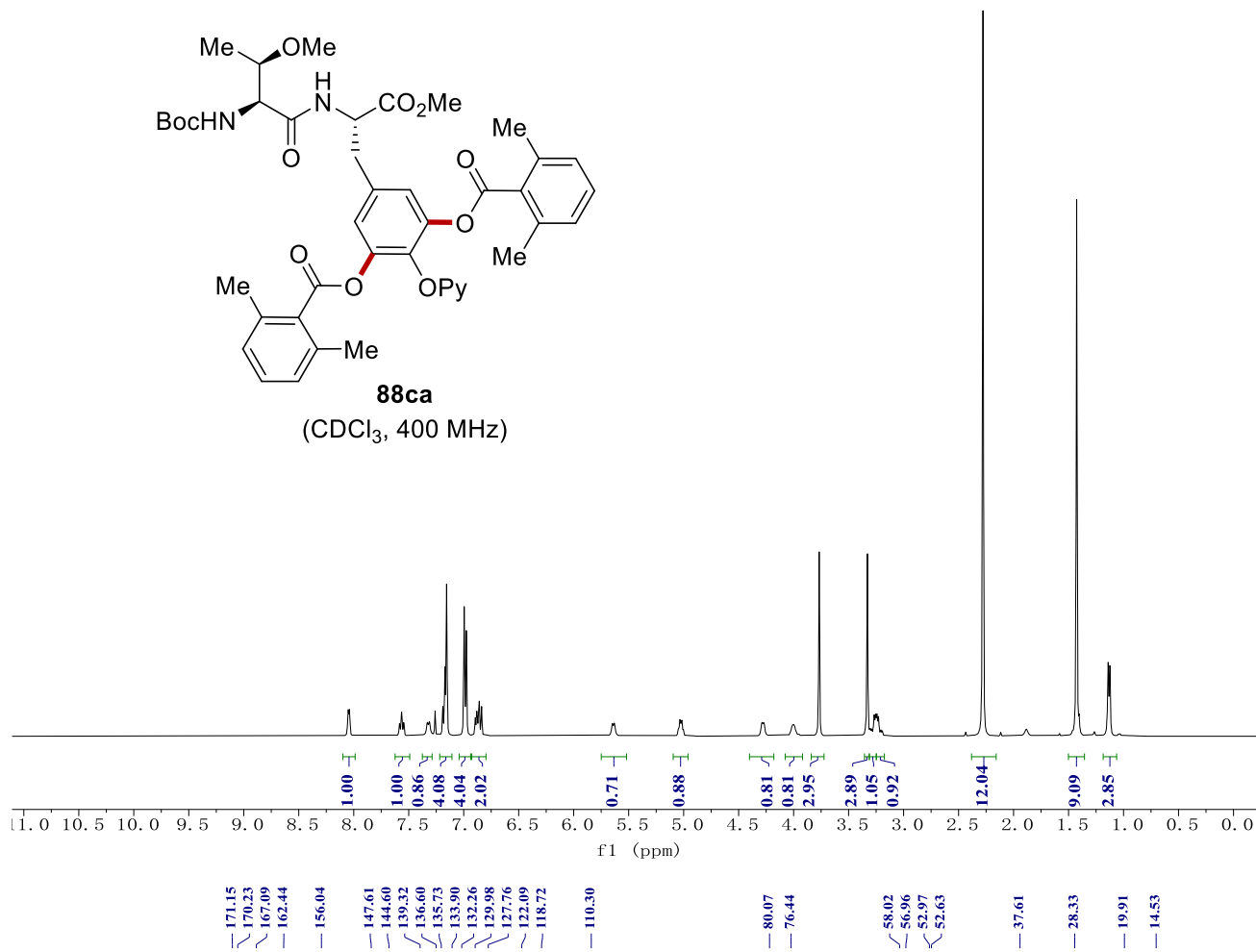
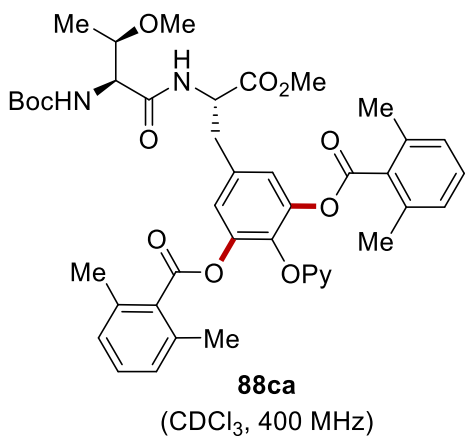
NMR Spectra



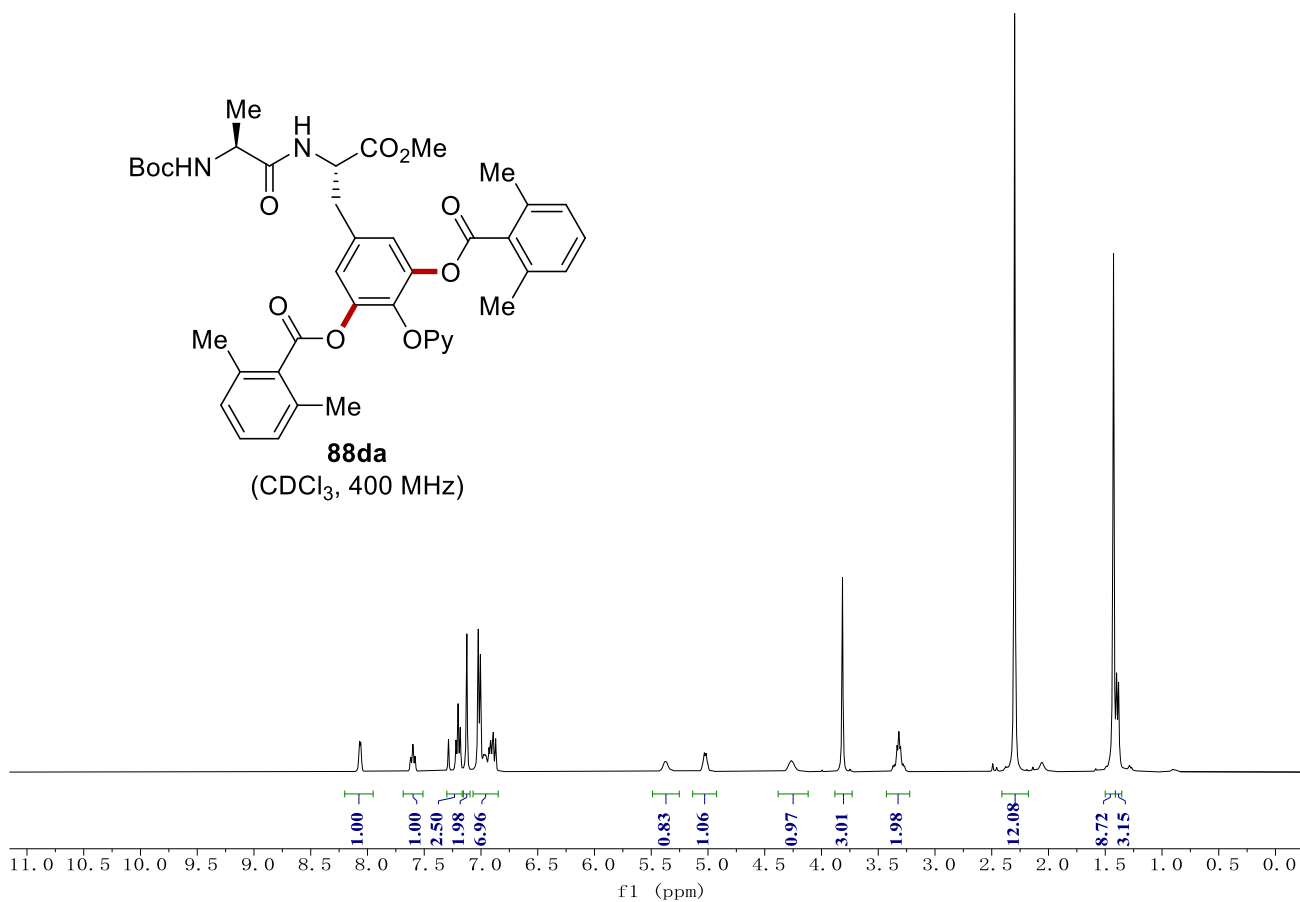
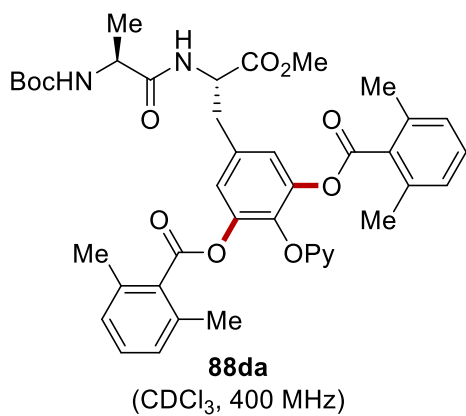
NMR Spectra



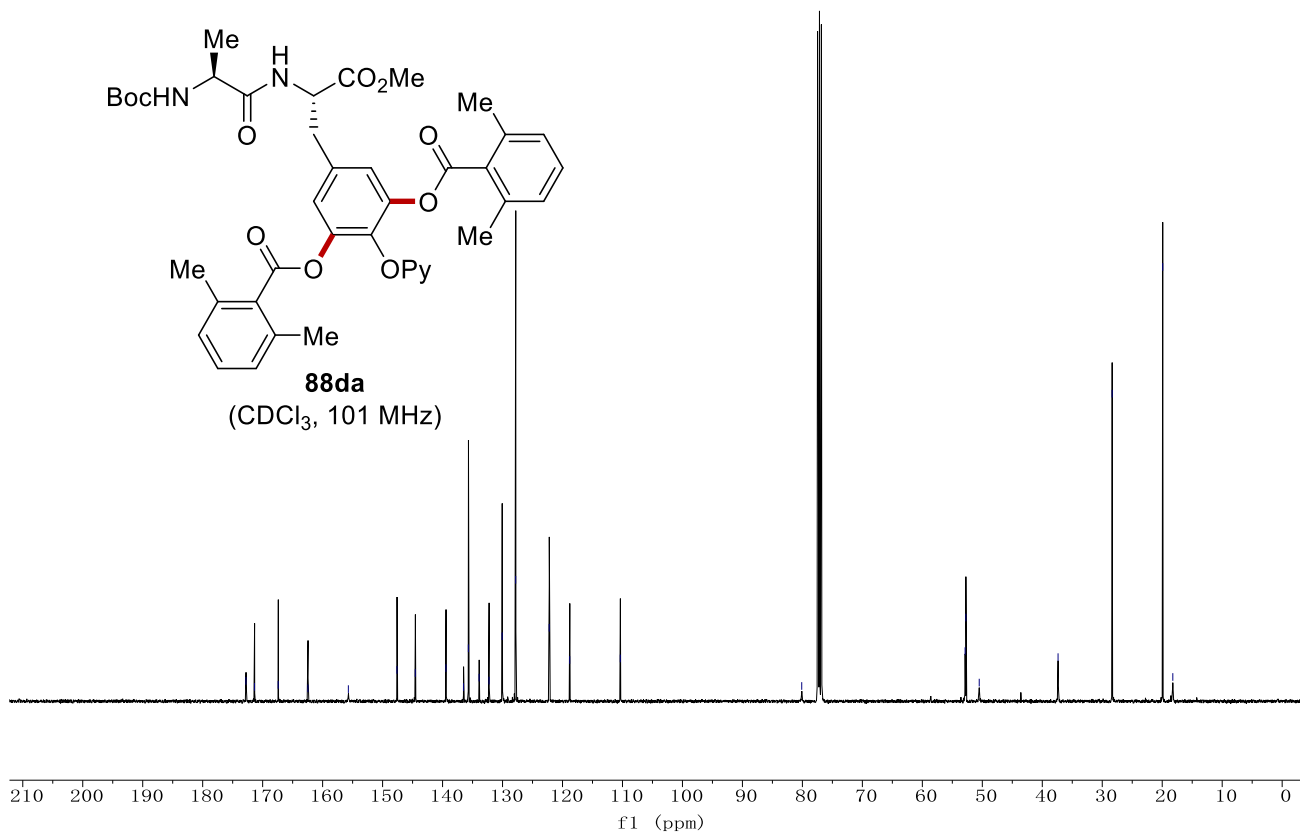
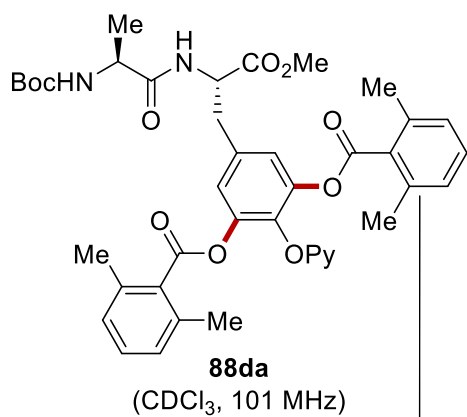
NMR Spectra



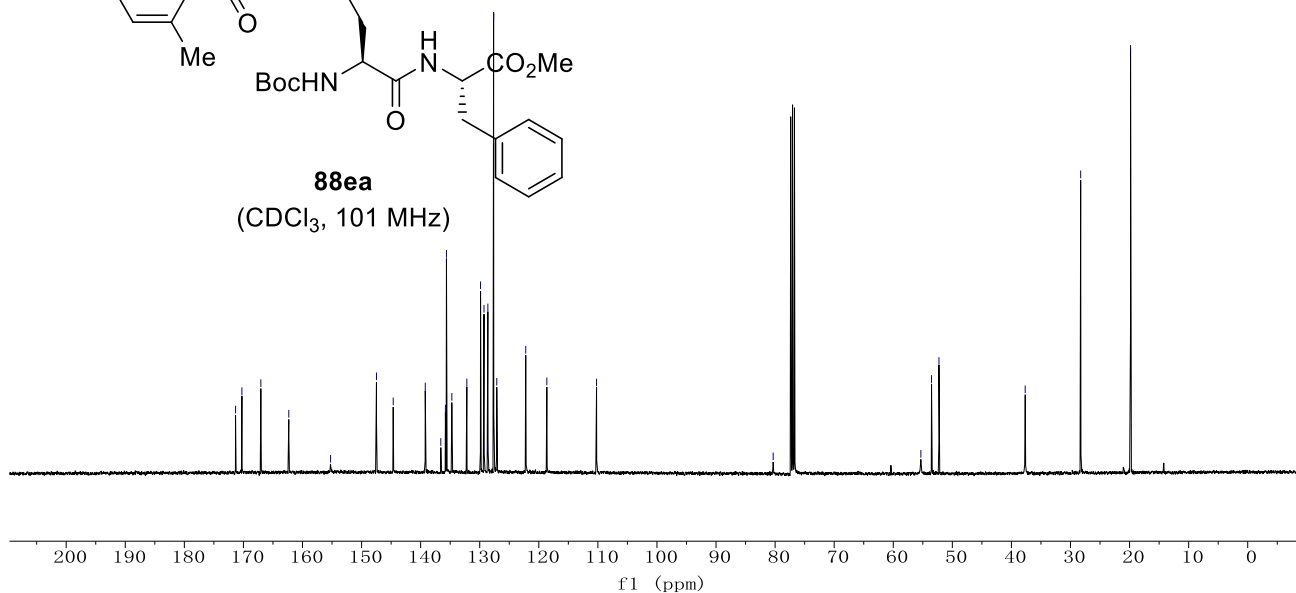
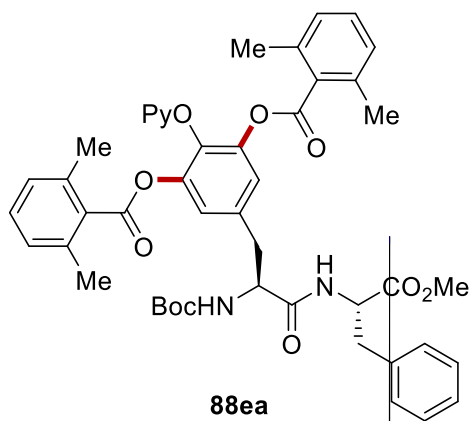
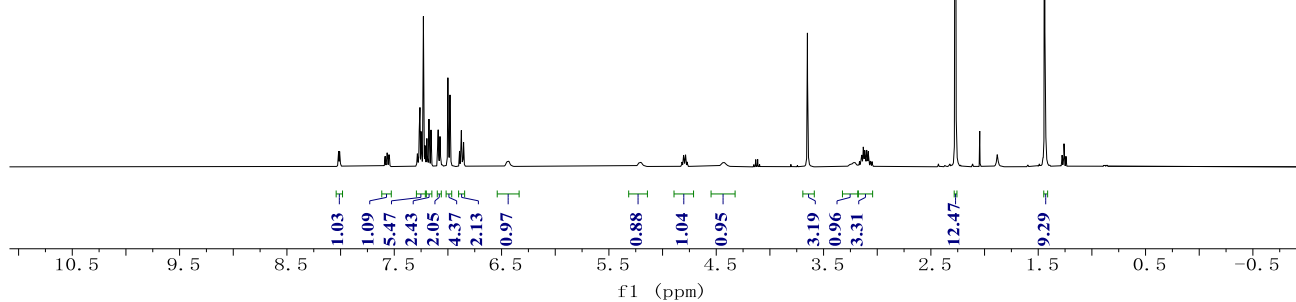
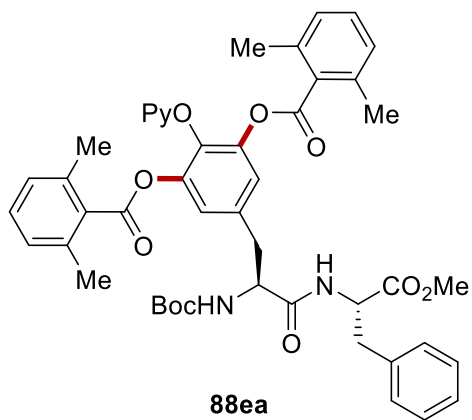
NMR Spectra



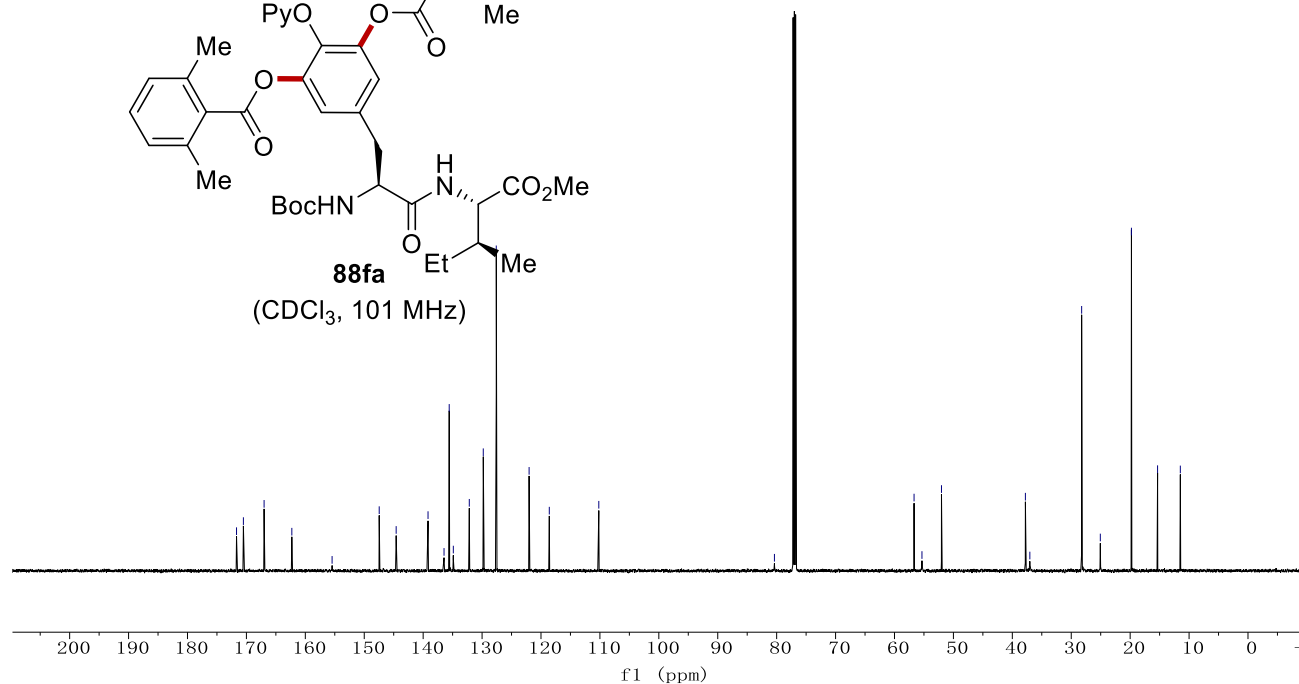
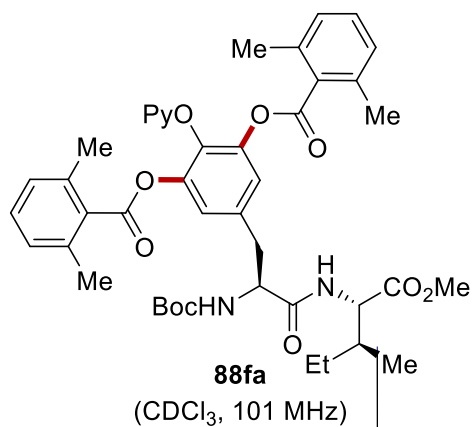
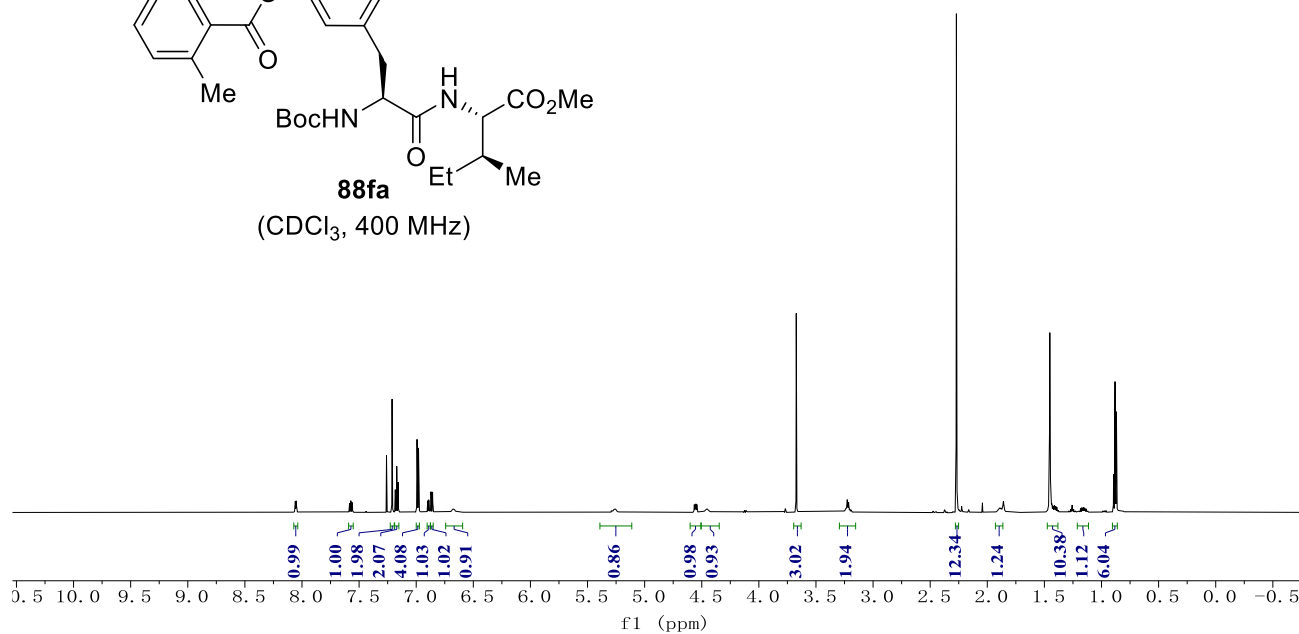
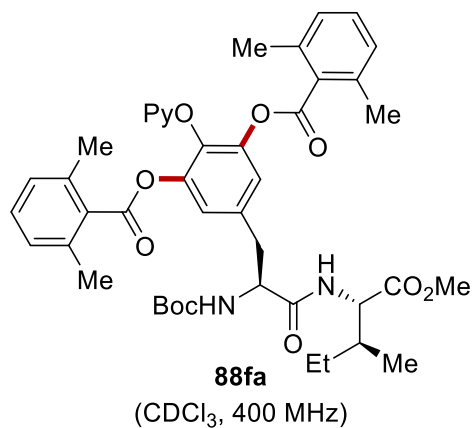
- 172.79
- 171.36
- 167.41
- 162.45
- 155.71
- 147.61
- 144.55
- 139.44
- 136.51
- 135.70
- 133.91
- 132.25
- 130.07
- 127.81
- 122.22
- 118.80
- 110.37
- 80.11
- 52.87
- 52.74
- 50.51
- 37.37
- 28.35
- 19.92
- 18.23



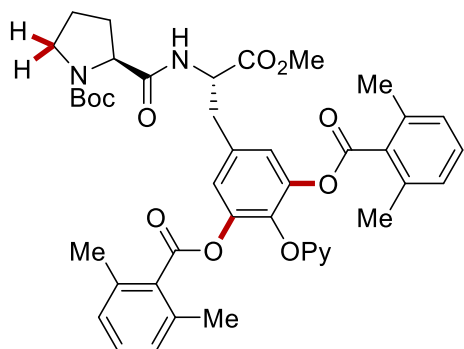
NMR Spectra



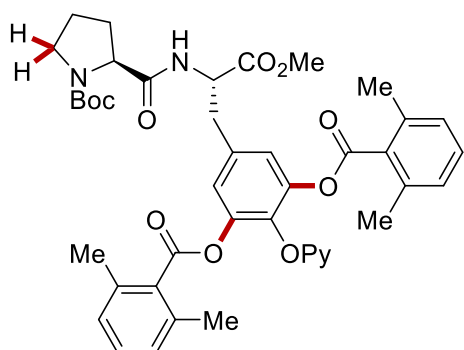
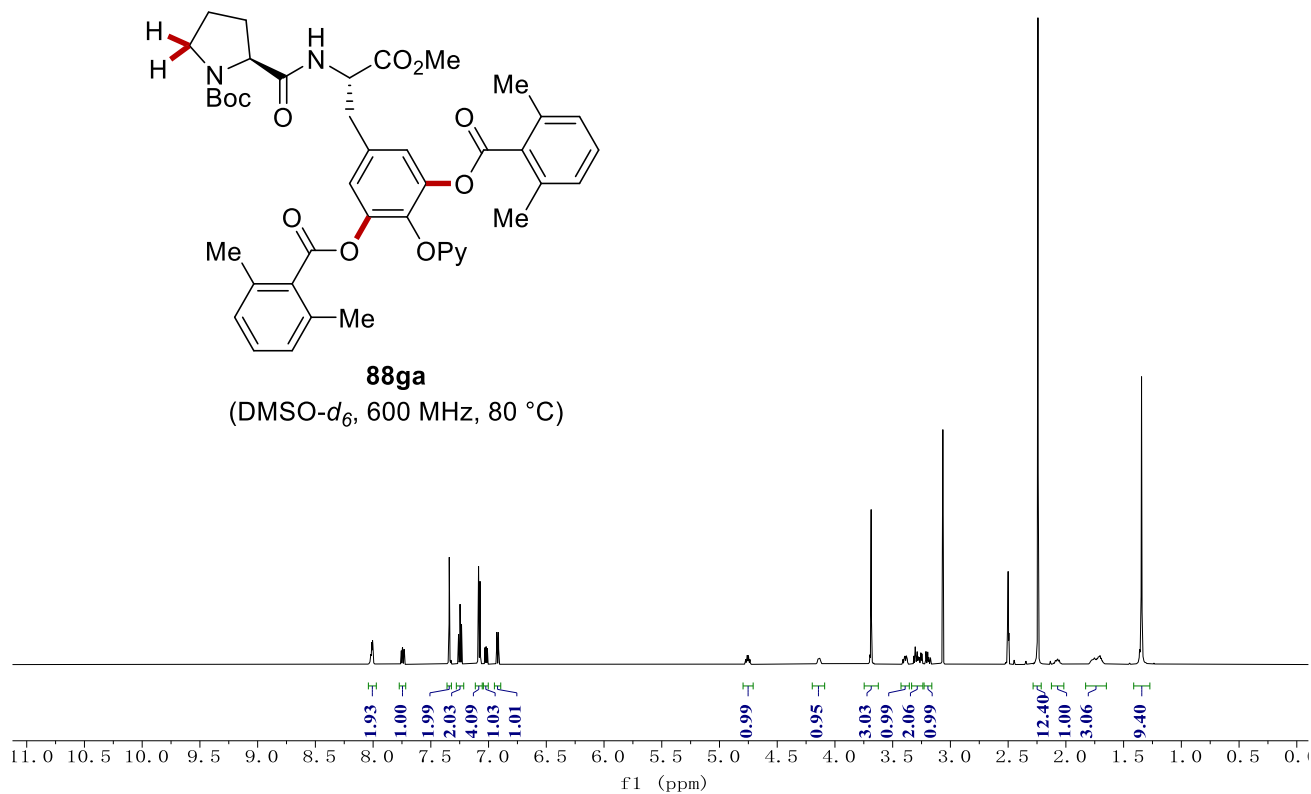
NMR Spectra



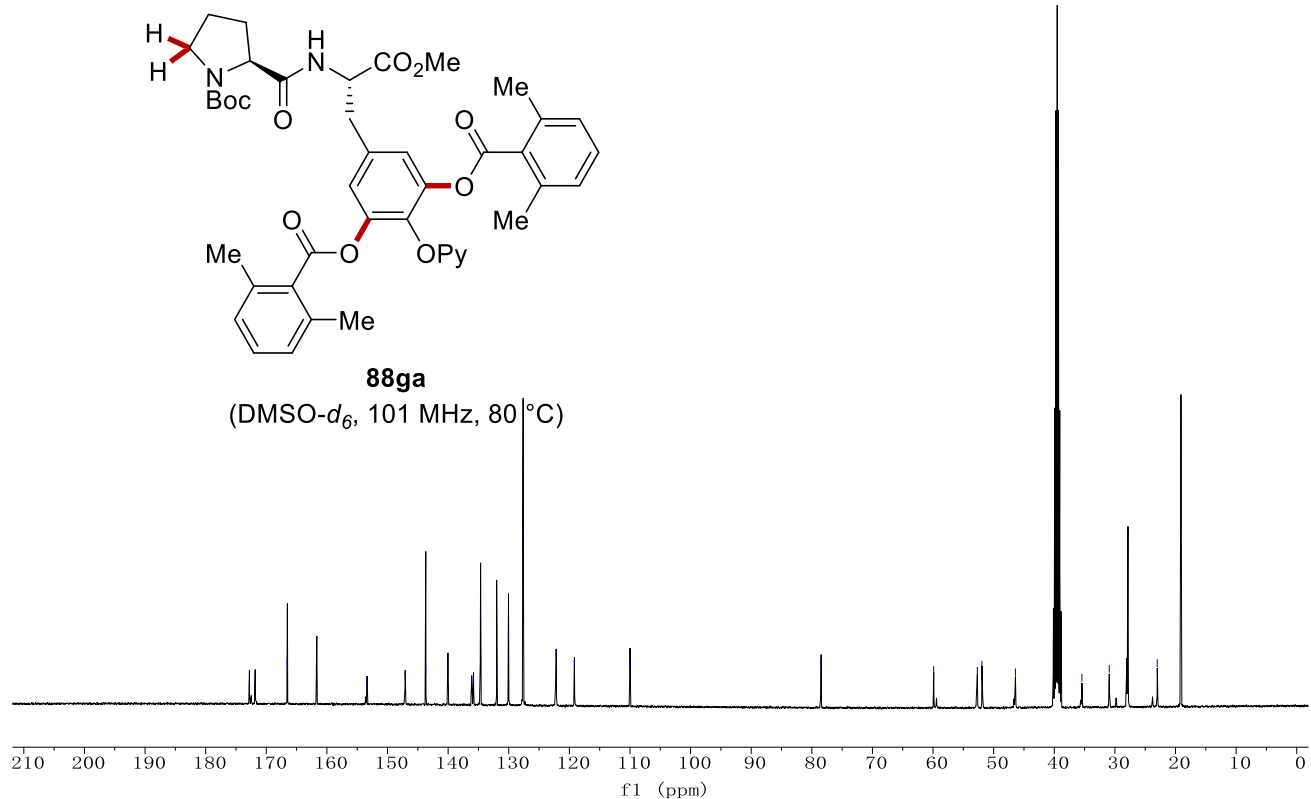
NMR Spectra



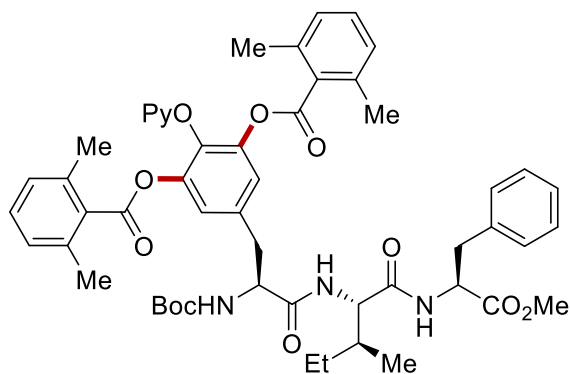
88ga
(DMSO- d_6 , 600 MHz, 80 °C)



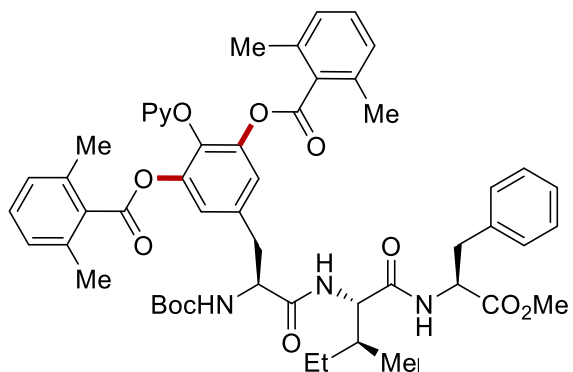
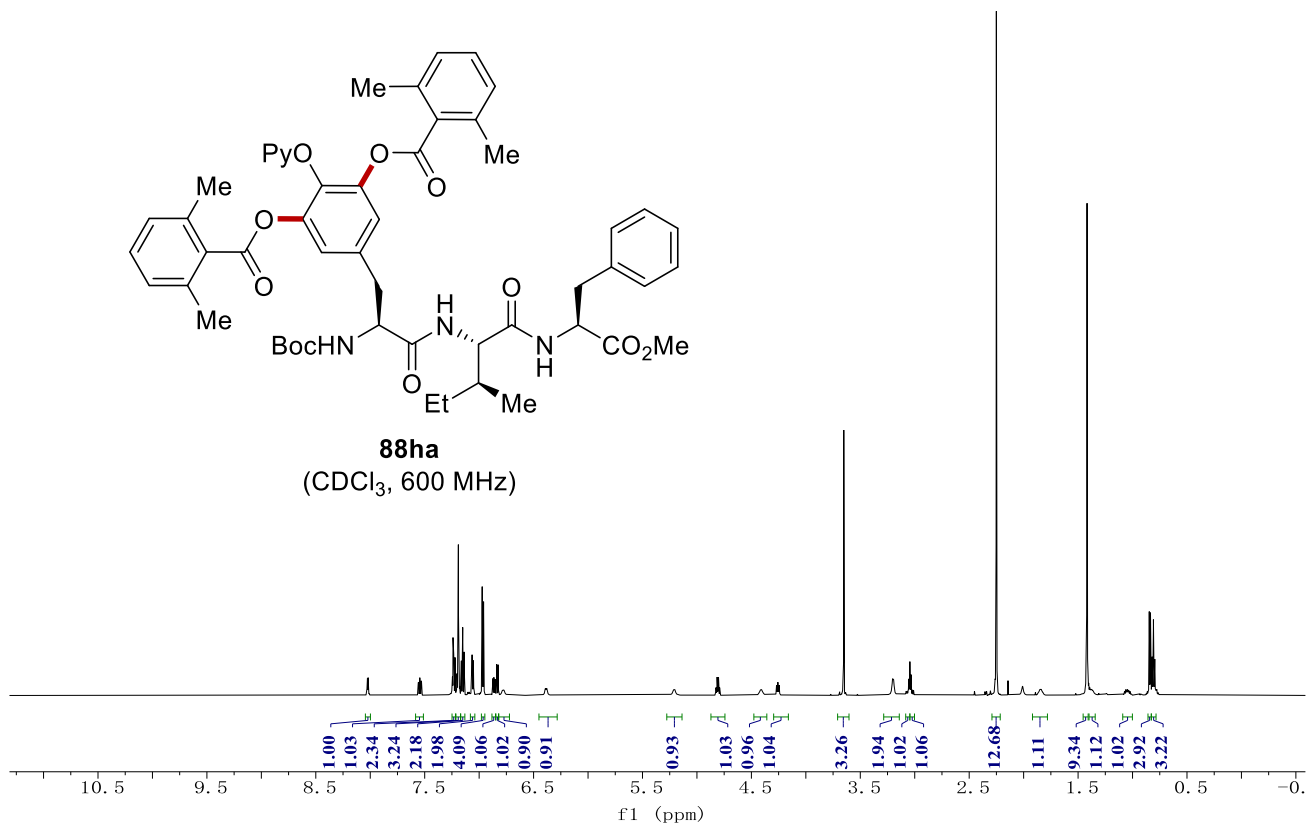
88ga
(DMSO- d_6 , 101 MHz, 80 °C)



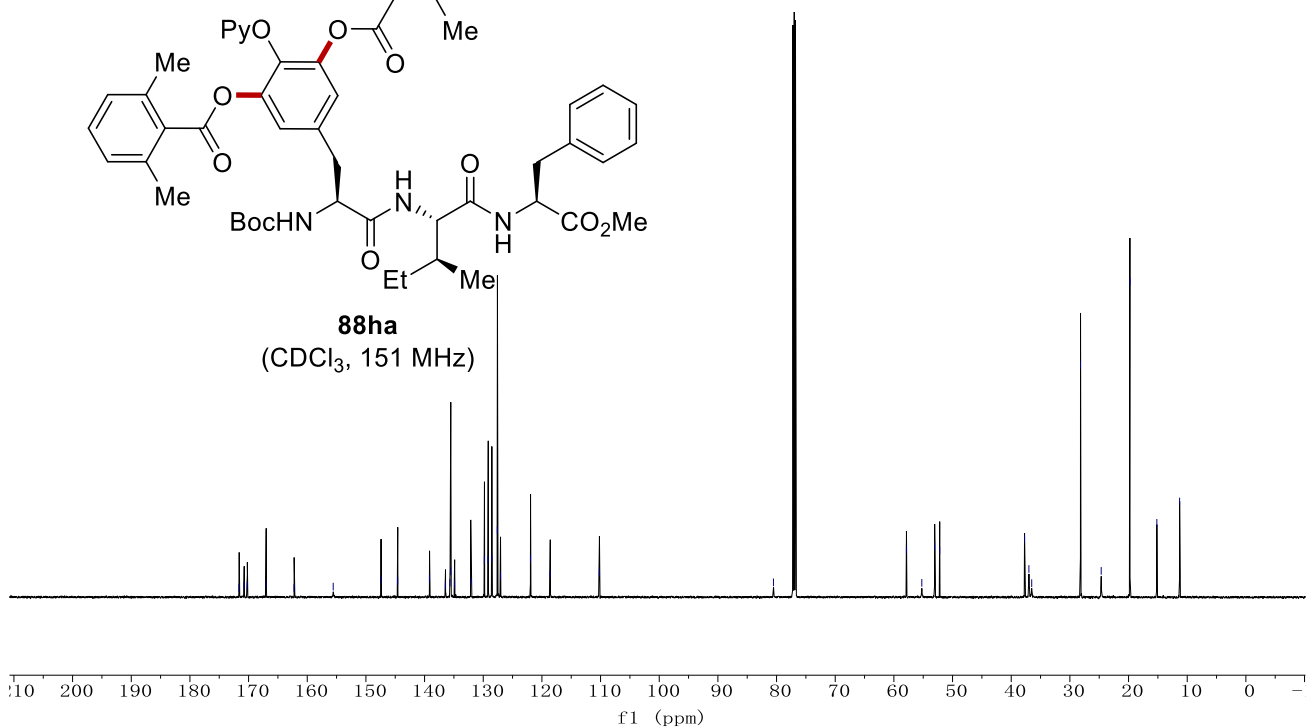
NMR Spectra



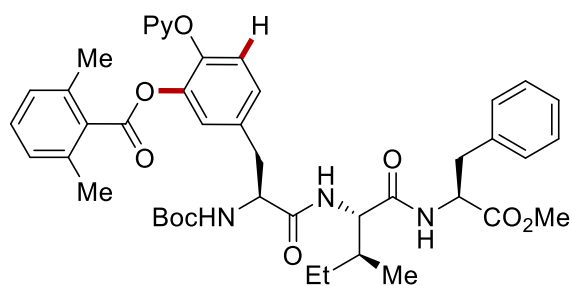
88ha
(CDCl₃, 600 MHz)



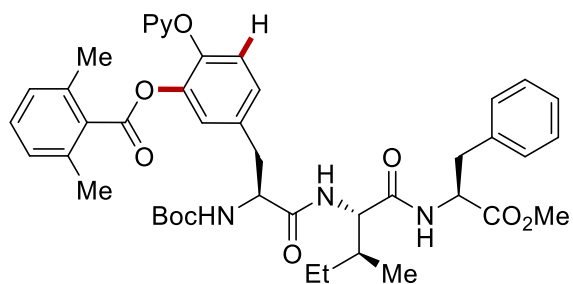
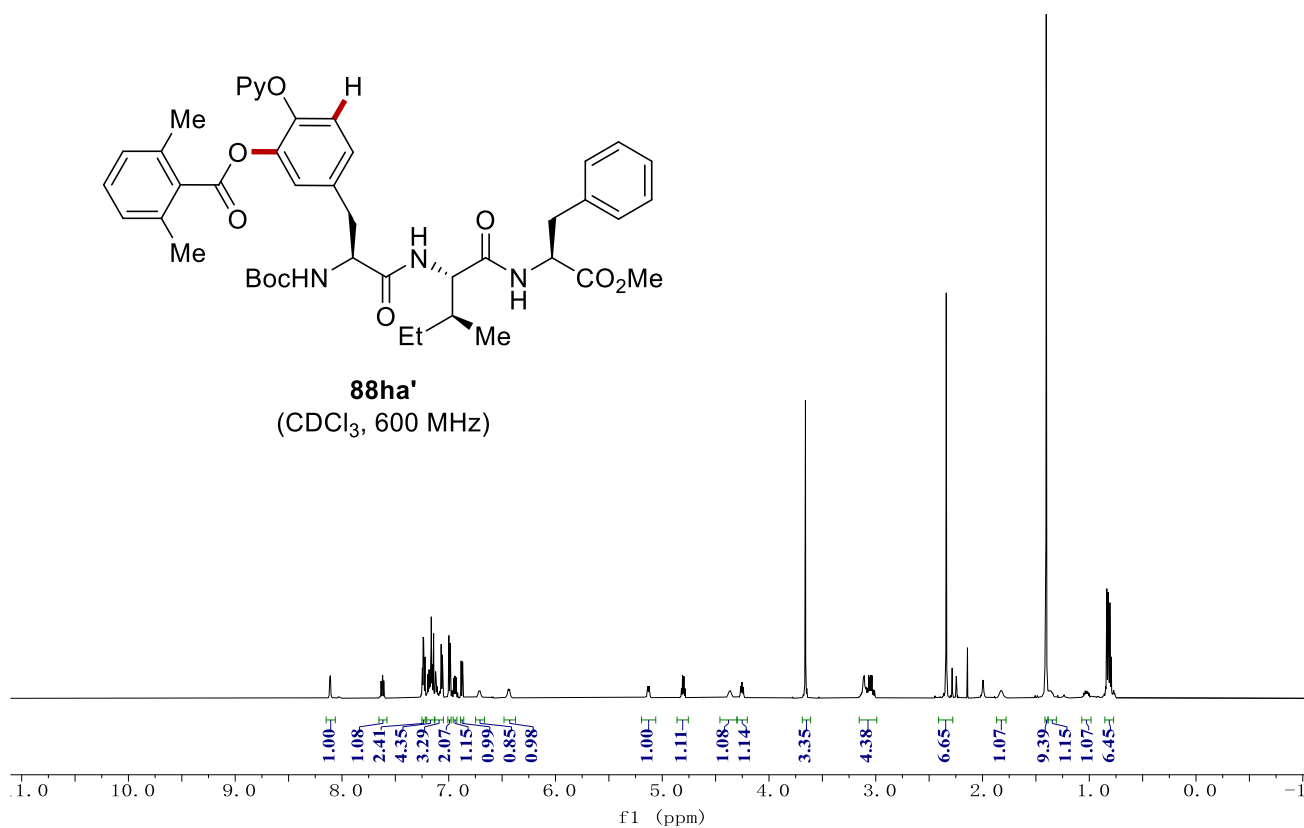
88ha
(CDCl₃, 151 MHz)



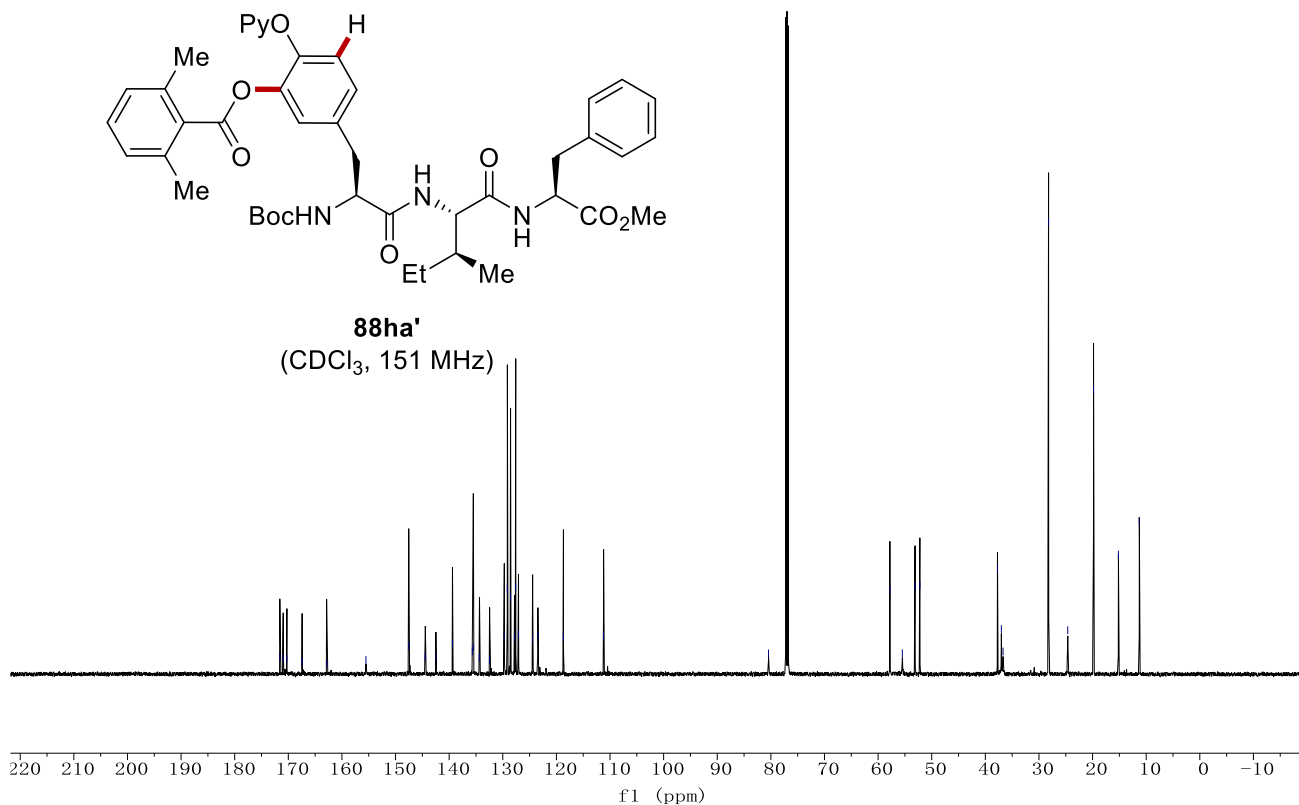
NMR Spectra



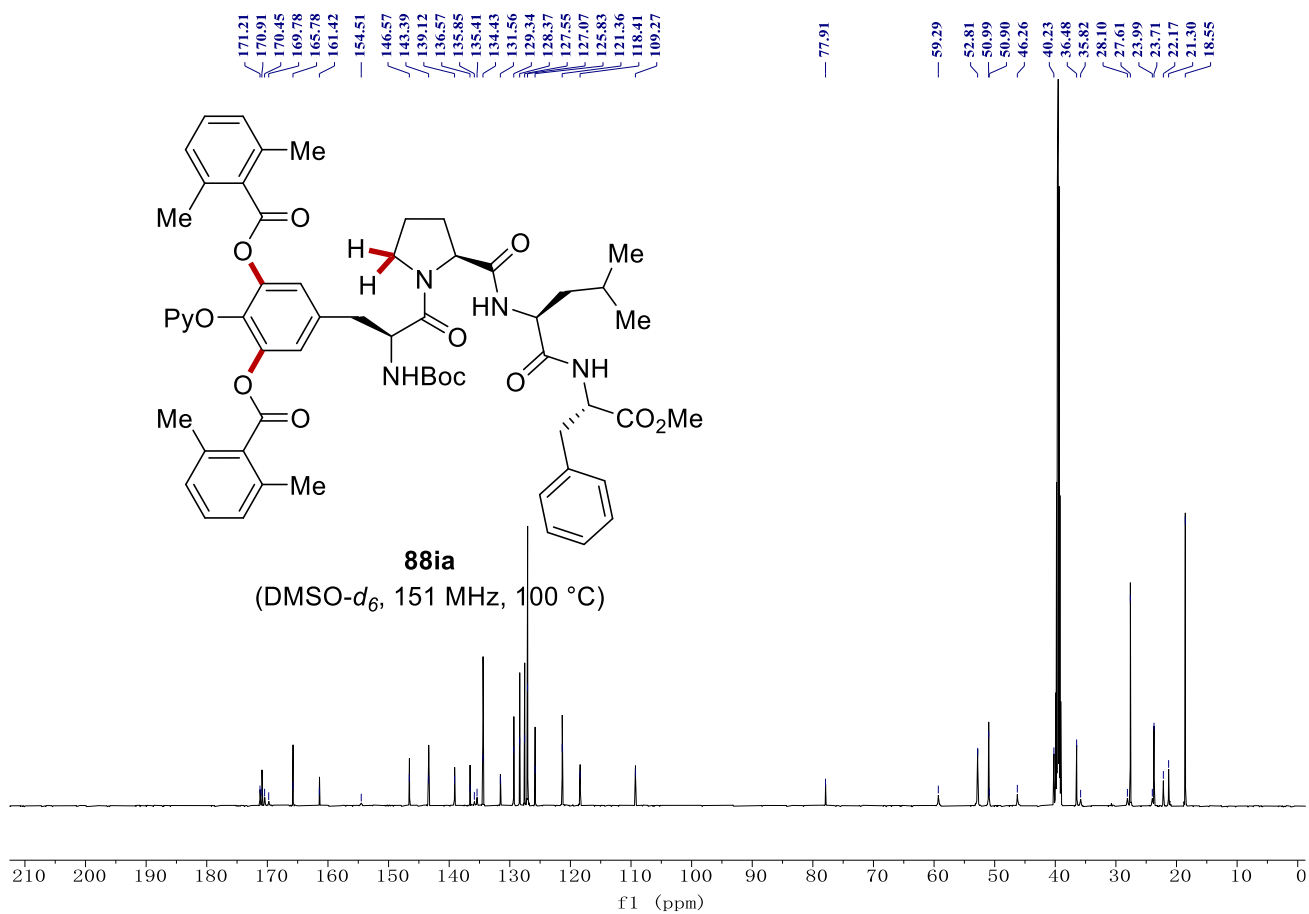
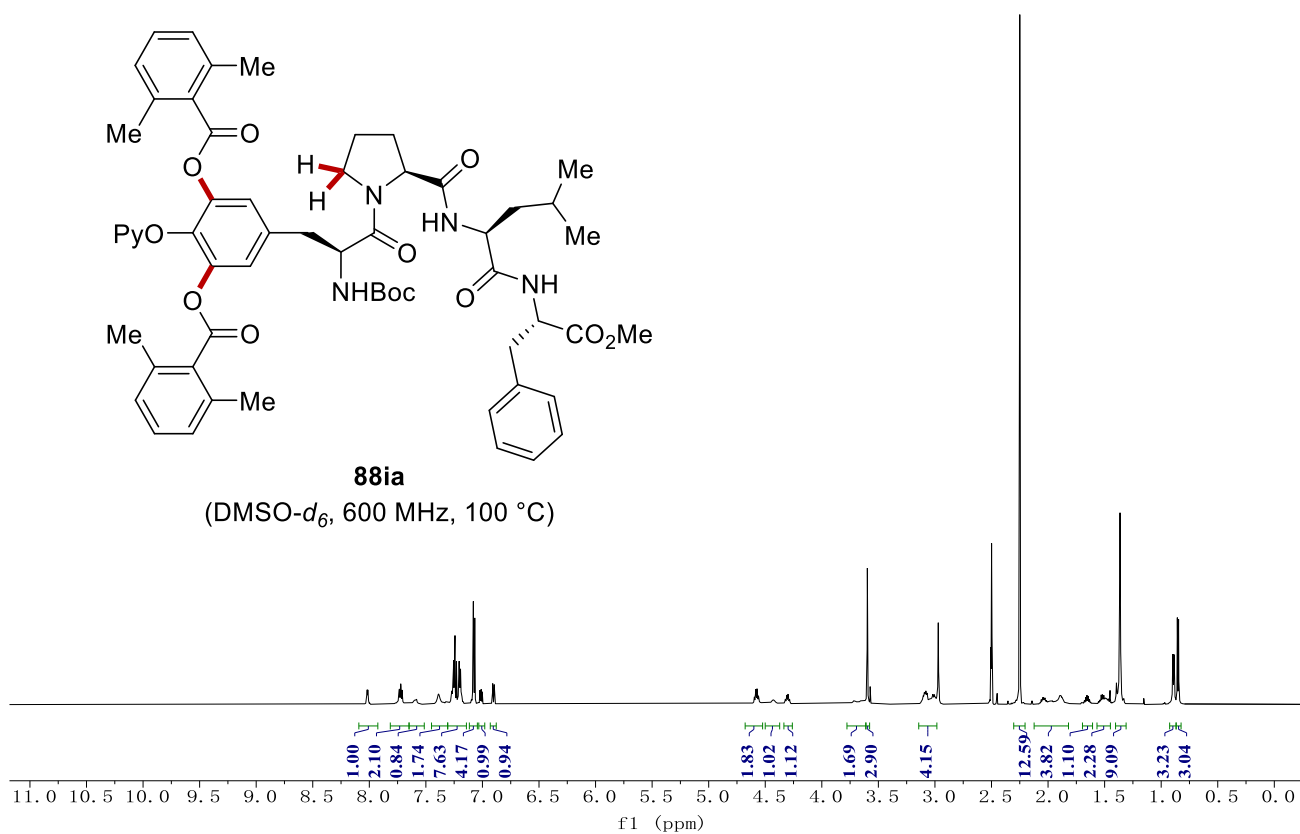
88ha'
(CDCl₃, 600 MHz)



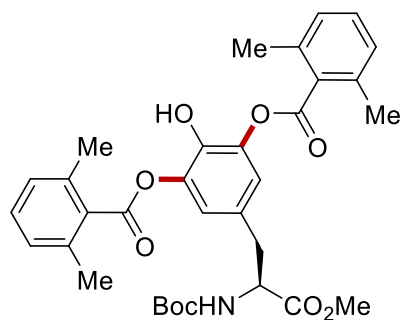
88ha'
(CDCl₃, 151 MHz)



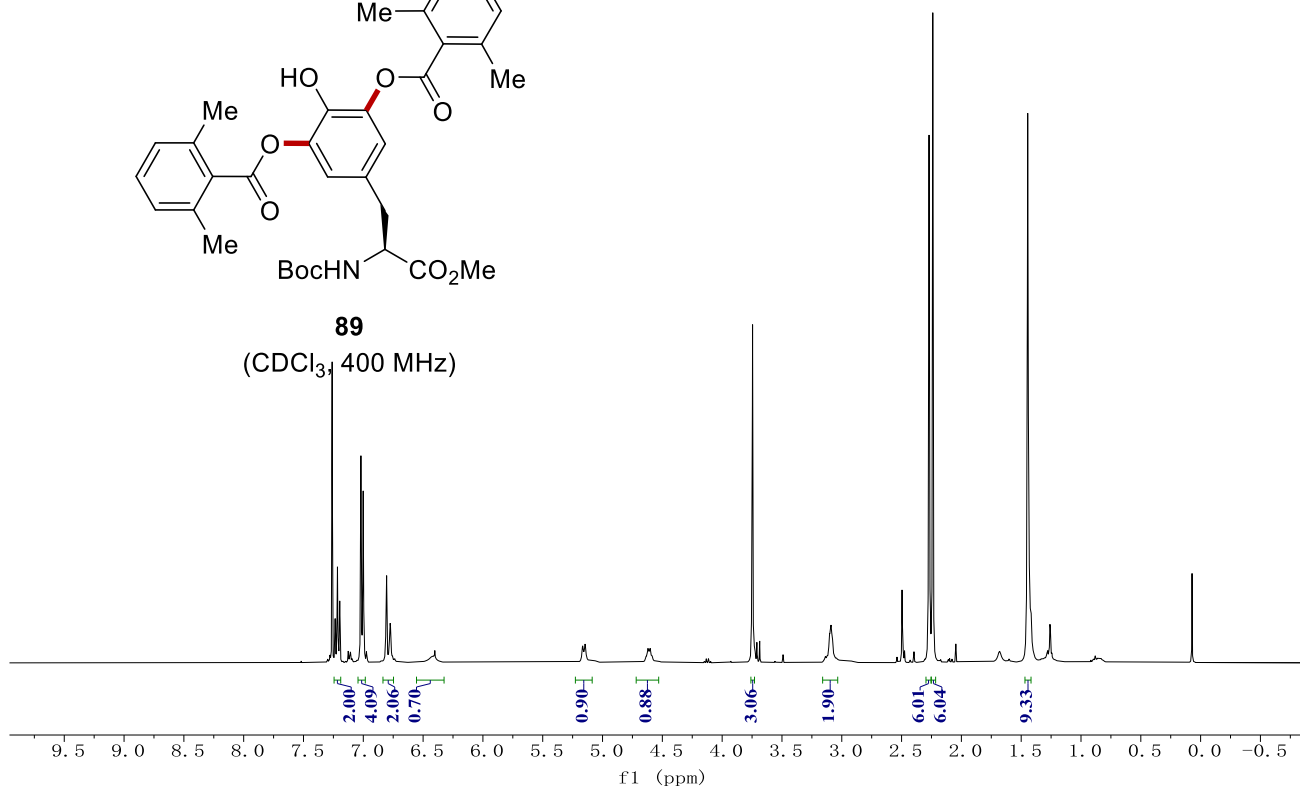
NMR Spectra



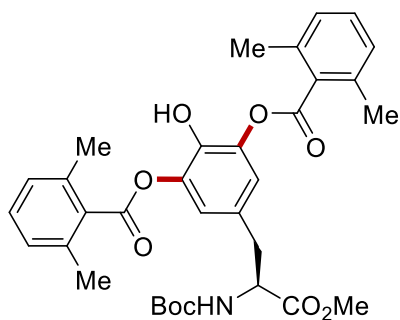
NMR Spectra



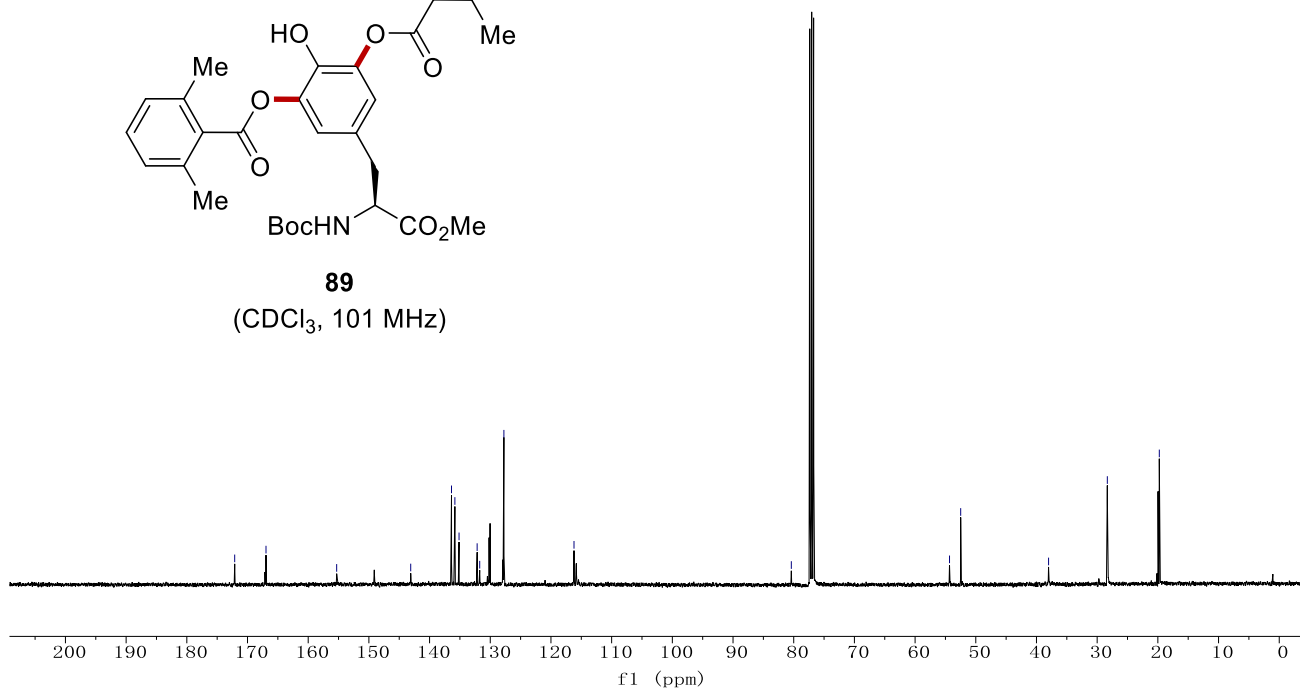
89
(CDCl₃, 400 MHz)



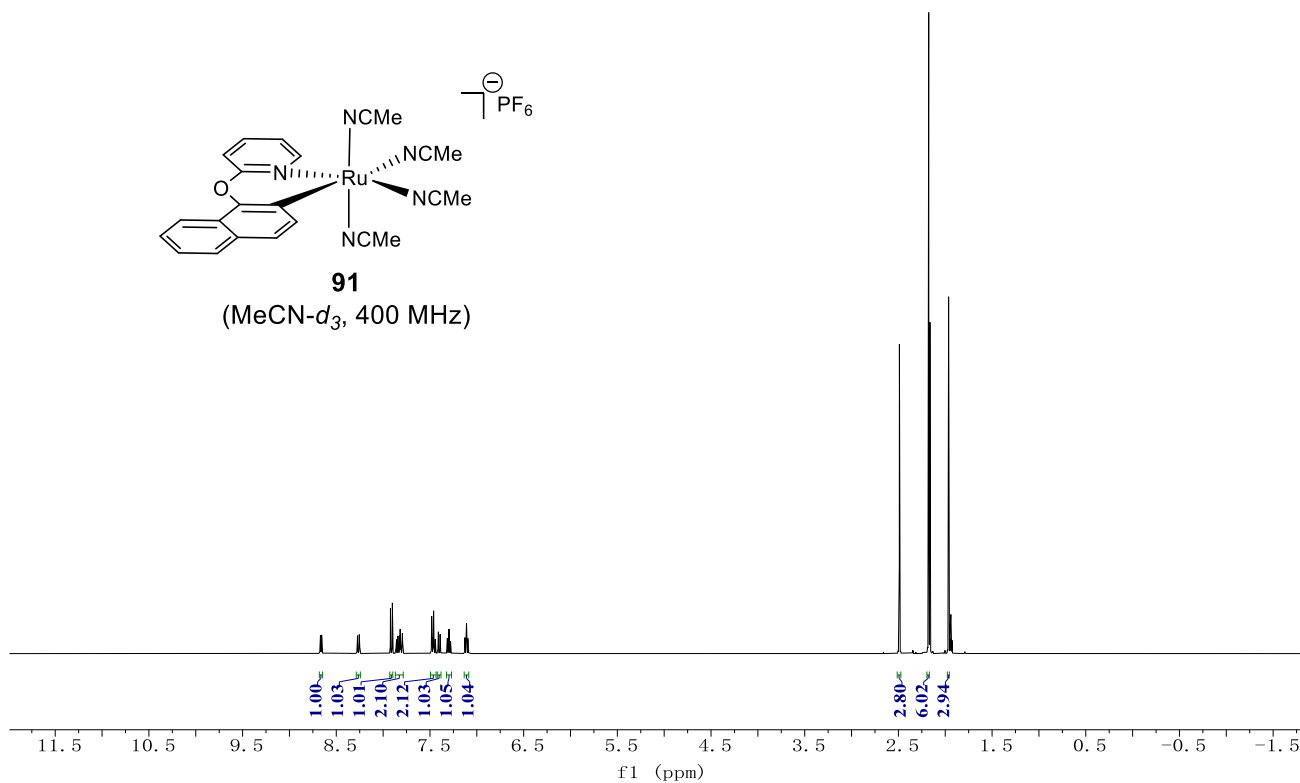
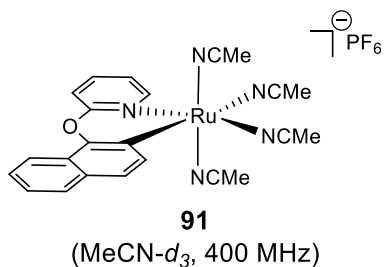
— 172.11 — 166.95 — 155.31 — 143.11 — 136.39 — 135.83 — 135.15 — 132.16 — 131.74 — 127.76 — 116.20 — 80.39 — 54.33 — 52.49 — 38.01 — 28.33 — 19.76



89
(CDCl₃, 101 MHz)

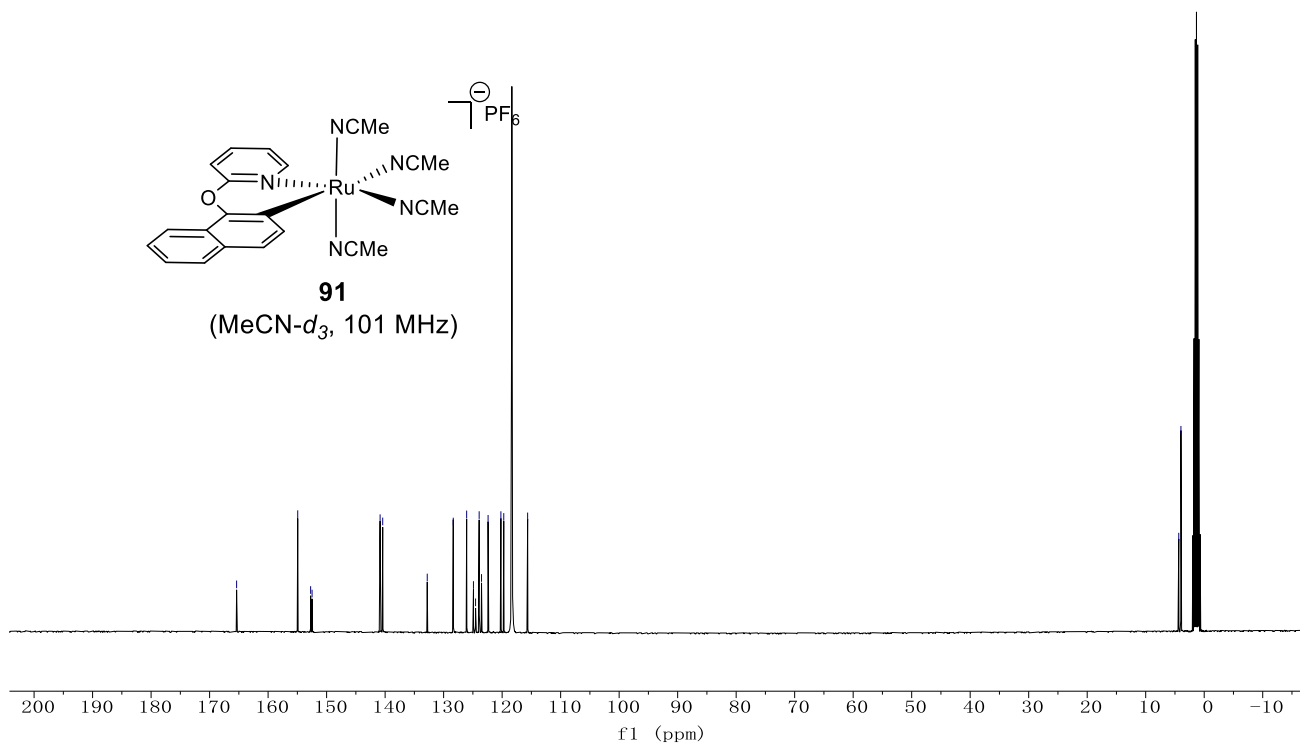
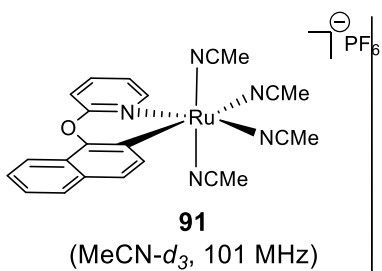


NMR Spectra

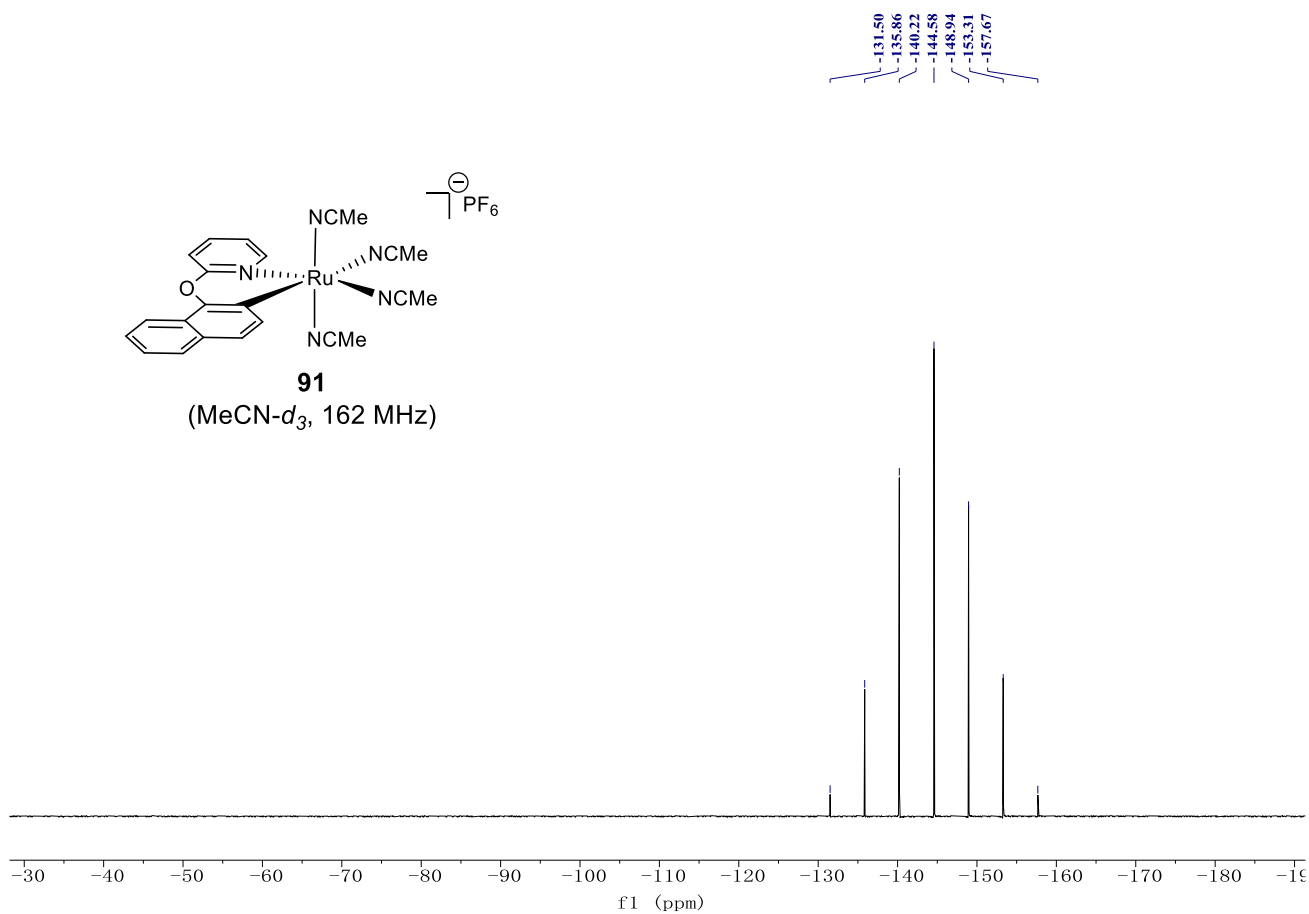
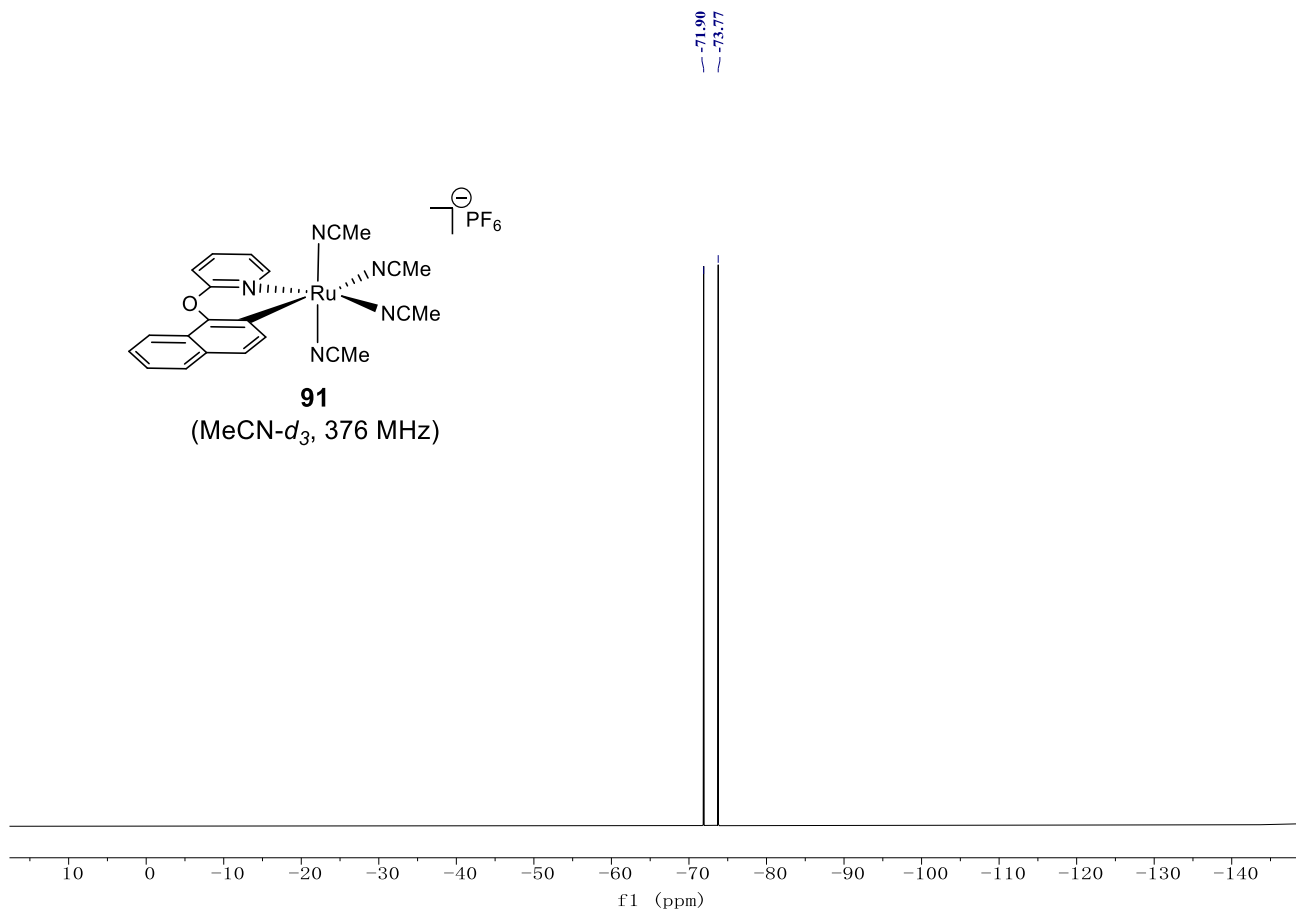


165.38
154.94
152.73
152.48
140.86
140.41
132.80
128.35
126.06
124.90
124.54
123.93
123.52
122.40
120.21
119.72
115.64

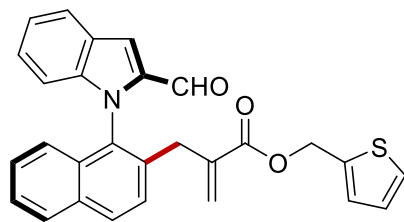
4.35
3.98



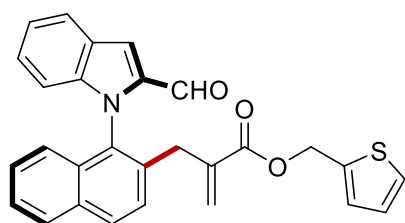
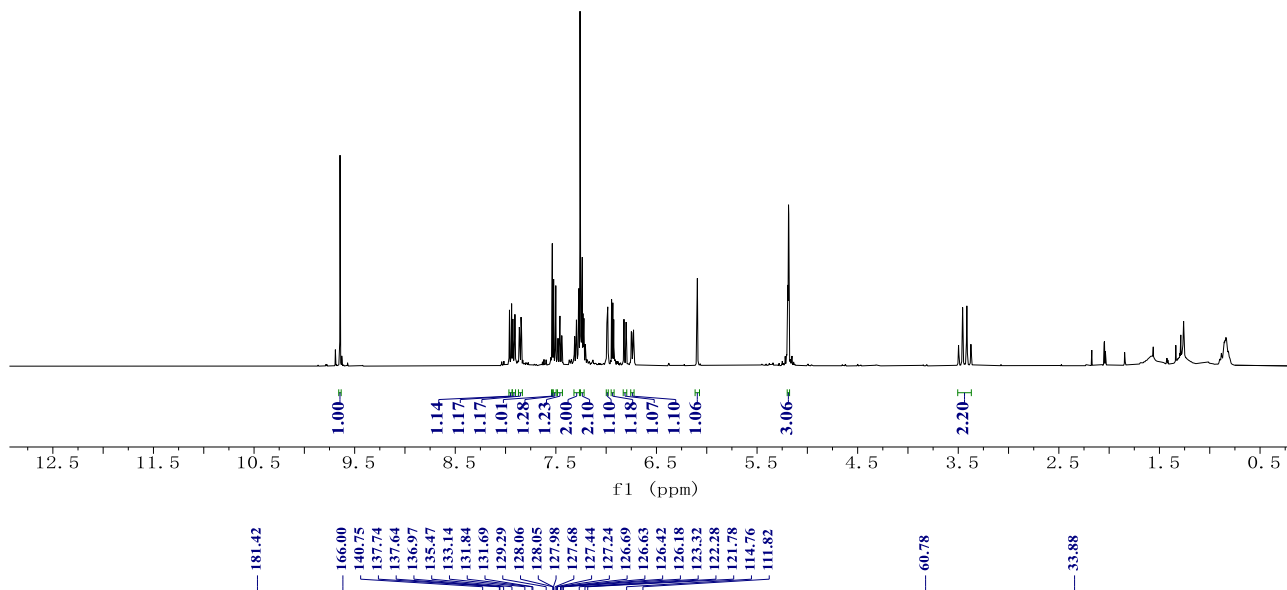
NMR Spectra



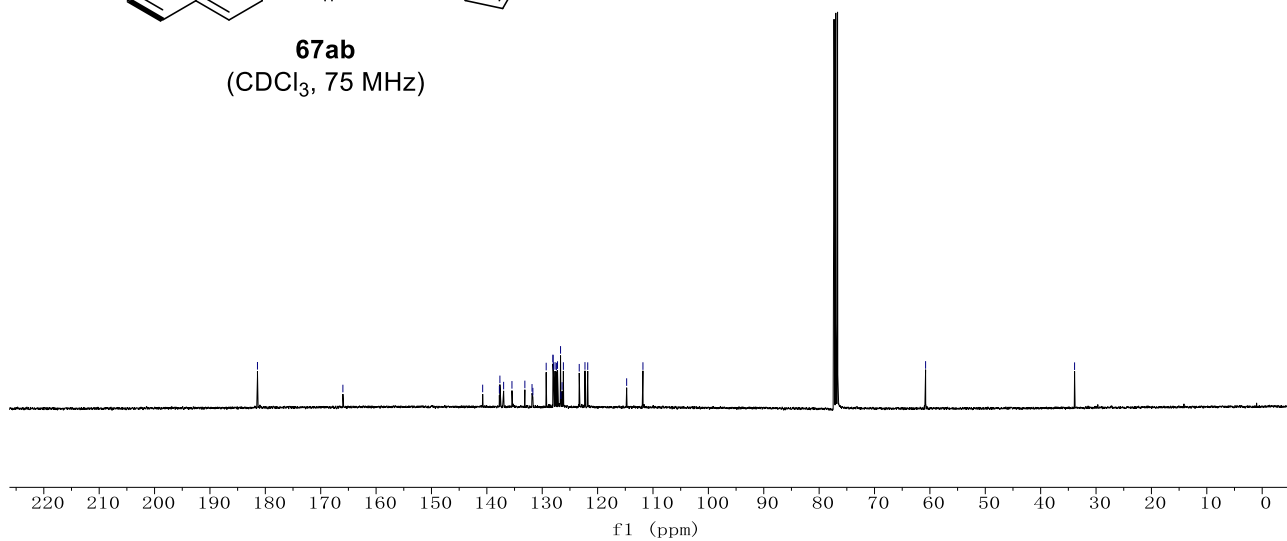
NMR Spectra



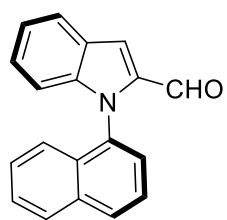
67ab
(CDCl₃, 400 MHz)



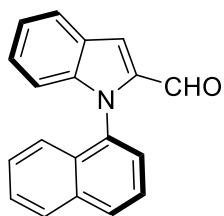
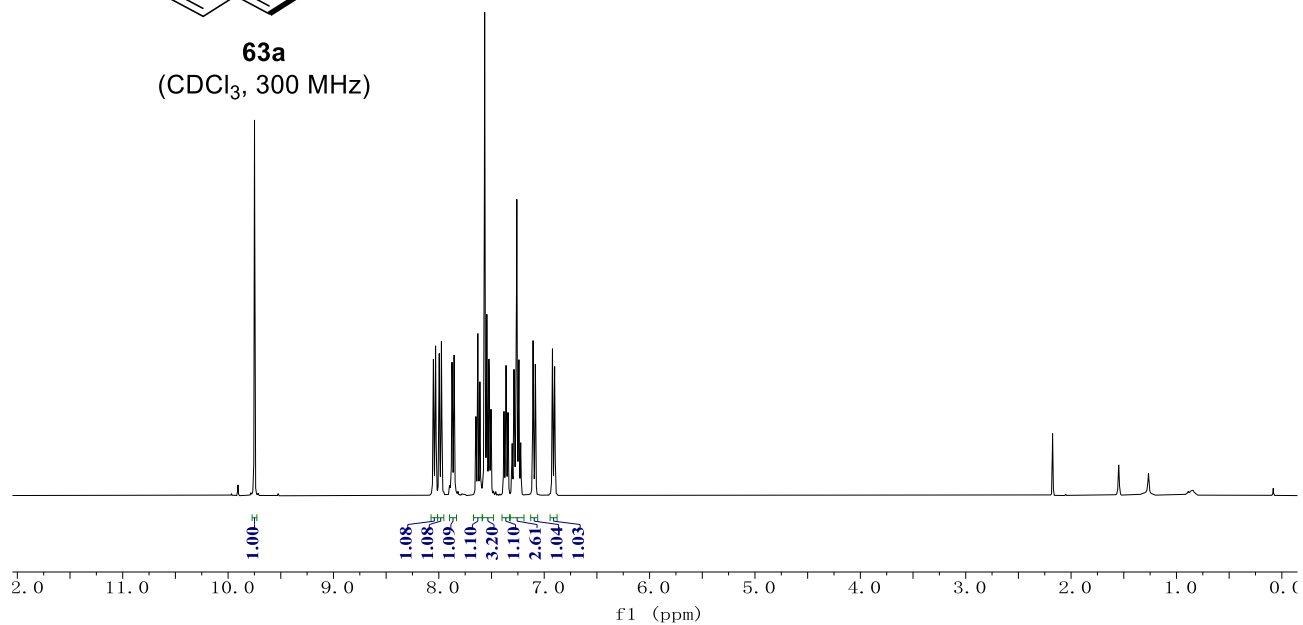
67ab
(CDCl₃, 75 MHz)



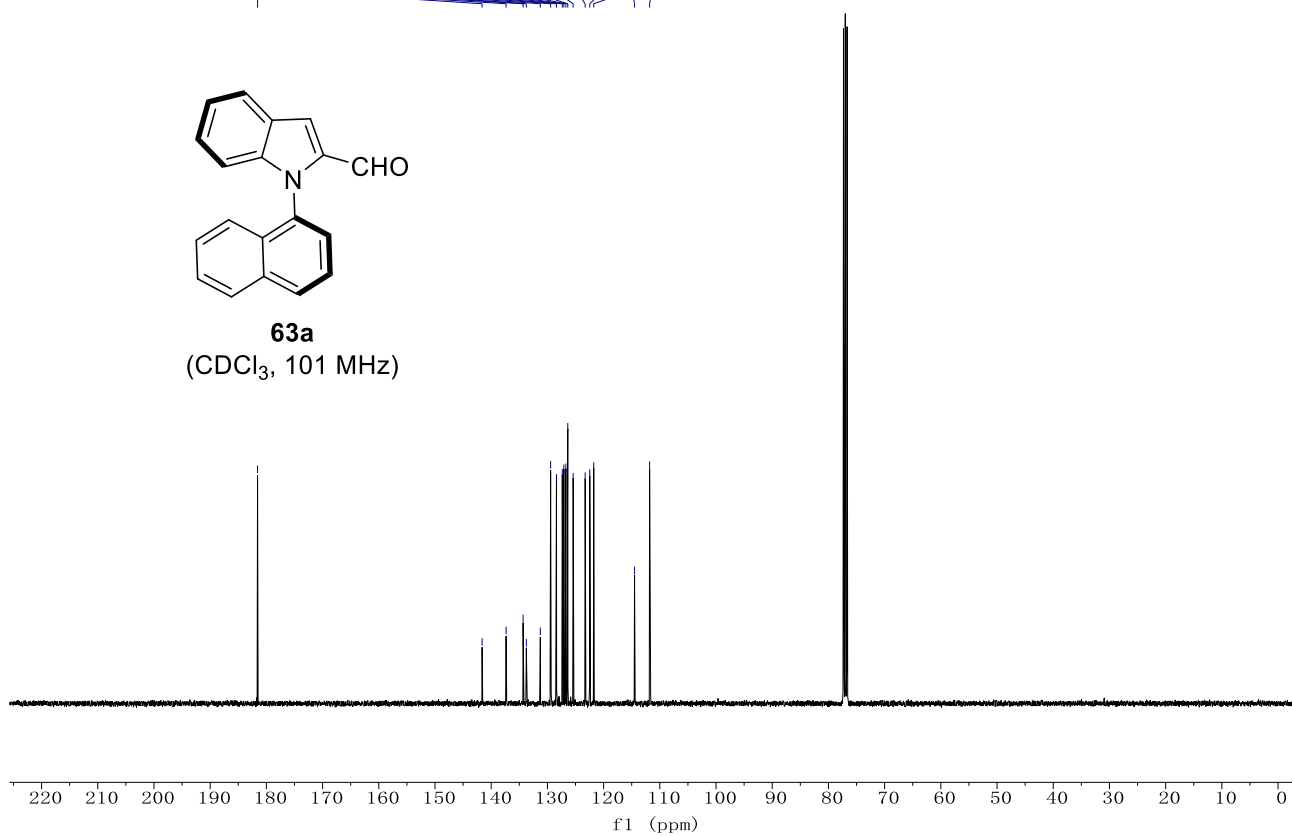
NMR Spectra



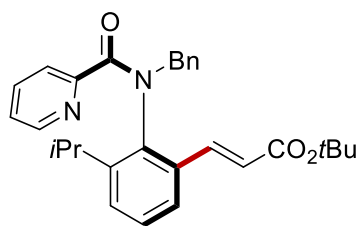
63a
(CDCl₃, 300 MHz)



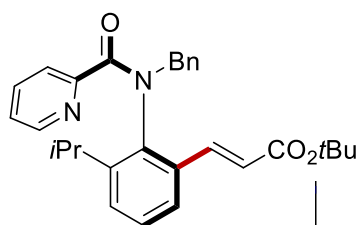
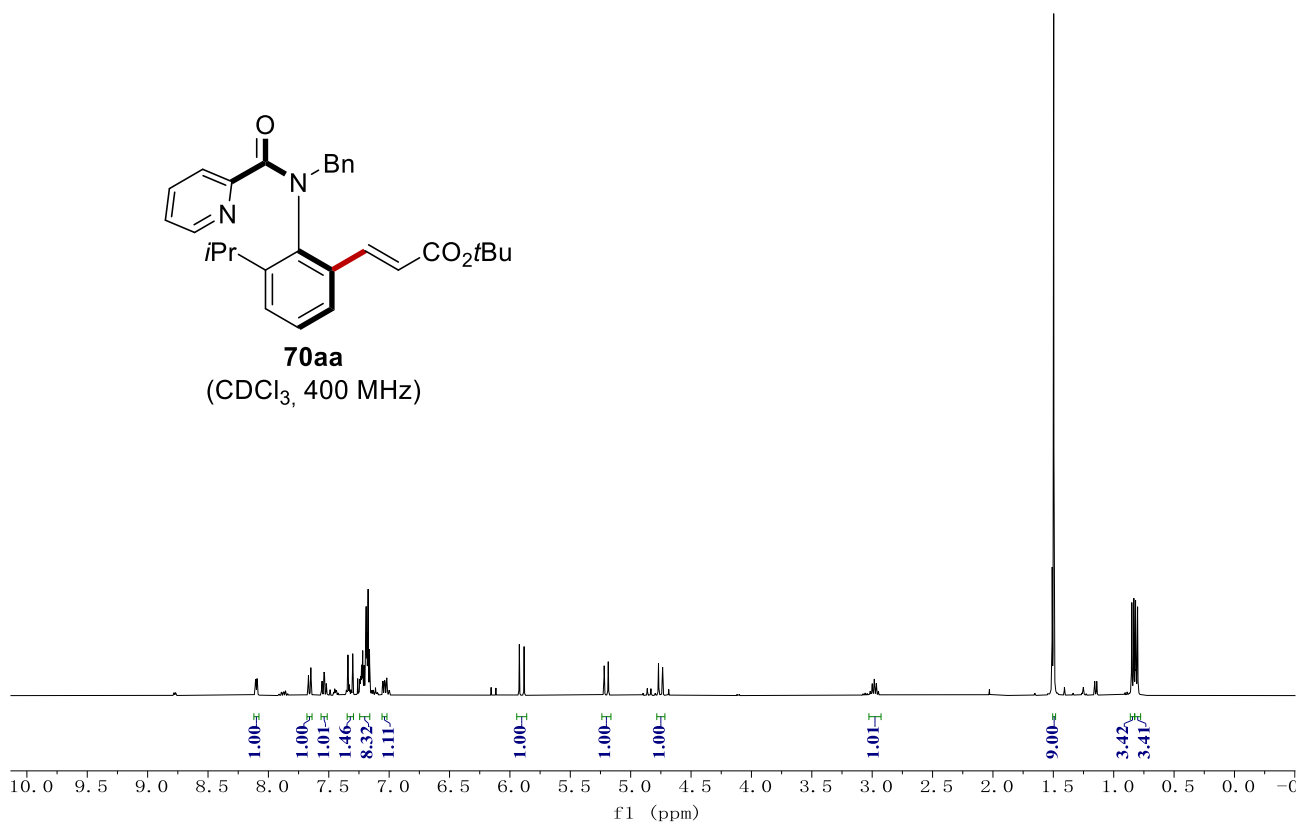
63a
(CDCl₃, 101 MHz)



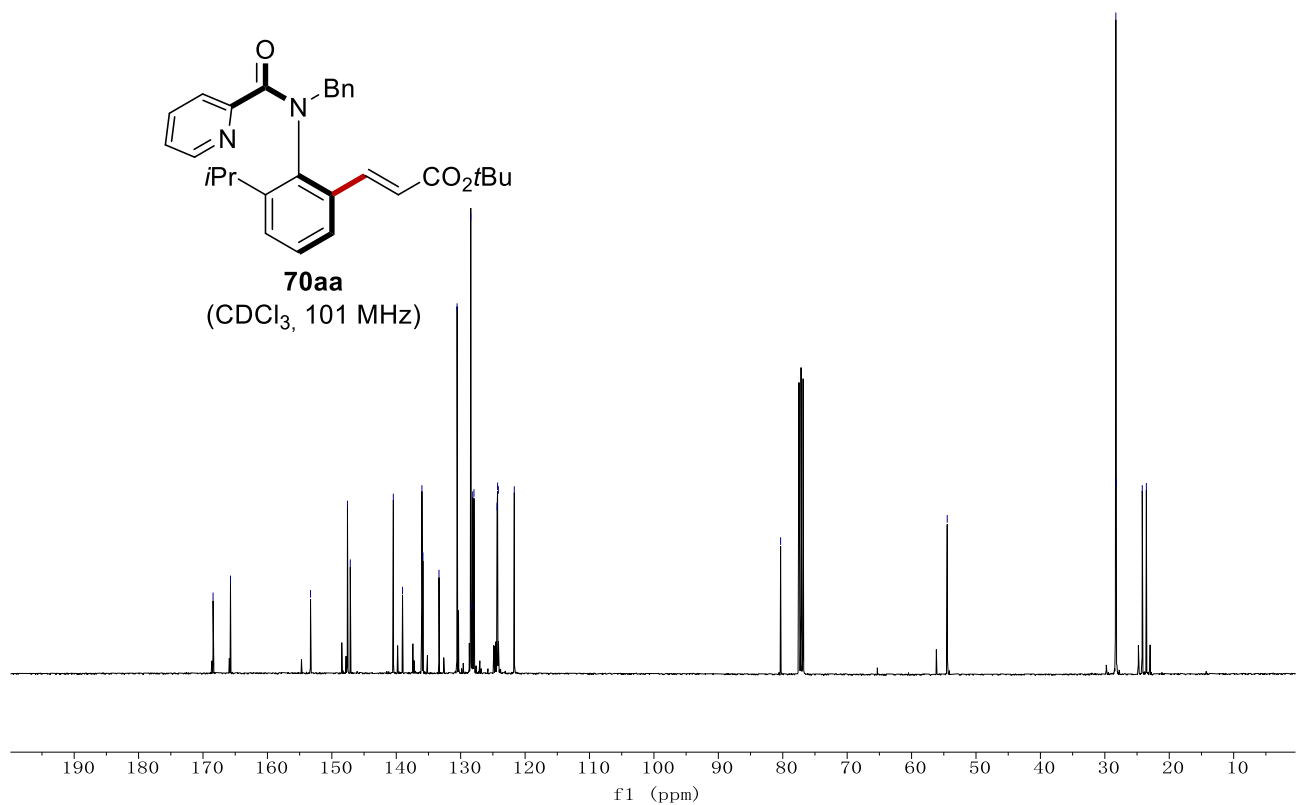
NMR Spectra



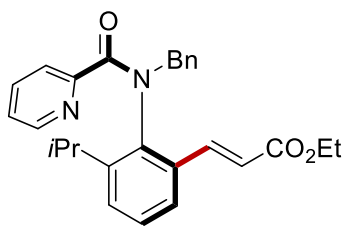
70aa
(CDCl₃, 400 MHz)



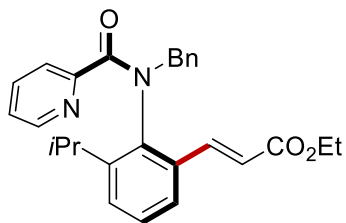
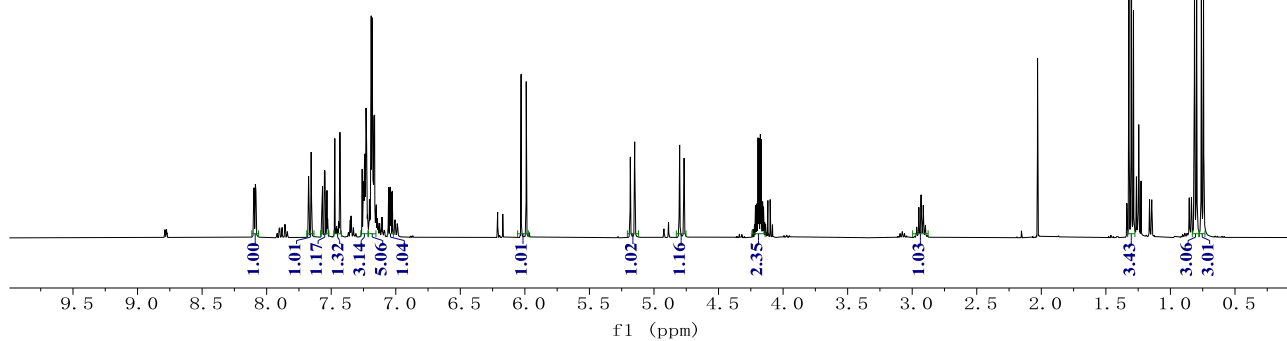
70aa
(CDCl₃, 101 MHz)



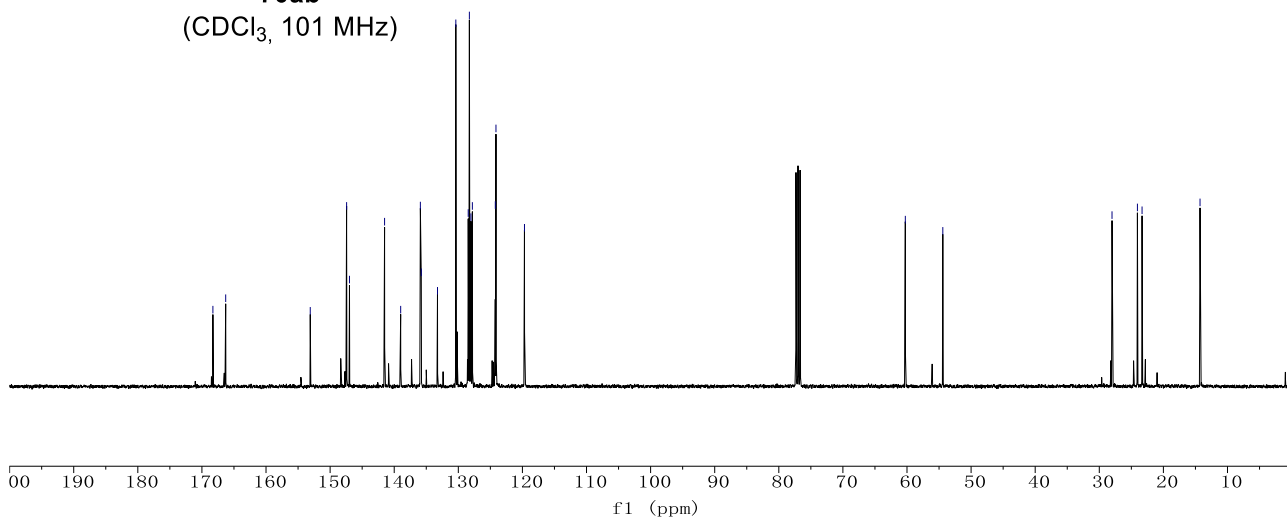
NMR Spectra



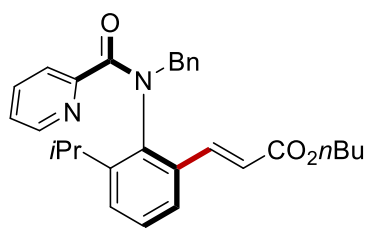
70ab
(CDCl₃, 400 MHz)



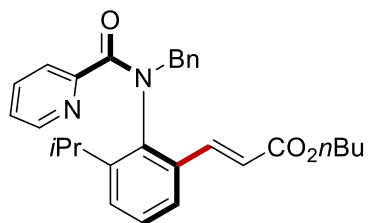
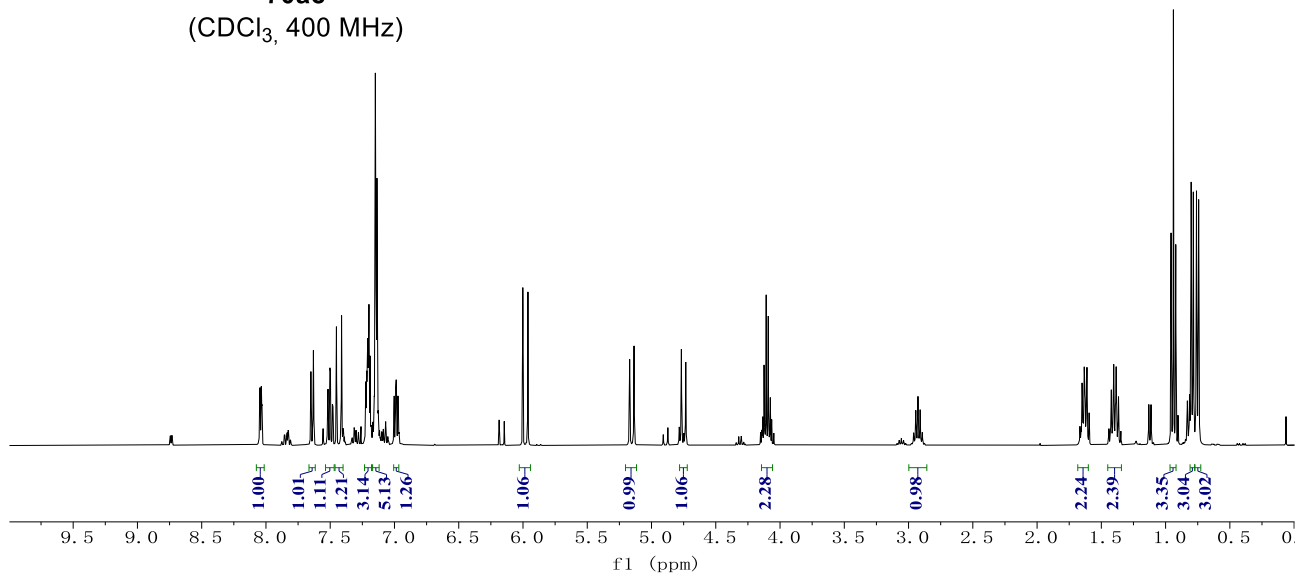
70ab
(CDCl₃, 101 MHz)



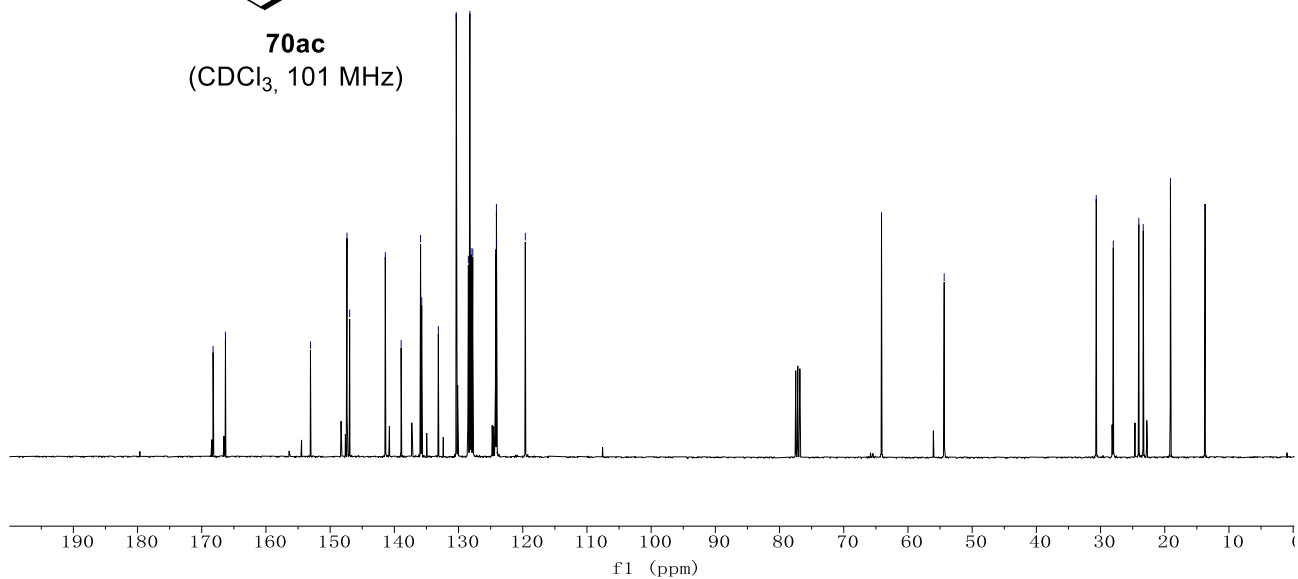
NMR Spectra



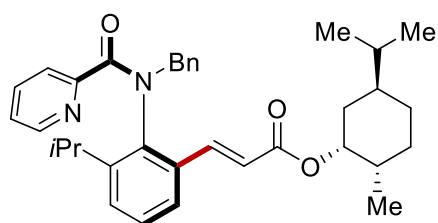
70ac
(CDCl₃, 400 MHz)



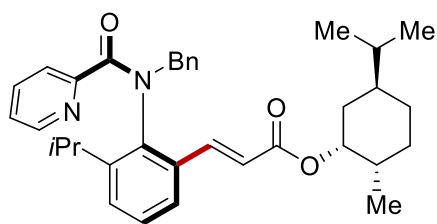
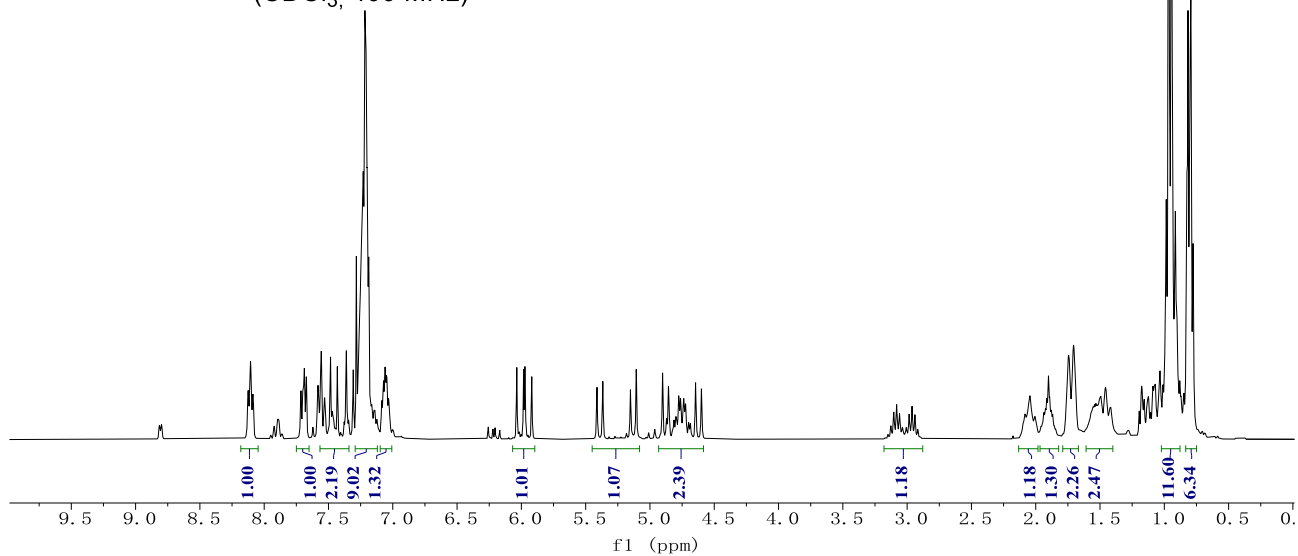
70ac
(CDCl₃, 101 MHz)



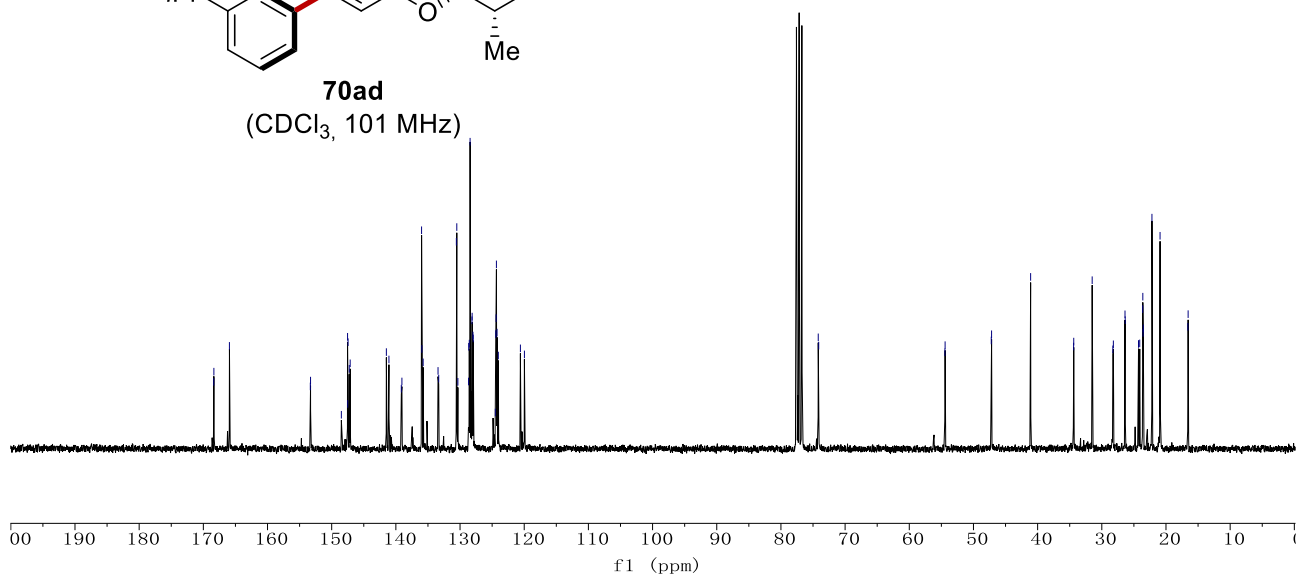
NMR Spectra



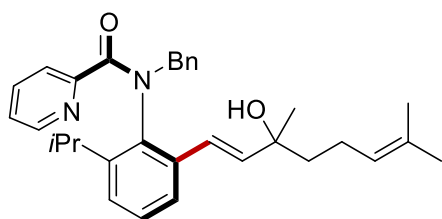
70ad
(CDCl₃, 400 MHz)



70ad
(CDCl₃, 101 MHz)



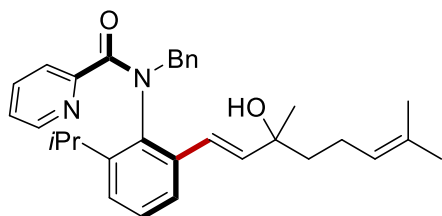
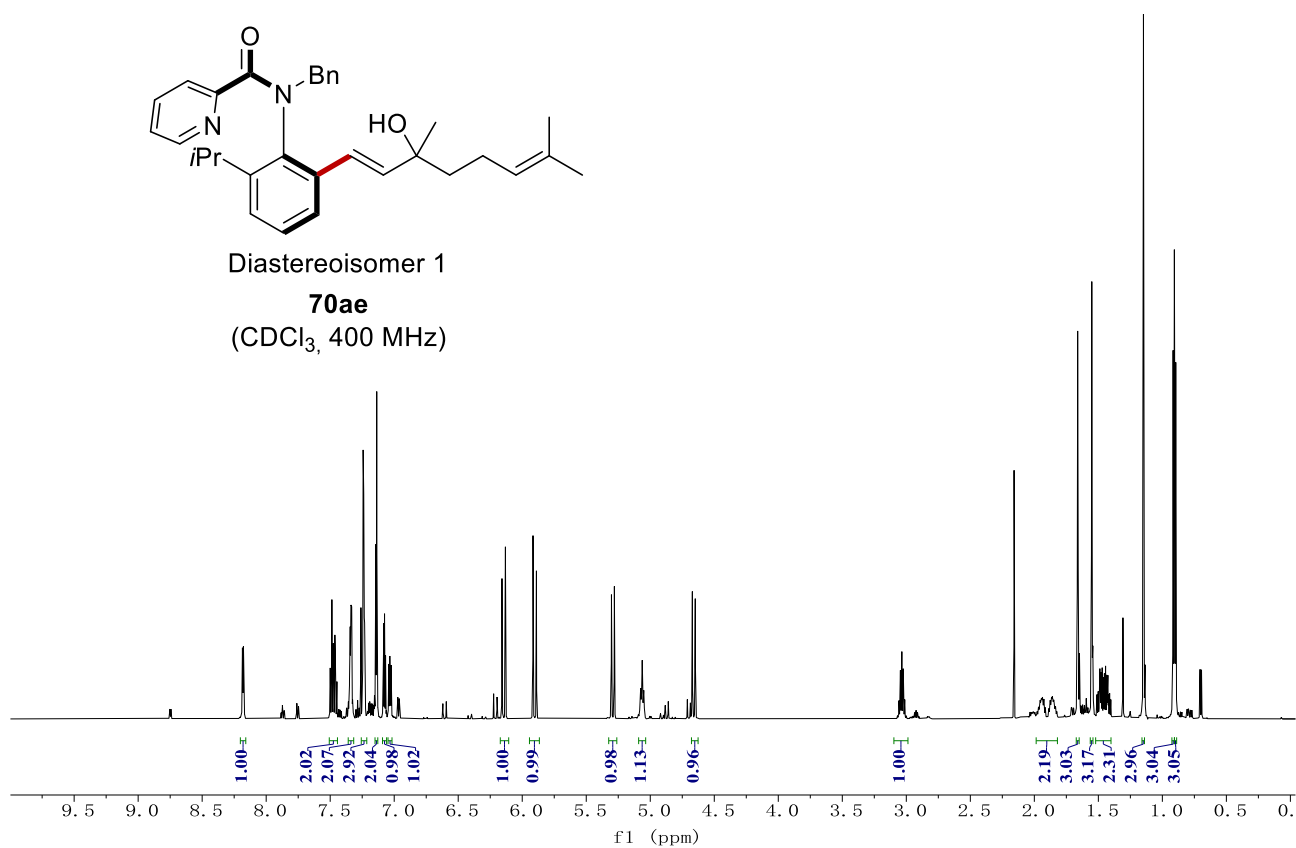
NMR Spectra



Diastereoisomer 1

70ae

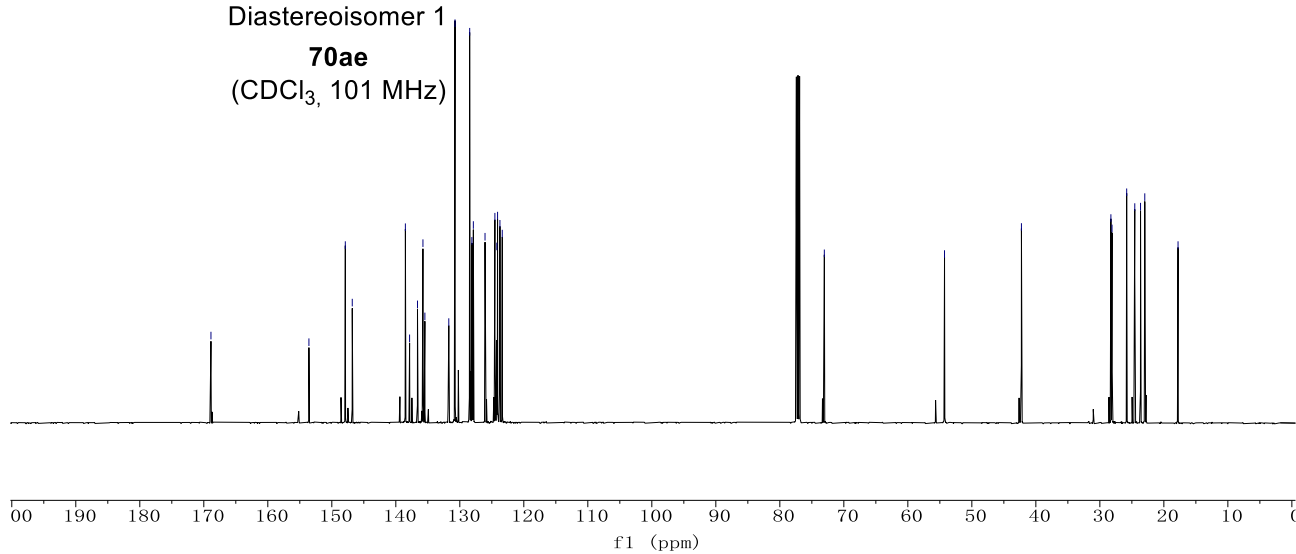
(CDCl₃, 400 MHz)



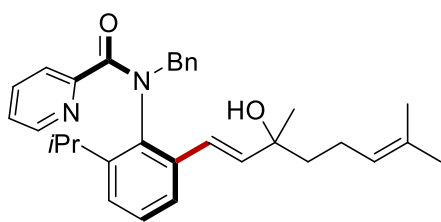
Diastereoisomer 1

70ae

(CDCl₃, 101 MHz)



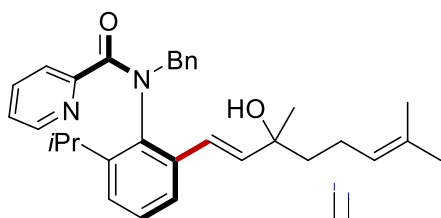
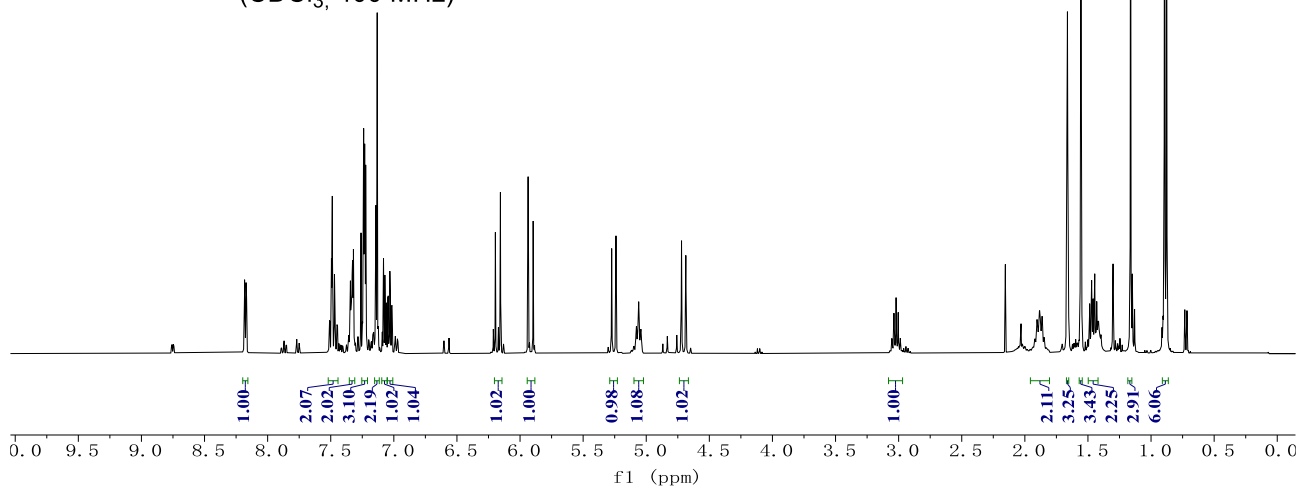
NMR Spectra



Diastereoisomer 2

70ae

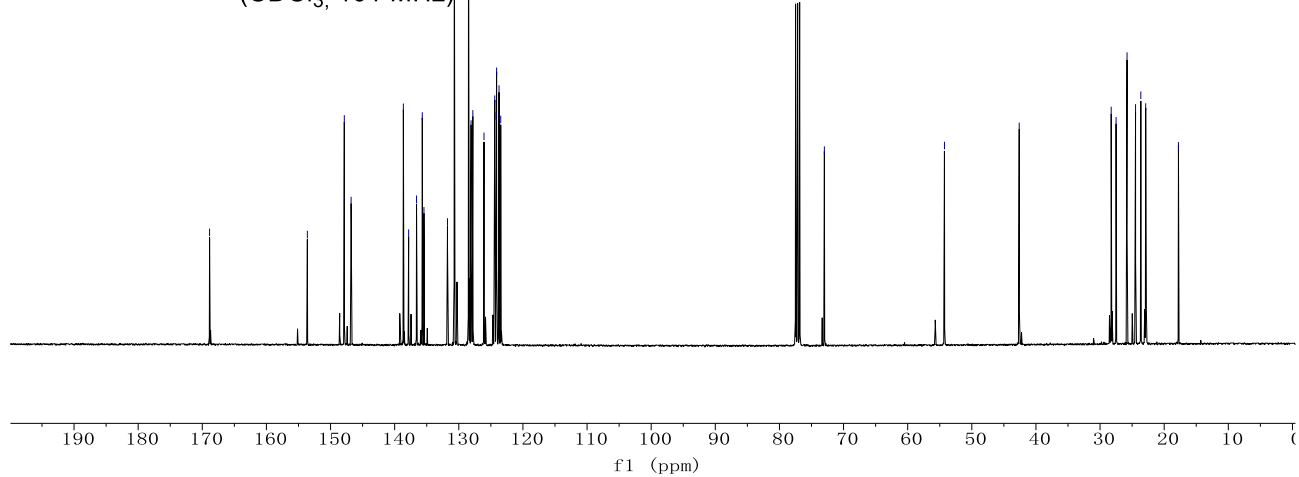
(CDCl₃, 400 MHz)



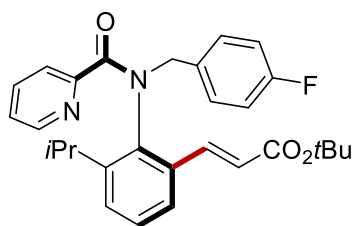
Diastereoisomer 2

70ae

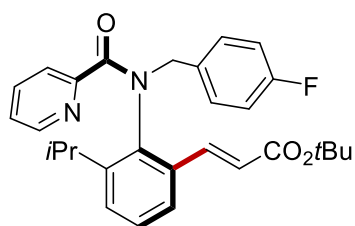
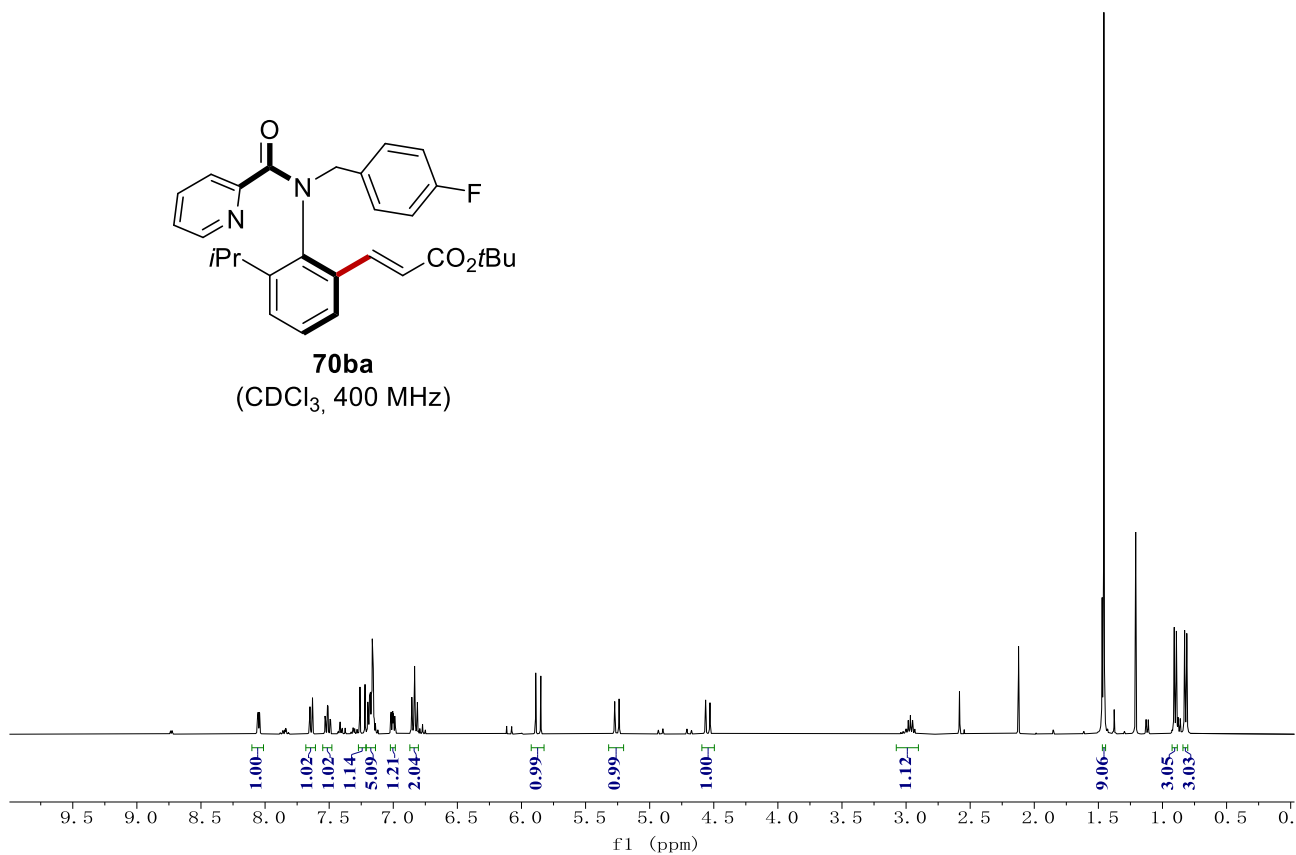
(CDCl₃, 101 MHz)



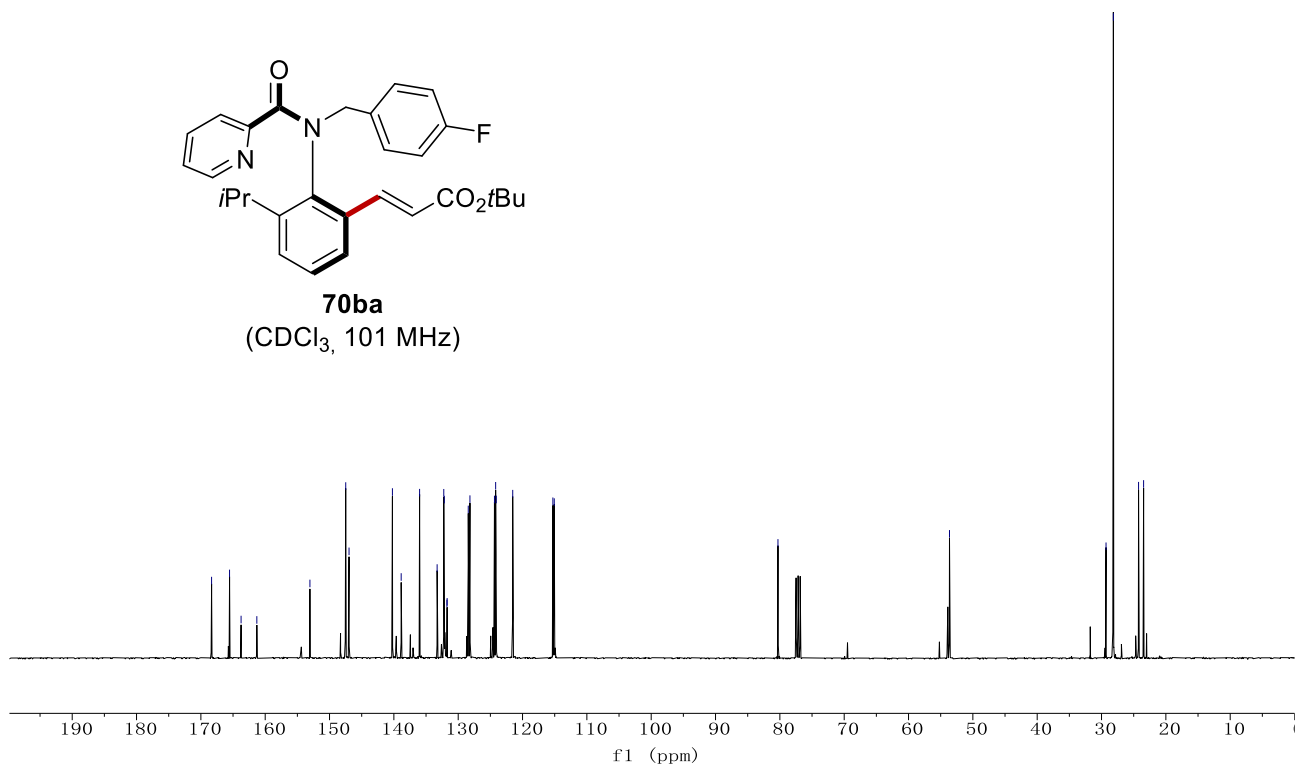
NMR Spectra



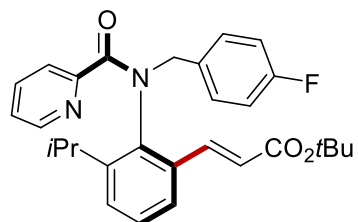
70ba
(CDCl₃, 400 MHz)



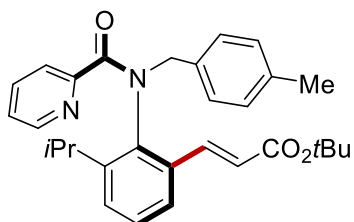
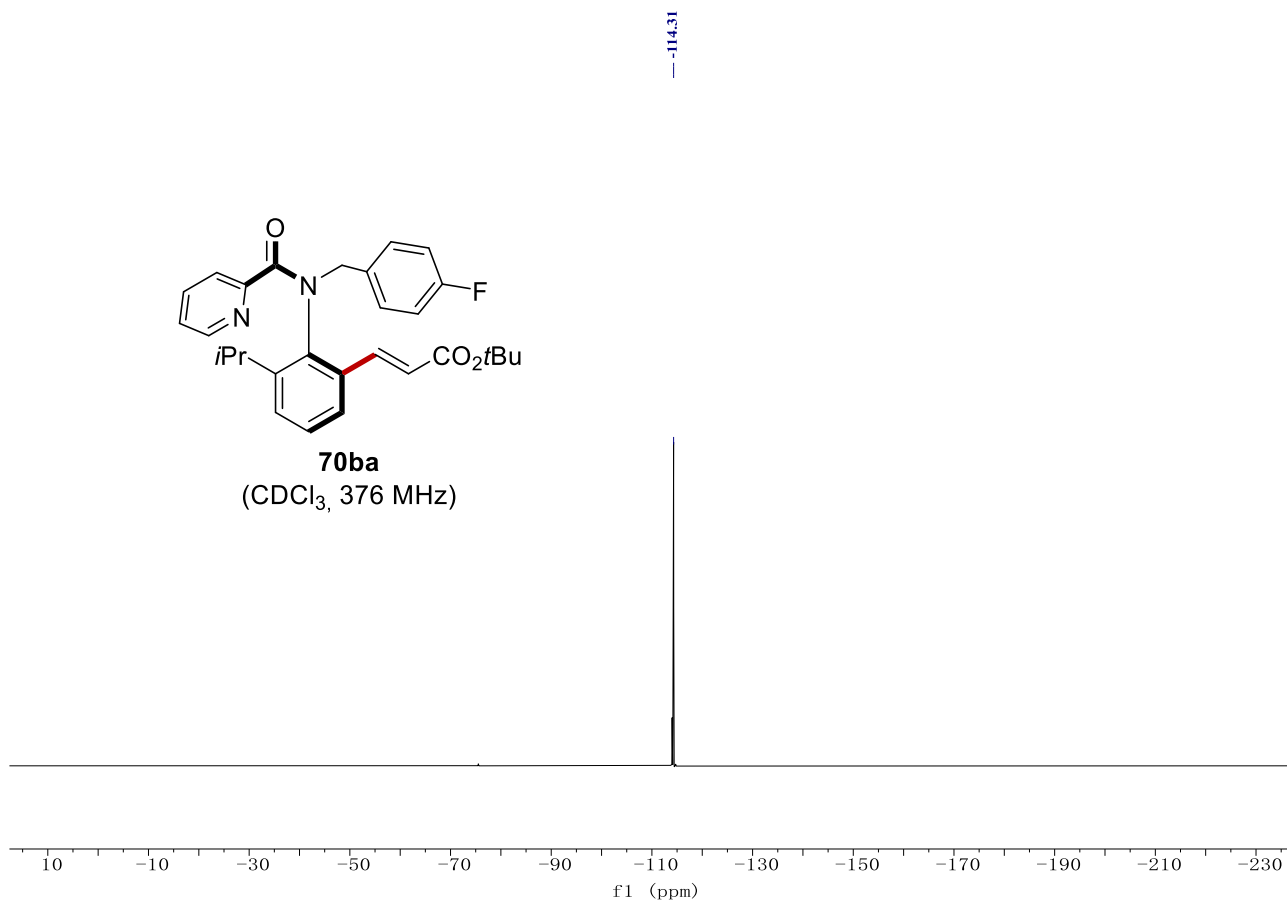
70ba
(CDCl₃, 101 MHz)



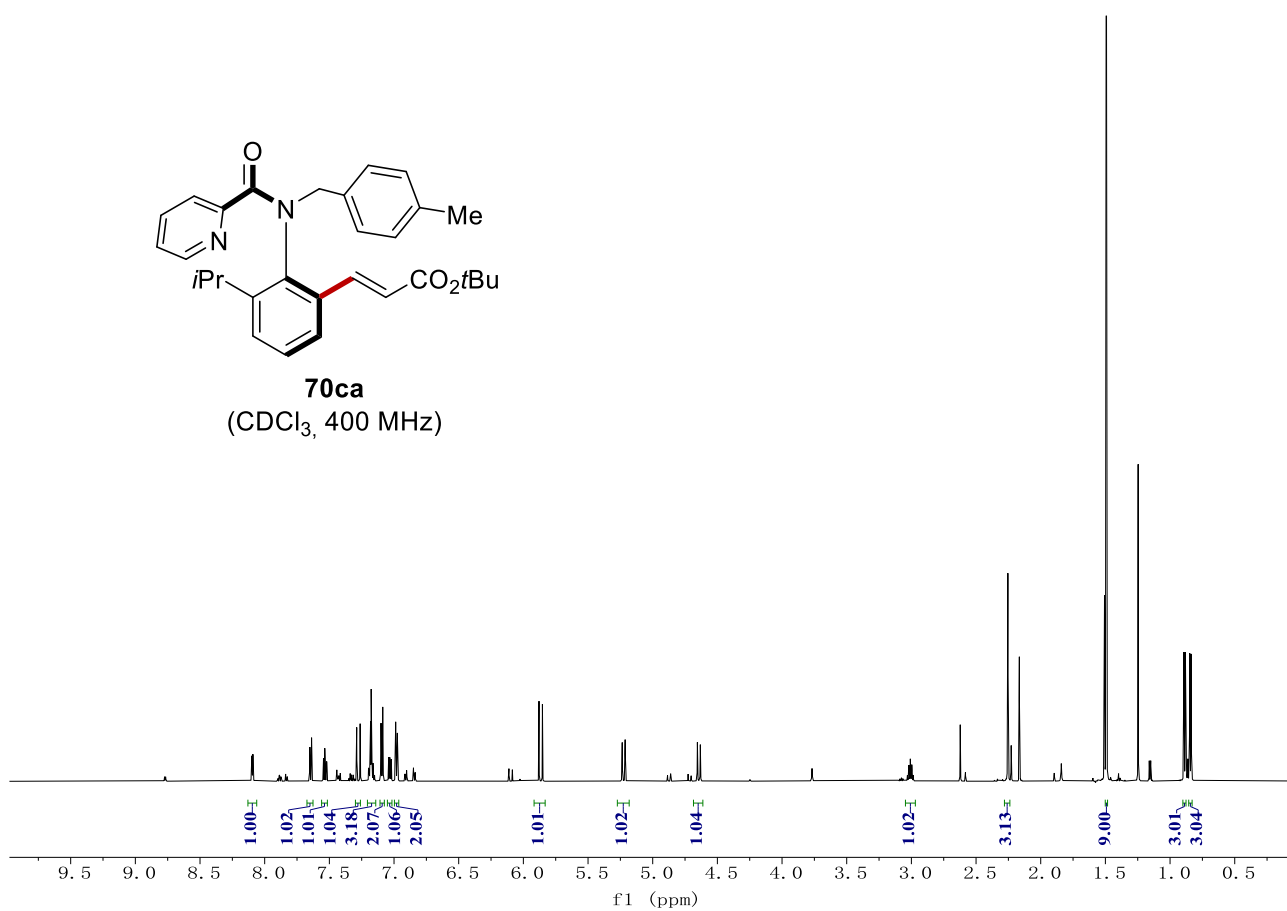
NMR Spectra



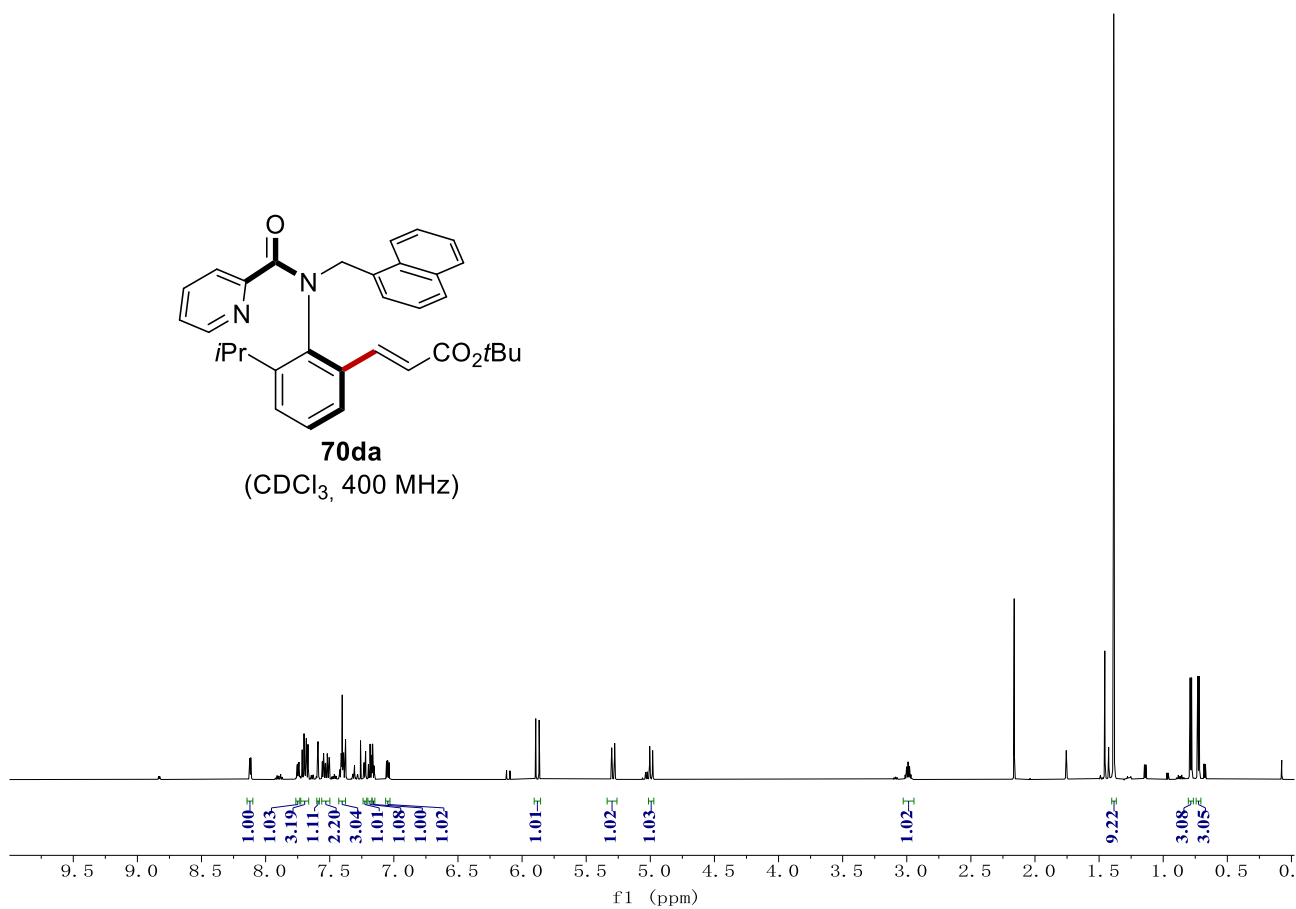
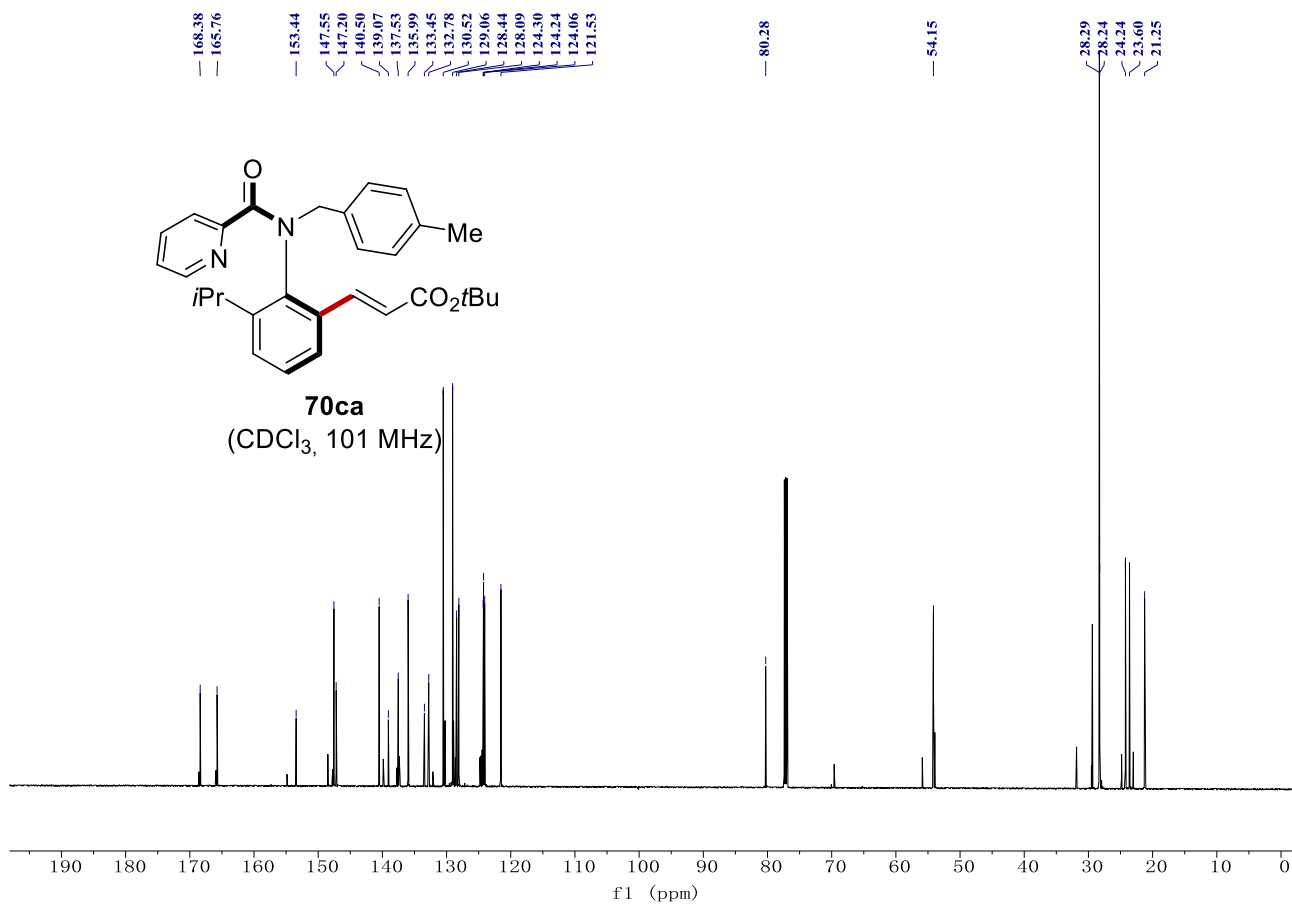
70ba
(CDCl₃, 376 MHz)



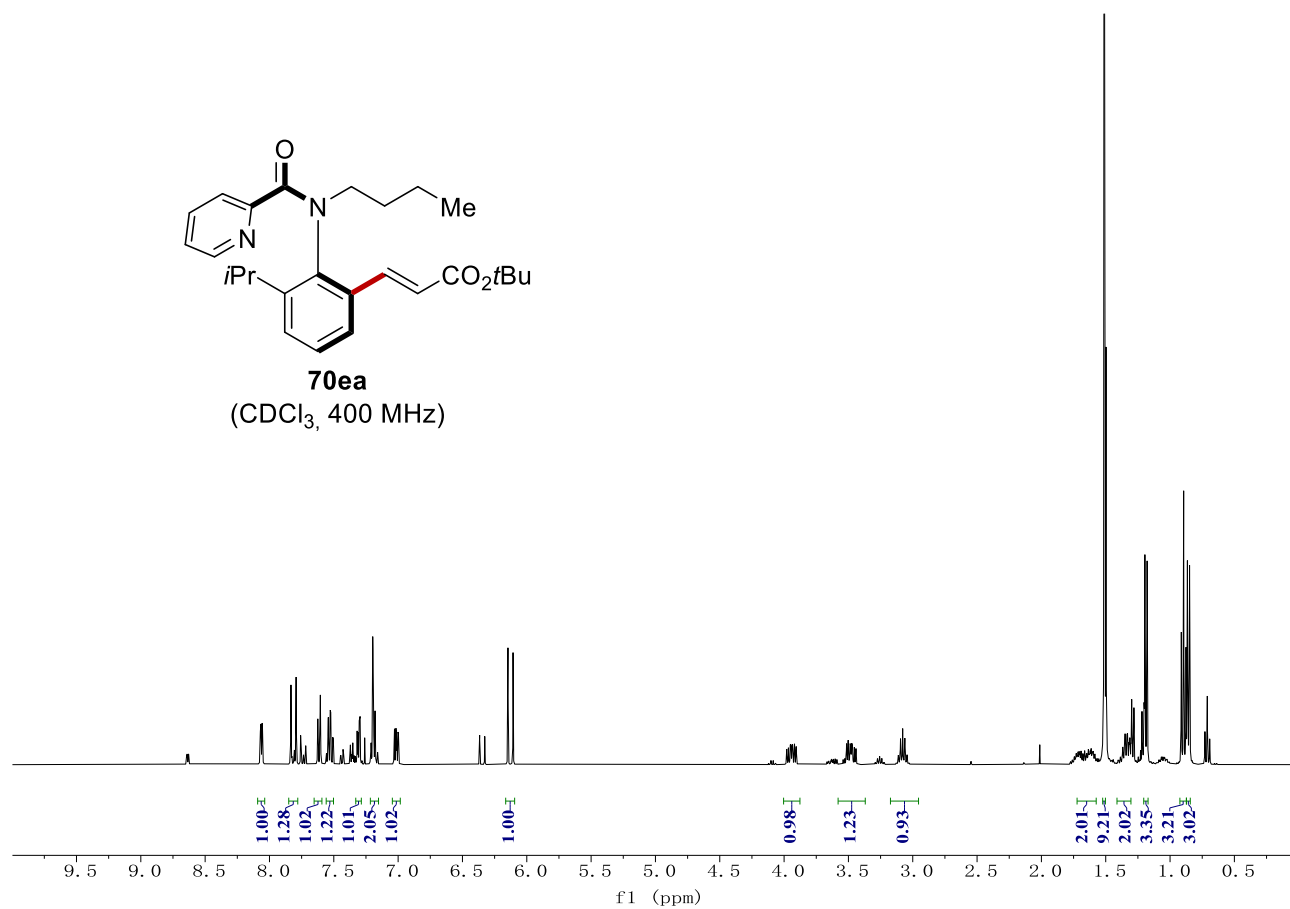
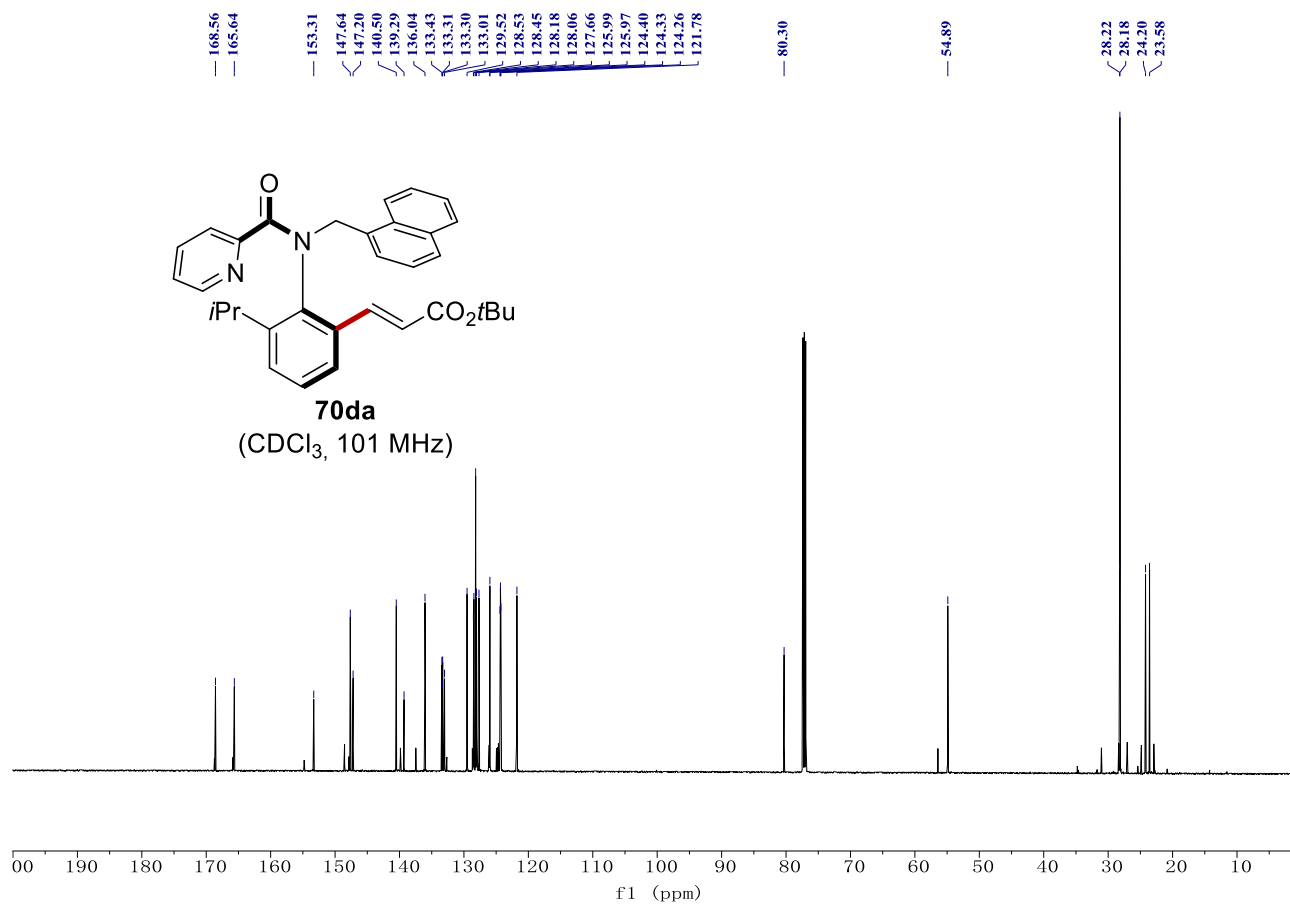
70ca
(CDCl₃, 400 MHz)



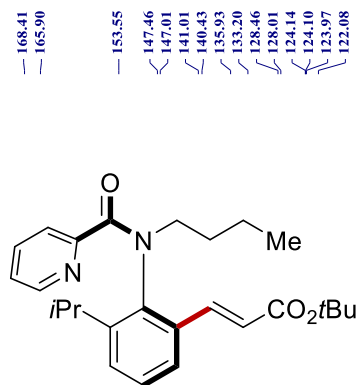
NMR Spectra



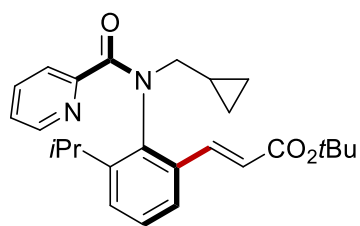
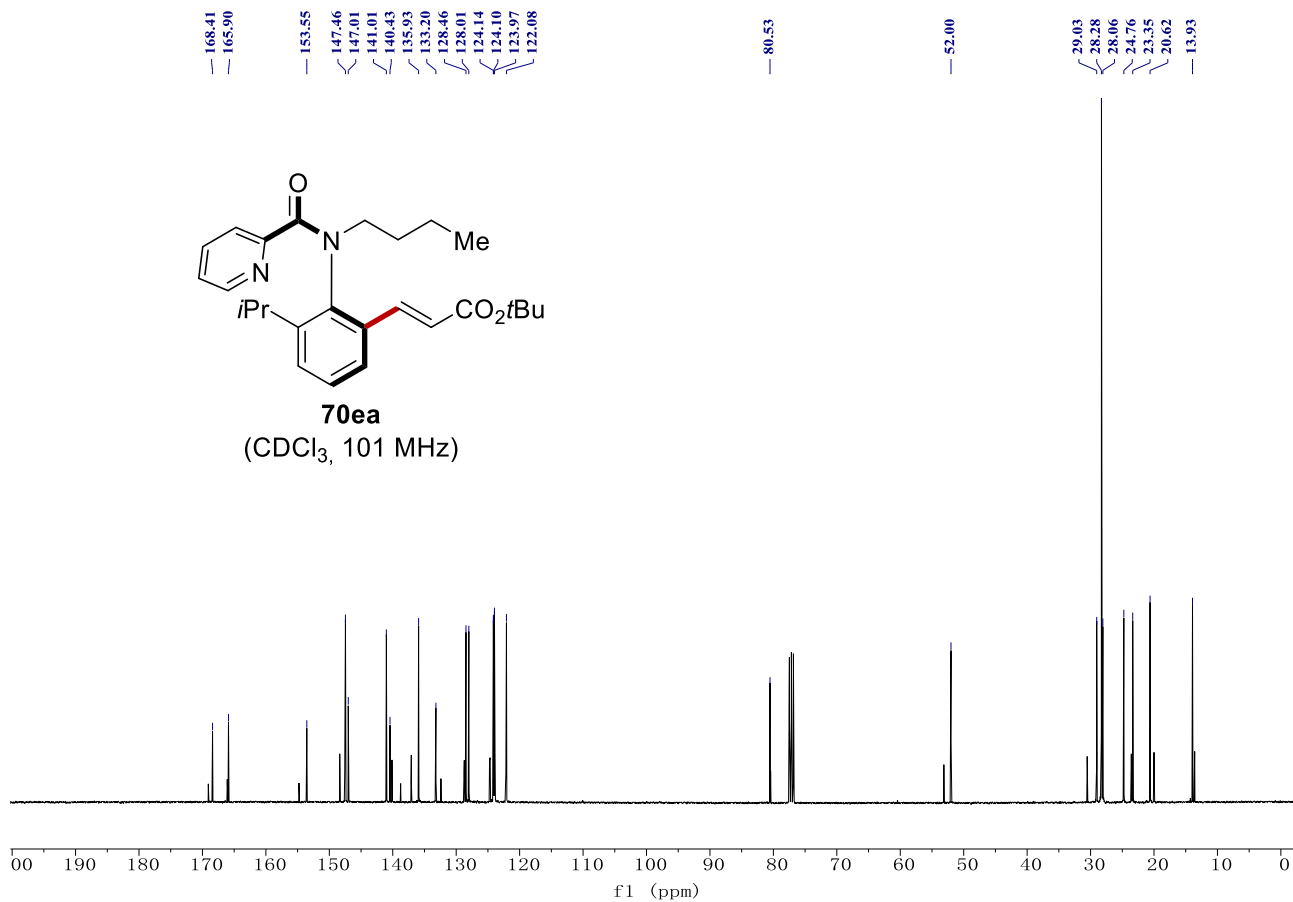
NMR Spectra



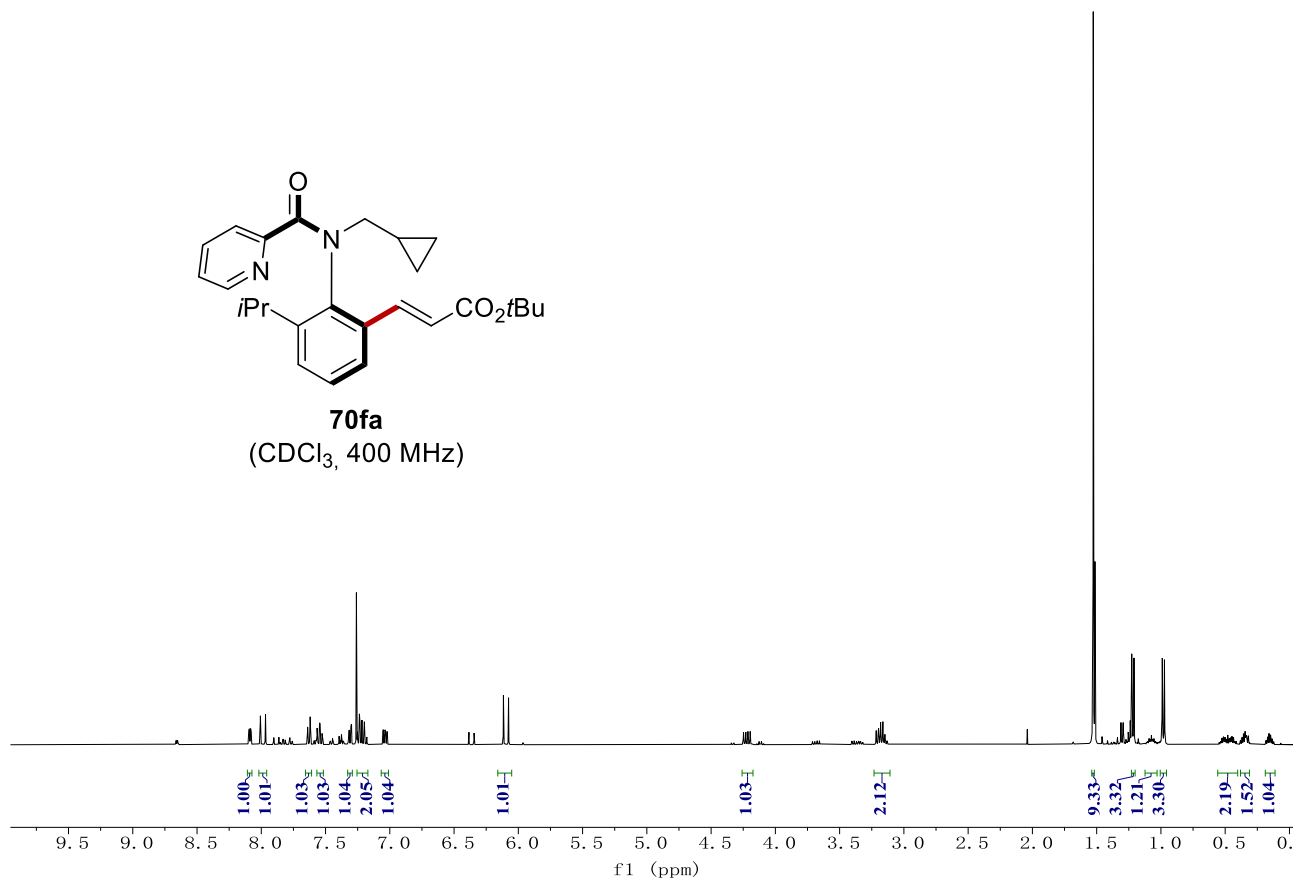
NMR Spectra



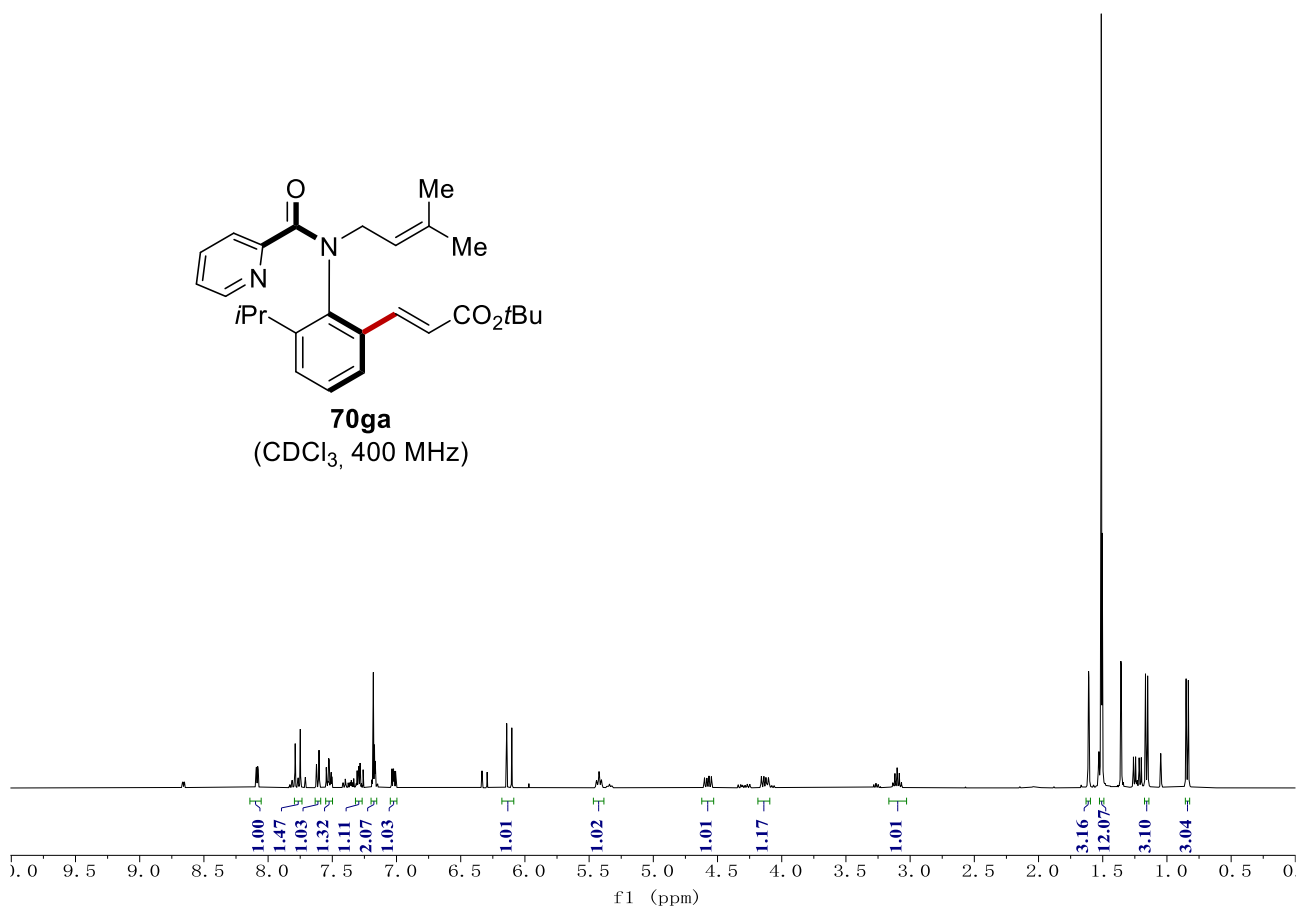
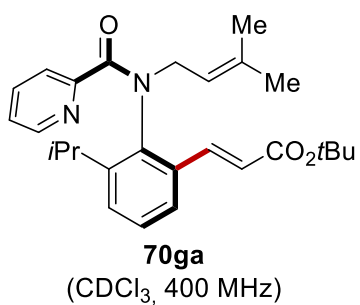
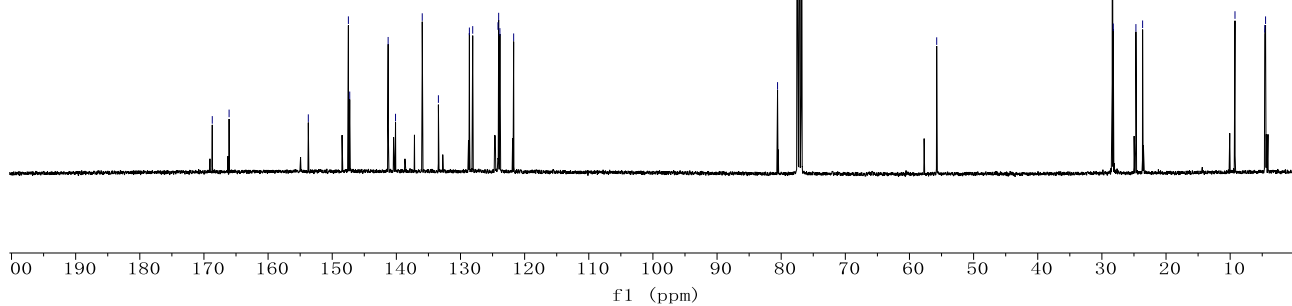
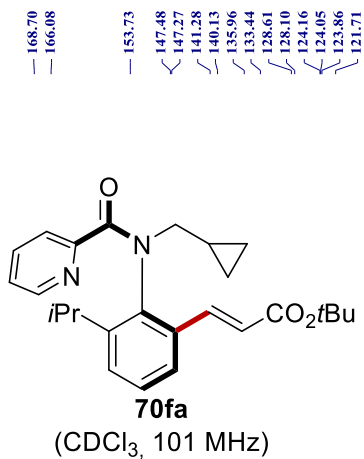
70ea
(CDCl₃, 101 MHz)



70fa
(CDCl₃, 400 MHz)

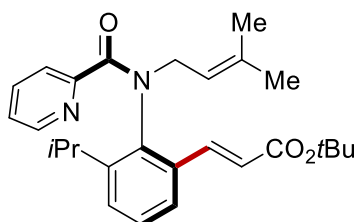


NMR Spectra

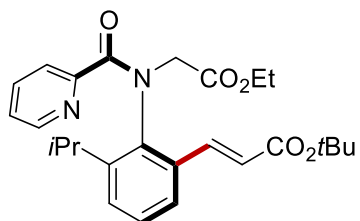
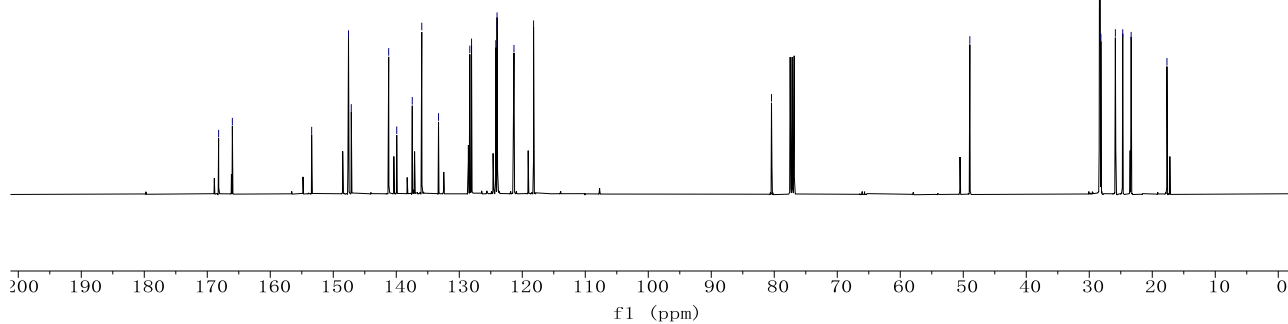


NMR Spectra

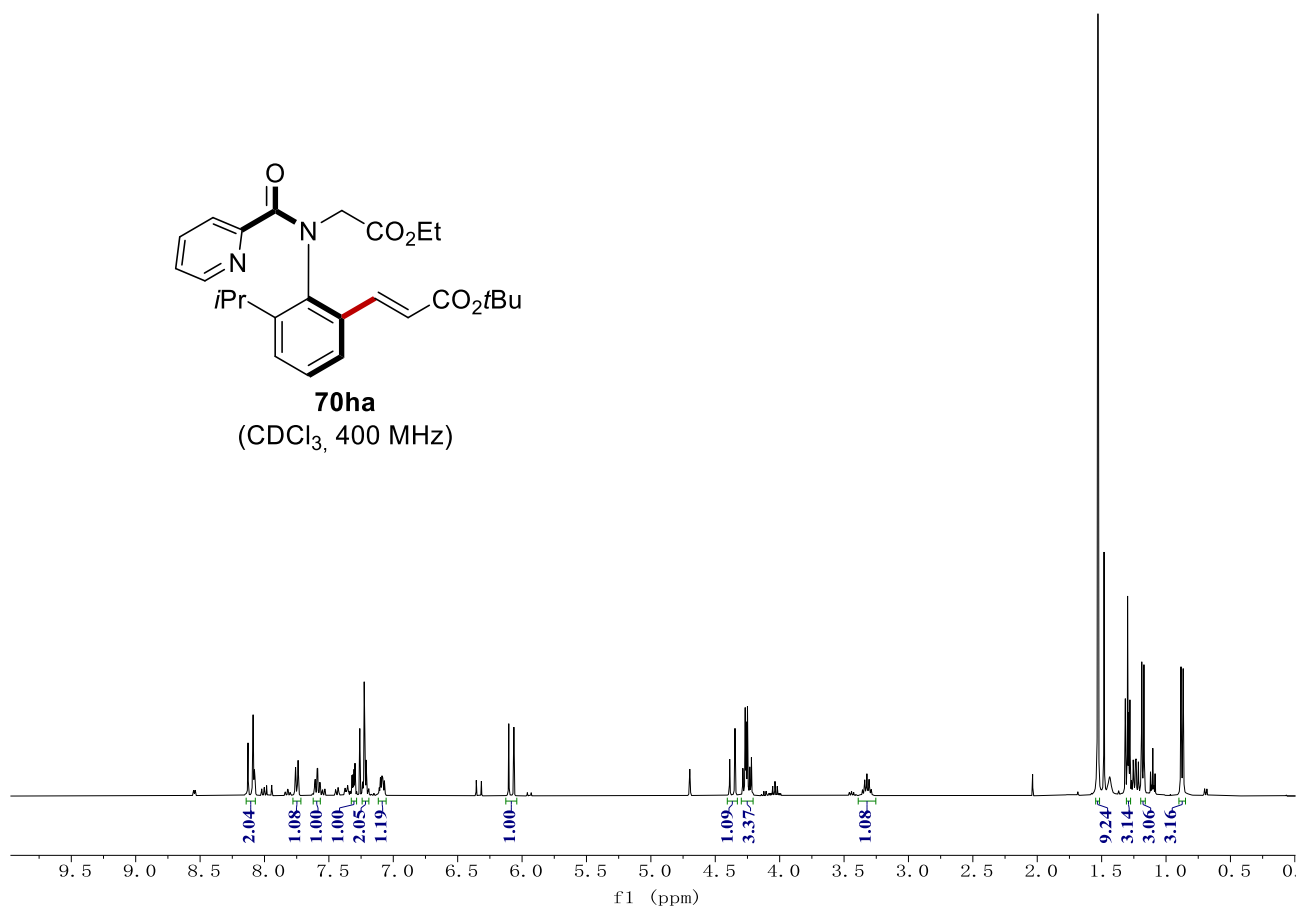
168.20
166.02
153.43
147.58
147.14
141.20
139.93
137.46
135.95
133.30
128.53
124.20
124.00
123.98
121.32
118.21
80.44
48.96
28.30
28.15
25.86
24.69
23.35
17.67



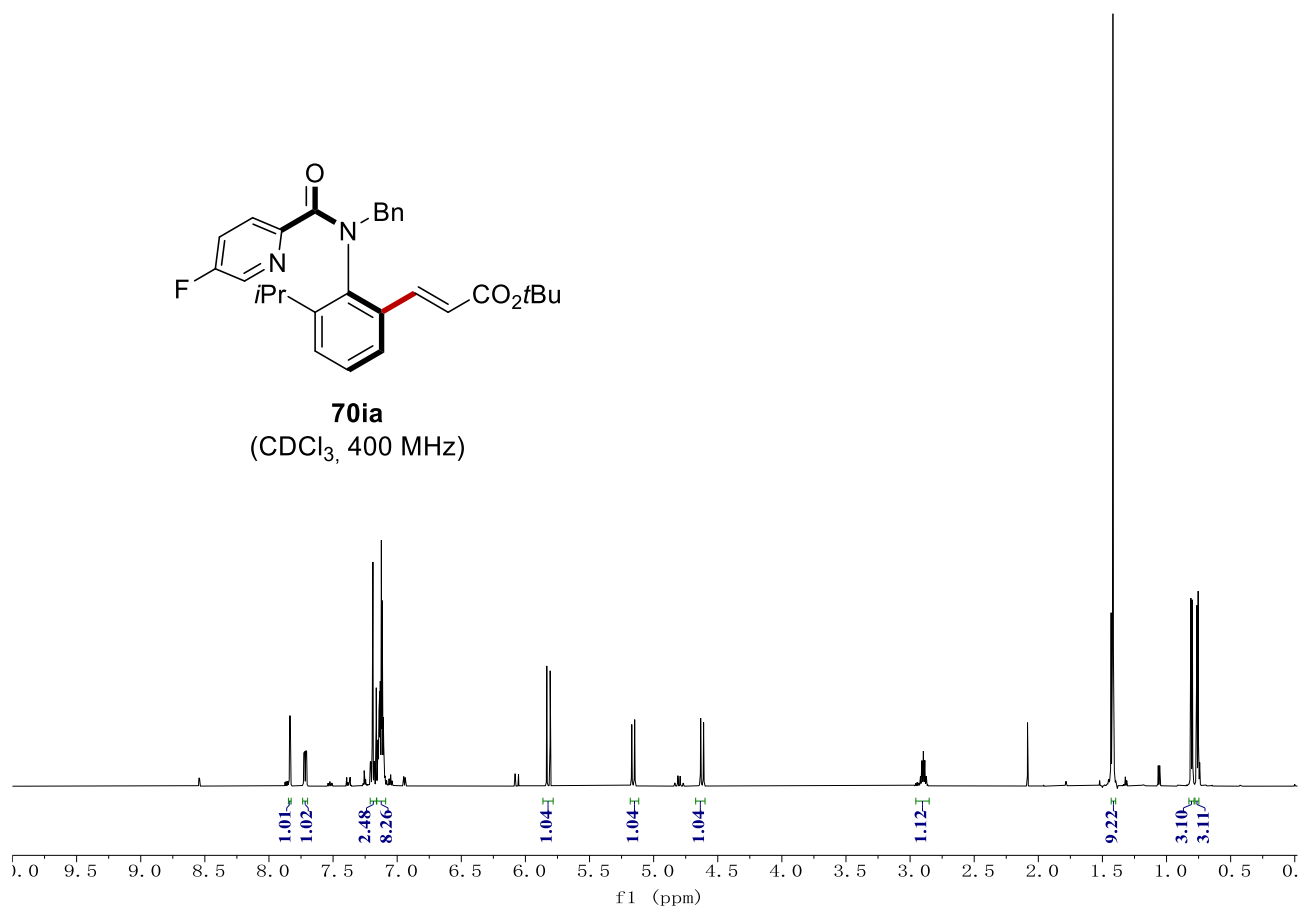
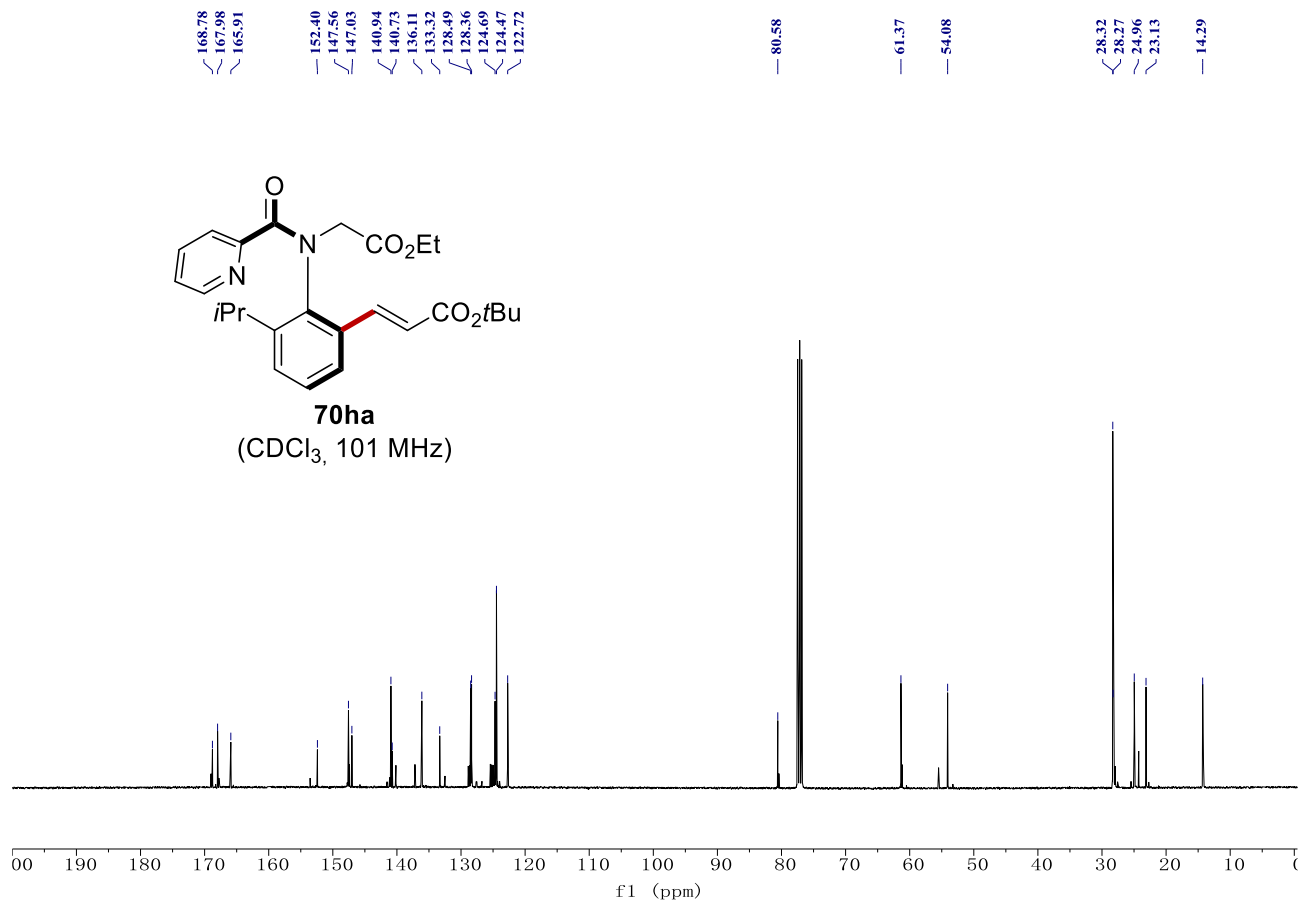
70ga
(CDCl₃, 101 MHz)



70ha
(CDCl₃, 400 MHz)

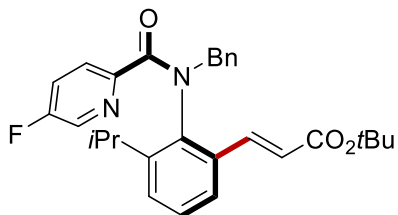


NMR Spectra

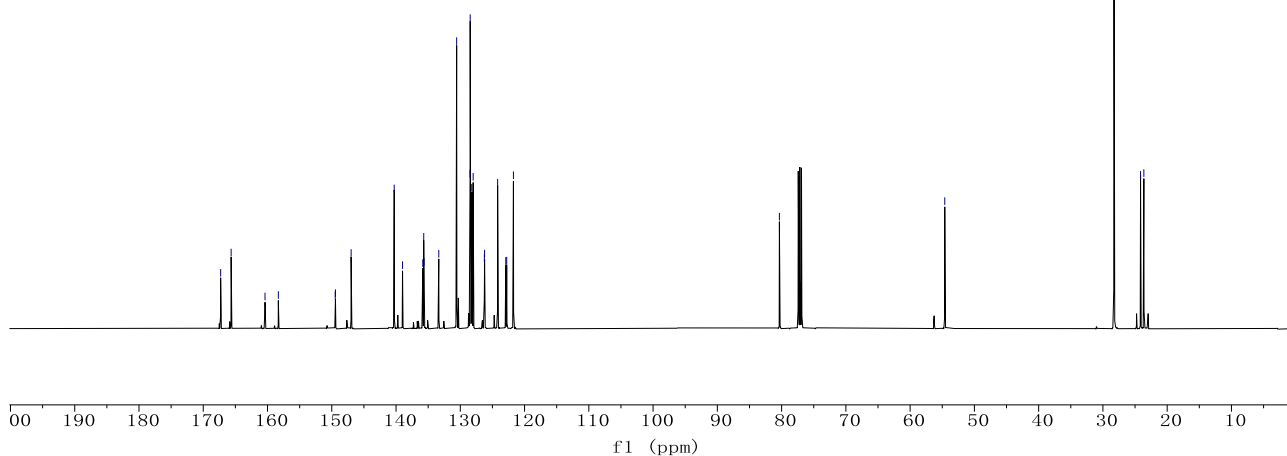


NMR Spectra

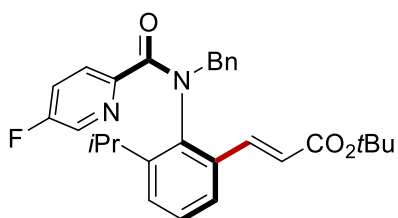
167.29, 165.66, 160.39, 158.32, 149.46, 149.43, 146.99, 140.29, 138.99, 135.84, 135.69, 135.65, 133.35, 130.57, 128.46, 128.48, 128.22, 128.00, 126.26, 126.22, 124.19, 122.92, 122.78, 121.73, 80.34, 54.61, 28.29, 24.14, 23.63



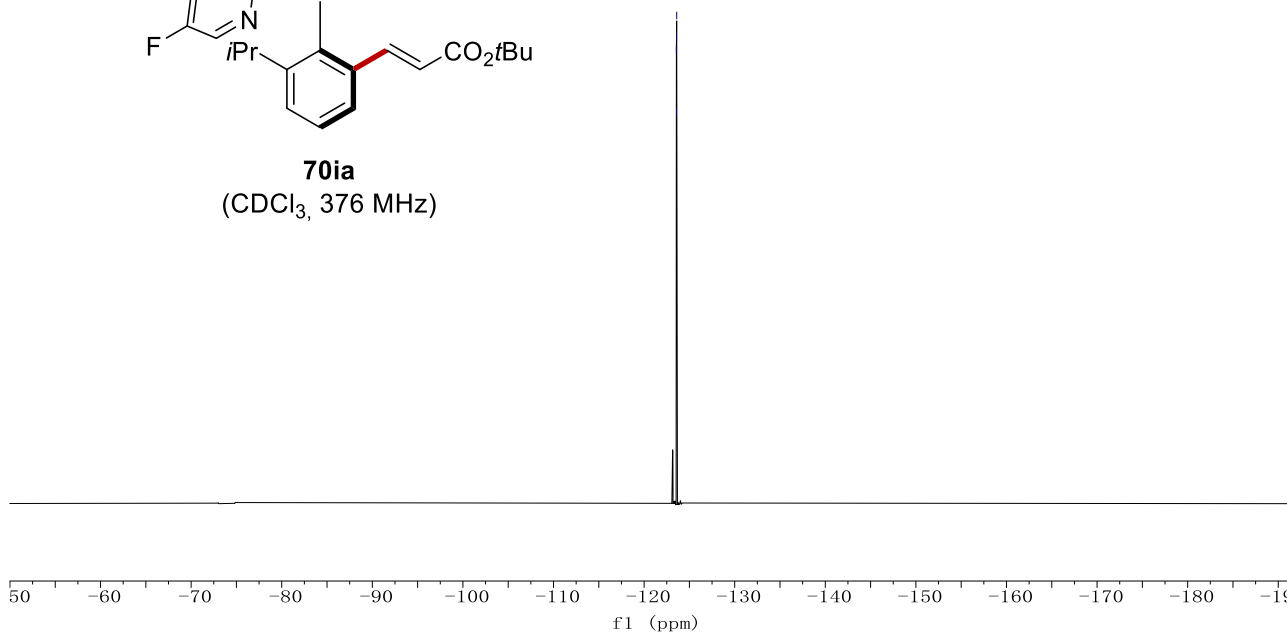
70ia
(CDCl₃, 101 MHz)



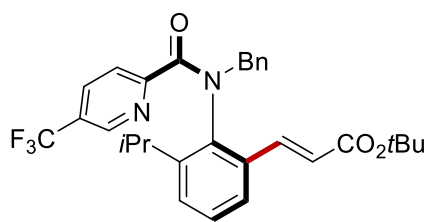
123.56, 123.58, 123.59, 123.60



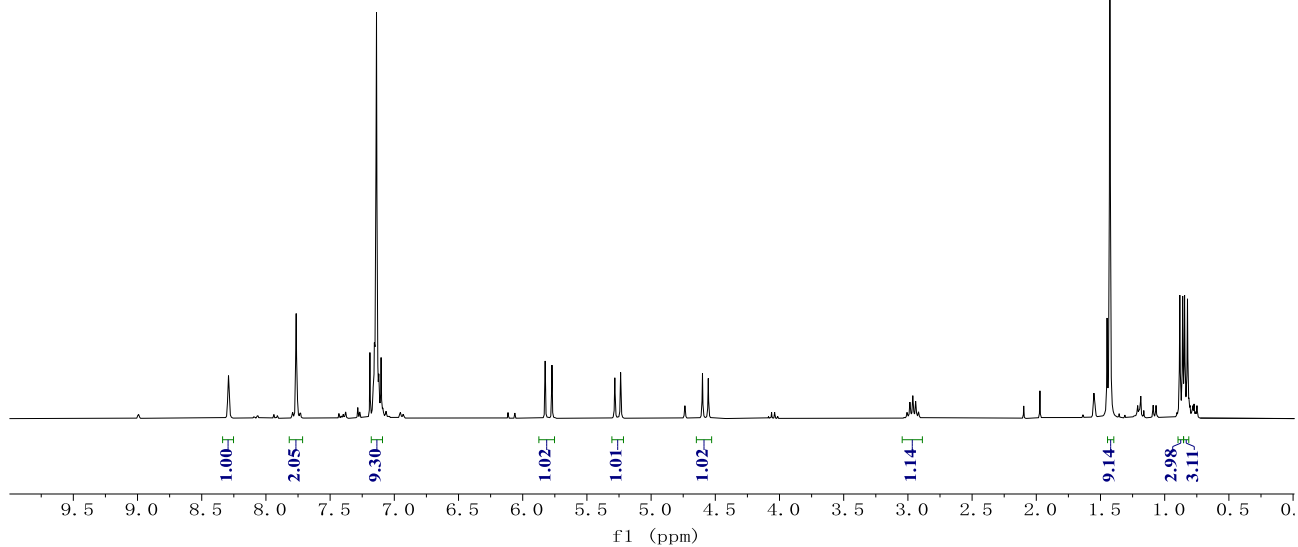
70ia
(CDCl₃, 376 MHz)



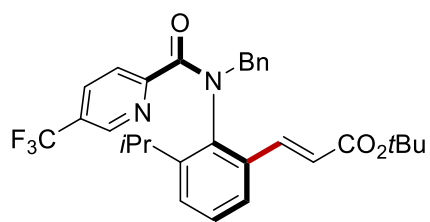
NMR Spectra



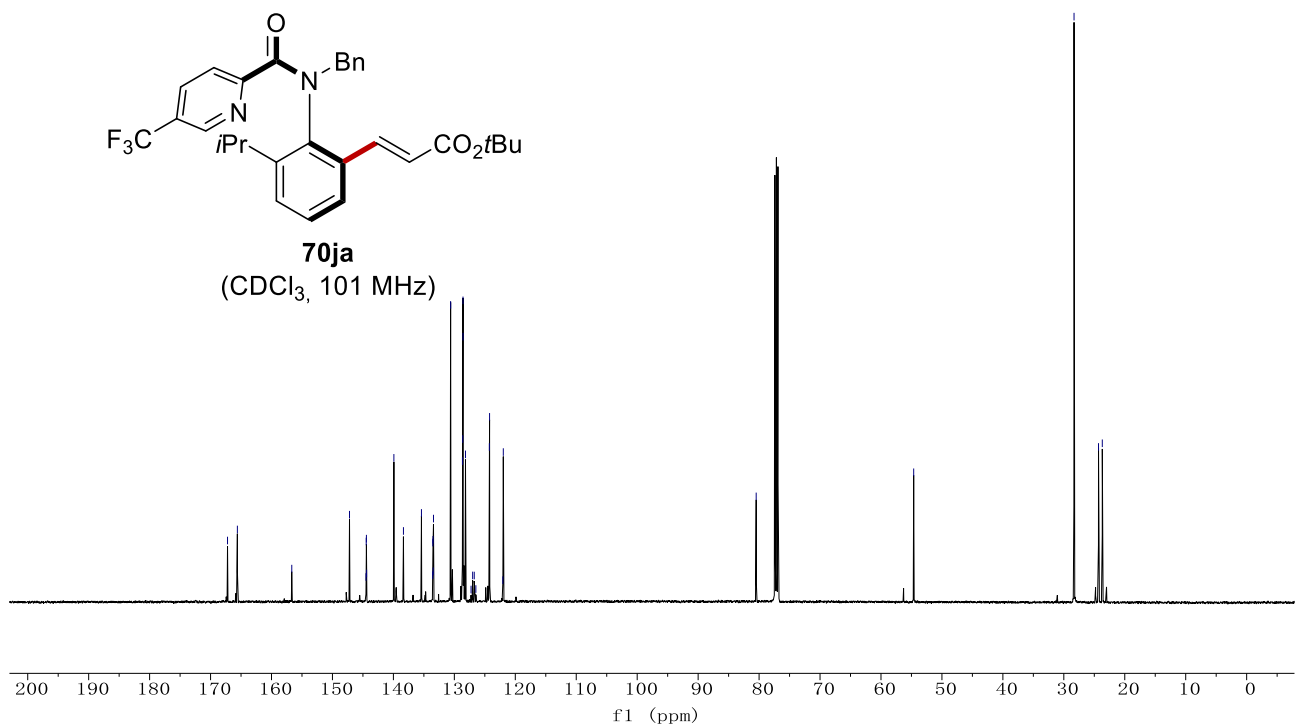
70ja
(CDCl₃, 400 MHz)



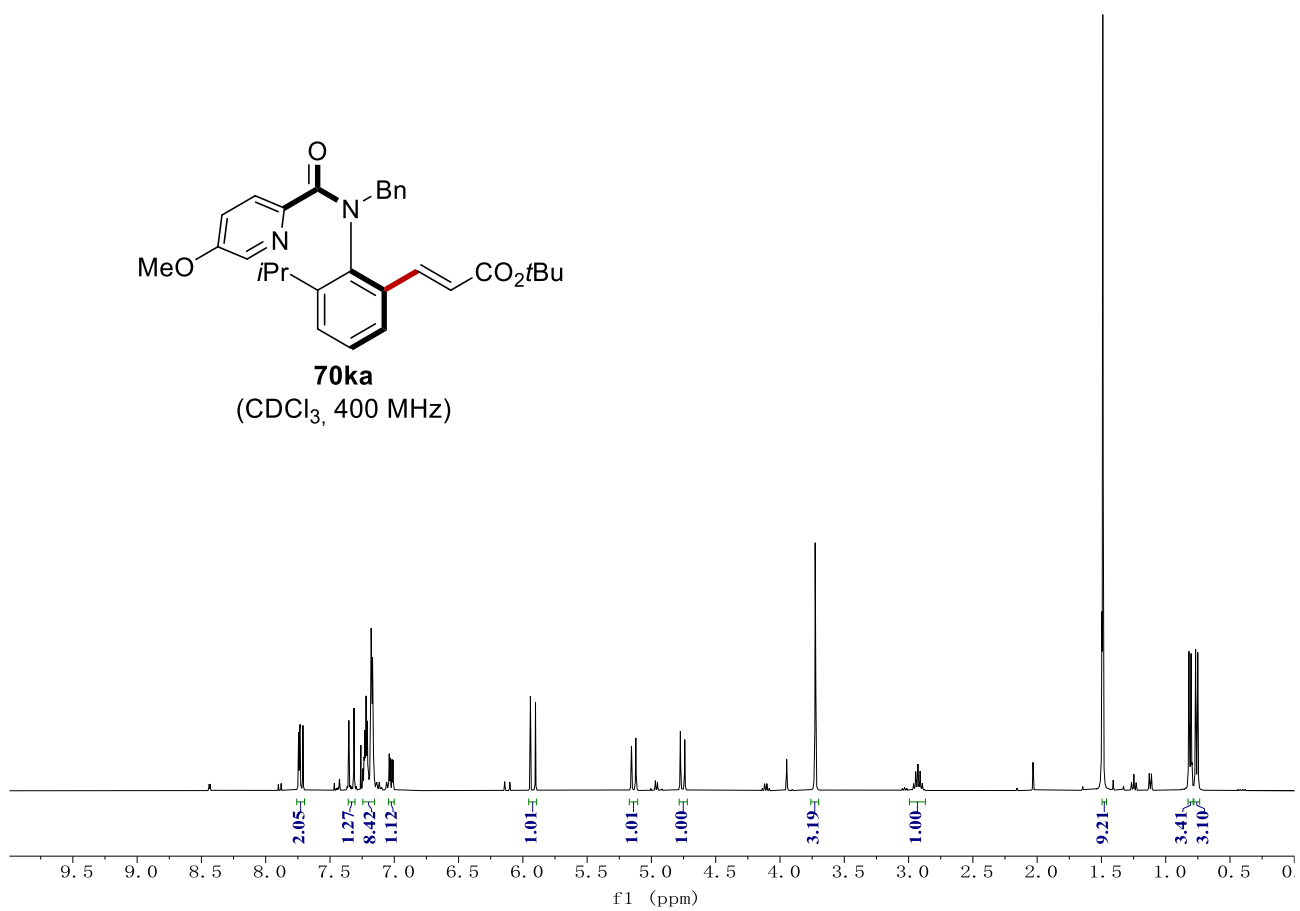
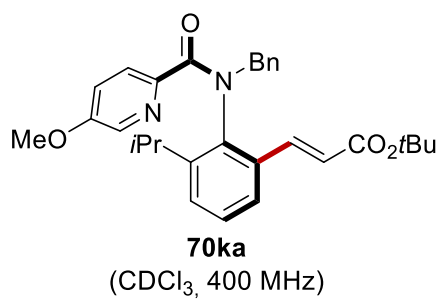
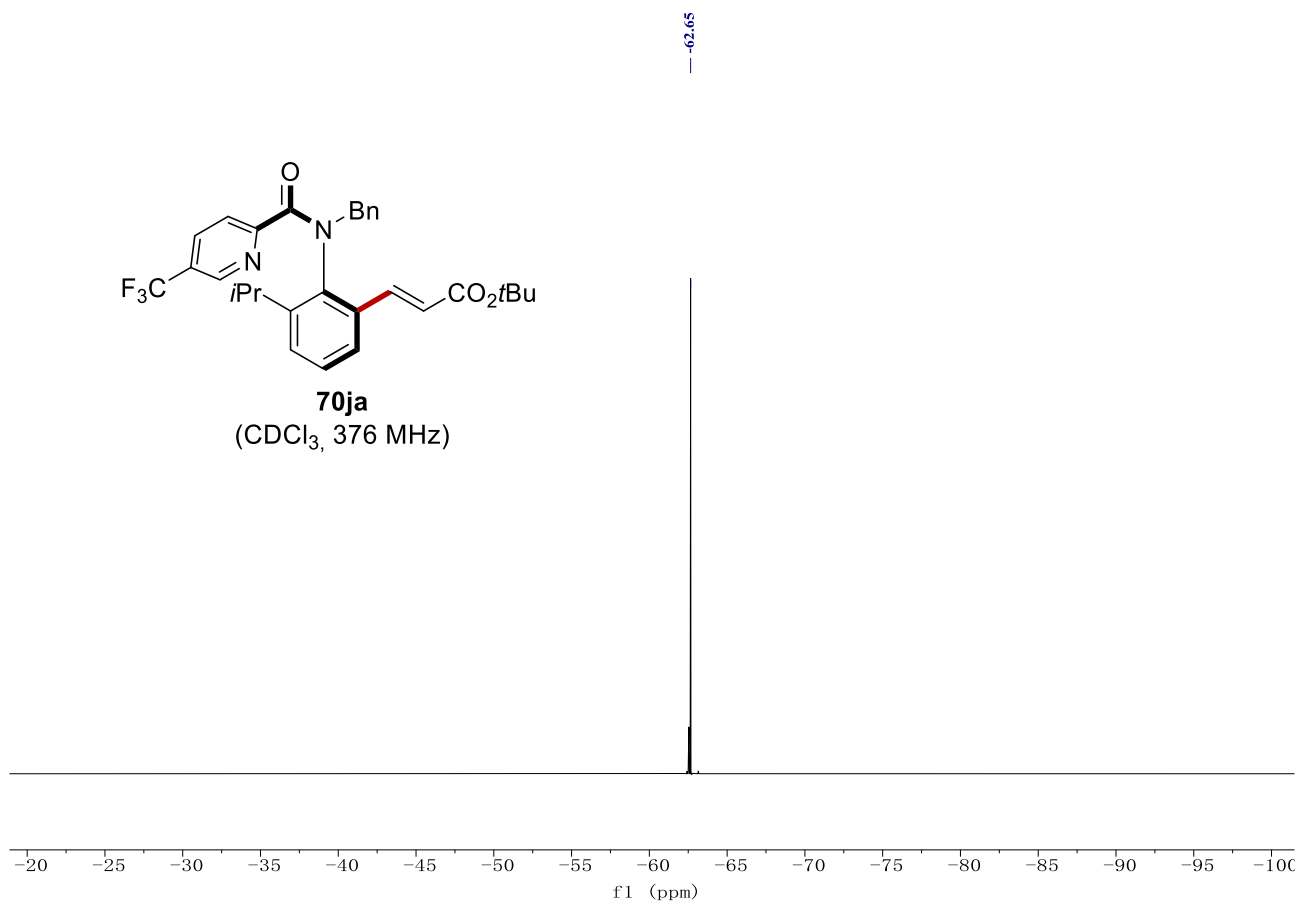
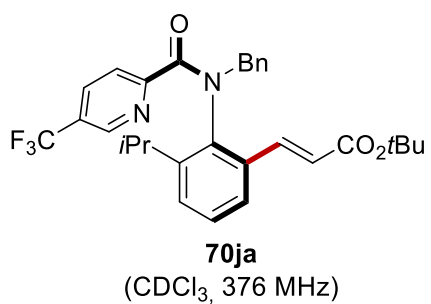
167.22
165.60
156.68
147.20
144.49
144.46
144.43
144.40
139.92
138.35
135.40
133.56
133.53
133.50
133.48
133.42
130.61
128.67
128.63
128.58
128.58
128.17
127.26
127.00
126.73
126.47
124.25
124.22
122.04
121.97
80.48
54.63
28.32
24.31
23.69



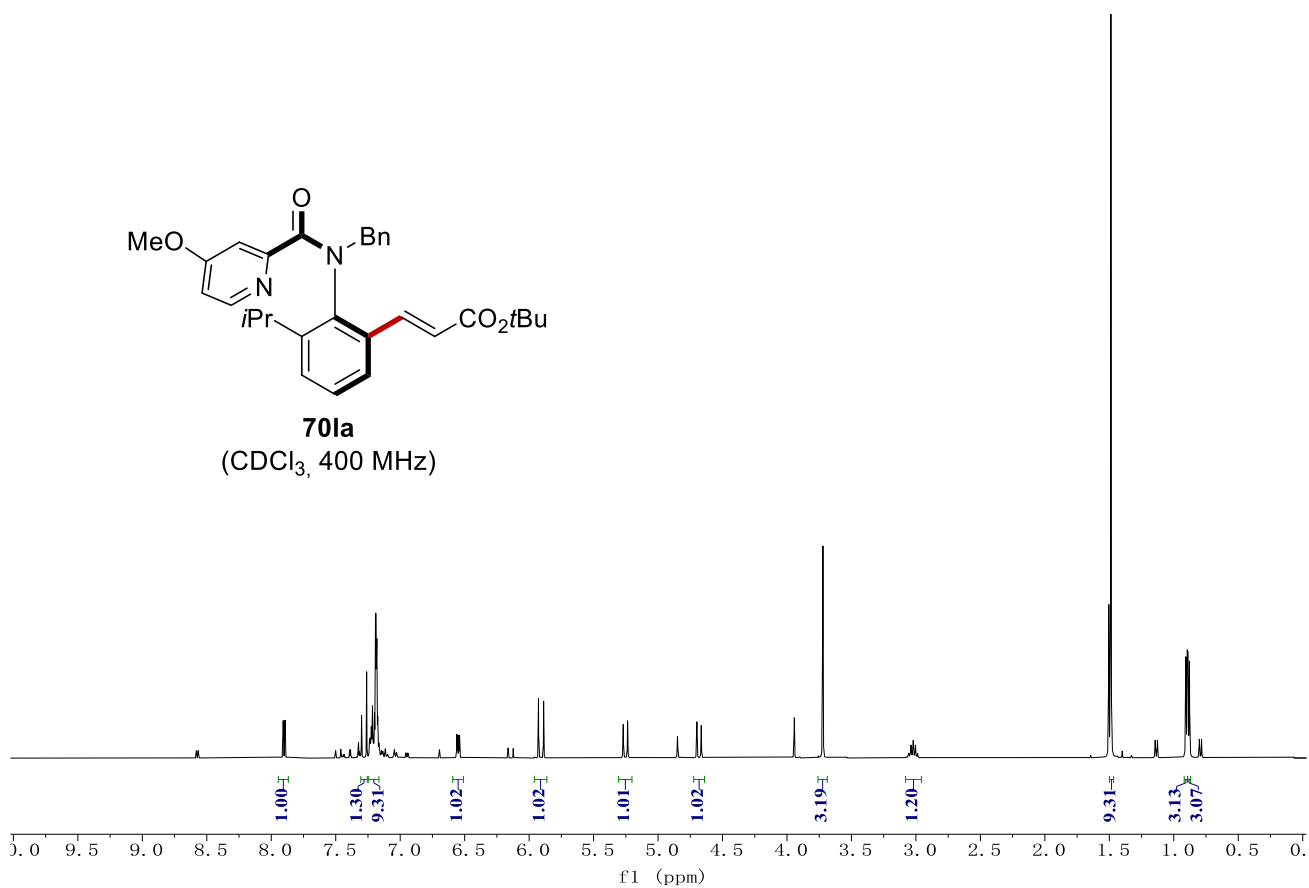
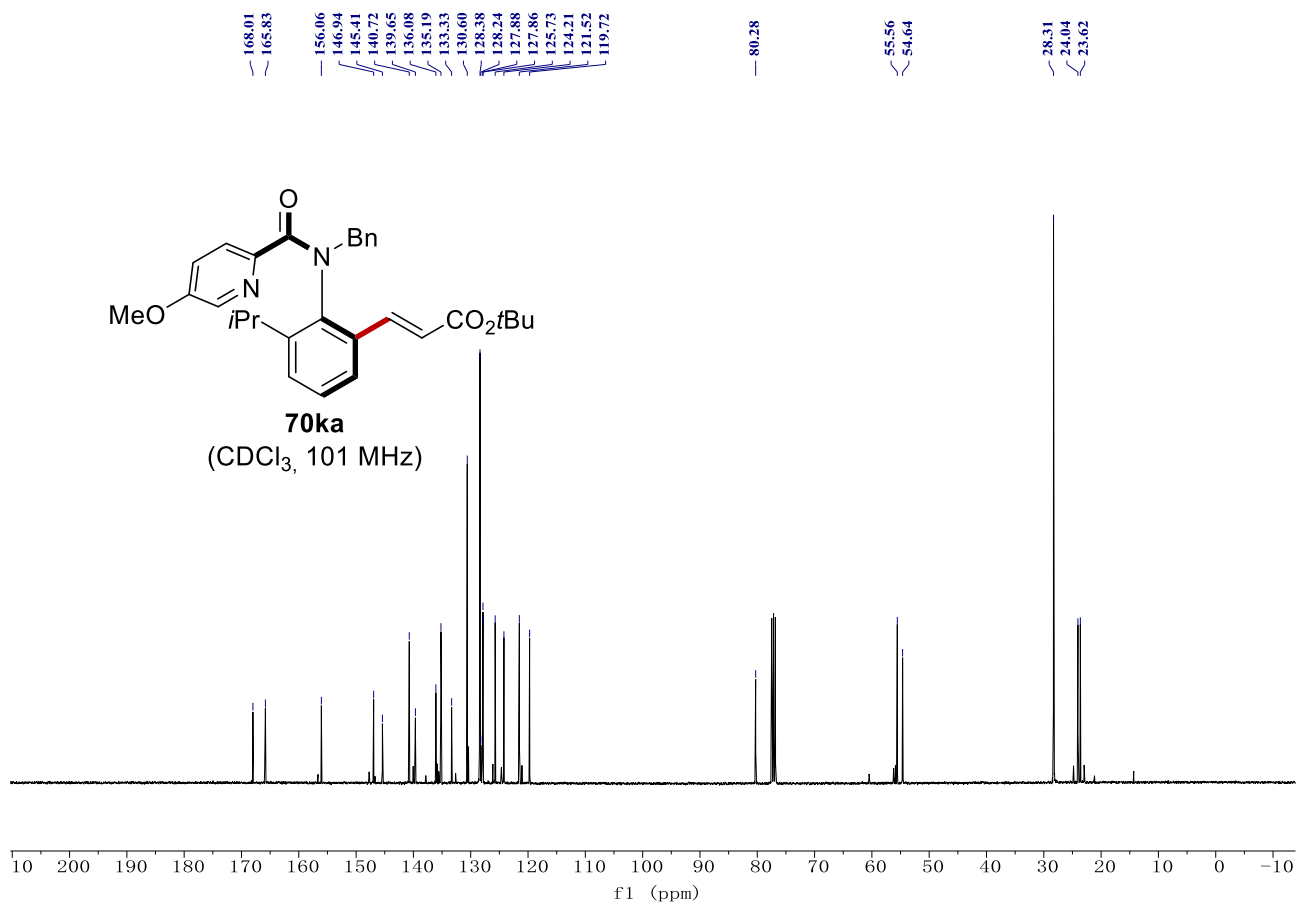
70ja
(CDCl₃, 101 MHz)



NMR Spectra

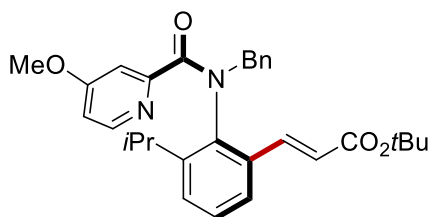


NMR Spectra

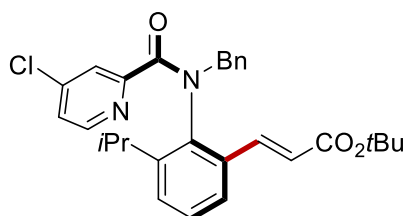
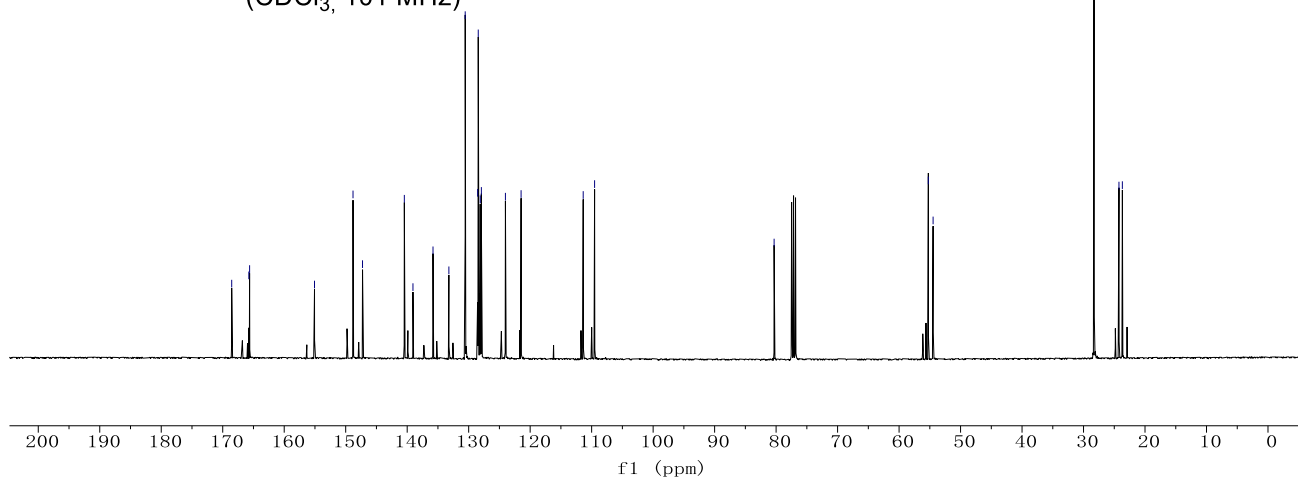


NMR Spectra

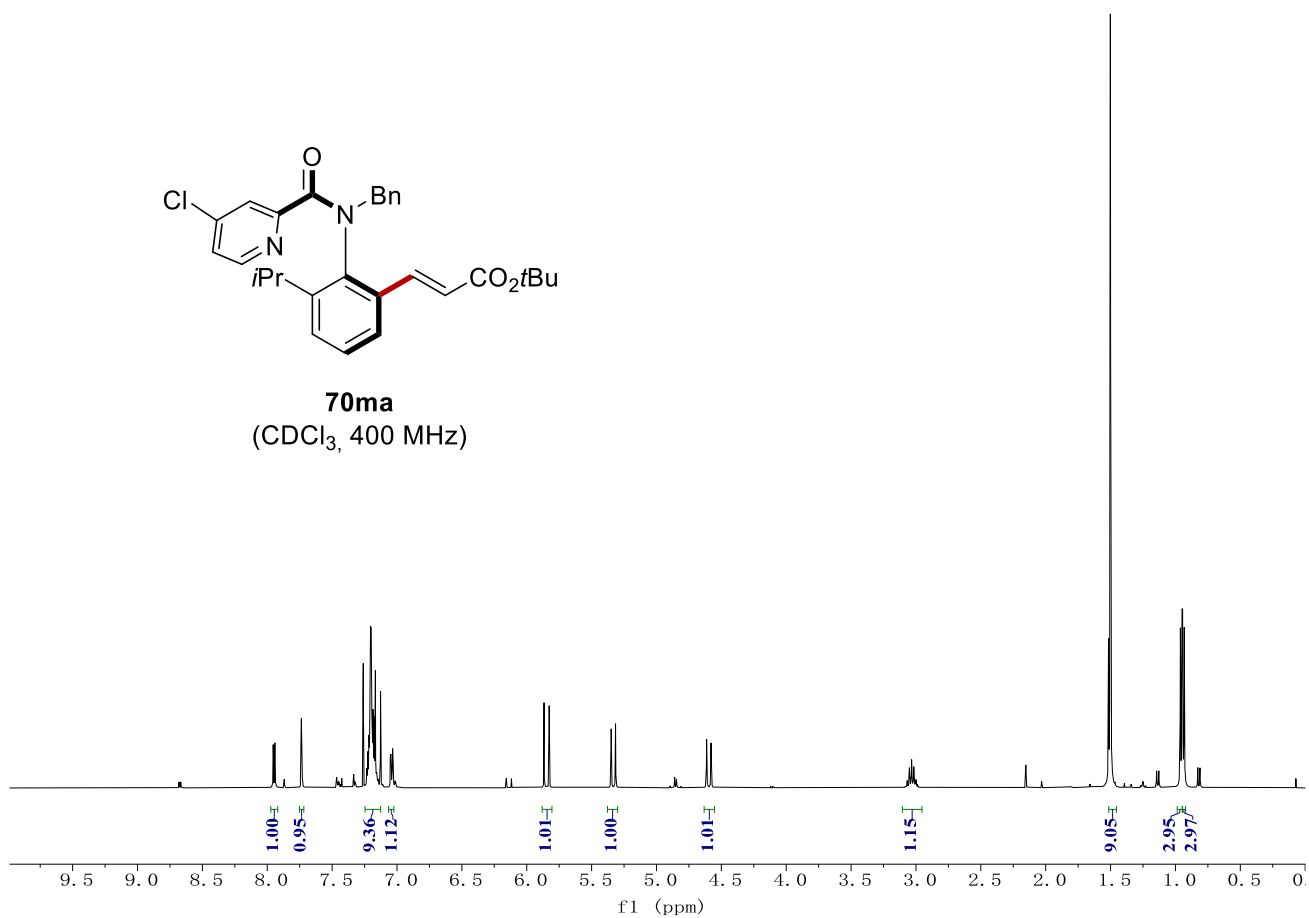
168.54
165.75
165.63
155.07
148.81
147.26
140.46
139.06
135.80
133.22
130.56
128.54
128.44
128.11
127.94
124.02
121.48
111.37
109.52
80.32
55.24
54.47
28.28
24.24
23.68



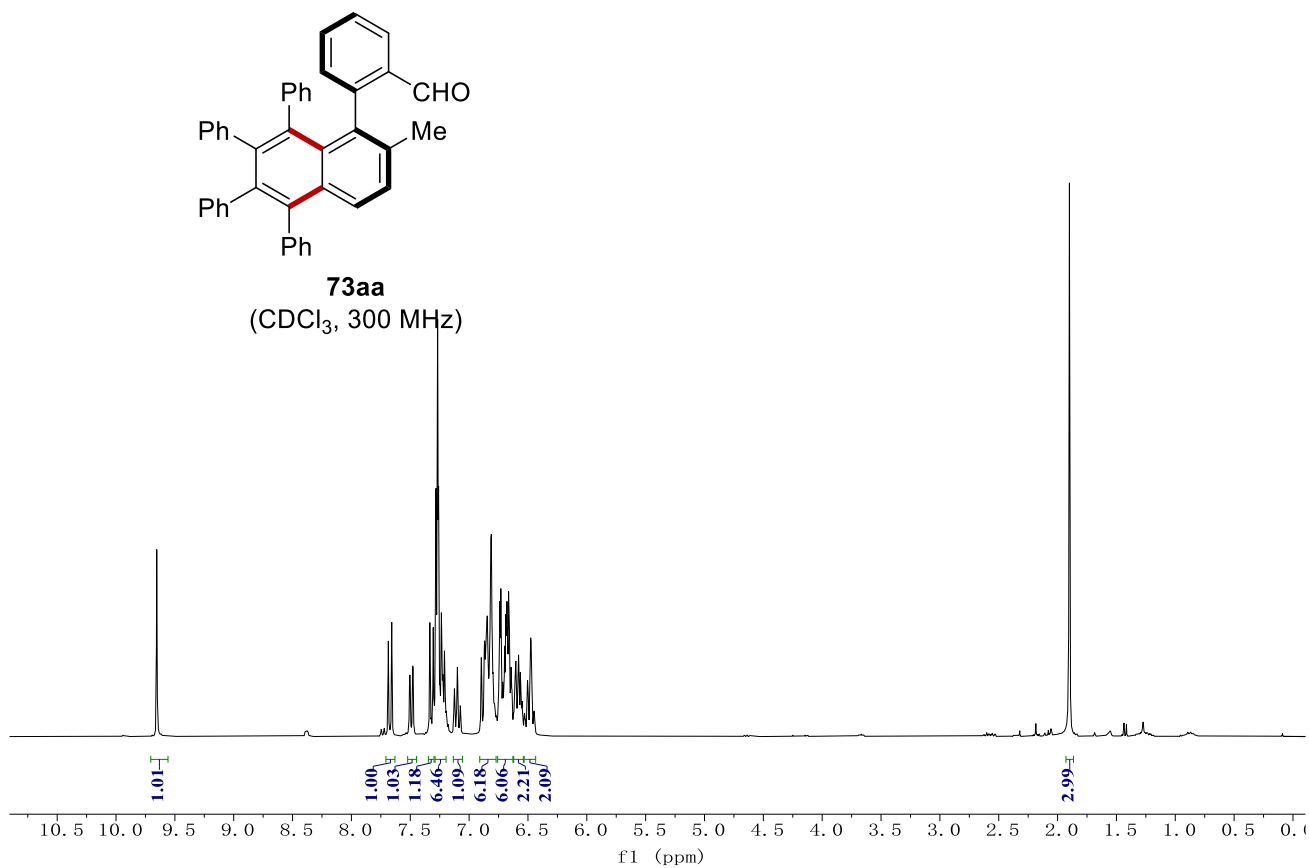
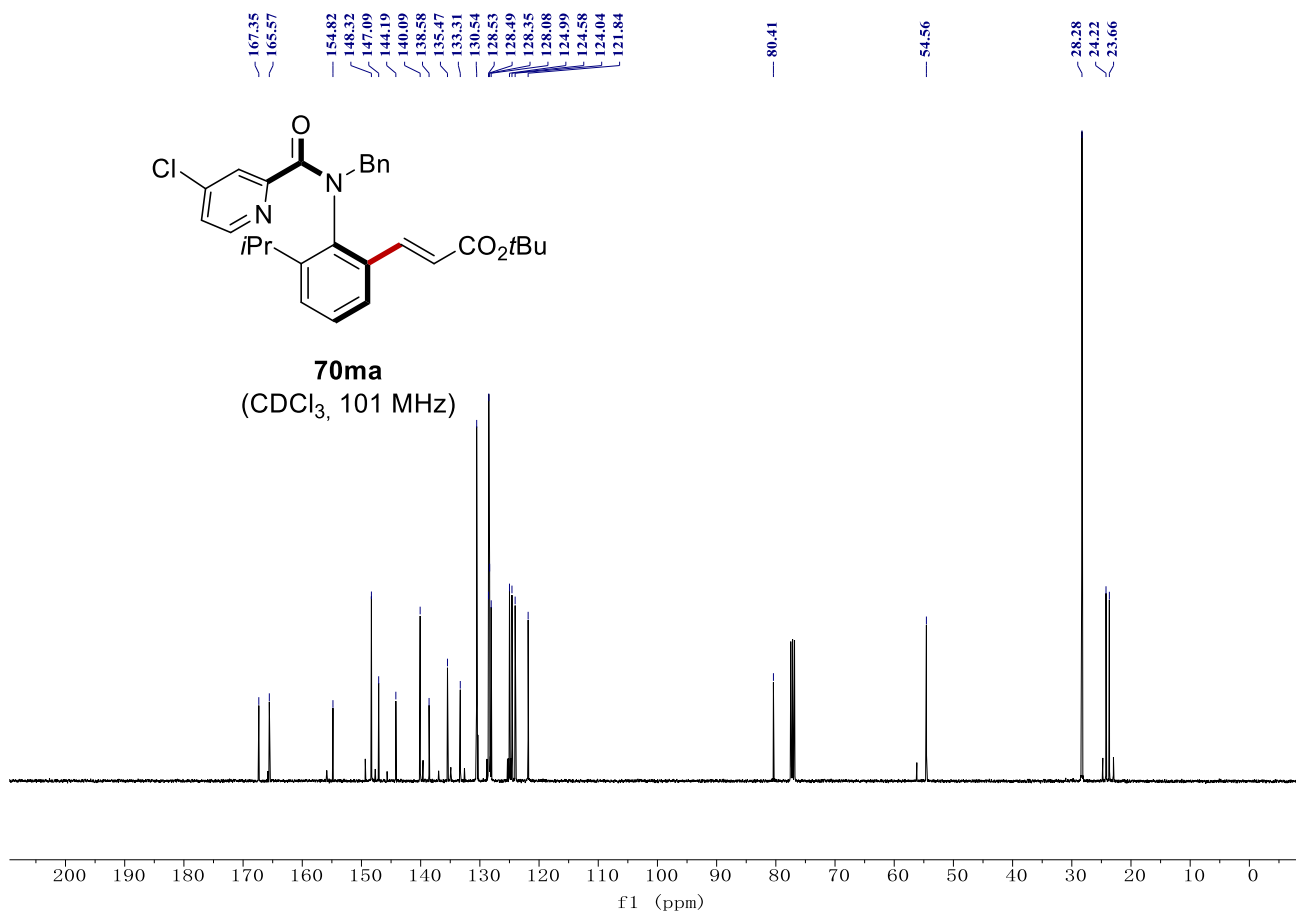
70la
(CDCl₃, 101 MHz)



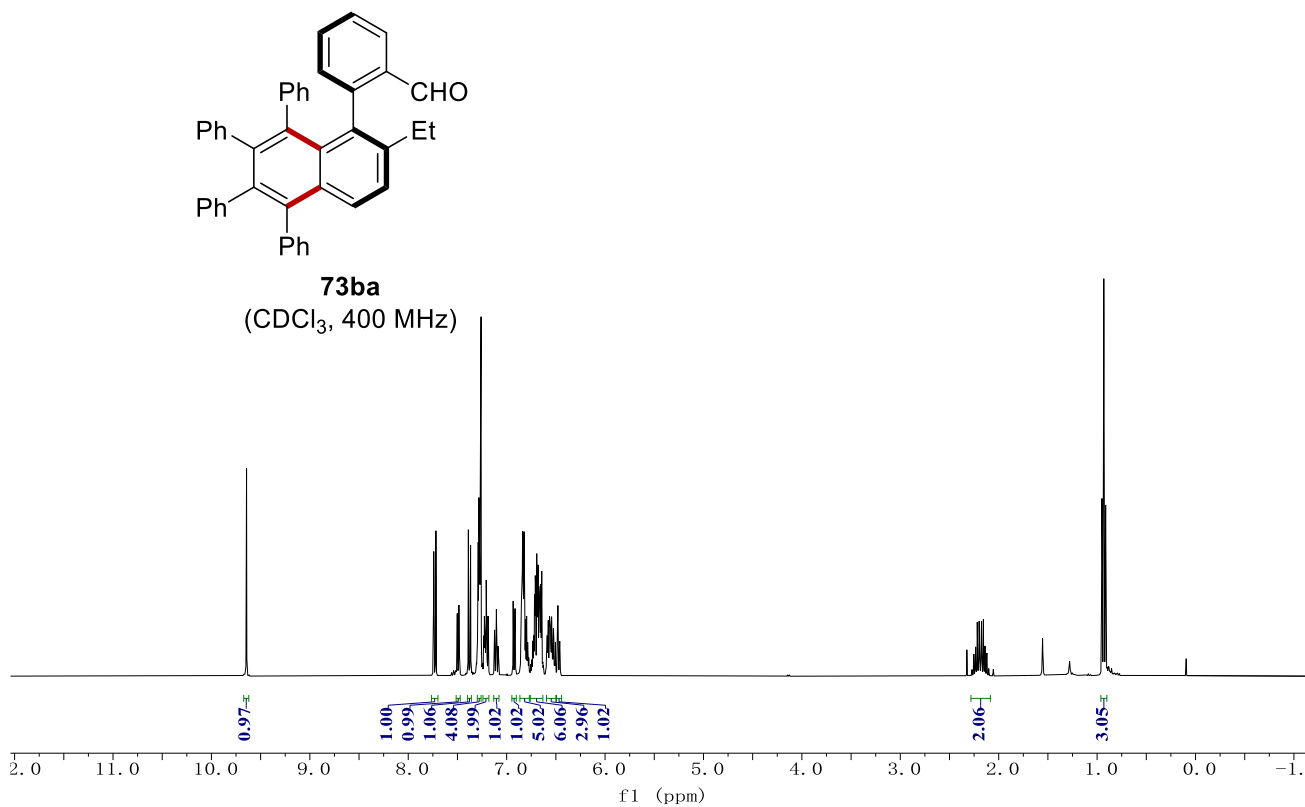
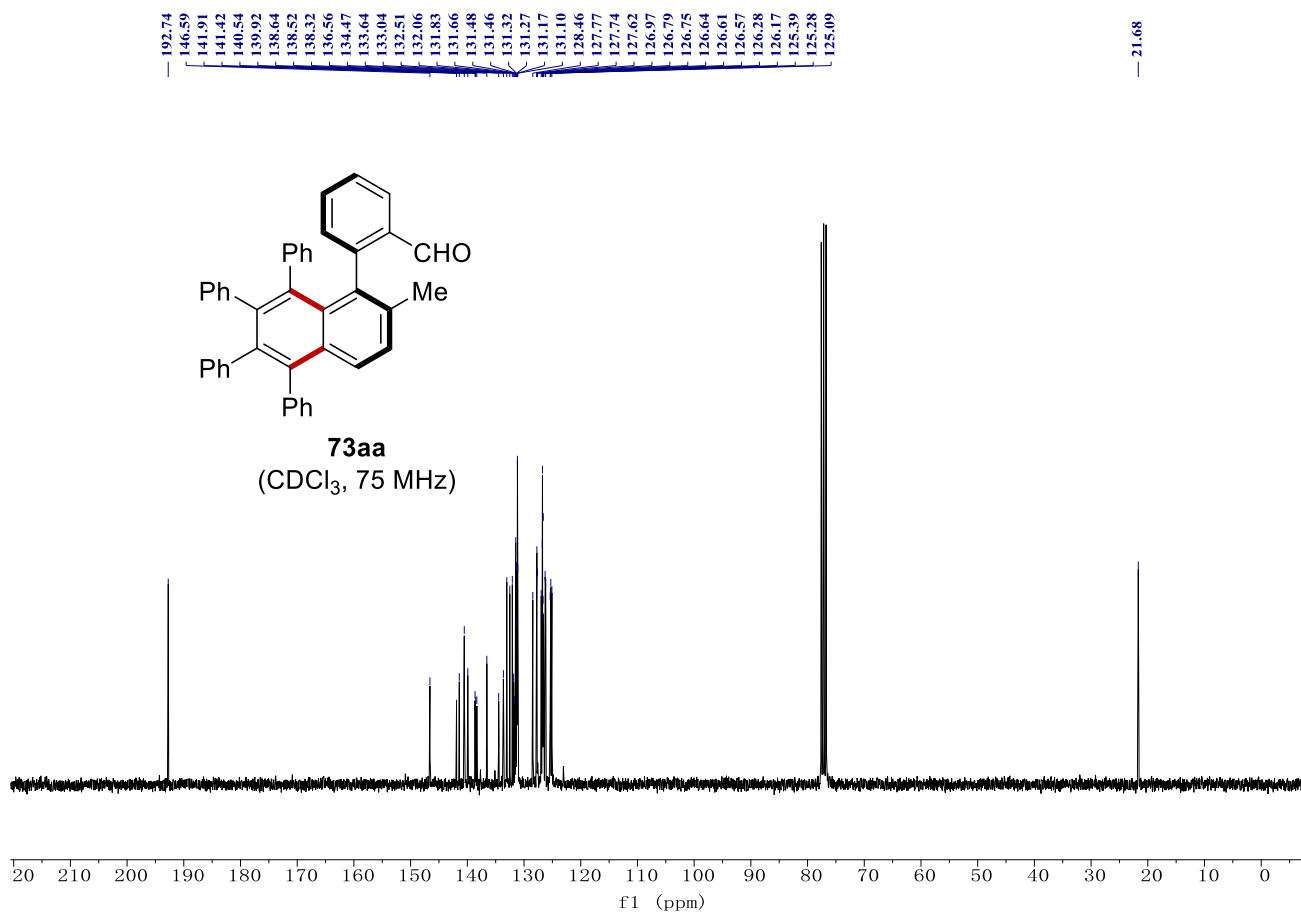
70ma
(CDCl₃, 400 MHz)



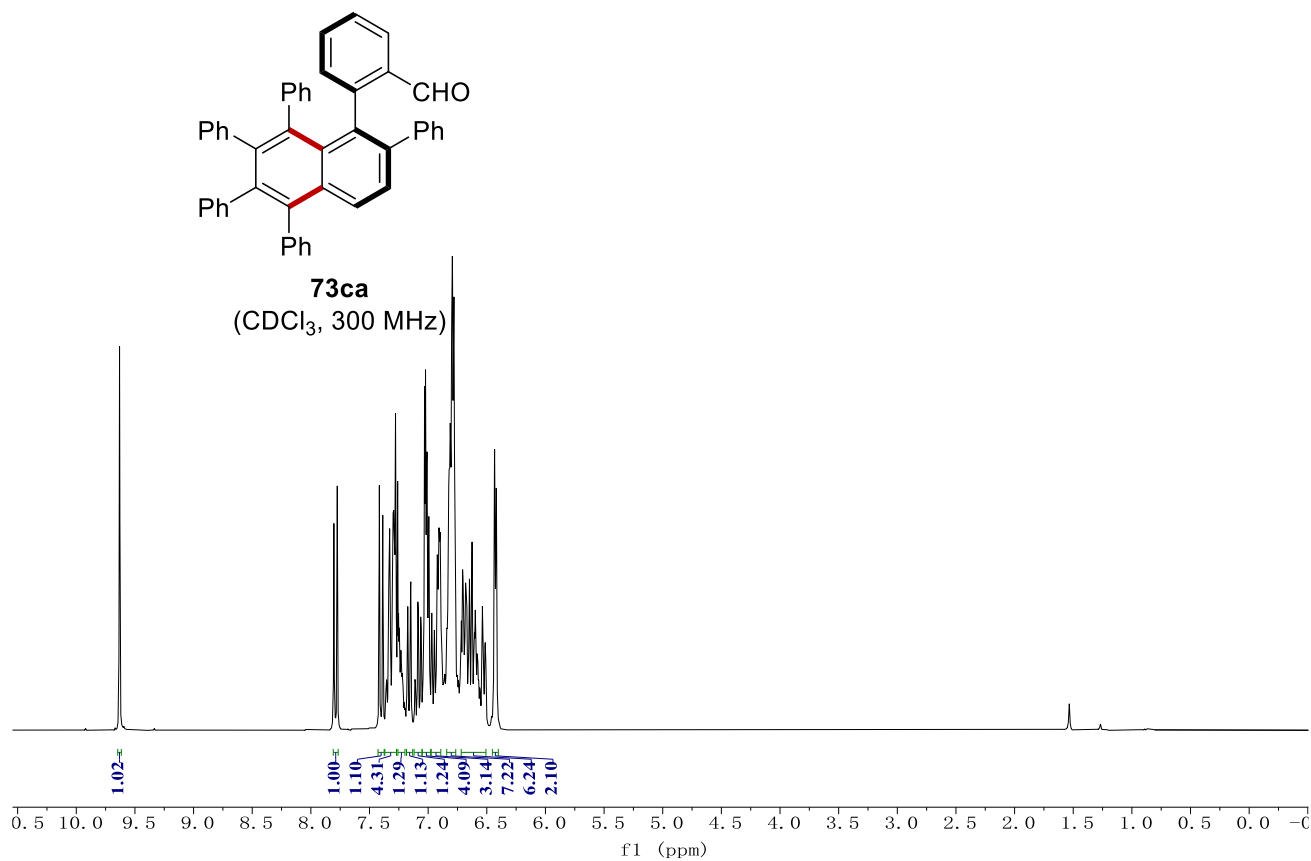
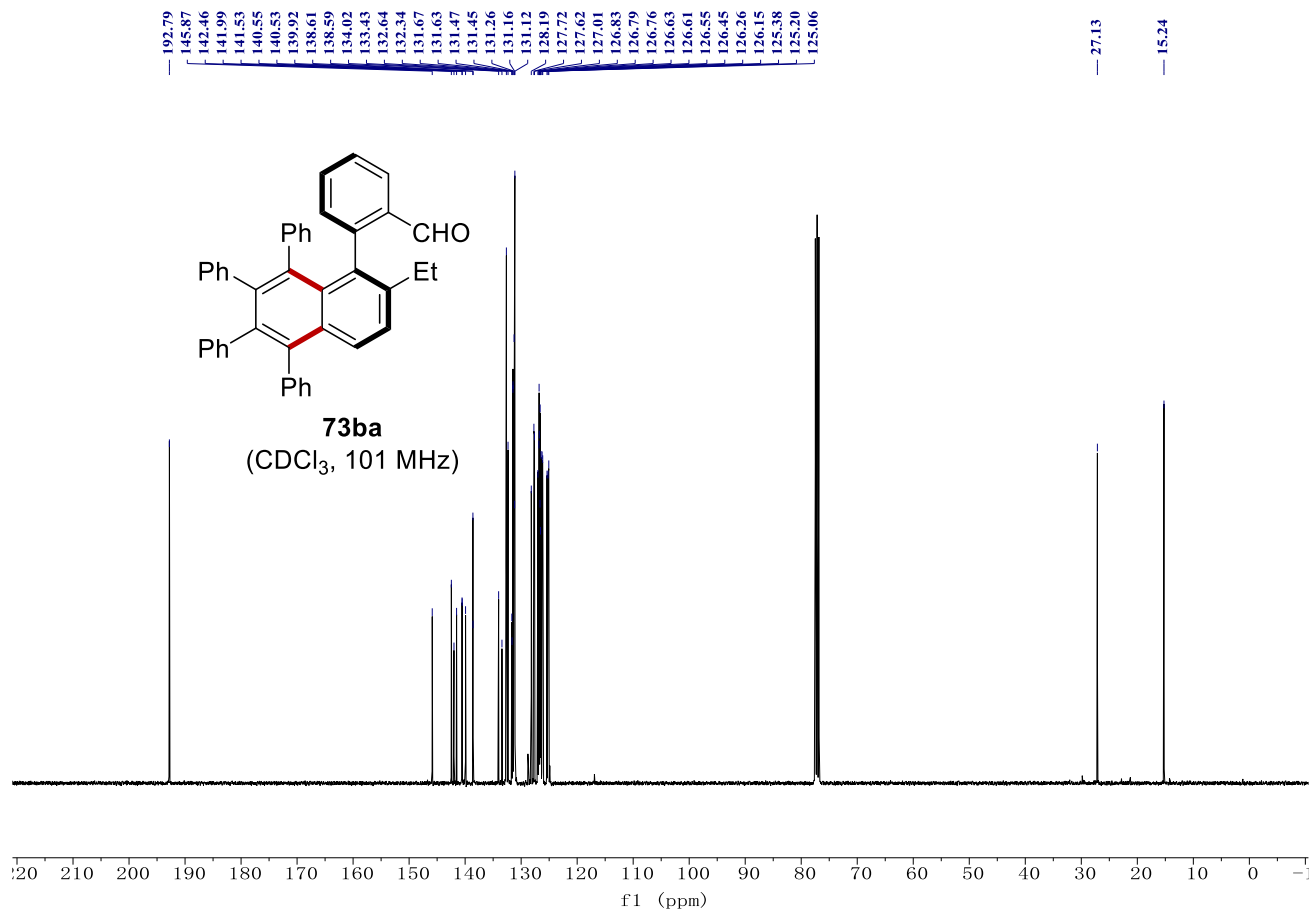
NMR Spectra



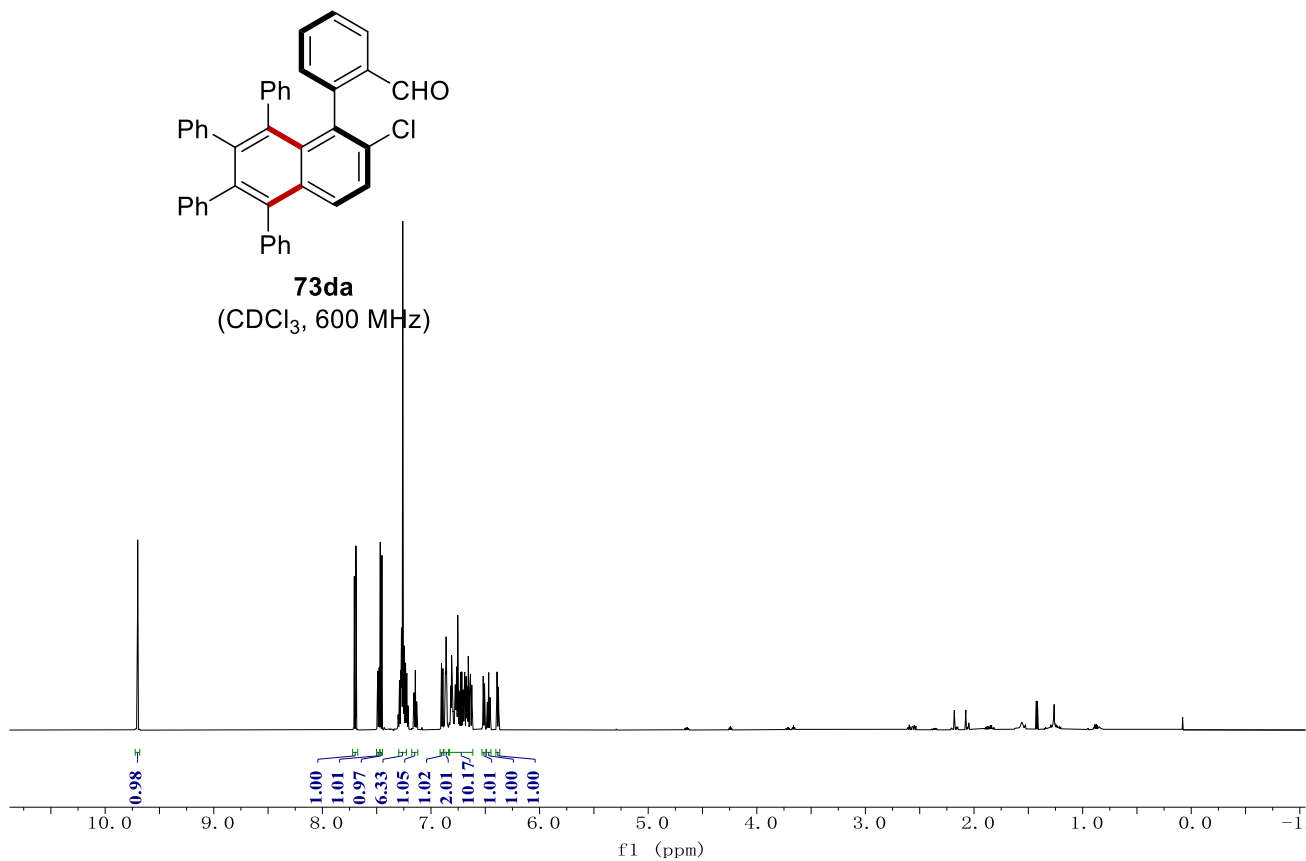
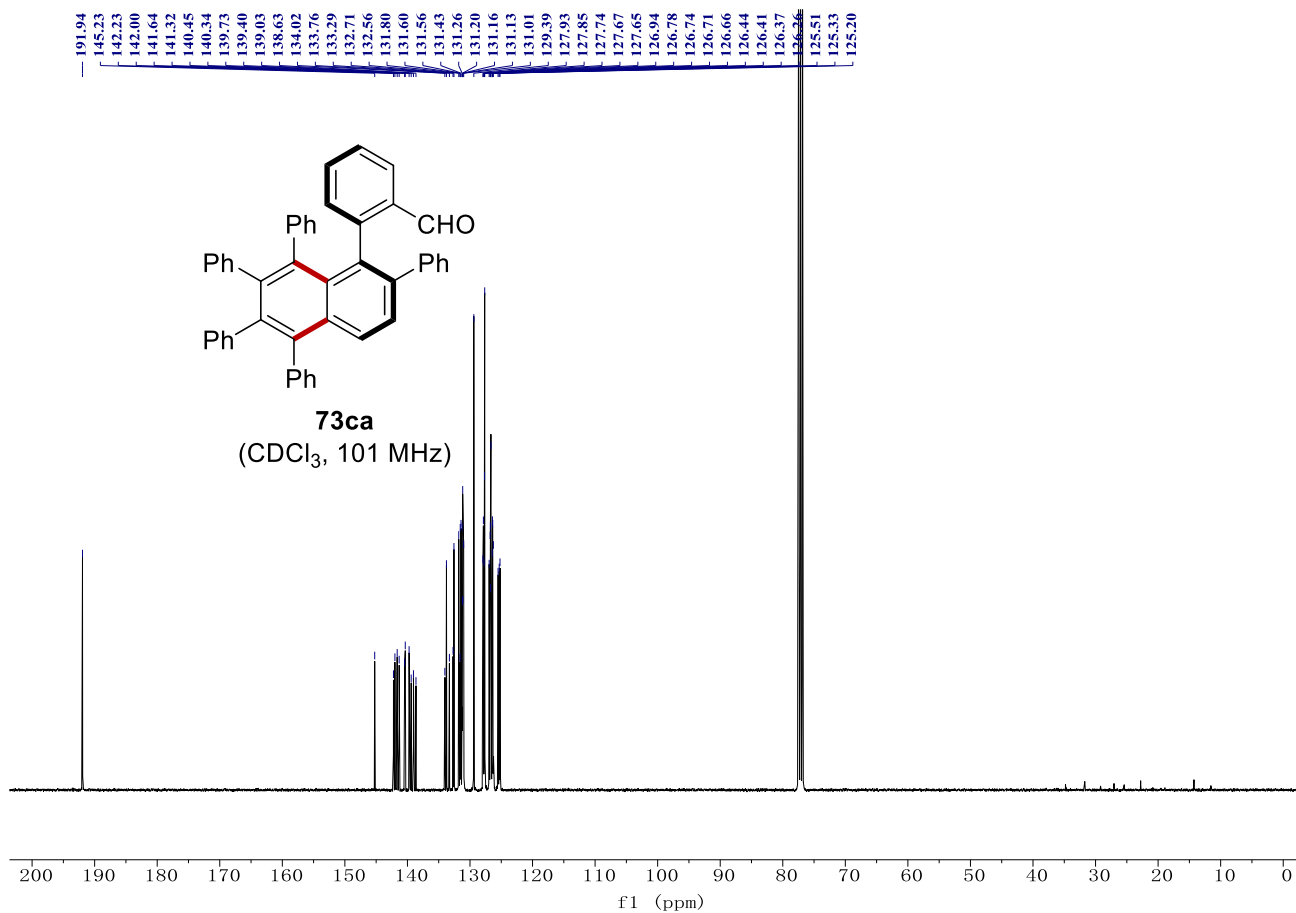
NMR Spectra



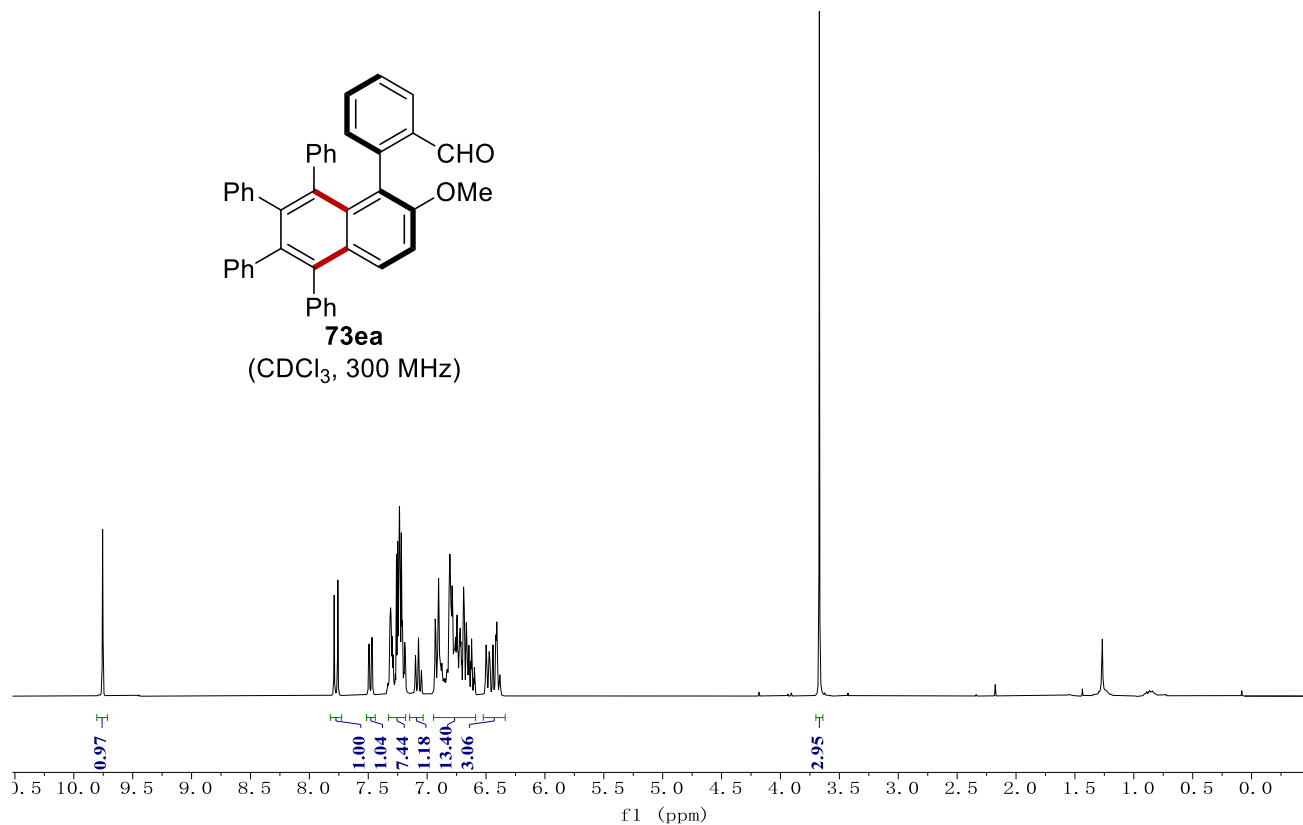
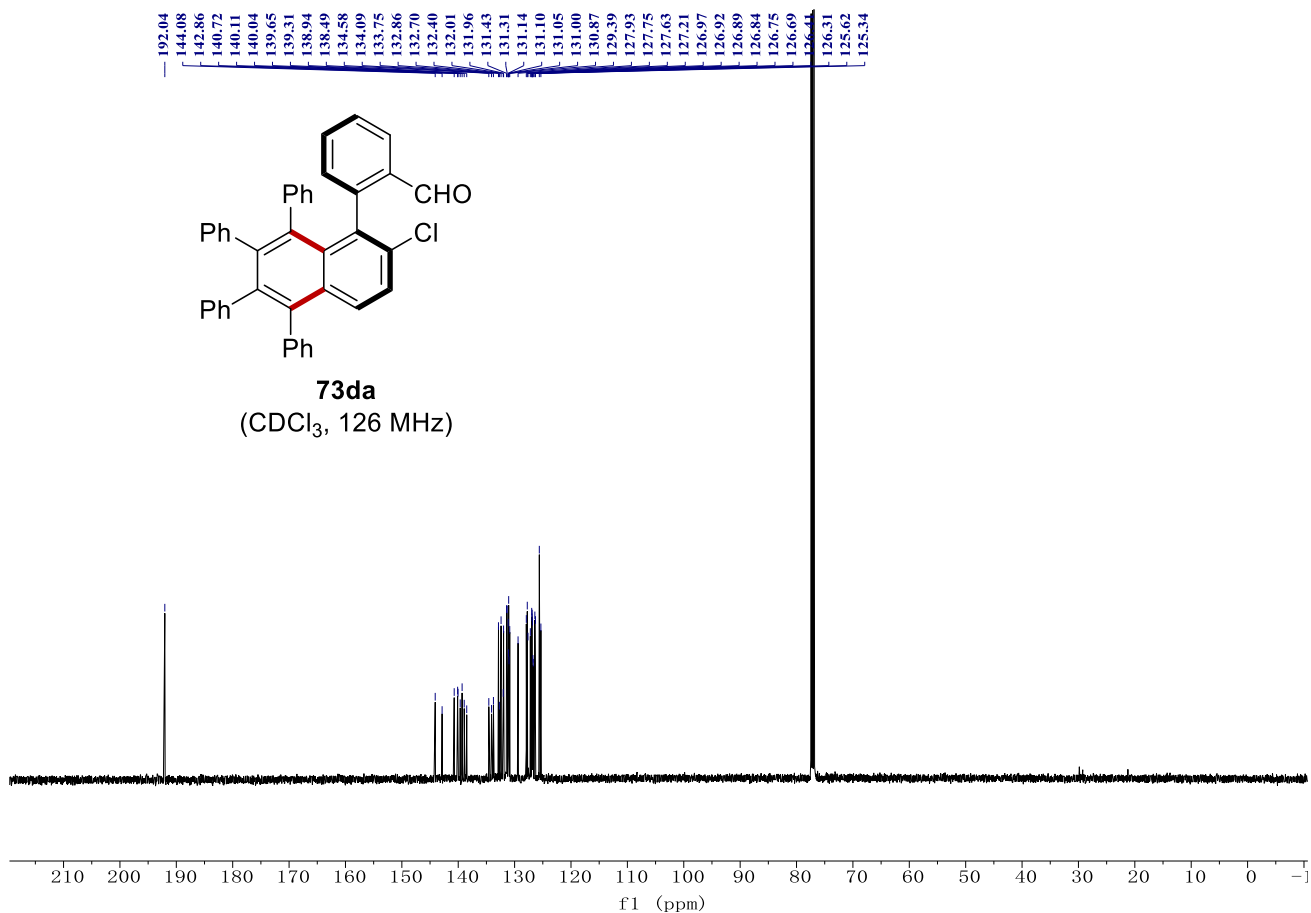
NMR Spectra



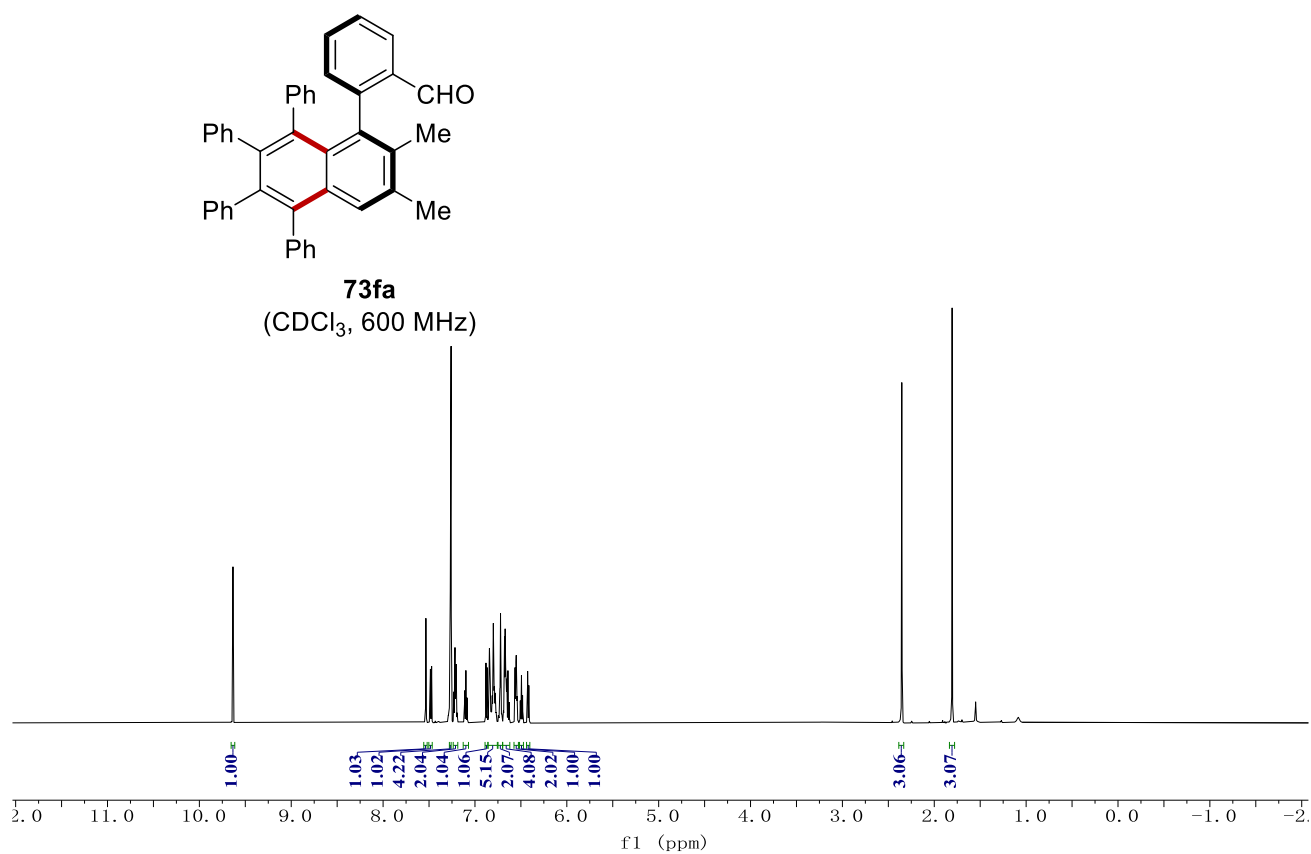
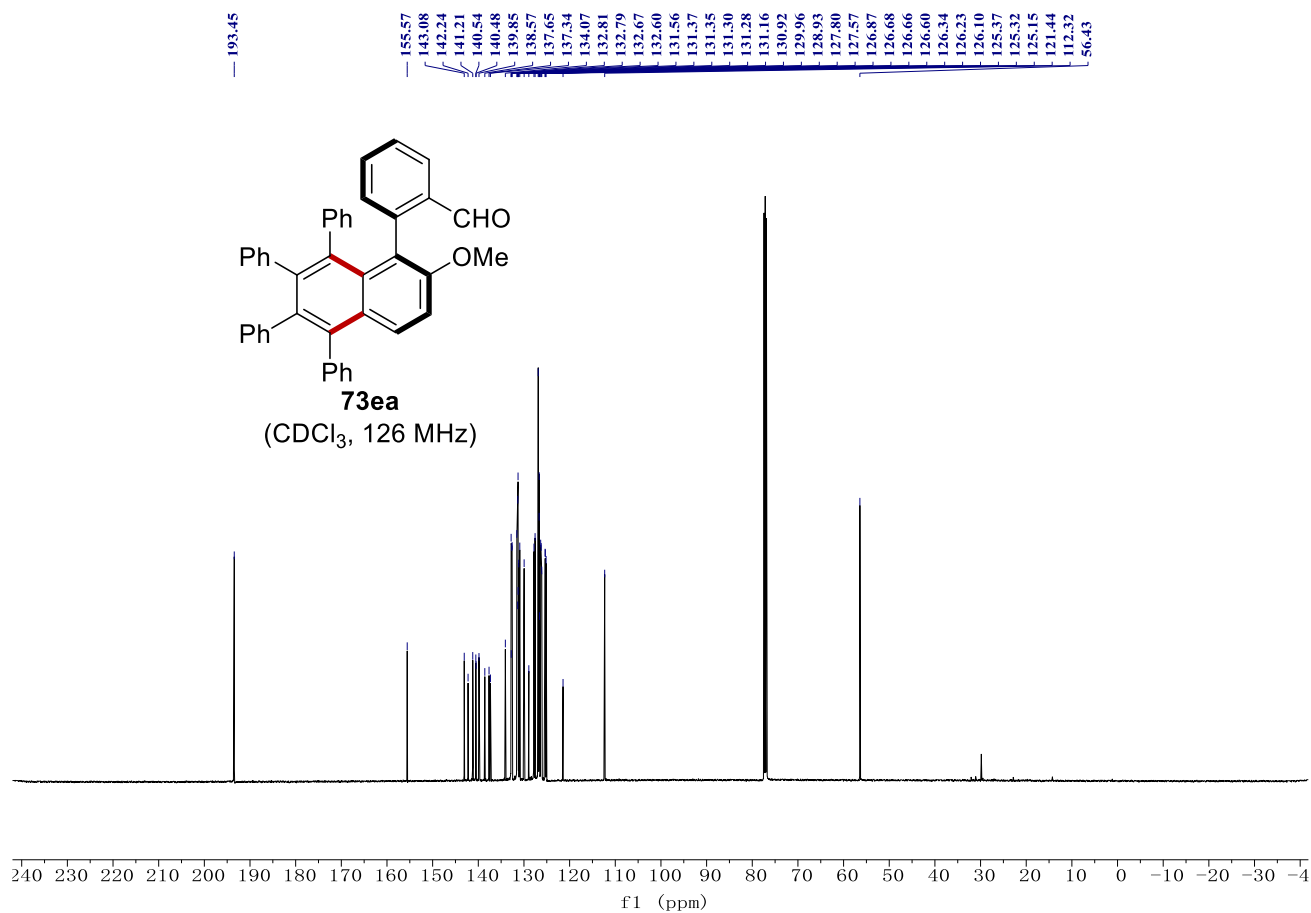
NMR Spectra



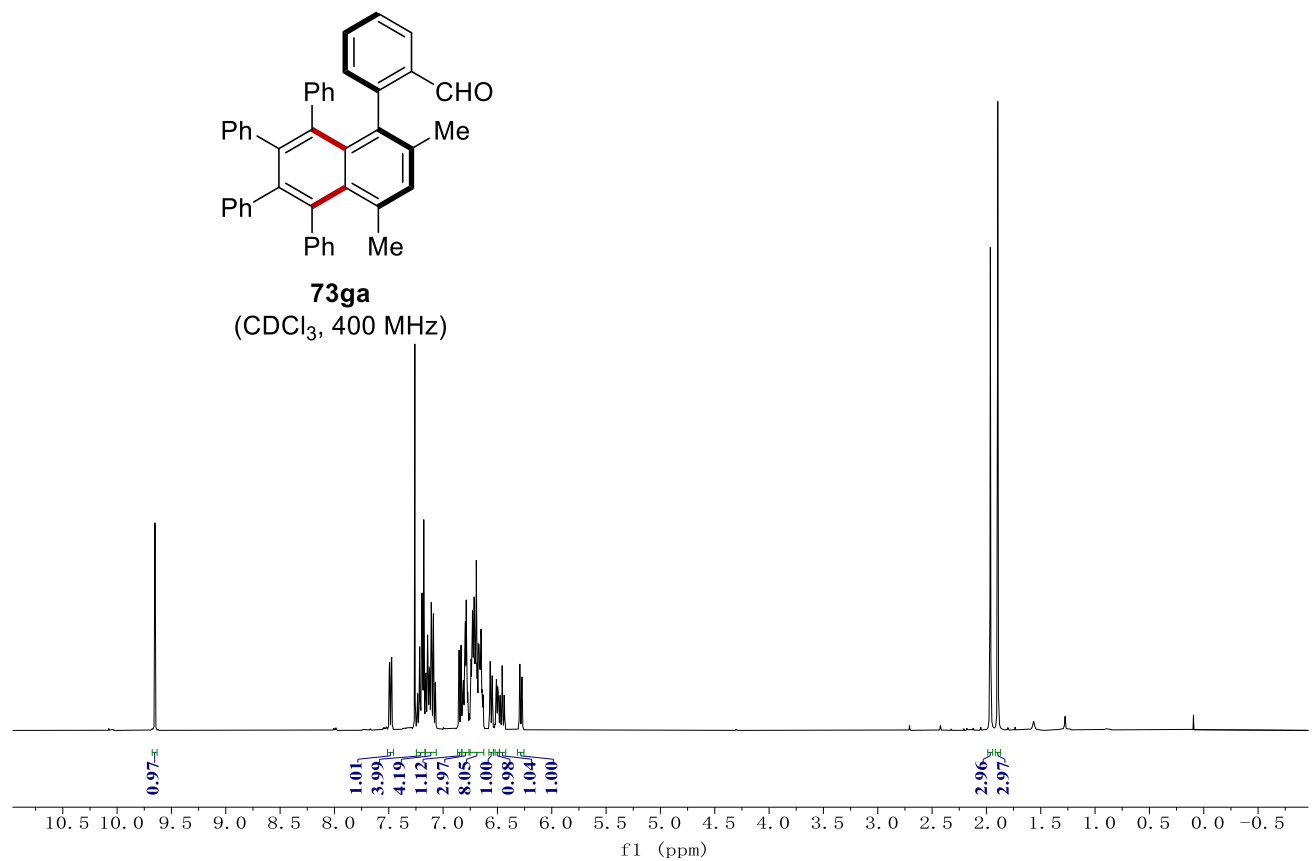
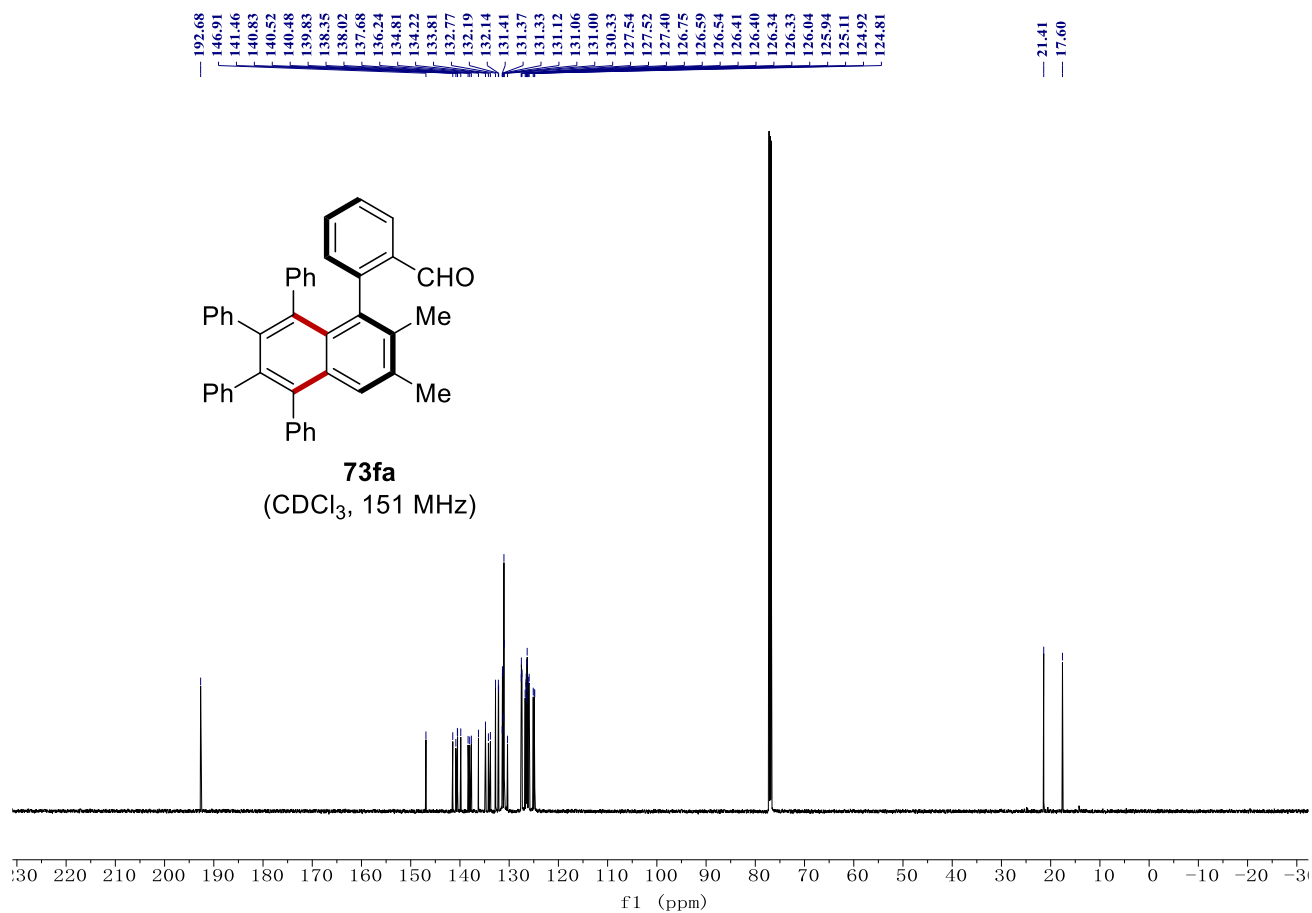
NMR Spectra



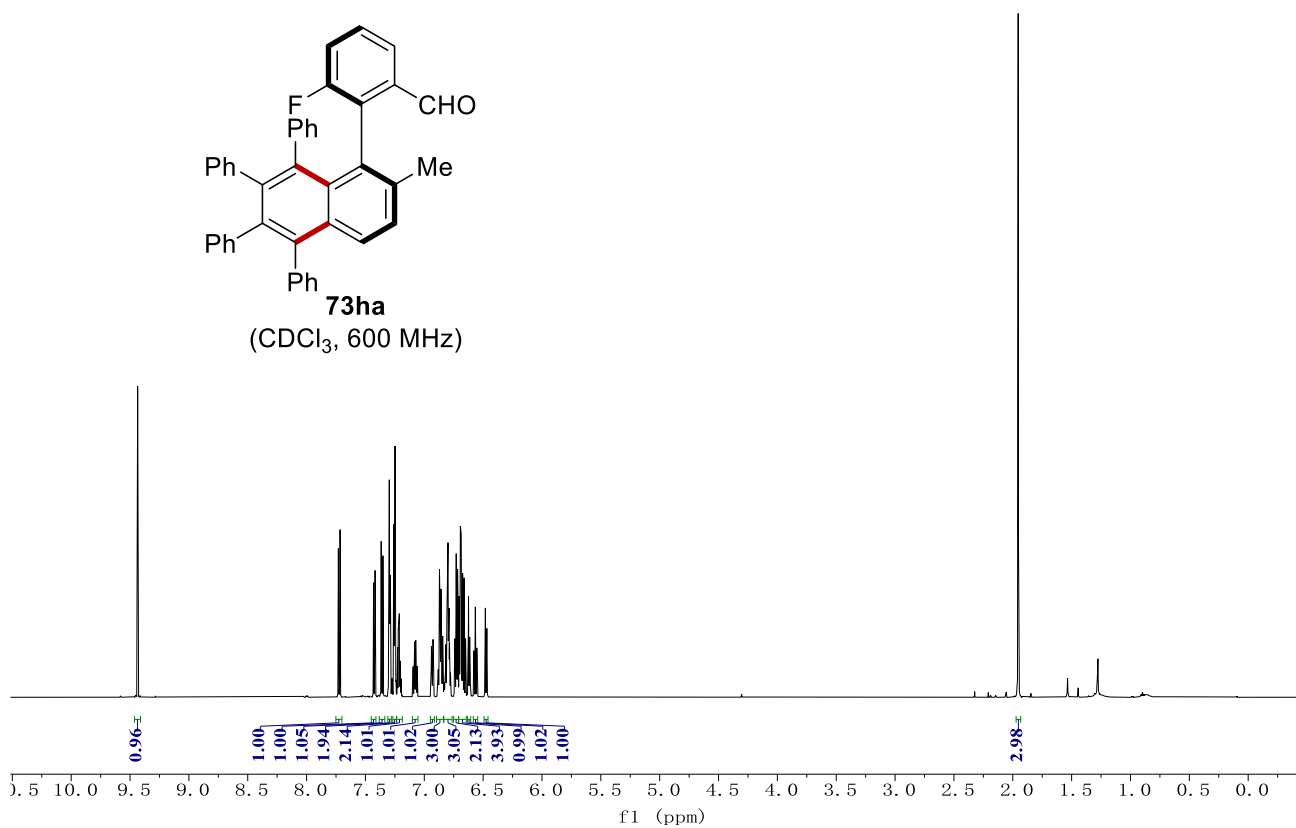
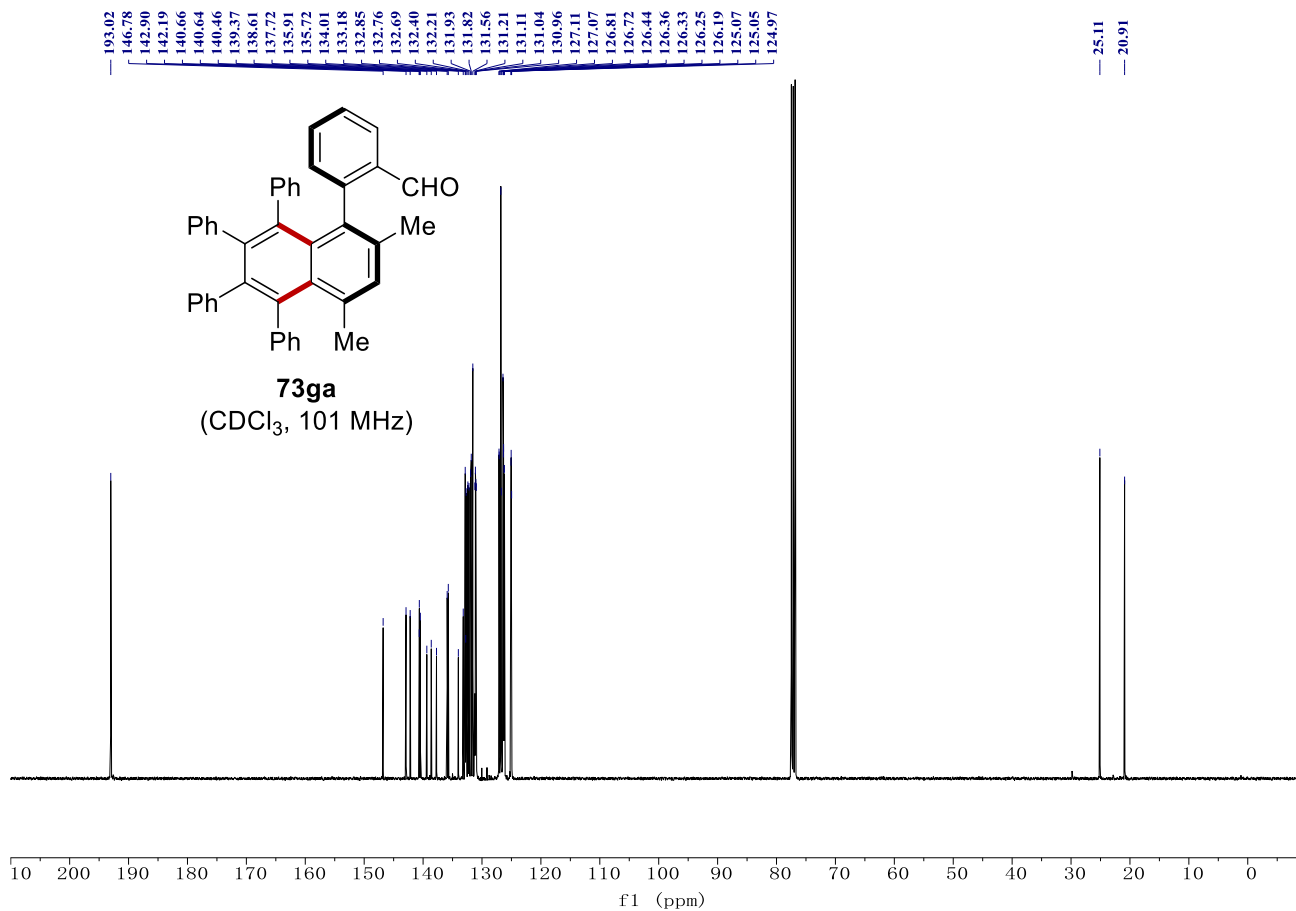
NMR Spectra



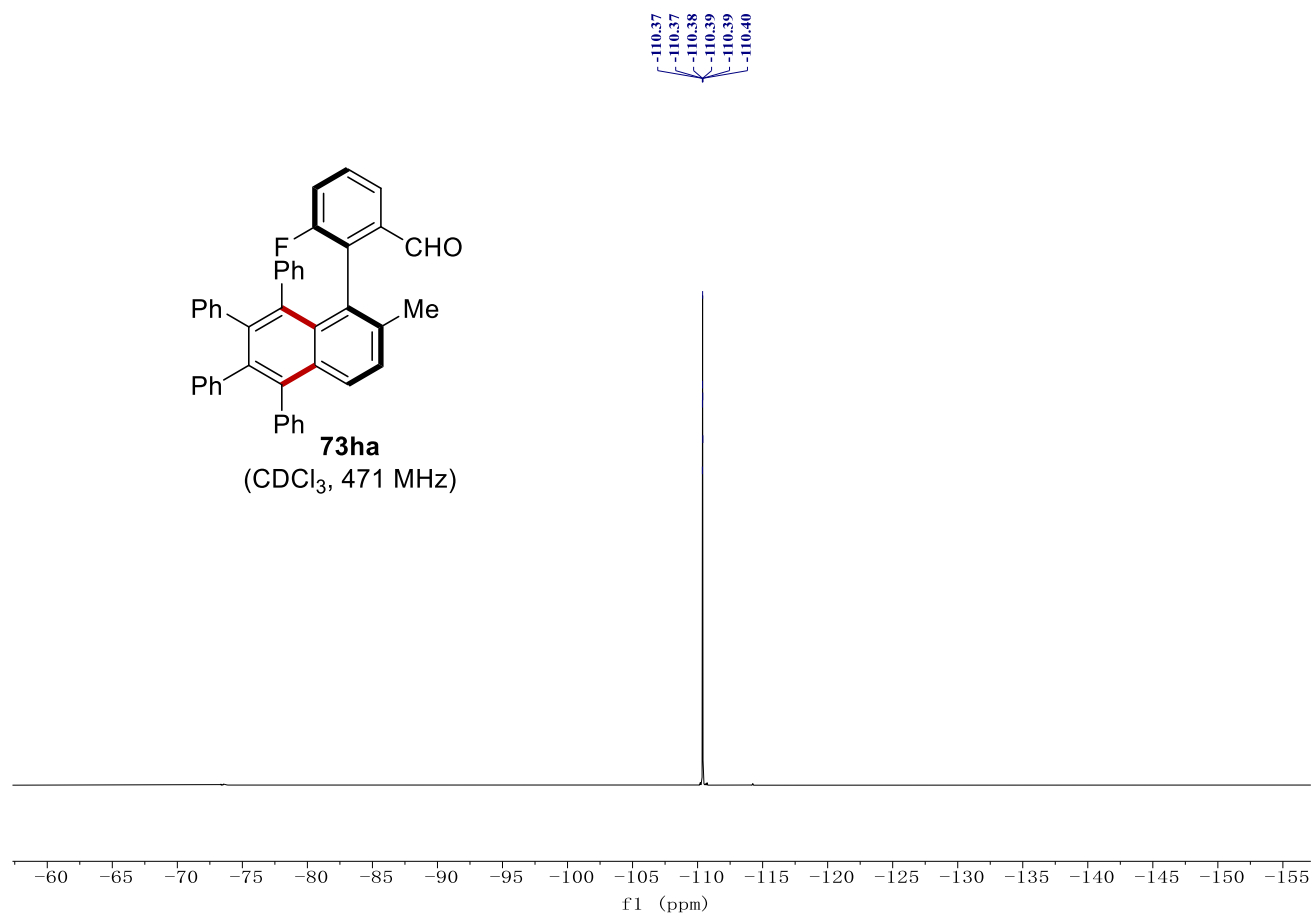
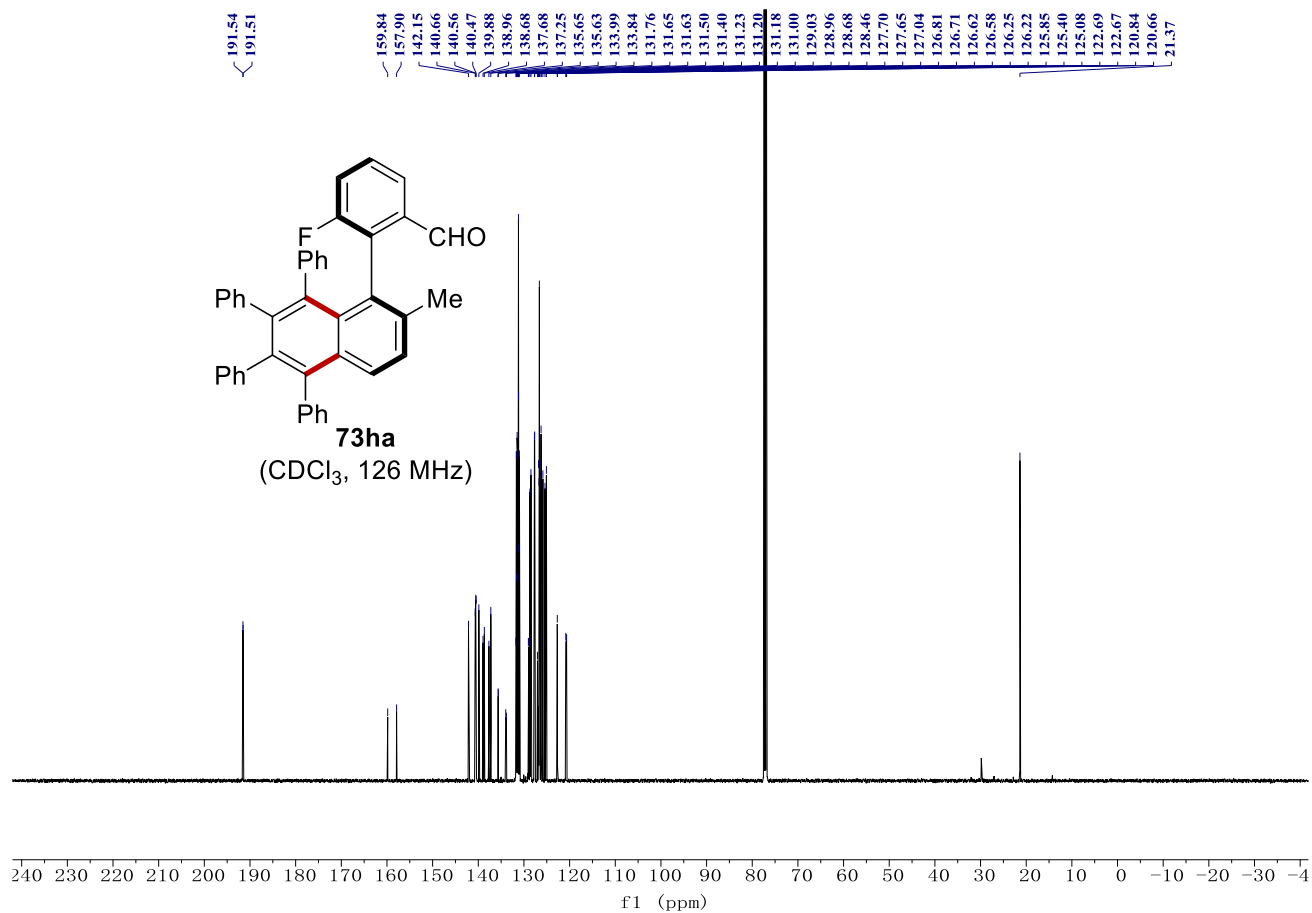
NMR Spectra



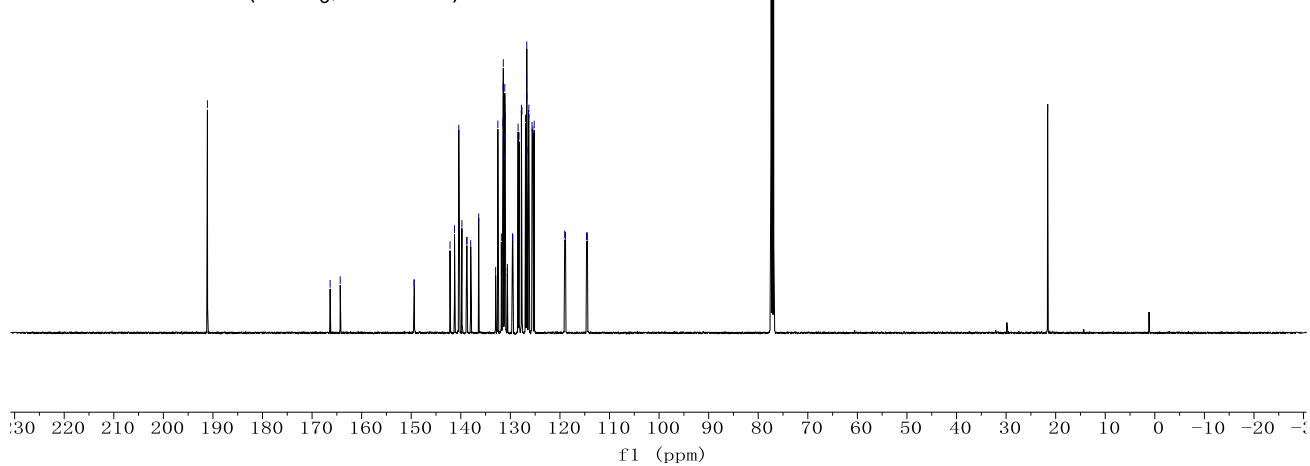
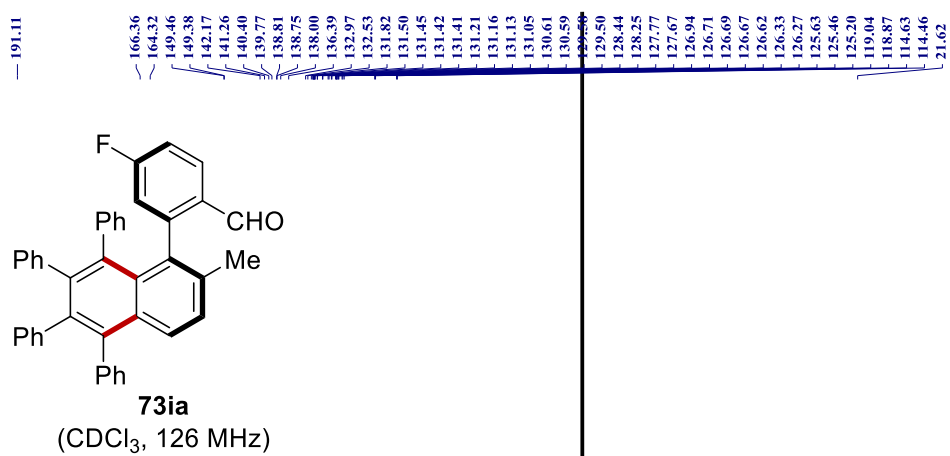
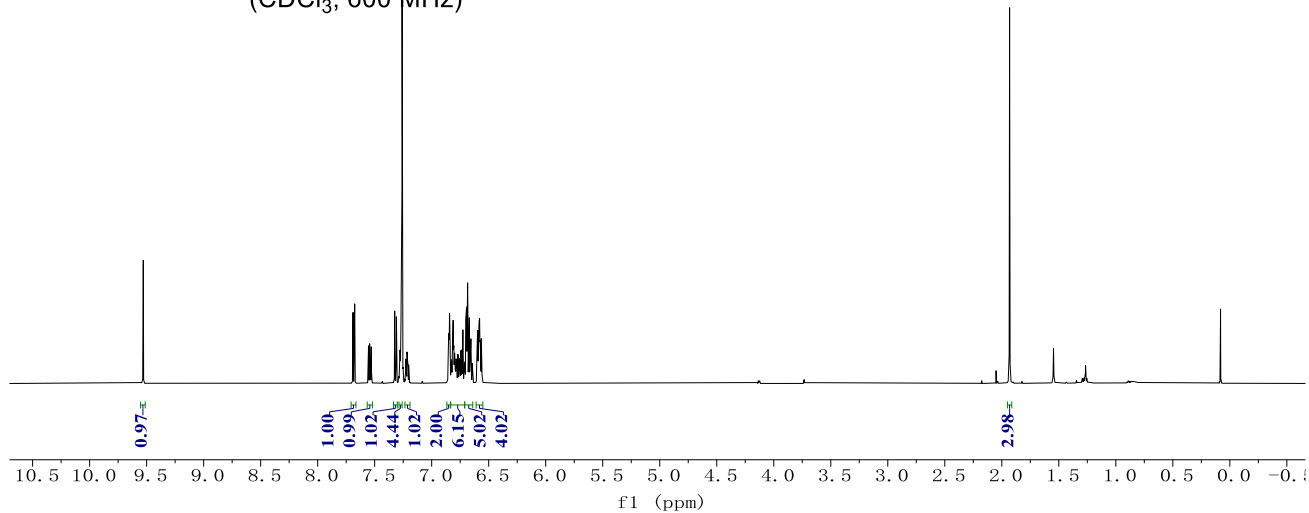
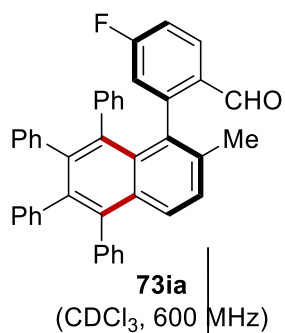
NMR Spectra



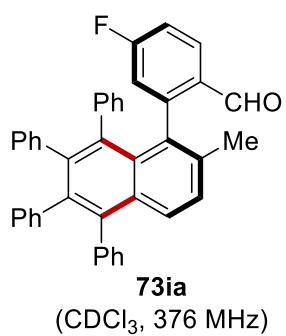
NMR Spectra



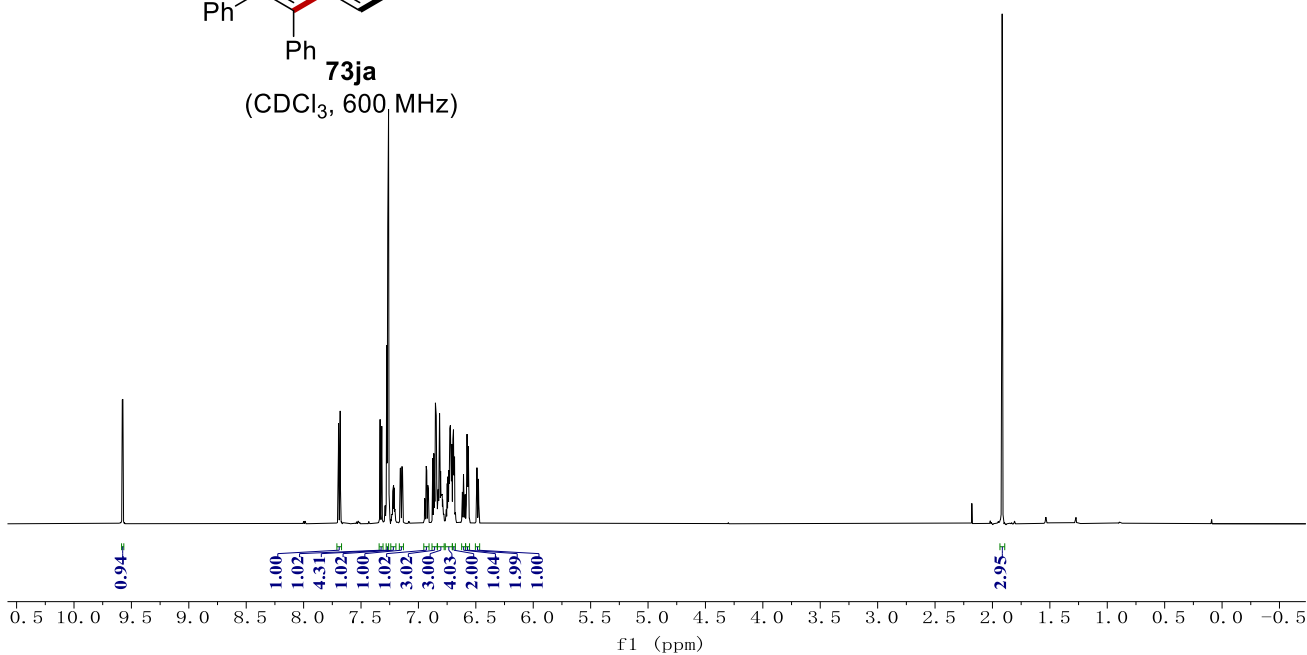
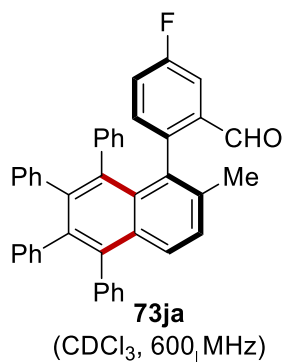
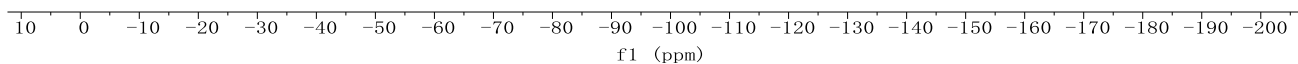
NMR Spectra



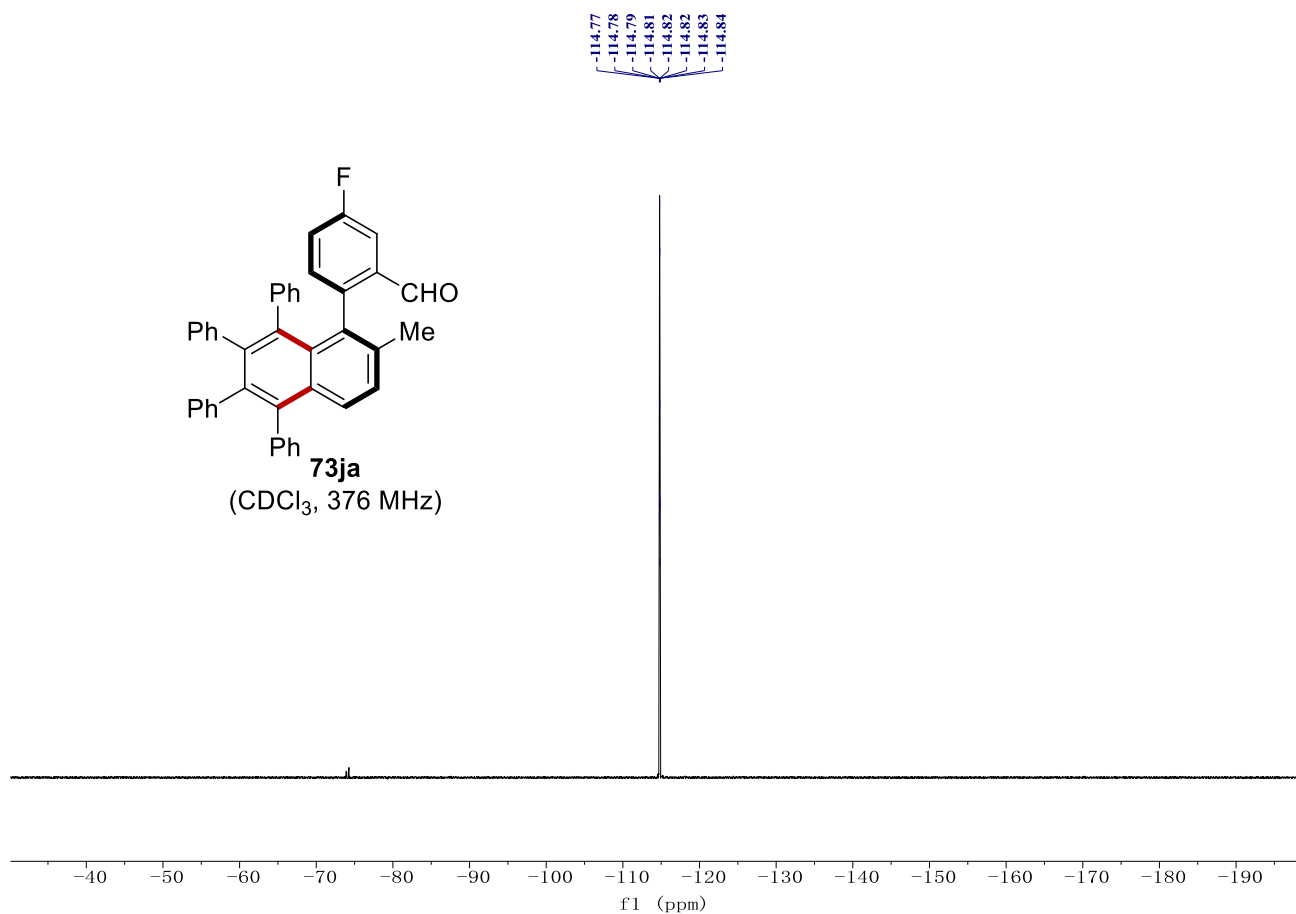
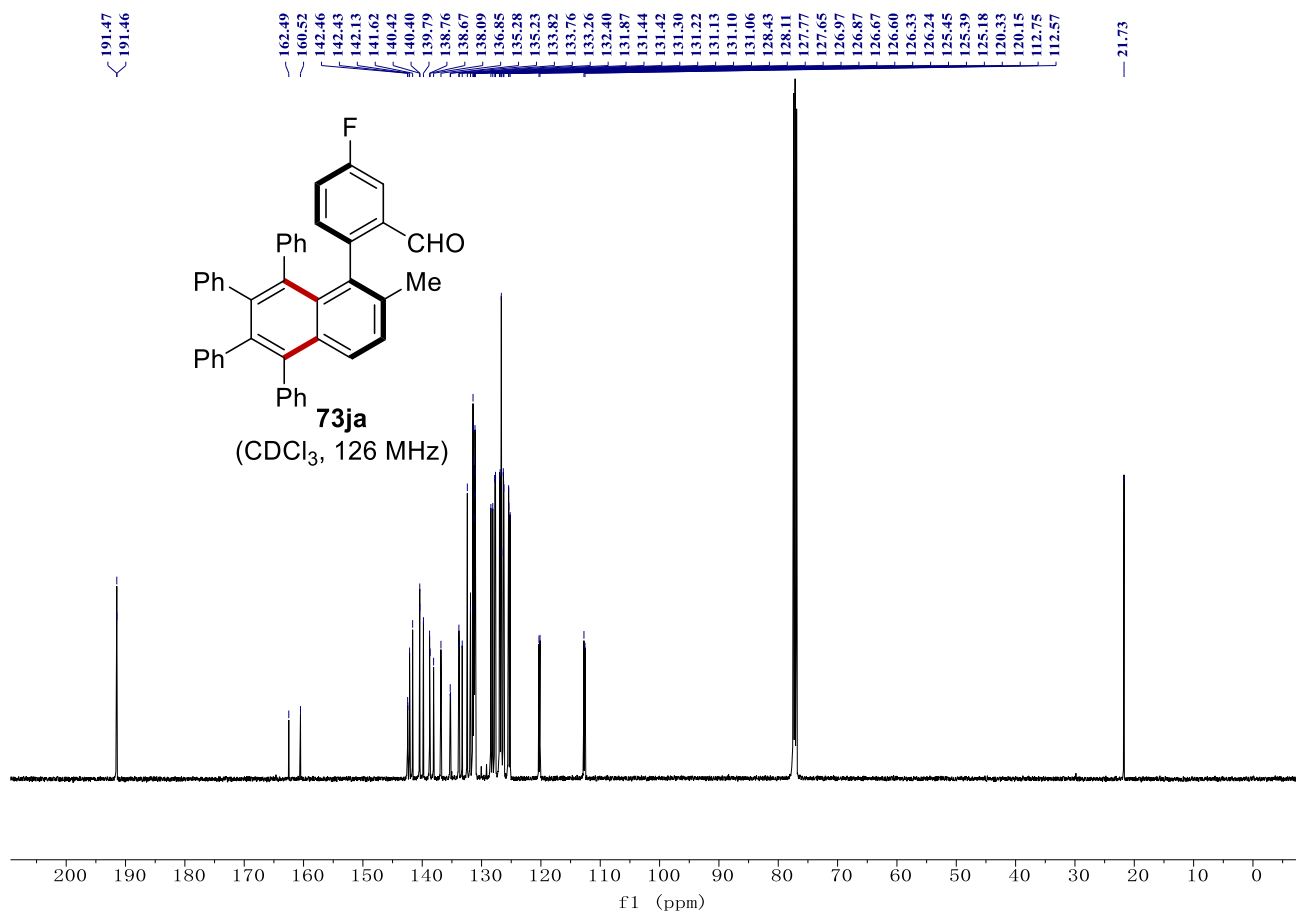
NMR Spectra



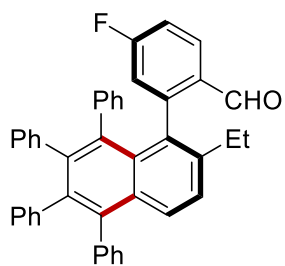
-105.67
-105.68
-105.69
-105.71
-105.72
-105.73



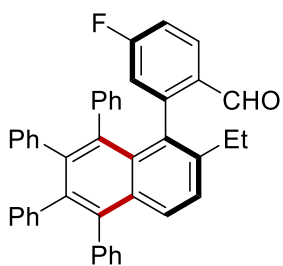
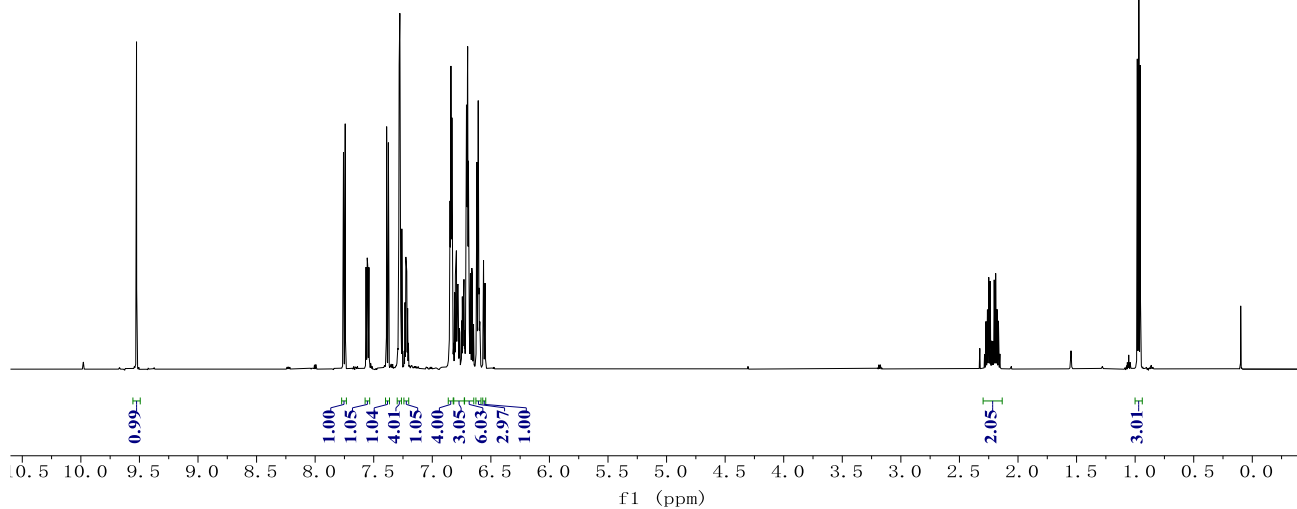
NMR Spectra



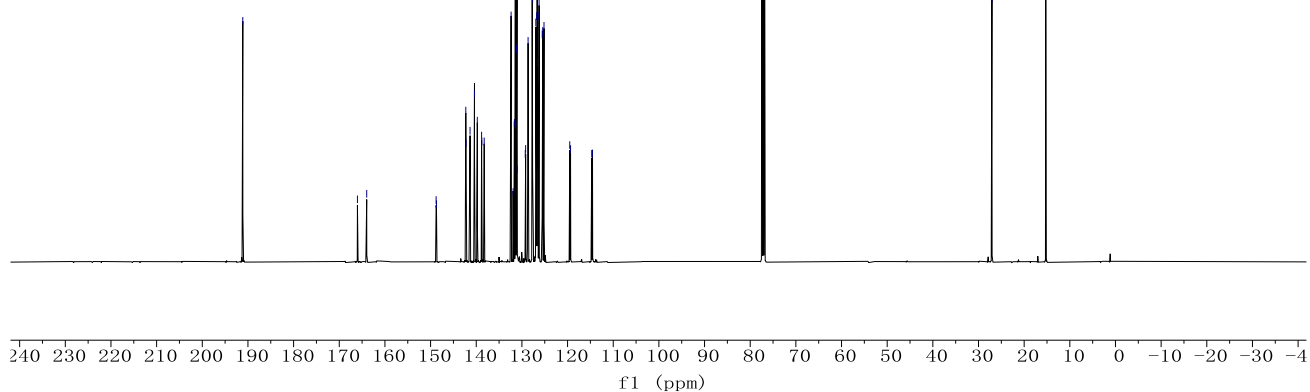
NMR Spectra



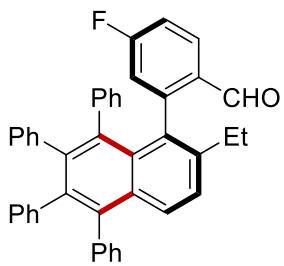
73ka
(CDCl₃, 600 MHz)



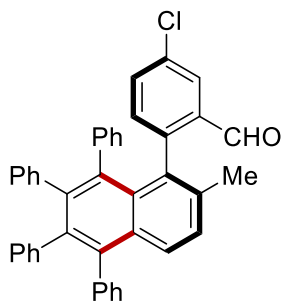
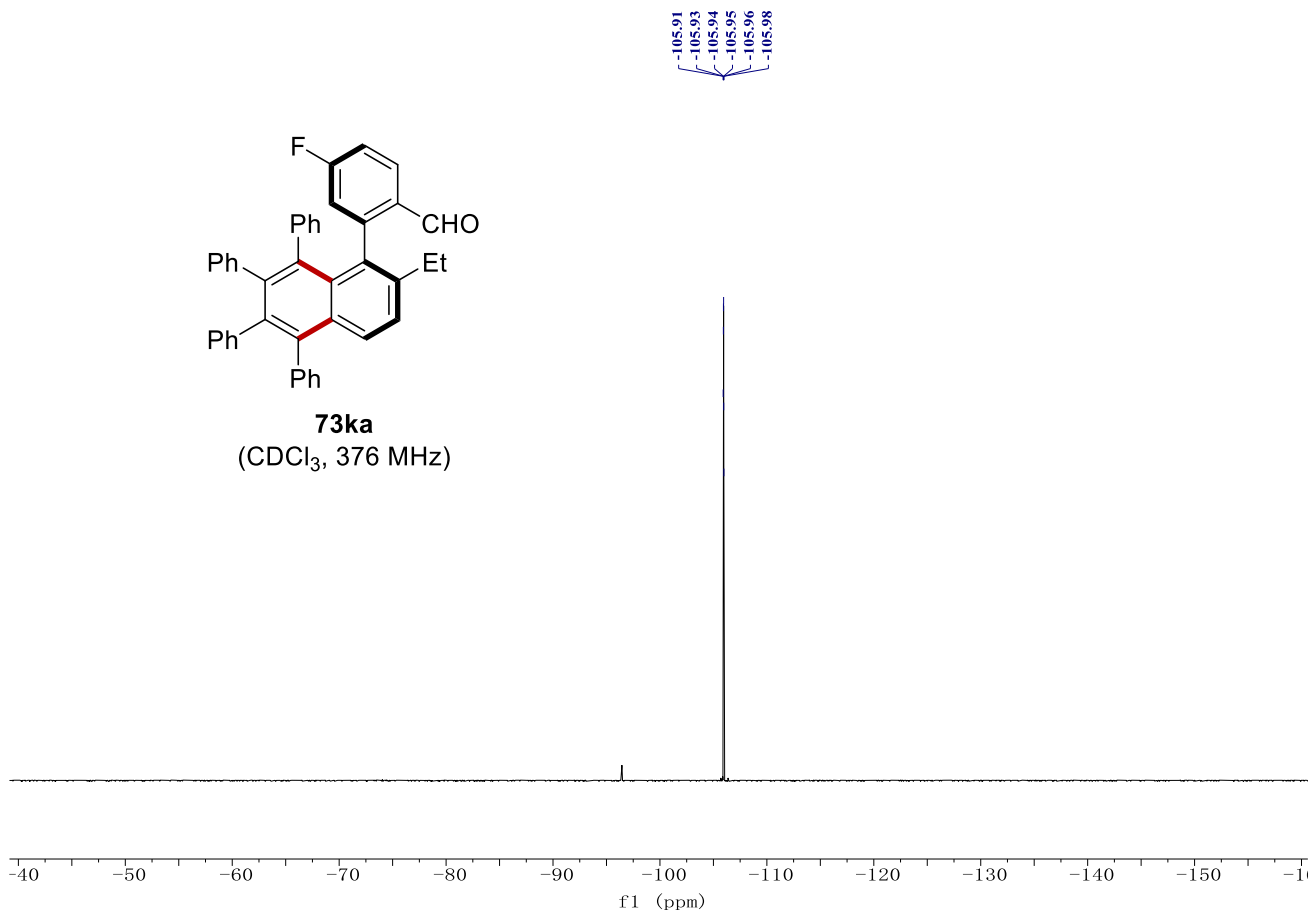
73ka
(CDCl₃, 126 MHz)



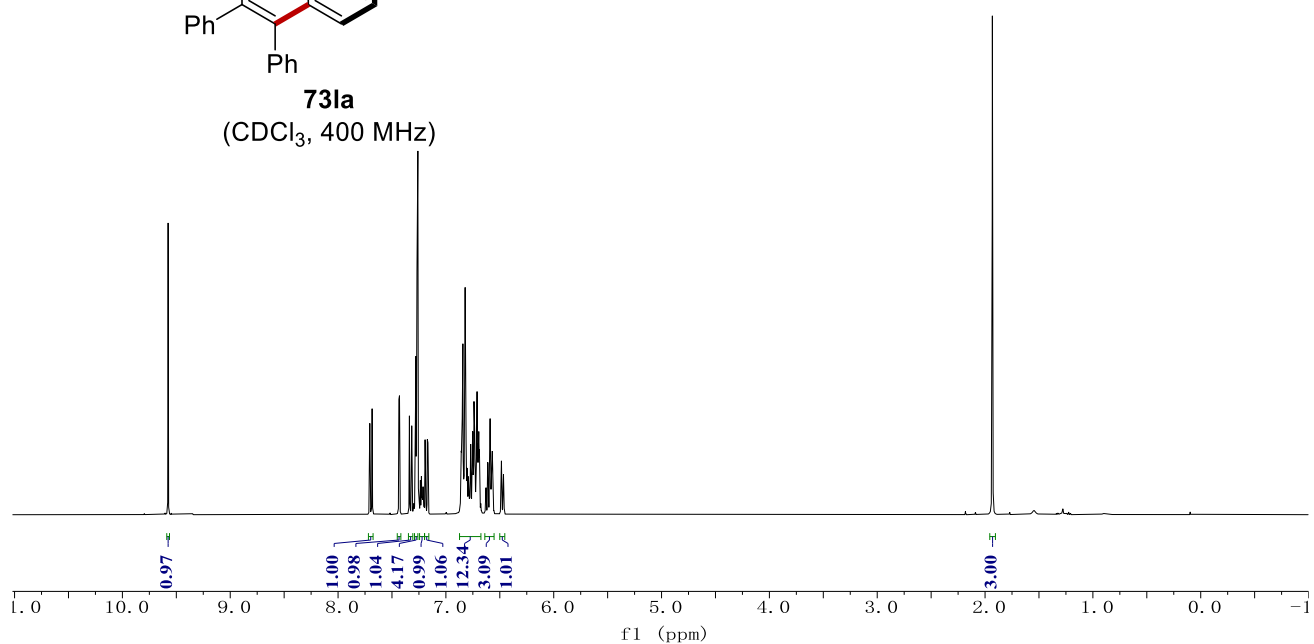
NMR Spectra



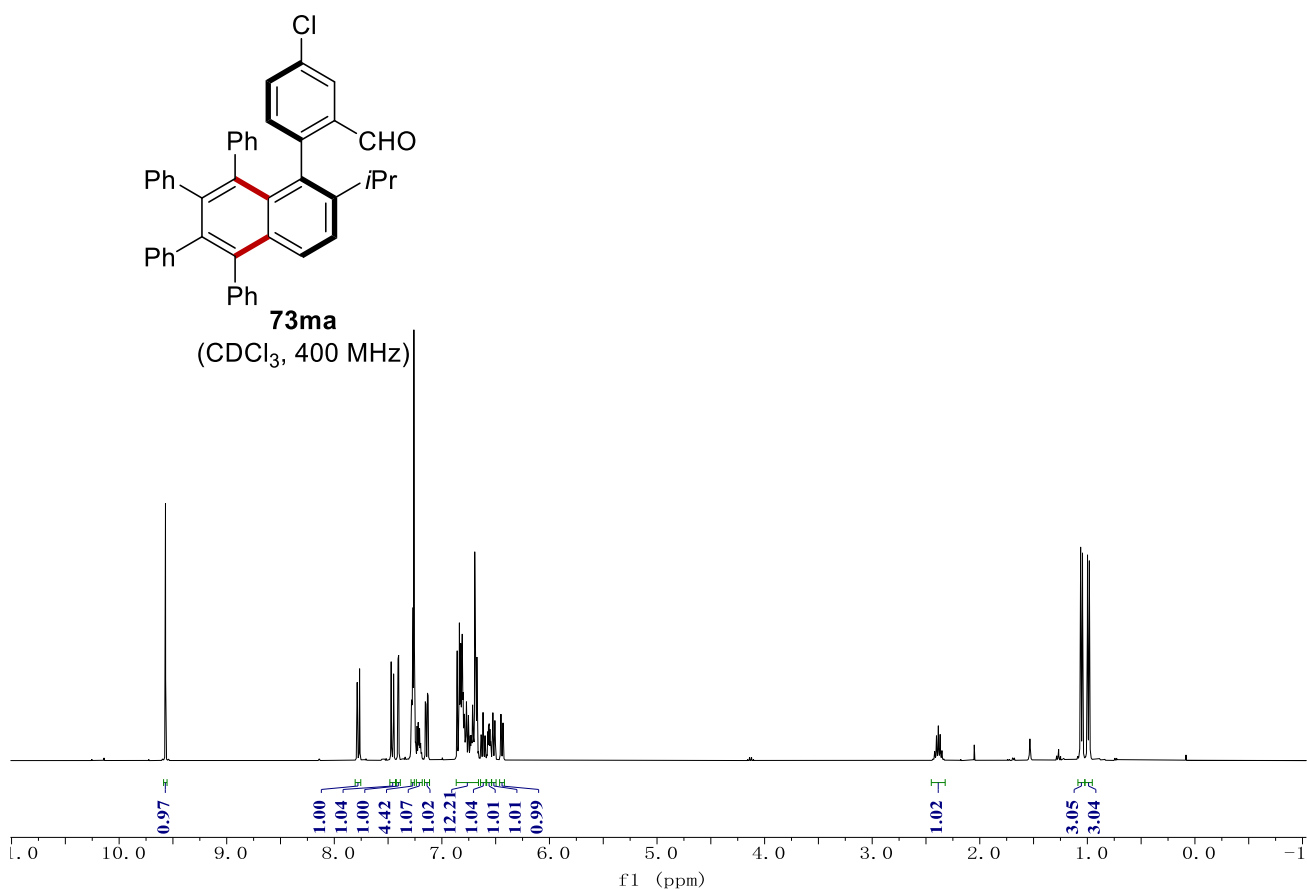
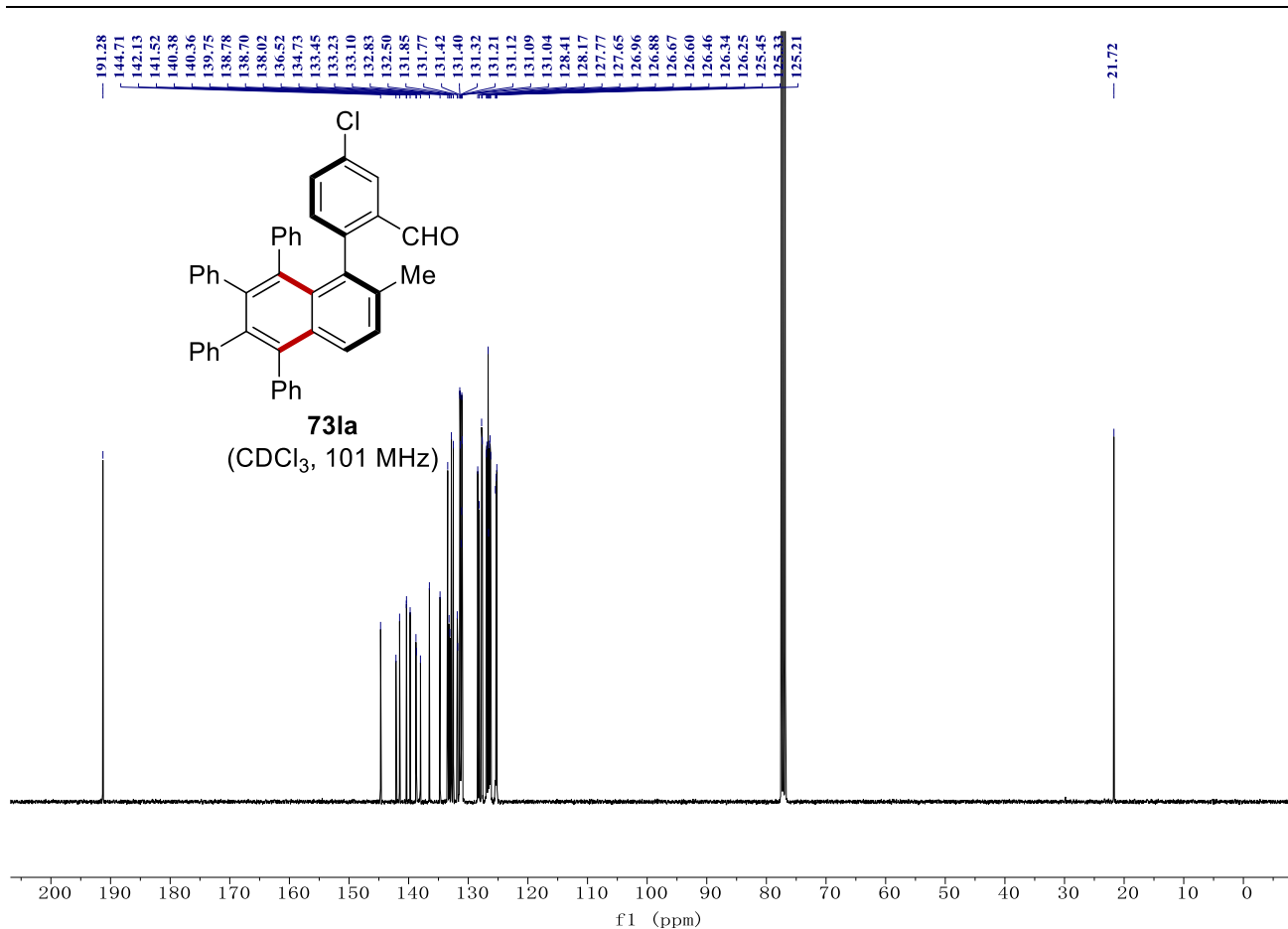
73ka
(CDCl₃, 376 MHz)



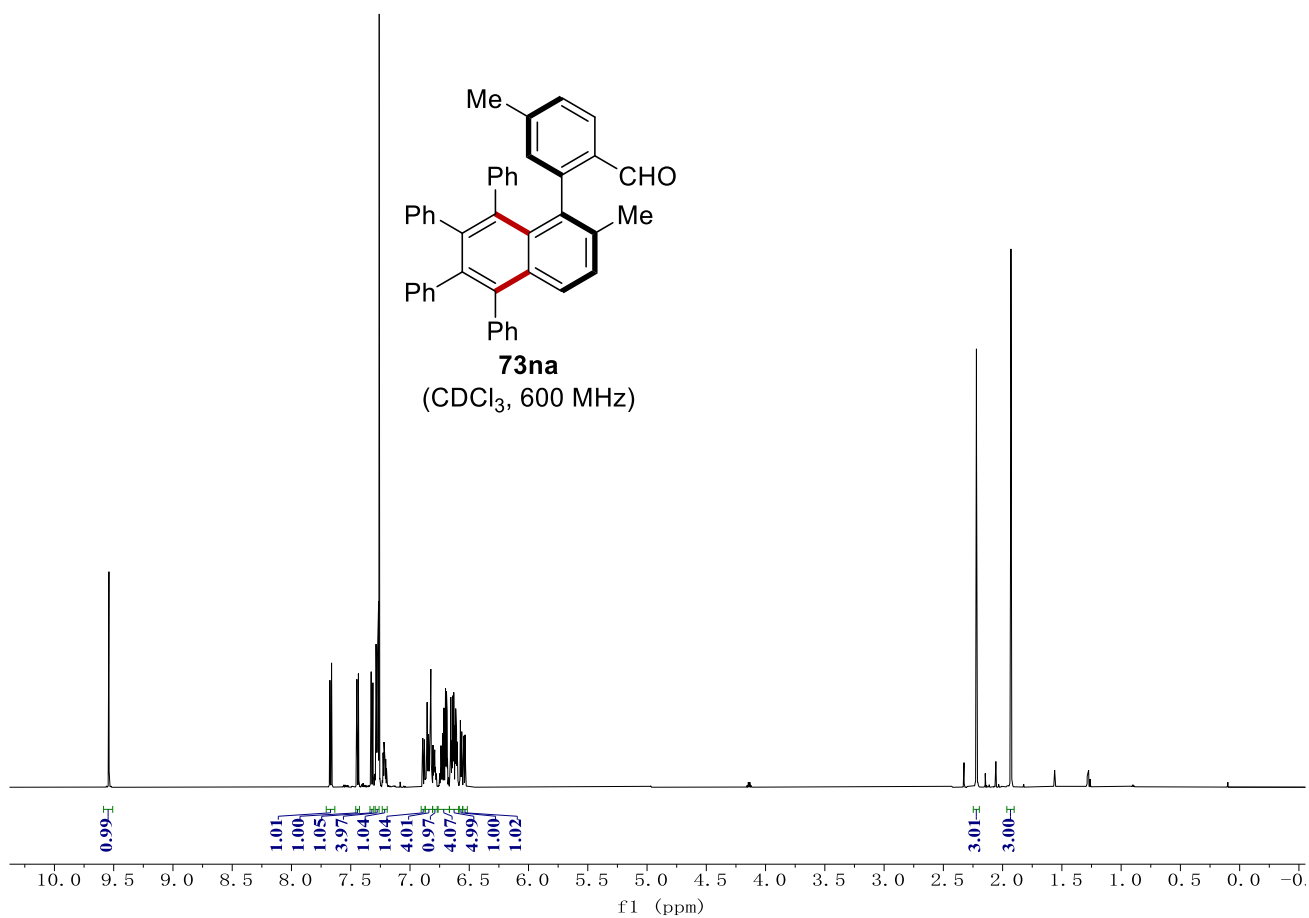
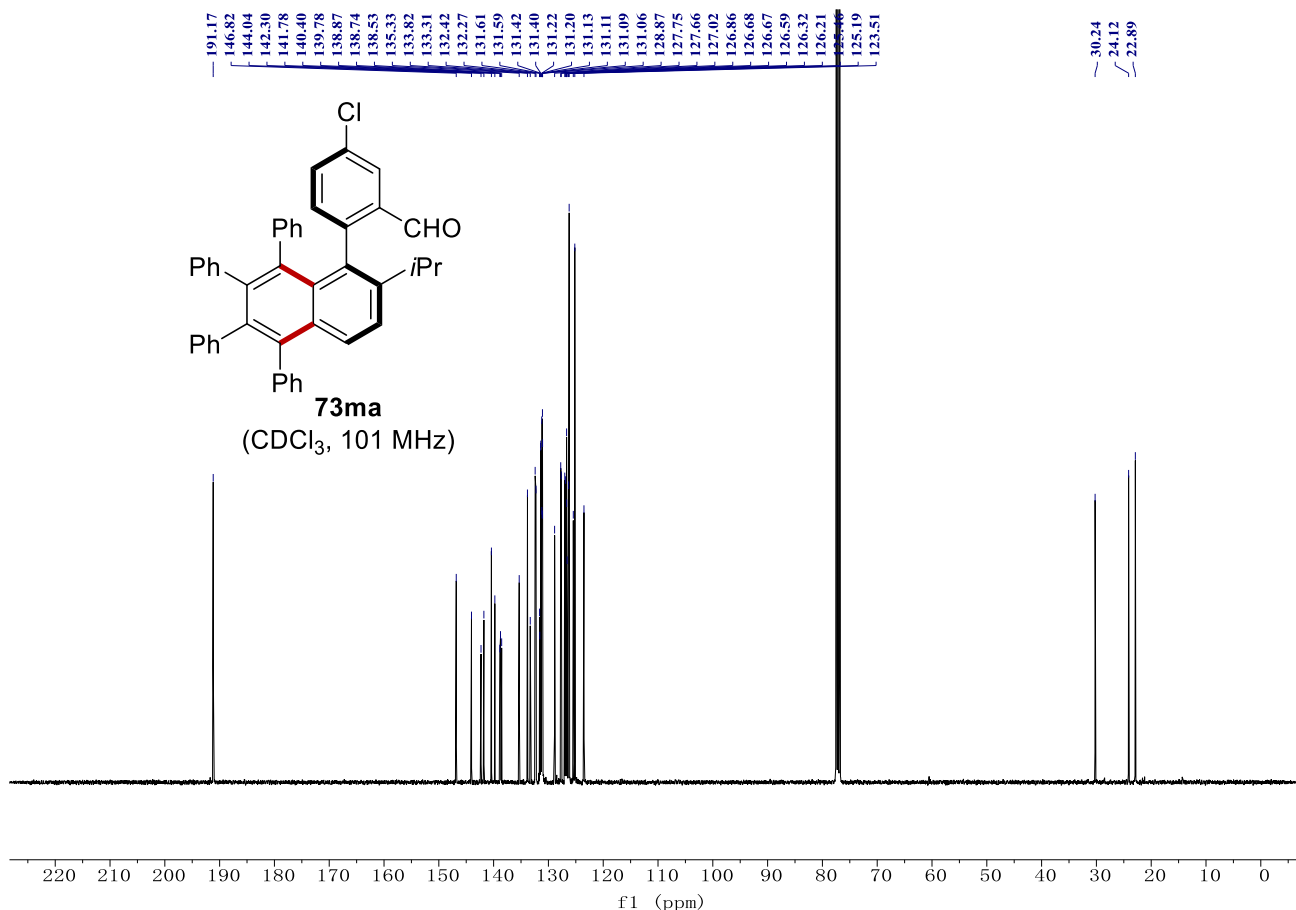
73la
(CDCl₃, 400 MHz)



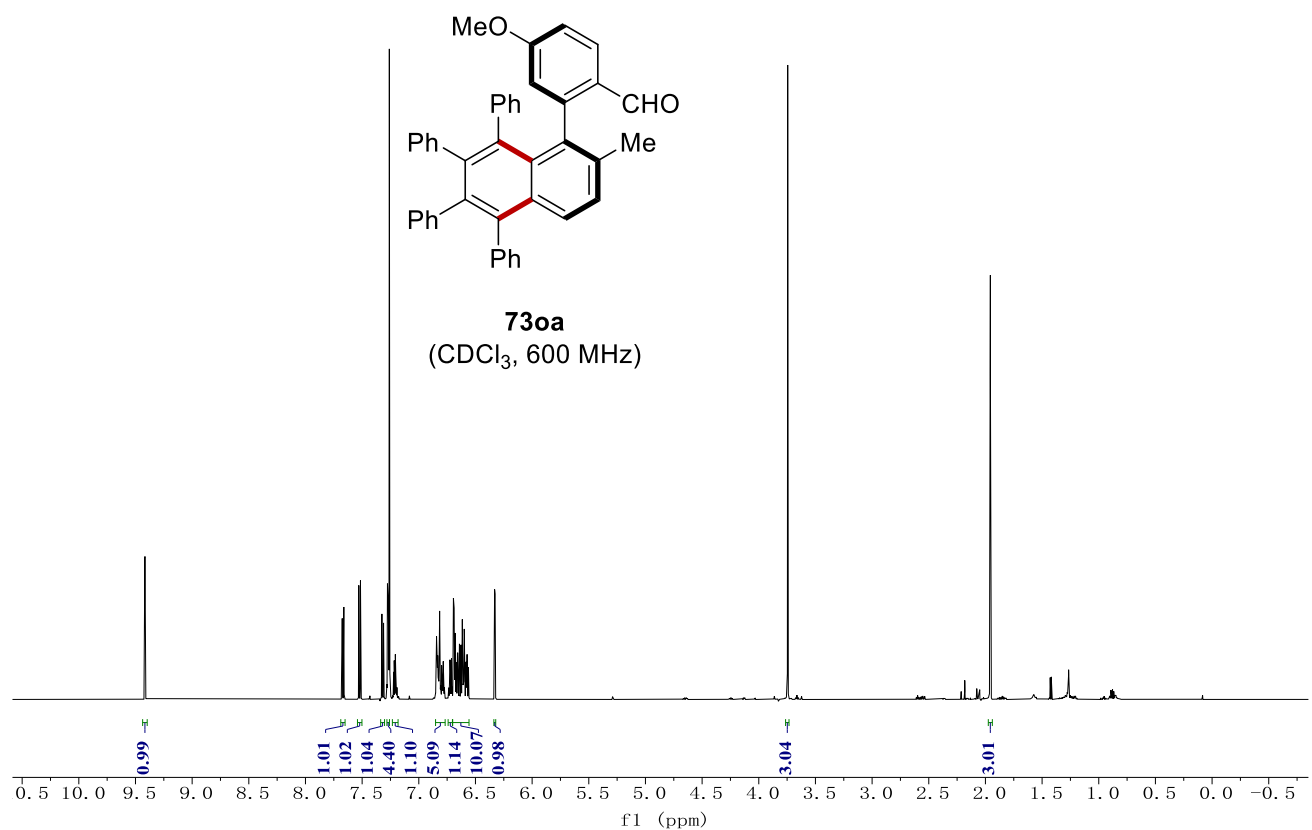
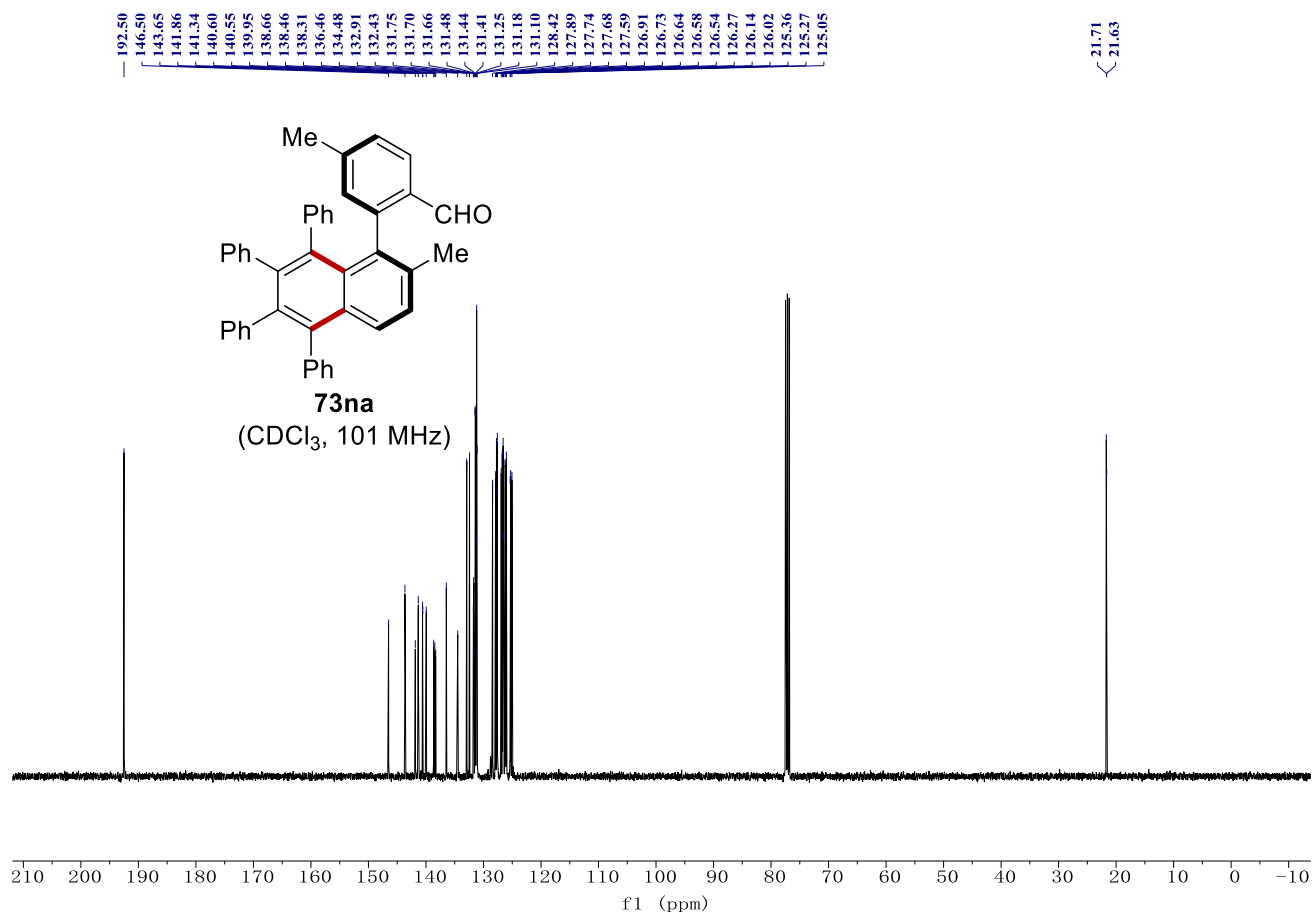
NMR Spectra



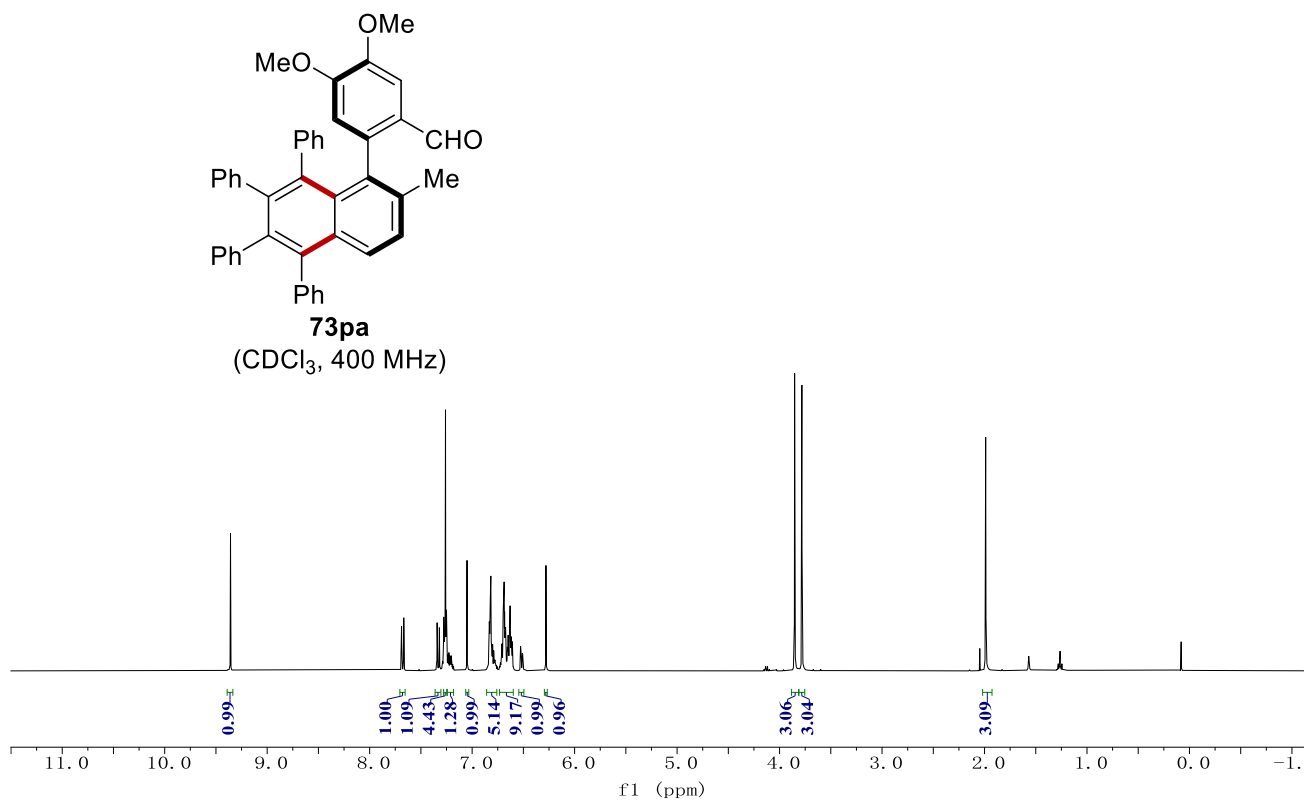
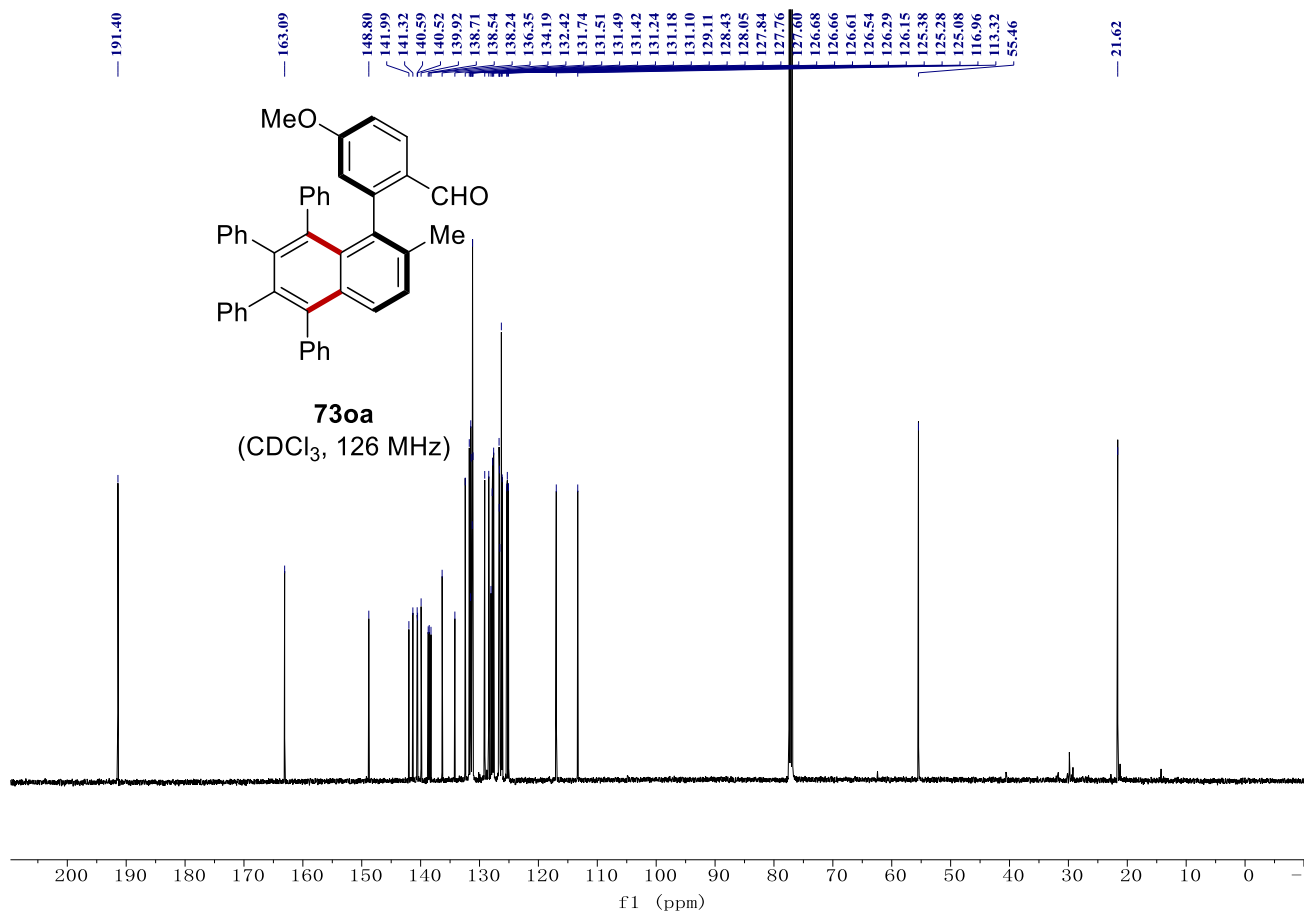
NMR Spectra



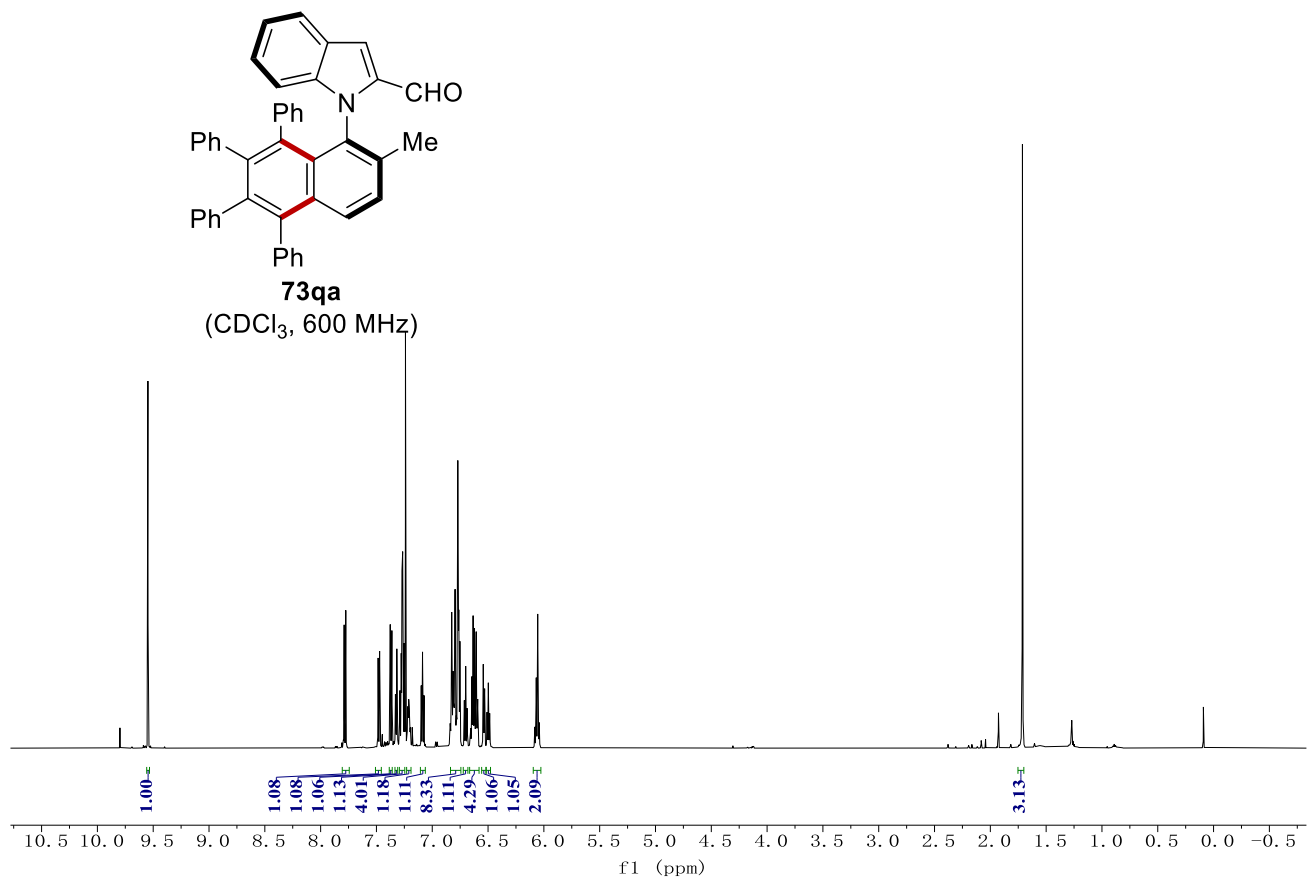
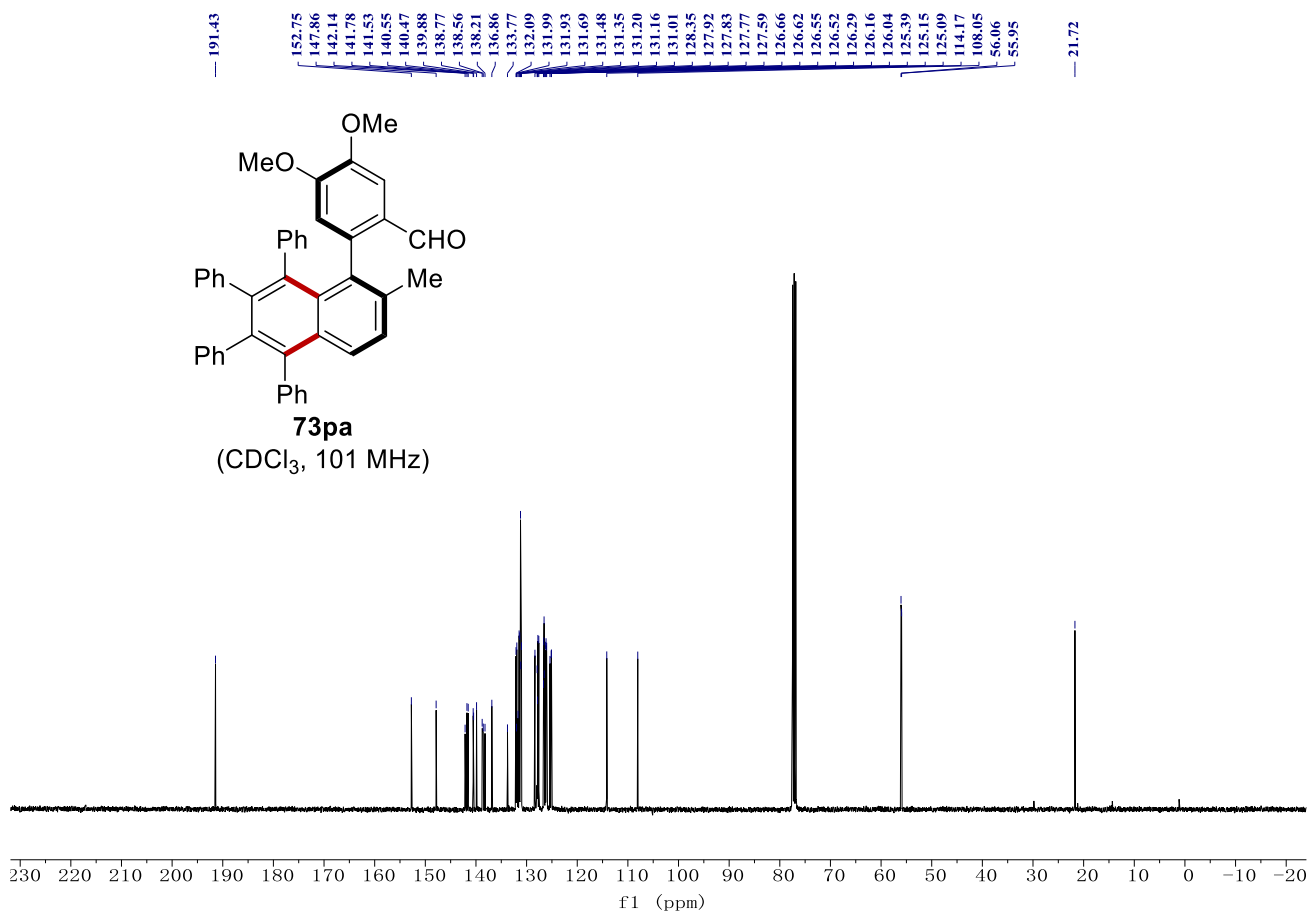
NMR Spectra



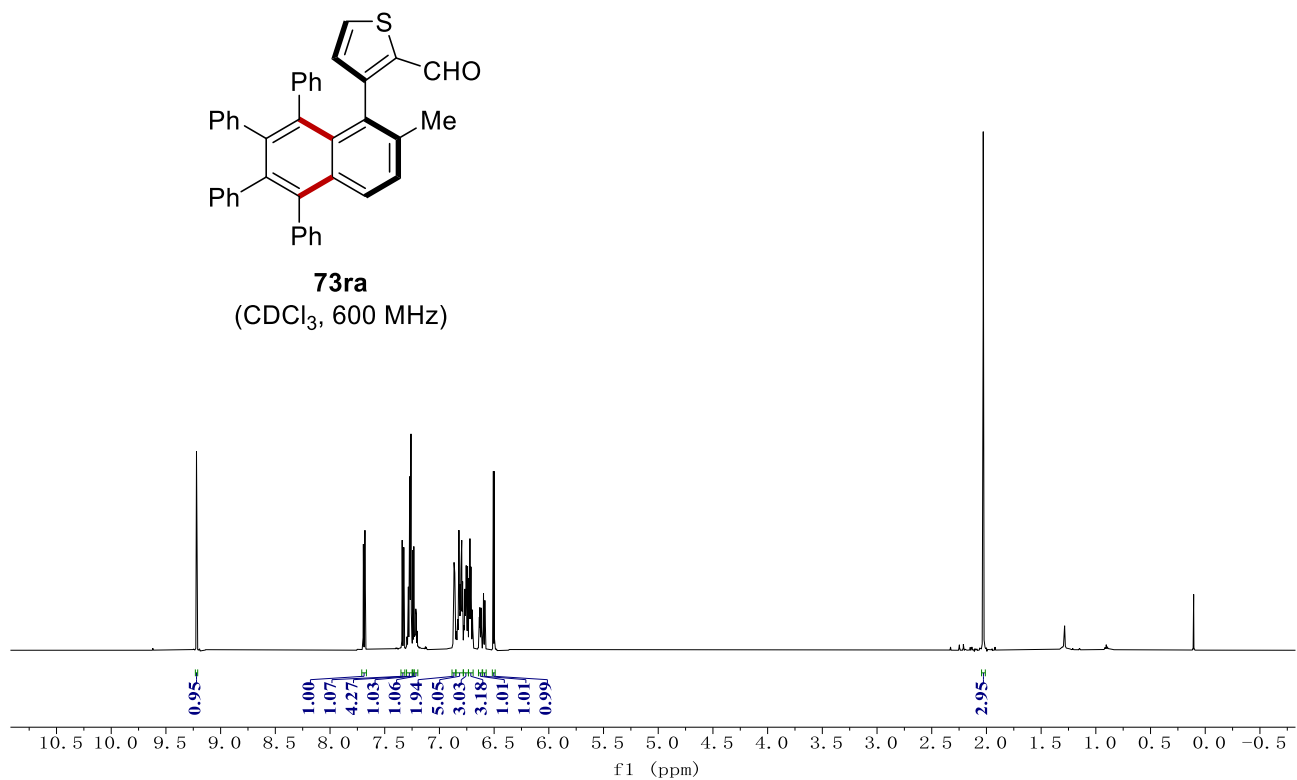
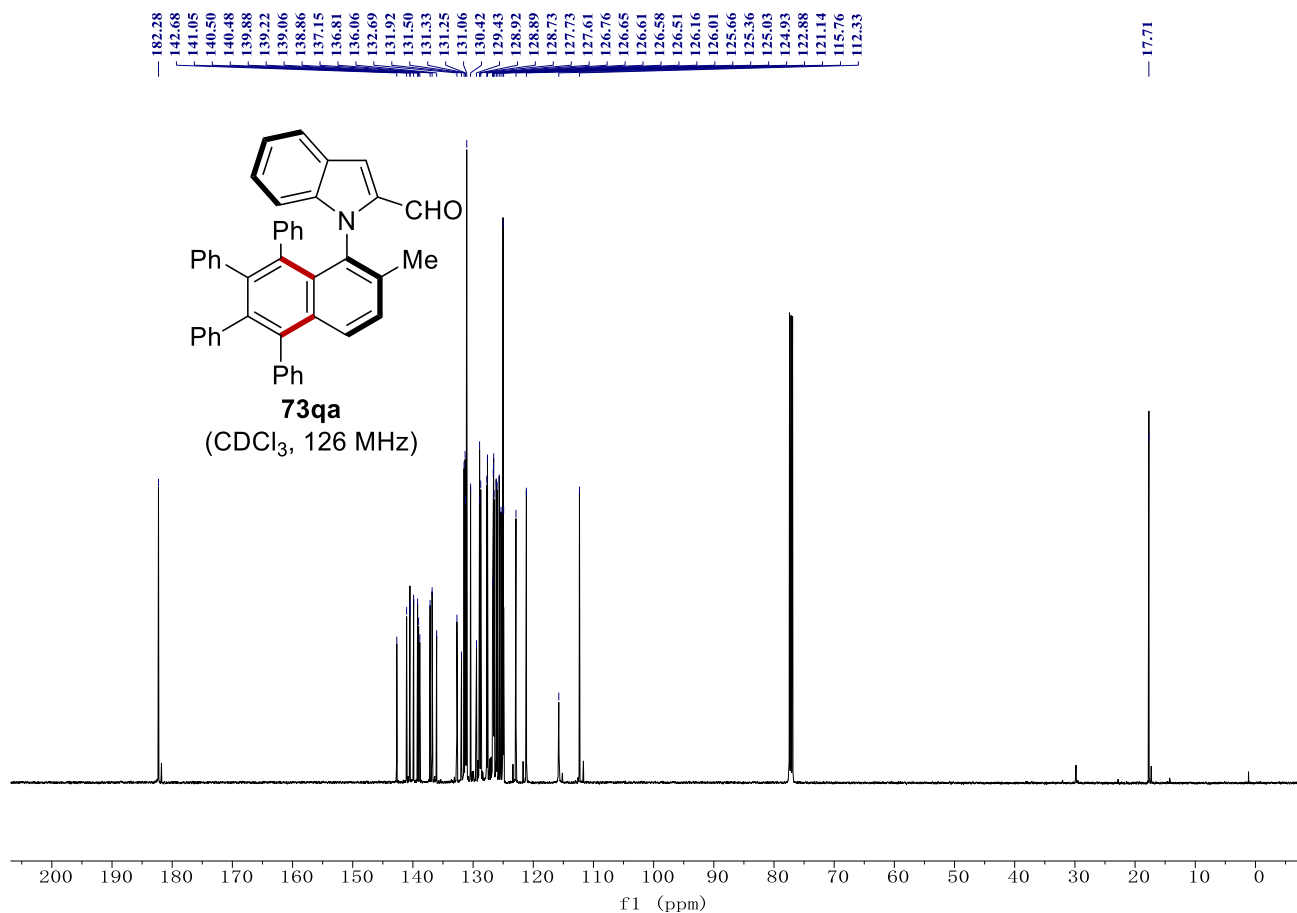
NMR Spectra



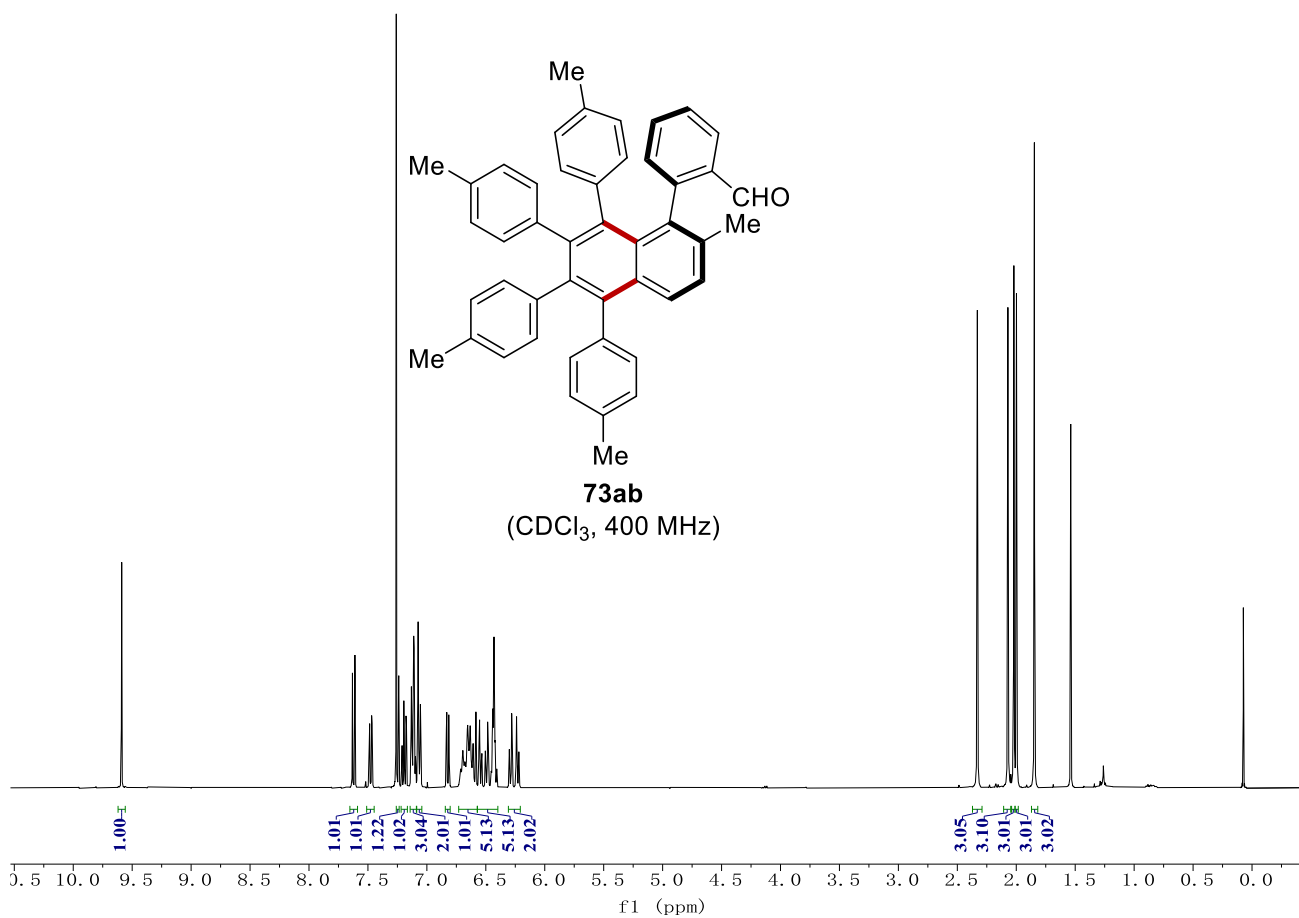
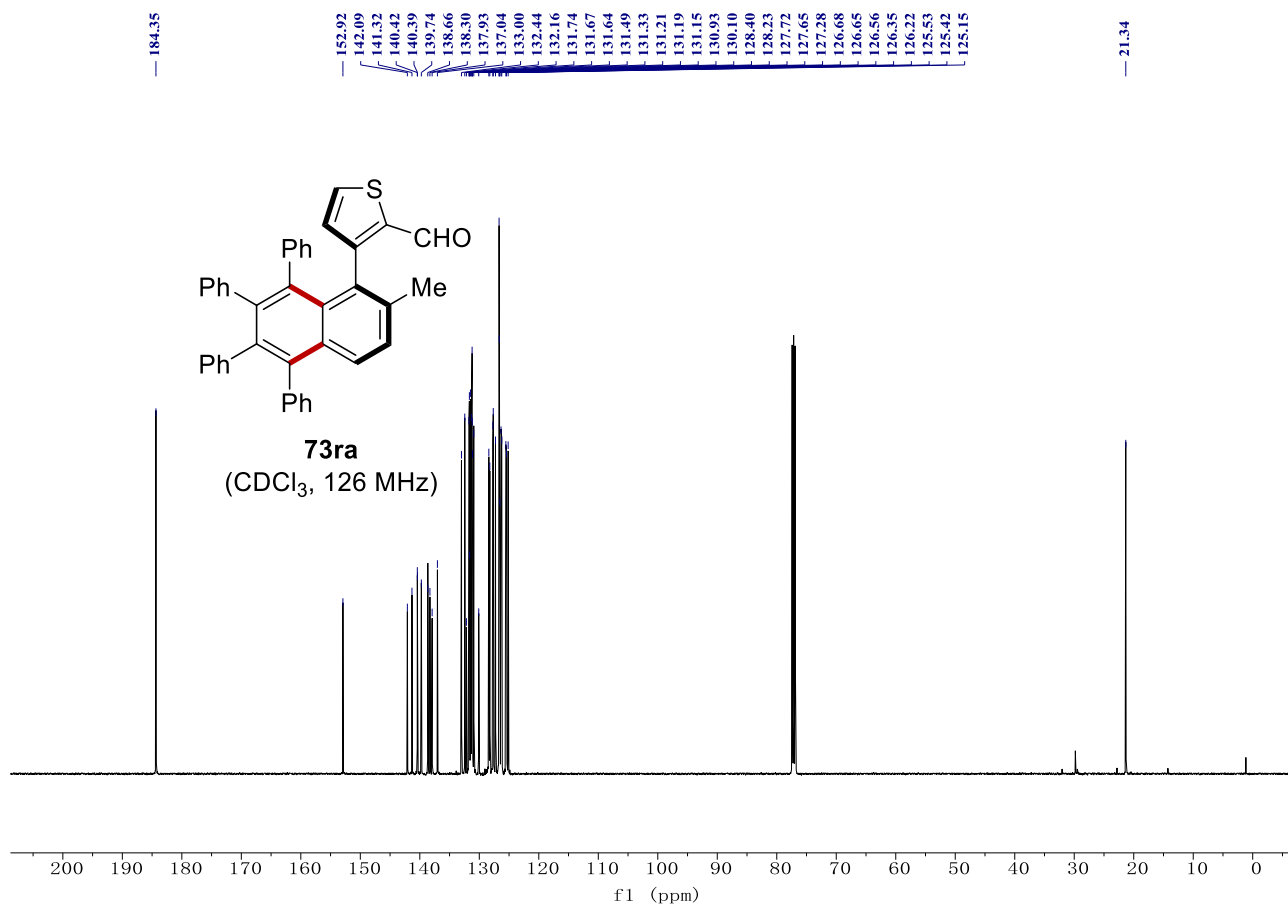
NMR Spectra



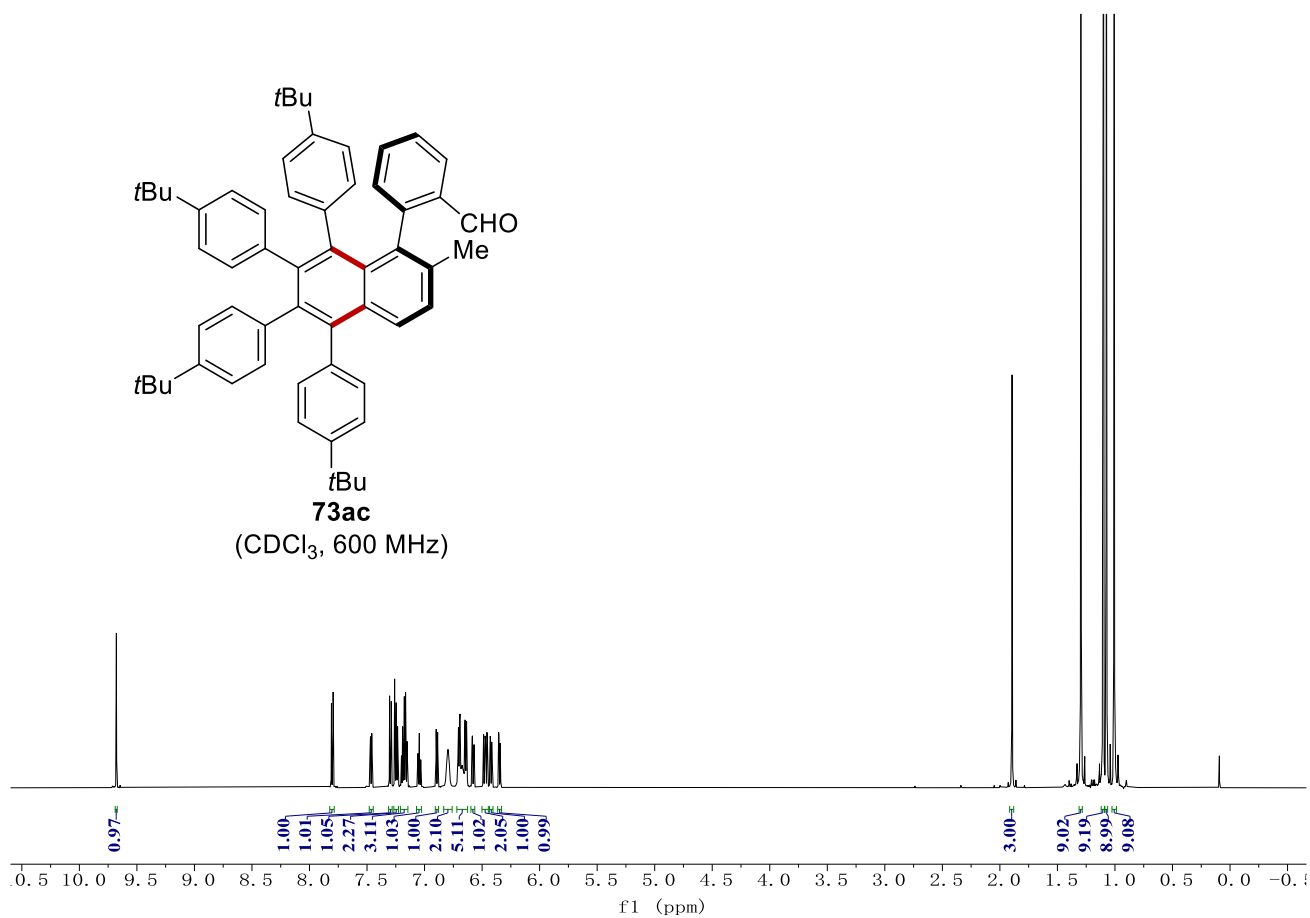
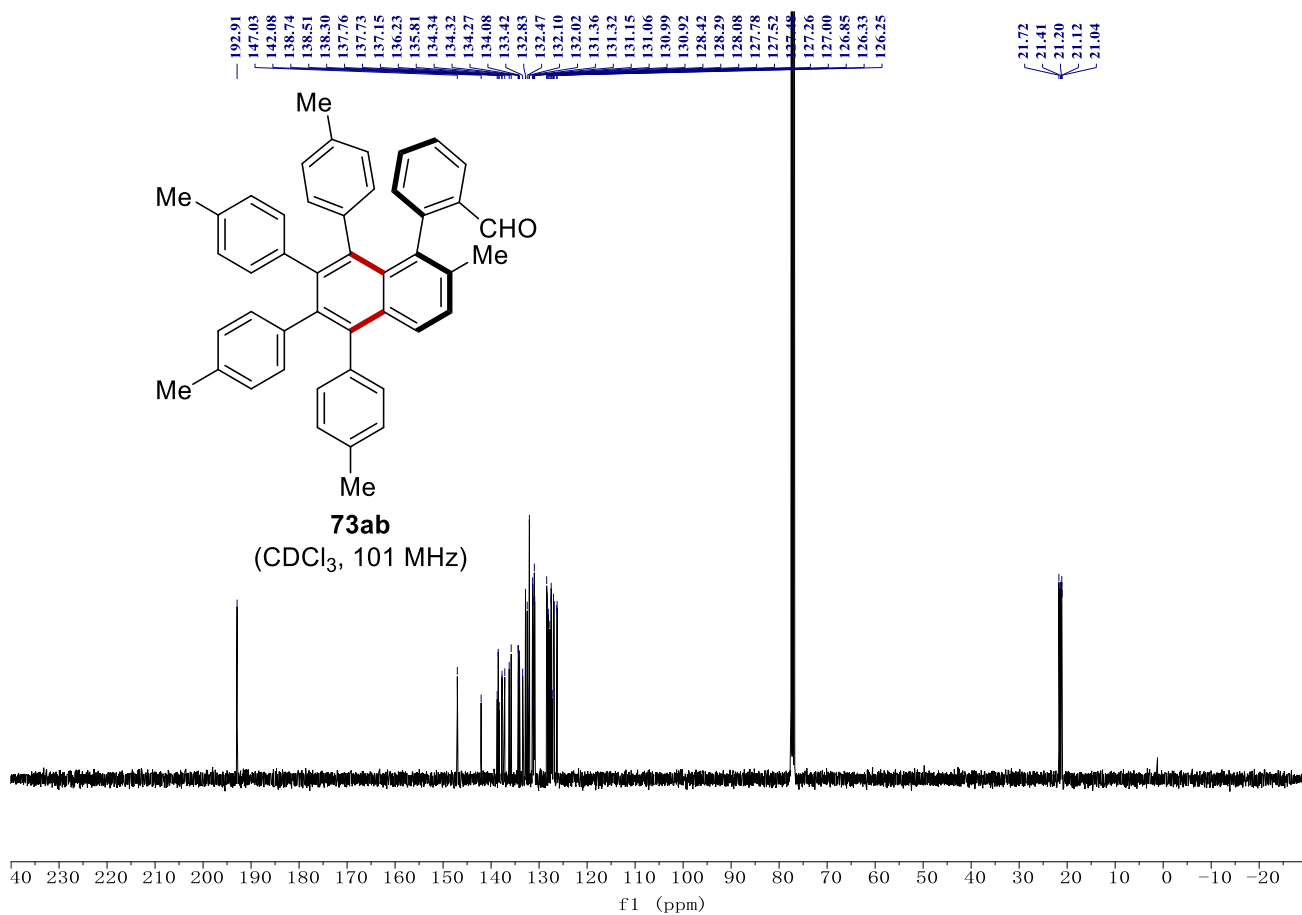
NMR Spectra



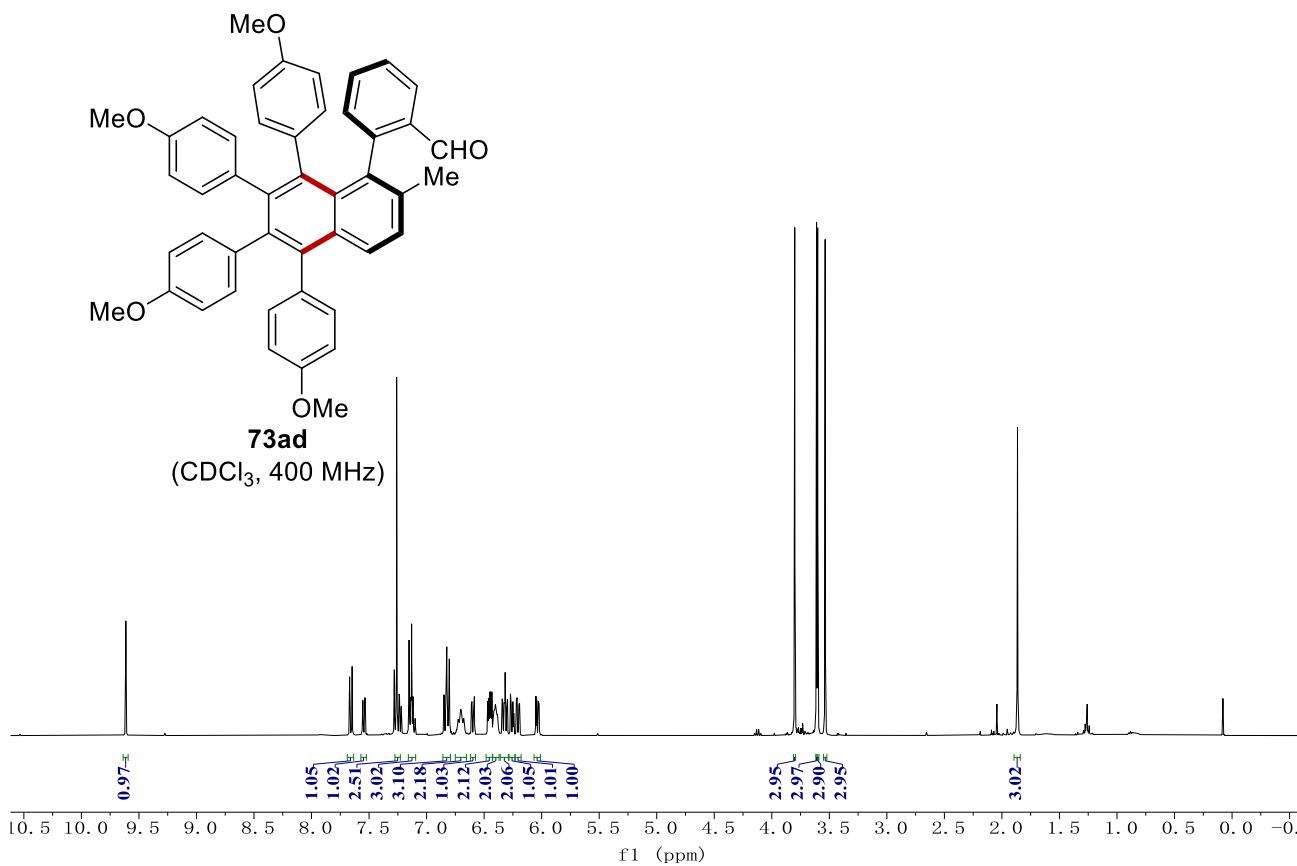
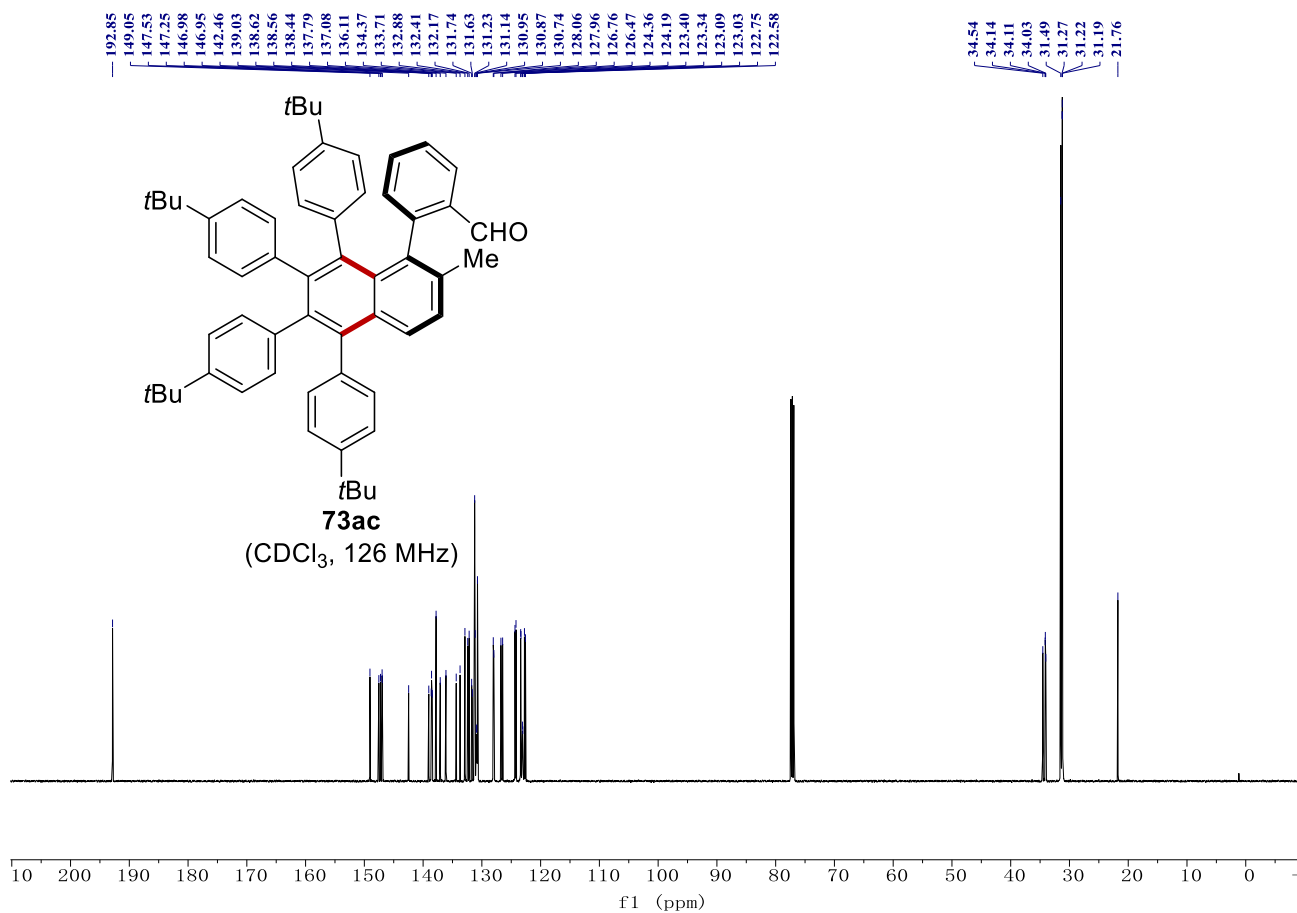
NMR Spectra



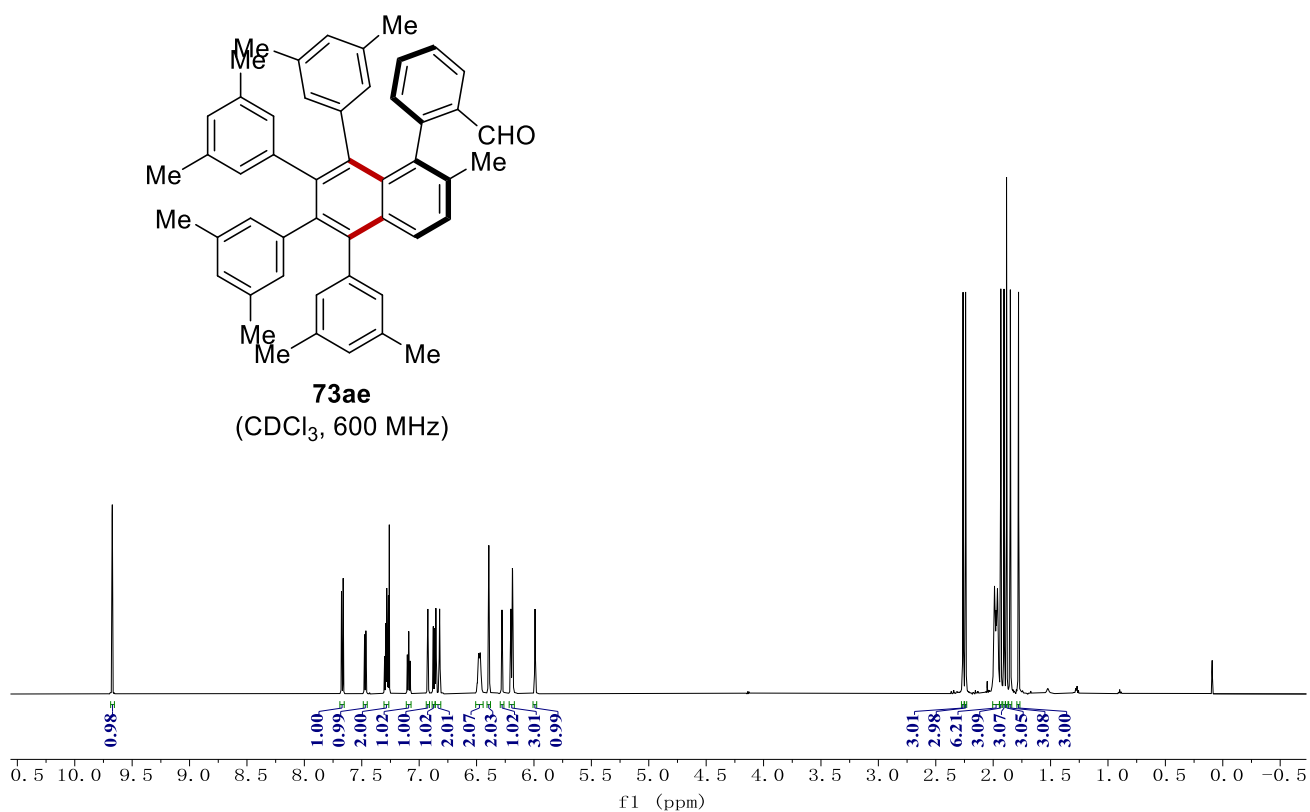
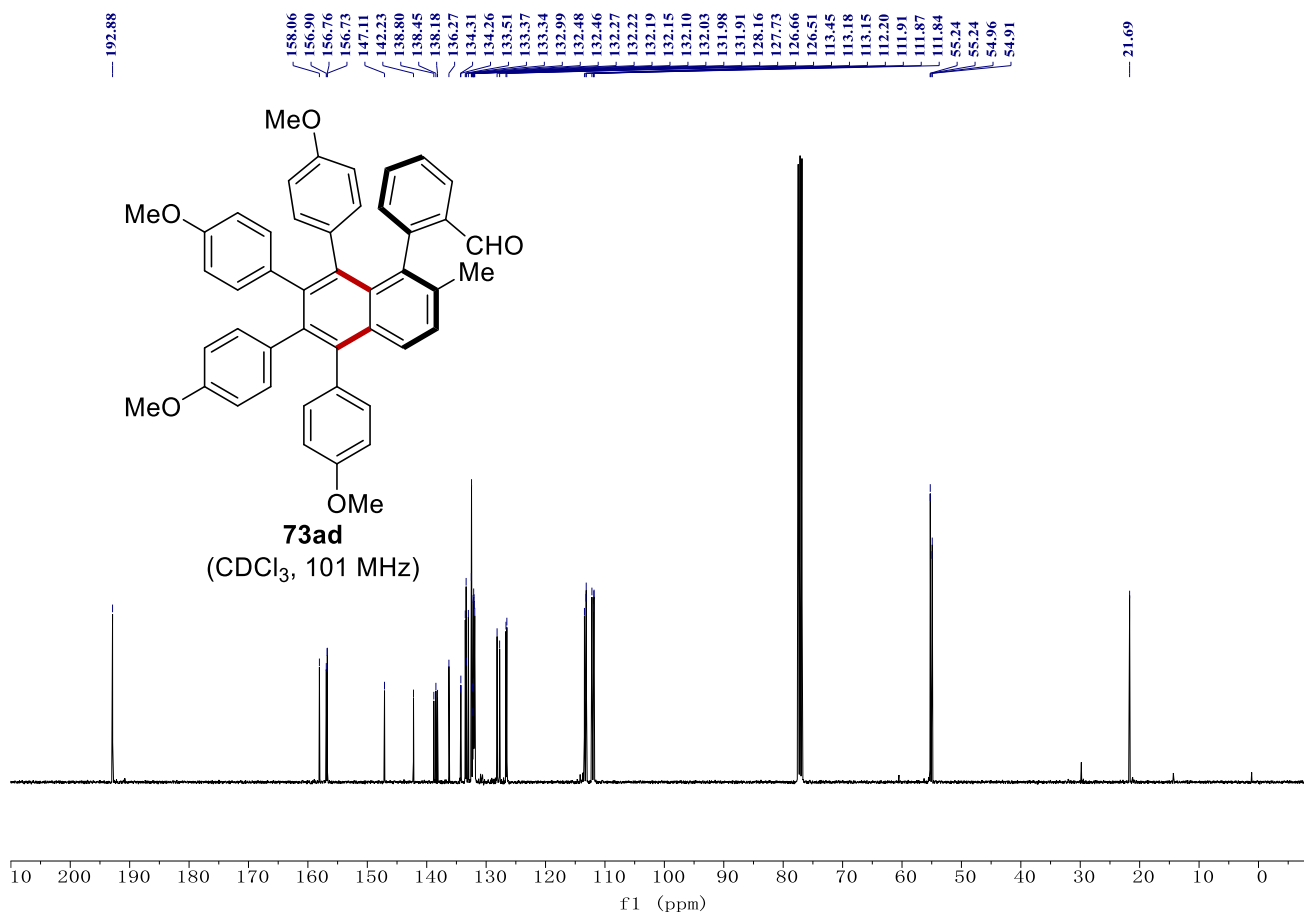
NMR Spectra



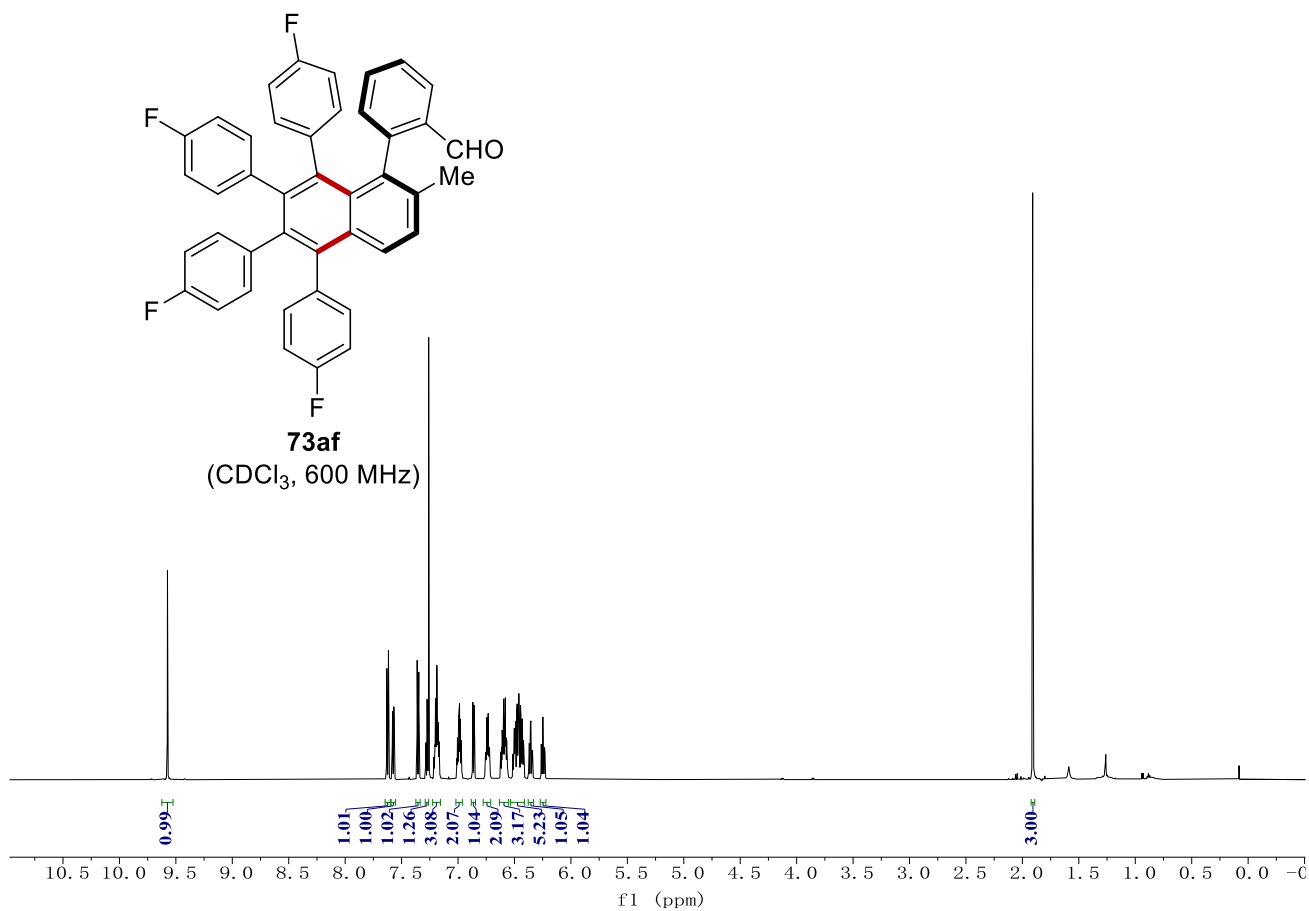
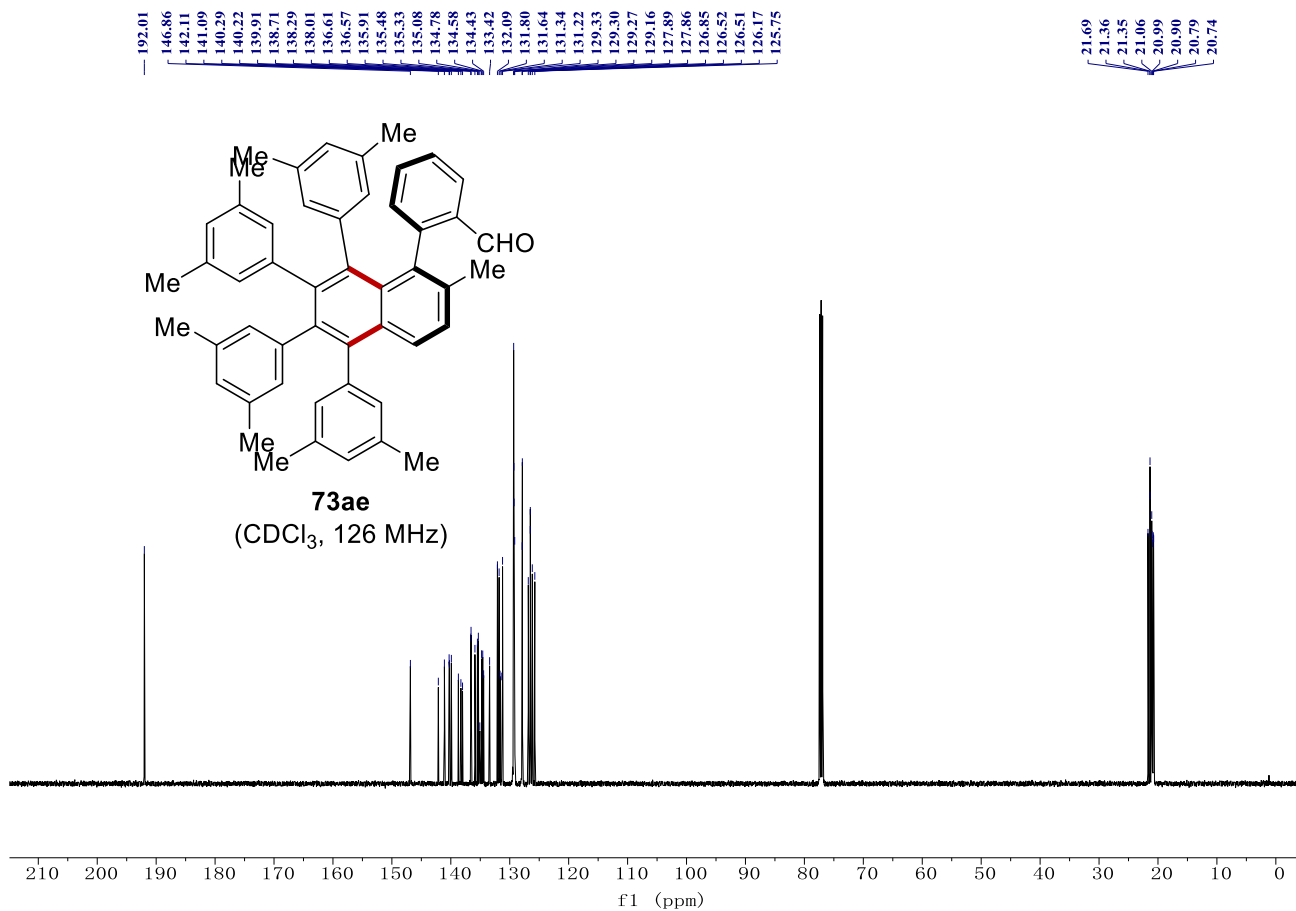
NMR Spectra



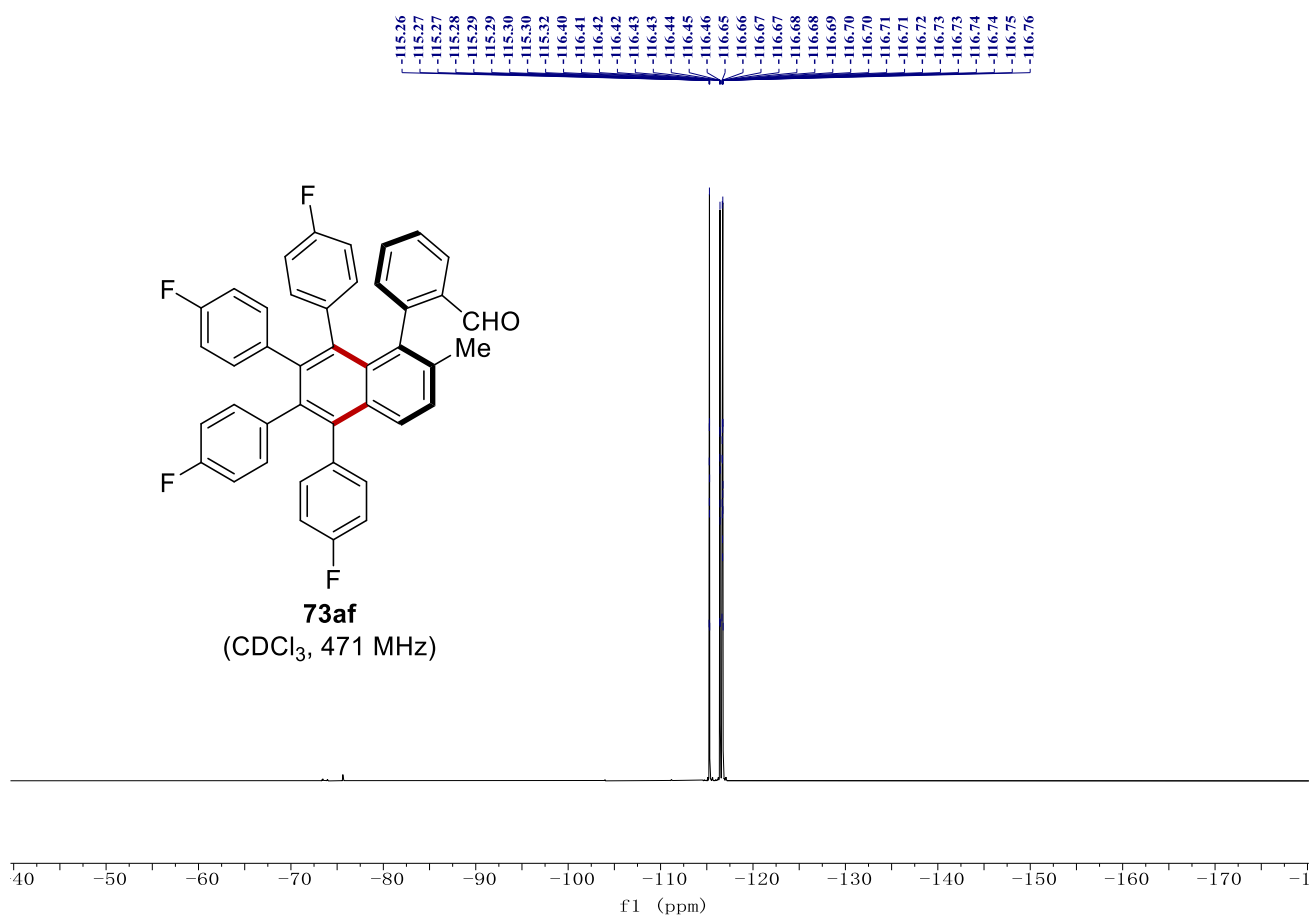
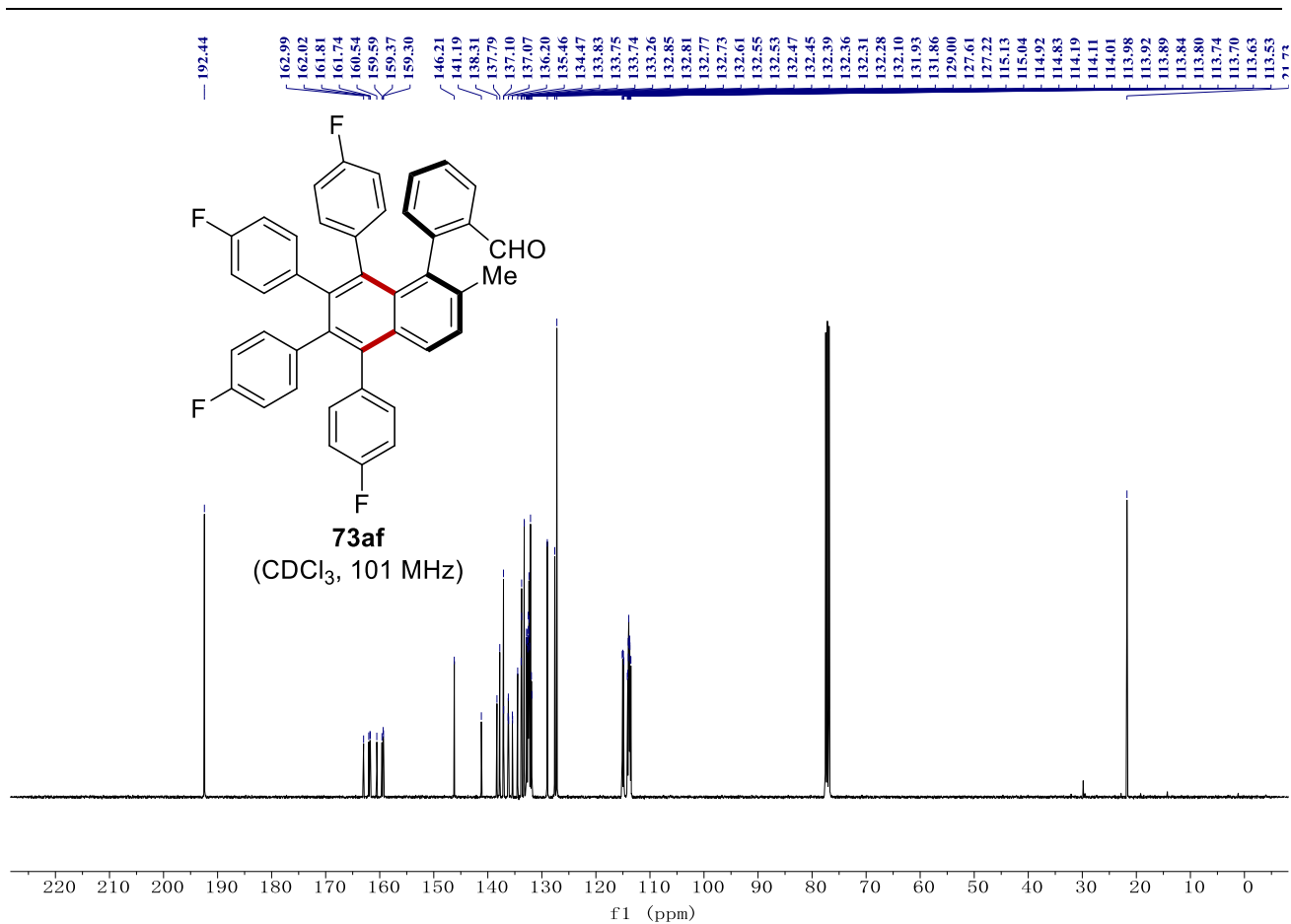
NMR Spectra



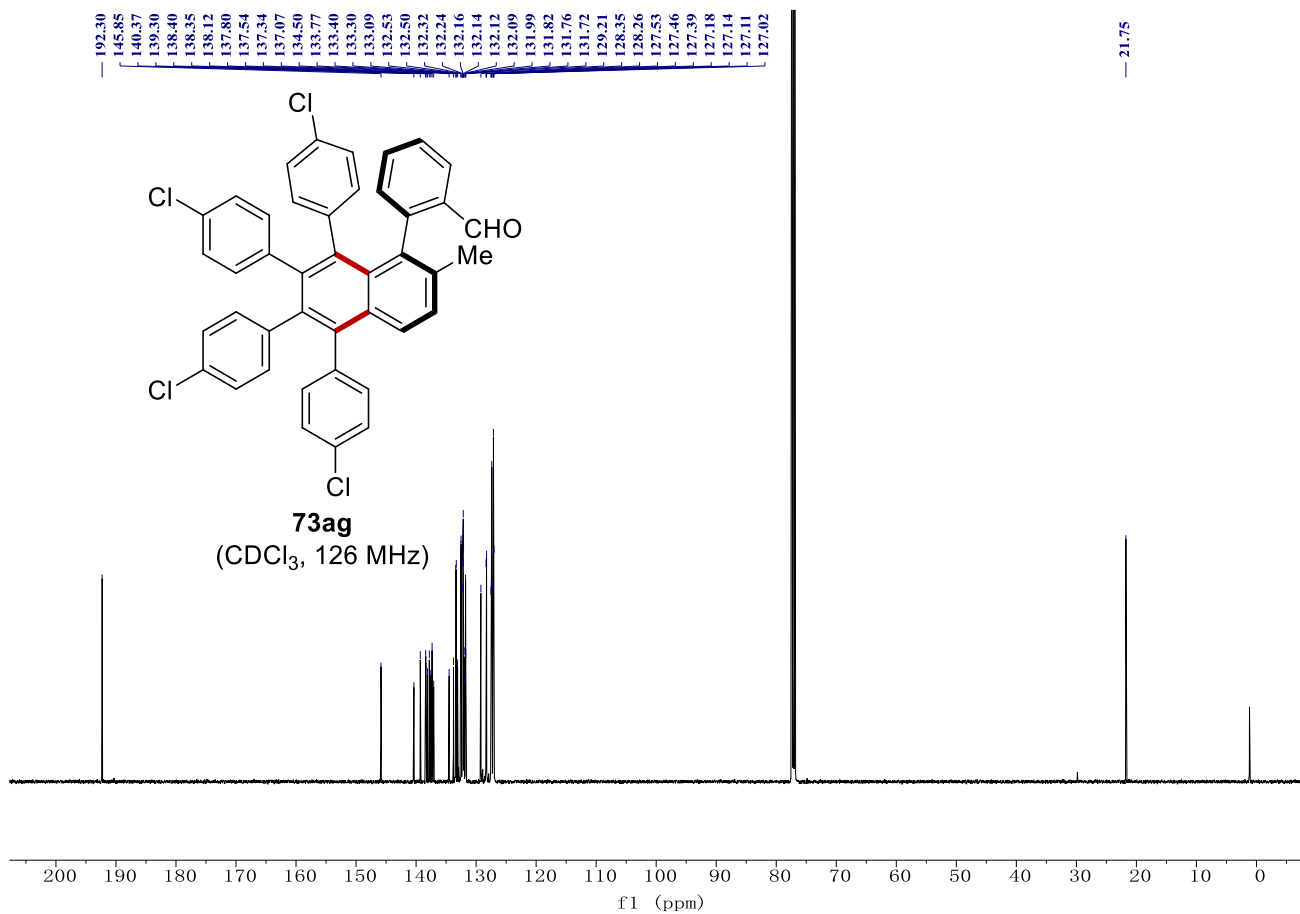
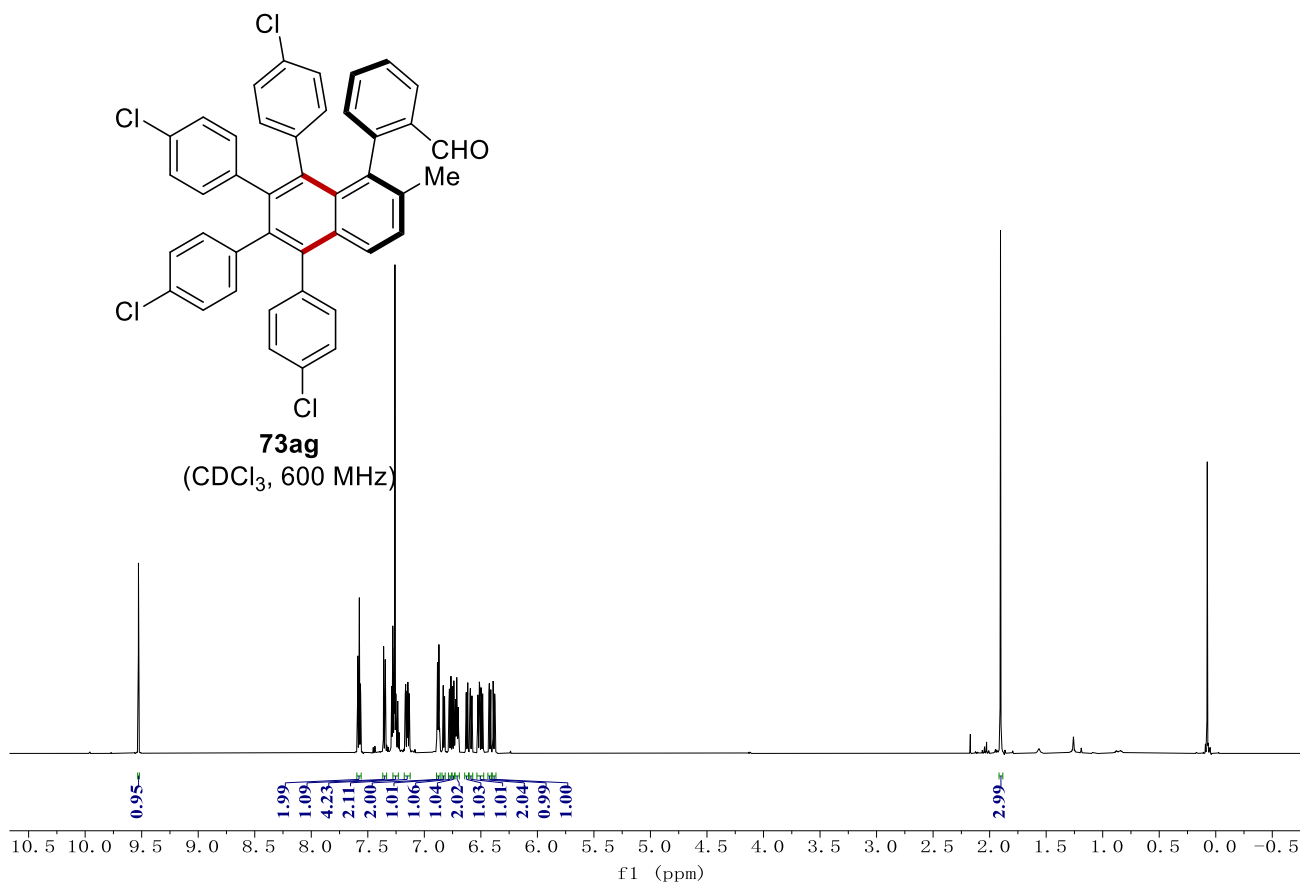
NMR Spectra



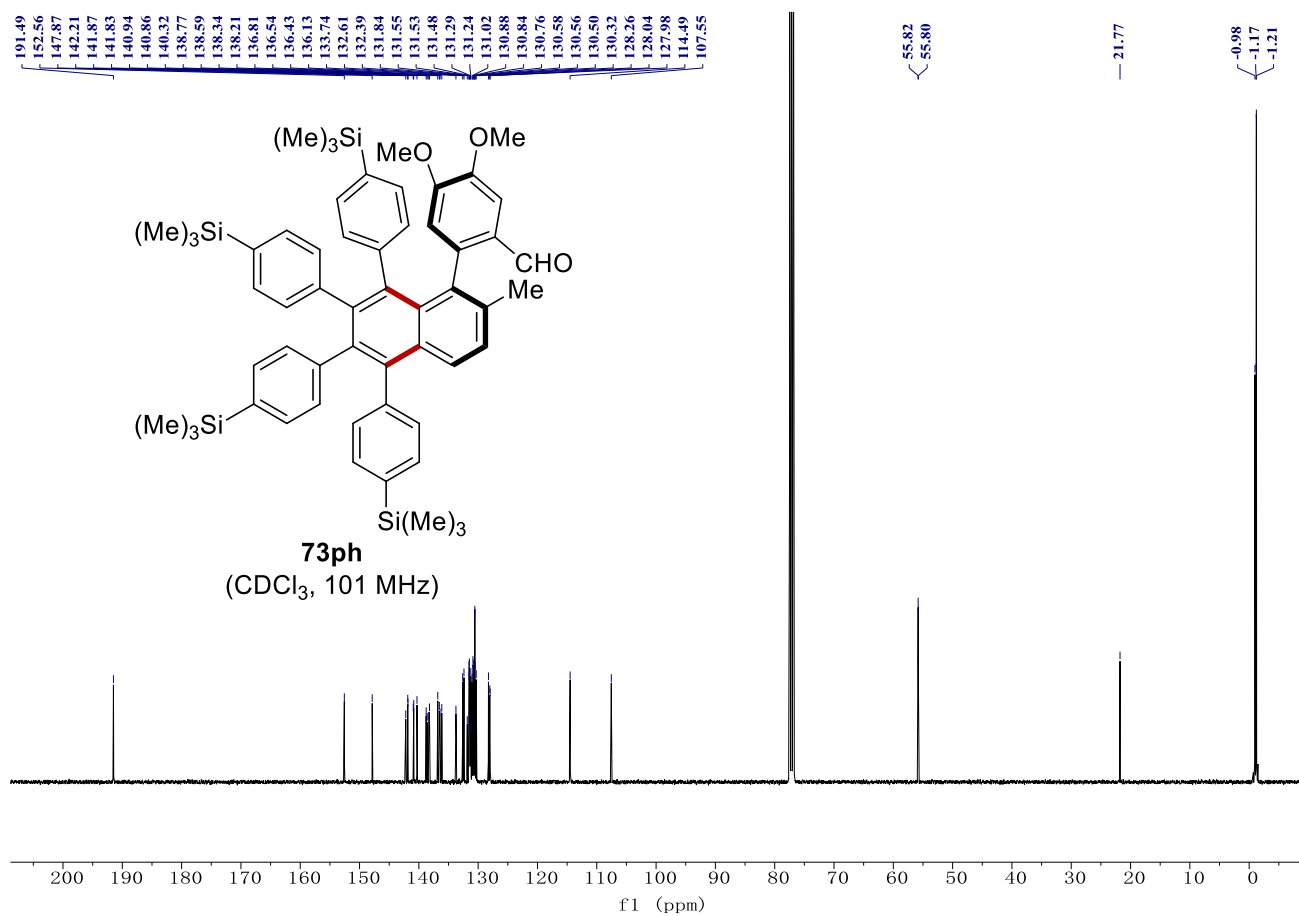
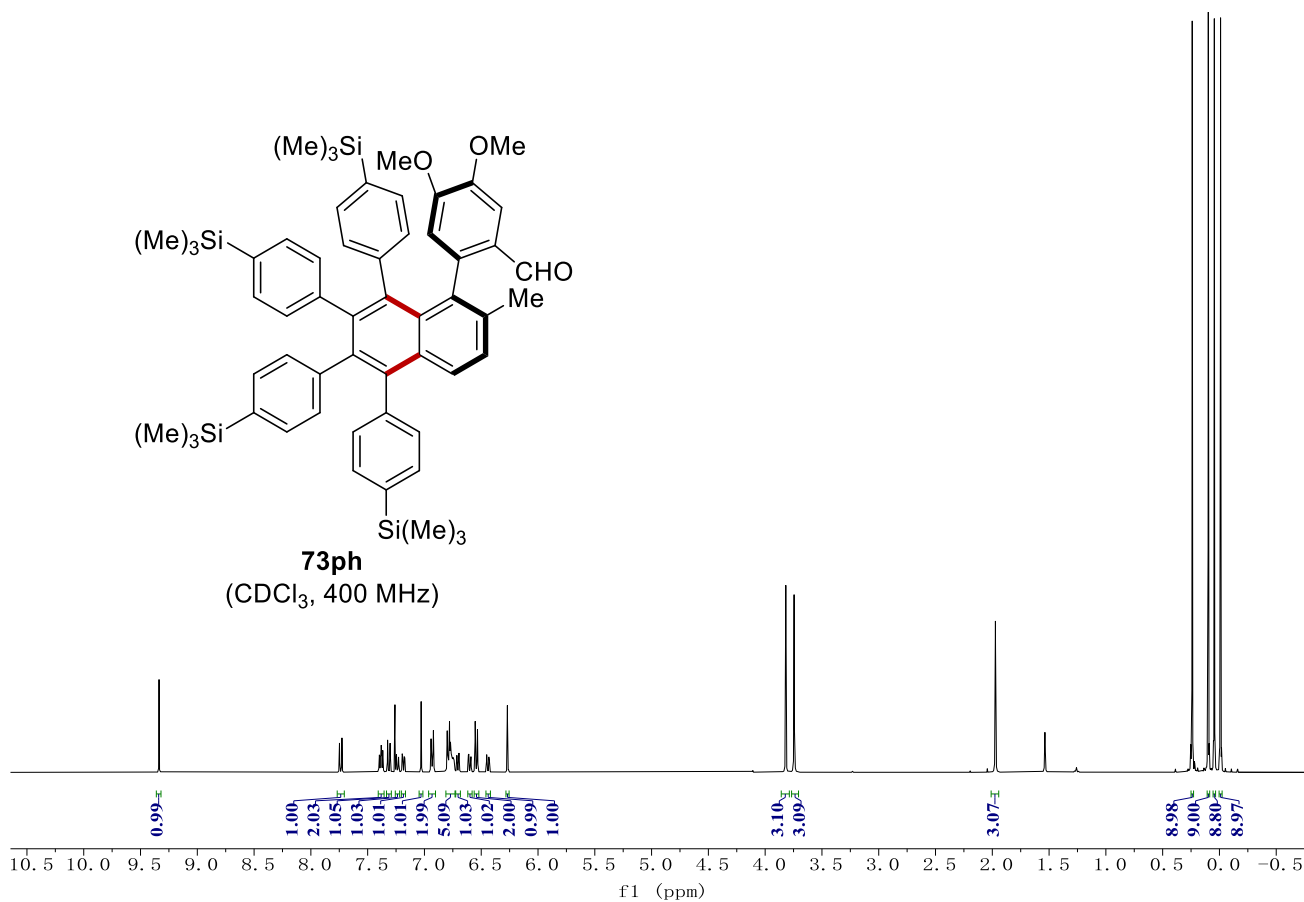
NMR Spectra



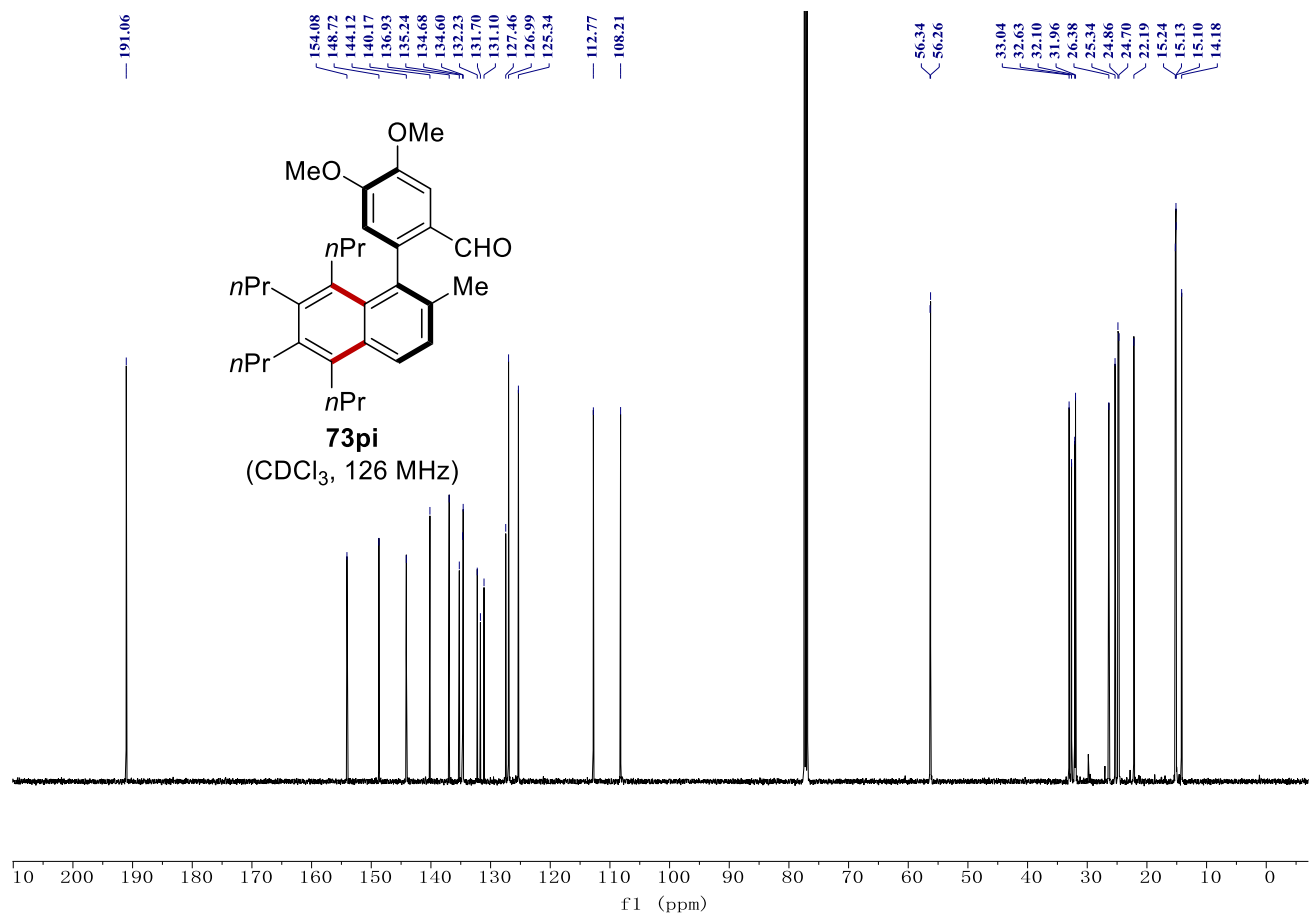
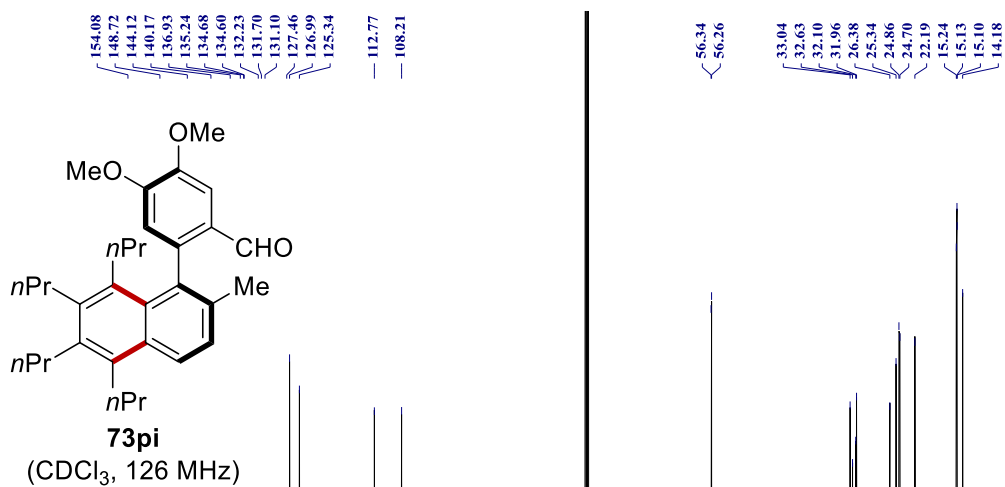
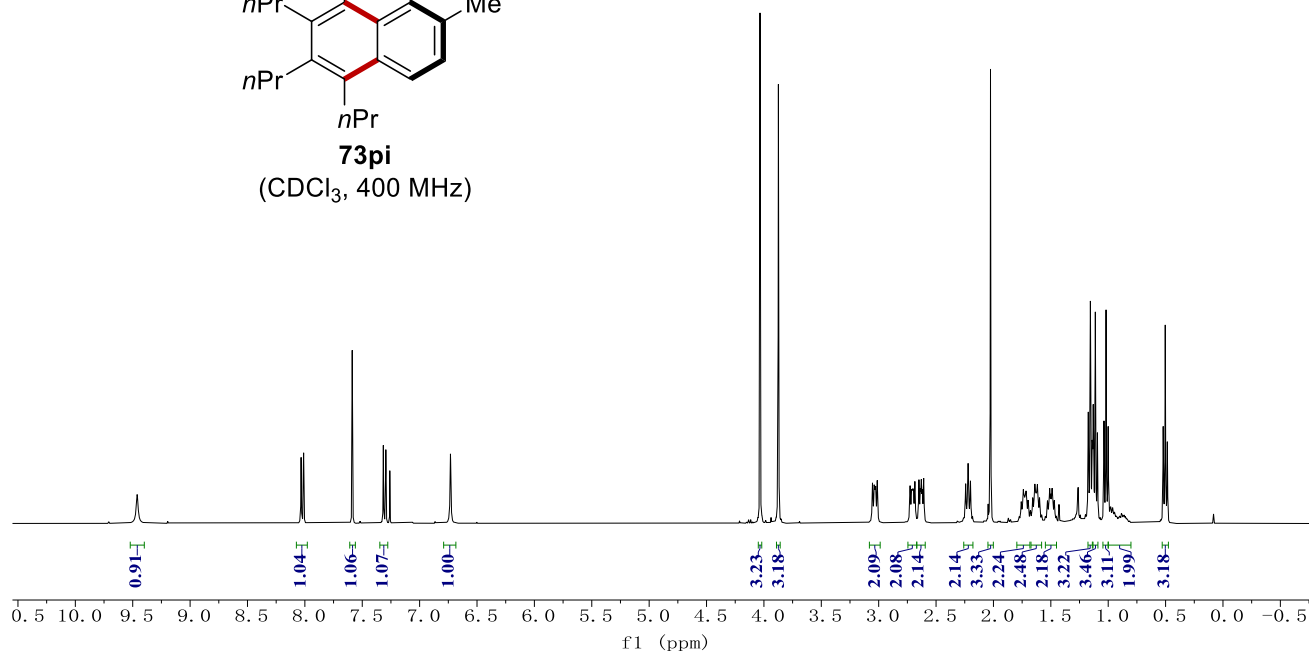
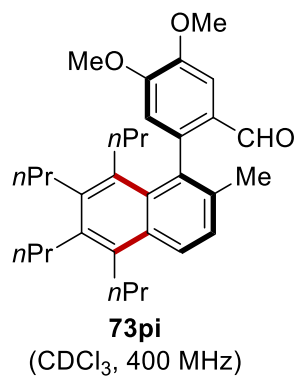
NMR Spectra



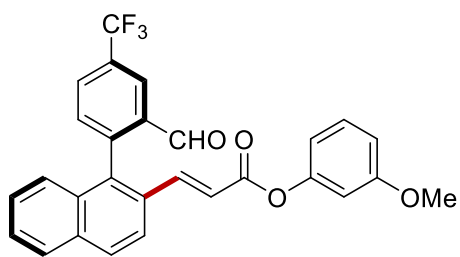
NMR Spectra



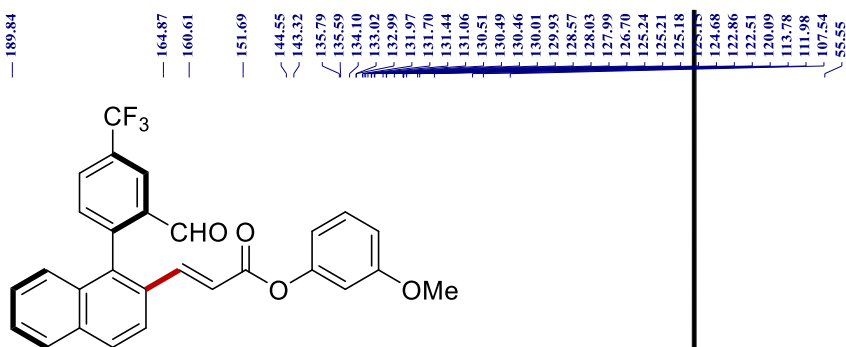
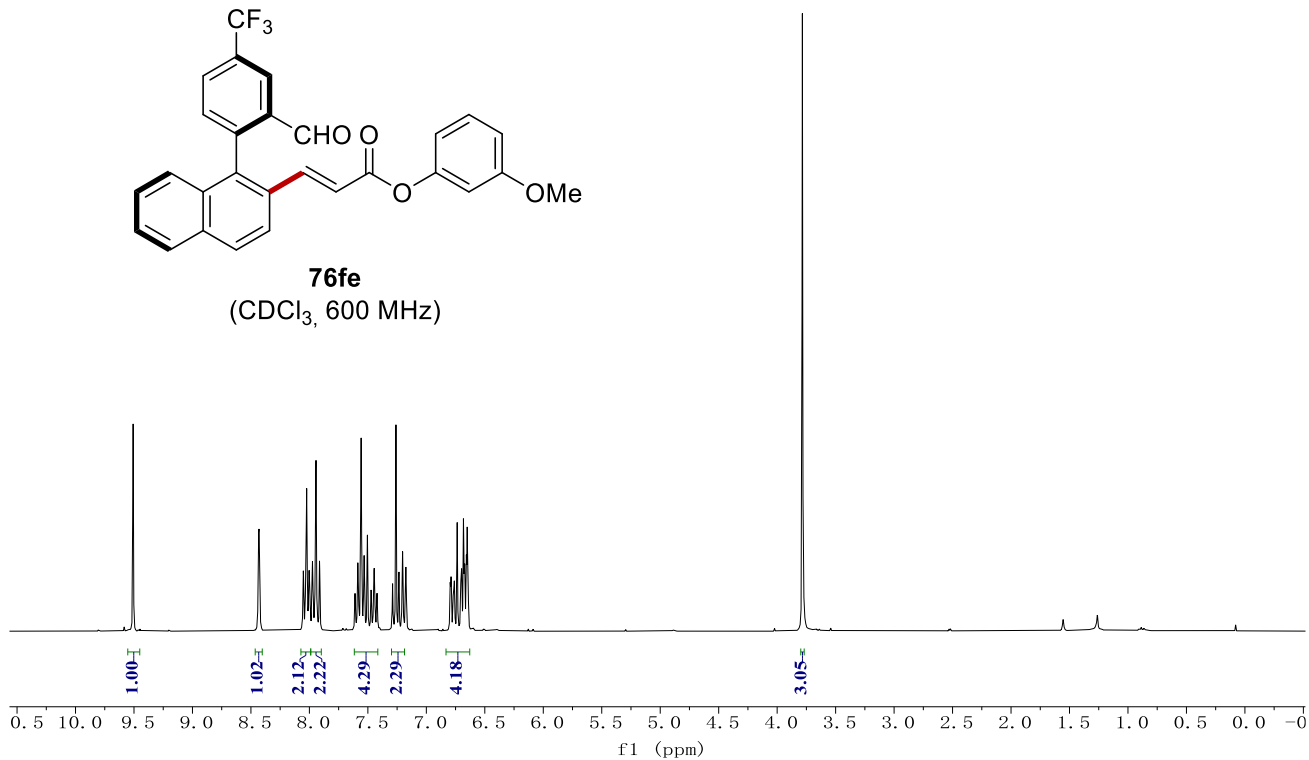
NMR Spectra



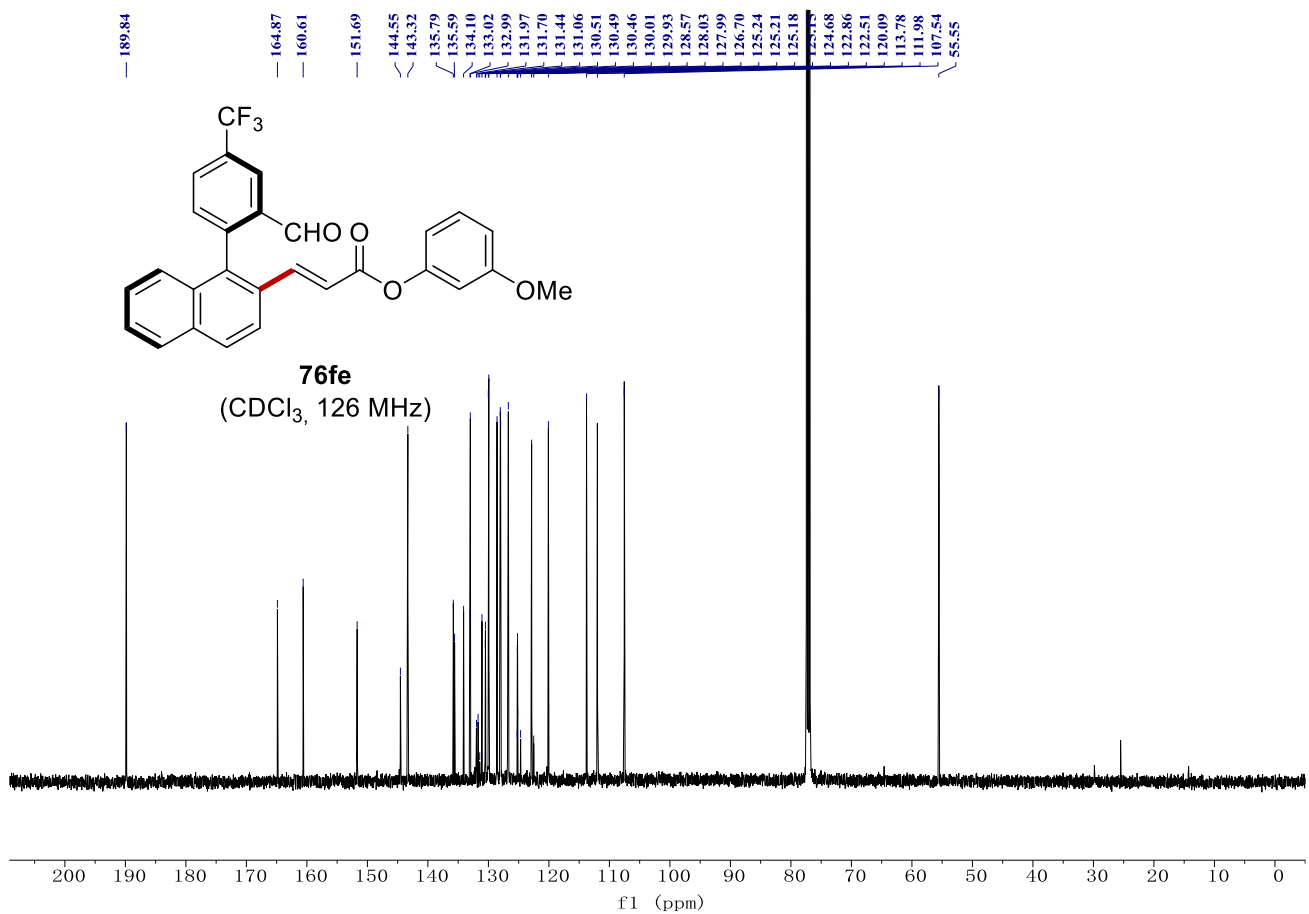
NMR Spectra



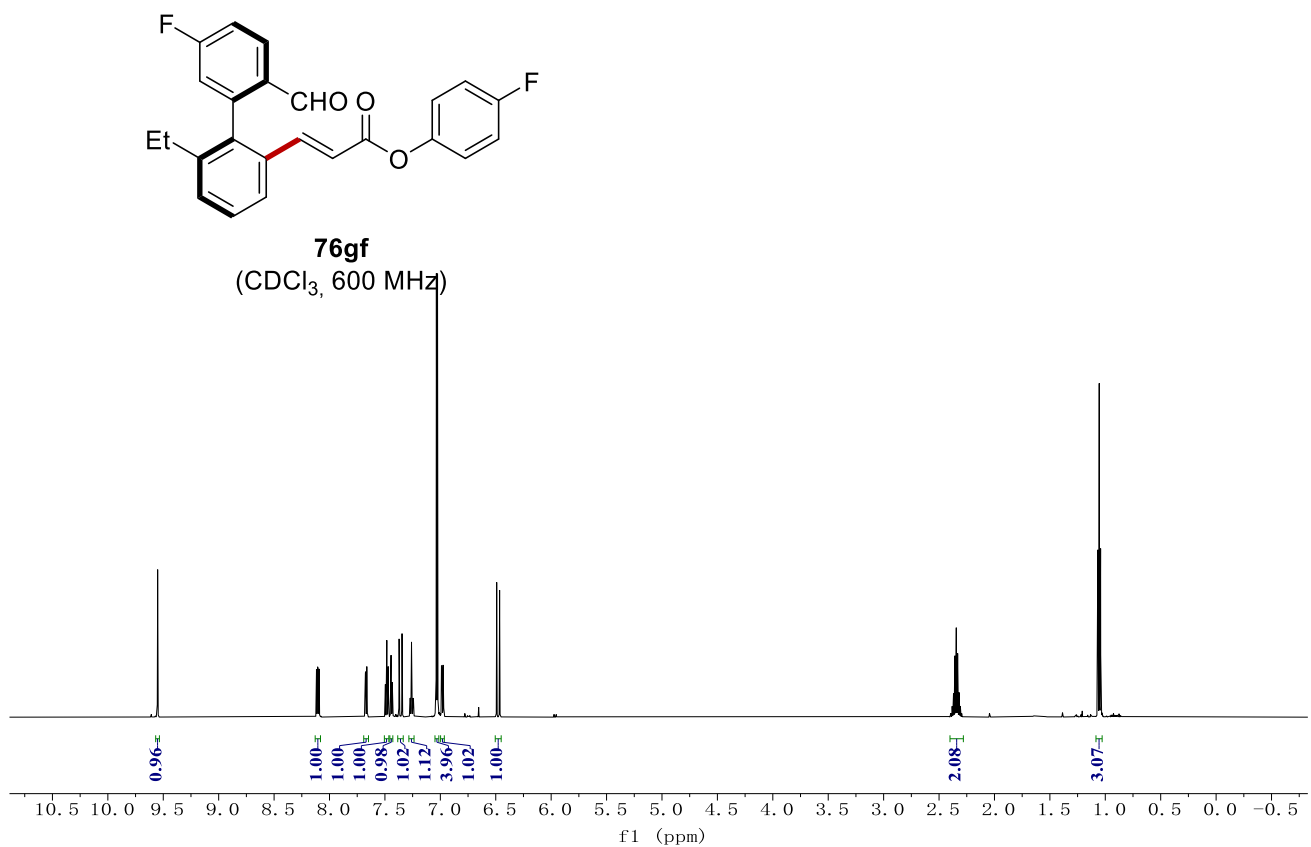
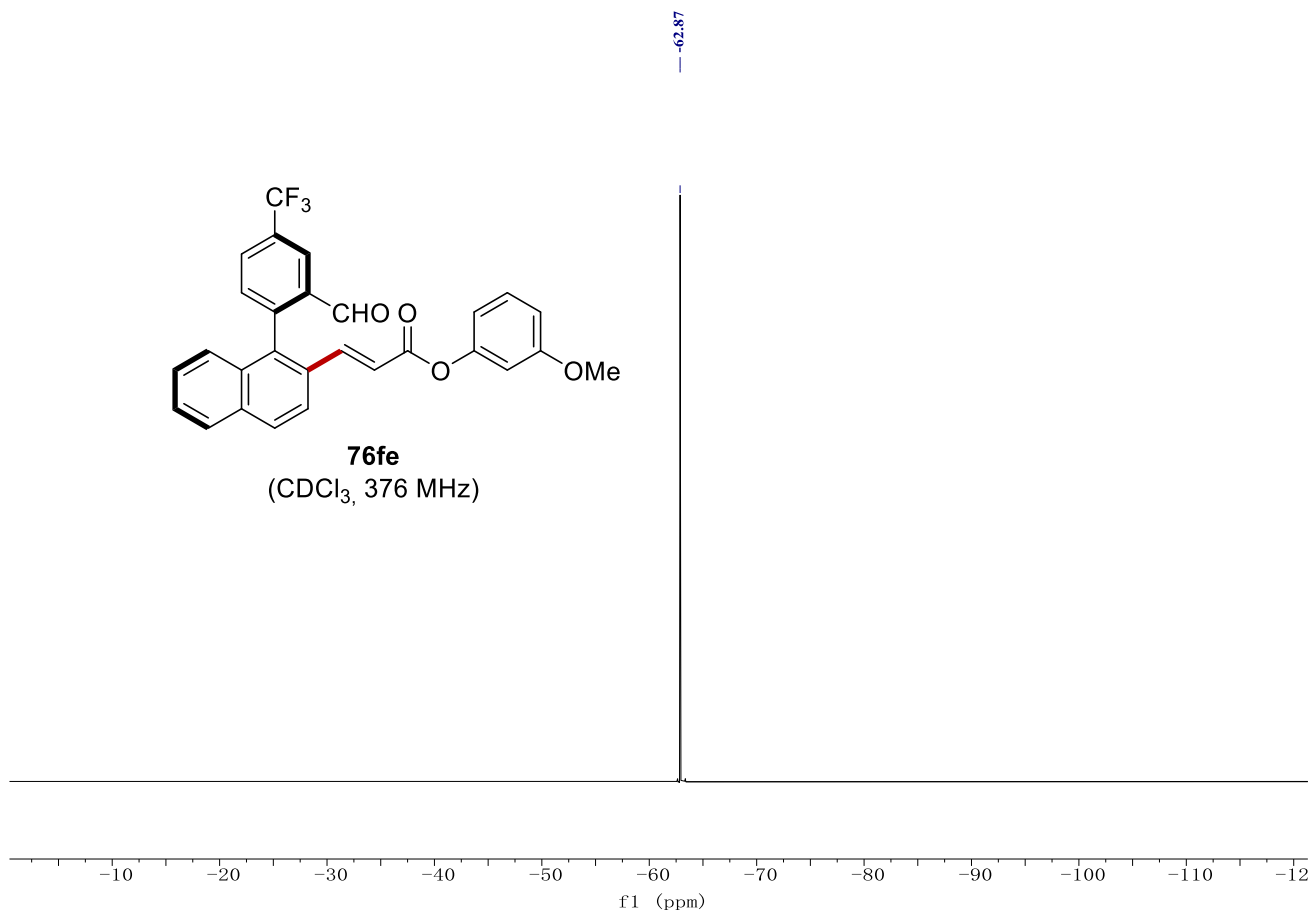
76fe
(CDCl₃, 600 MHz)



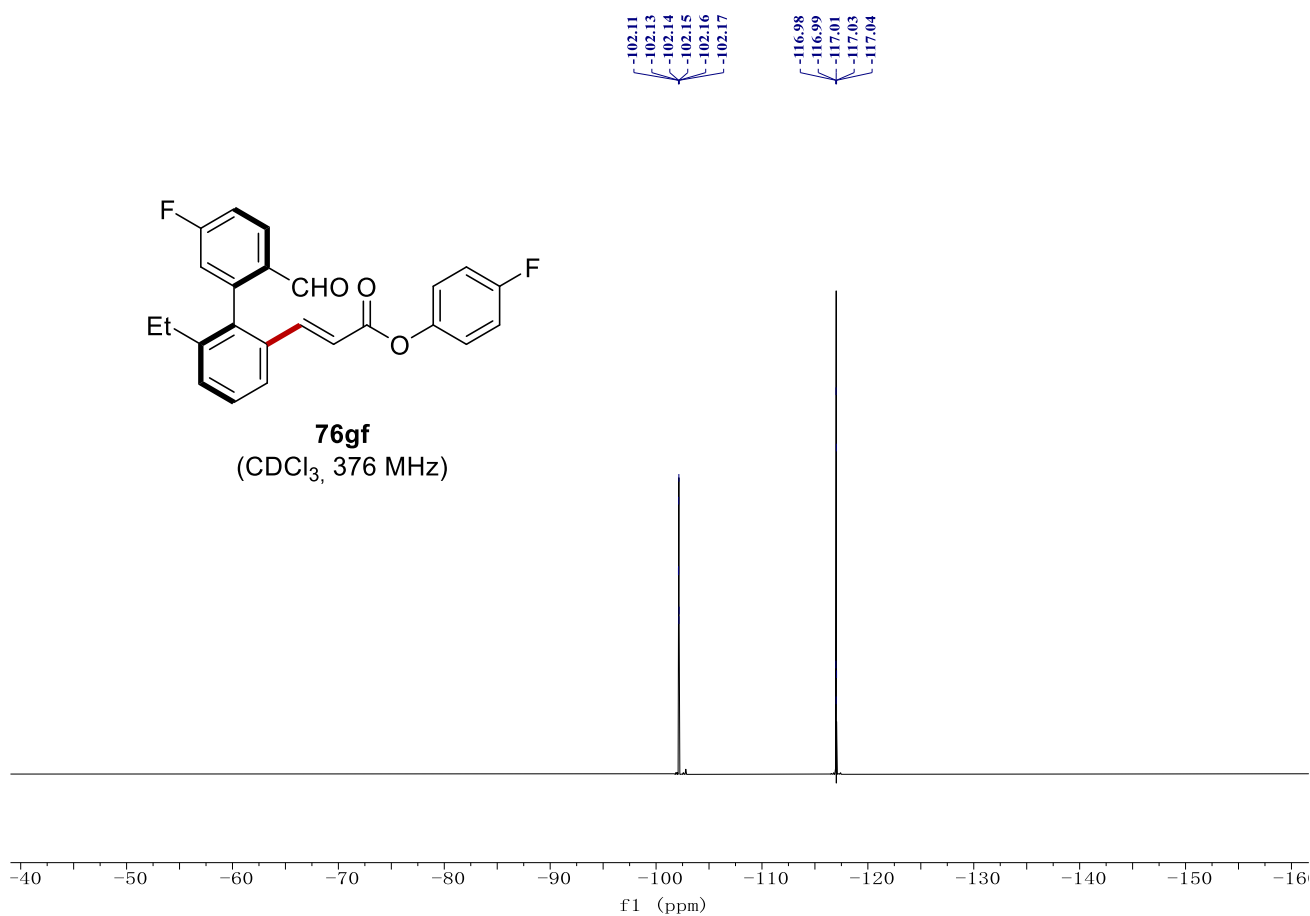
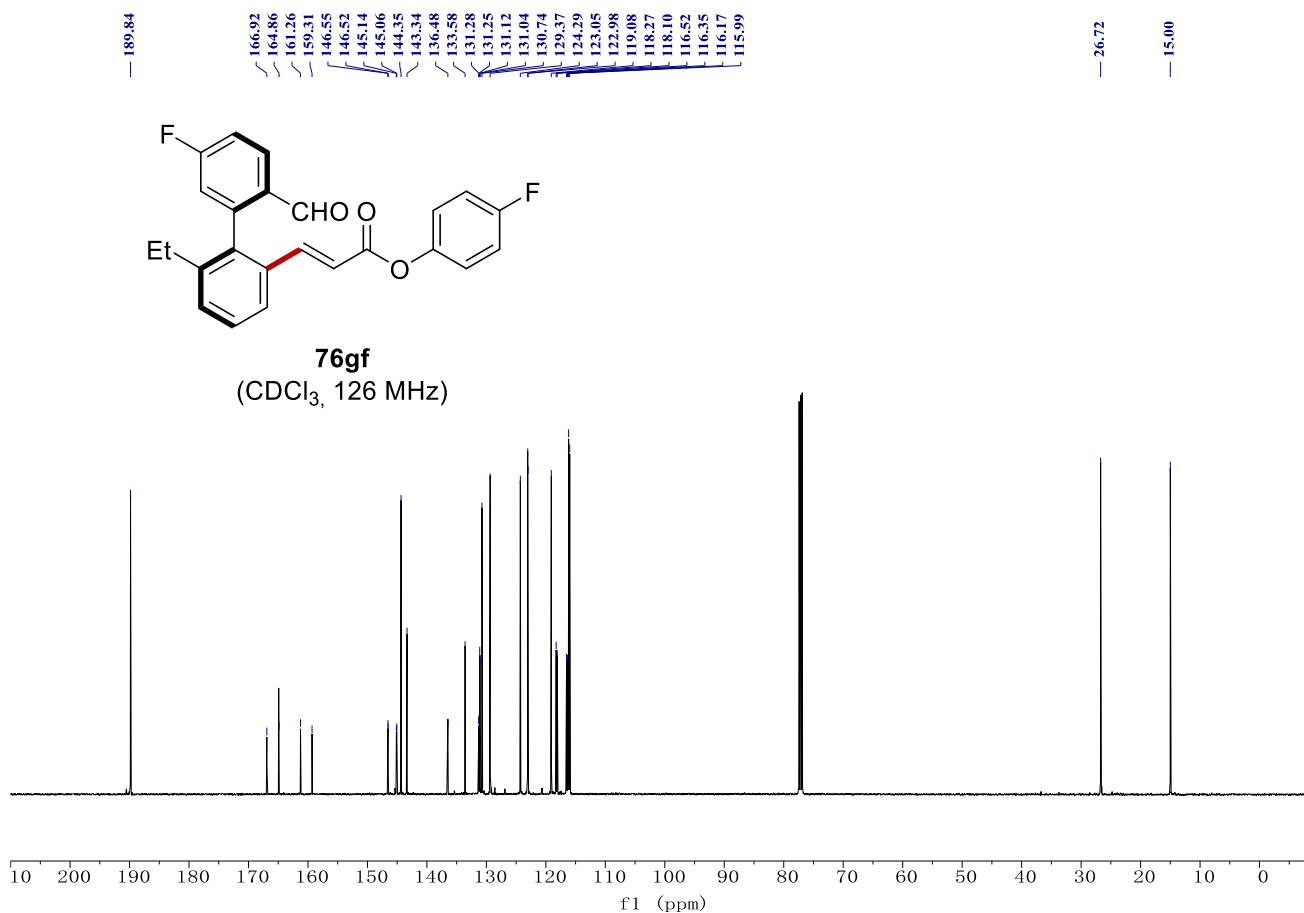
76fe
(CDCl₃, 126 MHz)



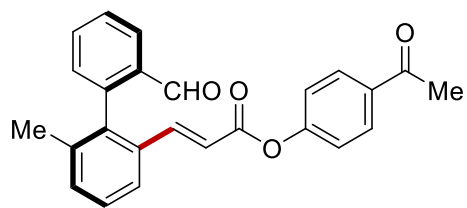
NMR Spectra



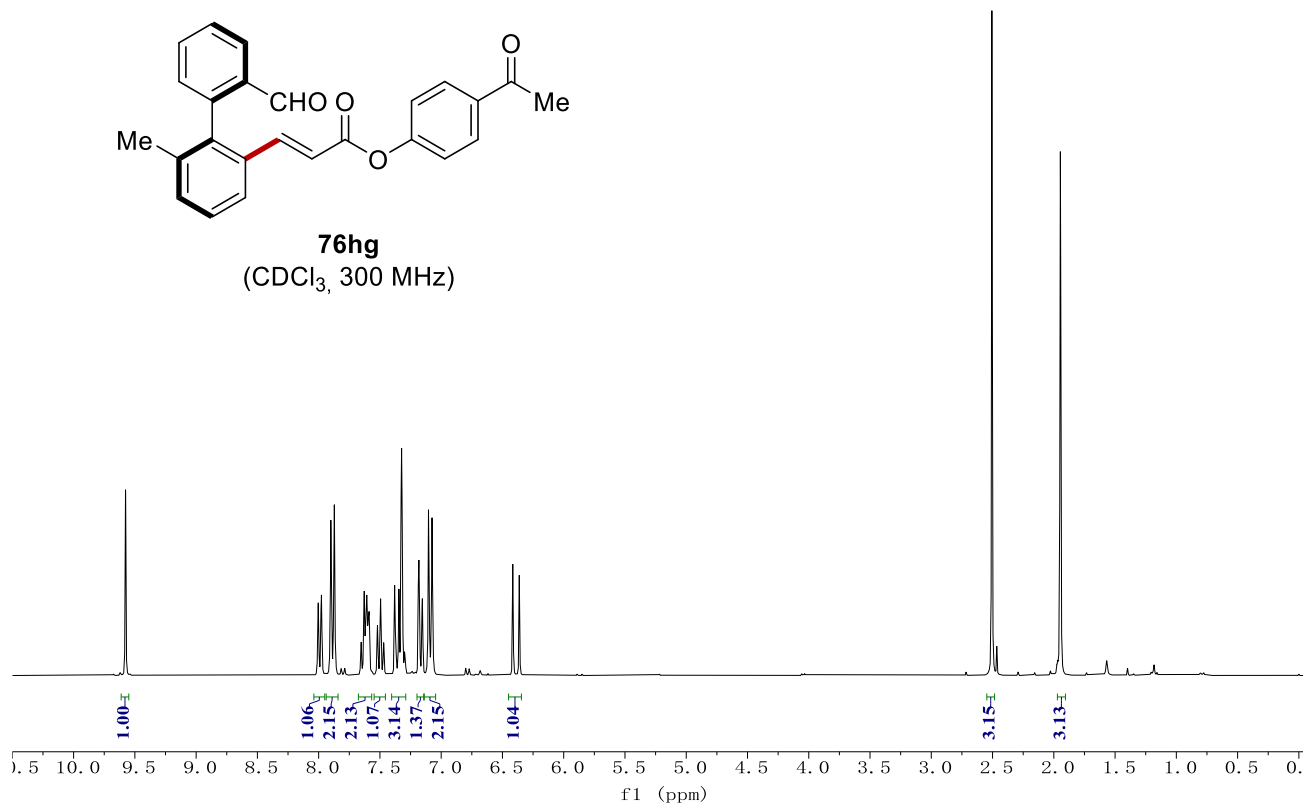
NMR Spectra



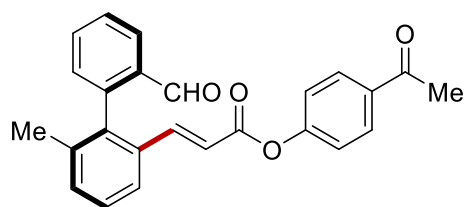
NMR Spectra



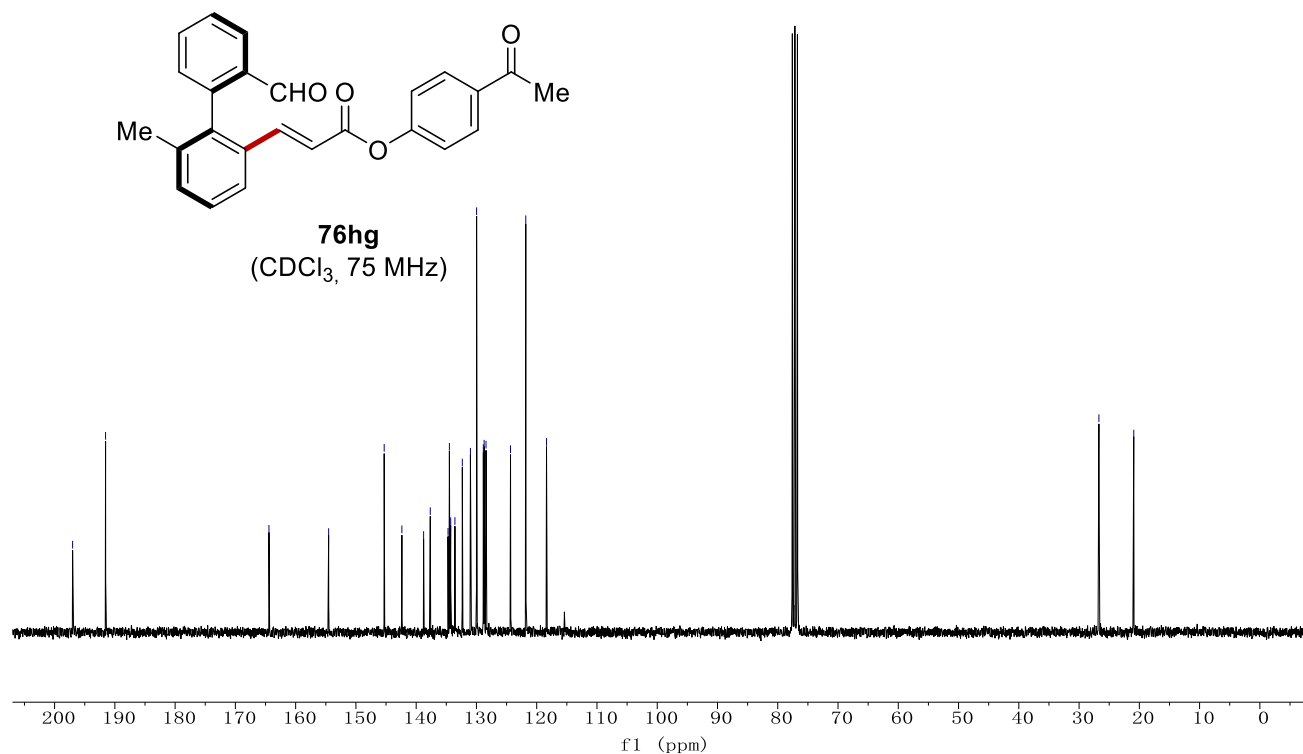
76hg
(CDCl₃, 300 MHz)



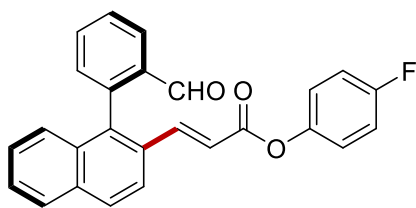
- 197.01
- 191.54
- 164.43
- 154.53
- 145.31
- 142.37
- 138.76
- 137.66
- 134.72
- 134.49
- 134.27
- 133.57
- 132.34
- 131.00
- 129.97
- 128.86
- 128.72
- 128.41
- 124.35
- 121.81
- 118.37
- 26.71
- 20.93



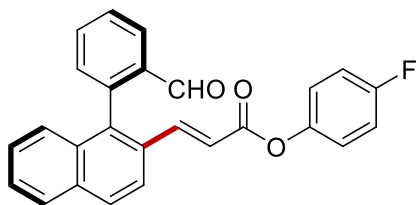
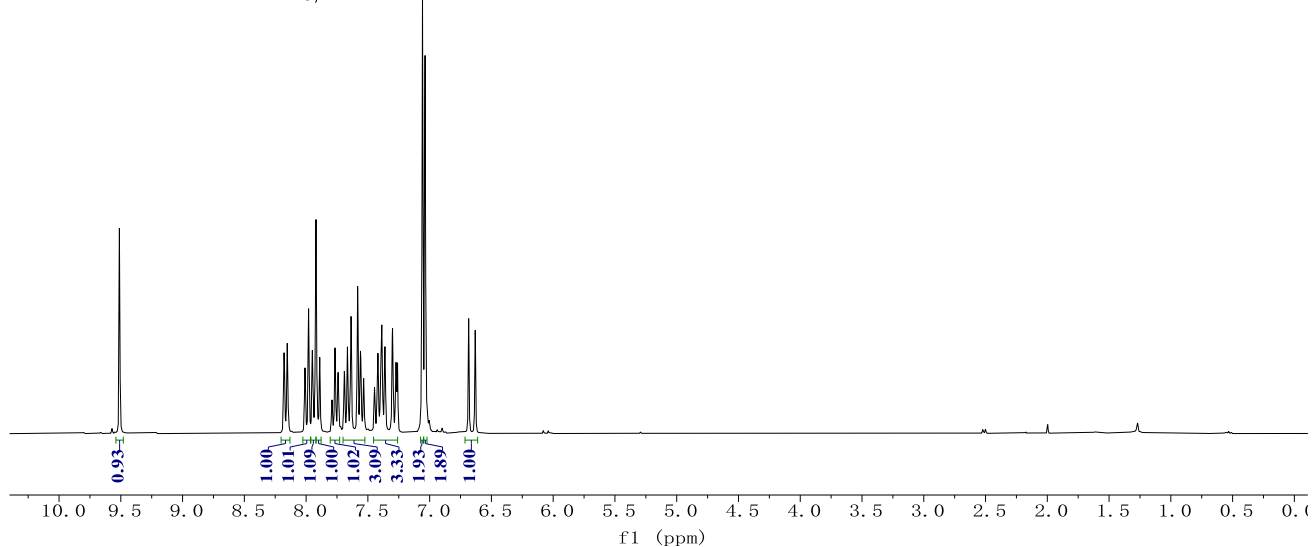
76hg
(CDCl₃, 75 MHz)



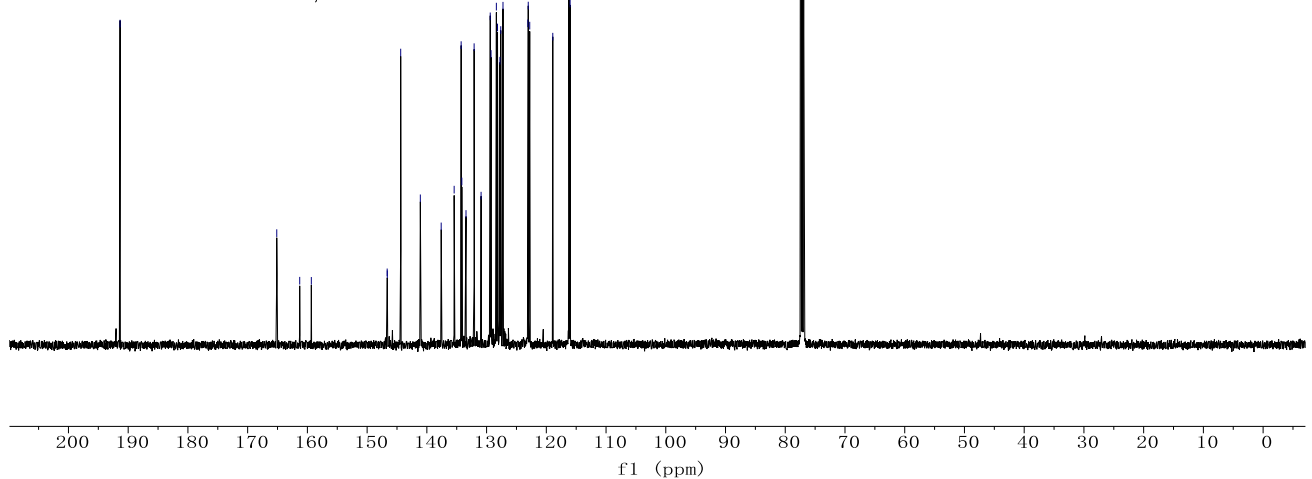
NMR Spectra



76ef
(CDCl₃, 600 MHz)

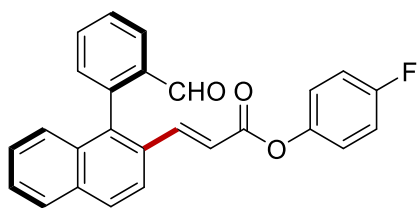


76ef
(CDCl₃, 126 MHz)

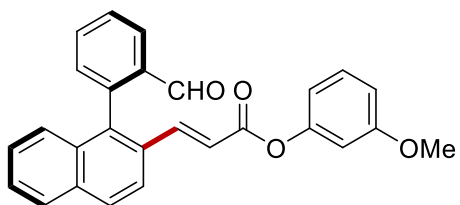
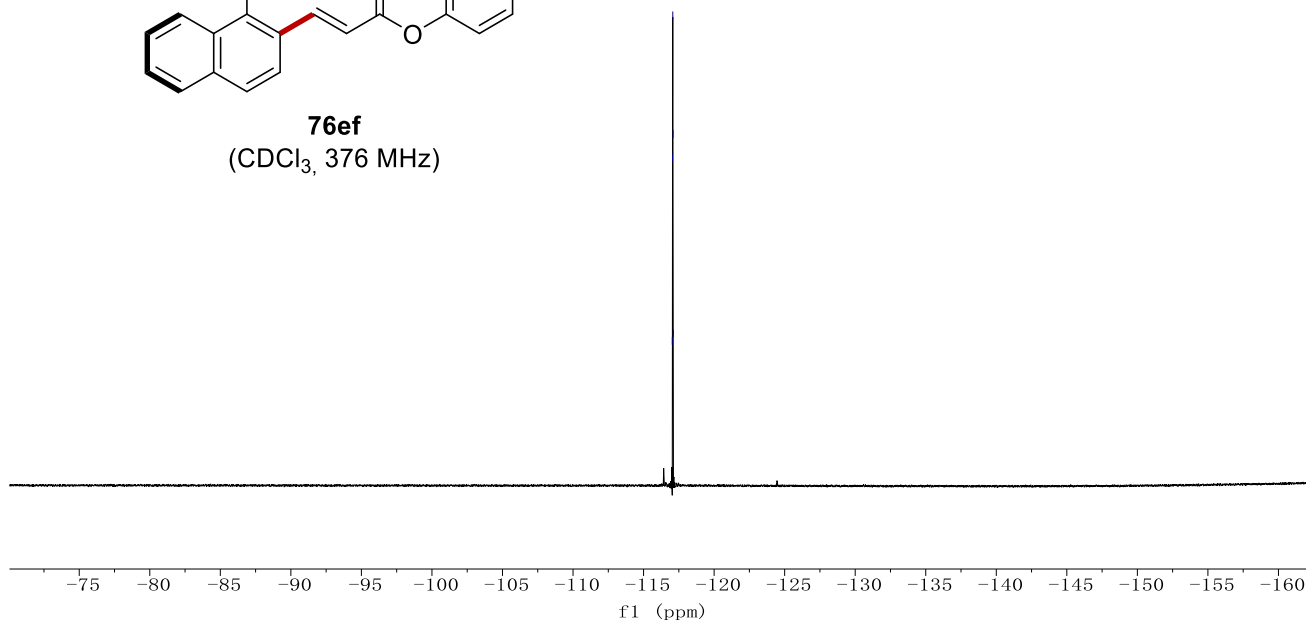


NMR Spectra

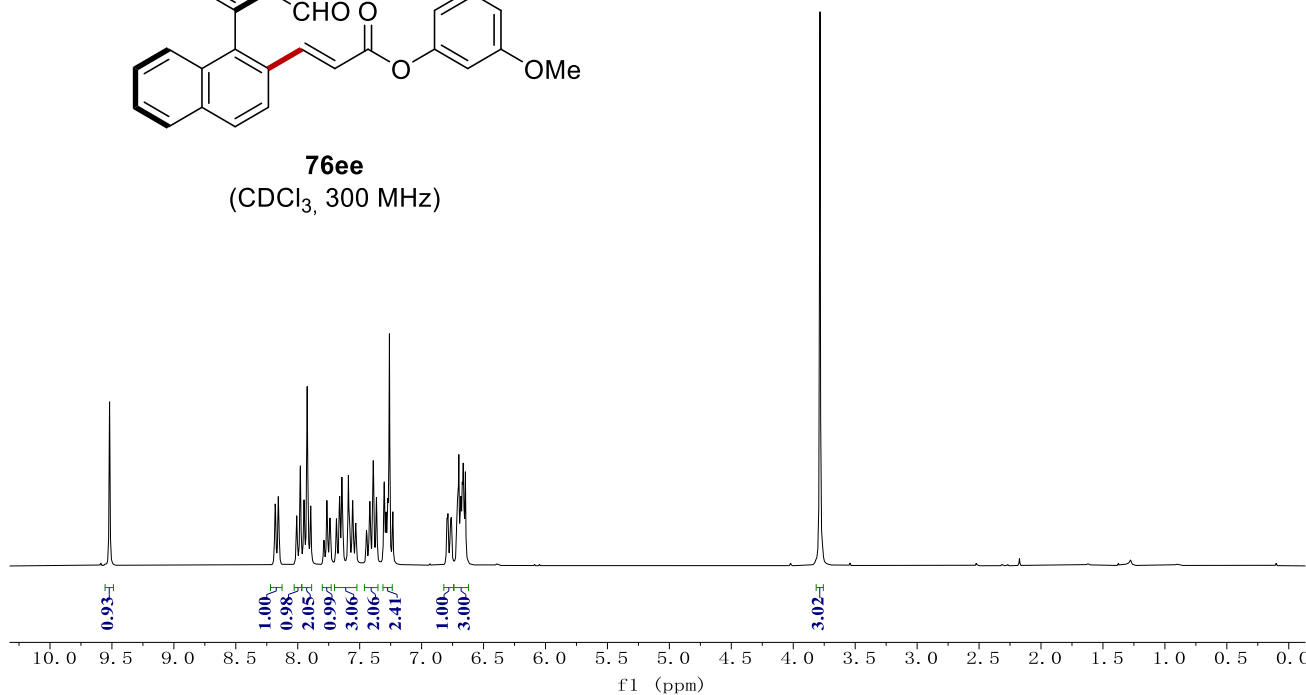
-117.04
-117.05
-117.07
-117.10



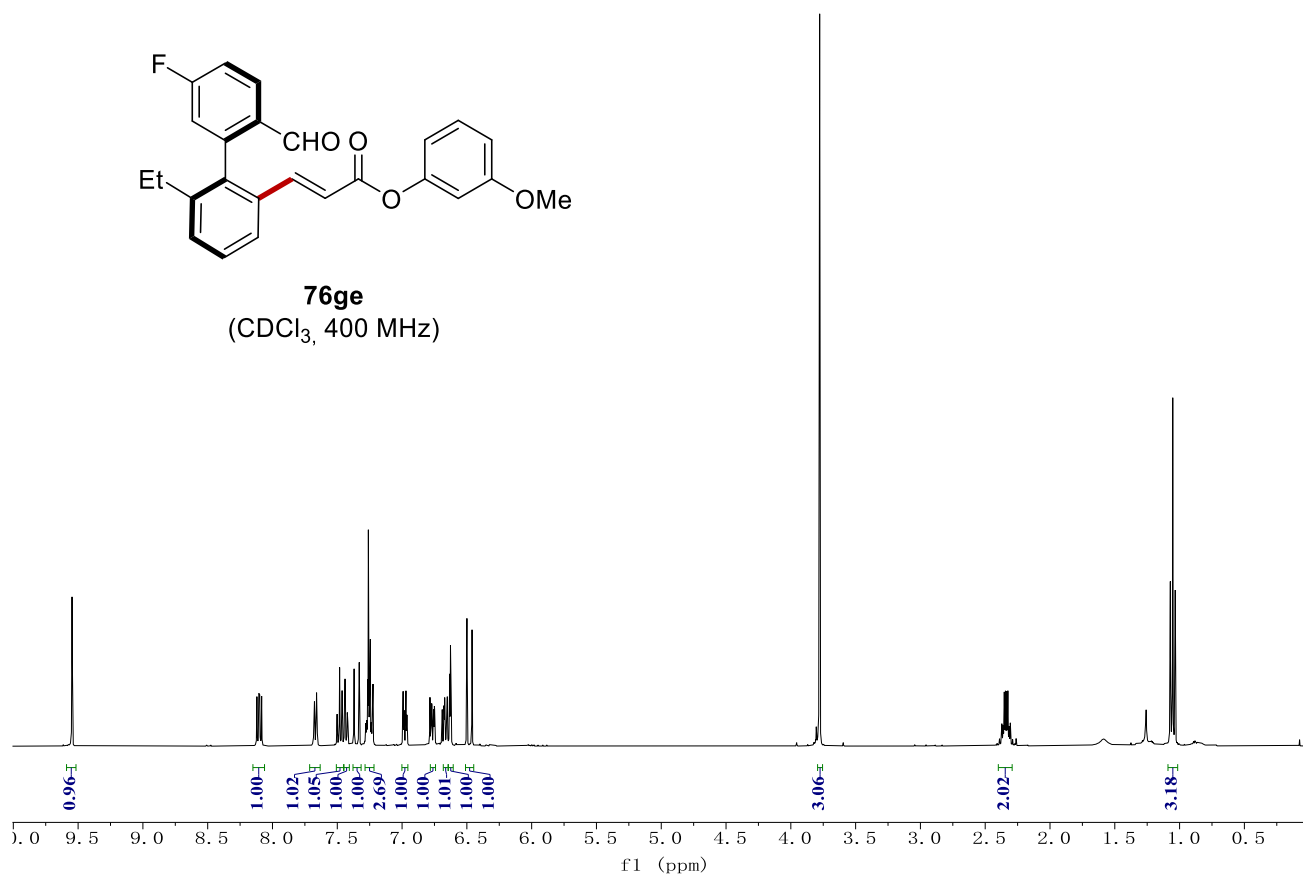
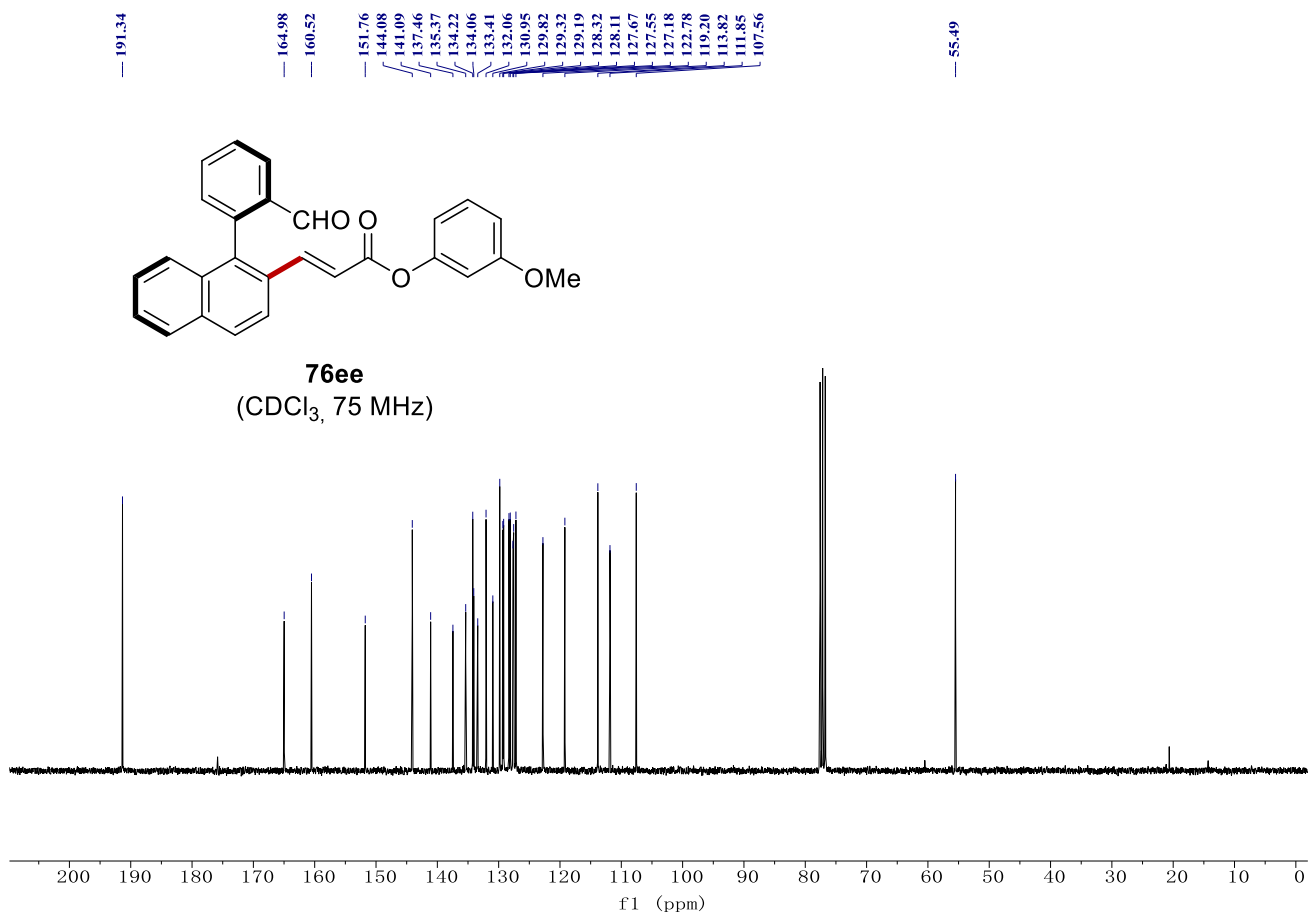
76ef
(CDCl₃, 376 MHz)



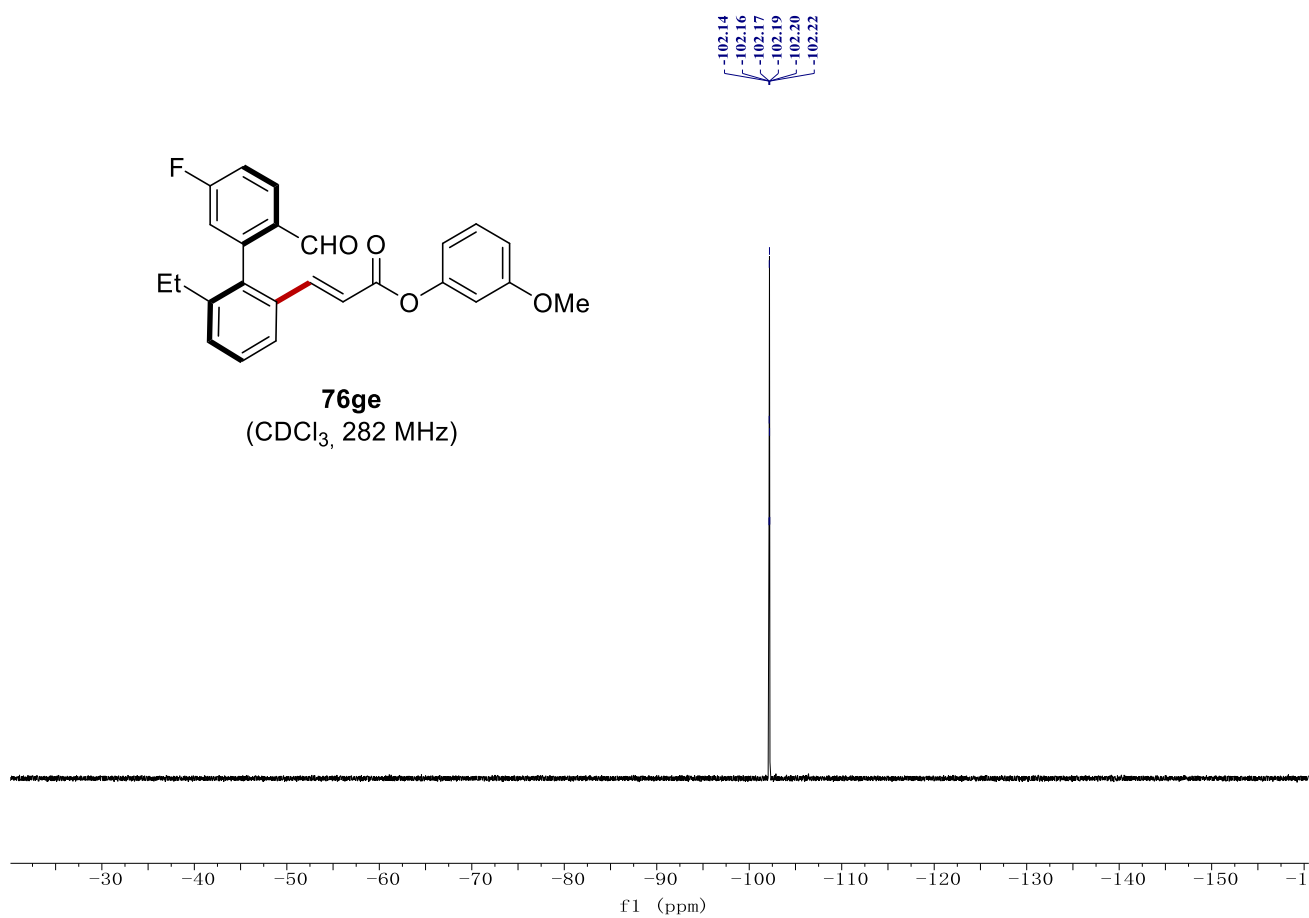
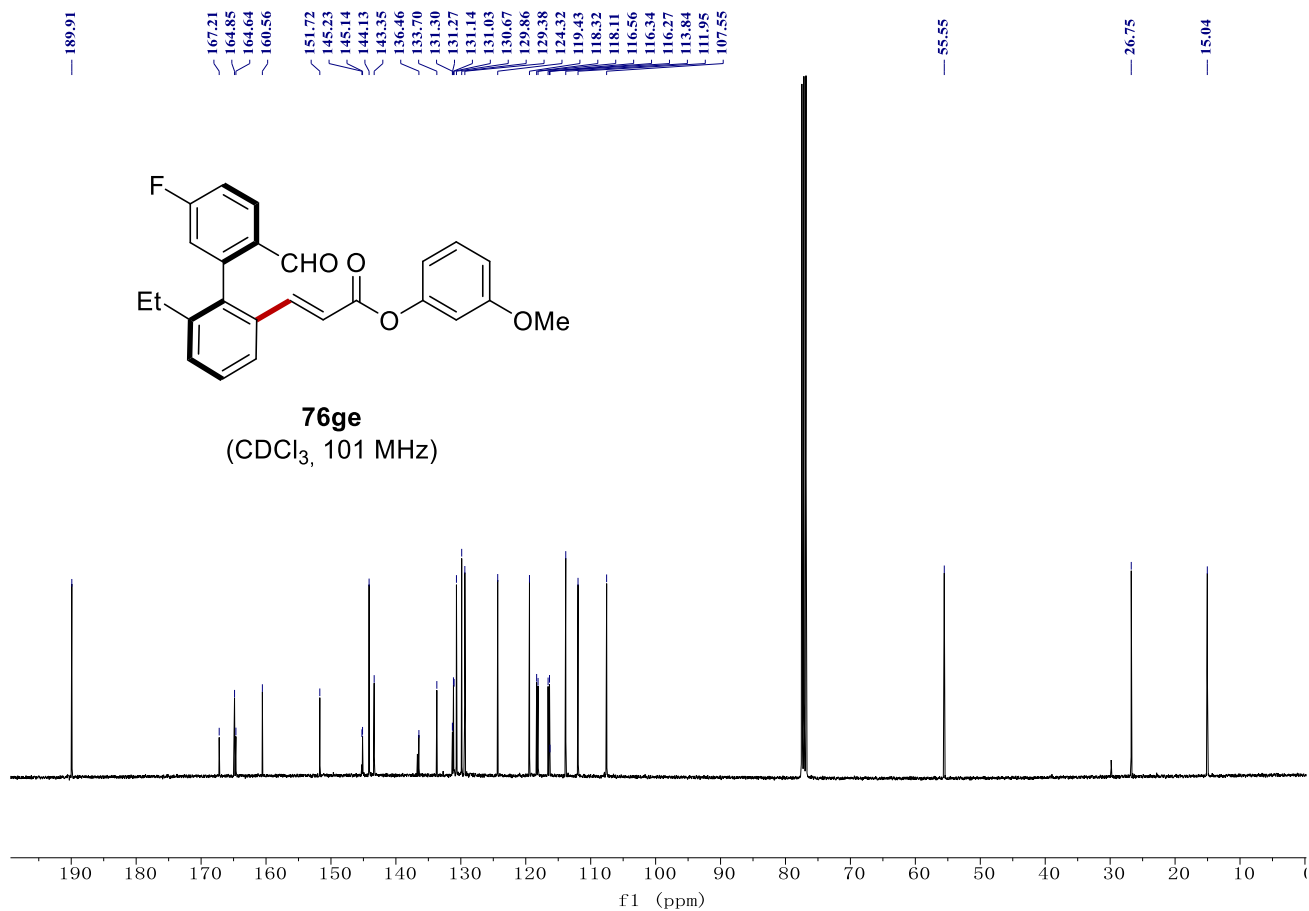
76ee
(CDCl₃, 300 MHz)



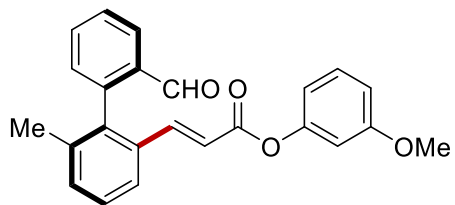
NMR Spectra



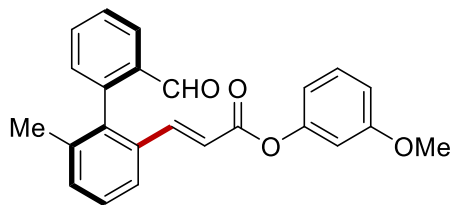
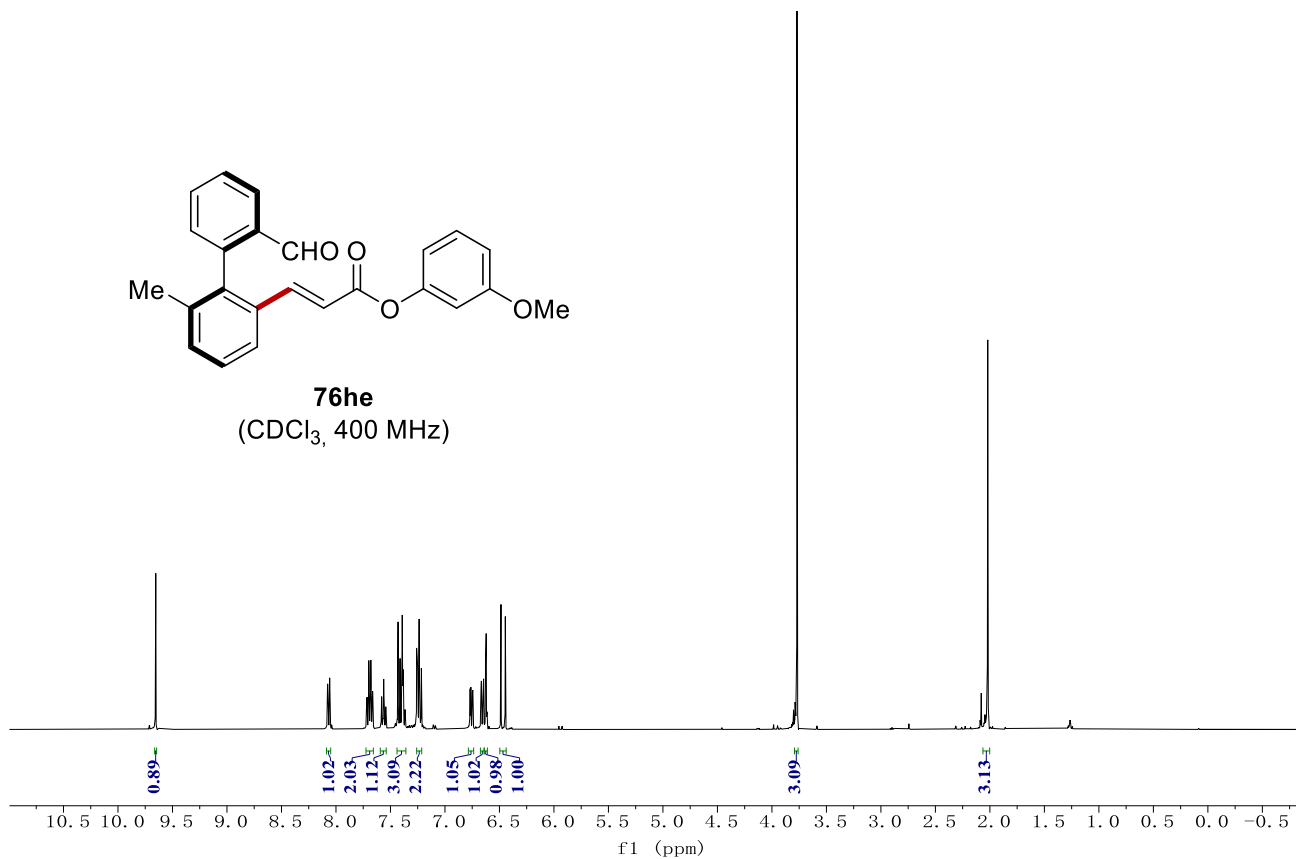
NMR Spectra



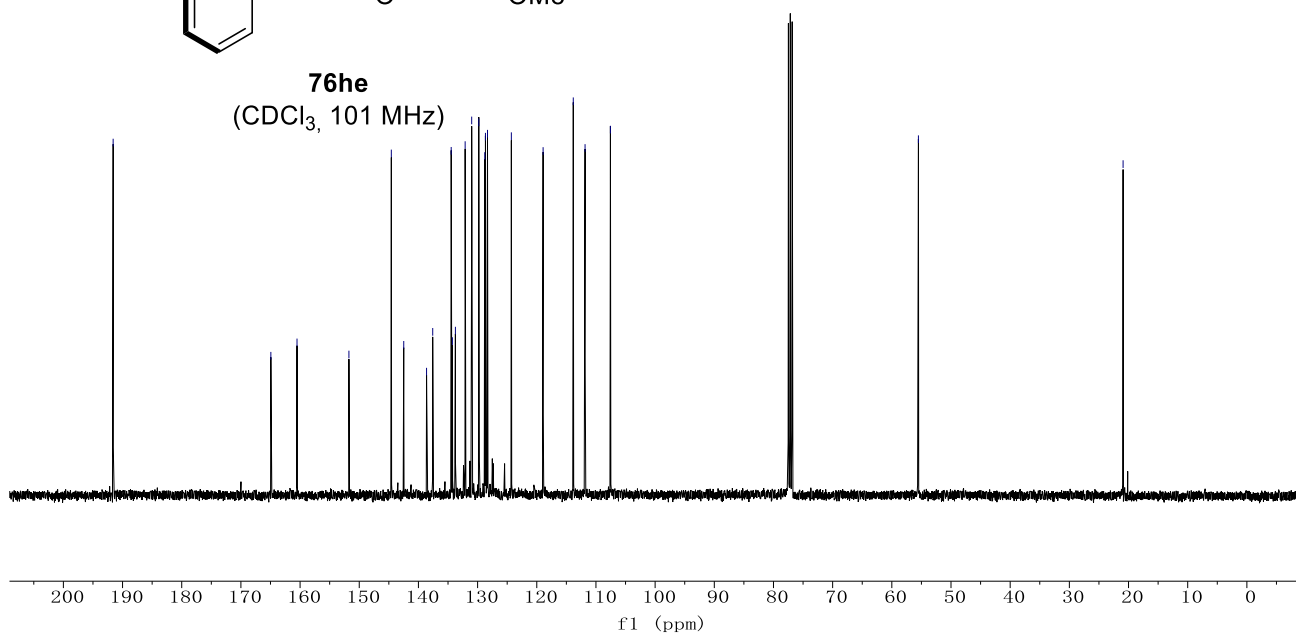
NMR Spectra



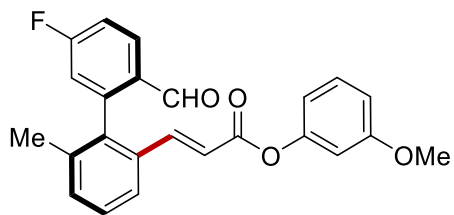
76he
(CDCl₃, 400 MHz)



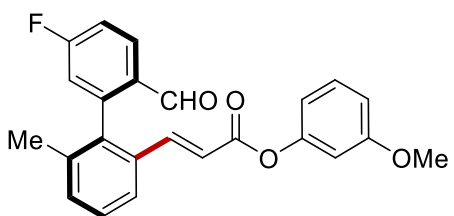
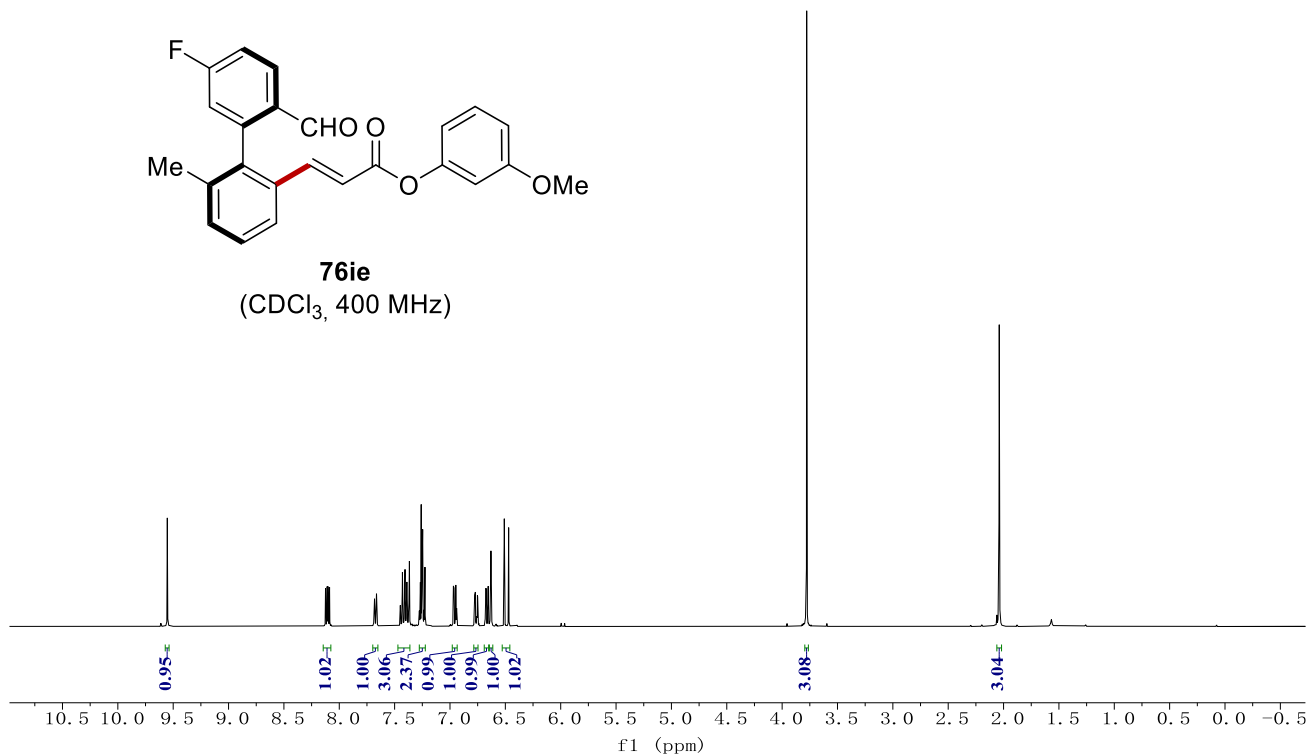
76he
(CDCl₃, 101 MHz)



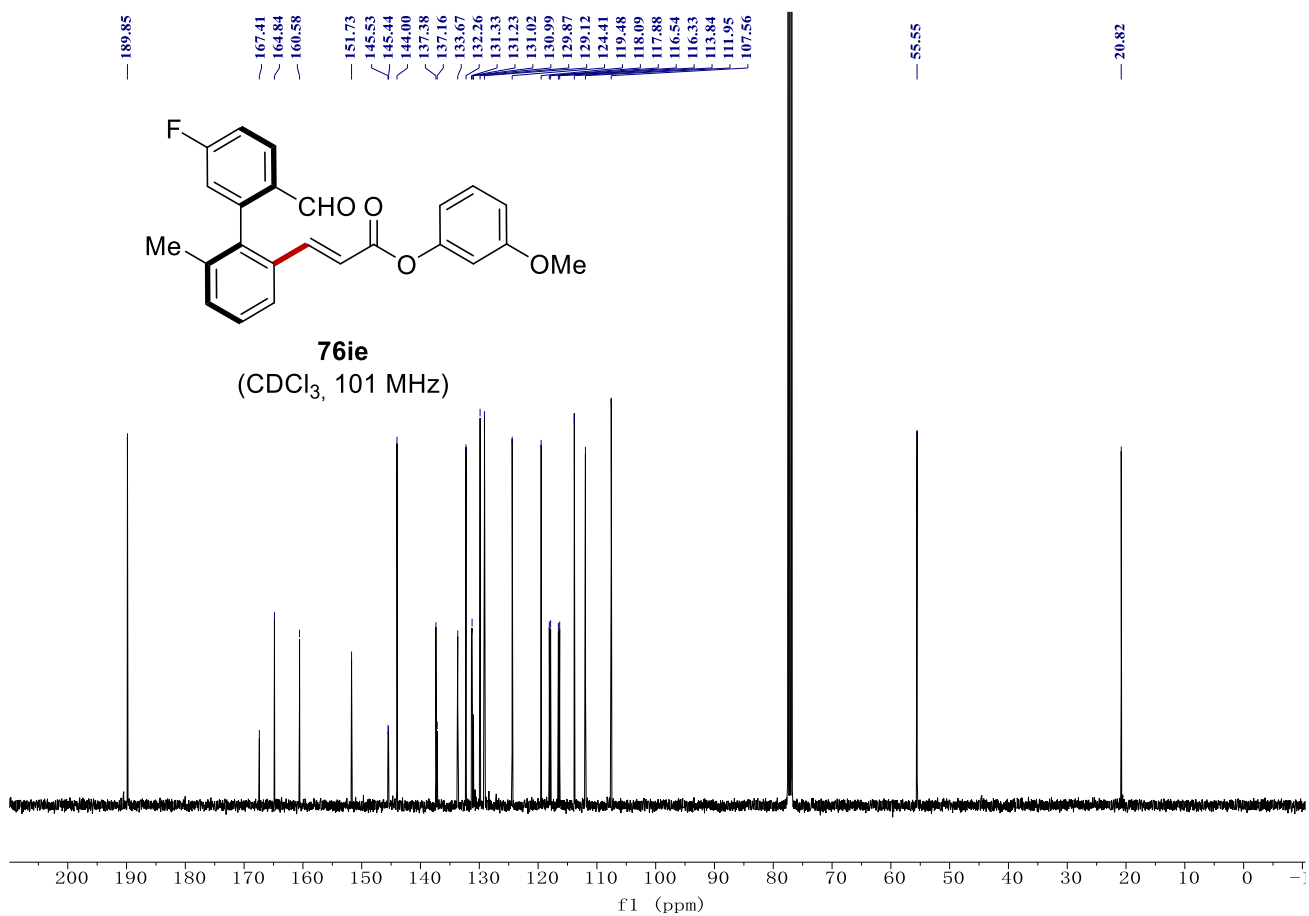
NMR Spectra



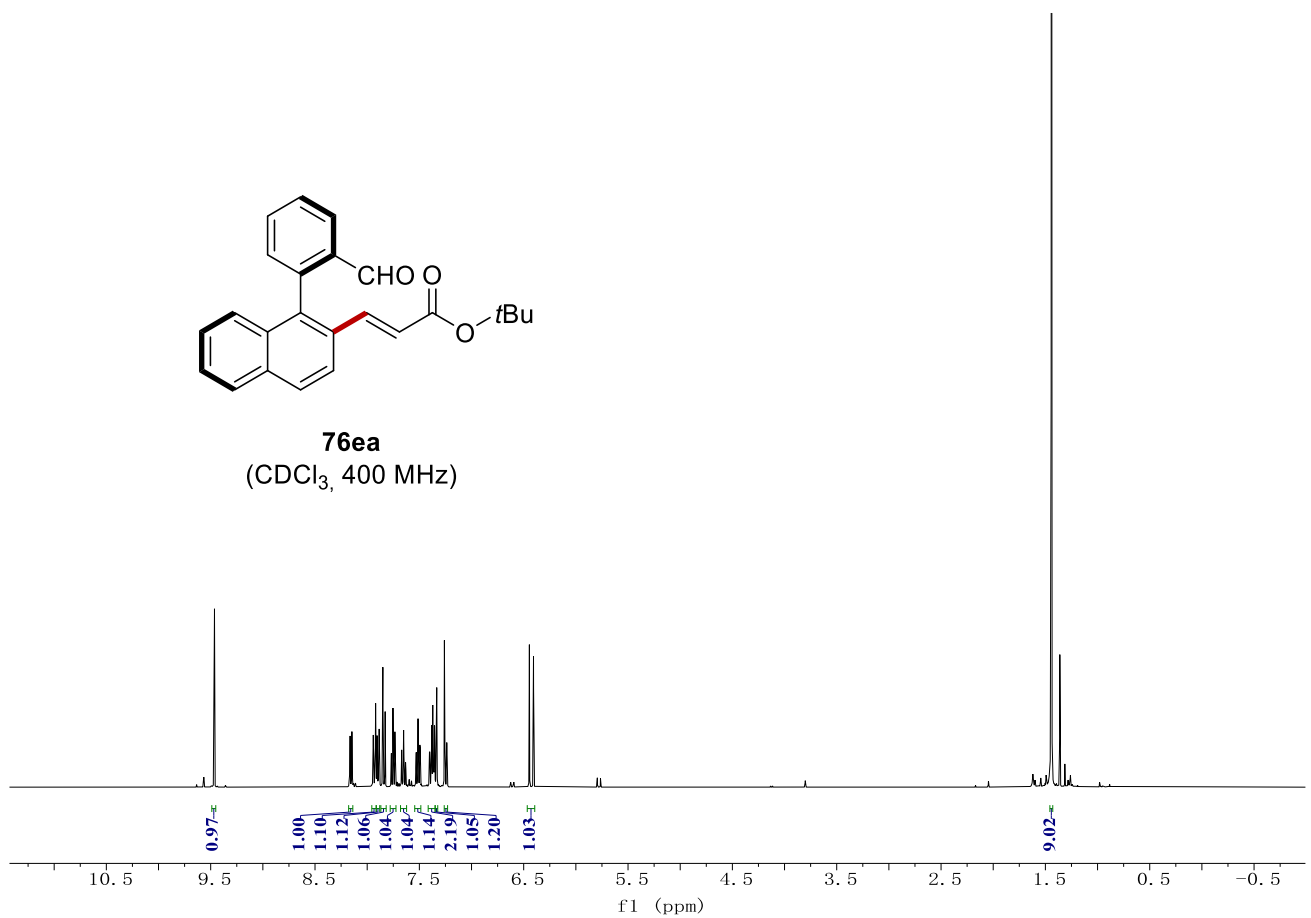
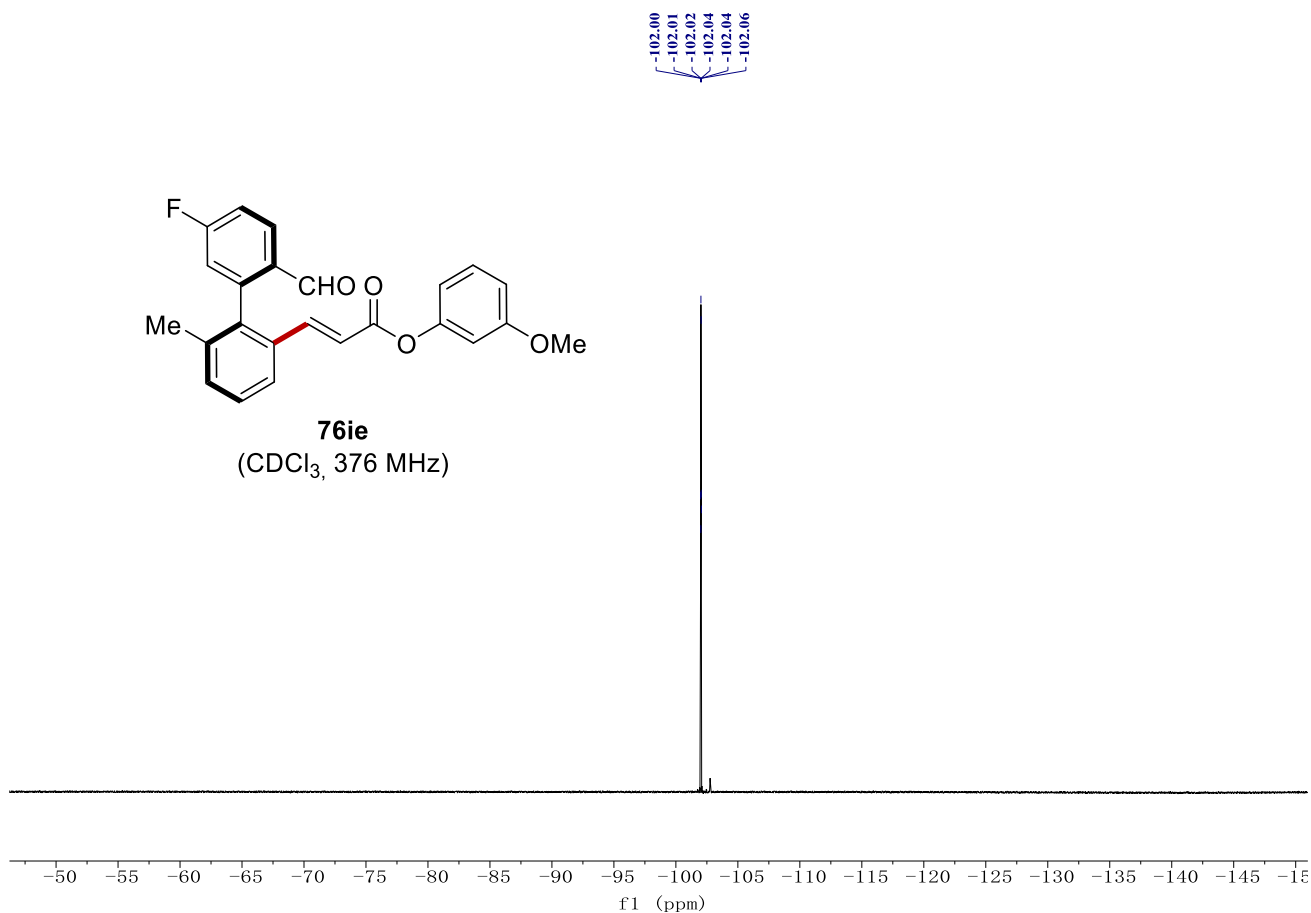
76ie
(CDCl₃, 400 MHz)



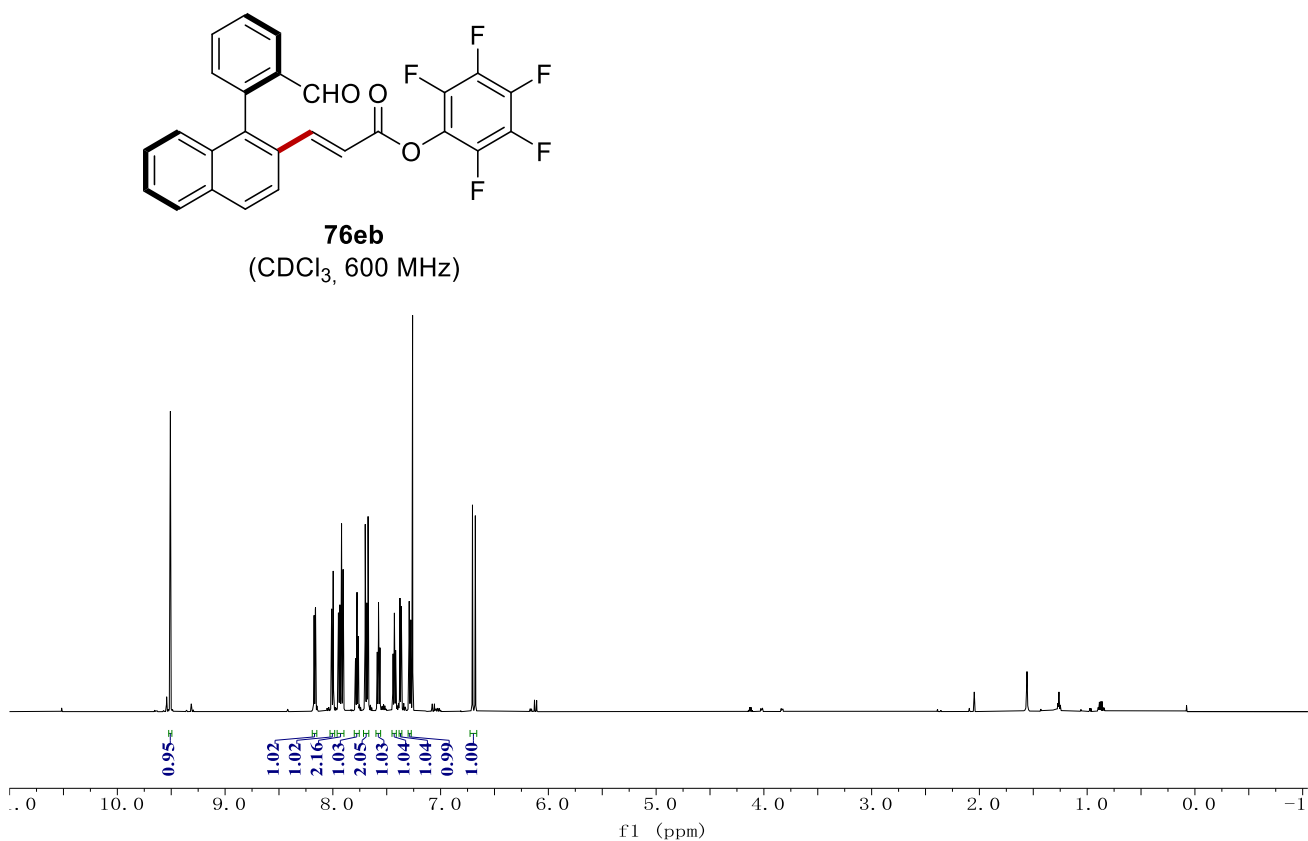
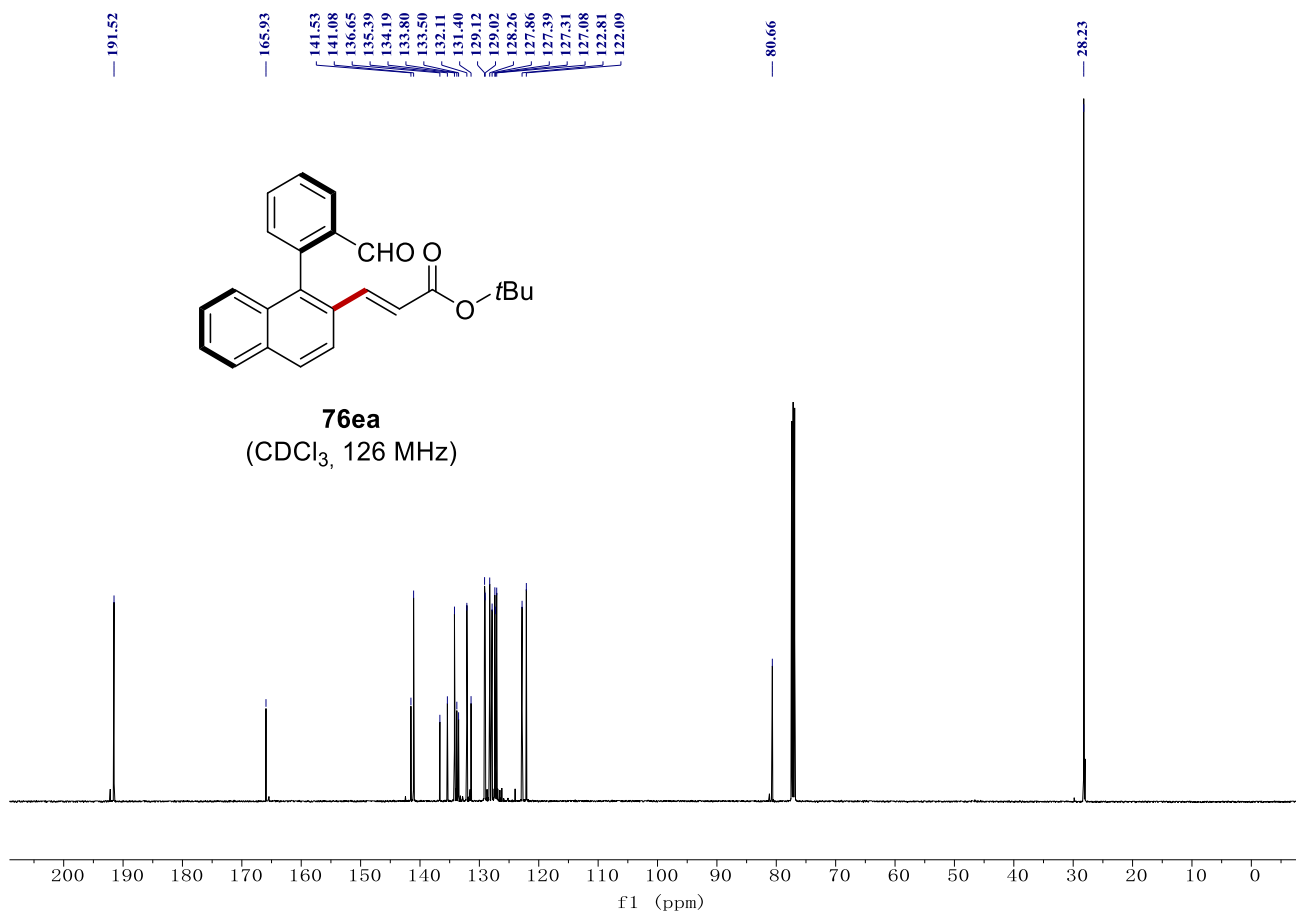
76ie
(CDCl₃, 101 MHz)



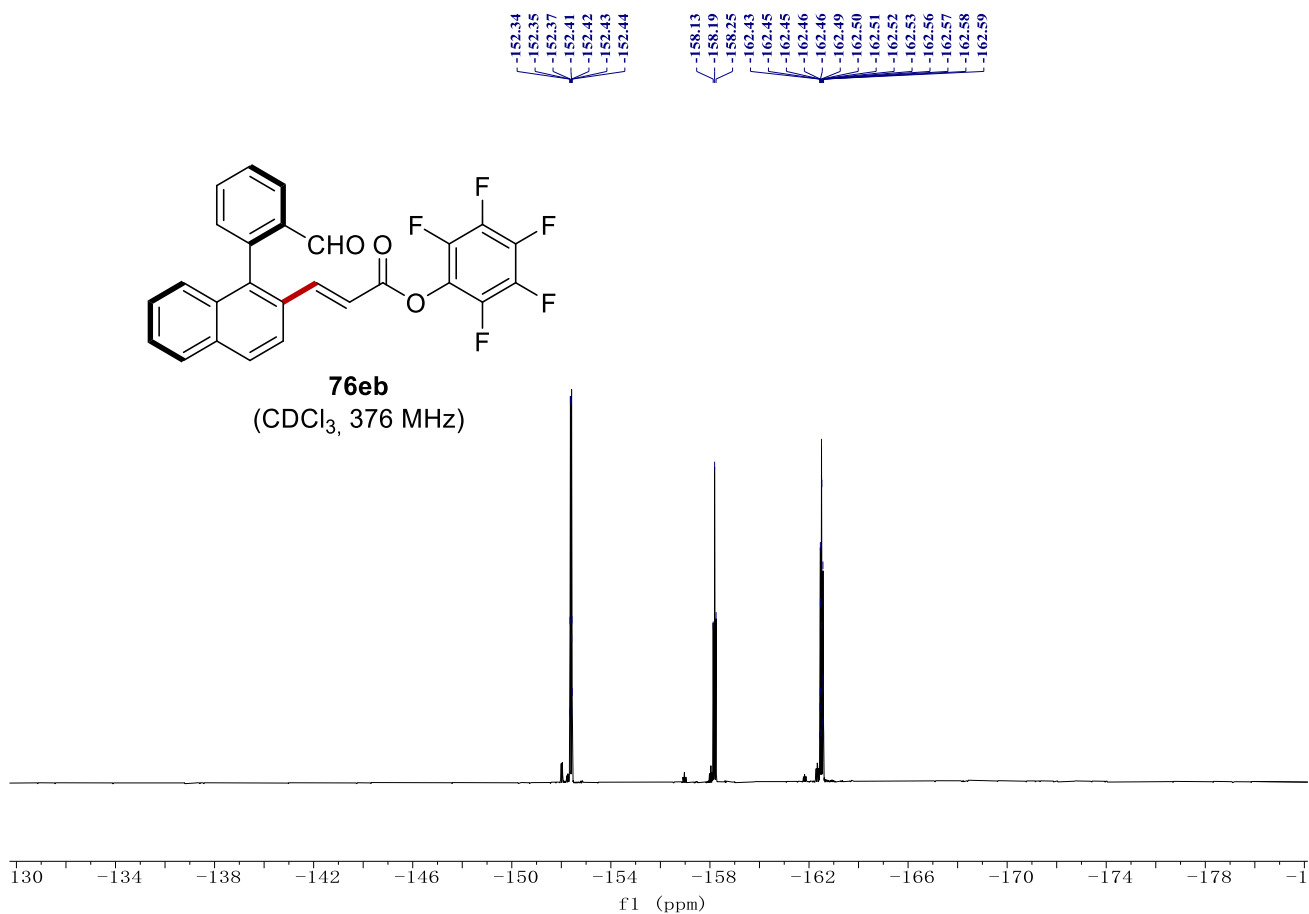
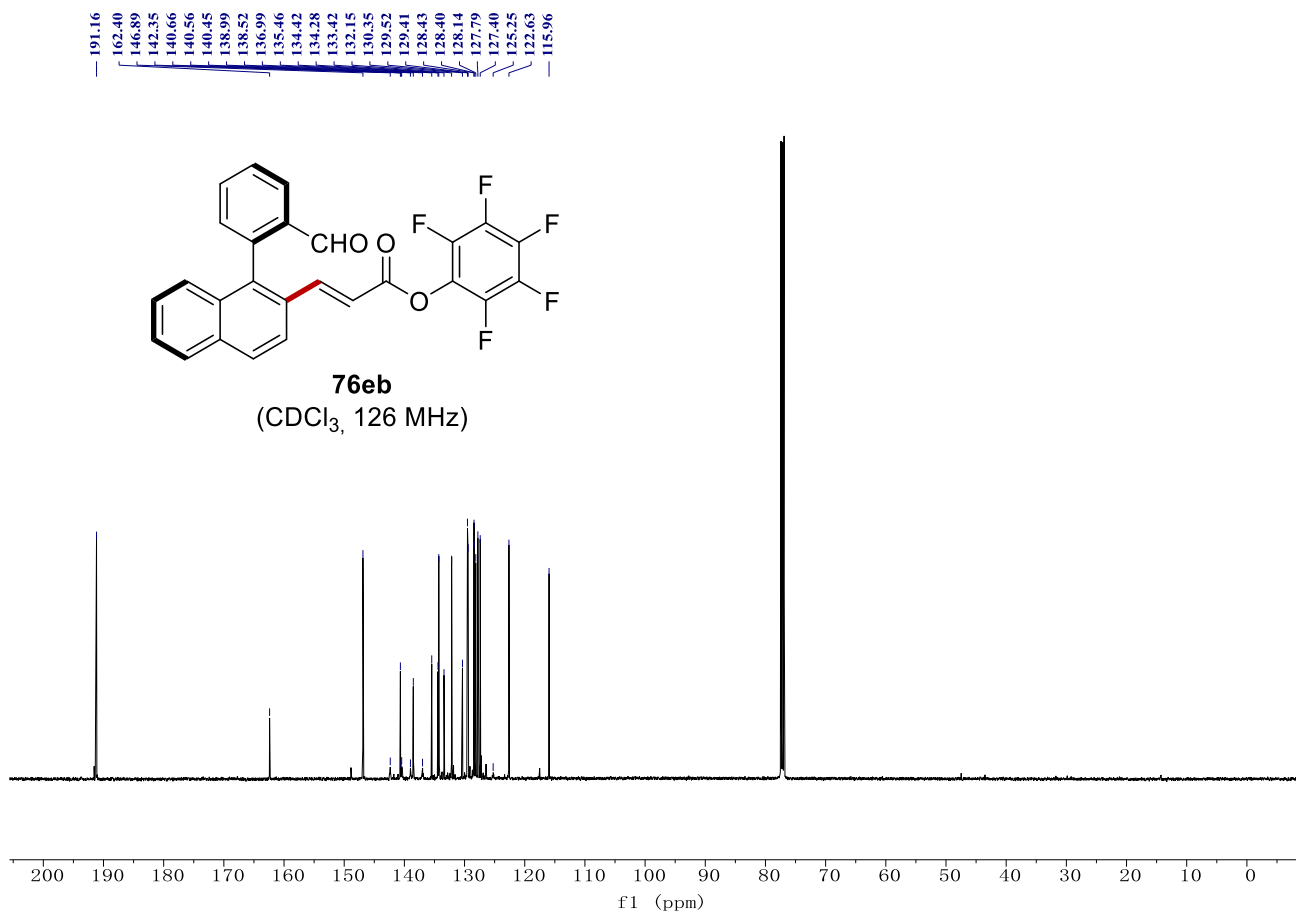
NMR Spectra



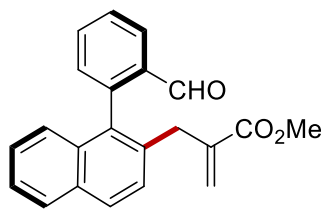
NMR Spectra



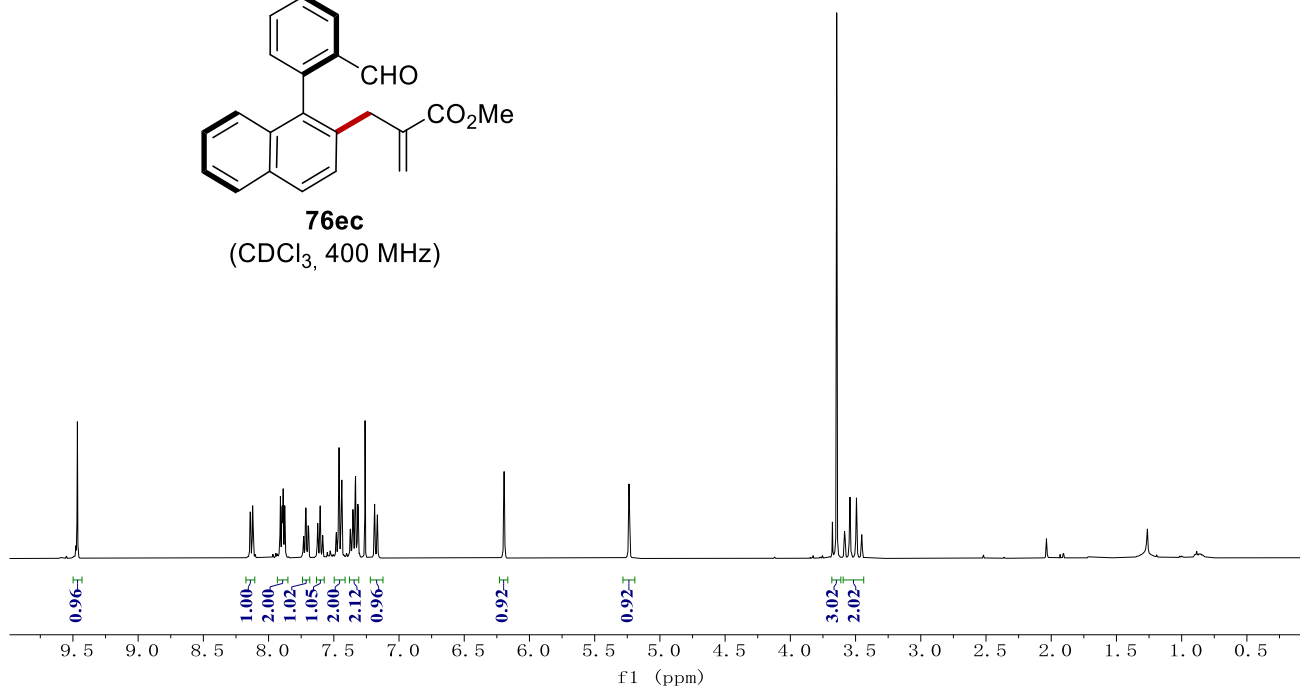
NMR Spectra



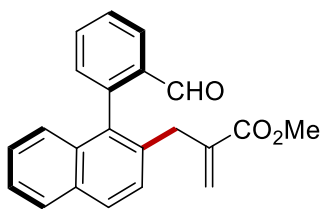
NMR Spectra



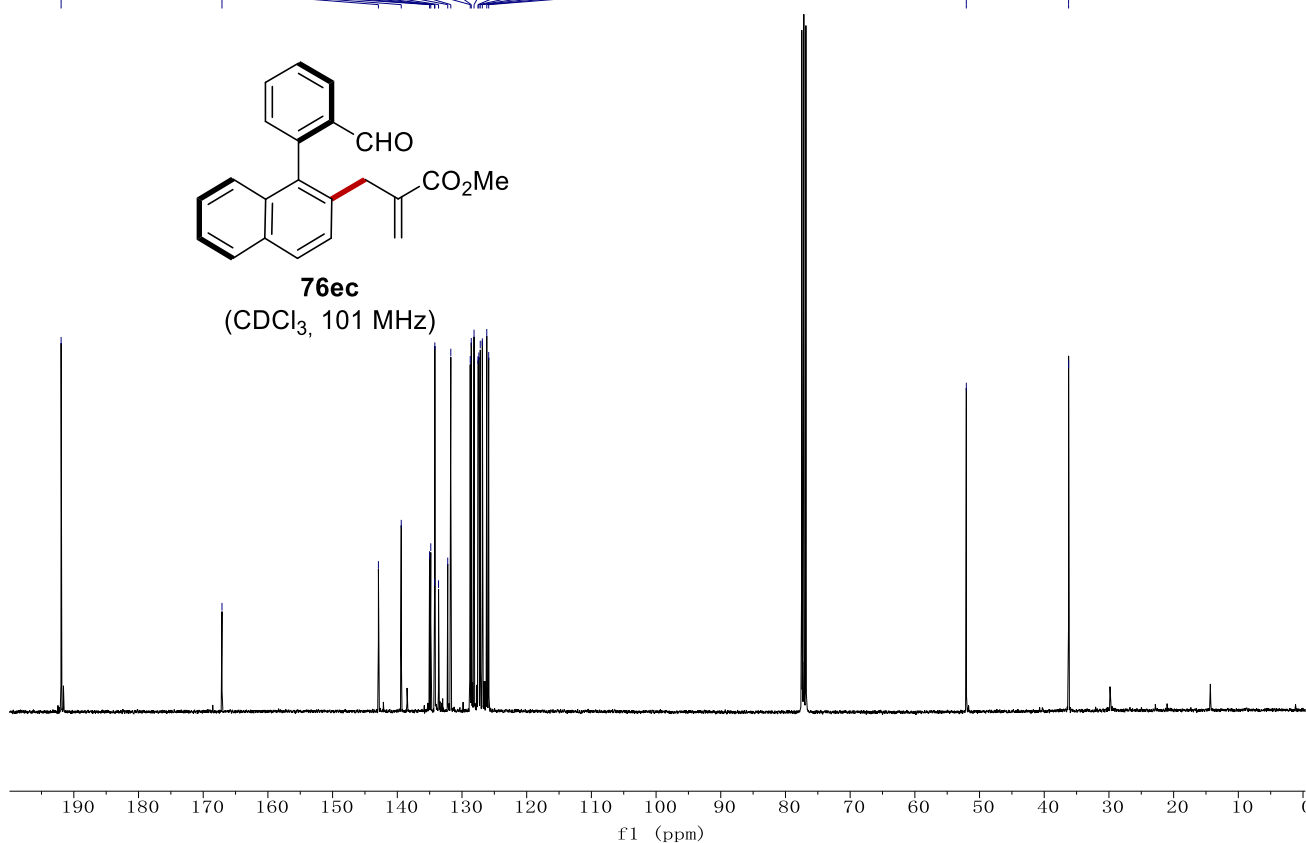
76ec
(CDCl₃, 400 MHz)



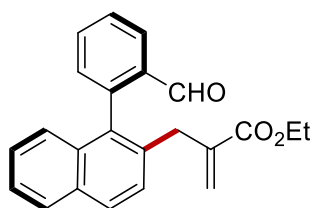
191.97
167.10
142.92
139.39
135.01
134.83
134.24
134.19
133.63
132.21
131.73
128.73
128.57
128.14
127.53
127.40
127.18
126.86
126.17
125.87
52.04
36.23



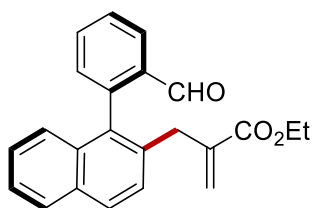
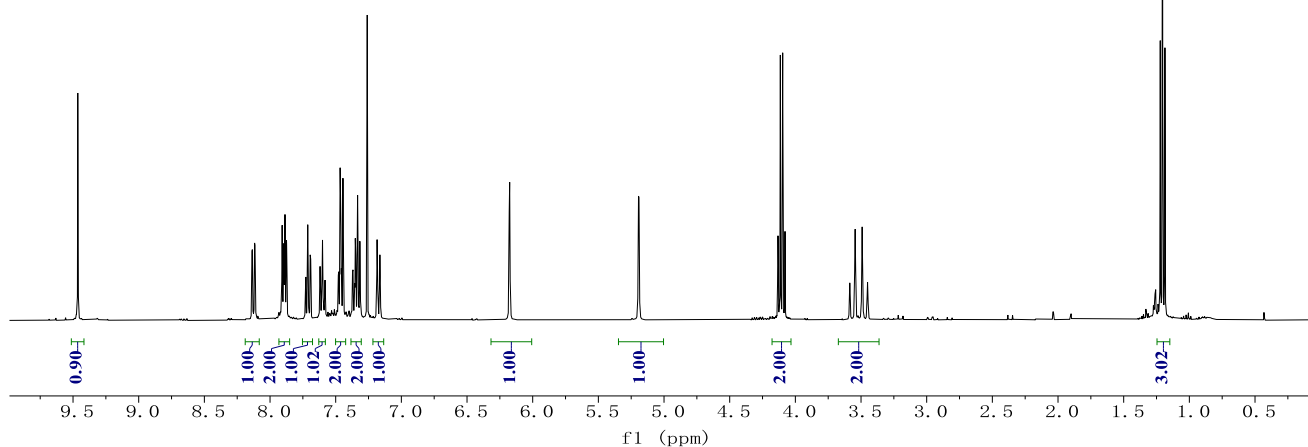
76ec
(CDCl₃, 101 MHz)



NMR Spectra



76ed
(CDCl₃, 400 MHz)



76ed
(CDCl₃, 101 MHz)

